The Formation of an Electrochemical Sensor for the Selective Detection of Dopamine

NUI MAYNOOTH
Ollscoil na hÉireann Má Nuad

Claire Harley BSc. (Hons)

Department of Chemistry
National University of Ireland Maynooth
July 2009

Thesis Submitted to the National University of Ireland in Fulfilment of the Requirements for the Degree of Doctor of Philosophy

Supervisors: Prof. Carmel Breslin and Dr. Denise Rooney

Head of Department: Prof. John Lowry

Table of Contents

Declaration

I hereby certify that this thesis, which I now submit for assessment on the programme of study leading to the award of PhD, has not been submitted, in whole or part, to this or any other university for any degree, and is, except where otherwise stated is the original work of the author.

Signed: _____   Date: _____

Dedication

Dedicated with love to my parents and my grandmothers

Kathleen 'Tattley' Davis and Sadie Harley.

Acknowledgements

First and foremost, I would like to thank my supervisors Prof. Carmel Breslin and Dr. Denise Rooney. Carmel in particular has been a constant source of support and encouragement throughout my time in Maynooth and I am deeply indebted to her for her guidance, understanding, patience and boundless knowledge.

I would also like to acknowledge the funding I received from the Irish Research Council for Science, Engineering and Technology (IRCSET) and the Endeavour Programme. In addition, my sincere thanks goes to Tyndall for the SEM imaging and Tencor analysis and to the staff in the CMAU at Trinity College Dublin for the EDX measurements. A special word of thanks also goes to all the lecturers and technicians who have helped me during the course of my research, especially Mr Noel Williams and Dr. Ken Maddock.

Regarding my time in Australia, I owe a big thank you to Prof. Gordon Wallace and all at IPRI for giving me the opportunity to study at the University of Wollongong. The experience and knowledge I gained in my five short months there was invaluable and I will cherish the memories both inside and outside the lab. Also, this experience would not have been as enjoyable or as memorable without my good friend and colleague Gillian by my side. It is rare in life to meet such a thoughtful and kind hearted person and I am truly honoured to be able to call her my friend. I wish her every success in the future.

To Eimear and Foxy, thank you so much for your camaraderie and support in the lab over the last few years. I can undoubtedly say that my time in Maynooth would not have been the same without your presence. Thanks for the laughs girls. My sincere thanks also goes to the rest of my colleagues in the electrochemistry research group both past and present. In particular, I would like to extend my thanks to Dr. John Colleran for his friendship and guidance. Since his arrival he has been a prolific source of positivity and knowledge within the group.

Thanks also to all my friends and colleagues at NUI Maynooth outside of the electrochemistry group, who made my time here so enjoyable. A special word of thanks

goes to Dr. Fiachra Bolger and Declan ('yer oul' one') for their patience and generosity of their time in proof reading and greatly reducing my errors.

To Andrea, Siabhra, Eva, Shauna, Selina, Nicole and all my friends outside of college, I would like to thank you for providing welcome distractions and friendship when needed.

Finally, and by no means least, I would like to thank my Mum, Dad and Elaine for their constant love and support. I would also like to thank another family member who played a significant role in my life, Granny Tattley, RIP.

Abstract

In this thesis results are presented and discussed on the formation, characterisation, optimisation and performance of a polypyrrole-sulfonated β-cyclodextrin (PPy-SCD) film that can be used as novel dopamine (DA) sensor. This material exhibited a higher sensitivity to DA in comparison to the several other polypyrrole modified electrodes that were investigated in this study and it was also highly selective towards DA in the presence of a wide variety of major interfering compounds.

The sulfonated β-cyclodextrins were immobilised in a polypyrrole film *via* a potentiostatic mode of growth from an aqueous solution of pyrrole and sulfonated β-cyclodextrin. No supporting electrolyte was used to ensure that the polymer was only doped by the anionic sulfonated β-cyclodextrin. The DA was detected at this material in a sulfate supporting electrolyte, giving peak oxidation and reduction currents at approximately 0.450 V vs. SCE and 0.320 V vs. SCE, respectively, for a 1.0×10^{-3} mol dm^{-3} DA solution. However, similar DA oxidation currents and potentials were obtained in a chloride supporting electrolyte solution. This increases the potential of the PPy-SCD film as a possible *in-vivo* DA sensor seeing as most biological samples have a high saline content.

The oxidation of DA at the PPy-SCD modified electrode was optimised by varying a range of factors and conditions. Using these optimised parameters a limit of detection of 3.36×10^{-6} mol dm^{-3} was evaluated using constant potential amperometry. An attempt to increase this sensitivity further by incorporating ultrathin fibers into the polymer matrix proved to be unsuccessful.

It was determined that a 1:1 inclusion complex was formed between the DA and the sulfonated β-cyclodextrin, whereby the hydrophobic moiety of the DA was included in the cavity. Complex formation constants of 199.54 ± 4.88 mol^{-1} dm^3 and 240.18 ± 5.87 mol^{-1} dm^3 were obtained, respectively, from cyclic voltammetry and rotation disk voltammetry in solution. In fact, this complexation in conjunction with oxidation at the polypyrrole film is responsible for the significant DA signal observed at the PPy-SCD modified electrode.

A wide variety of interfering compounds were also examined to establish their effect, if any, on the determination of DA at the PPy-SCD modified electrode. The interference from several major interfering compounds, such as ascorbic acid and uric acid, could be effectively blocked. No interference was exhibited from 5-hydroxytryptamine and 5-hydroxyindole acetic acid at low concentrations of DA and the oxidation peaks of DA and acetaminophen were effectively separated with the acetaminophen having no influence on the oxidation peak current or potential of the DA signal. However, the interference from epinephrine, homovanillic acid and 3,4-dihydroxyphenylacetic acid could not be eliminated.

Chapter 1

Introduction and Literature Review

1.1 Conducting Polymers

1.1.1 What is a Conducting Polymer?

Everyday polymers, generally referred to as plastics, are composed of simple repeating units called monomers and are generally known to have good insulating properties. It is this characteristic that has resulted in insulating polymers being used extensively by the electrical, electronics and packaging industry[1]. Conducting polymers differ from these everyday polymers in that they are intrinsically conducting. Three scientists, A.J. Heeger, A.G. MacDiarmid and H. Shirakawa, are credited for the discovery and development of electrically conducting polymers and they were awarded the Noble Prize in Chemistry in 2000. These polymers are comprised of carbon, hydrogen and simple heteroatoms such as nitrogen and sulfur and contain π-conjugation across the polymer backbone. Typical π-conjugated conducting polymers include polyaniline (PANi), polypyrrole (PPy) and polythiophene, Figure 1.1.
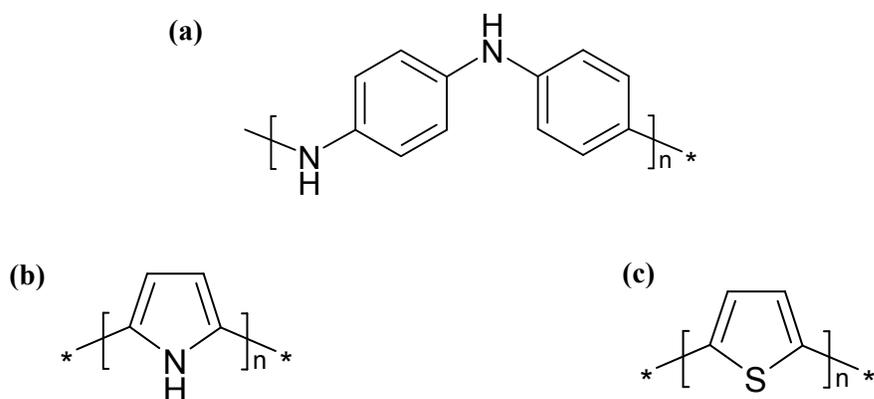
Figure 1.1: Structure of (a) polyaniline (PANi), (b) polypyrrole (PPy) and (c) polythiophene in the dedoped state.

An early explanation of the conductivity exhibited by conducting polymers was given by Bredas and Street[2]. The authors used the band theory of solids to determine the conductivity classification of conducting polymers. In general, materials can be classified into three categories depending on their electrical conductivity: insulators, semiconductors

and conductors. The difference in energy between the top of the outermost valence band and the bottom of the conduction band is referred to as the band gap, E_g, as shown in Figure 1.2. In insulators the electrons in the valence band are separated from the conduction band by a large band gap, $E_g > 10$ eV. Consequently, it is difficult to excite the electrons from the valence band into the conduction band. In semiconductors there is a small enough gap between the valence and conduction bands, $E_g \sim 1.0$ eV, and as a result the electrons can be excited from the valence band into the conduction band at room temperature. For conductors, the valence band overlaps the conduction band and so the conduction band is now partially filled with electrons. Bredas and Street[2] established that the band gap for conducting polymers was around 1.0 eV, and accordingly, categorised them as semiconductors. However, the conductivity associated with conducting polymers cannot be explained entirely using this band theory model.
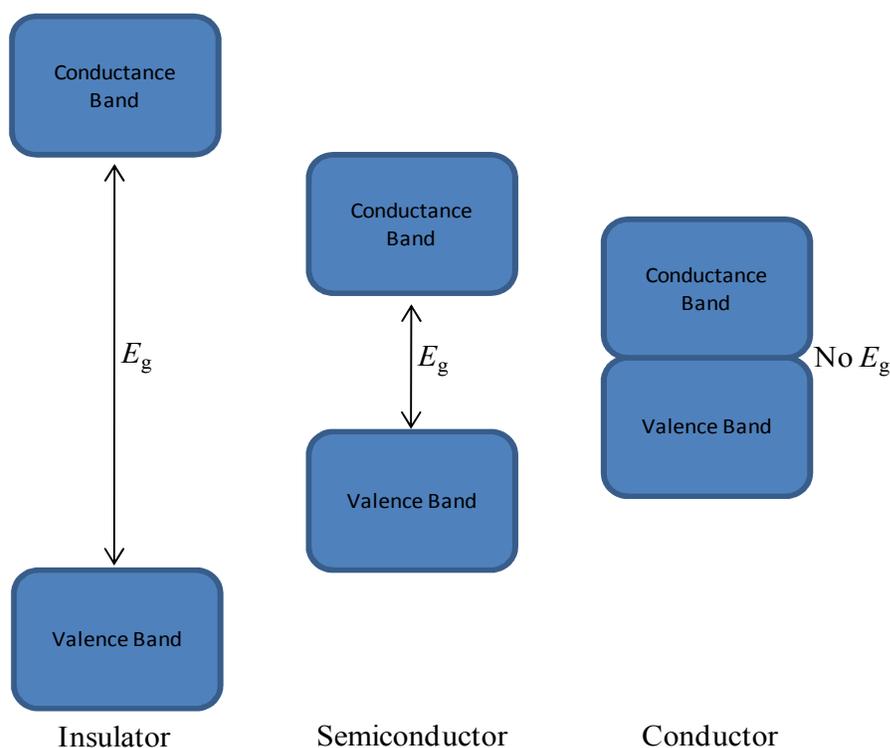
Figure 1.2: The difference in the band gap, E_g, for insulators, semiconductors and conductors.

The inherent conductivity of these conducting polymers results from the formation of various redox states upon oxidation or reduction of the conjugated backbone. This is associated with the formation of polarons (radical cations) and bipolarons[2-4] and this concept is explained in more detail in Sections 1.1.2 and 1.2.3. The charges generated along this polymer backbone during oxidation and reduction are compensated for by incorporating anionic or cationic species, generally known as dopants, into the polymer matrix, Equations 1.1 and 1.2. Here, P denotes the polymer in the neutral state, P^{n+} is the polymer in the oxidised state, P^{n-} is the polymer in the reduced state, X is any cation, F is any anion and n is the moles of the salt. Both the anionic and cationic doping processes enhance the conductive properties of the conducting polymer. This is because the conductivity increases as the doping level increases due to the creation of more mobile charges[5]. The maximum doping level varies for different conducting polymers and for different dopants. For example, the doping level for PPy ranges from 20% to 50% depending on the dopant used[6]. Therefore, the conductivity of the polymer is not only dependent on the redox state of the polymer but also on the degree of doping.

Anionic Doping: $\qquad\qquad\qquad P + nXF \rightarrow P^{n+}nF^- + nX^+$ $\qquad\qquad$ 1.1

Cationic Doping: $\qquad\qquad\qquad P + nXF \rightarrow nX^+P^{n-} + nF^-$ $\qquad\qquad$ 1.2
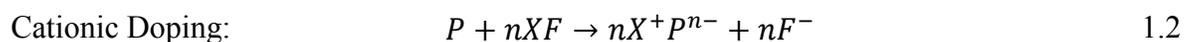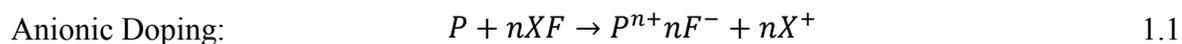
1.1.2 Conducting Polymer Formation

The synthesis of conducting polymers is primarily achieved either chemically or electrochemically. In both cases, the initial step of polymerisation involves the oxidation of the monomer to its radical cation, $M^{+\cdot}$. Once formed, the radicals react with each other, electrochemical polymerisation, or with other monomer molecules, M, in the case of chemical polymerisation. In the electrochemical case, the radical-radical coupling leads to a radical dication. This then looses two protons to form a neutral dimer, which can then be

oxidised to a radical cation, which reacts further to form the polymer, Scheme 1.1. In contrast, a dimer radical cation is generated during chemical polymerisation, Scheme 1.2, which leads to the formation of the polymer[5].

$$M^{+\cdot} + M^{+\cdot} \xrightarrow{-2H^+} \text{Radical Dication} \rightarrow \text{Neutral Dimer} \xrightarrow{-e^-} \text{Radical Cation} \rightarrow \text{Polymer}$$

Scheme 1.1: Electrochemical polymerisation.

$$M^{+\cdot} + M \rightarrow \text{Dimer Radical Cation} \xrightarrow{-2ne^-, -2nH^+} \text{Polymer}$$

Scheme 1.2: Chemical polymerisation.

Chemical synthesis is achieved when the monomer is exposed to relatively strong oxidising agents such as ammonium peroxydisulfate, potassium dichromate or ferric chloride[7]. This can be carried out in solution or directly onto a surface. The chemical deposition of a conducting polymer directly onto a surface involves coating the desired surface with the monomer solution and then subsequently treating the surface with the solution or vapour of the oxidising agent. This results in the polymer film being polymerised exclusively on the surface of preference. In solution, the polymer is precipitated from an acidic monomer solution upon the addition of the oxidising agent which normally results in bulk polymerisation. However, this bulk polymerisation can be impeded to some degree so that the conducting polymer can be deposited on a surface. This is achieved by varying several reaction conditions such as the concentration and ratio of oxidant and monomer, the reaction temperature and appropriate treatment of the surface to be coated by the polymer[8].

Electrochemical polymerisation occurs when a suitable anodic potential or current is applied to a conducting substrate that has been immersed in a monomer electrolyte. A counter and reference electrode are also needed for this to take place. A schematic representation of the electrochemical cell set up required for electropolymerisation is given in Section 2.5. Galvanostatic (constant current), potentiostatic (constant potential) and potential sweeping techniques such as cyclic voltammetry are the methods generally

employed for electropolymerisation. Electrochemical polymerisation, in particular galvanostatic and potentiostatic modes, has several advantageous over chemical polymerisation. An adherent polymer film can be grafted directly onto an electrode surface in one simple step. Reproducible films can be obtained as the film thickness can be controlled by monitoring the charge passed during deposition and the polymer films formed have fewer impurities as harsh oxidising agents are not used. In addition, it is also possible to perform *in situ* characterisation of the polymer while it is growing[9].

1.1.3 Applications of Conducting Polymers

The electrical properties of conducting polymers together with the fact that they retain the mechanical properties of traditional polymers have made them very useful in a wide variety of areas. These include sensors, actuators, corrosion resistance materials, batteries, optics, electronics and biomedical/biological applications[10].

In particular, the exchange properties of conducting polymers have been utilised to develop such applications. For example, conducting polymers doped with small mobile anions have anion exchange properties, whereas conducting polymers doped with large immobile anions generally have cation exchange properties[11]. This has resulted in the formation of actuators[12-14], drug delivery systems[15], selective sensors[16] and metal ion transporters[17] to name a few.

Conducting polymers have also been extensively used for various electrochromic and optoelectronic devices[18-21]. This is because the introduction of dopants into the polymer changes the optical properties of the polymer in the ultraviolet-visible (UV-vis) and the near infrared (NIR) regions, as well as increasing the electrical properties[22].

1.2 Polypyrrole

Polypyrrole (PPy), Figure 1.3, was first chemically synthesised in 1916 by the oxidation of pyrrole with hydrogen peroxide to give an amorphous black powder known as 'pyrrole

black'[23]. The first electrochemical synthesis of PPy was then reported some years later in 1968 by Dall'Ollio *et al.*[24]. The authors used an aqueous solution of pyrrole and sulfuric acid to electrosynthesise a layer of PPy on a platinum electrode. Since then, various PPy films and composite films of PPy have been polymerised on a wide variety of substrates from an array of different solutions.

Polypyrrole is one of the most extensively used and studied conducting polymers because of its ease of preparation, high conductivity and relative stability. Accordingly, PPy has found applications in a number of advanced technologies such as chemical sensors[25, 26], batteries[27, 28], supercapacitors[29, 30] and corrosion protection[31, 32]. An additional feature of PPy is that it forms a biologically compatible polymer matrix[33]. Therefore, it has been used in a broad number of biomedical fields including biosensors[34, 35], tissue engineering[36, 37] and implantable biodevices[38]. Another interesting and prominent property of PPy is its ability to switch its redox behaviour. This has resulted in the design of ion-selective electrodes, electrochromic displays, solar cells, drug delivery systems and actuators[39-43].
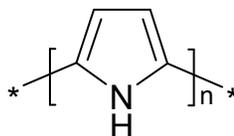
Figure 1.3: Structure of PPy in its neutral state.

1.2.1 Synthesis of Polypyrrole

There are two chief methods for the synthesis of PPy: chemical and electrochemical polymerisation. One of the easiest and most common ways of chemically synthesising PPy is in solution. Chemical synthesis in solution yields a black precipitate when the monomer, pyrrole, is exposed to an oxidising agent. The oxidising agent used in chemical polymerisation initiates polymerisation by oxidising the monomer and also provides dopant anions to neutralise the positive charge of the polymer in the oxidised state. The radical cation formed upon oxidation then attacks another monomer molecule generating a dimer

radical cation which is further oxidised and, coupled with the loss of hydrogen, the polymer chain grows until termination, Scheme 1.3. The most often used oxidising agents for pyrrole polymerisation are salts of transition metal ions, such as Fe^{3+}, Cu^{2+}, Cr^{6+}, Ce^{4+}, Ru^{3+} and Mn^{7+}. Several other oxidising agents, including organic acids and peroxides have been employed however, films generated from these oxidants usually exhibit lower conductivity[44]. One major disadvantage of this method is that the PPy is produced in the bulk of the solution and only some of the PPy will cover the surface of a material that has been introduced into the solution. This process can be hindered, Section 1.1.2, however it is complicated and dependant on many parameters.

Another way of chemically synthesising PPy is to directly deposit the polymer film onto a surface. One way to achieve this is to use a process that has been coined vapour phase polymerisation. Vapour phase polymerisation involves applying the oxidant to the surface using a solvent coating process and then exposing the coated surface to the vapour of the monomer. The vapour phase polymerisation method was first described by Mohammadi and co-workers[45]. The authors used $FeCl_3$ or H_2O_2 as oxidants to polymerise PPy films. Since then the vapour phase polymerisation of pyrrole has been carried out using Fe(III) *p*-toluenesulfonic acid and a range of other Fe(III) sulfonates as oxidising agents[46, 47].
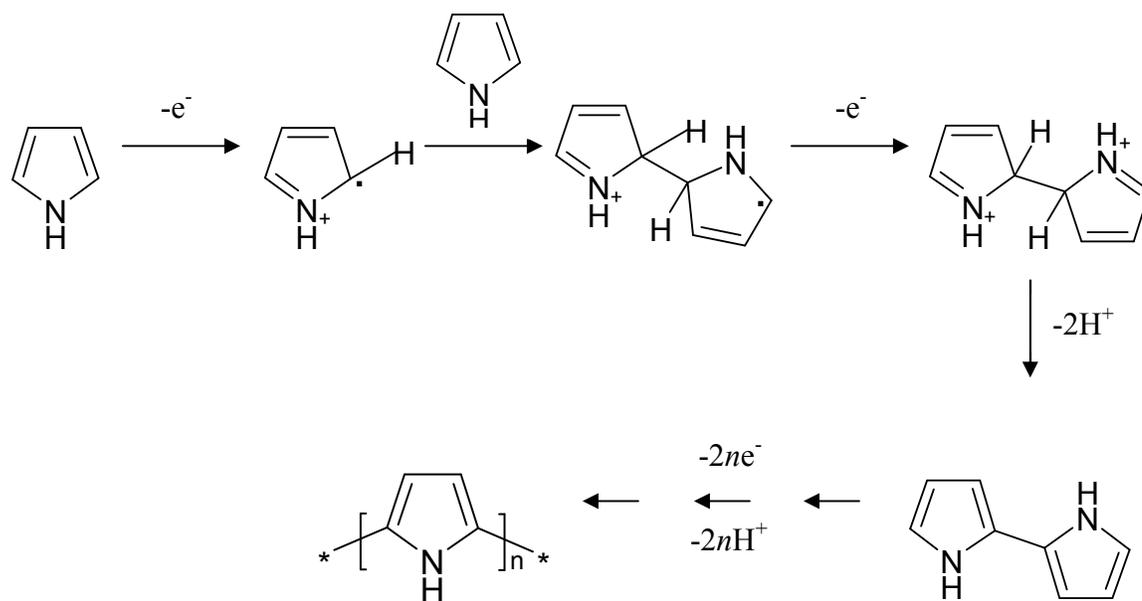
Scheme 1.3: Mechanism for the chemical synthesis of PPy.

Electrochemical polymerisation of pyrrole is achieved when an anodic potential or current is applied to a conducting substrate that has been immersed in a suitable electrolyte containing the monomer and the desired doping salt. Different electrochemical techniques including galvanostatic[48], potentiostatic[49] and potentiodynamic[50] methods have been used to do this. Electrochemically synthesised PPy has some attractive features, highlighted in Section 1.1.2, and as a result is used more extensively than chemical deposition. Various mechanisms for the electropolymerisation process have been proposed[51-53]. However, the mechanism described by Genies *et al.*[54] is the most common one encountered in the literature, Scheme 1.4. The initial step involves the oxidation of the monomer to a radical cation. This takes place at the surface of the electrode or substrate. Radical-radical coupling then occurs at the α-position of each radical resulting in a radical dication. The radical-radical coupling arises because the concentration of radical cations at the electrode surface is much larger than that of the neutral monomer[5]. Two protons are subsequently lost from the radical dication to generate a neutral dimer which is oxidised into a radical dimer. At this point the radical dimer reacts with a monomer radical to form a trimer. The propagation continues *via* the same sequence; oxidation, coupling and deprotonation until the final polymer product is obtained.

It would appear from the mechanisms given in Schemes 1.3 and 1.4 that the final PPy chain is neutral. This, however, is not the case. The final PPy chain synthesised from both chemical and electrochemical polymerisation will actually be in an oxidised/doped state[55], Figure 1.4. This is explained in more detail in Section 1.2.3.
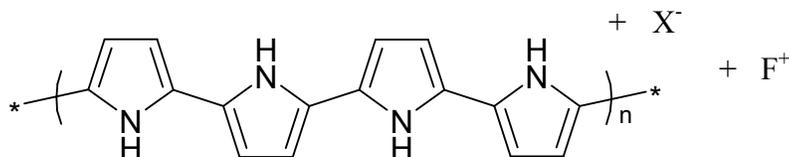
Figure 1.4: The final doped polymer, where X^- and F^+ are the anion and cation from a simple XF salt, which was dissolved in a suitable solvent with the monomer.
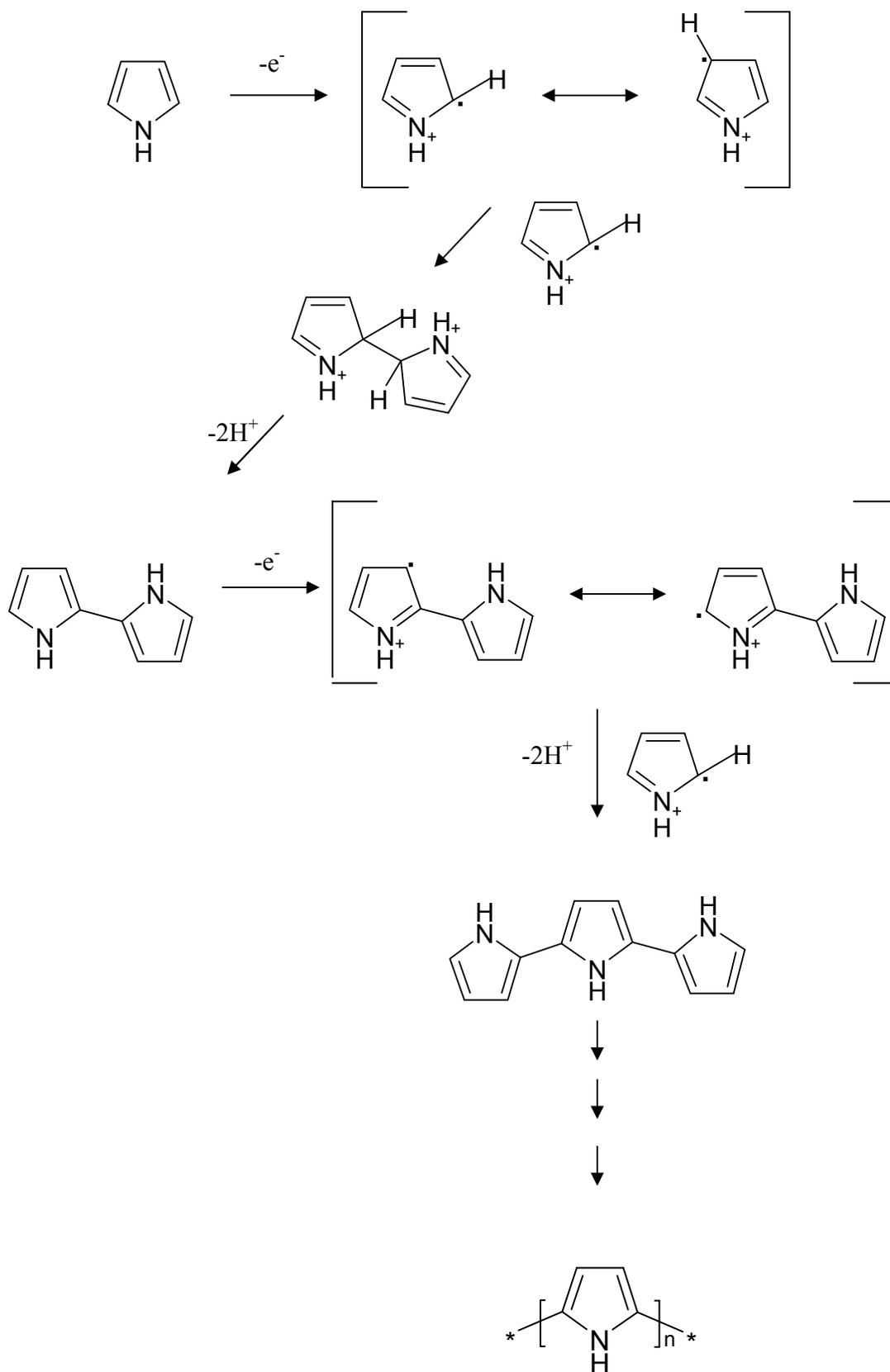
Scheme 1.4: Mechanism for the electrochemical synthesis of PPy.

1.2.2 Factors affecting Electropolymerisation

The electrochemical polymerisation of pyrrole is affected by a number of conditions used for the synthesis. These include the potential, solvent, nature of electrode, concentration and nature of the supporting electolyte, temperature, pH and mode of polymerisation.

The nature of the electrode is a critical parameter for the preparation of PPy films. The electrode used must not be oxidisable as this would compete with the oxidation of the pyrrole monomer. For this reason, most studies have focused on the electrodeposition of PPy at inert anodes such as, platinum, glassy carbon or gold[56-58]. However, a range of active metals which form oxides have also been used[59-61]. In these circumstances, the potential of pyrrole oxidation usually increases and the current density generally decreases[62]. Apart from metals, PPy has also been electropolymerised on a wide variety of other materials including indium tin oxide glass (ITO)[63] and silicon[64].

The supporting electrolyte also plays a major role in the electropolymerisation process. This is because it usually determines the type of anion/dopant that will be incorporated into the polymer to balance the positive charge. The size of the anion can influence various characteristics such as the porosity and redox properties of the film[55]. A vast variety of dopants have been used to electrosynthesise PPy. These include anions such as Cl^-, Br^-, ClO_4^-, NO_3^-, BF_4^-, PF_6^-, benzenesulfonate, dodecylsulfonate and polyvinylsulfonate[65]. Mono, di and trisulfonated naphthalene have also been incorporated into PPy films by Suematsu and co-workers[66]. The electrolyte concentration is also important. Li and Yong[67] have shown that the doping degree, conductivity and tensile strength of a PPy/NO_3 film increases as the electrolyte concentration increases until a concentration of 1.0 mol dm^{-3} has been surpassed.

Accordingly, the solvent used will also have a very strong influence on the electrochemical polymerisation of pyrrole. The main requirement of the solvent is that it has good ionic conductivity and a good electrochemical resistance against decomposition at the monomer oxidation potentials[23]. A range of aqueous, organic and ionic liquids have been used to electropolymerise pyrrole[68-70]. Aqueous solutions usually require a reasonably high amount of supporting electrolyte to achieve the desired conductivity. Likewise, organic solutions

generally need a suitable organic salt. The characteristics of PPy grown from aqueous, non aqueous and mixed solutions have been investigated by Carquigny and co-workers[71]. The authors found that thin PPy films were deposited from the pure acetronitrile/$LiClO_4$ solutions. In contrast, the films grown from the water/$LiClO_4$ solution and the mixed solution of acetronitrile/water/$LiClO_4$ were thicker but more porous. This result is consistent with Ko *et al.*[72] who also found that the PPy films prepared in acetonitrile/tetraethylammonium perchlorate had superior electron transfer characteristics and conductivities to those prepared in the aqueous medium. The addition of surfactants, in particular the anionic type, to the monomer electrolyte will also have an effect on the electropolymerisation of pyrrole. This is because they tend to increase the conductivity, smoothness and mechanical properties of the films prepared[73].

The potential is also significant in the electropolymeristion of pyrrole. Asavapiriyanont *et al.*[52] showed that the oxidation of pyrrole occurs between 0.65 V vs. SCE and 0.90 V vs. SCE. Oxidation at potentials higher than this leads to a decrease in the conductivity of the polymer. This process, known as the overoxidation process, is irreversible and occurs gradually with increasing potential. The mechanism for overoxidation still remains unclear. To date, the most accepted mechanism for the overoxidation of PPy is the nucleophillic attack of PPy by strong aqueous nucleophiles such as OH^-, Br^- and H_2O[74]. This in turn causes the formation of carbonyl groups on the α-carbons of the pyrrole ring which breaks the conjugation of the polymeric chain[75].

Asavapiriyanont *et al.*[52] also investigated the electrodepostion of PPy films on a Pt electrode from acidic, neutral and basic aqueous solutions and found that polymerisation favours a neutral or weakly acidic pH. Zhou and Heinze[76] also found this to be the case when they investigated the effect of pH on the electropolymerisation of pyrrole from an acetonitrile solution. A major disadvantage associated with the polymerisation of pyrrole from acidic solutions is that the conductivity of the film deteriorates. This is because an acid catalysed non-conjugated trimer is formed that will react further to form a partly conjugated PPy[55]. Alkaline solutions tend to inhibit the polymerisation as it causes the cation radicals to deprotonate to neutral radicals. This interferes with the radical-radical coupling reaction and results in non-conducting films[77]. There are various exceptions to

these assertions and it is important to stress that the effect of the pH is dependent on a number of variables such as, the buffer species, the supporting electrolyte and the substrate anode material[77].

The polymerisation temperature is another key factor. In general, the rate of polymerisation will increase with increasing temperature. This is because the kinetics of the synthesis reaction are being accelerated. There is usually a corresponding decrease in the conductivity and redox properties of the PPy film as the temperature increases, however, films produced at lower temperatures are generally of a lower quality[55].

Finally, the mode of polymerisation will also exert an effect on the polymerisation of pyrrole. PPy films are most commonly electrosynthesised *via* galvanostatic, potentiostatic and poteniodynamic methods. The films formed from a constant current or constant potential mode of polymerisation are usually more porous and uneven, while the films obtained using cyclic voltammetry are generally more smooth and compact[78]. However, more recent studies carried out by Hernandez-Perez *et al.*[79] showed that poteniostatic methods give rise to smooth surfaces. The authors used atomic force microscopy (AFM) to investigate the surface morphology of PPy films prepared at platinum electrodes by potentiostatic and voltammetric methods. They concluded that the potentiostatic mode of growth was better for obtaining thin films with a smooth surface morphology. Furthermore, the PPy film growth was easier to control using this method.

1.2.3 Redox Properties of Polypyrrole

The most important electrochemical property of PPy is its redox switching behaviour. PPy can be easily switched between the neutral, partially oxidised and fully oxidised sate, as shown in Figure 1.5. When the neutral form of PPy is oxidised an electron is removed from the polymer backbone and a polaron (radical cation) is formed. At this point the polymer is said to be in the partially oxidised state, Figure 1.5(b). Further oxidation then causes an electron to be removed from the polaron and a bipolaron is formed, Figure 1.5(c).

When PPy is oxidised an influx of anions are incorporated into the polymer to counterbalance the positive charges formed, Figure 1.6(a). Conversely, when PPy is reduced to the neutral state, the anions are subsequently expelled from the polymer, Figure 1.6(b). This scenario is especially true for small mobile anions such as chlorides. However, larger anions such as *p*-dodecylbenzene sulfonate[80] and poly(styrenesulfonate)[81] are permanently anchored into the polymer matrix. In this situation, the electroneutrality during the reduction of the polymer is maintained by the flux of mobile cations from the electrolyte solution into the polymer, Figure 1.7(b). Medium sized anions on the other hand generally exhibit both anionic and cationic exchange. Khalkhali *et al.*[80] found that this was the case for *p*-toluene sulfonate and dodecyl sulfate.

(a)

(b)

(c)
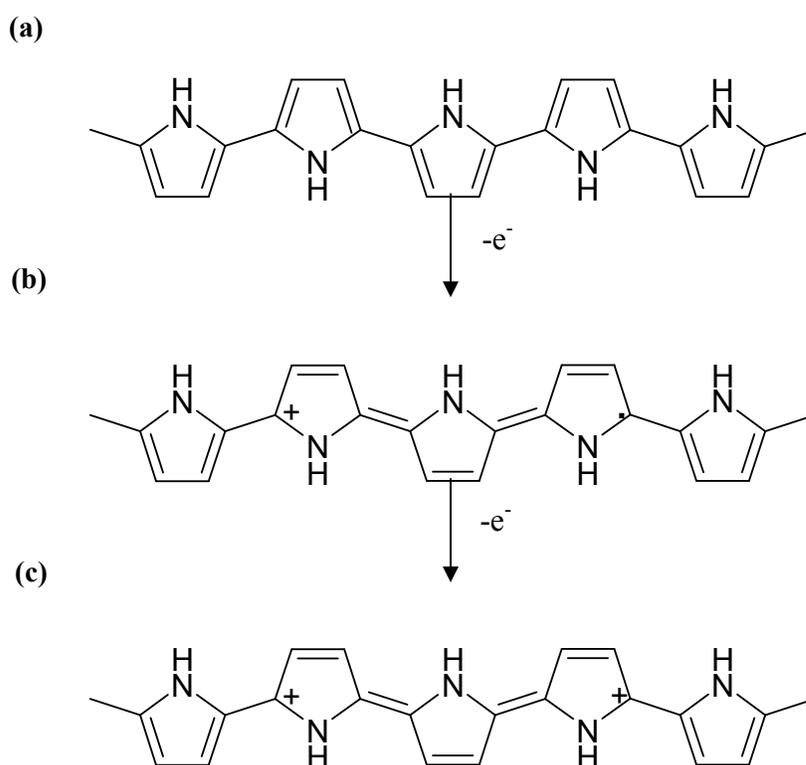
Figure 1.5: Formation of a polaron and bipolaron where, (a) is the neutral PPy, (b) is the partially oxidised PPy (polaron) and (c) is the fully oxidised PPy (bipolaron).
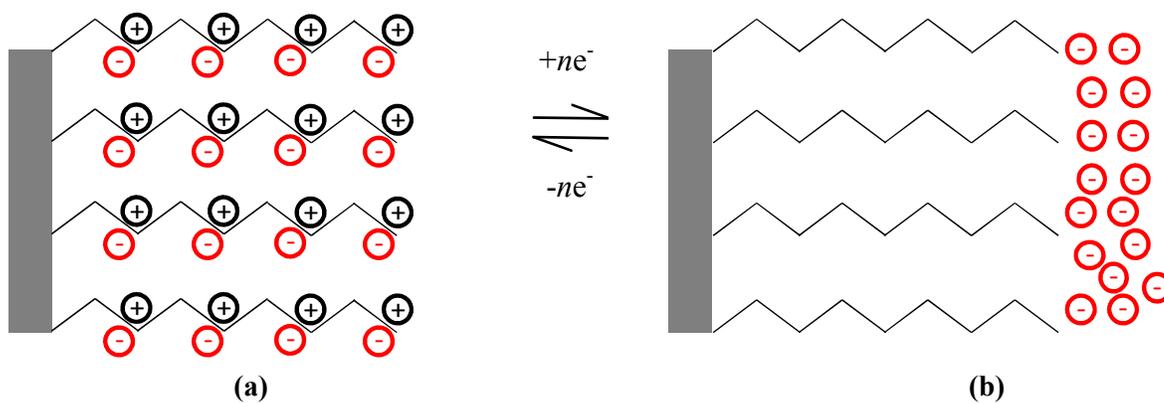
Figure 1.6: (a) Incorporation of anions into PPy film and (b) release of anions from PPy film.
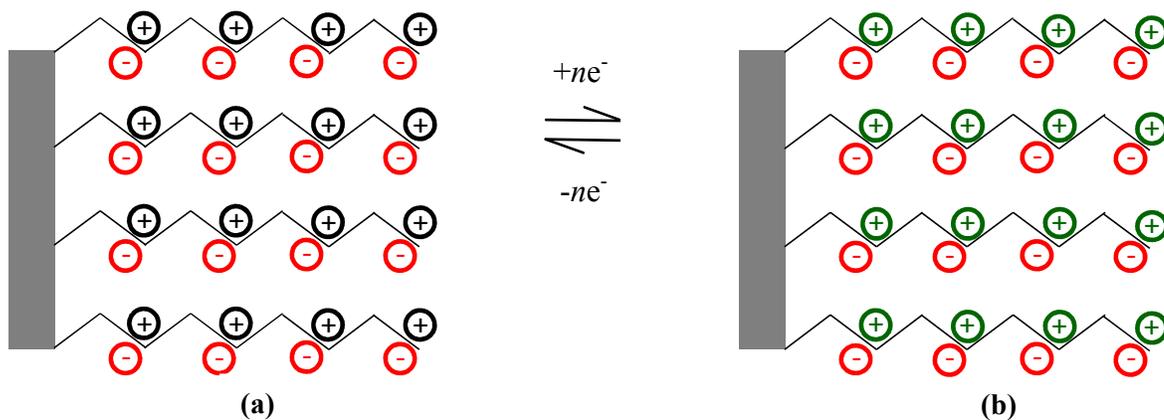
Figure 1.7: (a) Cation expulsion from PPy film and (b) cation incorporation into PPy film where + is the charge on the PPy, - is the anions and + is the cations.

1.3 Cyclodextrins

Cyclodextrins are naturally occurring macrocyclic oligosaccharides built from α-1,4-linked $_D$-glucopyranose units. The most common and readily available cyclodextrins are the α-, β- and γ-cyclodextrins. These cyclodextrins are composed of six, seven and eight glucopyranose units, respectively, Figure 1.8.

Cyclodextrins were first discovered in 1891 by Villiers[82] and later developed by Schardinger[83]. Since then, the number of cyclodextrin related publications has increased exponentially[84]. This is due to the structural features and interesting properties of cyclodextrins, discussed in Sections 1.3.1 and 1.3.2.

Cyclodextrins can be produced *via* a relatively simple enzymatic conversion involving enzyme glycosyl transferase and starch. The addition of the enzyme to an aqueous solution of starch causes the linkages of the starch to split forming maltodextrinyl radicals. This occurs every sixth, seventh or eighth unit for the α-, β- or γ-cyclodextrin. These radicals then react with their own non-reducing end to form a six, seven or eight membered ring structure[85].

1.3.1 Structural Features

The chemical structures of the α-, β- and γ-cyclodextrin are given in Figure 1.8. The glucose units are connected through glycosidic α-1,4 bonds, as illustrated in Figure 1.9. It is this bonding mode that gives cyclodextrins their distinctive truncated cone structure, Figure 1.10(a). The cavity sizes corresponding to the α-, β- and γ-cyclodextrin are given in Figure 1.10(b). On the basis of X-ray measurements it has been deduced that the primary hydroxyl groups (C_6) are located on one edge of the cyclodextrin, the primary face, while, the secondary hydroxyl groups (C_2 and C_3) are located on the other edge, the secondary face. The cavity of the cyclodextrin is then lined with C_3 and C_5 hydrogens and ether-like oxygens[86]. The primary and secondary hydroxyl groups on the exterior of the cyclodextrin are polar while the hydrogens inside of the cyclodextrin are apolar. Consequently, cyclodextrins can be dissolved in an aqueous medium but still retain their cavity matrix. It

is this characteristic that gives cyclodextrins their unique complexation ability in aqueous solutions. This is discussed further in Section 1.3.2.
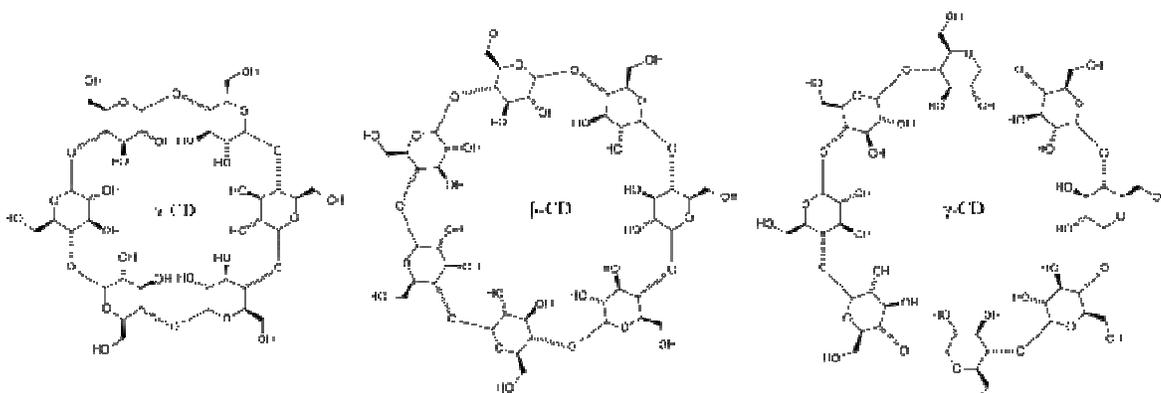
Figure 1.8: Chemical structures of the α-, β- and γ-cyclodextrin.
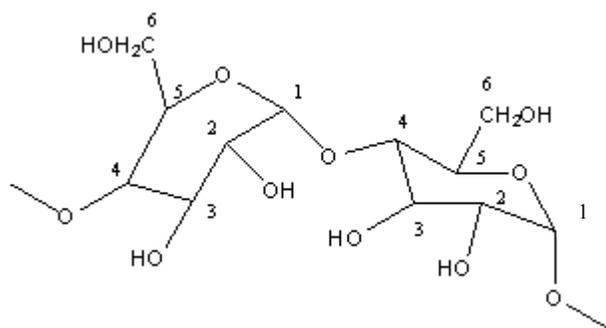
Figure 1.9: The 1,4 link that joins the $_D$-glucopyranoside units.
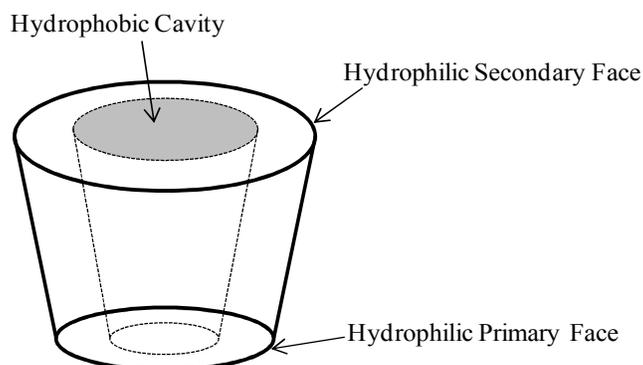
Figure 1.10(a): The truncated cone structure of cyclodextrins.
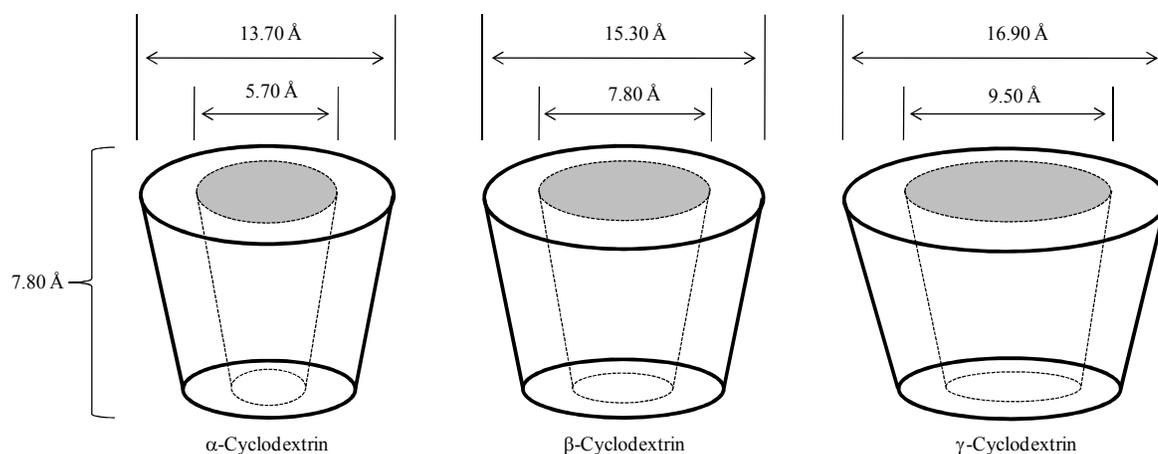
Figure 1.10(b): Geometric dimensions of the α-, β- and γ-cyclodextrins.

A wide variety of cyclodextrin derivatives have been prepared from the native α-, β-, and γ-cyclodextrins. This is particularly true of the β-cyclodextrin. In total, 21 hydroxyl groups on the β-cyclodextrin can be modified by substituting the hydrogen atom or the hydroxyl group with an appropriate substituting group such as an alkyl or thio group[84]. Out of the 21 hydroxyl groups on the β-cyclodextrin that can be modified, 7 are on the primary face and 14 are on the secondary face. Chemical modifications of cyclodextrins are usually carried out to enhance the solubility of the cyclodextrin and the inclusion complex. They can also be used to improve, or in some cases, inhibit the binding affinity of the complexation[87]. The cyclodextrin used in this study was a sulfonated β-cyclodextrin. Commercially available sulfonated β-cyclodextrin has approximately 7-11 sulfonated groups per cyclodextrin, Figure 1.11. The structure of the sulfonated β-cyclodextrin has been investigated by Chen *et al.*[88] and Amini and co-workers[89]. Both authors found that sulfation was occurring at the C_6 and C_2 positions but not at the C_3 position. Furthermore, the C_6 positions are preferentially sulfated over the C_2 positions according to Chen and co-workers[88]. This indicates that the entire primary face and some of the secondary face are substituted with sulfonated groups. In terms of application, sulfonated β-cyclodextrins have been used as chiral separating agents in capillary electrophoresis[88-90]. They also have biomedical potential as the sulfonated β-cyclodextrin is non-toxic[91] and apparently it can reduce the blood supply of tumor tissues by inhibiting the formation of new arteries[84].
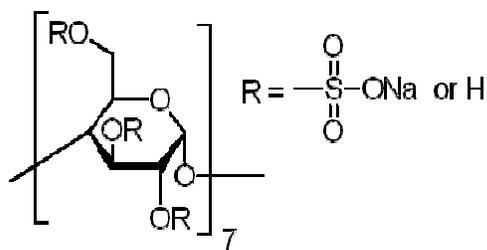
Figure 1.11: Structural representation of the sulfonated β-cyclodextrin.

1.3.2 Inclusion Complexation

The inclusion chemistry of cyclodextrins can be divided into two categories, aqueous complexation and solid state complexation. Naturally, the formation of aqueous inclusion complexes is prominent given the extraordinary hydrophobic and hydrophilic qualities of cyclodextrins. Cyclodextrins are well-known to bind with suitable guest molecules in aqueous solutions to form inclusion complexes. The formation of such inclusion complexes occurs without the formation of any covalent bonds. Moreover, no covalent bonds are broken[86]. In general, the complex formed between a cyclodextrin (CD) and a guest molecule (D) is a 1:1 association. However, more complicated associations do exist[92]. The inclusion complex formed for the simplest case (1:1) is governed by an equilibrium process with a complex formation constant, *K*, Equations 1.3 and 1.4.

$$CD + D \rightleftharpoons CD\text{-}D \qquad\qquad 1.3$$

$$K = \frac{[CD\text{-}D]}{[CD][D]} \qquad\qquad 1.4$$

The formation of cyclodextrin complexes in aqueous solutions has been studied intensively over the past couple of decades using a variety of electrochemical and spectroscopic approaches. The most common spectroscopic techniques used include nuclear magnetic

resonance (NMR)[93, 94], UV-vis spectroscopy[95, 96] and fluorescence spectrometry[97, 98]. In terms of electrochemical analysis, both cyclic voltammetry[99, 100] and rotating disc voltammetry[101, 102] have been widely used. Cyclodextrins will alter the electrochemical and spectral behavior of the guest molecule if an inclusion complex is formed. Therefore, one of the most straightforward and easiest ways of not only confirming complexation but determining the complex formation constant, *K*, is to carry out a titration[103]. This involves keeping the concentration of the guest molecule constant while varying the concentration of the cyclodextrin. If an inclusion complex is formed there will be a marked difference in the behavior of the guest molecule and this change becomes more evident as the concentration of the cyclodextrin is increased.

There are two key factors which influence the formation and stability of complexes in aqueous solutions: steric and thermodynamic. The majority of scientists agree that the relative size of the cavity to the size of the guest is a critical factor in the complexation process. However, some of the thermodynamic interactions between the different components of the system are still a matter of some debate. The most widely studied thermodynamic factors include hydrophobic effects, electrostatic interactions, hydrogen bonding and van der Waals forces.

The role of hydrophobic effects in cyclodextrin complexation is debatable. This is because the thermodynamic factors which give rise to the hydrophobic effect are complex and still not totally understood. According to the Equation 1.5, the inclusion complex will only be formed if there is a net driving force, ie. $\Delta G < 0$. The association of nonpolar molecules in water will result in positive enthalpy and positive entropy changes and the association is said to be 'entropy driven'. This entropic hydrophobic effect arises because the hydration shells of the two molecules are destroyed when they combine. The structured hydration water is then released and stabilised by other water molecules.

$$\Delta G = \Delta H - T\Delta S \qquad\qquad 1.5$$

The experimental observation in most cases for cyclodextrin complexation is that entropy and enthalpy changes are negative[104]. This would seem to imply that the hydrophobic effect is not an important driving force and consequently has led many scientists to believe that it is not an important contributor.

However, several other methods have shown that hydrophobic interactions play a significant role. For example, guest molecules can contain moieties that are more hydrophillic. In this situation, the less polar part of the molecular binds with the internal surface of the cyclodextrin, while the more polar part of the molecule remains as far as possible from the outer edge of the complex[105, 106]. Furthermore, the strength of the inclusion complex will also increase as the hydrophobicity of the guest molecule is increased. Alvira *et al.*[107] reported that the interaction energy between the β-cyclodextrin and an acrylic ester increased as the hydrophobicity of the alkyl group in the ester was increased.

Other evidence to support hydrophobic effects is that the complex formed is usually weakened when an organic co-solvent is added and strengthened when an inorganic co-solvent is added[108]. The addition of an inorganic salt to the solvent will strengthen the binding because the bulk solution is now more polar. On the other hand, the organic salt competes with the guest molecule which decreases the binding. Viernstein *et al.*[109] found that the equilibrium constant of a triflumizole-β-cyclodextrin complex decreased as the concentration of a number of organic co-solvents, alcohols in this case, increased. In addition, the equilibrium constant decreased as the apolar nature of the alcohol increased. This further highlights the importance of the hydrophobic effect in cyclodextrin complexation.

Van der Waals forces have also been deemed crucial in the binding of cyclodextrins and guest molecules. Generally, van der Waals forces describe induction (dipole induced dipole interaction) and dispersion forces. Cyclodextrins have a relatively large dipole moment and so it is not surprising that the involvement of these forces in cyclodextrin complexes has been widely claimed. Nevertheless, a vast majority of these claims are based on the fact that a negative enthalpy change in complexation is observed, leaving by default van der Waals forces. Also, based on theoretical calculations many authors concluded that van der

Waals forces were the main driving force in the formation of cyclodextrin complexes. However, these calculations were usually carried out in the gas phase and did not take into account solvent effects[108].

Various other methods have been used to highlight the importance of van der Waals forces. Both induction and dispersion forces depend on polarisability and experimental evidence has shown that the stability of complexation increases as the factors that contribute to polarisability are increased. The fact that the bulky side of the guest molecule can enter the cavity of the cyclodextrins and that they can form inclusion complexes in pure organic solvents such as DMF and DMSO, also demonstrates the involvement of van der Waals forces in cyclodextrin complexation[108].

The influence of electrostatic interactions in the formation of cyclodextrin inclusion complexes has also been noted. There are three significant types of electrostatic interactions: ion-ion interactions, ion-dipole interactions and dipole-dipole interactions. Ion-ion interactions in complexation are only significant when the cyclodextrin has been appropriately substituted. For example, Okimoto *et al.*[110] have shown that binding between a neutral/positive guest molecule and an anionically charged cyclodextrin is superior to the binding of the same guest molecules with a neutral cyclodextrin. In contrast, the neutral cyclodextrin exhibited enhanced binding with the negatively charged guest molecules.

The ion-dipole interaction is expected to occur given that cyclodextrins are polar molecules. In general, the ion-dipole interaction and hence the complexation should increase as the size of the ion increases. It has been shown that simple anions such as ClO_4^- and NO_3^- complex with cyclodextrins however, dianions such as SO_4^{2-} and CO_3^{2-} do not. This is because the interaction between the guest and water is strong. Consequently, the ion-dipole interactions are not significant in complexation. In contrast, dipole-dipole interactions do seem to have an influence on not only the stability but in some cases the orientation of the complex[108].

The role of hydrogen bonding in aqueous complexation is rather controversial. This is because water molecules can compete with the cyclodextrins to form hydrogen bonds with

the guest molecule. Some authors suggest it does play a part[111, 112] however many authors have discounted it[113, 114].

1.3.3 Applications of Cyclodextrins

Cyclodextrins have been applied to a wide variety of products and processes due to their host-guest complexation abilities and excellent biocompatibility. In the pharmaceutical industry, cyclodextrins have been extensively used for drug delivery systems and drug formulations[115, 116]. They have also been used in the food, cosmetic, agricultural and chemical industries. Furthermore, they have been used in adhesives, coatings, plastics and rubbers and photographic and recording materials[83-86].

One of the most successful and commercially available applications of cyclodextrins is Febreeze®, a household odour eliminator. The active ingredient in Febreeze® is a modified β-cyclodextrin. These cyclodextrins capture malodorous molecules in their cavities and as a result they are no longer detected.

1.4 Dopamine

Dopamine (DA), Figure 1.12, is a catecholamine neurotransmitter that is widely present in both the brain and the peripheral nervous system. The bio-synthetic pathway for DA is quite simple, Scheme 1.5. Tyrosine, a naturally occurring amino acid in protein foods, is converted into L-Dopa by the enzyme tyrosine hydroxylase. The L-Dopa can then be converted to DA, which subsequently can be converted to norepinephrine and finally epinephrine by a series of enzymes. Neurons that use DA as a neurotransmitter have the first and second enzymes but not the rest, and so the tyrosine is converted only as far as DA[117].
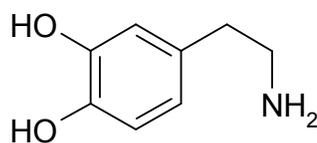
Figure 1.12: Structure of DA.
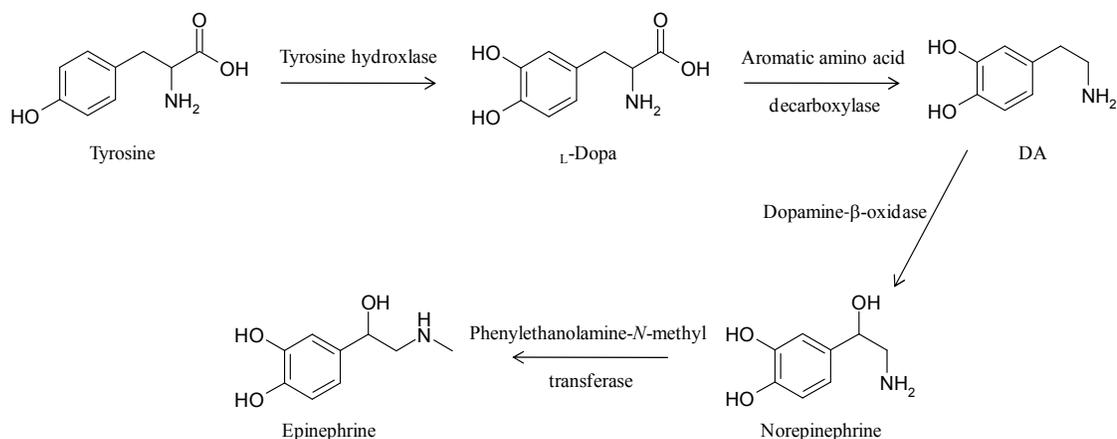
Scheme 1.5: The synthetic pathway of DA[117].

DA has been linked with the debilitating ailment, Parkinson's disease and the severe mental disorder, schizophrenia. The symptoms of Parkinson's disease arise when the DA containing neurons in the brain start to deteriorate. They eventually disappear as the disease progresses. Currently, there is no immediate cure for patients with Parkinson's disease. The administration of L-Dopa has been found to be helpful but it becomes less effective over time[118].

Schizophrenia occurs because the number of DA receptors in the schizophrenic brain are believed to be higher than in the normal brain. Therefore, the normal amount of DA in the schizophrenic brain has too powerful an action. Again, there is no instant cure, however, the sensitivity of the system can be reduced by blocking the DA receptors with antipsychotic drugs[117].

DA is also believed to play a central role in Huntington's disease, a fatal, genetic neurodegenerative movement disorder for which there is no cure. However, decreasing the release of DA with tetrabenazine has emerged as an effective treatment in suppressing Huntington's disease[119]. Furthermore, it has been shown that DA plays a very important role in drug addiction[120] and attention disorders[121] and it has even been associated with HIV infection[122]. Accordingly, the development of simple analytical methods for the determination of DA concentrations is important.

1.5 Dopamine Sensors

DA is one of the most important catecholamine neurotransmitters in the mammalian central nervous system. Abnormalities in DA concentrations have been linked with several neurological disorders, as highlighted in Section 1.4. Consequently, it is not surprising that the measurement of DA has been the focus of much recent research work.

In particular, there has been much interest in the development of electrochemical sensors. This is because DA is electroactive and thus the oxidation of DA can be followed using electrochemical techniques. Electrochemical sensors are usually inexpensive to manufacture, highly sensitive and easy to employ. Furthermore, the electrodes used in the sensing can be miniaturised and conveniently placed in the living organism for real time analysis. This is not possible with non-electrochemical techniques.

The electrochemical oxidation of DA occurs *via* an ECE mechanism[123, 124], Scheme 1.6. A two electron exchange results in the formation of dopamine-o-quinone. This molecule can then undergo an intermolecular addition, which results in a cyclisation reaction generating leucodopaminechrome which, in turn, is oxidised further *via* another two electron transfer to dopaminochrome. In this scheme, 'E' denotes the electrochemical reactions and 'C' denotes the chemical reactions. However, it is well known that the dopaminochrome can be further oxidised to indolic-o-quinone to generate the insoluble melanin polymer, which fouls and poisons the electrode[125], Scheme 1.7.

Monitoring the concentration of DA is particularly challenging using electrochemical methods because DA co-exists with many interfering compounds in biological samples. These interfering compounds are usually present at concentrations much higher than DA and, moreover, they are oxidised at similar potentials to DA at most solid electrodes. This is particularly true of ascorbic acid (AA), the main interfering compound in the determination of DA. Furthermore, the electrochemical detection of DA using solid electrodes usually suffers from the fouling effect described in Scheme 1.7. Consequently, modified electrodes have been employed for the determination of DA. The most popular strategies include polymer modified electrodes[126], self-assembled monolayer modified electrodes[127] and surfactant modified electrodes[128]. However, a wide variety of other modified electrodes have also been used.

The electrochemical sensor investigated in this study is a platinum electrode modified with a polypyrrole-sulfonated β-cyclodextrin (PPy-SCD) film. Accordingly, the application of cyclodextrins in DA sensors is addressed in this section, along with the most popular approaches mentioned above. A different electrochemical approach and the various non-electrochemical approaches that have been used to sense DA will be discussed to a lesser degree in Section 1.5.5.
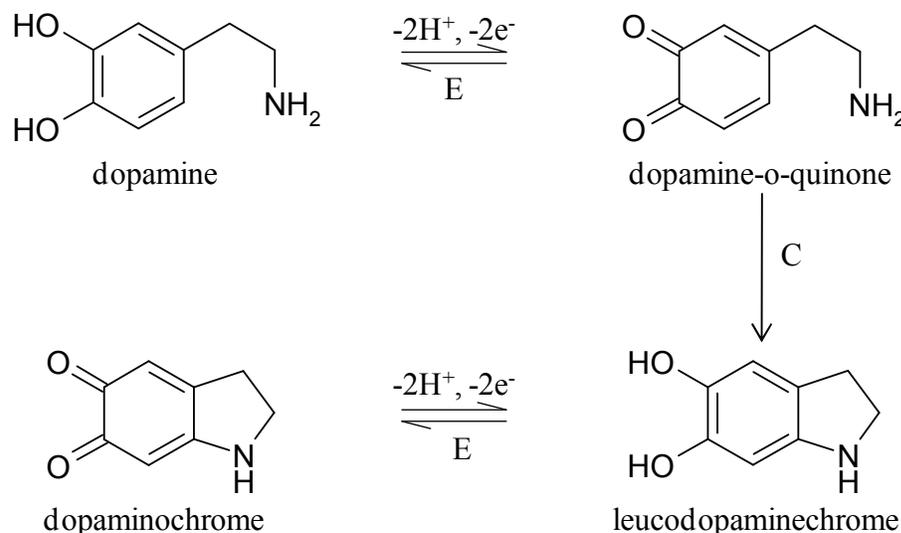
Scheme 1.6: The ECE mechanism for DA oxidation[124].
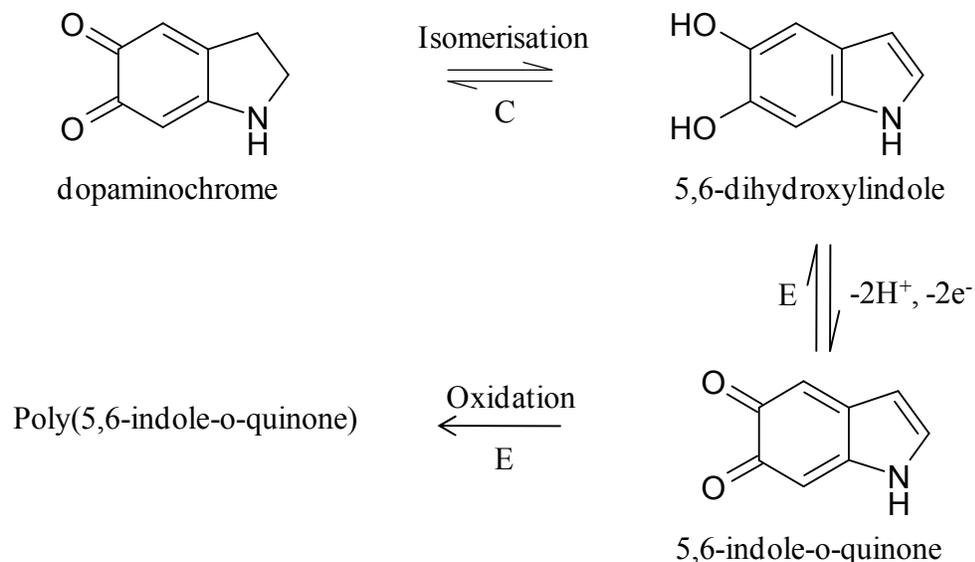
Scheme 1.7: The formation of the insoluble melanin polymer[125].

1.5.1 Polymer Modified Electrodes

The development of DA sensors based on electrodes modified with polymeric films is the most widely investigated. These materials can be divided into two categories: those that can selectively detect DA in the presence of AA and those that can simultaneously detect DA and AA by resolving the oxidation peaks. This is because AA is the most problematic interfering compound in the determination of DA. It is oxidised in the same potential region as DA and is present in most biological samples at much higher concentrations. Furthermore, a reaction between the oxidised DA and the AA can occur, which results in the regeneration of the DA. This regenerated DA can then be re-oxidised at the electrode surface resulting in a higher DA signal than expected. Accordingly, it is used by the majority of researchers as a standard to evaluate the performance of the sensor.

The majority of the reports for polymer modified electrodes in the literature are related to the simultaneous determination of DA and AA, Table 1.1. In general, the limit of detection given for the simultaneous determination of DA and AA was established in the presence of AA unless otherwise stated. This holds true throughout the rest of Section 1.5. As shown in Table 1.1, the limit of detection of DA ranges from 3.9×10^{-5} mol dm^{-3} to 2.0×10^{-7} mol dm^{-3} depending on both the technique used and the polymeric material used.

Overoxidised polymer modified electrodes have also been employed to sense DA. Li *et al.*[129] used an overoxidised polypyrrole film with single walled nanotubes to simultaneously detect DA, AA and uric acid (UA). A limit of detection of 3.8×10^{-7} mol dm^{-3} was determined for DA using differential pulse voltammetry. The detection of DA in the presence of AA was also attempted by Ghita and Arrigan[130] using an overoxidised polyindole electrode. However, AA was found to be a major interferent.

Table 1.1: Polymer modified electrodes capable of simultaneously determining DA and AA.

Reference	Material	Limit of Detection of DA / mol dm^{-3}	Technique
131	Polypyrrole/ferrocyanide film	3.9×10^{-5} / 1.5×10^{-5}	Linear Sweep Voltammetry / Differential Pulse Voltammetry
132	Poly(*N,N*-dimethylaniline) film	2.0×10^{-7}	Square Wave Voltammetry
133	Poly(*p*-nitrobenzenazo resorcinol) film	3.9×10^{-7}	Differential Pulse Voltammetry
134	Poly(chromotrope 2B) film	4.5×10^{-7}	Differential Pulse Voltammetry
135	Poly(Evans Blue) film	2.5×10^{-7}	Differential Pulse Voltammetry
136	Poly(vinyl alcohol) film	1.4×10^{-6}	Differential Pulse Voltammetry
137	Poly(acid chrome blue K) film	5.0×10^{-7}	Differential Pulse Voltammetry

Polymer films with incorporated nanoparticles have also been used for the electrochemical sensing of DA. For example, Mathiyarasu *et al.*[138] used a poly(3,4-ethylenedioxythiophene)/gold nanoparticle film and Gopalan *et al.*[139] used a poly(4-aminothiophenol)/gold nanopaticle film to simultaneously detect DA, AA and UA. In both cases, differential pulse voltammetry was used.

Nafion®, a perfluorinated polymer, has also been used extensively in DA sensors. Nafion® has terminal sulfonate groups that can repel the negatively charged anions from the electrode surface. Accordingly, it has been used in a number of modified electrodes, Table 1.2.

The fabrication of Langmuir-Blodgett films and layer-by-layer films from various conducting polymers has also been established for DA sensing. These films contain one or more monolayers of an organic material. Ferreira *et al.*[140] produced Langmuir-Blodgett films from polyaniline and a ruthenium complex. The oxidation peaks of DA and AA could be separated even when the concentration of AA was three times higher than the concentration of DA. However, when the concentrations of DA and AA were the same the film could not distinguish between them. A detection limit of 4.0×10^{-5} mol dm^{-3} was obtained in the absence of AA using cyclic voltammetry, which according to the authors is sufficient to detect DA in a pharmaceutical product.

Layer-by-layer films of nanostructured polyaniline with one of three tetrasulfonated metallic phthalocyanines (TsPc) have been fabricated by Zucolotto *et al.*[141] for the determination of DA. These films could distinguish between AA and DA, which were present in the solution at concentrations of 6.4×10^{-3} mol dm^{-3} and 6.0×10^{-3} mol dm^{-3}, respectively. The DA signal at the polyaniline/iron TsPc film exhibited the most promising results. The DA signal was more defined at this film and the DA and AA peaks were more resolved. Cyclic voltammetry was the only electrochemical technique employed in this study and a detection limit of 1.0×10^{-5} mol dm^{-3} was achieved in the absence of the AA.

Table 1.2: Examples of Nafion® modified electrodes.

Ref.	Material	Result	LOD / mol dm^{-3}
142	An ordered mesoporous carbon / Nafion® composite film	Simultaneous determination of DA, AA and UA. The limit of detection was evaluated using differential pulse voltammetry.	5.0×10^{-7}
143	Glassy carbon electrode modified with a catechin hydrate / Nafion® film	The oxidation current of DA in the presence of 1.0×10^{-3} mol dm^{-3} AA is about 5% higher than in the absence of AA. This is reduced to less than 3% when the concentration of AA is lowered to 3.0×10^{-4} mol dm^{-3}. This was achieved using constant potential amperometry.	1.1×10^{-8}
144	Nafion® coated clinoptilolite modified carbon paste electrode	Authors claim that a 200 fold excess of AA has virtually no interference on the DA response using differential pulse anodic stripping voltammetry. However, there is no evidence given to support these claims.	1.0×10^{-8}
145	Nafion® / carbon-coated iron nanoparticle-chitosan composite film	No electrochemical response for 1.0×10^{-3} mol dm^{-3} AA at the modified electrode. This concentration of AA had no effect on the peak potential or current of the differential pulse voltammogram of 1.0×10^{-5} mol dm^{-3} DA. However, there is no evidence given to support these results.	8.3×10^{-7}
146	Glassy carbon electrode modified with TiO$_2$ nanoparticles / Nafion®	AA peak observed at -0.1 V vs. SCE. 5.0×10^{-3} mol dm^{-3} AA had no effect on peak current of 8.0×10^{-6} mol dm^{-3} DA. However, as the concentration of AA was increased the response of DA decreased. This was investigated using square wave voltammetry.	9.5×10^{-9}

1.5.2 Self-Assembled Monolayer Modified Electrodes

Self-assembled monolayers (SAMs) of organosulfur compounds on gold surfaces are often used as a means of sensing DA. The simultaneous determination of DA and AA has been achieved by Shervedani *et al.*[147], Zhang *et al.*[148] and Liu *et al.*[149], to name a few. A detection limit of 2.3×10^{-6} mol dm^{-3} DA was established by Shervedani *et al.*[147] using a gold cysteamine self-assembled monolayer with differential pulse voltammetry. Zhang *et al.*[148] used a redox active monolayer of 4'-mercapto-*N*-phenylquinone diimine and differential pulse voltammetry to attain a limit of detection of 1.2×10^{-6} mol dm^{-3}. Cyclic voltammetry was the electrochemical technique of choice for Liu *et al.*[149] who obtained a limit of detection of 8.0×10^{-7} mol dm^{-3} with an *N*-acetylcysteine self assembled monolayer in the absence of AA.

The voltametric response of DA in the presence of AA was also explored by Wang *et al.*[150] using a thiolactic acid self-assembled monolayer. In this case, the anodic peaks of DA and AA could not be distinguished when a 5-fold excess of AA was added to a 2.0×10^{-4} mol dm^{-3} DA solution. A limit of detection of 3.0×10^{-6} mol dm^{-3} was subsequently determined in the absence of AA using cyclic voltammetry.

Self-assembled monolayers with nanoparticles have also been utilised for DA sensing. Several authors have used this approach. Hu *et al.*[151] used a cysteamine/gold nanoparticle monolayer, Zhang and Jiang[152] used a sulfhydryl-terminated/gold nanoparticle monolayer and Thiagarajan and Chen[153] used an L-cysteine/platinum/gold nanparticle monolayer. The simultaneous determination of DA in the presence of AA was achieved by the materials developed by Zhang and Jiang[152] and Thiagarajan and Chen[153]. Hu *et al.*[151] claim that the cysteamine/gold nanoparticle monolayer can selectively detect DA in the presence of AA. However, AA was oxidised at the electrode surface and two well resolved peaks were observed in the differential pulse voltammogram of the DA and AA solution.

To the best of our knowledge, the selective detection of DA in the presence of AA has not been reported by a self-assembled modified electrode.

1.5.3 Surfactant Modified Electrodes

Modifying the electrode surface with a surfactant has become an increasingly popular means for sensing DA. Chen and Chzo[128] modified a glassy carbon electrode with a didodecyldimethylammonium bromide film and used this material to simultaneously detect DA and AA. A similar result was also achieved by Shahrokhian *et al.*[154] using a tetraoctylammonium bromide/cobalt-5-nitrosalophen modified carbon paste electrode.

The selective detection of DA was achieved by Zheng and Zhou[155] using a sodium dodecyl sulfate modified carbon paste electrode. AA (4.0×10^{-3} mol dm^{-3}) had no electrochemical response at the modified electrode surface and a 100 fold excess of AA had no effect on the differential pulse voltammogram of DA.

1.5.4 Applications of Cyclodextrins in Dopamine Sensing

Cyclodextrins have been incorporated into many DA sensors[156-158]. For example, Alarcon-Angeles *et al.*[159] modified a glassy carbon electrode with a multiwalled carbon nanotubes/β-cyclodextrin film. This film was subsequently able to simultaneously detect DA and AA, giving an oxidation peak at approximately 0.3 V for the DA and 0.1 V for the AA. A limit of detection of 3.7×10^{-5} mol dm^{-3} was evaluated using cyclic voltammetry. Another example of a cyclodextrin based material that can separate the oxidation peaks of AA and DA is that reported by Izaoumen *et al.*[160]. The authors used a β-cyclodextrin/sonogel carbon electrode and adsorptive differential pulse voltammetry to achieve this and to determine a detection limit of 1.6×10^{-7} mol dm^{-3} DA in the absence of AA.

Polymer modified electrodes with incorporated cyclodextrins have also been employed for the determination of DA. Bouchta *et al.*[161] used a poly-3-methylthiophene-γ-cyclodextrin film to simultaneously detect DA and AA, while Yin *et al.*[162] used a polyaniline/multi-walled carbon nanotubes/β-cyclodextrin film to achieve a similar result. A detection limit of 2.0×10^{-7} mol dm^{-3} and 1.2×10^{-8} mol dm^{-3} was calculated from both films, respectively. A polypyrrole/β-cyclodextrin modified electrode for the determination of DA has also been

reported by Izaoumen *et al.*[163]. This film was able to separate the oxidation peaks of AA and DA and a limit of detection of 6.0 x 10^{-6} mol dm^{-3} was estimated for DA using cyclic voltammetry. However, the nature of the cyclodextrin and the parameters used to form the polymer modified electrodes described by Bouchta *et al.*[161] and Izaoumen *et al.*[163] are very questionable. For example, the polymer film used by Izaoumen *et al.*[163] was electrosyntheised from a monomer solution containing the neutral-β-cyclodextrin and a LiClO$_4$ supporting electrolyte. The neutral-β-cyclodextrin possesses no negative charge and so it is unlikely that it will be incorporated into the polymer matrix to balance out the positive charge. In this situation, it is more probable that the perchlorate anions will dope the polymer. A similar situation arises with Bouchta *et al.*[161] in that, the anions from the supporting electrolyte are probably incorporated into the polymer matrix and not the neutral-γ-cyclodextrin. Furthermore, the polymer modified electrodes used by both authors were formed by cycling the applied potential from 0.0 V vs. SCE to 1.8 V vs. SCE at a scan rate at 50 mV s^{-1} for 25 cycles (Izaoumen *et al.*[163]) and 40 cycles (Bouchta *et al.*[161]). These high potential conditions are well known to generate an overoxidised and highly porous polymer film. Therefore, the DA signals observed by both authors may be simply due to the underlying substrate.

1.5.5 Another Electrochemical Approach and Non-Electrochemical DA Sensors

The electrochemical detection of DA can be achieved without the use of modified electrodes. The most common way of doing this is to use electrochemistry at the interface between two immiscible electrolyte solutions[164, 165]. Berduque *et al.*[164] found that a large excess of AA did not affect the electrochemical response of DA and Beni *et al.*[165] concluded that AA had no influence on the determination of DA. However, this approach can never be used as an *in-vivo* sensing method.

Various non-electrochemical techniques have been employed for the determination of DA. These techniques usually work by simultaneously detecting DA and a wide range of other compounds and some of them are used in conjunction with each other and with electrochemical techniques. Examples of such techniques include flow injection analysis[166],

microchip capillary electrophoresis[167], high performance liquid chromatography[168] and Raman spectroscopy[169]. Nevertheless, these approaches can not be used as an *in-vivo* sensor for real-time analysis.

1.6 Introduction to Work in this Thesis

As shown in Section 1.5, a number of approaches have been used in the electrochemical sensing of DA. Films modified with cyclodextrins are particularly interesting, as they offer the possibility of forming inclusion complexes with DA. However, as shown in Section 1.5.4, there are very few reports on using cyclodextrins in the sensing of DA. Furthermore, the majority of cyclodextrins that have been investigated to date are neutral.

In this thesis, a novel approach was employed, whereby a sulfonated β-cyclodextrin was chosen. The β-cyclodextrin cavity, Figure 1.10, is sufficiently large to accommodate the DA molecule, while the anionic sulfonated groups on the rim of the cavity have the capacity to repel the anionic ascorbate and urate anions.

These sulfonated β-cyclodextrins were immobilised in a polypyrrole film. As detailed in Chapter 3, the pyrrole monomer was electropolymerised in the presence of the anionic cyclodextrin without any additional supporting electrolyte to give a polypyrrole film doped with the sulfonated β-cyclodextrin (PPy-SCD). These films were characterised in detail and then optimised for the sensing of DA. In Chapter 4, further optimisation of the PPy-SCD film is described. The PPy-SCD film was deposited onto ultrathin fibers generated by electrospinning, in an attempt to increase the surface area of the electrode. In Chapters 5 and 6, the performance of the PPy-SCD film in the electrochemical sensing of DA in the presence of a wide variety of interfering compounds is described. No oxidation peak was observed for AA, even at very high concentrations of 1.0×10^{-2} mol dm^{-3} AA, giving highly selective detection of DA in the presence of AA. Clear evidence for the formation of an inclusion complex between DA and the sulfonated β-cyclodextrin was obtained, while the anionic sulfonated groups promoted the formation of the inclusion complex and served to repel the anionic ascorbate.

1.7 References

1.   A. Azapagic, A. Emsley and I. Hamerton*, Polymers: the environment and sustainable development*, John Wiley and Sons, 219, (2003).
2.   J. L. Bredas and G. B. Street, *Accounts of Chemical Research*, **18**, 309, (1985).
3.   B. Scrosati*, Applications of Electroactive Polymers*, Springer, 354, (1993).
4.   J. van Haare, E. E. Havinga, J. L. J. van Dongen, R. A. J. Janssen, J. Cornil and J. L. Bredas, *Chemistry-a European Journal*, **4**, 1509, (1998).
5.   P. Chandrasekhar*, Conducting Polymers, Fundamentals and Applications: A Practical Approach*, Kluwer Academic Publishers, 718, (1999).
6.   A. L. Briseno, A. Baca, Q. Z. Zhou, R. Lai and F. M. Zhou, *Anal. Chim. Acta*, **441**, 123, (2001).
7.   H. S. Nalwa*, Advanced Functional Molecules and Polymers: Volume 3: Electronic and Photonic Properties*, Taylor & Francis, 386, (2001).
8.   A. Malinauskas, *Polymer*, **42**, 3957, (2001).
9.   M. Nuñez*, Progress in electrochemistry research*, Nova Publishers, 190, (2005).
10.   G. G. Wallace, G. M. Spinks, L. A. P. Kane-Maguire and P. R. Teasdale*, Conductive Electroactive Polymers: Intelligent Polymer Systems*, CRC Press, 270, (2008).
11.   G. Bidan, B. Ehui and M. Lapkowski, *Journal of Physics D-Applied Physics*, **21**, 1043, (1988).
12.   G. Han and G. Shi, *Sensors and Actuators B: Chemical*, **99**, 525, (2004).
13.   M. S. Cho, H. J. Seo, J. D. Nam, H. R. Choi, J. C. Koo and Y. Lee, *Smart Mater. Struct.*, **16**, S237, (2007).
14.   P. A. Anquetil, H. H. Yu, J. D. Madden, P. G. Madden, T. M. Swager and I. W. Hunter, *Smart Structures and Materials 2002: Electroactive Polymer Actuators and Devices (Eapad)*, **4695**, 424, (2002).
15.   P. M. George, D. A. LaVan, J. A. Burdick, C. Y. Chen, E. Liang and R. Langer, *Advanced Materials*, **18**, 577, (2006).
16.   A. R. Zanganeh and M. K. Amini, *Sens. Actuator B-Chem.*, **135**, 358, (2008).
17.   D. A. Reece, S. F. Ralph and G. G. Wallace, *Journal of Membrane Science*, **249**, 9, (2005).
18.   K. Gurunathan, A. V. Murugan, R. Marimuthu, U. P. Mulik and D. P. Amalnerkar, *Materials Chemistry and Physics*, **61**, 173, (1999).
19.   M. E. Nicho, H. Hu, C. López-Mata and J. Escalante, *Solar Energy Materials and Solar Cells*, **82**, 105, (2004).
20.   R. J. Mortimer, A. L. Dyer and J. R. Reynolds, *Displays*, **27**, 2, (2006).
21.   M.-C. Choi, Y. Kim and C.-S. Ha, *Progress in Polymer Science*, **33**, 581, (2008).
22.   U. Lange, N. V. Roznyatovskaya and V. M. Mirsky, *Analytica Chimica Acta*, **614**, 1, (2008).
23.   H. S. Nalwa*, Handbook of Advanced Electronic and Photonic Materials and Devices*, Academic Press, 3366, (2000).
24.   A. Dallolio, G. Dascola, V. Varacca and V. Bocchi, *Comptes Rendus Hebdomadaires Des Seances De L Academie Des Sciences Serie C*, **267**, 433, (1968).
25.   S. Carquigny, J.-B. Sanchez, F. Berger, B. Lakard and F. Lallemand, *Talanta*, **78**, 199, (2009).

26. S. A. Waghuley, S. M. Yenorkar, S. S. Yawale and S. P. Yawale, *Sensors and Actuators B: Chemical*, **128**, 366, (2008).

27. N. Mermilliod, J. Tanguy and F. Petiot, *Journal of the Electrochemical Society*, **133**, 1073, (1986).

28. H. K. Song and G. T. R. Palmore, *Advanced Materials*, **18**, 1764, (2006).

29. B. Muthulakshmi, D. Kalpana, S. Pitchumani and N. G. Renganathan, *Journal of Power Sources*, **158**, 1533, (2006).

30. M. D. Ingram, H. Staesche and K. S. Ryder, *Solid State Ionics*, **169**, 51, (2004).

31. A. M. Fenelon and C. B. Breslin, *Electrochim. Acta*, **47**, 4467, (2002).

32. R. Zhu, G. Li and G. Huang, *Materials and Corrosion-Werkstoffe Und Korrosion*, **60**, 34, (2009).

33. S. Geetha, C. R. K. Rao, M. Vijayan and D. C. Trivedi, *Analytica Chimica Acta*, **568**, 119, (2006).

34. J. Wang and M. Musameh, *Analytica Chimica Acta*, **539**, 209, (2005).

35. K. Ghanbari, S. Z. Bathaie and M. F. Mousavi, *Biosens. Bioelectron.*, **23**, 1825, (2008).

36. J. H. Collier, J. P. Camp, T. W. Hudson and C. E. Schmidt, *Journal of Biomedical Materials Research*, **50**, 574, (2000).

37. M. Martina and D. W. Hutmacher, *Polymer International*, **56**, 145, (2007).

38. P. M. George, A. W. Lyckman, D. A. LaVan, A. Hegde, Y. Leung, R. Avasare, C. Testa, P. M. Alexander, R. Langer and M. Sur, *Biomaterials*, **26**, 3511, (2005).

39. J.-D. Kwon, P.-H. Kim, J.-H. Keum and J. S. Kim, *Solar Energy Materials and Solar Cells*, **83**, 311, (2004).

40. R. T. Richardson, B. Thompson, S. Moulton, C. Newbold, M. G. Lum, A. Cameron, G. Wallace, R. Kapsa, G. Clark and S. O'Leary, *Biomaterials*, **28**, 513, (2007).

41. A. M. Rocco, M.-A. De Paoli, A. Zanelli and M. Mastragostino, *Electrochim. Acta*, **41**, 2805, (1996).

42. G. M. Spinks, B. Xi, D. Zhou, V.-T. Truong and G. G. Wallace, *Synthetic Metals*, **140**, 273, (2004).

43. J. Migdalski, T. Blaz and A. Lewenstam, *Analytica Chimica Acta*, **322**, 141, (1996).

44. S. K. Ghosh, *Functional Coatings: By Polymer Microencapsulation*, Wiley-VCH, 371, (2006).

45. A. Mohammadi, M. A. Hasan, B. Liedberg, I. Lundstrom and W. R. Salaneck, *Synthetic Metals*, **14**, 189, (1986).

46. P. Subramanian, N. B. Clark, L. Spiccia, D. R. MacFarlane, B. Winther-Jensen and C. Forsyth, *Synthetic Metals*, **158**, 704, (2008).

47. B. Winther-Jensen, J. Chen, K. West and G. Wallace, *Macromolecules*, **37**, 5930, (2004).

48. A. S. Liu and M. A. S. Oliveira, *Materials Research* **10**, 205, (2007).

49. W. Prissanaroon-Ouajai, P. J. Pigram, R. Jones and A. Sirivat, *Sensors and Actuators B: Chemical*, **135**, 366, (2008).

50. J. Tietje-Girault, C. Ponce de León and F. C. Walsh, *Surface and Coatings Technology*, **201**, 6025, (2007).

51. K. J. Kim, H. S. Song, J. D. Kim and J. K. Chon, *Bulletin of the Korean Chemical Society*, **9**, 248, (1988).

52. S. Asavapiriyanont, G. K. Chandler, G. A. Gunawardena and D. Pletcher, *J. Electroanal. Chem*, **177**, 229, (1984).

53.   Y. J. Qiu and J. R. Reynolds, *Journal of Polymer Science Part a-Polymer Chemistry*, **30**, 1315, (1992).

54.   E. M. Genies, G. Bidan and A. F. Diaz, *J. Electroanal. Chem*, **149**, 101, (1983).

55.   S. Sadki, P. Schottland, N. Brodie and G. Sabouraud, *Chemical Society Reviews*, **29**, 283, (2000).

56.   M. Zhou and J. Heinze, *Electrochim. Acta*, **44**, 1733, (1999).

57.   H. Korri-Youssoufi, N. Desbenoit, R. Ricoux, J. P. Mahy and S. Lecomte, *Materials Science and Engineering: C*, **28**, 855, (2008).

58.   H. B. Fredj, S. Helali, C. Esseghaier, L. Vonna, L. Vidal and A. Abdelghani, *Talanta*, **75**, 740, (2008).

59.   M. Bazzaoui, L. Martins, E. A. Bazzaoui and J. I. Martins, *Electrochim. Acta*, **47**, 2953, (2002).

60.   I. L. Lehr and S. B. Saidman, *Materials Chemistry and Physics*, **100**, 262, (2006).

61.   S. T. Earley, D. P. Dowling, J. P. Lowry and C. B. Breslin, *Synthetic Metals*, **148**, 111, (2005).

62.   D. L. Wise, *Electrical and optical polymer systems*, CRC Press, 1239, (1998).

63.   L. Tian, Y. Qi and B. Wang, *Journal of Colloid and Interface Science*, **333**, 249, (2009).

64.   R. K. Sharma, A. C. Rastogi and S. B. Desu, *Physica B: Condensed Matter*, **388**, 344, (2007).

65.   U. Johanson, M. Marandi, T. Tamm and J. Tamm, *Electrochim. Acta*, **50**, 1523, (2005).

66.   S. Suematsu, Y. Oura, H. Tsujimoto, H. Kanno and K. Naoi, *Electrochim. Acta*, **45**, 3813, (2000).

67.   Y. F. Li and J. Yang, *Journal of Applied Polymer Science*, **65**, 2739, (1997).

68.   E. De Giglio, M. R. Guascito, L. Sabbatini and G. Zambonin, *Biomaterials*, **22**, 2609, (2001).

69.   J. C. Wu, X. M. Yu, H. Lord and J. Pawliszyn, *Analyst*, **125**, 391, (2000).

70.   M. Deepa and S. Ahmad, *European Polymer Journal*, **44**, 3288, (2008).

71.   S. Carquigny, O. Segut, B. Lakard, F. Lallemand and P. Fievet, *Synthetic Metals*, **158**, 453, (2008).

72.   J. M. Ko, H. W. Rhee, S. M. Park and C. Y. Kim, *Journal of the Electrochemical Society*, **137**, 905, (1990).

73.   Y. Li and J. Ouyang, *Synthetic Metals*, **113**, 23, (2000).

74.   F. Beck, P. Braun and M. Oberst, *Berichte Der Bunsen-Gesellschaft-Physical Chemistry Chemical Physics*, **91**, 967, (1987).

75.   H. L. Ge, G. J. Qi, E. T. Kang and K. G. Neoh, *Polymer*, **35**, 504, (1994).

76.   M. Zhou and J. Heinze, *Journal of Physical Chemistry B*, **103**, 8443, (1999).

77.   S. Shimoda and E. Smela, *Electrochim. Acta*, **44**, 219, (1998).

78.   T. F. Otero and E. Delarreta, *Synthetic Metals*, **26**, 79, (1988).

79.   T. Hernandez-Perez, M. Morales, N. Batina and M. Salmon, *Journal of the Electrochemical Society*, **148**, C369, (2001).

80.   R. Ansari Khalkhali, W. E. Price and G. G. Wallace, *Reactive and Functional Polymers*, **56**, 141, (2003).

81.   C. K. Baker, Y. J. Qiu and J. R. Reynolds, *Journal of Physical Chemistry*, **95**, 4446, (1991).

82.   A. Villiers, *Compt. Rend.*, **112**, 536, (1891).

83.   J. Szejtli, *Chemical Reviews*, **98**, 1743, (1998).
84.   J. Szejtli, *Pure and Applied Chemistry*, **76**, 1825, (2004).
85.   J. Szejtli, *Journal of Materials Chemistry*, **7**, 575, (1997).
86.   E. M. M. Del Valle, *Process Biochemistry*, **39**, 1033, (2004).
87.   S. Hbaieb, R. Kalfat, Y. Chevalier, N. Amdouni and H. Parrot-Lopez, *Mater. Sci. Eng. C-Biomimetic Supramol. Syst.*, **28**, 697, (2008).
88.   F.-T. A. Chen, G. Shen and R. A. Evangelista, *J. Chromatogr. A*, **924**, 523, (2001).
89.   A. Amini, T. Rundlof, M. B. G. Rydberg and T. Arvidsson, *Journal of Separation Science*, **27**, 1102, (2004).
90.   A. M. Stalcup and K. H. Gahm, *Anal. Chem.*, **68**, 1360, (1996).
91.   T. Loftssona and T. Järvinen, *Advanced Drug Delivery Reviews*, **36**, 59, (1999).
92.   K. A. Connors, *Chemical Reviews*, **97**, 1325, (1997).
93.   K. J. Liao, X. H. Yan, D. Y. Zhao and X. Y. Ma, *Chinese Chemical Letters*, **13**, 227, (2002).
94.   A. Bernini, O. Spiga, A. Ciutti, M. Scarselli, G. Bottoni, P. Mascagni and N. Niccolai, *European Journal of Pharmaceutical Sciences*, **22**, 445, (2004).
95.   X.-J. Dang, M.-Y. Nie, T. Jian and H.-L. Li, *J. Electroanal. Chem*, **448**, 61, (1998).
96.   C. Yáñez, R. Salazar, L. J. Núñez-Vergara and J. A. Squella, *Journal of Pharmaceutical and Biomedical Analysis*, **35**, 51, (2004).
97.   Y. Y. Zhou, C. Liu, H. P. Yu, H. W. Xu, Q. Lu and L. Wang, *Spectroscopy Letters*, **39**, 409, (2006).
98.   D. K. Roy, N. Deb, B. C. Ghosh and A. K. Mukherjee, *Spectrochimica Acta Part A: Molecular and Biomolecular Spectroscopy*, **73**, 201, (2009).
99.   G.-C. Zhao, J.-J. Zhu, J.-J. Zhang and H.-Y. Chen, *Anal. Chim. Acta*, **394**, 337, (1999).
100.   M. S. Ibrahim, I. S. Shehatta and A. A. Al-Nayeli, *Journal of Pharmaceutical and Biomedical Analysis*, **28**, 217, (2002).
101.   E. Coutouli-Argyropoulou, A. Kelaidopoulou, C. Sideris and G. Kokkinidis, *J. Electroanal. Chem*, **477**, 130, (1999).
102.   J.-F. Bergamini, M. Belabbas, M. Jouini*, S. Aeiyach, J.-C. Lacroix, K. I. Chane-Ching and P.-C. Lacaze*, *J. Electroanal. Chem*, **482**, 156, (2000).
103.   H. Dodziuk, *Cyclodextrins and their complexes: chemistry, analytical methods, applications*, Wiley-VCH, 489, (2006).
104.   M. V. Rekharsky and Y. Inoue, *Chemical Reviews*, **98**, 1875, (1998).
105.   M. Zhang, J. Li, L. Zhang and J. Chao, *Spectroc. Acta Pt. A-Molec. Biomolec. Spectr.*, **71**, 1891, (2009).
106.   C. Yanez, L. J. Nunez-Vergara and J. A. Squella, *Electroanalysis*, **15**, 1771, (2003).
107.   E. Alvira, J. A. Mayoral and J. I. García, *Chem. Phys. Lett.*, **245**, 335, (1995).
108.   L. Liu and Q. X. Guo, *Journal of Inclusion Phenomena and Macrocyclic Chemistry*, **42**, 1, (2002).
109.   H. Viernstein, P. Weiss-Greiler and P. Wolschann, *International Journal of Pharmaceutics*, **256**, 85, (2003).
110.   K. Okimoto, R. A. Rajewski, K. Uekama, J. A. Jona and V. J. Stella, *Pharmaceutical Research*, **13**, 256, (1996).
111.   X.-M. Wang and H.-Y. Chen, *Spectrochimica Acta Part A: Molecular and Biomolecular Spectroscopy*, **51**, 333, (1995).

112.   L. Leclercq, M. Bria, M. Morcellet and B. Martel, *Journal of Inclusion Phenomena and Molecular Recognition in Chemistry*, **30**, 215, (1998).
113.   L. Liu and Q. X. Guo, *Journal of Physical Chemistry B*, **103**, 3461, (1999).
114.   S. P. Vanhelden, B. P. Vaneijck and L. H. M. Janssen, *Journal of Biomolecular Structure & Dynamics*, **9**, 1269, (1992).
115.   V. J. Stella and R. A. Rajewski, *Pharmaceutical Research*, **14**, 556, (1997).
116.   K. Uekama, F. Hirayama and T. Irie, *Chemical Reviews*, **98**, 2045, (1998).
117.   R. F. Thompson, *The Brain: A Neuroscience Primer*, W. H. Freeman and Company, 475, (1993).
118.   P. Revest and A. Longstaff, *Molecular neuroscience*, Taylor & Francis, 237, (1998).
119.   G. S. Wilson and M. A. Johnson, *Chemical Reviews*, **108**, 2462, (2008).
120.   P. E. M. Phillips, G. D. Stuber, M. Heien, R. M. Wightman and R. M. Carelli, *Nature*, **422**, 614, (2003).
121.   R. D. O'Neill, *Sensors*, **5**, 317, (2005).
122.   E. Koutsilieri, V. ter Meulen and P. Riederer, *Journal of Neural Transmission*, **108**, 767, (2001).
123.   A. Afkhami, D. Nematollahi, L. Khalafi and M. Rafiee, *International Journal of Chemical Kinetics*, **37**, 17, (2005).
124.   T. Luczak, *Electroanalysis*, **20**, 1639, (2008).
125.   Y. Li, M. Liu, C. Xiang, Q. Xie and S. Yao, *Thin Solid Films*, **497**, 270, (2006).
126.   S. Hou, N. Zheng, H. Feng, X. Li and Z. Yuan, *Anal. Biochem.*, **381**, 179, (2008).
127.   J. Weng, J. Xue, J. Wang, J.-S. Ye, H. Cui, F.-S. Sheu and Q. Zhang, *Adv. Funct. Mater.*, **15**, 639, (2005).
128.   S. M. Chen and W. Y. Chzo, *J. Electroanal. Chem*, **587**, 226, (2006).
129.   Y. Li, P. Wang, L. Wang and X. Lin, *Biosens. Bioelectron.*, **22**, 3120, (2007).
130.   M. Ghita and D. W. M. Arrigan, *Electrochim. Acta*, **49**, 4743, (2004).
131.   J.-B. Raoof, R. Ojani and S. Rashid-Nadimi, *Electrochim. Acta*, **50**, 4694, (2005).
132.   P. R. Roy, T. Okajima and T. Ohsaka, *Bioelectrochemistry*, **59**, 11, (2003).
133.   X. Lin, Y. Zhang, W. Chen and P. Wu, *Sens. Actuator B-Chem.*, **122**, 309, (2007).
134.   X. Lin, Q. Zhuang, J. Chen, S. Zhang and Y. Zheng, *Sens. Actuator B-Chem.*, **125**, 240, (2007).
135.   L. Lin, J. Chen, H. Yao, Y. Chen, Y. Zheng and X. Lin, *Bioelectrochemistry*, **73**, 11, (2008).
136.   Y. Li and X. Lin, *Sens. Actuator B-Chem.*, **115**, 134, (2006).
137.   W. J. Kang, L. M. Niu and L. Ma, *Chin. Chem. Lett.*, (2008).
138.   J. Mathiyarasu, S. Senthilkumar, K. L. N. Phani and V. Yegnaraman, *Materials Letters*, **62**, 571, (2008).
139.   A. I. Gopalan, K.-P. Lee, K. M. Manesh, P. Santhosh, J. H. Kim and J. S. Kang, *Talanta*, **71**, 1774, (2007).
140.   M. Ferreira, L. R. Dinelli, K. Wohnrath, A. A. Batista and O. N. Oliveira, *Thin Solid Films*, **446**, 301, (2004).
141.   V. Zucolotto, M. Ferreira, M. R. Cordeiro, C. J. L. Constantino, W. C. Moreira and J. O. N. Oliveira, *Sensors and Actuators B: Chemical*, **113**, 809, (2006).
142.   D. Zheng, J. Ye, L. Zhou, Y. Zhang and C. Yu, *J. Electroanal. Chem*, **625**, 82, (2009).
143.   A. Salimi, K. Abdi and G. R. Khayatian, *Microchim. Acta*, **144**, 161, (2004).

144. S. Alpat, S. K. Alpat and A. Telefoncu, *Anal. Bioanal. Chem.*, **383**, 695, (2005).
145. G.-S. Lai, H.-L. Zhang and D.-Y. Han, *Microchim. Acta*, **160**, 233, (2008).
146. S. Yuan, W. Chen and S. Hu, *Materials Science and Engineering: C*, **25**, 479, (2005).
147. R. K. Shervedani, M. Bagherzadeh and S. A. Mozaffari, *Sens. Actuator B-Chem.*, **115**, 614, (2006).
148. L. Zhang, J. Jia, X. Zou and S. Dong, *Electroanalysis*, **16**, 1413, (2004).
149. T. Liu, M. Li and Q. Li, *Talanta*, **63**, 1053, (2004).
150. Q. Wang, N. Jiang and N. Li, *Microchemical Journal*, **68**, 77, (2001).
151. G.-Z. Hu, D.-P. Zhang, W.-L. Wu and Z.-S. Yang, *Colloids and Surfaces B: Biointerfaces*, **62**, 199, (2008).
152. L. Zhang and X. Jiang, *J. Electroanal. Chem.*, **583**, 292, (2005).
153. S. Thiagarajan and S.-M. Chen, *Talanta*, **74**, 212, (2007).
154. S. Shahrokhian and H. R. Zare-Mehrjardi, *Sensors and Actuators B: Chemical*, **121**, 530, (2007).
155. J. Zheng and X. Zhou, *Bioelectrochemistry*, **70**, 408, (2007).
156. A. Fragoso, E. Almirall, R. Cao, L. Echegoyen and R. G. Jonte, *Chem. Commun.*, **19**, 2230, (2004).
157. B. Kong, J. Zeng, G. Luo, S. Luo, W. Wei and J. Li, *Bioelectrochemistry*, **In Press, Corrected Proof**.
158. U. E. Majewska, K. Chmurski, K. Biesiada, A. R. Olszyna and R. Bilewicz, *Electroanalysis*, **18**, 1463, (2006).
159. G. Alarcon-Angeles, B. Perez-Lopez, M. Palomar-Pardave, M. T. Ramirez-Silva, S. Alegret and A. Merkoci, *Carbon*, **46**, 898, (2008).
160. N. Izaoumen, L. M. Cubillana-Aguilera, I. Naranjo-Rodríguez, J. L. H.-H. de Cisneros, D. Bouchta, K. R. Temsamani and J. M. Palacios-Santander, *Talanta*, **In Press, Corrected Proof**.
161. D. Bouchta, N. Izaoumen, H. Zejli, M. E. Kaoutit and K. R. Temsamani, *Biosens. Bioelectron.*, **20**, 2228, (2005).
162. T. J. Yin, W. Z. Wei and J. X. Zeng, *Analytical and Bioanalytical Chemistry*, **386**, 2087, (2006).
163. N. Izaoumen, D. Bouchta, H. Zejli, M. E. Kaoutit and K. R. Temsamani, *Analytical Letters*, **38**, 1869, (2005).
164. A. Berduque, R. Zazpe and D. W. M. Arrigan, *Anal. Chim. Acta*, **611**, 156, (2008).
165. V. Beni, M. Ghita and D. W. M. Arrigan, *Biosens. Bioelectron.*, **20**, 2097, (2005).
166. H. J. Leu and M. S. Lin, *Electroanalysis*, **18**, 307, (2006).
167. D. J. Fischer, W. R. Vandaveer, R. J. Grigsby and S. M. Lunte, *Electroanalysis*, **17**, 1153, (2005).
168. Y. Wang, D. S. Fice and P. K. F. Yeung, *Journal of Pharmaceutical and Biomedical Analysis*, **21**, 519, (1999).
169. H. G. Schulze, L. S. Greek, C. J. Barbosa, M. W. Blades, B. B. Gorzalka and R. F. B. Turner, *Journal of Neuroscience Methods*, **92**, 15, (1999).

Chapter 2

Experimental

2.1 Introduction

In this chapter the experimental techniques and apparatus used in the course of this research are outlined. The procedures for the experiments are also detailed. In addition, an overview of the theories and related equations are described.

2.2 Experimental Techniques

The chief electrochemical / analytical techniques used throughout this study were cyclic voltammetry, potentiostatic measurements, rotating disc voltammetry, electrochemical quartz crystal microbalance measurements (EQCM), ultraviolet–visible spectroscopy (UV-Vis), nuclear magnetic resonance spectroscopy (NMR) and scanning electron microscopy (SEM) coupled with energy dispersive x-ray analysis (EDX). A brief overview of each technique is given below.

2.2.1 Cyclic Voltammetry

Cyclic voltammetry is often the first experiment performed in an electroanalytical study and can be used to obtain information about simple and complicated electrode reactions. As a result, cyclic voltammetry is one of the most useful and widely applied techniques in electrochemistry[1]. Cyclic voltammetry is a dynamic electrochemical technique wherein the applied potential at the working electrode is swept between two chosen potential limits and the change in current is monitored. This is done at a constant rate known as the scan rate. The initial applied potential, E_i, is swept to a vertex potential, E_v, where the scan is reversed and swept back to the final potential, E_f, which usually equals the original potential, E_i. This process creates a cyclic effect and is typically repeated a number of times. For a simple redox reaction, Equation 2.1, where only R is present, the current response of the forward scan is the linear potential sweep voltammogram as R is oxidised to O which produces an anodic peak. On the reverse scan, the reduction of O to R occurs, resulting in a

cathodic peak. A plot of applied potential (V vs. SCE) versus current (A cm^{-2}) is used to depict such generated cyclic voltammograms, Figure 2.1.

$$O + n e^- \quad \rightleftharpoons \quad R \qquad \qquad 2.1$$
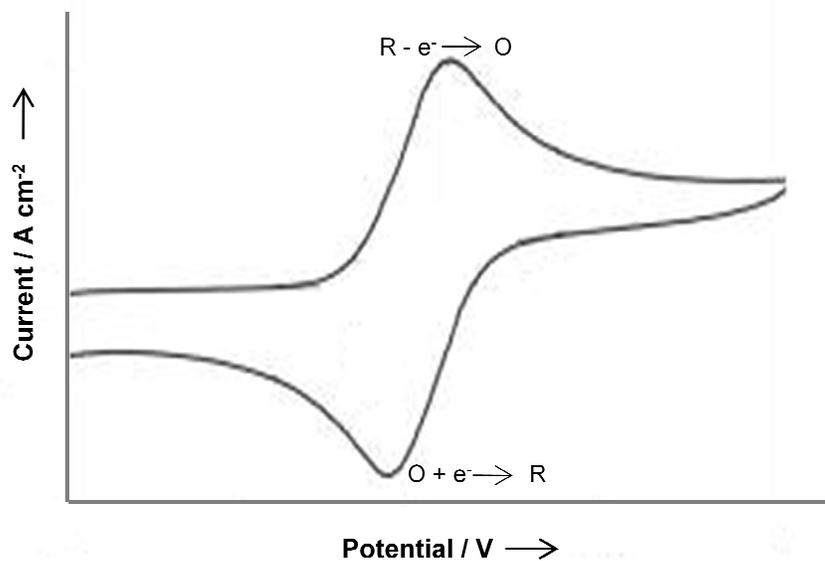
Figure 2.1: Typical current-potential profile for a cyclic voltammogram of a reversible redox species.

Cyclic voltammetry was used primarily in the study of the electrochemical behaviour of the polypyrrole-sulfonated β-cyclodextrin (PPy-SCD) modified electrode towards the oxidation and reduction of dopamine (DA). It was also used to investigate the effect of numerous interfering compounds on the DA signal and as an alternative approach to synthesise the PPy-SCD films. Furthermore, it was used to determine if an inclusion complex was formed between certain compounds and the sulfonated β-cyclodextrin.

2.2.2 Potentiostatic Measurements

Potentiostatic measurements were utilised for a variety of different processes in this study. A potentiostatic mode was employed to grow the PPy-SCD film. This was carried out by applying a constant potential to the working electrode in the polymer forming electrolyte for a fixed amount of time, or until a desired charge had passed. The growth of the polymer was recorded by monitoring the current response (A cm^{-2}) as a function of time (s). This technique was also used to over-oxidise or reduce the PPy-SCD film by holding the working electrode at a substantially higher or lower potential for a fixed amount of time. Another potentiostatic measurement carried out in this research was constant potential amperometry (CPA). CPA is a technique where a constant potential, sufficient to oxidise or reduce the analyte of interest, is applied to the electrode and the current is monitored[2]. CPA was used as a tool to calibrate the PPy-SCD modified electrode to DA. This involved rotating the working electrode at high speeds until the non-faradaic current had reached a stable background level. When a basal current level was achieved, a series of injections of DA were made to the cell while the working electrode was still being rotated and the changes in the current were monitored. This produces a step-wise pattern of time (s) versus current (A cm^{-2}), Figure 2.2. Further details of this experiment are given in Section 2.8
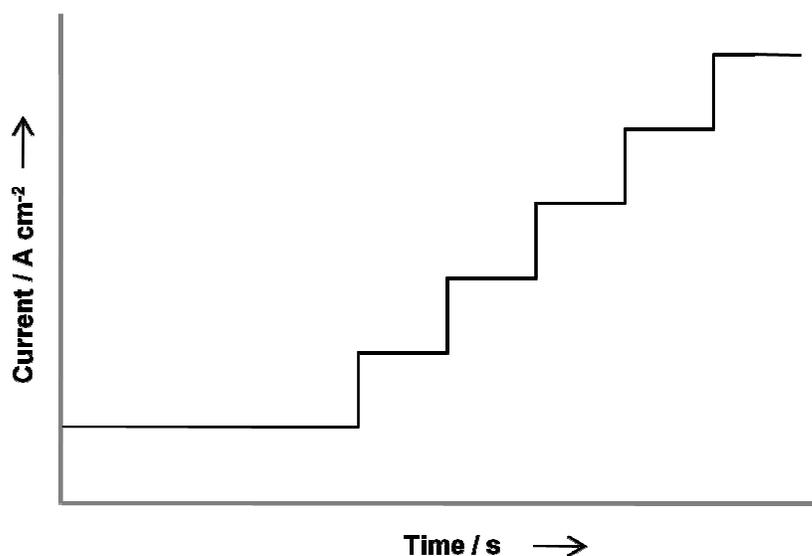

Figure 2.2: Typical constant potential amperometry response.

2.2.3 Electrochemical Quartz Crystal Microbalance Measurements

The electrochemical quartz crystal microbalance (EQCM) technique is a very useful tool in electrochemistry as it can monitor extremely small mass changes at the electrode surface during electrochemical experiments[3]. EQCM utilises the piezoelectric qualities of a quartz crystal which becomes deformed in the presence of an electric field. The quartz crystal microbalance consists of a quartz crystal wafer, sandwiched between two metal electrodes. In this study, a 1.47 cm^2 quartz crystal was used with gold electrodes placed either side of it. Applying an alternating electric field between the two gold electrodes causes the quartz crystal to oscillate. The resonant frequency of this oscillation is inversely proportional to the mass of the quartz crystal. Therefore, the change in the crystal mass (Δm) can be determined by measuring the changes in the crystal's resonant frequency (Δf). The relationship between Δm and Δf is given by the Sauerbrey equation, Equation 2.2.

$$\Delta f = \frac{-2f_0^2}{A\sqrt{\mu\rho}}\Delta m \qquad\qquad 2.2$$

where, f_o is the resonant frequency of the crystal prior to a mass change (8.0 MHz), A is the surface area of the gold (0.202 cm^2), μ is the crystal density (2.648 g cm^{-3}) and ρ is the sheer modulus (2.947 x 10^{11} g cm^{-1} s^{-2})[4].

The above relationship shows that a change in the resonance frequency of the crystal gives the opposite change in the crystal mass load. Therefore, an increase in the mass will result in a decrease in oscillation and thus a decrease in frequency.

A schematic representation of the EQCM set up is given in Figure 2.3. During each experiment only one of the metal electrode surfaces is in contact with the electrolyte. The quartz wafer is supported by two wires, one to carry current to the gold layer and the other to allow for crystal vibration and to record changes in the frequency. The reference electrode is a custom-made Ag/AgCl electrode and the counter electrode is a fine platinum wire.

In this work the EQCM technique was used to investigate the ion-exchange properties of the PPy-SCD film. It was also used to try and determine the approximate doping levels of the PPy-SCD film. This was done by recording the current (A cm^{-2}) and the frequency change (Hz) as a function of time (s) and potential (V vs. SCE). Further details of this experiment are given in Section 3.3.5.5.
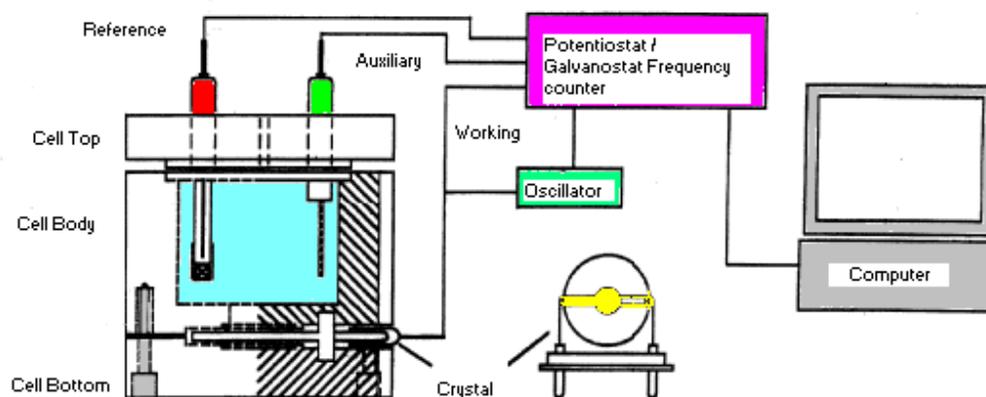

Figure 2.3: Schematic set-up of the electrochemical quartz microbalance.

2.2.4 Rotating Disc Voltammetry

Rotating disc voltammetry is similar to cyclic voltammetry in that the potential of the working electrode is swept between two chosen potential limits and the change in current is monitored. However, it differs significantly because the working electrode itself is rotated[5]. The rotating disc electrode (RDE) consists of a flat disc of suitable electrode material (Pt, Au or GC) centrally embedded in a rod of insulating material. It is attached to a motor by a rotating shaft and subsequently immersed in the electrolyte solution and rotated at a certain frequency, f, where the angular velocity, $\omega = 2\pi f/60$[1]. A schematic representation of the set-up is shown in Figure 2.4. The current is measured as a function of the potential and the resulting voltammograms generally exhibit a sigmoid shaped wave, Figure 2.5, at a sufficiently fast rotation rate. The rotational motion sets up a well defined flow of solution towards the surface of the rotating disc electrode. It acts like a pump, pulling the solution upwards and then throwing it outwards, Figures 2.6(a) and (b)[6]. However, the layer of

solution immediately adjacent to the surface of the electrode behaves as if it was stuck to the electrode and appears from the perspective of the rotating electrode to be motionless. This layer is called the stagnant layer. The analyte is brought to the surface of the electrode by a combination of two types of transport, vortex flow and simple molecule diffusion. First, the vortex flow continuously brings fresh analyte to the outer edge of the stagnant layer and then the analyte diffuses across the stagnant layer. The thinner the stagnant layer, the faster the analyte can diffuse across it. The size of the stagnant layer is governed by the rate of rotation. In general, faster electrode rotation makes the stagnant layer thinner. Therefore, the diffusion of the analyte to the electrode surface will be faster at higher rotation speeds resulting in higher currents[5]. It is this high rate of mass transport that results in the sigmoidal shaped wave. If the rotation rate is not sufficiently fast, voltammograms resembling those of cyclic voltammetry are obtained.
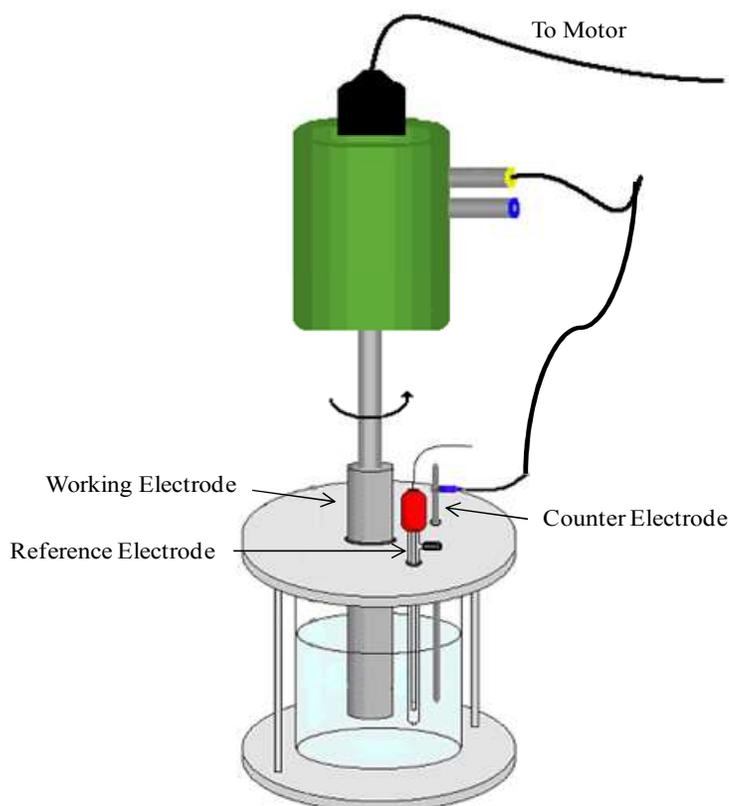
Figure 2.4: Schematic representation of the experimental set-up for rotation disc voltammetry.

Since the observed current using rotating disc voltammetry is limited by diffusion, the current can be related to the rotation rate of the electrode using the Levich equation, Equation 2.3.

$$i_L = (0.62)nFAD^{2/3}\omega^{1/2}v^{-1/6}C_o \qquad\qquad 2.3$$

where, i_L is the limiting current, n is the number of electrons transferred, F is the Faraday constant, A is the electrode area, D is the diffusion coefficient, ω is the rotation speed, v is the kinematic viscosity and C is the concentration of reactant in solution[6]. It can be seen from this equation that the diffusion coefficient is linearly dependent on the square root of the rotational speed and the limiting current. Therefore, a plot of $\omega^{1/2}$ versus i_L yields a linear plot and the diffusion coefficient can be calculated from the slope of this line.

For the purpose of this study, rotation disc voltammetry was used to prove that an inclusion complex was formed between the DA and the sulfonated β-cyclodextrin. The data were subsequently used to calculate the complex formation constant between the DA and the sulfonated β-cyclodextrin. Further details are given in Section 2.11.
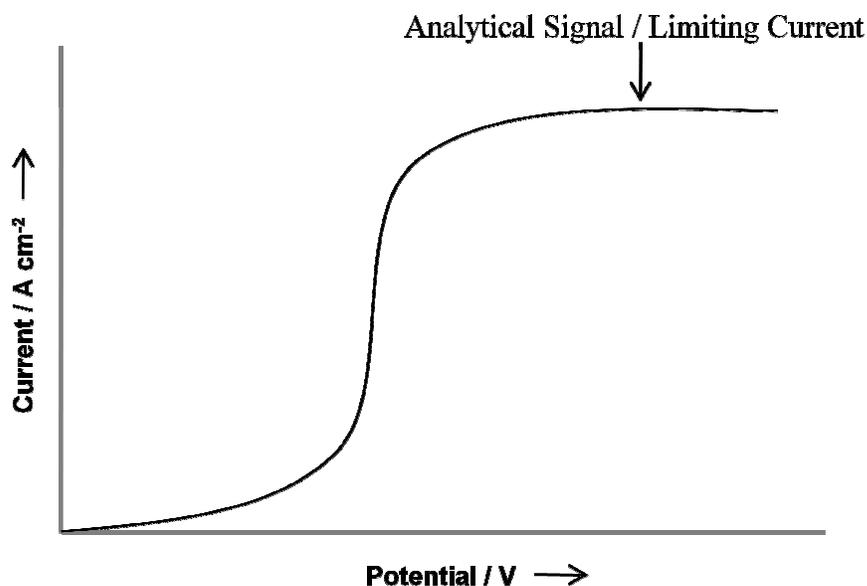

Figure 2.5: Typical rotation disc voltammetry response.
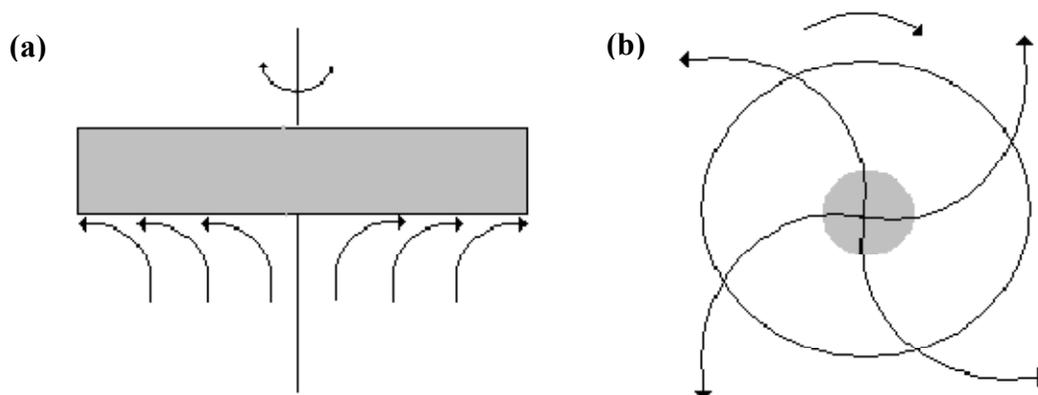
Figure 2.6: Schematic showing the flow pattern from (a) a side view and (b) from below.

2.2.5 Differential Pulse Voltammetry

Pulse voltammetry was developed to improve the sensitivity of voltammetric measurements. This is achieved by reducing the double layer capacitance to zero so that the current recorded is totally faradaic[6]. There are several types of pulse voltammetry including normal, differential and square wave. In differential pulse voltammetry, the base potential is incremented and increased at a fixed rate as shown in Figure 2.7. The pulses applied are of the same magnitude each time. The current is measured shortly before the pulse is applied and at the end of the pulse, Figure 2.7. The difference between these two values is recorded and plotted as a function of the applied potential. Information on the parameters used is given in Section 2.8.

In this study, differential pulse voltammetry was used to investigate the effect of pH on the oxidation peak potential of the DA.
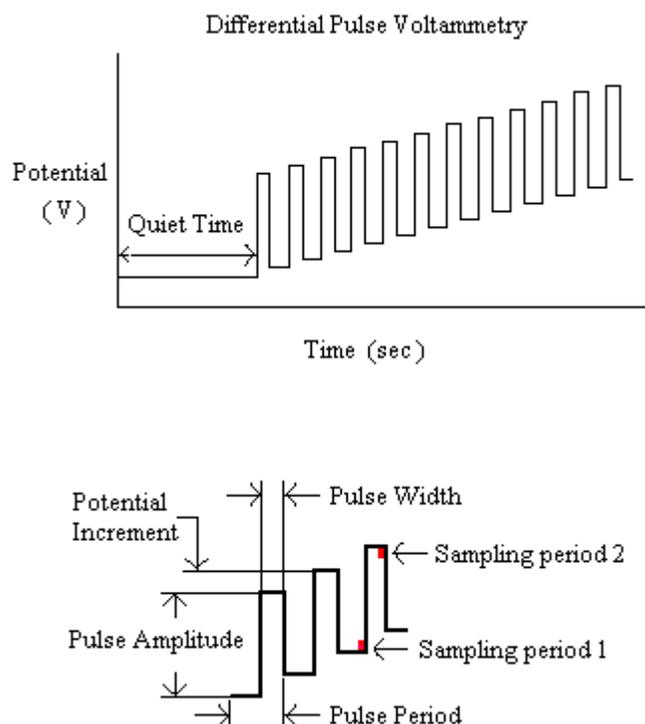
Figure 2.7: Schematic of differential pulse voltammetry technique, showing the step method applied and the parameter settings required. The red tabs denote at which point the current is measured.

2.2.6 Ultraviolet–Visible Spectroscopy

Ultraviolet–visible (UV-Vis) spectroscopy is a very useful analytical technique as it can be used to determine the amount of substance present in a sample. This is because the absorbance is proportional to the concentration of the absorbing species given by the Beer-Lambert law, Equation 2.4.

$$A = \varepsilon bc \hspace{6cm} 2.4$$

where, A is the absorbance, ε is the molar absorbtivity, b is the path length and c is the concentration of the absorbing species. For the purposes of this study, UV-Vis spectroscopy was employed to investigate the stoichiometry of the DA and sulfonated β-cyclodextrin complex by Job's method. Further details on how this was carried out are presented in Section 2.11.4.

2.2.7 Nuclear Magnetic Resonance Spectroscopy

Nuclear magnetic resonance spectroscopy (NMR) is the principal technique used for determining the structure of organic compounds. It is a phenomenon which occurs when the nuclei of certain atoms, notably ^{1}H, ^{13}C, ^{19}F and ^{31}P are exposed to an external magnetic field. ^{1}H NMR is the most frequently used and can provide information on a wide variety of factors including the number of different hydrogens present in a molecule and the electronic environment of the different types of hydrogens[7].

Every chemically equivalent hydrogen or group of hydrogens will give a signal in the ^{1}H NMR spectra. Consequently, this reveals how many sets of equivalent protons a molecule contains. The area under the ^{1}H NMR signal is directly proportional to the number of hydrogens giving rise to the signal. Therefore, by integrating the different ^{1}H NMR signals, information about the relative numbers of chemically distinct hydrogens can be obtained. Chemically different hydrogens in a molecule do not experience the same magnetic field. For example, hydrogens bound to carbons attached to electron withdrawing groups tend to resonate at higher frequencies (more downfield). This is because the nucleus is de-shielded and thus the magnetic field is increased and more energy is required to bring about resonance. Accordingly, the position of the signal in the ^{1}H NMR can determine what kind of protons the molecule contains. ^{1}H NMR also provides information about the amount of hydrogens that are coupled to a particular hydrogen or group of equivalent hydrogens. In general, an NMR signal will be split into $n + 1$ peaks, where n is the number of hydrogens on the adjacent atom or atoms. If there are no hydrogens on the adjacent atoms, then the signal will remain as a single peak, a singlet. If there is one, two or three hydrogens on the adjacent atoms then the signal will be split into two peaks of equal size (doublet), three peaks with an area in the ratio of 1:2:1 (triplet) or four peaks with an area in the ratio 1:3:3:1 (quartet), respectively[8].

In this study, ^{1}H NMR was used to investigate the manner in which the DA was including inside the cavity of the sulfonated β-cyclodextrin. This was achieved by monitoring the environment of the individual atoms and of the complex and was carried out by Miss Gillian Hendy, a fellow researcher in the group. Further information on how this was carried out is given in Section 2.11.3.

2.2.8 Scanning Electron Microscopy (SEM) and Energy Dispersive X-Ray Analysis (EDX)

The scanning electron microscope (SEM) is a microscope that uses electrons rather than light to form an image. It is routinely used to generate high-resolution images of objects to reveal information about the external morphology and topography. In order to generate such images, the surface of the sample under investigation is bombarded with a high energy beam of electrons (primary electrons). This in turn causes the electrons from the sample to dislodge (secondary electrons). These secondary electrons are attracted and collected by a positive detector and translated into signals which are amplified, analyzed and translated into images. The preparation of samples for SEM analysis is relatively easy since most SEMs only require the sample to be conductive. This can be done by coating the sample to be analysed with gold using a sputter coater[9].

The SEM is usually equipped with an energy dispersive X-ray analysis (EDX) system to enable it to perform compositional analysis on specimens. In this case, it measures the X-rays omitted from the sample when the sample is bombarded by the SEM's electron beam. The X-ray energy is characteristic of the element from which it was emitted and thus EDX analysis is useful for identifying the chemical composition of the sample[9].

In this study, SEM and EDX were used to investigate the morphology and chemical compositions of the polymer films. SEM was also employed to study the size and structure of the nanofibers and the polymer modified nanofibers, Chapter 4.

2.3 Instrumentation, Software and Ancillary Equipment

Potentiostatic and cyclic voltammetry experiments were carried out using one of two potentiostats; a Solartron Potentiostat Model 1285A and a Solartron Potentiostat Model 1287. In the case of the Solartron Potentiostat Model 1285A, the electrochemical experiments were performed using Scribner Associates Corrware for Windows Version 2.2. The Solartron Potentiostat Model 1287 used Scribner Associates Corrware for Windows Version 2.1. The resulting data in all cases were analysed using Scribner Associates

CorrView Version 2.3a. The remaining apparatus information is outlined in Table 2.1. During the CPA experiments, the working electrode was rotated using the Princeton Applied Research Model 636 Ring-Disc Electrode System apparatus. General analysis of data and plotting of calibration graphs were performed in Microsoft Excel 2000 and Sigmaplot 2001. The NMR data were processed with the Bruker Topspin 1.3 software. An overview of the ancillary equipment used throughout this study is given in Table 2.2. The Tencor and SEM analysis was carried out in the Tyndall National Institute, University College Cork under the National Access Programme (NAP) which was funded by Science Foundation Ireland (SFI), while the EDX was carried out in the CMAU at Trinity College Dublin.

Table 2.1: Analytical techniques used with model information.

Analytical Technique	Model
UV-Vis spectroscopy	Varian Cary 50 UV-Vis. Spectrometer
Rotating Disc Voltammetry	Princeton Applied Research Model 636 Ring-Disc Electrode System
EQCM	Chi EQCM, Model 440
^{1}H NMR	300 MHz Bruker Spectometer
SEM	Leica Stereoscan 440 / Joel 840 SEM / Hitachi S400
EDX	Tescan Mira XMU VPFE
Surface Profilometer (Thickness of Films)	Tencor Veeco Dektac 6M Stylus Profilometer

Table 2.2: Ancillary equipment used with model information.

Equipment	Model
Sonicator	Branson 1510
Electronic Balances	Sartorius Models TE612 and TE124S
pH Meter	Orion Model 720A
Conductivity Meter	Jenway 4510
Gold Sputter Coater	Emitech K550x / Agar Scientific

2.4 Chemicals and Solutions

The chemicals used throughout this study were purchased from Sigma-Aldrich or its subsidiary company Fluka. All chemicals were used as supplied except for pyrrole which was distilled and stored at -4^0 C before use. All solutions were made from distilled water unless stated otherwise. All DA solutions were prepared freshly before each experiment as DA is easily oxidised. The composition of the buffer solutions used in Chapter 4 are outlined in Table 2.3. Where necessary, the pH of the solutions was changed using concentrated H_2SO_4 or NaOH.

Table 2.3: Composition of buffer solutions used in Chapter 4.

Buffer Solution	Composition
Phosphate	0.08 M of NaH_2PO_4 and 0.02 M Na_2HPO_4
Saline Phosphate	8.0 g of NaCl, 0.2 g of KCl, 1.4 g of Na_2HPO_4 and 0.24 g of KH_2PO_4 in 1 L of distilled water
Acetate	0.10 M CH_3COONa and 10 µl CH_3COOH
Succinate	0.035 M Succinic Acid and 0.065 M NaOH
Maleate	0.04 M Maleic Acid and 0.06 M NaOH
MES	0.07 M MES and 0.03 M NaOH

2.5 The Electrochemical Cell Set-up

A standard three-electrode electrochemical cell configuration was employed for all electrochemical experiments. This consists of a working electrode (WE), a reference electrode (RE) and finally a counter/auxiliary electrode (CE), as shown in Figure 2.8. The WE used was generally a platinum (Pt) disc supported inside a Teflon$^®$ holder. The manufacture of the WE is discussed in Section 2.6. The RE was a saturated calomel electrode (SCE) and the CE consisted of a high surface area Pt wire. This cell was then connected to a potentiostat and the results were recorded by a computer in the manner shown in Figure 2.9. In general, the potential is measured between the RE and the WE and the current is measured between the WE and the CE. The electrochemical cell consisted of these three electrodes, unless otherwise stated.
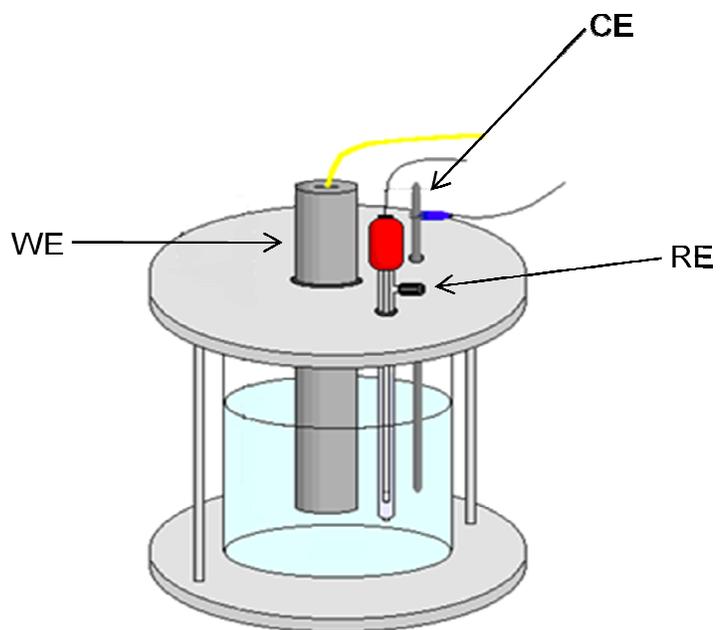
**Figure 2.8: Schematic of the electrochemical cell used for electrochemical measurements.**
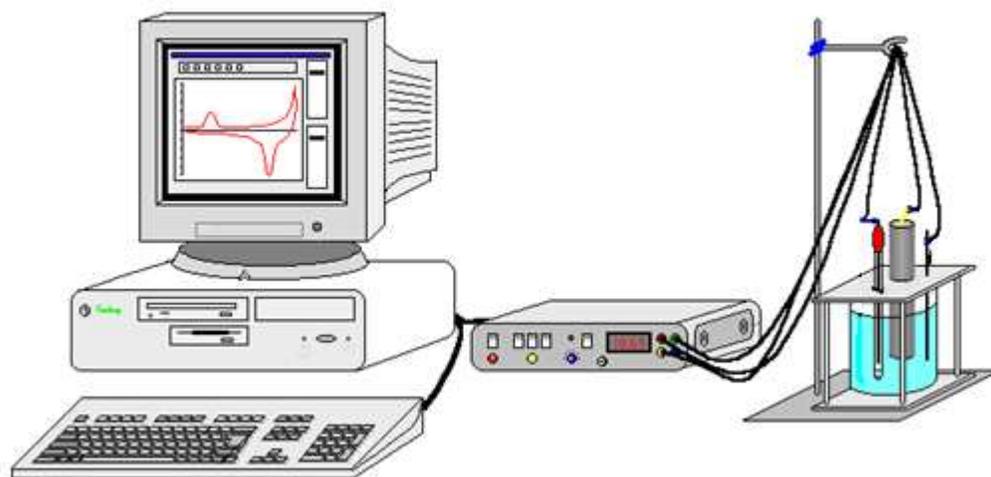
Figure 2.9: Experimental set-up used to record all electrochemical measurements.

2.6 Preparation of the Working Electrodes

The chemical composition and exposed surface area of each of the working electrodes used over the course of this study are presented in Table 2.4. The substrates used in each of the working electrodes were supplied by GoodFellow or Alfa Aesar in rod form and were then cut into lengths of 3 cm. An electrical contact between the substrate and the external circuit was achieved by attaching a copper wire to the substrate with a conducting epoxy resin. The wire was then threaded through the Teflon holder leaving the substrate exposed at one end. The end of the electrode with the copper wire was sealed with silicone and the end of the electrode with the substrate exposed was sealed using a non-conducting epoxy resin. A schematic representation of the electrode assembly is shown in Figure 2.10. The rotating disc electrodes (Pt and GC) were purchased from Princeton Applied Research and had a geometric surface area of 0.1963 cm^2 (GC) and 0.1257 cm^2 (Pt).

Prior to each experiment the exposed electrode surface was hand polished using Buehler MetaDi monocrystalline diamond suspension and a Buehler polishing microcloth. The samples were polished to a smooth finish with successively finer grades ranging from 30 µm to 1 µm. They were rinsed with distilled water and sonicated for 30 s in the ultrasonic bath in between each polish grade. If a polymer film was on the surface of the electrode, a Buehler METASERV grinder polisher with Buehler SiC grinding paper (Grit P 2500) was used to remove the polymer before polishing with the diamond suspension.
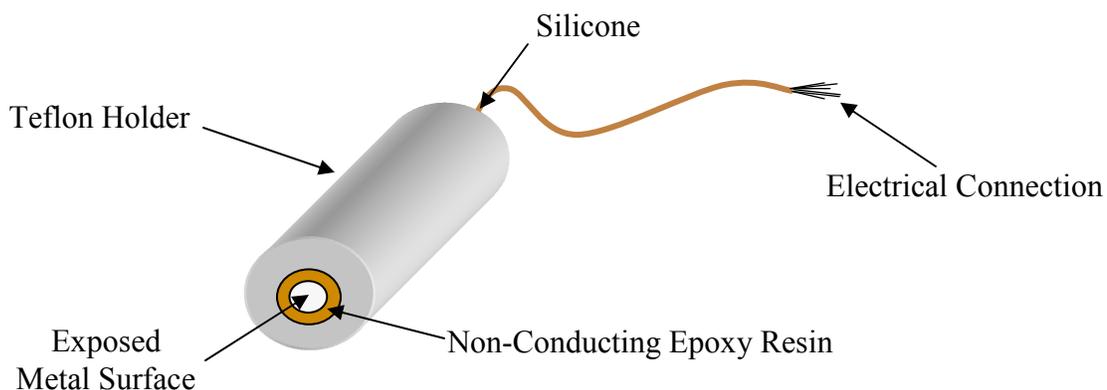

Figure 2.10: Schematic diagram of electrode structure.

Table 2.4. Chemical composition and surface area of electrodes.

Metal	Composition Purity	Geometric Surface Area / cm^2
Pt	99.95 %	0.1257
GC	N/A	0.1257
Au	99.95 %	0.1257

2.7 Fabrication and Characterisation of the Polypyrrole Films

In general, the PPy films were electrosynthesised at the working electrode using an oxidation potential of 0.800 V vs. SCE from a solution of 0.20 mol dm^{-3} pyrrole and 0.01 mol dm^{-3} of the appropriate electrolyte until a charge of 0.24 C cm^{-2} was reached. Any variation in the potentials, charge passed or polymer forming electrolyte is presented in the figure captions or corresponding text in the results section. The morphology and chemical composition of the PPy films were analysed using scanning electron microscopy (SEM) and energy dispersive X-ray analysis (EDX). The samples were gold coated prior to SEM imaging. The thickness of the polymer films was studied using Tencor. Information on the apparatus used to carry this out is given in Table 2.1. In addition to the above analysis, EQCM was also used to acquire information about the ion exchange properties of the PPy-SCD film and the doping levels of the film. For this analysis the PPy-SCD films were grown until a charge of 0.12 C cm^{-2} had been reached from a monomer solution containing 0.20 mol dm^{-3} pyrrole and 0.01 mol dm^{-3} sulfonated β-cyclodextrin. The films were then cycled in 0.10 mol dm^{-3} NaCl for 10 cycles from -1.100 to +0.800 V vs. Ag/AgCl.

2.8 Dopamine Analysis

Cyclic voltammetry was primarily used in the analysis of DA. In most cases, the modified electrodes and the bare electrodes were first cycled in the background electrolyte, 0.10 mol

dm^{-3} Na_2SO_4, between -0.100 V vs. SCE and 0.900 V vs. SCE for 10 cycles. It will be stated in the text in the results section if this was not performed. The electrodes were then transferred to the various concentrations of DA / 0.10 mol dm^{-3} Na_2SO_4 solutions and cycled from -0.100 V vs. SCE and 0.900 V vs. SCE for 10 cycles. Any fluctuations in these parameters or solutions will be clearly stated in the text or figure captions. The scan rate used in this study was varied depending on the experimental conditions. However, the most frequently used scan rate was 100 mV s^{-1}. The scan rate employed in each experiment is presented in the figure captions or corresponding text in the results section. In order to determine the true peak current of each cyclic voltammogram a straight line was drawn from the start point of the peak and a vertical straight line was then drawn through the mid-point of the peak. The current at which the two lines crossed was the background current and this was then subtracted from the measured current at the peak potential. This is schematically illustrated in Figure 2.11. It will be stated in the text if the background was not subtracted. The charge associated with a peak was calculated by integrating under the curve using the integration function in the CorrView programme. This was performed in Section 3.3.5.3 to give information on the surface coverage of the electrode.

The performance of the sensor was also evaluated using constant potential amperometry. This was performed by rotating the polymer modified working electrode at 2000 rpm in a 0.10 mol dm^{-3} Na_2SO_4 solution at a constant potential of 0.650 V vs. SCE until a steady state was achieved. At this point a series of injections of DA ranging from 50 μL to 5 mL were made to the cell.

Differential pulse voltammetry was employed to investigate the effect of pH on the DA oxidation peak potentials. The parameters used to carry this out are given in Table 2.5. In these experiments, the modified electrodes were only cycled in the 0.10 mol dm^{-3} Na_2SO_4 solution for two cycles before being transferred to the DA solutions for 5 cycles.
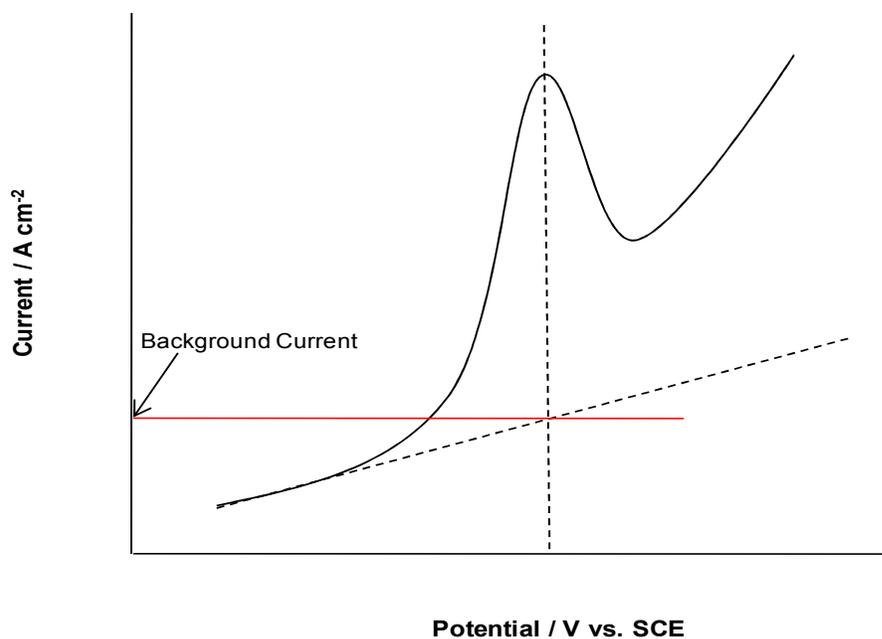
Figure 2.11: The calculation of the background current of each cyclic voltammogram.

Table 2.5: Parameters used for differential pulse voltammetry experiments

Parameters	Values
Pulse Amplitude	50 mV
Pulse Width	0.07 s
Sampling Width	0.03 s
Pulse Period	0.30 s
Scan Rate	5 mV s^{-1}

2.9 Kinetic Analysis

The voltammogram response at different scan rates can reveal kinetic information concerning the electrocatalytic process, such as diffusion and adsorption effects. Furthermore, it can be used to determine the reversible behaviour of a system. The factors

that influence the behaviour and magnitude of the peak current can be described by the Randles-Sevcik equation, Equation 2.5. The use of this equation is limited to processes that are reversible. A reversible cyclic voltammogram can only be observed if both the oxidation and reduction species are stable and if the kinetics of the electron transfer process are fast[6].

$$i_p = (2.69 \times 10^5)n^{3/2}D^{1/2}v^{1/2}C_o \qquad\qquad 2.5$$

In Equation 2.5, i_p is the peak current (A cm^{-2}), n is the electron stoichiometry, D is the diffusion coefficient (cm^2 s^{-1}), v is the scan rate (V s^{-1}) and C_o is the concentration (mol cm^{-3})[4].

It can be seen from this equation that the peak current is proportional to the concentration of electroactive species and to the square root of the scan rate and diffusion coefficient. Therefore, a linear relationship between the current and the square root of the scan rate indicates that the redox reaction of the electroactive species conforms to the Randles-Sevcik equation and is governed to some extent by a diffusion-controlled process. Consequently, the process is considered adsorption free. If a plot of the peak current against the square root of the scan rate yields a straight line then the diffusion coefficient can be determined from the slope of this line if n, A and C_o are all known. This equation was used in Chapter 5 to evaluate the diffusion coefficient of DA at the PPy-SCD modified electrode.

One of the tests of the reversibility of a system is that the plot of i_p as a function of $v^{1/2}$ is linear. If this is true, then other tests can be applied, all of which should be satisfied over the range of scan rates investigated if the system is reversible. The ratio of the forward and reverse peak currents for a reversible reaction is equal to unity, Equation 2.6, and the peak potentials are independent of the scan rate. The peak separations comply with Equation 2.7 and the difference in the peak potentials and the half-wave peak potentials satisfy Equation 2.8. A failure to satisfy one or more of the conditions above suggests that the electron

transfer is not reversible on the timescale of the experiment and that the process is more complex[6].

$$\frac{i_p^A}{i_p^C} = 1 \qquad\qquad 2.6$$

$$\Delta E_p = E_p^A - E_p^C = \frac{59}{n} mV \qquad\qquad 2.7$$

$$E_p - E_{p/2} = \frac{59}{n} mV \qquad\qquad 2.8$$

Here, i_p^A is the oxidation peak current, i_p^C is the reduction peak current, E_p^A is the peak potential of the oxidation peak, E_p^C is the peak potential of the reduction peak, $E_{p/2}$ is the half-wave potential and n is the number of electrons transferred[6].

When the electron transfer process is very slow, the system can be described as irreversible. The peak current of an irreversible system can be described by Equation 2.9, where n_α is the number of electrons transferred up to and including the rate-determining step and α_c is the charge-transfer coefficient of the reaction.

$$i_p = -(2.99 \, x \, 10^5)n(\alpha_c n_\alpha)^{1/2}C_o D^{1/2} v^{1/2} \qquad\qquad 2.9$$

The main characteristic feature of a cyclic voltammogram of a totally irreversible system is the absence of a reverse peak. In addition, although the oxidation peak currents are proportional to the square root of the scan rate, the peak potential will shift by $30/\alpha_c n_\alpha$ mV for each decade change in v. Furthermore, the difference in the peak potentials and the half-wave peak potentials should adhere to Equation 2.10[6].

$$E_p - E_{p/2} = \frac{48}{\alpha_c n_\alpha} mV \qquad\qquad 2.10$$

In between these two extremes, a quasi-reversible system exists, whereby the kinetics are not very fast or very slow. In this case, both the forward and back reactions make a contribution to the current and the system is bound by Equation 2.11, where k^θ is the standard rate constant.

$$0.3v^{1/2} \geq k^\theta \geq 2 \; x \; 10^{-5}v^{1/2} \; cm \; s^{-1} \qquad\qquad 2.11$$

For a quasi-reversible system the peak currents increase with the square root of the scan rate but are not always proportional to it. The ratio of the peak oxidation and reduction currents is equal to unity, provided that α_c and α_A are equal to 0.5. The anodic and cathodic peaks are separated by more than $59/n$ mV and this separation increases and the peak potential shifts with increasing scan rate[6].

2.10 Interference Study

2.10.1 Solutions

In all cases, bar that of uric acid (UA), a stock solution of 1.0 x 10^{-3} mol dm^{-3} of each of the interfering compounds was prepared using 0.10 mol dm^{-3} Na$_2$SO$_4$. The stock solution of UA was diluted ten-fold to 1.0 x 10^{-4} mol dm^{-3} because UA has a lower solubility in the aqueous electrolyte. These stock solutions were then used to prepare the different concentrations of DA which varied from 6.0 x 10^{-5} mol dm^{-3} to 1.0 x 10^{-3} mol dm^{-3}. This ensured that a fixed concentration of the interfering compound was present with each concentration of DA explored. The pH of the combined solution of DA and interfering compound was not altered unless otherwise specified. For large variations between the pH

of DA and the pH of the combined DA and interfering compound, the pH was adjusted using concentrated H_2SO_4 or NaOH.

2.10.2 Electrochemical Methodology

In these experiments, the PPy-SCD film was electro-synthesised as outlined in Section 2.7. In each experiment, a fresh PPy-SCD film was used. The response of every interfering compound was firstly investigated at the bare Pt substrate and then at the PPy-SCD modified electrode. The peak currents and peak potentials for the oxidation of DA at the polymer modified electrode in the presence of each interfering compound were subsequently recorded. A comparison between the mean oxidation currents and mean oxidation potentials of DA with and without the interfering compound was then made. This comparison was made without subtracting the background currents, as the background currents remained constant. This analysis was carried out using cyclic voltammetry and the relevant parameters are given in Section 2.8. All electrodes, both bare and polymer-modified, were first cycled in the background electrolyte, Na_2SO_4, under the same conditions before being placed in the interfering compound solution or the combined solution of DA and interfering compound.

2.11 Complexation Analysis

2.11.1 Complexation between Dopamine and the Sulfonated β-cyclodextrin

Both cyclic voltammetry and rotation disc voltammetry were used to investigate if an inclusion complex was formed between the DA and the sulfonated β-cyclodextrin. This was done in solution at a bare glassy carbon electrode in a 0.30 mol dm^{-3} citrate phosphate buffer solution (pH = 6.0). A 250 mL citrate phosphate buffer solution (pH = 6.0) was prepared by mixing 150 mL of 0.2 mol dm^{-3} disodium hydrogen phosphate (Na_2HPO_4) and 100 mL of 0.1 mol dm^{-3} citric acid ($C_6H_8O_7$). The concentration of the sulfonated β-cyclodextrin was varied from 2.5 x 10^{-3} mol dm^{-3} to 2.0 x 10^{-2} mol dm^{-3} while the

concentration of DA remained fixed at 5.0 x 10^{-4} mol dm^{-3} to give DA-containing solutions with an excess of anionic sulfonated β-cyclodextrin. Voltammograms for each solution and a pure 5.0 x 10^{-4} mol dm^{-3} DA solution were then recorded using the parameters given in Table 2.6.

Table 2.6: The parameters used in cyclic voltammetry and rotation disc voltammetry to investigate if an inclusion complex was formed between the DA and the sulfonated β-cyclodextrin.

	Cyclic Voltammetry	**Rotation Disc Voltammetry**
Scan Rate	50 mV s^{-1}	50 mV s^{-1}
Cycles	10	10 at 50, 300, 500, 700, 1000 and 2000 rpm
Electrochemical Window	-0.250 V vs. SCE to 0.800 V vs.SCE	-0.500 V vs. SCE to 0.800 V vs.SCE

2.11.2 Calculation of the Complex Formation Constant between Dopamine and the Sulfonated β-cyclodextrin

The complexation between a cyclodextrin (CD) and a guest molecule (D) where a 1:1 association complex is formed is governed by the following equilibrium, given in Equation 2.12.

$$CD + D \quad \rightleftharpoons \quad CD\text{-}D \qquad\qquad 2.12$$

The corresponding complex formation constant for this equilibrium is denoted as *K*, and is defined by,

$$K = \frac{[CD - D]}{[CD][D]} \qquad\qquad 2.13$$

where the concentrations represent the equilibrium concentrations. The equations used in this study to calculate the complex formation constants are subject to some stipulations. The concentration of CD must be larger than the total concentration of D in solution and a 1:1 association complex must be formed.

Cyclodextrins are well known to form inclusion complexes with guest molecules in solution. In doing so, the cyclodextrin alters the electrochemical behaviour of the guest molecule causing the peak currents to decrease and the peak potentials to shift. The decrease in the peak currents is due to the fact that the complexes have lower diffusion coefficients than that of the guest molecule alone, while the shift in the potential reveals that the oxidation of the guest molecule is more difficult when it is included in the cavity[10].

One of the most common ways of calculating the complex formation constant, K, between cyclodextrins and guest molecules in solution is to carry out a titration[11, 12]. This analysis involves keeping the concentration of the guest molecule constant while varying the concentration of the cyclodextrin. This titration procedure was applied to the cyclic voltammetry data to calculate the complex formation constant between the DA and the sulfonated β-cyclodextrin. The current titration equation is, as follows:

$$\frac{1}{C_p} = K \frac{(1-A)}{1-i/i_0} - K$$

2.14

where C_p is the concentration of sulfonated β-cyclodextrin, A is the proportional constant, i_o and i are the peak currents without and with sulfonated β-cyclodextrin and K is the complex formation constant.

Variations in the peak potential were monitored using rotation disc voltammetry. Using these data, the complex formation constant between the DA and the sulfonated β-cyclodextrin was determined using Equation 2.15.

$$\frac{F}{RT}\left\{\left(E_{\frac{1}{2}}\right)_{app} - \left(E_{\frac{1}{2}}\right)_f\right\} = ln\,(1 + K[SCD]) + ln\,(\frac{D_c}{D_f})^{1/2}$$

2.15

Here, F is the Faraday constant, R is the gas constant, T is the temperature, $(E_{1/2})_{app}$ and $(E_{1/2})_f$ are the half-wave potentials in the presence and absence of the sulfonated β-cyclodextrin, respectively. K is the complex formation constant and D_c and D_f are the diffusion coefficients in the presence and absence of the sulfonated β-cyclodextrin, respectively[13]. The diffusion coefficients in this equation were evaluated using Equation 2.4, also known as the Levich equation.

2.11.3 NMR Analysis

^{1}H NMR spectroscopy is one of the most powerful techniques for examining host-guest chemistry in solution. It can provide complete information on the stoichiometry, binding constant, orientation and geometry of a host-guest interaction[14]. For the purposes of this research, ^{1}H NMR was used to investigate the manner in which the DA was including inside the cavity of the sulfonated β-cyclodextrin. This was achieved by monitoring the environment of the individual atoms and the complex. The ^{1}H NMR analysis presented in this study was carried out by Gillian Hendy. The samples were prepared by dissolving 5.0×10^{-3} mol dm^{-3} of DA or 2.0×10^{-2} mol dm^{-3} sulfonated β-cyclodextrin or 5.0×10^{-3} mol dm^{-3} of DA and 2.0×10^{-2} mol dm^{-3} sulfonated β-cyclodextrin in 0.5 mL of D$_2$O (99.72%) / 0.10 mol dm^{-3} KCl. The KCl was employed to maintain a near constant ionic strength.

2.11.4 Job's Analysis

One of the most commonly used techniques for the determination of the stoichiometry of intermolecular complexes is Job's method. To implement Job's method experimentally, a series of solutions containing a fixed total number of moles of A and B are prepared. The volume of these solutions remain constant, however the molar ratio of each solution is systematically varied from large to small ratios. The amount of product in each solution can then be measured using the appropriate physicochemical parameter (absorbance, chemical shift, solubility, etc). This is then plotted against the molar ratio of the components with the maximum of the plot representing the stoichiometry of the complex[14]. Job's method by

UV-Vis spectroscopy was used in Section 5.3.5 to determine the stoichiometry of the DA and sulfonated β-cyclodextrin complex. The solutions used for this analysis are given in Table 2.7 together with the mole fraction of each solution. The mole fraction of each solution was calculated using Equation 2.16. The absorbance of each of these solutions was measured from 200 nm to 500 nm and the change in the absorbance of each solution was calculated using Equation 2.17. The Job's plot was constructed by plotting the difference in the absorbance times the mole fraction against the mole fraction of DA in each solution.

$$\text{Mole Fraction} = \frac{[DA]}{[DA] + [SCD]} \qquad \qquad 2.16$$

$$\Delta A = A_{\text{DA}} - A_{\text{DA+SCD}} \qquad \qquad 2.17$$

Table 2.7: The amount of DA and sulfonated β-cyclodextrin used to make the solutions and the corresponding mole fractions of each of these solutions.

1.0 x 10⁻⁴ mol dm⁻³ DA / mL	1.0 x 10⁻⁴ mol dm⁻³ SCD / mL	Mole Fraction
3.0	0.0	1.0
2.7	0.3	0.9
2.4	0.6	0.8
2.1	0.9	0.7
1.8	1.2	0.6
1.5	1.5	0.5
1.2	1.8	0.4
0.9	2.1	0.3
0.6	2.4	0.2
0.3	2.7	0.1
0.0	3.0	0.0

2.11.5 Complexation between Dopamine and the Neutral β-Cyclodextrin

The formation of an inclusion complex between the DA and the neutral β-cyclodextrin was examined using rotation disc voltammetry. The scan rate and electrochemical window in Table 2.6 together with the citrate phosphate buffer solution (pH = 6.0) were utilised. In contrast, only 10 cycles were performed at 50 rpm and voltammograms were only recorded for a pure 1.0×10^{-4} mol dm^{-3} DA solution and a mixed solution of 1.0×10^{-4} mol dm^{-3} DA and 2.0×10^{-3} mol dm^{-3} neutral β-cyclodextrin. The concentration of neutral β-cyclodextrin, and accordingly the concentration of DA were lowered as the neutral β-cyclodextrin is less soluble in an aqueous medium than the sulfonated β-cyclodextrin.

2.11.6 Complexation between Several Interfering Compounds and the Sulfonated β-Cyclodextrin

In this case cyclic voltammetry was the technique of choice. The same scan rate, number of cycles and buffer solution used in Section 2.11.1 were employed but only the voltammograms of a 5.0×10^{-4} mol dm^{-3} interfering compound solution and a mixed solution of 1.0×10^{-2} mol dm^{-3} sulfonated β-cyclodextrin and 5.0×10^{-4} mol dm^{-3} interfering compound were recorded. In addition, the same electrochemical window was not always used, however it will be stated in the figure caption what electrochemical window was used. Furthermore, the pH of the buffer solution was altered in some cases. This was done by varying the concentrations of disodium hydrogen phosphate and citric acid.

2.12 Increasing the Sensitivity *via* Nanostructures

2.12.1 Electrochemical Set-Up / Instrumentation

The electrochemical experiments were performed using an EDAQ Potentiostat Model EA160 with a conventional three-electrode cell. The working electrode was the PLA fibers

or the polymer coated PLA fibers and they were cut to give a surface area of 0.25 mm^2. The auxiliary electrode consisted of a platinum wire and the reference electrode was a silver chloride electrode. The data were analysed using the corresponding EDAQ software and Microsoft Excel®2000 Version.

2.12.2 Electrospinning

A schematic diagram to illustrate electrospinning of polymer nanofibers is shown in Figure 2.12. It consists of three major components: a high voltage power supply, a needle and a grounded metal collector which can be covered with a variety of materials including fabric, glass and gold mylar. The needle is connected to a syringe containing the polymer solution and the solution is fed through the needle at a constant and controllable rate using a syringe pump. The electrospinning process is based on applying a high electric field to a droplet of polymer solution which causes the formation of an electrified jet that continuously elongates becoming long and thin[15].

Several poly($_L$-lactide) acid (PLA) (inherent viscosity 0.90-1.20 dL/g) solutions were prepared in various solvents with the aid of mechanical stirring. The solvents investigated included 1,1,1,3,3,3-hexafluoro-2-propanol (HFIP) and chloroform (CH_3Cl) and a solvent mixture of CH_3Cl and dimethylformamide (DMF) (70:30). The electrospinning process was carried out at various voltages using a high voltage power supply (Gamma High Voltage) and at a variety of flow rates which were controlled by a digital syringe pump (KdScientific Pump Infusion Single Syringe QF3139). The polymer solution was drawn from a syringe with a diameter of 4.9 mm and was fed through a needle tip with a diameter of 1.0 mm. The resulting fibers were collected on an iron grounded target covered with either gold mylar or glass which was placed at a distance of approximately 10 cm from the syringe tip.
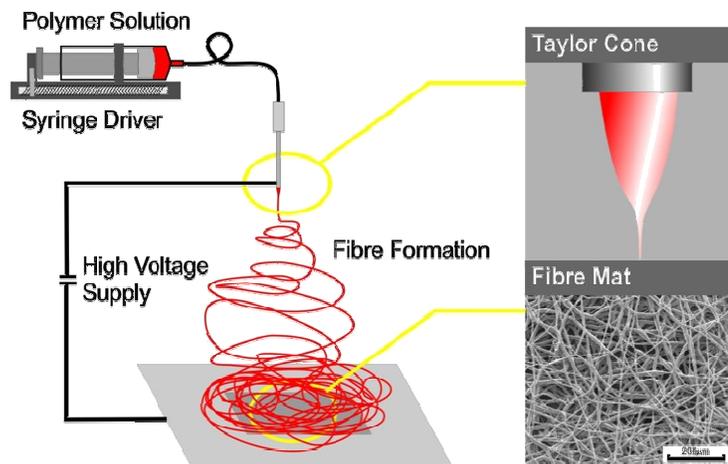
Figure 2.12: The electrospinning apparatus.

2.12.3 Characterisation of Fibers / Electropolymerisation of the PPy-SCD / Sensing of Dopamine

The electrochemical characterisation of the PLA nanofibers and the electropolymerisation of PPy-SCD onto the PLA nanofibers were primarily achieved using cyclic voltammetry. The electrochemical characterisation of the PLA nanofibers was carried out in a 0.01 mol dm^{-3} FeCN$_6$/KCl solution using a range of electrochemical windows and various scan rates. The scan rate and electrochemical window employed in each experiment is presented in the figure captions or corresponding text in the results section. The electropolymerisation of PPy-SCD onto the PLA nanofibers was carried out in 0.20 mol dm^{-3} pyrrole / 0.01 mol dm^{-3} sulfonated β-cyclodextrin solution using a scan rate of 100 mV s^{-1} and an electrochemical window of -0.600 V vs. Ag/AgCl to 0.800 V vs. Ag/AgCl. The number of cycles varied from experiment to experiment, however it will be stated in the text how many were used. In addition to cyclic voltammetry, constant potential and constant current modes were used to electropolymerise a layer of polypyrrole onto the fibers. These were carried out in a 0.20 mol dm^{-3} pyrrole / 0.10 mol dm^{-3} *p*-toluenesulfonic acid (PTS) solution until a certain charge or time was reached. The polymer modified PLA nanofibers were then transferred to a DA / 0.10 mol dm^{-3} Na$_2$SO$_4$ solution and cyclic

voltammetry was used to detect the DA by polarising the polymer from -0.100 V vs. Ag/AgCl to 0.900 V vs. Ag/AgCl at 100 mV s^{-1}.

2.12.4 Vapour Phase Polymerisation

A 20% oxidant solution was firstly prepared from a 40% Fe(III)PTS/ethanol solution. A 10% Fe(III)PTS/sulfonated β-cyclodextrin solution was subsequently prepared by taking 1.0 mL of the 20% Fe(III)PTS solution and 1.0 mL of a 0.02 mol dm^{-3} sulfonated β-cyclodextrin/H$_2$0 solution. A thin film of this solution was spin coated onto bare gold mylar and onto the 1 min-electrospun PLA nanofibers using a rotation speed of 3000 rpm. These samples were then placed onto a hot plate for 30 s where the ethanol was evaporated off and then transferred to a chamber containing pyrrole monomer at the bottom. After approximately 30 min in the chamber a polymer film had grown on both the samples. The samples were then removed, washed in ethanol for 20 min and left to dry for 60 min. The polymer modified substrates were then transferred to a DA solution and cycled from -0.800 V vs. Ag/AgCl to 0.800 V vs. Ag/AgCl at 100 mV s^{-1}.

2.12.5 Analysis of Fibers

The morphologies of the simple PLA fibers were observed using an optical microscope (Leica DFC 280) and SEM images were obtained by using a Leica Stereoscan 440 SEM. The morphology of the polymer coated PLA nanofibers was observed using an SEM (Joel 840 SEM). Prior to acquiring SEM images, the substrates were gold coated for 3 min using an Emitech K550x sputter coater.

2.13 Michaelis-Menten Kinetics and Lineweaver-Burk Analysis

The simple enzyme-catalysed production of a product (*P*) from a substrate (*S*) follows Equation 2.18. The enzyme (*E*) binds to the substrate to form an enzyme-substrate complex (*E-S*) which dissociates to free enzyme and product.

$$[E] + [S] \underset{k_{-1}}{\overset{k_1}{\rightleftharpoons}} [E-S] \xrightarrow{k_2} [E] + [P] \qquad 2.18$$
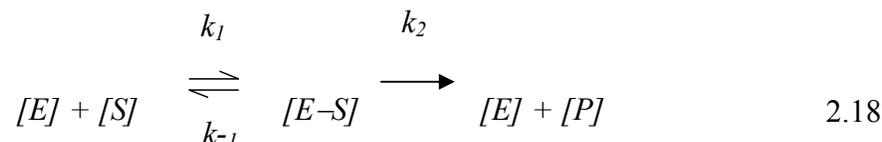
In this equation k_1 and k_{-1} are rate constants for the association of substrate and enzyme and the dissociation of unconverted substrate from the enzyme, respectively. k_2 is the rate constant for the dissociation of converted substrate. Two major assumptions are made about this equation. The first is that there must be a vast excess of substrate so that *[S] >> [E]*. Secondly, the *[E-S]* complex should be formed and broken down at the same rate, ie., the system is at steady-state[16].

The Michaelis-Menten equation, Equation 2.19, describes the relationship between the rate of substrate conversion by an enzyme to the concentration of the substrate. In this equation, *V* is the rate of substrate conversion, V_{max} is the maximum rate of substrate conversion, *[S]* is the substrate concentration and K_m is the Michaelis constant. A plot of *[S]* versus *V* generates a hyperbolic curve. This is because the enzyme sites are becoming more saturated as *[S]* is increased and consequently a V_{max} will be reached. However, the V_{max} is never really reached and therefore an accurate determination of V_{max} is not possible. Instead, an estimate of V_{max} is used. K_m is an indicator of the stability of the enzyme-substrate complex. K_m is equivalent to the *[S]* at which the *V* reaches half of the estimated V_{max}. This in turn also means that the K_m value calculated from the curve is only an approximate value. A low K_m value indicates tight binding, whereas a high K_m value suggests weak binding.

$$V = \frac{V_{max}[S]}{K_m + [S]} \qquad 2.19$$

where
$$K_m = \frac{k_{-1} + k_2}{k_1}$$
2.20

and
$$V_{max} = k_2([E] + [E - S])$$
2.21

A simpler representation of this analysis can be obtained with the Lineweaver-Burk equation, Equation 2.22. This is a linear transformation of the Michaelis-Menten equation generated by taking the reciprocal of both sides. Using this equation a straight line is generated from plotting *1/V* as a function of *1/[S]*. The y-intercept of this line is equivalent to the inverse of *V*$_{max}$ and the x-intercept of this line represents *1/K*$_m$.

$$\frac{1}{V} = \frac{1}{V_{max}} + \frac{K_m}{V_{max}[S]}$$
2.22

In this study, the Michaelis-Menten equation and the Lineweaver-Burk equation were used to determine if there was any binding interaction between the PPy-SCD and the DA. Despite the fact that the PPy-SCD film is not an enzyme, this analysis can still be applied to the system as cyclodextins are well known to mimic enzyme-catalysed reactions[17].

2.14 References

1. A. J. Bard and L. R. Faulkner*, Electrochemical Methods: Fundamentals and Applications*, John Wiley & Sons, Inc, 833, (2001).
2. J. P. Lowry and R. D. O'Neill, *Encyclopedia of Sensors, Neuroanalytical Chemistry In Vivo Using Electrochemical Sensors*, C. A. Grimes, E. C. Dicky, and M. V. Pishko, American Scientific Publishers, **10**, 1, (2006).
3. I. Rubinstein*, Physical Electrochemistry: Principles, Methods, and Applications*, CRC Press, 595, (1995).
4. J. Wang*, Analytical Electrochemistry*, Wiley-Interscience, 250, (2006).
5. J. G. Vos, R. J. Forster and T. E. Keyes*, Interfacial Supramolecular Assemblies*, John Wiley and Sons, 317, (2003).
6. R. Greef, R. Peat, L. M. Peter, D. Pletcher and J. Robinson*, Instrumental Methods in Electrochemistry*, T. J. Kemp, Ellis Horwood Limited, 443, (1985).
7. L. G. Wade*, Organic Chemistry*, Prentice Hall International, 1221, (1999).
8. R. T. Morrison and R. N. Boyd*, Organic Chemistry*, Prentice Hall International, 1325, (1992).
9. J. Goldstein, D. E. Newbury, P. Echlin, C. E. Lyman, D. C. Joy, E. Lifshin, L. Sawyer and J. R. Michael*, Scanning Electron Microscopy and X-ray Microanalysis*, Springer, 689, (2003).
10. H. Dodziuk*, Cyclodextrins and Their Complexes: Chemistry, Analytical Methods, Applications*, Wiley-VCH, 489, (2006).
11. G.-C. Zhao, J.-J. Zhu, J.-J. Zhang and H.-Y. Chen, *Anal. Chim. Acta*, **394**, 337, (1999).
12. C. Yanez, L. J. Nunez-Vergara and J. A. Squella, *Electroanalysis*, **15**, 1771, (2003).
13. E. Coutouli-Argyropoulou, A. Kelaidopoulou, C. Sideris and G. Kokkinidis, *J. Electroanal. Chem*, **477**, 130, (1999).
14. U. Holzgrabe, I. Wawer and B. Diehl*, NMR Spectroscopy in Drug Development and Analysis*, Wiley-VCH, 299, (1999).
15. D. Li and Y. N. Xia, *Advanced Materials*, **16**, 1151, (2004).
16. L. Buckberry and P. Teesdale*, Essentials of Biological Chemistry*, John Wiley & Sons, Ltd, **1**, 145, (2001).
17. R. Kataky and E. Morgan, *Biosens. Bioelectron.*, **18**, 1407, (2003).

Chapter 3

Development and Optimisation of the Dopamine Sensor-A Polypyrrole Sulfonated β-Cyclodextrin Modified Electrode

3.1 Introduction

Dopamine (DA) is one of the most important catecholamine neurotransmitters in the mammalian central nervous system. Abnormalities in DA concentrations have been linked to several neurological disorders such as Parkinson's disease[1] and schizophrenia[2]. DA also plays a central role in drug addiction[3], attention disorders[4] and regulating movement in Huntington's disease[5]. Furthermore, DA has been associated with HIV infection[6]. Accordingly, the development of simple analytical methods for the determination of DA concentrations is important and is the topic of much recent research work. In particular, there is considerable interest in the development of electrochemical sensors, as DA is electroactive and these sensors are usually inexpensive to manufacture, highly sensitive and easy to employ. Also, the electrodes used can be miniaturised and conveniently placed in the living organism to give data at the sub-second timescale. This is not possible with non-electrochemical techniques, which involve taking samples from the biological tissues, followed by further analyses.

However, monitoring the concentration of DA is particularly challenging because it co-exists with many interfering compounds in biological samples. These interfering compounds are usually present at concentrations much higher than DA and, moreover, they are oxidised at similar potentials to DA at most solid electrodes. As a result, the ability to develop an electrochemical sensor, where both sensitivity and selectivity are of equal significance, is extremely important. One way to overcome the selectivity and sensitivity issues associated with the measurement of DA is to modify the electrode surface. Several strategies including polymer modified electrodes[7-10], self-assembled monolayer modified electrodes[11], surfactant modified electrodes[12], RNA modified electrodes[13], metal nanoparticle modified electrodes[14] and metal oxide modified electrodes[15] have all been used to detect DA in the presence of potential interfering compounds. Generally, these materials function by separating the oxidation waves of DA and the interferent.

In this chapter, several polymer modified electrodes are formed and their ability to oxidise DA is investigated. In particular, the oxidation of DA at polypyrrole-sulfonated β-cyclodextrin (PPy-SCD) modified electrode is explored. This material exhibited a higher

sensitivity to DA in comparison to the other polymer modified electrodes. The properties, characteristics and factors affecting the growth of the PPy-SCD films are firstly examined. In the latter stages of the chapter a range of parameters are considered and varied in order to achieve the optimum DA signal, and from here the sensitivity of the PPy-SCD modified electrode is evaluated using both cyclic voltammetry measurements and constant potential amperometry. The influence of interfering compounds on the determination of DA at the PPy-SCD modified electrode is investigated in Chapters 5 and 6.

3.2 Experimental

The instrumentation and software employed are described in Section 2.3. All chemicals, electrochemical experiments and solutions are described in detail in Chapter 2. The SEM and surface profilometer (Tencor) analysis was performed in the Tyndall National Institute at University College Cork, while the EDX analysis was carried out in the CMAU at Trinity College Dublin. In all cases, except for the scan rate and the rotation disc voltammetry experiments, the modified electrodes were first cycled in the background electrolyte, 0.10 mol dm^3 Na_2SO_4, between -0.100 V vs. SCE and +0.900 V vs. SCE to ensure the release of any pyrrole or oligomers at the surface. This was generally done for 10 cycles or 2 cycles as in the case of the differential pulse voltammetry analysis. Then, the electrodes were transferred to the DA solutions. Unless otherwise stated, the background current was subtracted from the DA peak currents to give the true peak current for the oxidation of DA. The error bars in the current measurements were calculated using the formula below with *n* representing the number of experiments carried out.

$$Standard\ Error = Standard\ Deviation\ of\ n\ experiments \div \sqrt{n}$$

3.3 Results and Discussion

3.3.1 Oxidation of Dopamine at Bare Electrodes

The working electrodes explored in this study were platinum (Pt), glassy carbon (GC) and gold (Au). Figure 3.1 shows the cyclic voltammetric behaviour of DA at a bare GC, Au and Pt electrode. The electrochemical oxidation of DA in an aqueous solution is shown in Scheme 3.1. A two electron exchange results in the formation of dopamine-o-quinone (DOQ) (Equation 3.1). This molecule can undergo an intermolecular addition, which results in a cyclization reaction generating leucodopaminechrome (Equation 3.2), which, in turn, is oxidised further *via* another two electron transfer to dopaminochrome (Equation 3.3)[16, 17].

It can be seen in Figure 3.1 that the oxidation of DA, at all three electrodes, exhibits two pairs of redox peaks. The pair of redox peaks observed at the higher potentials corresponds to the redox process described in Equation 3.1, whereas the pair of redox peaks observed at the lower potentials relates to Equation 3.3. These redox peaks were only observed after the first cycle (5th cycle is shown in Figure 3.1) consistent with the mechanism outlined in Equations 3.1 to 3.3. Although the peak currents are considerably smaller for this second redox couple, these data clearly show that the dopaminochrome is formed at the three unmodified electrodes. It is well known that the dopaminochrome can be further oxidised to indolic-o-quinone to generate an insoluble melanin, which fouls and poisons the electrode[18, 19]. Accordingly, all three electrodes are susceptible to poisoning in the electrochemical sensing of DA.

The peak currents and potentials observed for the DA/DOQ, Equation 3.1, at each electrode are highlighted in Table 3.1. The ratio of the oxidation and reduction peak currents and the potential difference between the oxidation and reduction peaks are also provided. The peak separations vary from 0.350 to 0.410 V and indicate a quasi-reversible redox system, in agreement with literature reports[20]. Although the redox behaviour of DA at the Pt electrode is somewhat more reversible, it is clear that these unmodified electrodes are rather poor in the electrochemical sensing of DA.

$$\text{(3.1)}$$

$$\text{(3.2)}$$

$$\text{(3.3)}$$
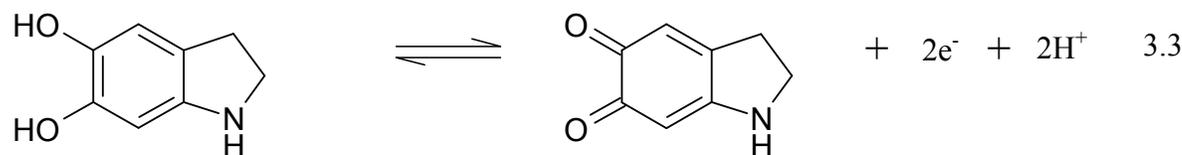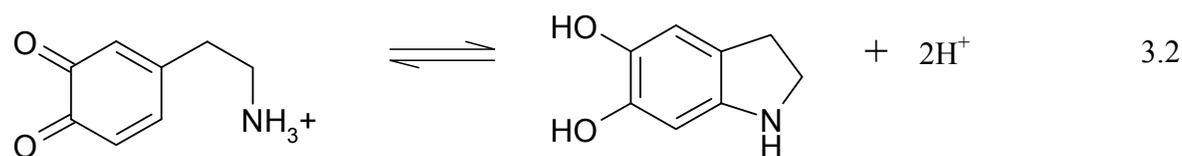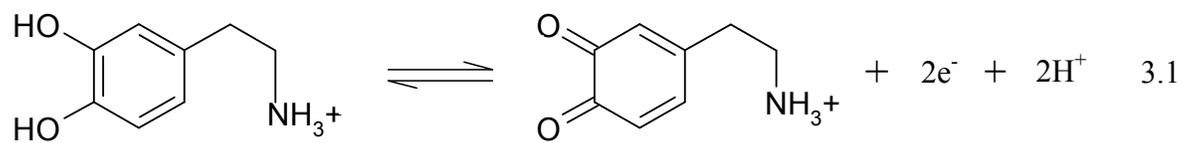
Scheme 3.1: Mechanism of DA oxidation[16, 17].
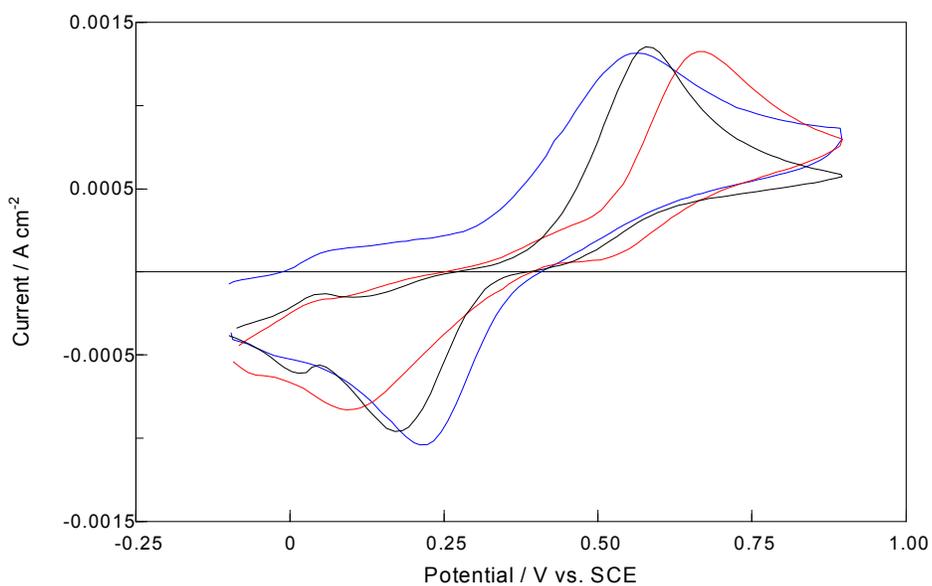
Figure 3.1: Cyclic voltammograms of a ▬ bare GC electrode, a ▬ bare Au electrode and a ▬ bare Pt electrode in a 5.0 x 10^{-3} mol dm^{-3} DA / 0.10 mol dm^{-3} Na$_2$SO$_4$ solution (pH~6.0). Scan rate = 100 mV s^{-1}.

Table 3.1: Peak currents and potentials observed for the redox pair corresponding to the oxidation of DA and reduction of DOQ.

Electrode	I_p^A / A cm^{-2}	I_p^C / A cm^{-2}	I_p^A / I_p^C	E_p^A / V vs. SCE	E_p^C / V vs. SCE	ΔE / V
GC	0.001355	0.000958	**1.41**	0.5770	0.1710	**0.4060**
Au	0.001325	0.000830	**1.60**	0.6625	0.0920	**0.5705**
Pt	0.001318	0.001043	**1.26**	0.5658	0.2114	**0.3544**

3.3.2 Oxidation of Dopamine at Polypyrrole Modified Electrodes

The results from Section 3.3.1 show that DA can be oxidised at solid Pt, GC and Au electrodes. However, the electrochemical detection of DA using these solid electrodes is ineffective, as they usually suffer from a fouling effect due to the accumulation of oxidised products on the electrode surface[21]. The loss of the activity of the electrodes during the oxidation process has been mainly attributed to the adherent deposition of an electropolymerised film (melanin formation) on the surface of the electrodes[18]. In addition, ascorbic acid (AA), the main interferent in the electrochemical detection of DA in biological samples, is oxidised at similar potentials to DA at these solid electrodes. This results in an overlapping voltammetric signal which makes the selective detection of DA impossible[22]. To overcome the above problems, modified Pt, GC and Au electrodes have been used for the determination of DA[23-25]. In particular, there has been much interest in the development of sensors based on electrodes modified with polymeric films. Electropolymerised films of pyrrole, aniline, 3-methylthiophene, acridine red, sulfosalicylic acid, 3,5-dihydroxy benzoic acid and acid chrome K have all been reported for the determination of DA in the presence of AA[24, 26-29]. Among the wide range of polymers that can be used to design a bioanalytical sensor, polypyrrole (PPy), Figure 3.2, is one of the most attractive and extensively used materials[30]. This is due to its large surface area, good environmental stability, controllable surface biochemical properties, simple electrochemical preparation and also because of its good biocompatibility properties[31]. PPy may be synthesised electrochemically or chemically, however electrochemical methods have several advantages over the chemical polymerisation approaches because the film thickness

and morphology, permeation and charge transport can be controlled by adjusting the electrochemical parameters[32]. Furthermore, electropolymerised PPy films have a strong adherence to the electrode surface and also exhibit good conductivity[30].

In this study, PPy films doped with various anions were electropolymerised at a Pt electrode using a potentiostatic mode. This technique is based on the well-known reaction that the electropolymerisation of pyrrole yields a positively charged polymer backbone and the anions that are present in the electrolyte solution are incorporated into the polymer matrix to balance the charge[33], as illustrated in Scheme 3.2. The dopant anions considered in this study included, chloride (Cl^-), sulfate (SO_4^{2-} or HSO_4^-), dodecyl sulfate (SDS^-), neutral β-cyclodextrin (βCD) and sulfonated β-cyclodextrin (SCD^{n-}).
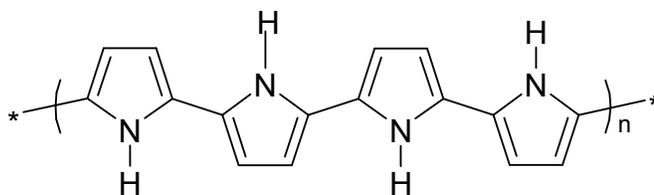
Figure 3.2: Structure of polypyrrole (PPy) in the reduced non-doped state.
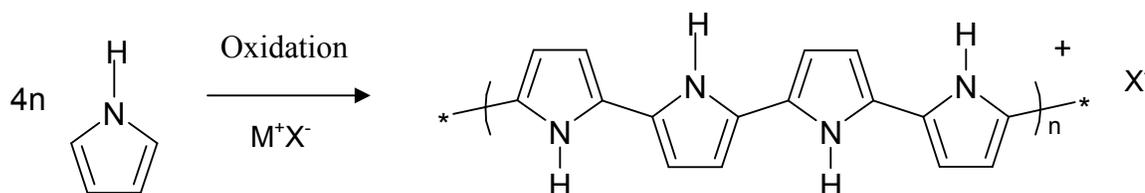
Scheme 3.2: Overall polymerisation reaction of pyrrole in the presence of an MX electrolyte.

Typical growth profiles for the formation of PPy with each dopant are shown in Figures 3.3(a) and (b), where the logarithm of the current is plotted as a function of time in Figure 3.3(a) and the corresponding charge-time plots are shown in Figure 3.3(b). It can be seen that the polymer formed by incorporating the anionic sulfonated β-cyclodextrin as a dopant

grows at a much faster rate than the other polymers. In terms of the dopant anions, the rate of polymer growth decreases in the order SCD^{n-} > SO_4^{2-} > SDS^- > Cl^- >> βCD. This is somewhat unusual as the sulfonated β-cyclodextrin is a large bulky molecule with lower mobility than the smaller anions. As a result it will have a significantly lower diffusion rate. However, the solution formed by dissolving the sulfonated β-cyclodextrin in water is highly conducting. Conductivity, defined by Equation 3.4, is a measure of a materials ability to conduct an electric current and therefore the higher the conductivity, the higher the current flow. Here, I is the current, σ is the conductivity and E is the electric field[34].

$$I = \sigma E \qquad\qquad 3.4$$

The conductivity of a 1×10^{-2} mol dm^{-3} sulfonated β-cyclodextrin solution was recorded and it was found it be 4.5 mS. In contrast, the conductivity of a 1×10^{-2} mol dm^{-3} sodium chloride solution is 1080 µS. This enhanced conductivity of the sulfonated β-cyclodextrin solution can be attributed to the high number of ionised sulfonated groups on the cyclodextrin. Indeed, sulfonated groups tend to be fully ionised. Sulfonic acids have high dissociation constants of about 10^{-2} and are generally considered as strong organic acids[35]. This concept is verified in Table 3.2, where the ionic strength of each of the dopant solutions was calculated using Equation 3.5,

$$I = \frac{1}{2}\sum_i m_i\, z_i^2 \qquad\qquad 3.5$$

where, m_i and z_i are the molarity and the charge of the ith ion, respectively[36].
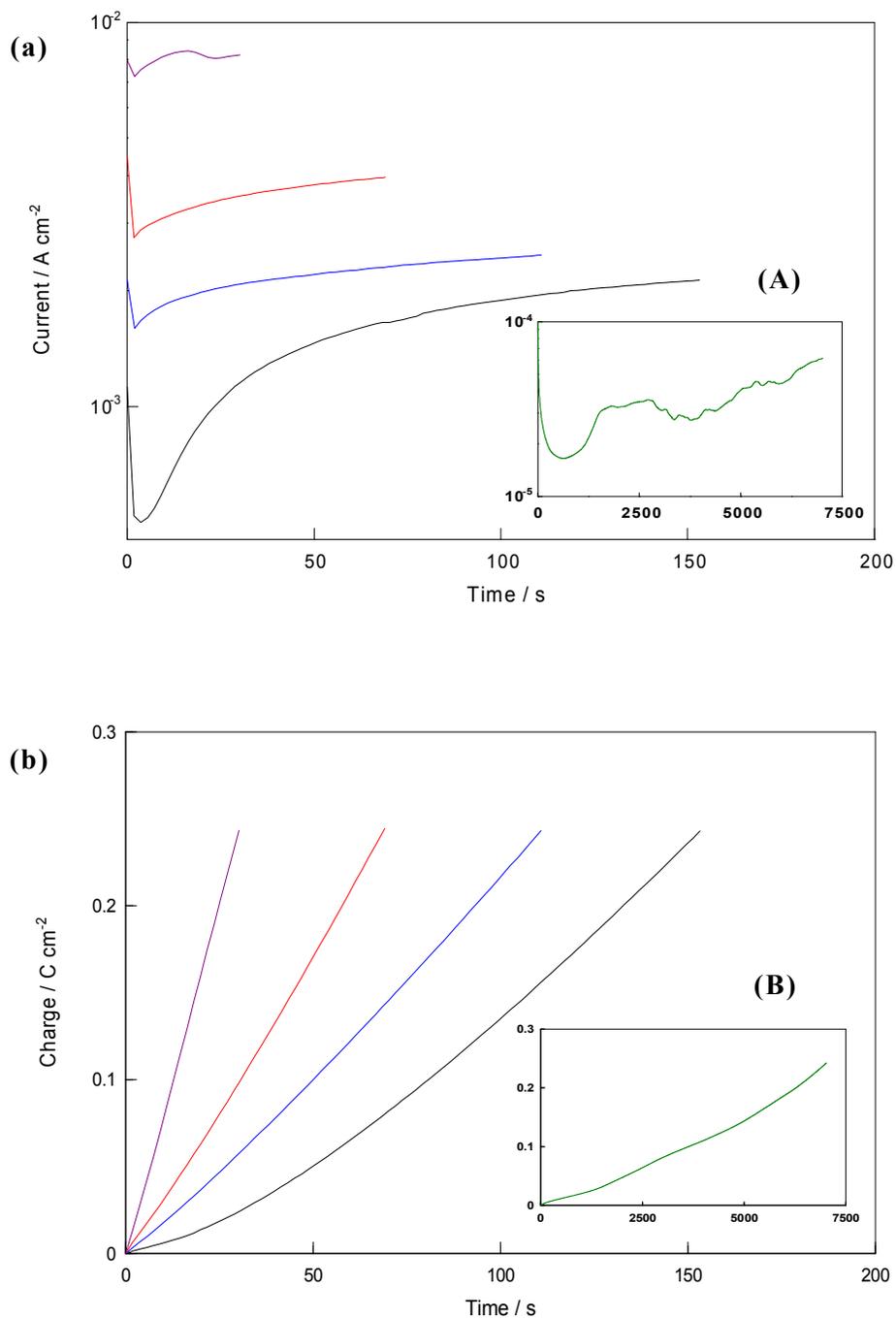
Figure 3.3: (a) Current-time plot and (b) charge-time plot for the formation of PPy on a Pt electrode at 0.800 V vs. SCE from monomer solutions containing 0.20 mol dm^{-3} pyrrole and 0.01 mol dm^{-3} ▬ sodium chloride, ▬ sodium sulfate, ▬ sodium dodecyl sulfate and ▬ sulfonated β-cyclodextrin. Inset: (A) Current-time plot and (B) charge-time plot for the formation of PPy on a Pt electrode at 0.800 V vs. SCE from monomer solution containing 0.20 mol dm^{-3} pyrrole and 0.01 mol dm^{-3} β-cyclodextrin. Axes are identical to Figures 3.3(a) and (b). All polymer films were grown until a charge of 0.24 C cm^{-2} was reached.

The ionic strength is proportional to the conductivity and it can be seen from Table 3.2 that the ionic strength varies in the order SCD > Na_2SO_4 > SDS = NaCl > βCD. Gratifyingly, the sulfonated β-cyclodextrin solution exhibits the highest conductivity and ionic strength followed by the sodium sulfate solution, while the neutral β-cyclodextrin solution has little or no conductivity. Indeed, when higher concentrations of NaCl were used to give conductivities close to that of the SCD, similar current-time and charge-time transients were recorded with the chloride and SCD anions. This verifies that conductivity has a major influence on the electropolymerisation of pyrrole and accounts for the apparently higher rates observed with the SCD anions, Figure 3.3.

As the ionic strength of the sodium dodecyl sulfate solution is similar to that of the sodium chloride solution and the dodecyl sulfate is much larger in size, the higher rates of electropolymerisation in the sodium dodecyl sulfate solutions, Figures 3.3(a) and (b), are probably connected to the surfactant properties of the dodecyl sulfate. Sodium dodecyl sulfate is a well-known surfactant and it is widely reported in the literature that the presence of surfactants in the monomer solution increase the conductivity of the PPy films prepared[37].

Table 3.2: Ionic strengths of the 0.01 mol dm^{-3} dopant solutions.

Dopant Solution	Ionic Strength / mol dm^{-3}
NaCl	0.01
Na_2SO_4	0.03
SDS	0.01
βCD	0.00
SCD	0.45

The DA response at each of the PPy films was then examined using cyclic voltammetry, as illustrated in Figure 3.4. The electrodes were cycled in a 1.0 x 10^{-3} mol dm^{-3} DA solution dissolved in a 0.1 mol dm^{-3} Na_2SO_4 supporting electrolyte, between -0.100 V and 0.900 V vs SCE at a scan rate of 100 mV s^{-1}. In total 10 cycles were measured and the data presented in the figure are taken from the 5th cycle. From Figure 3.4, it can be seen that DA is detected at the polypyrrole chloride (PPy-Cl), polypyrrole sulfate (PPy-SO_4), polypyrrole dodecyl sulfate (PPy-SDS) and polypyrrole sulfonated β-cyclodextrin (PPy-SCD) films. Only one pair of redox peaks was observed at each of these polymer films corresponding to the redox process of Equation 3.1. The oxidation of DA occurs at potentials ranging from 0.430 to 0.460 V vs. SCE, while the reduction of the DOQ occurs at about 0.270 V vs. SCE.

Another characteristic of the voltammograms recorded by these polymer films is that the peak currents have increased dramatically in comparison to a bare Pt electrode, Figure 3.1. This marked increase in the current can be attributed to the polymer and not the metal surface. Indeed, this is further supported by the fact that the oxidation potential of DA at the polymer-modified electrodes is some 100 mV lower than that observed at the bare Pt electrode. In addition, the presence of these polymers on the Pt electrode has decreased the potential difference between the oxidation and reduction peaks of DA, making the reaction more reversible than that observed at a bare Pt electrode, Table 3.3. The peak potential separations vary from approximately 140 to 180 mV at the polymer modified electrodes, compared to 350 mV at the bare Pt electrode, indicating a significant increase in the reversibility of the system.

Table 3.3: Peak oxidation currents, I_p^A, peak oxidation potentials, E_p^A, and peak separations, ΔE, obtained at each polymer modified electrode and at a bare Pt electrode in a 1.0×10^{-3} mol dm^{-3} DA / 0.10 mol dm^{-3} Na$_2$SO$_4$ solution, pH ~ 6.0, using cyclic voltammetry at 100 mV s^{-1}.

Electrode	I_p^A / A cm^{-2}	E_p^A / V vs. SCE	ΔE / V
PPy-Cl	0.000139	0.4414	0.1513
PPy-SO$_4$	0.000814	0.4318	0.1851
PPy-SDS	0.000316	0.4501	0.1338
PPy-SCD	0.001742	0.4599	0.1534
PPy-βCD	-	-	-
Bare Pt	0.000308	0.5509	0.3563

It is evident from Figure 3.4 that the oxidation of DA at the PPy-SCD modified electrode is superior to the oxidation of DA at the other polymer films. This is further emphasised in Table 3.3, where the DA oxidation peak currents and peak potentials recorded at each of the PPy-modified electrodes and at the bare Pt electrode are tabulated. Furthermore, the interference of AA is eliminated at the PPy-SCD modified electrode, Section 5.3.1. Although the reversibility of the DA signal is improved by the presence of the PPy-Cl and the PPy-SDS modified electrodes, it can be seen from Table 3.3 and Figure 3.4 that relatively low DA oxidation currents are measured with these systems. The DA response at the polypyrrole β-cyclodextrin (PPy-βCD) film is exceptionally weak and this is highlighted in Figure 3.5, where it can be seen that a better DA signal is observed at a bare Pt electrode.

The results in this section clearly show that the presence of the sulfonated β-cyclodextrin in the PPy film significantly increases the reversibility and sensitivity of the DA signal relative to the other PPy films studied and the bare Pt electrode. DA displayed similar reversible behaviour at all the PPy films studied, however the peak currents for the oxidation of the DA were only increased by the PPy-SCD film and to a lesser degree the PPy-SO$_4$ film compared with the bare Pt electrode. To the best of our knowledge, the

electrochemical synthesis of PPy-SCD films has only been reported by Temsamani *et al.*[38], Bidan *et al.*[39] and Reece and co-workers[40]. Temsamani *et al.*[38] used cyclic voltammetry to grow the polymer films on Au electrodes whereas, Bidan *et al.*[39] deposited the films on a Pt electrode using a constant potential of 0.40 V vs. SCE. Reece *et al.*[40] used galvanostatic, potentiostatic and poteniodynamic methods to prepare the polymer films on Pt electrodes. In contrast to the monomer solution used in this work, Temsamani *et al.*[38] used lithium perchlorate ($LiClO_4$) as a supporting electrolyte in the monomer solution. This can result in the doping of the polymer by perchlorate anions instead of the sulfonated β-cyclodextrin, or indeed both may be incorporated. However, Temsamani *et al.*[38] claim that the perchlorate anion is selectively excluded as a dopant anion. No supporting electrolyte was used in this study, which ensured that the polymer was only doped by the anionic sulfonated β-cyclodextrin.
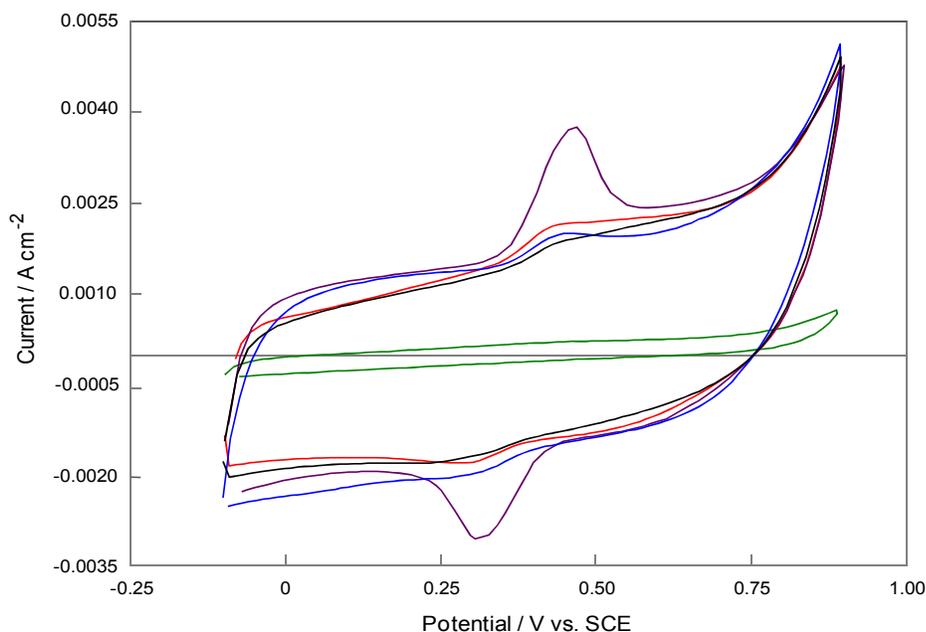
Figure 3.4: Cyclic voltammograms of a ▬ PPy-Cl modified electrode, ▬ PPy-SO$_4$ modified electrode, ▬ PPy-SDS modified electrode, ▬ PPy-βCD modified electrode and a ▬ PPy-SCD modified electrode in a 1.0 x 10^{-3} mol dm^{-3} DA / 0.10 mol dm^{-3} Na$_2$SO$_4$ solution (pH~6.0). Scan rate = 100 mV s^{-1}.
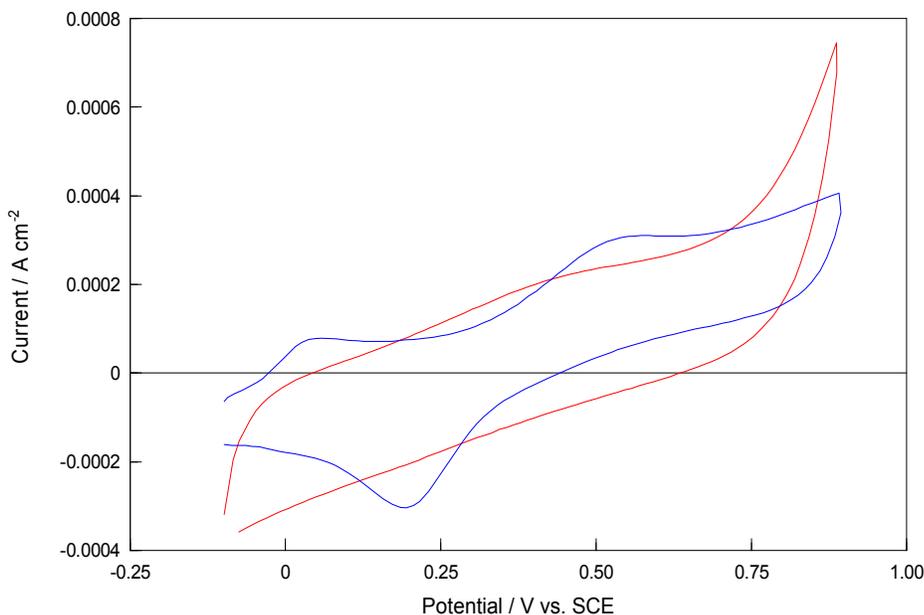
Figure 3.5: Cyclic voltammograms of a — **PPy-βCD modified electrode and a** — **bare Pt electrode in a 1.0 x 10^{-3} mol dm^{-3} DA / 0.10 mol dm^{-3} Na$_2$SO$_4$ solution (pH~6.0). Scan rate = 100 mV s^{-1}.**

In terms of potential applications, these PPy-SCD films have been shown to have relevance in electrochemically aided solid-phase microextraction[41] and the controlled delivery of neutral drugs[39]. They also have potential for preconcentration/sampling devices and selective electrodes[38] and the transport of metal ions[40]. However, there are no reports, to the best of our knowledge, on the use of the PPy-SCD films for the selective detection or simultaneous determination of DA.

3.3.3 Oxidation of Dopamine at PPy-βCD Modified Electrode

It is clearly obvious from Figure 3.5 that the DA response at the PPy-βCD modified electrode (neutral cyclodextrin) is extremely weak, yielding a broad oxidation wave with no corresponding reduction peak. In contrast, Izaoumen *et al.*[42] have shown that the DA signal at a PPy-βCD modified glassy carbon electrode is well-resolved and reversible. One of the differences, in terms of the electrosynthesis of the PPy-βCD films in this work and that reported by the group, is that Izaoumen and co-workers[42] used LiClO$_4$ as a supporting

electrolyte in the monomer solution. To investigate if the presence of a supporting electrolyte in the monomer solution had any role, a polymer film was electropolymerised on a Pt electrode from a solution of 0.20 mol dm^{-3} pyrrole / 0.01 mol dm^{-3} βCD / 0.10 mol dm^{-3} NaCl. The growth of this polymer was then compared to the growth of a polymer electrosynthesised from a solution of 0.20 mol dm^{-3} pyrrole / 0.10 mol dm^{-3} NaCl, as illustrated in Figure 3.6(a). From Figure 3.6(a), it can be seen that both polymer films take approximately the same time to reach the required charge and that the growth of both films occurs at very similar rates. The DA response at the resultant polymers was then recorded, as shown in Figure 3.6(b). However, no difference in the DA signal was observed at the PPy film formed in NaCl only and in NaCl with the neutral β-CD. These results suggest that it is indeed the chloride anions from the supporting electrolyte that are responsible for doping the polymer and not the neutral β-CD. The fact that the chloride anions are preferentially doped in the polymer over the neutral β-CD makes sense bearing in mind that when the polymer is oxidised it becomes positively charged and requires a negatively charged dopant to balance the charge.
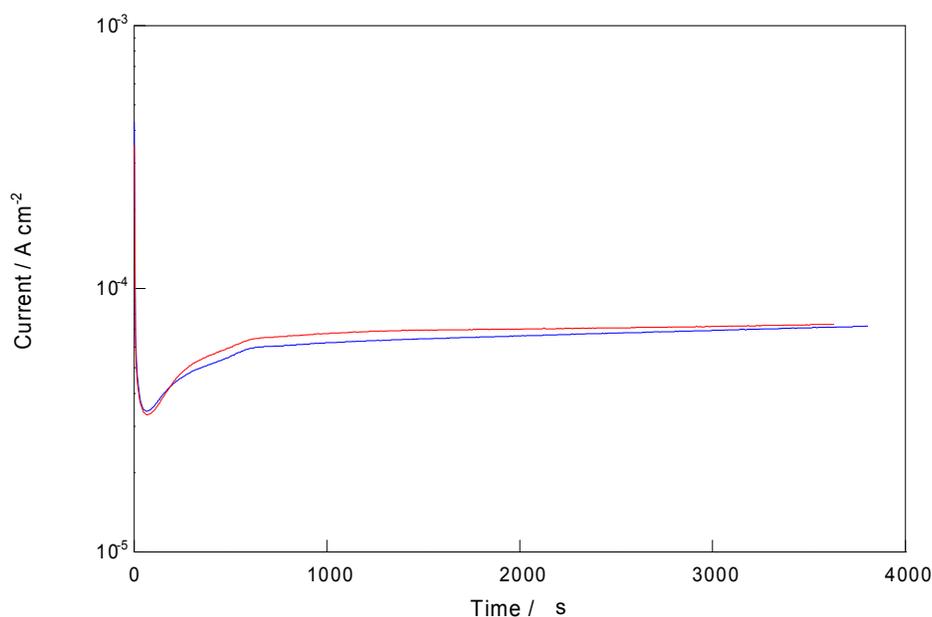
Figure 3.6(a): Current as a function of time for the formation of PPy on a Pt electrode at 0.500 V vs. SCE from monomer solutions containing ▬ 0.20 mol dm^{-3} pyrrole / 0.10 mol dm^{-3} sodium chloride and ▬ 0.20 mol dm^{-3} pyrrole / 0.01 mol dm^{-3} neutral β-CD / 0.10 mol dm^{-3} sodium chloride.
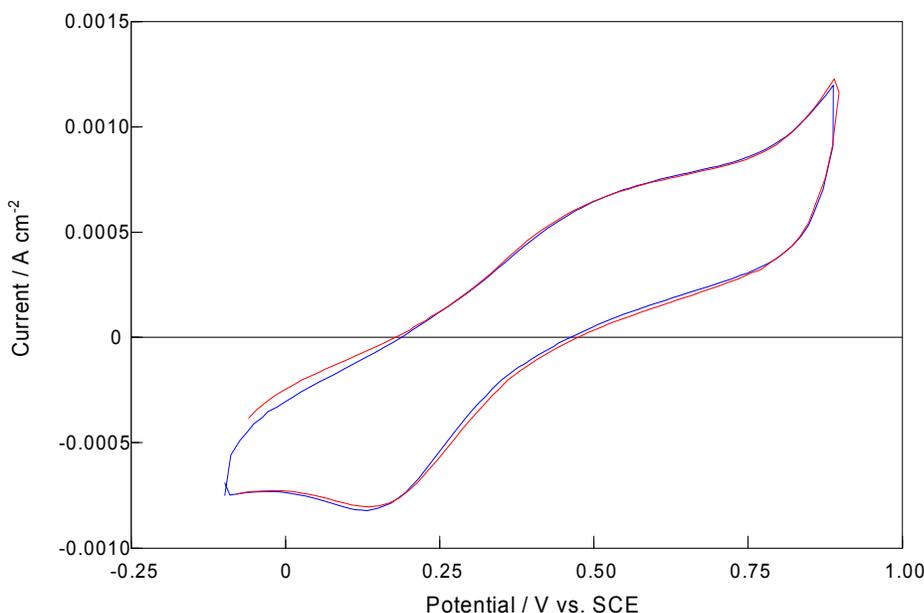
Figure 3.6(b): Cyclic voltammograms of the polymer formed from the — 0.20 mol dm^{-3} pyrrole / 0.10 mol dm^{-3} sodium chloride solution and from the — 0.20 mol dm^{-3} pyrrole / 0.01 mol dm^{-3} β-CD / 0.10 mol dm^{-3} sodium chloride solution cycled in a 5.0 x 10^{-3} mol dm^{-3} DA / 0.10 mol dm^{-3} Na$_2$SO$_4$ solution (pH~6.0). Scan rate = 100 mV s^{-1}.

Clearly, the chloride anions from the sodium chloride supporting electrolyte dope the polymer and not the neutral β-CD. This suggests that the polymer films used by Izaoumen *et al.*[42,43] may be doped with the perchlorate anions from the LiClO$_4$ supporting electrolyte instead of the neutral β-CD. In the paper by Izaoumen *et al.*[42] the cyclic voltammograms of 1.0 x 10^{-3} mol dm^{-3} DA at a PPy-βCD modified electrode and at a PPy modified electrode were compared in 0.10 mol dm^{-3} H$_2$SO$_4$. The DA was oxidised at a lower potential at the PPy-βCD modified electrode than at the PPy modified electrode and the oxidation current was slightly higher. An oxidation peak potential of 0.510 V vs. SCE was recorded at the PPy-βCD modified electrode for 1.0 x 10^{-3} mol dm^{-3} DA in 0.10 mol dm^{-3} H$_2$SO$_4$, (Figure 1 in Izaoumen's paper). These results are quite different to those presented here in Figures 3.3 and 3.5 which clearly show that the PPy films formed in the presence of the neutral β-CD grow at a very slow rate and are very poor in the sensing of DA, while the films formed in the presence of the neutral β-CD with a supporting NaCl electrolyte exhibit properties very similar to the polymer films doped only with chloride anions, Figure 3.6. Again, these films are rather poor in the sensing of DA.

Interestingly, Izaoumen *et al.*[42,43] formed the PPy-βCD modified electrodes by cycling the applied potential from 0.000 to 1.800 V vs. SCE at 50 mV s^{-1} for 25 cycles. These high potential conditions are well known to generate an overoxidised and highly porous polymer film and the DA signals observed by Izaoumen and co-workers may be simply due to the underlying substrate. Indeed, the DA oxidation peak potentials observed by the group and shown in Figure 3 of their paper, 0.565 V vs. SCE at pH 3.0 and approximately 0.545 V vs. SCE at a pH of 6.0, are very similar to the peak potentials shown here in Table 3.1 for the bare electrodes.

3.3.4 Factors Affecting the Growth of the PPy-SCD Films

As the PPy-SCD polymer films are clearly more superior in the electrochemical detection of DA, experiments were carried out to investigate how the growth of the PPy-SCD films were affected by varying the concentration of the pyrrole monomer, the concentration of sulfonated β-cyclodextrin, the applied potential and the working electrode. In addition, the presence of a supporting electrolyte in the monomer solution was also explored to see the effect, if any, it had on the growth of the PPy-SCD film. In these experiments the rate of the polymer growth was initially monitored by the period, or the time taken, for the electropolymerisation charge to reach a value of 0.24 C cm^{-2}. Then, a more detailed kinetic analysis was performed in an attempt to evaluate the reaction order for the monomer and the anionic sulfonated cyclodextrin.

From Figure 3.7 it can be seen that the time taken for the polymer to reach the target charge of 0.24 C cm^{-2} decreases with increasing concentrations of pyrrole, varying from times exceeding 3000 s, at low concentrations to much shorter periods of 400 s for pyrrole concentrations higher than 0.10 mol dm^{-3}. A similar result was achieved when the concentration of sulfonated β-cyclodextrin was varied, Figure 3.8. However, concentrations greater than 5.0 x 10^{-3} mol dm^{-3} appear to have no additional influence on the rate of polymer growth.
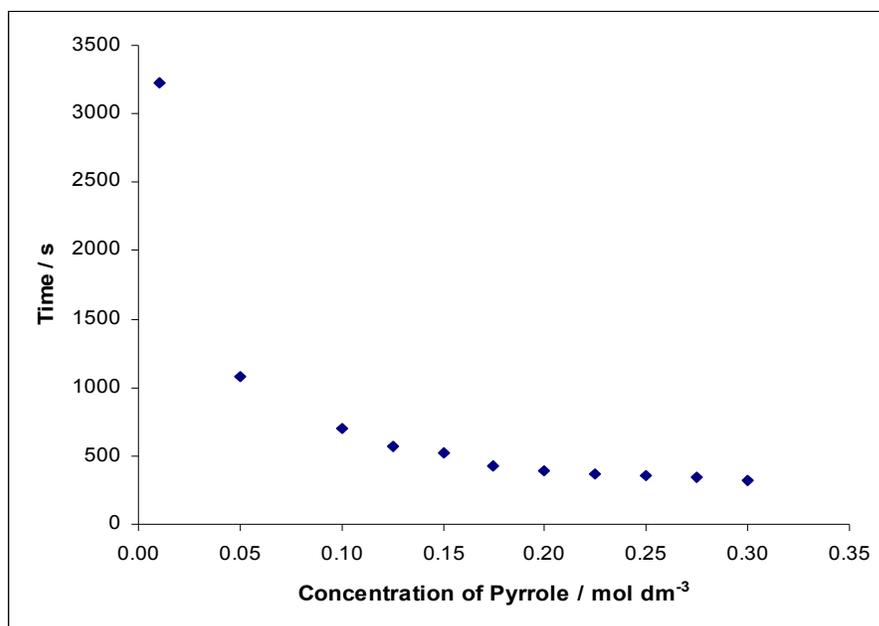
Figure 3.7: Electropolymerisation time required to reach 0.24 C cm^{-2} as a function of the pyrrole concentration. The PPy-SCD films were grown from a monomer solution containing various concentrations of pyrrole and a fixed concentration of 0.01 mol dm^{-3} sulfonated β-cyclodextrin at a potential of 0.500 V vs. SCE.
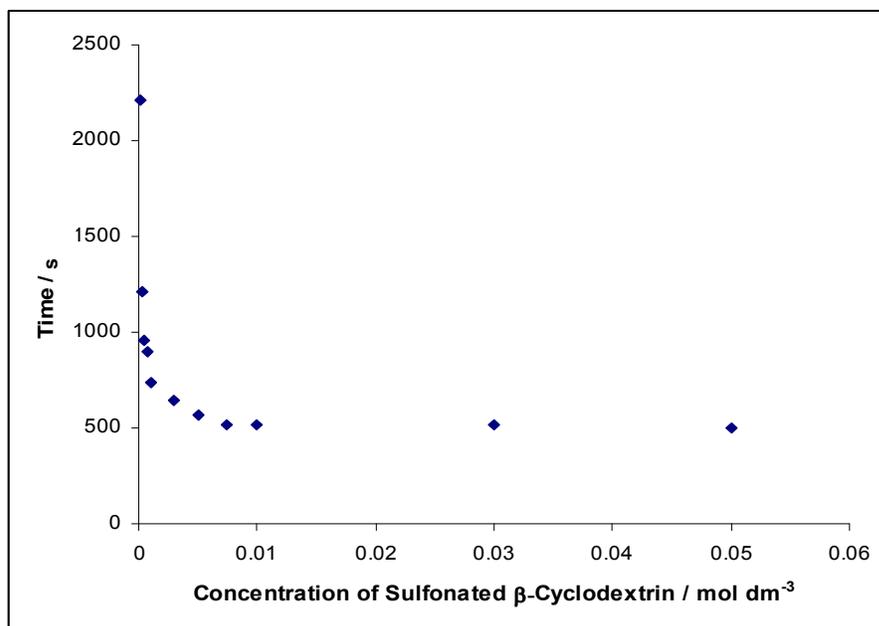
Figure 3.8: Electropolymerisation time required to reach 0.24 C cm^{-2} as a function of the concentration of sulfonated β-cyclodextrin. The PPy-SCD films were grown from a monomer solution containing various concentrations of sulfonated β-cyclodextrin and a fixed concentration of 0.20 mol dm^{-3} pyrrole at a potential of 0.500 V vs. SCE.

The effect of altering the applied potential is illustrated in Figure 3.9, where it can be seen that the rate of polymer growth increases considerably with increasing the applied potential from 0.400 to 0.800 V vs. SCE. Although it is possible to form the polymer at 0.400 V vs SCE, the rate of the electropolymerisation reaction is very low, requiring nearly 4000 s to reach the selected charge.

These data are in good agreement with literature reports on other dopants, indicating that the anionic sulfonated β-cyclodextrin behaves, at least to some extent, like the more traditional dopants during electropolymerisation.
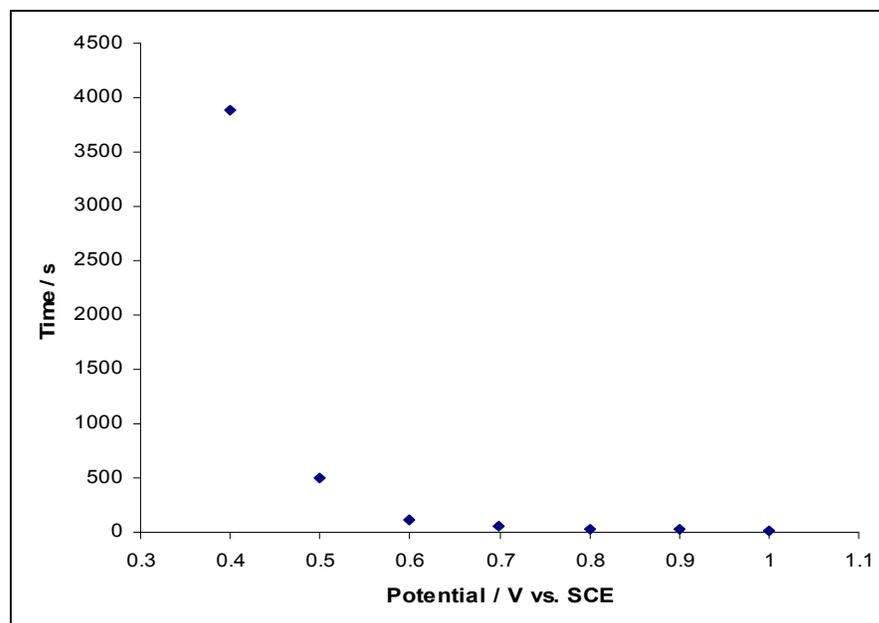
Figure 3.9: Electropolymerisation time required to reach 0.24 C cm^{-2} as a function of the applied potential. The PPy-SCD films were grown from a monomer solution containing 0.20 mol dm^{-3} pyrrole and 0.01 mol dm^{-3} sulfonated β-cyclodextrin.

The rate of electropolymerisation at a constant applied potential can be related to the monomer and dopant concentrations by using the rate law given in Equation 3.6. In this analysis, R represents the rate of the electropolymerisation reaction, Py represents the monomer concentration, SCD represents the dopant concentration, k represents the rate constant and α and β are the partial orders of the reaction.

$$R = k[Py]^{\alpha}[SCD]^{\beta} \qquad\qquad 3.6$$

The charge consumed during the growth of the polymer, Q, can be related to the amount of polymer deposited and accordingly, the rate of the electropolymerisation reaction can be given in terms of dQ/dt. Thus, Equation 3.6 can be expressed in terms of Equation 3.7 and modified to give Equation 3.8.

$$\frac{dQ}{dt} = k[\text{Py}]^{\alpha}[\text{SCD}]^{\beta} \qquad\qquad 3.7$$

$$\log\left(\frac{dQ}{dt}\right) = \log k + \alpha \log[Py] + \beta \log[SCD] \qquad\qquad 3.8$$

In these experiments, the applied potential was fixed at 0.500 V vs. SCE and the concentrations of pyrrole and the sulfonated β-cyclodextrin were varied. The rate of electropolymerisation, dQ/dt, was found by plotting the electropolymerisation charge as a function of time. This was then fitted to Equation 3.8 and α, β and k were determined. These values were obtained from the slopes of Figure 3.10 and Figure 3.11, respectively.
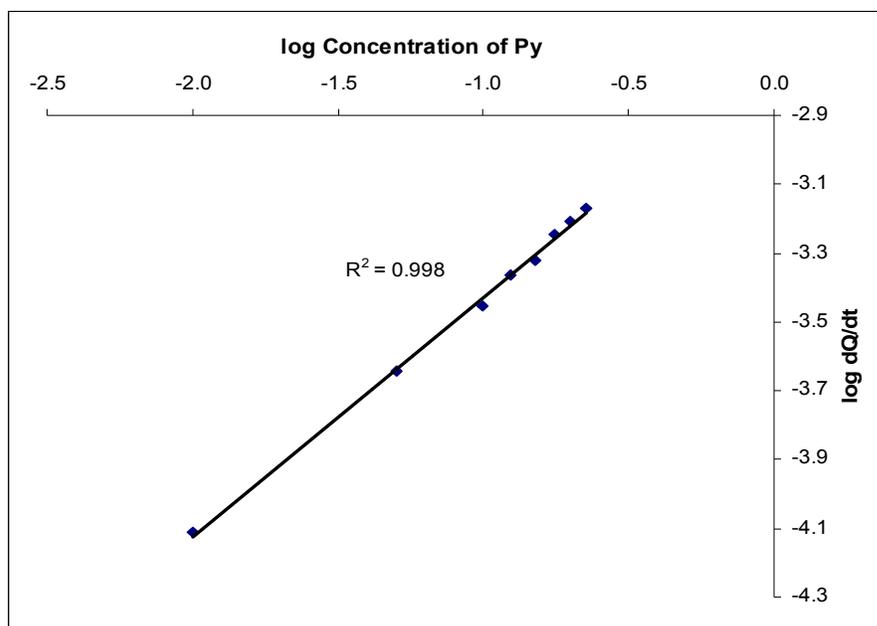
Figure 3.10: Plot of the logarithm of the rate of electropolymerisation, dQ/dt, as a function of the logarithm of the concentration of pyrrole.
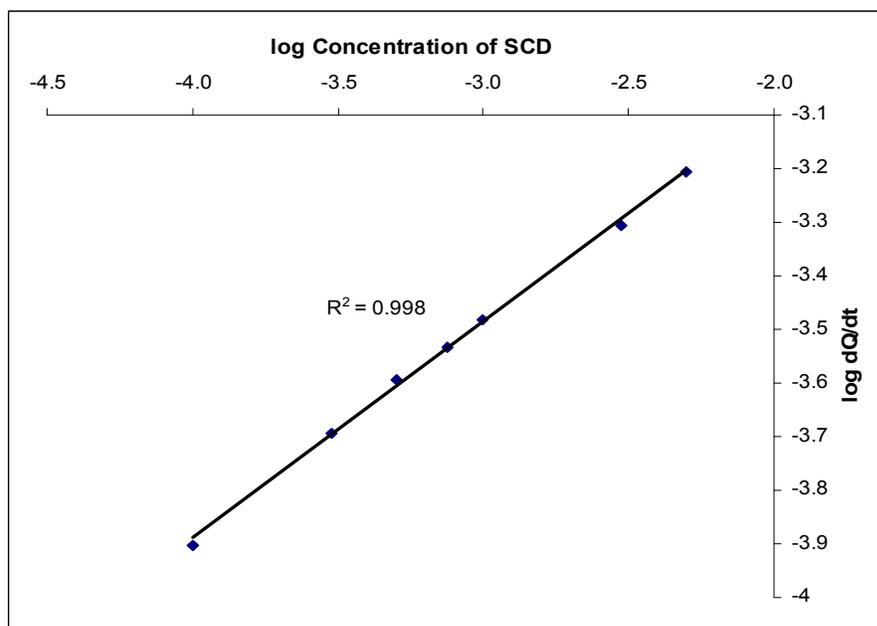
Figure 3.11: Plot of the logarithm of the rate of electropolymerisation, dQ/dt, as a function of the logarithm of the concentration of sulfonated β-cyclodextrin.

The partial order of the reaction with respect to the monomer concentration, α, was found to be 0.7, while a lower value of 0.4 was acquired for β, the partial order of the reaction for the sulfonated β-cyclodextrin dopant anion. These values were then substituted into Equation 3.7 and a value of 0.0140 ± 0.0006 C cm^{-2} s^{-1} (mol dm^{-3})$^{-1.1}$ was calculated for the rate constant, k. These reaction orders are in good agreement with previous publications. For example, Serra Moreno et al.[44] obtained reaction orders of 0.58 and 0.56 corresponding to α and β for the formation of a polypyrrole-perchlorate film (PPy-ClO$_4$), giving a near 1:1 ratio of the two partial reaction orders. Iroh and Wood[45], on studying the kinetics of pyrrole electropolymerisation in toluene sulfonic acid, sulfuric acid and dodecylbenzene sulfonate, obtained partial orders for pyrrole in the range 0.8 to 1.0, and partial orders of 0.7 to 1.0 for the electrolyte dopant anions.

The fractional values of the partial orders reflect the complex electropolymerisation process. Taking the rate-determining step as the oxidation of the monomer (Py $\rightarrow$ Py$^{\bullet+}$ + e^{-}) and neglecting diffusion limitations, then the rate should be first order with respect to the pyrrole monomer concentration. The α value obtained from Figure 3.10 is less than unity and indicates a more complex system, where the propagation of the polymer and/or the incorporation of the dopant contribute to the slow step of the reaction.

As pointed out, the ratio of the partial reaction orders with respect to the monomer and dopant is usually close to 1:1. The approximate 2:1 ratio obtained in this study and the relatively low partial order of 0.4 obtained for the sulfonated β-cyclodextrin show that the rate of the reaction is less dependent on the sulfonated β-cyclodextrin. Indeed, this is very clear from Figure 3.8, where concentrations higher than 0.01 mol dm^{-3} have little effect on the rate of electropolymerisation. This can be attributed to the large number of sulfonated groups on the β-cyclodextrin and the fact that the sulfonated β-cyclodextrin gives rise to a lower doping of the polymer compared to a simple chloride, Section 3.3.5.5.

In another set of experiments the influence of the nature of the substrate was investigated. Three substrates were chosen, Pt, Au and GC, while a constant applied potential and constant pyrrole and sulfonated β-cyclodextrin concentrations were maintained. The results obtained from growing the PPy-SCD modified films on these different electrode substrates

are shown in Figure 3.12, where the current is plotted as a function of time. The polymers were grown to a constant charge. It can be seen that the polymer film grows much slower on the Au electrode with a lower current than that measured at the GC or Pt electrodes. This may be connected to the formation of a gold oxide, which in turn, limits the rate of electron transfer at the gold interface. The current increases rapidly for the first few seconds, at all three electrodes, corresponding to the nucleation of the polymer, then a near constant current is obtained, indicating a constant rate of electropolymerisation.
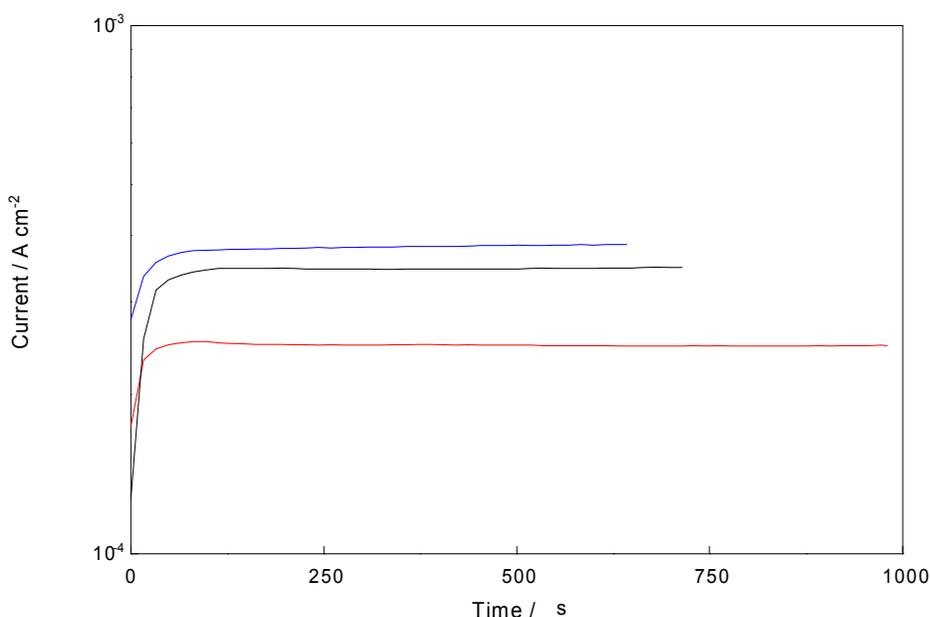
Figure 3.12: Current plotted as a function of time for the formation of PPy-SCD on ▬ Pt, ▬ GC and ▬ Au electrodes at 0.500 V vs. SCE from a monomer solution containing 0.20 mol dm^{-3} pyrrole / 0.01 mol dm^{-3} sulfonated β-cyclodextrin.

In order to gain information on the role, if any, of a supporting electrolyte during the growth of the PPy-SCD films, NaCl was added to the electropolymerisation solution. Typical growth profiles for a polymer film grown at a Pt electrode from a monomer solution containing no supporting electrolyte and for a polymer film grown from a monomer solution with a supporting electrolyte (0.10 mol dm^{-3} NaCl) are depicted in Figure 3.13. It can be seen that the growth of the polymer films is different, particularly

during the early stages of polymer formation. The currents observed for the growth of the polymer film from a monomer solution containing 0.10 mol dm⁻³ NaCl are much lower and continue to decrease during the first 20 s, at which point they start to increase and eventually mimic the currents observed for the polymer film grown from a monomer solution containing no supporting electrolyte. Furthermore, the polymer film grown from the monomer solution containing the supporting electrolyte takes longer to reach the required charge. This is not connected to variations in conductivity, as the concentration of the highly ionised sulfonated β-cyclodextrin is maintained constant.

The comparatively low current measured during the early stages of polymer formation in the mixed electrolyte suggests that the polymer is preferentially doped with the chloride anions from the supporting electrolyte for the first few layers of polymer growth. This is not surprising as the concentration of chloride is 10-fold higher and the small chloride anions are more mobile than the large and bulky sulfonated β-cyclodextrin.
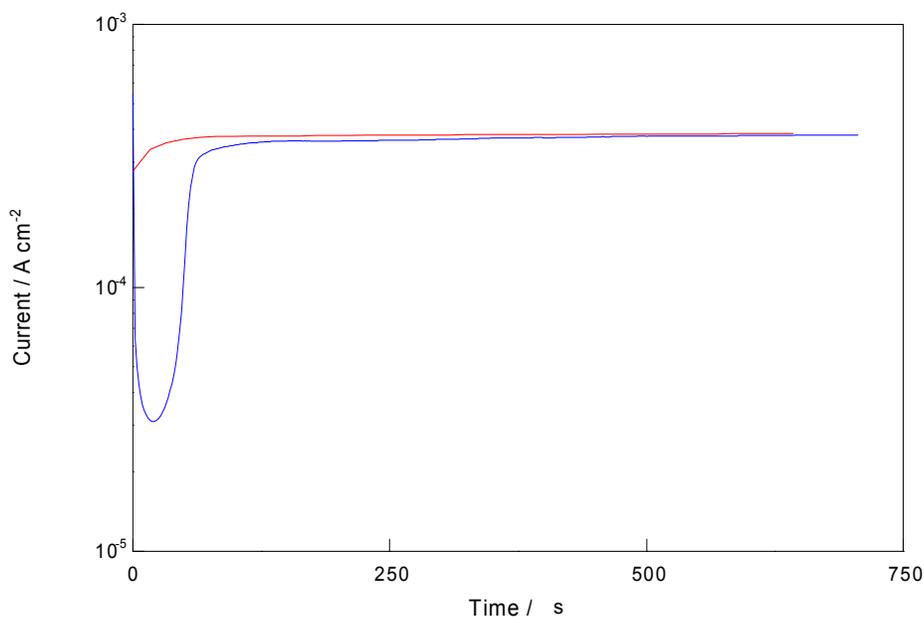
Figure 3.13: Current plotted as a function of time for the formation of PPy on a Pt electrode at 0.500 V vs. SCE from a monomer solution containing — 0.20 mol dm⁻³ pyrrole / 0.01 mol dm⁻³ sulfonated β-cyclodextrin and — 0.20 mol dm⁻³ pyrrole / 0.01 mol dm⁻³ sulfonated β-cyclodextrin / 0.10 mol dm⁻³ NaCl.

Indeed, this is highlighted in Figure 3.14 where it can be seen that this relatively low current is very comparable to the currents observed for the formation of a PPy-Cl film. The subsequent increase in the current may indicate that the sulfonated β-cyclodextrin is now incorporated into the polymer in addition to the chloride anions. Therefore, both the sulfonated β-cyclodextrin and the chloride anions from the supporting electrolyte are incorporated into the polymer film. Further confirmation of this theory is provided in Section 3.3.5.1. This contradicts the findings of Temsamani *et al.*[38] who claimed that the perchlorate anions from the supporting electrolyte were selectively excluded as a dopant in the polymer film.
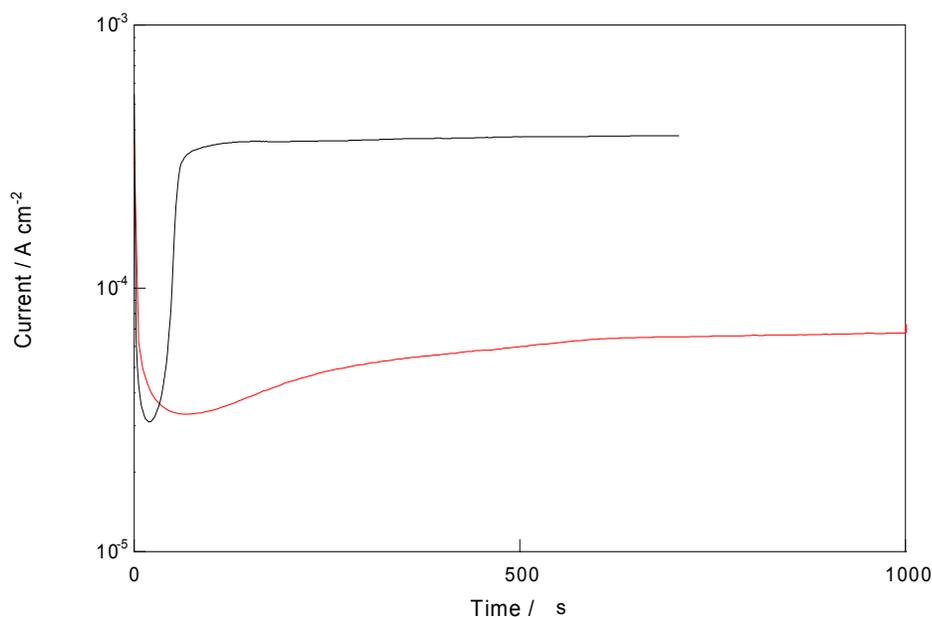
Figure 3.14: Current plotted as a function of time for the formation of PPy on a Pt electrode at 0.500 V vs. SCE from a monomer solution containing ▬ 0.20 mol dm⁻³ pyrrole / 0.01 mol dm⁻³ sulfonated β-cyclodextrin / 0.10 mol dm⁻³ NaCl and ▬ 0.20 mol dm⁻³ pyrrole / 0.10 mol dm⁻³ NaCl.

It is clear from Figures 3.3 and 3.12 that the electropolymerisation of pyrrole in the presence of the anionic sulfonated β-cyclodextrin occurs with considerable ease and without the need of a supporting electrolyte. In order to obtain more detailed information on the manner in which the PPy-SCD film nucleates at the Pt substrate, the current-time

transients were analysed in terms of progressive and instantaneous nucleation models. In instantaneous nucleation, the nuclei are formed only at the beginning of the pulse. Therefore, the number of nuclei is constant and the deposit grows at these sites without the formation of any new nuclei. This generally gives rise to nuclei with large radii and surfaces with rough morphology. In the case of progressive nucleation, the nuclei are formed continuously during the growth period. This results in smaller nuclei with a less rough morphology. Scharifker and Hills[46] derived a series of relationships between the measured current and time for these two types of nucleation. Equations 3.9 and 3.10 give simple expressions for the instantaneous and progressive models, respectively.

$$I = zFD^{3/2}c^{1/2}Nkt^{1/2} \qquad\qquad 3.9$$

$$I = zFD^{3/2}c^{1/2}AN_\infty k't^{3/2} \qquad\qquad 3.10$$

The constants, k and k' are given by Equations 3.11 and 3.12, respectively.

$$k = \left(\frac{8\pi cM}{\sigma}\right)^{1/2} \qquad\qquad 3.11$$

$$k' = \frac{4}{3}\left(\frac{8\pi cM}{\sigma}\right)^{1/2} \qquad\qquad 3.12$$

In this analysis, I represents the current density, t is time, D is the diffusion coefficient, c is the bulk concentration, zF is the molar charge, M is the molar mass of the deposit, σ is the density of the deposit, N is the total number of nuclei, N_∞ is the number density of active sites and A is the steady state nucleation rate constant.

Equations 3.9 and 3.10 correspond to the rising part of the current-time transients, i.e., before the current maximum is observed. Figures 3.15 and 3.16 show plots of the current density recorded during the growth of the PPy film in the anionic sulfonated cyclodextrin with the current plotted as a function of $t^{1/2}$ and $t^{3/2}$ in accordance with Equations 3.9 and 3.10, respectively. A clear linear relationship is observed when the current is plotted as a function of the square root of time, indicating that the nucleation of the PPy film is an instantaneous process. On the other hand, when the same data are plotted in accordance with Equation 3.10, poor agreement is obtained, ruling out a progressive nucleation mechanism during the very early stages of nucleation.

A more detailed quantitative analysis can be performed using the current-time transients in the vicinity of the current maxima. Scharifker and Hills[46] derived expressions relating the measured current density with time for 3D instantaneous and 3D progressive nucleation models, as shown in Equations 3.13 and 3.14, respectively.

$$\left(\frac{I}{I_{max}}\right)^2 = \frac{1.9542}{t/t_{max}}\left[1 - exp\left(-1.2564\left(\frac{t}{t_{max}}\right)\right)\right]^2 \qquad 3.13$$

$$\left(\frac{I}{I_{max}}\right)^2 = \frac{1.2254}{t/t_{max}}\left[1 - exp\left(-2.3367\left(\frac{t}{t_{max}}\right)^2\right)\right]^2 \qquad 3.14$$

These dimensionless plots are used frequently to distinguish between 3D progressive and 3D instantaneous nucleation[47, 48]. Typical plots comparing the experimental data with the theoretical progressive and theoretical instantaneous profiles are provided in Figure 3.17. The theoretical profiles were generated with Equations 3.13 and 3.14.

Again, the experimental data are more typical of an instantaneous 3D nucleation process and have a better agreement with the theoretical instantaneous profile. These analyses clearly show that during the early stages of deposition of the PPy film from the anionic sulfonated cyclodextrin the nuclei are only formed at the beginning of the pulse. However, the high polymer growth rate soon leads to overlapping nuclei which ensures a continued high growth rate for the PPy-SCD film.
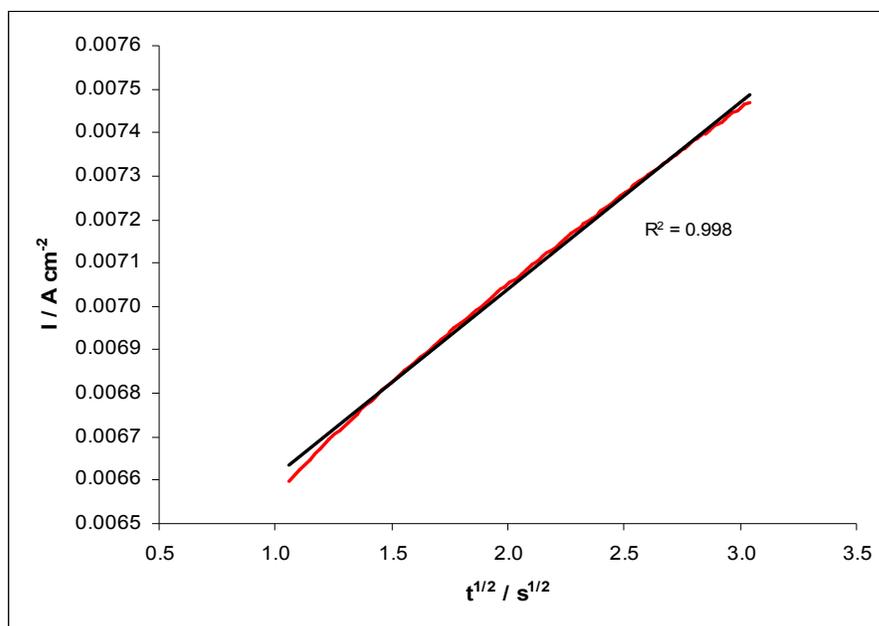
Figure 3.15: The current as a function of $t^{1/2}$ for the formation of the PPy-SCD film.
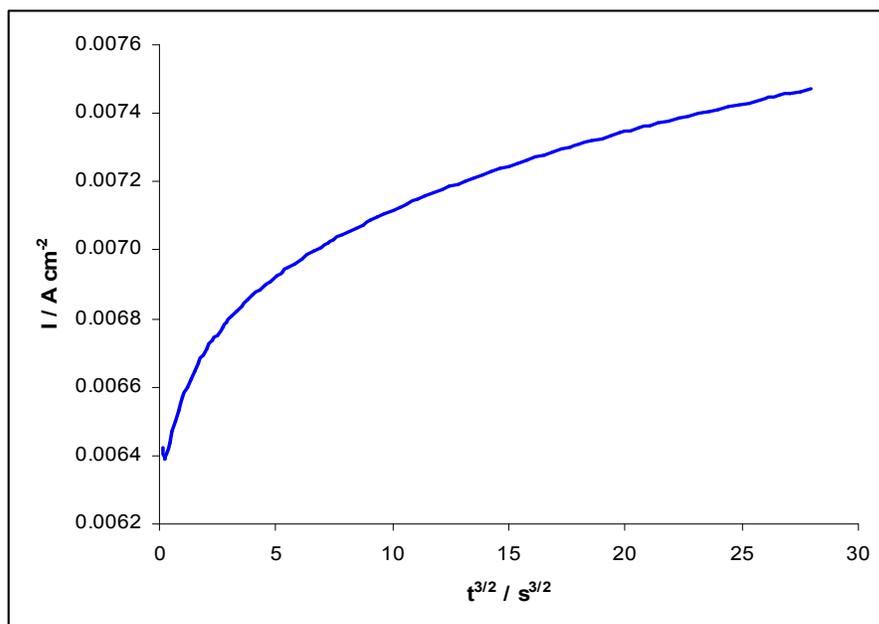
Figure 3.16: The current as a function of $t^{3/2}$ for the formation of the PPy-SCD film.
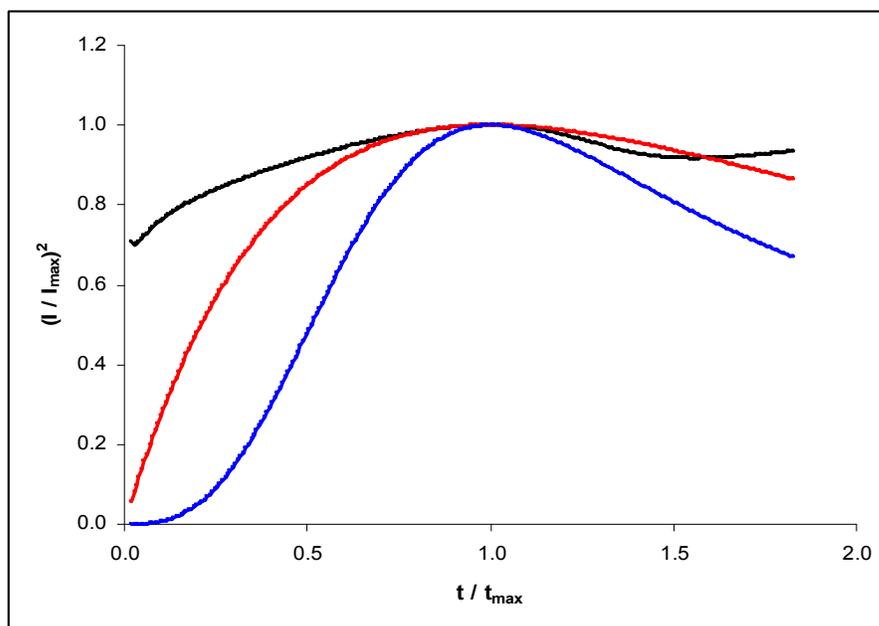
**Figure 3.17: A plot of $(I/I_{max})^2$ as a function of t/t_{max} for the — experimental data, the —
theoretical progressive profile and the — theoretical instantaneous profile.**

## 3.3.5 Characteristics and Properties of the PPy-SCD Films

3.3.5.1 SEM and EDX

SEM measurements were performed on a PPy-SCD film, Figure 3.18, in the Tyndall
National Institute at University College Cork. From this figure it can be seen that the PPy-
SCD film exhibits a 'cauliflower' morphology typically seen for PPy films[49]. However, its
morphology seems to be more structured and organised and this is not normally observed
with a characteristic PPy film.

EDX measurements were subsequently performed on a PPy-Cl film, a PPy-SCD film and a
PPy-SCD film electrosynthesised in the presence of 0.10 mol dm^{-3} NaCl. This analysis was
carried out in the CMAU at Trinity College Dublin and the results are shown in Figure
3.19. The EDX spectrum of the PPy-Cl film, Figure 3.19(a), shows that chlorine is present
in the polymer film, while the EDX spectrum of the PPy-SCD film, Figure 3.19(b), shows
that sulfur is present in the polymer film. Naturally, no chlorine is present in the PPy-SCD

film and no sulfur is present in the PPy-Cl film. However, Figure 3.20 clearly shows that sulfur and chlorine are present in the PPy-SCD film electrosynthesised in the presence of 0.10 mol dm^{-3} NaCl. This proves that both the anionic β-cyclodextrin and the chloride anions from the NaCl supporting electrolyte are incorporated into the polymer film and contradicts the claims made by Temsamani *et al.*[38] that the negatively charged sulfonated β-cyclodextrin is selectively incorporated into the polymer film over the anion from the supporting electrolyte.
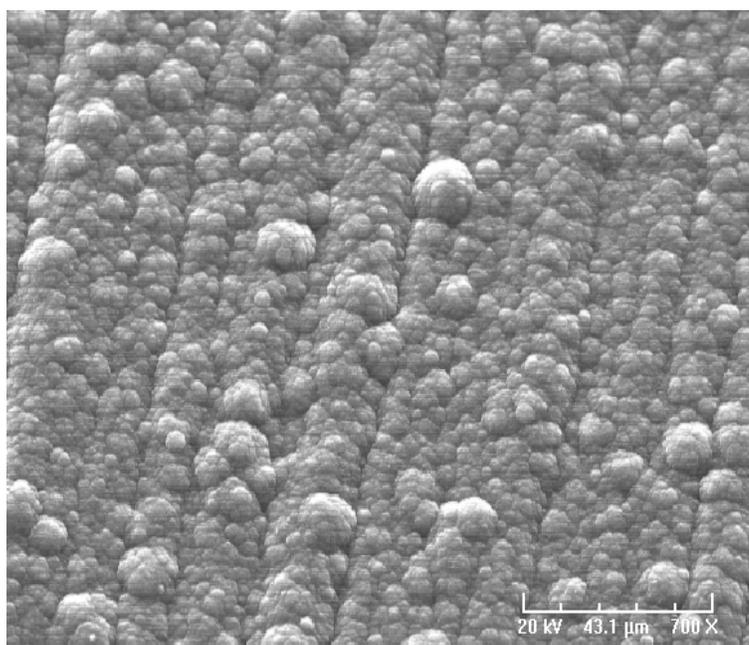
Figure 3.18: SEM micrograph of a PPy-SCD film electrosynthesised at 0.900 V vs. SCE from a monomer solution containing 0.20 mol dm^{-3} pyrrole and 0.01 mol dm^{-3} sulfonated β-cyclodextrin until a charge of 3.00 C cm^{-2} had been reached.

(a)

(b)
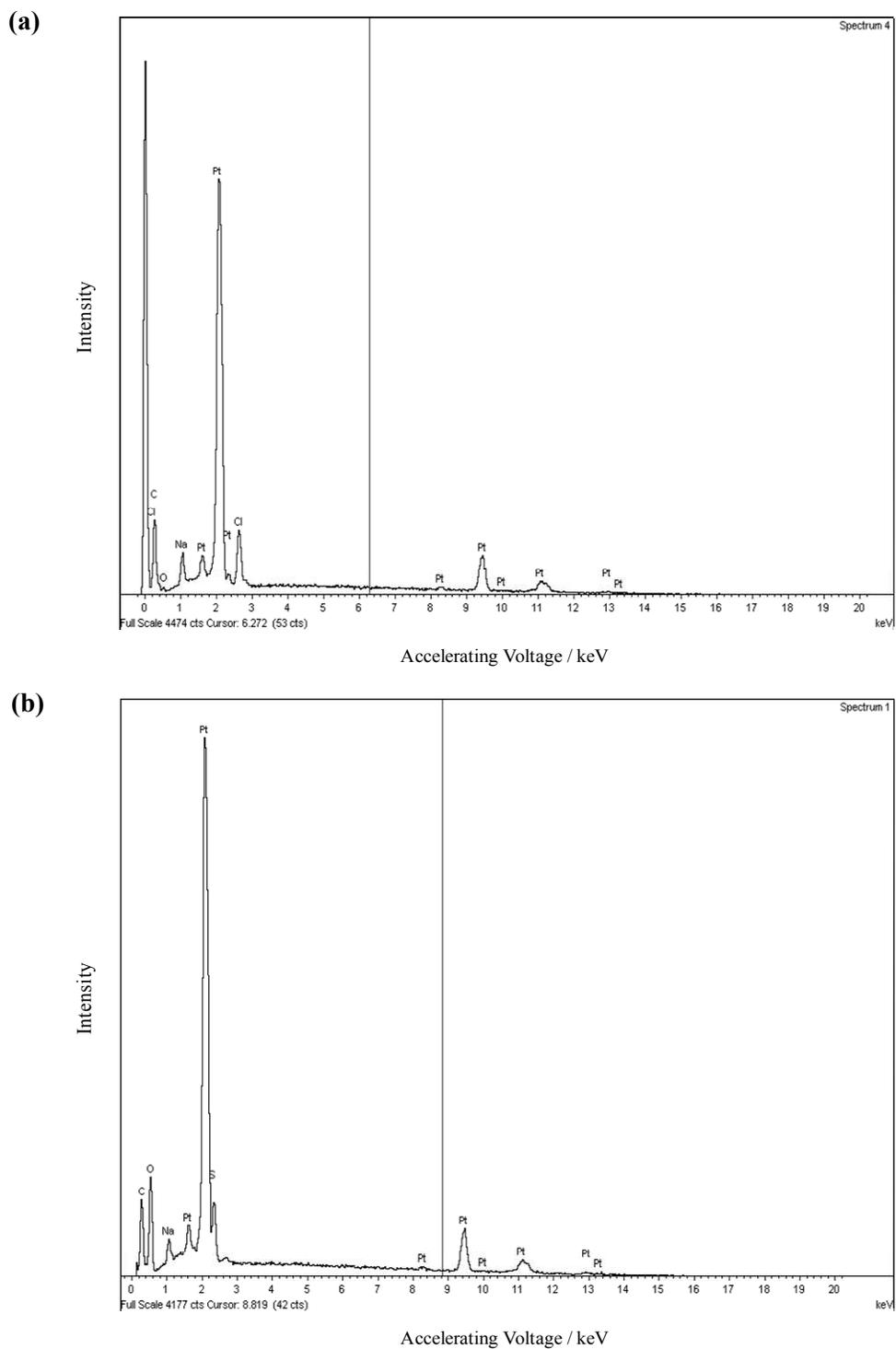
Figure 3.19: EDX spectra of (a) PPy-Cl film and (b) PPy-SCD film. The PPy-Cl film was electrodeposited from a monomer solution containing 0.20 mol dm^{-3} pyrrole and 0.10 mol dm^{-3} NaCl, while the PPy-SCD film was prepared from a monomer solution containing 0.20 mol dm^{-3} pyrrole and 0.01 mol dm^{-3} sulfonated β-cyclodextrin. In both cases, a potential of 0.800 V vs. SCE was used and the films were grown until a charge of 0.24 C cm^{-2} had been reached.

Accelerating Voltage / keV
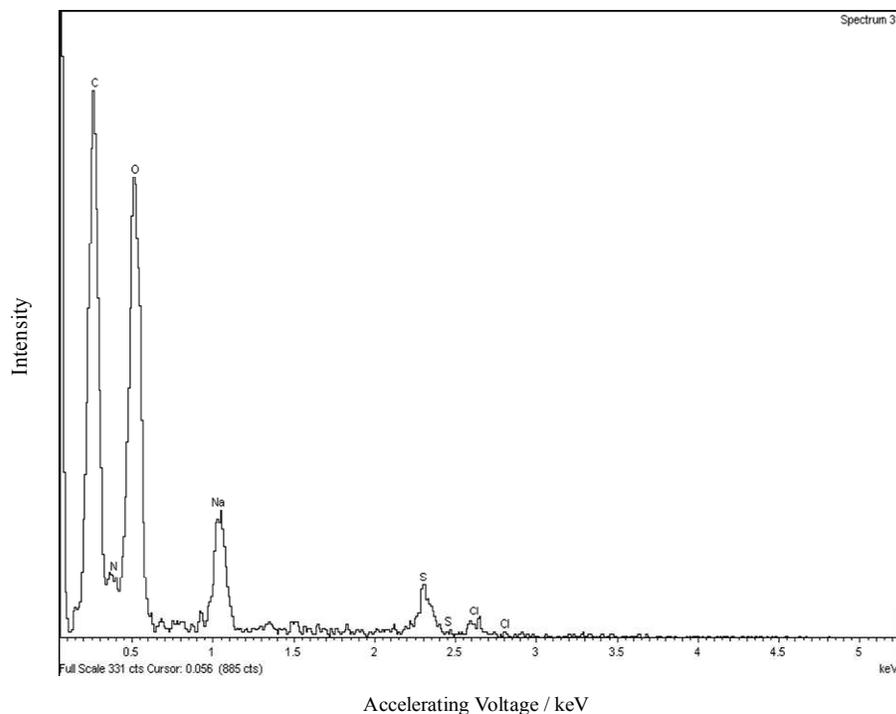
Figure 3.20: PPy-SCD film electrosynthesised in the presence of 0.10 mol dm^{-3} NaCl at 0.800 V vs. SCE until a charge of 0.24 C cm^{-2} had been reached.

3.3.5.2 Thickness of PPy-SCD Film

The thickness of the PPy-SCD film was determined using a Tencor profilometer in the Tyndall National Institute at University College Cork. PPy-SCD films were electrosythesised on one half of a Pt flat disk electrode at 0.800 V vs. SCE until a charge of 0.24 C cm^{-2} had been reached. Two separate measurements were carried out and the thickness of each of these films was found to be 510 nm $\pm$ 50 nm and 500 nm $\pm$ 10 nm.

The thickness of the films can also be theoretically calculated from the total charge passed using a relationship derived by Diaz *et al.*[50] that assumes that 1 C cm^{-2} is equivalent to 2.5 μm of polymer growth. Using this approximation and the charge used to grow the PPy-SCD films, 0.24 C cm^{-2}, a thickness of approximately 600 nm can be established. This is slightly higher than the experimental analysis however, it is important to highlight that the relationship quoted by Diaz and co-workers[50] was for a simple chloride dopant, which has

been shown to form thicker films than PPy films doped with tosylate and polystyrene sulfonate when the same amount of charge has been passed[51].

Equation 3.15 can also be used to theoretically calculate the thickness of the PPy-SCD film. Variations of this equation have been used by a number of authors including Fonner *et al.*[51] and Tietje-Girault *et al.*[52] to calculate the thickness of several PPy films. Here, *T* is the thickness of the film, *M*(Py) is the molar mass of the monomer, *x* is the number of dopant molecules per monomeric unit, *M*(SCD) is the molar mass of the dopant, *d* is the density of PPy, *F* is Faraday's constant and *q* is the charge passed. The thickness of the PPy-SCD film was calculated assuming that *M*(SCD) was equivalent to nine sulfonated groups, *x* was 0.125 and *d* was 1.5 g cm^{-3}. The equation also assumes 100% current efficiency for the PPy formation. Under these stipulations the thickness of the PPy-SCD film was estimated at 746 nm, which is considerably higher than the experimental analysis. However, the assumptions made in this analysis together with the fact that the equation assumes the current efficiency for the electropolymerisation of pyrrole is 100% are not precise. For example, the density of a PPy film doped with a simple chloride anion will be 1.5 g cm^{-3}. This may not be the case for the PPy-SCD film. Furthermore, the number of sulfonated groups on the β-cyclodextrin are variable. Therefore, it is impossible to know the exact number of dopant molecules incorporated into the polymer. Also, the value for *x* is an estimated value based on nine of the β-cyclodextrin sites being sulfonated, Section 3.3.5.5. Accordingly, estimating the thickness of the PPy-SCD film using Equation 3.15 is very unreliable.

$$T = \frac{M(Py) + xM(SCD)}{d(2 + x)F} q \qquad\qquad 3.15$$

3.3.5.3 Surface Coverage of Electroactive Centres

An estimation of the surface coverage of the electrode was made using Equation 3.16. Here, Γ is the surface coverage of electroactive centres (mol cm^{-2}), *n* represents the number of electrons involved in the reaction, *F* is the Faraday constant (C mol^{-1}), *A* is the surface area of the electrode (cm^2) and *Q* is the total amount of charge calculated from the

integration of the oxidation peak of PPy recorded using cyclic voltammetry[53]. If it is assumed that the sulfonated cyclodextrins are the electroactive centres, then the surface coverage gives an estimation of the number of anionic cyclodextrins distributed within the PPy film, which in turn can be equated with the oxidation of DA. However, as detailed in Section 5.3.4, the oxidation of DA also takes place at the PPy backbone.

$$\Gamma = \frac{Q}{nFA} \qquad\qquad 3.16$$

The oxidation and subsequent reduction of the PPy-SCD film is shown in Figure 3.21, where the film was cycled between -0.800 and +0.100 V vs. SCE at a slow scan rate of 5 mV s^{-1}. In this case, the redox properties of the PPy-SCD are clearly visible with the reduction of the polymer occurring at a peak potential of -0.52 V vs. SCE and the corresponding oxidation wave centred at -0.36 V vs. SCE. Using the computed oxidation peak charge, the surface coverage, Γ, was estimated at 4.3 x 10^{-8} mol cm^{-2}.
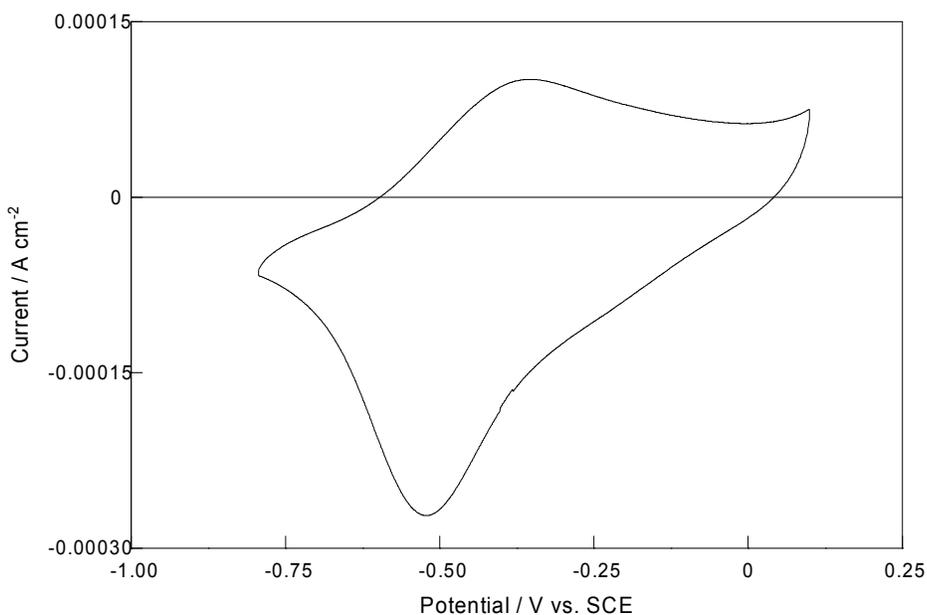
Figure 3.21: Cyclic voltammogram of a PPy-SCD modified electrode grown from a monomer solution containing 0.20 mol dm^{-3} pyrrole / 0.01 mol dm^{-3} sulfonated β-cyclodextrin in a 0.10 mol dm^{-3} Na$_2$SO$_4$ solution (pH~6.0). Scan rate = 5 mV s^{-1}.

An interesting feature of the cyclic voltammogram depicted in Figure 3.21 is the fact that the reduction peak is sharper than the corresponding oxidation peak, indicating a considerable variation in the kinetics of the two processes. The broad oxidation peak indicates a slow conversion of the polymer from the reduced to oxidised state, while the sharper reduction peak indicates a faster rate of reduction. This is somewhat unexpected. During the oxidation of PPy, or indeed other conducting polymers, the layer next to the electrode surface is generally oxidised first giving a conducting layer. The adjacent polymer layers are then oxidised and this continues until the conducting zone reaches the solution interface. Conversely, on reduction of the polymer, the layer adjacent to the electrode is reduced first to give an insulating interface, making the overall reduction process less efficient and slower. The sharper reduction wave in Figure 3.21 is a clear indication that the incorporation of Na^+ during the reduction of the polymer is a relatively fast and efficient process, $PPy^{n+}S\beta\text{-}CD^{n-} + ne^- \rightarrow PPy^oS\beta\text{-}CD^{n-}(nNa^+)$, whereas the oxidation of the polymer is much slower due to the slow release of Na^+, or alternatively the slow ingress of electrolyte anions, to balance the positive charge on the oxidised PPy. However, the incorporation of anions would not be favoured due to the high density of negative charge on the sulfonated β-cyclodextrins.

3.3.5.4 Capacitance Measurements

As evident in Figure 3.4, the background current in the cyclic voltammograms is large, indicating a high charging capacitance. This capacitance was calculated for the PPy-SCD film and compared with a PPy-Cl polymer film. The capacitance was calculated by means of the following relation, Equation 3.17, where, C is the capacitance (F cm^{-2}), I is the current density (A cm^{-2}) and dV/dt is the scan rate (V s^{-1})[54].

$$C = \frac{I}{dV/dt}$$ 3.17

The PPy-Cl and PPy-SCD films were cycled in 0.10 mol dm^{-3} Na$_2$SO$_4$ at different scan rates. The electrochemical window was reduced to 0.100 to 0.200 V vs. SCE to avoid any faradic currents and the current was obtained at 0.150 V vs. SCE. A plot of I versus dV/dt yields a straight line, as shown in Figure 3.22. Correlation coefficients of 0.998 and 0.999 were obtained on fitting the data to Equation 3.17 for the PPy-SCD and PPy-Cl films, respectively. The capacitance of the PPy-SCD film was found to be 1.2 x 10^{-3} F cm^{-2}, while the capacitance of the PPy-Cl film was established as 6.1 x 10^{-4} F cm^{-2}. These high values are typical of the capacitance recorded for conducting polymers. The fact that the capacitance of the PPy-SCD film is higher than that of the PPy-Cl film by a factor of two indicates that considerably more negative charge is stored in the PPy-SCD film, and consequently more cations are attracted to the surface of the film.

This is in good agreement with recent reports by Suematsu *et al.*[55] who studied the properties of PPy films doped with naphthalene rings substituted with sulfonated groups. They showed that the tri-sulfonated doped PPy film had a higher capacitance than the di- or mono-sulfonated doped films. This was attributed to the presence of free sulfonated groups in the films, which in turn enhances the concentration of cations bound within the polymer. Ingram *et al.*[56] using similar naphthalene substituted sulfonated salts, prepared thick (10 μm) PPy films for use in electrochemical supercapacitors. They showed that the polymers had an open structure that enabled the rapid insertion and ejection of cations and anions from the aqueous solution.
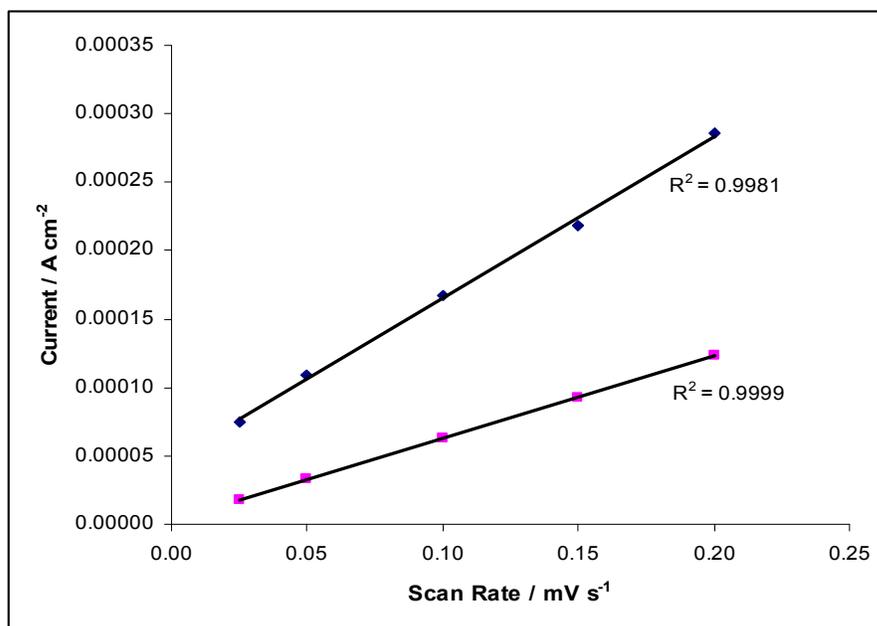
Figure 3.22: Current versus the scan rate. The PPy-SCD film was grown from 0.20 mol dm^{-3} pyrrole and 0.01 mol dm^{-3} sulfonated β-cyclodextrin, while the PPy-Cl film was grown from 0.20 mol dm^{-3} pyrrole and 0.10 mol dm^{-3} sodium chloride. Both films were formed at 0.800 V vs. SCE until a charge of 0.24 C cm^{-2} was reached and then cycled in 0.10 mol dm^{-3} sodium sulfate from 0.100 V vs. SCE to 0.200 V vs. SCE at different scan rates.

3.3.5.5 Ion Exchange Properties and Doping Levels of the PPy-SCD Film

It has been well reported in the literature that the electropolymerisation of pyrrole with fairly large dopant anions results in these dopant anions being permanently trapped in the polymer matrix[57, 58]. In this situation, the electroneutrality during the reduction of the polymer is maintained by the flux of mobile cations in the electrolyte solution into the polymer matrix. Consequently, the polymer system behaves like a cation exchange material and its ion transport properties are dominated by cation transport. In contrast, PPy films doped with small anions exhibit anion exchange properties. This is because the small anions are expelled from the polymer film during the reduction process[33, 59].

Electrochemical quartz crystal microbalance (EQCM) was employed to investigate the ion exchange properties of the PPy-SCD film. Essentially the change in the mass (Δm) can be computed from the change in the frequency (Δf) of a quartz crystal using Equation 3.18. Here, f_o is the resonant frequency of the crystal prior to a mass change, A is the surface area

of the metal electrodes which sandwich the crystal, μ is the crystal density (2.648 g cm^{-3}) and ρ is the sheer modulus (2.947 x 10^{11} g cm^{-1} s^{-2})[60]. A detailed explanation of this technique is given in Section 2.2.3.

$$\Delta f = \frac{-2f_0^2}{A\sqrt{\mu\rho}}\Delta m$$

3.18

In these experiments, the PPy-SCD films were electrochemically deposited at a potential of 0.800 V vs. Ag/AgCl to a final charge of 1.20 x 10^{-2} C cm^{-2} from a 0.20 mol dm^{-3} solution of pyrrole dissolved in 0.01 mol dm^{-3} sulfonated β-cyclodextrin. The films were then cycled in a fresh chloride electrolyte and both the mass and current were recorded.

It can be seen from Figure 3.23 that the mass increases as the PPy-SCD film is reduced in a 0.10 mol dm^{-3} NaCl solution. The increase in the mass can be attributed to the incorporation of sodium cations into the polymer matrix to balance the charge. Assuming that the entire mass increase is due to the insertion of Na$^+$ and that solvent, H$_2$O, intake is negligible, then approximately 2.3 μg and 1.0 x 10^{-7} moles of Na$^+$ are incorporated during the reduction step. This indicates that the PPy-SCD film is indeed a cationic exchange material. This result is not surprising, considering that the sulfonated β-cyclodextrin is a large immobile polyanion. The cationic exchange properties of the PPy-SCD film have previously been reported by Temsamani *et al.*[38] and Bidan *et al.*[39] by means of EDX and optical beam deflection measurements, respectively.
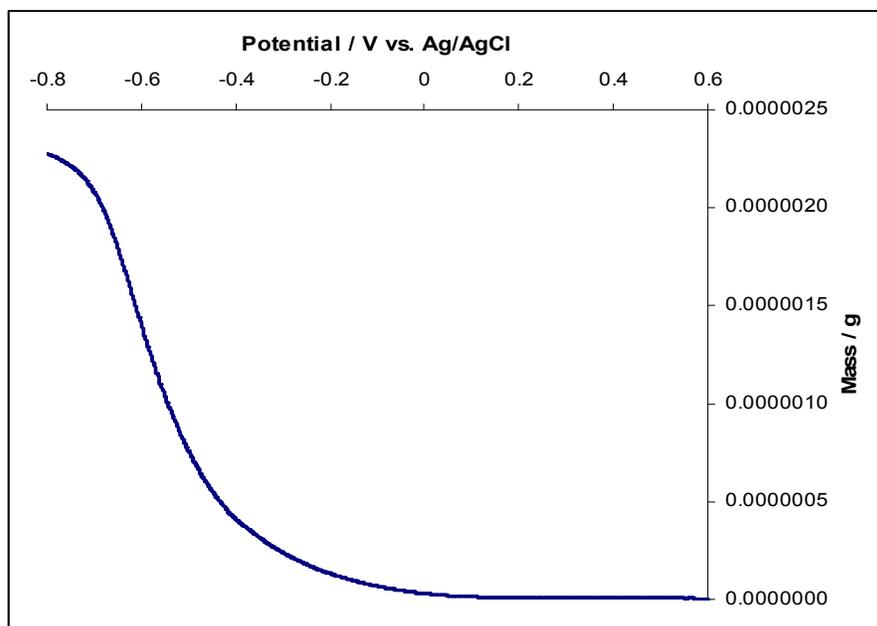
Figure 3.23: Plot of mass versus potential for PPy-SCD cycled in a 0.10 mol dm^{-3} NaCl solution, pH ~ 6.0 at 50 mV s^{-1}. The PPy-SCD film was formed in 0.20 mol dm^{-3} pyrrole and 0.01 mol dm^{-3} sulfonated β-cyclodextrin at 0.800 V vs. Ag/AgCl until a charge of 1.20 x 10^{-2} C cm^{-2}.

EQCM was also used to try and determine the approximate doping levels of the PPy-SCD film. This was done by monitoring the growth of the PPy-SCD film. During PPy electrosynthesis, the amount and nature of the anions doped into the polymer depends on the composition of the monomer electrolyte. In this study the monomer electrolyte consisted of simply pyrrole and sulfonated β-cyclodextrin, therefore the sulfonated β-cyclodextrin is the only anion that can dope the oxidised polymer. The variation in the mass of the polymer (Δm) can be related to the variation in the anodic charge (ΔQ) by Equation 3.19. In this equation M(Py) is the molar mass of the monomer, x is the number of dopant molecules per monomeric unit, M(SCD) is the molar mass of the dopant and F is Faraday's constant[61]. This equation assumes that the current efficiency for the electropolymerisation of the monomer is 100% and that no water is incorporated into the film[62].

$$\frac{\Delta m}{\Delta Q} = \frac{M(Py) + xM(SCD)}{(2+x)F} \qquad\qquad 3.19$$

The value of x for PPy has been reported to range from 0.2 to 0.5 dopant molecules per pyrrole unit[63]. For simple dopant anions such as HSO_4^-, the value of x is approximately 0.33, i.e., a 1:3 doping level[61]. Using this value of x and the experimentally measured charge, the theoretical mass associated with the formation of the PPy-SCD film was calculated and then compared to the mass recorded experimentally. Since the degree of sulfonation on the commercially available sulfonated β-cyclodextrin varies from 7-11, theoretical masses for each situation were considered. In addition, it was assumed that all the anionic sulfonated groups participated in the charge balance, i.e., there are no free sulfonated groups.

It is clearly evident from Figure 3.24 that the experimental mass is much lower than each of the calculated masses. This suggests that the doping level in the film cannot be the simple 1:3 relationship. Again, this result is not unexpected bearing in mind the size of the sulfonated β-cyclodextrin.

In general, dopant anions that are relatively large will have a lower x value. For example, 0.2 molecules of poly(styrene-4-sulfonate) are required for one molecule of pyrrole in the doping of PPy[64]. To investigate the effect of a lower x value on the mass of the PPy-SCD polymer, doping levels of 0.20 and 0.125 were substituted into Equation 3.19, presuming that nine of the β-cyclodextrin sites were sulfonated and that each of these anionic sulfonated groups participated in the doping process. It is clear from Figure 3.25 that the calculated mass of the polymer film decreases as x decreases and that the mass of the polymer film when x is equal to 0.125 is getting very close to that of the experimental mass. This value of x corresponds to one sulfonated β-cyclodextrin for every eight pyrrole units and suggests that the dopant ratio is in the vicinity of this value.

It is important to stress that calculating the exact number of dopant molecules incorporated into the polymer is not possible. This is because the number of sulfonated groups on the β-cyclodextrin is variable. Also, the equation used to calculate the theoretical mass does not take into account solvent participation and it also assumes the current efficiency for the electropolymerisation of pyrrole is 100%. Moreover, it is difficult to estimate the number of sulfonated groups on any given cyclodextrin that are involved in charge compensation and

doping and that are free and uncompensated. Nevertheless, the results presented clearly show that a simple 1:3 dopant ratio between the sulfonated β-cyclodextrin and the pyrrole is not possible in these PPy-SCD films. A good estimate is a 1:8 or a 12.5% doping level.
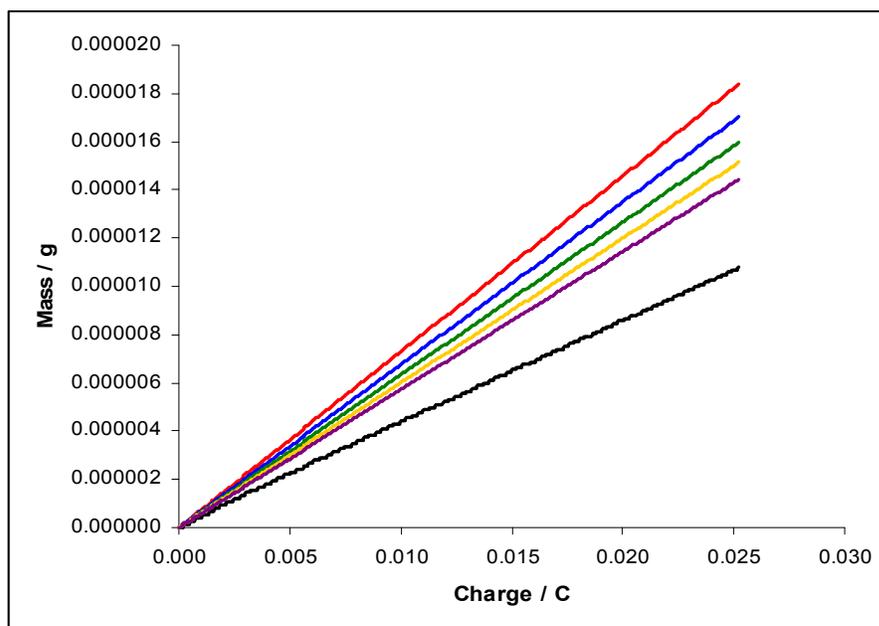

Figure 3.24: Plot of mass versus charge for the ▬ experimental mass of PPy-SCD and the theoretical mass of PPy-SCD calculated presuming that *x* was equal to 0.33 and the number of sulfonated sites on the β-cyclodextrin involved in doping were ▬ 7, ▬ 8, ▬ 9, ▬ 10 and ▬ 11.

An important consideration is the number of sulfonated groups on each cyclodextrin that takes part in the doping process. If all the sulfonated groups on the β-cyclodextrin were involved in charge balance this would not only place strain on the cyclodextrin but also lead to considerable steric hindrance in the polymer matrix. Therefore, it is highly probable that some free sulfonated groups are present within the polymer. As already discussed in Section 3.3.5.4, the high capacitance measured for the PPy-SCD film is consistent with a number of 'free' sulfonated groups. Furthermore, Naoi and co-workers[55], in studying the doping of PPy with mono-, di- and tri-sulfonated naphthalene, concluded that the PPy-trisulfonate doped films possessed free sulfonated groups without any charge compensation.
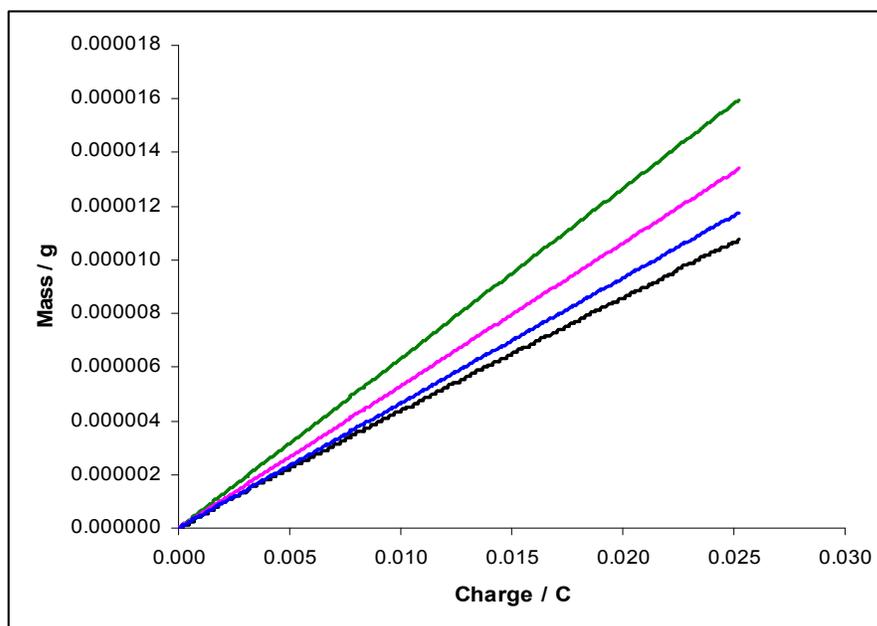
Figure 3.25: Plot of mass versus charge for the ▬ experimental mass of PPy-SCD and the theoretical mass of PPy-SCD calculated presuming that the 9 sulfonated groups on the β-cyclodextrin are involved in the doping with *x* equal to ▬ 0.33, ▬ 0.20 and ▬ 0.125.

3.3.6 Optimisation of the Dopamine Signal at the PPy-SCD Films

The results from Section 3.3.2 show that the PPy-SCD modified electrode exhibits excellent catalytic behaviour towards DA, facilitating the oxidation and reduction of the compound, and that the signal is attributable to the sulfonated β-cyclodextrin. To optimise the response of the DA at the PPy-SCD modified electrode, several parameters were altered and the resulting DA signal was recorded. Factors such as the potential that the polymer films are grown at and the charge that the polymer films are grown to were considered. Various other parameters were also investigated and these are discussed in detail below.

3.3.6.1 The Working Electrode

PPy-SCD films were electrosynthesised on Pt, GC and Au electrodes using an oxidation potential of 0.800 V vs. SCE. The response of 1.0 x 10^{-3} mol dm^{-3} DA was examined at each of the modified electrodes using cyclic voltammetry, as illustrated in Figure 3.26.

From this figure it can be seen that the DA is oxidised at the same potentials at each of the three polymer-modified electrodes. However, the oxidation and reduction peaks at the unmodified electrodes occur at different potentials, Figure 3.1. In addition, identical currents are observed at each of the modified electrodes which are highlighted in Table 3.4, along with the oxidation peak potentials. This indicates that the substrate on which the PPy-SCD film is electrodeposited has no influence on the oxidation of DA. Furthermore, these results show clearly that the DA is not interacting with, or being oxidised, at the underlying metal substrate.
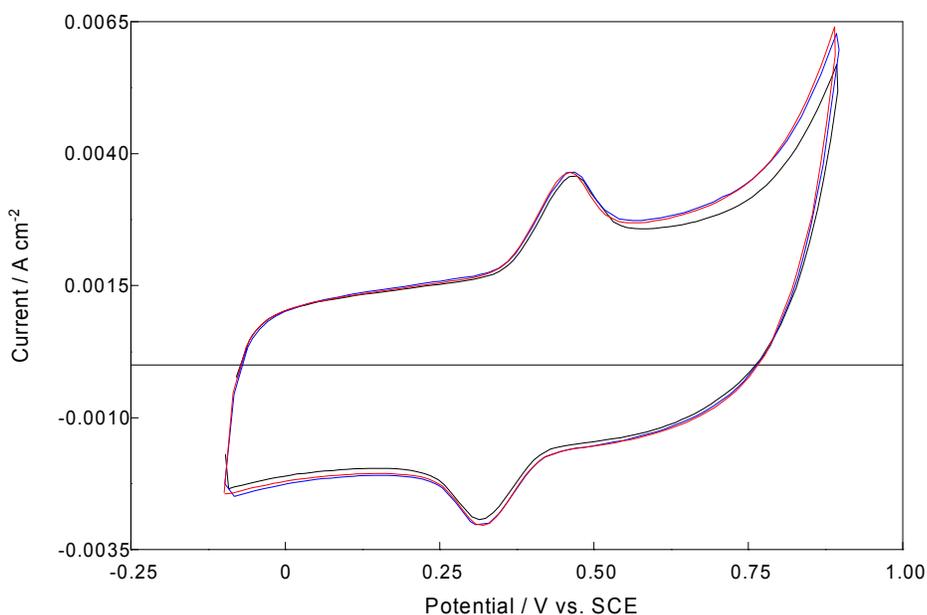
Figure 3.26: Cyclic voltammograms recorded in a 1.0 x 10^{-3} mol dm^{-3} DA / 0.10 mol dm^{-3} Na$_2$SO$_4$ solution (pH~6.0) at a scan rate of 100 mV s^{-1} for a PPy-SCD films electrosynthesisd at 0.800 V vs. SCE on ▬ Pt, ▬ GC and ▬ Au electrodes from 0.20 mol dm^{-3} pyrrole / 0.01 mol dm^{-3} sulfonated β-cyclodextrin (pH~6.0).

Table 3.4: Peak oxidation currents and potentials obtained at each of the PPy-SCD modified electrodes cycled at 100 mV s^{-1} in a 1.0 x 10^{-3} mol dm^{-3} DA / 0.10 mol dm^{-3} Na$_2$SO$_4$ solution, pH ~ 6.0.

Electrode	I_p^A / A cm^{-2}	E_p^A / V vs. SCE
Pt	0.001742	0.4599
Au	0.001737	0.4602
GC	0.001745	0.4609

3.3.6.2 The Concentration of Pyrrole

The concentration of pyrrole in the monomer solution was varied to determine its influence, if any, on the ability of the subsequent polymer films to sense DA. From Figure 3.27 and Table 3.5, it can be seen that similar currents and potentials are recorded for concentrations of 5.0 x 10^{-2} mol dm^{-3} pyrrole and higher, indicating no significant effect. However, no DA signal is observed from a PPy-SCD film electrosynthesised from an aqueous solution of 1.0 x 10^{-2} mol dm^{-3} pyrrole / 1.0 x 10^{-2} mol dm^{-3} sulfonated β-cyclodextrin. It is obvious from Figure 3.27 that the voltammogram recorded by this polymer film in the DA solution is at a significantly lower current than the other polymer films. The reason for this is that there is not enough monomer in the solution to form the conducting polymer. Instead, short chain oligomers, which will be less conducting and have a lower doping level, will form. The formation of these short chain polymers, resulting from an inadequate concentration of monomer in solution, has been well documented in the growth of conducting polymers, particularly, polyaniline.

Table 3.5: Peak oxidation currents and potentials obtained at each PPy-SCD modified electrode cycled at 100 mV s^{-1} in a 1.0 x 10^{-3} mol dm^{-3} DA / 0.10 mol dm^{-3} Na$_2$SO$_4$ solution, pH ~ 6.0. The PPy-SCD films were electrosynthesised at 0.800 V vs. SCE from the monomer solution with 0.01 mol dm^{-3} sulfonated β-cyclodextrin to a constant charge of 0.24 C cm^{-2}.

Concentration of Pyrrole / mol dm^{-3}	I_p^A / A cm^{-2}	E_p^A / V vs. SCE
0.01	-	-
0.05	0.001728	0.4561
0.10	0.001751	0.4628
0.20	0.001742	0.4599
0.30	0.001737	0.4635
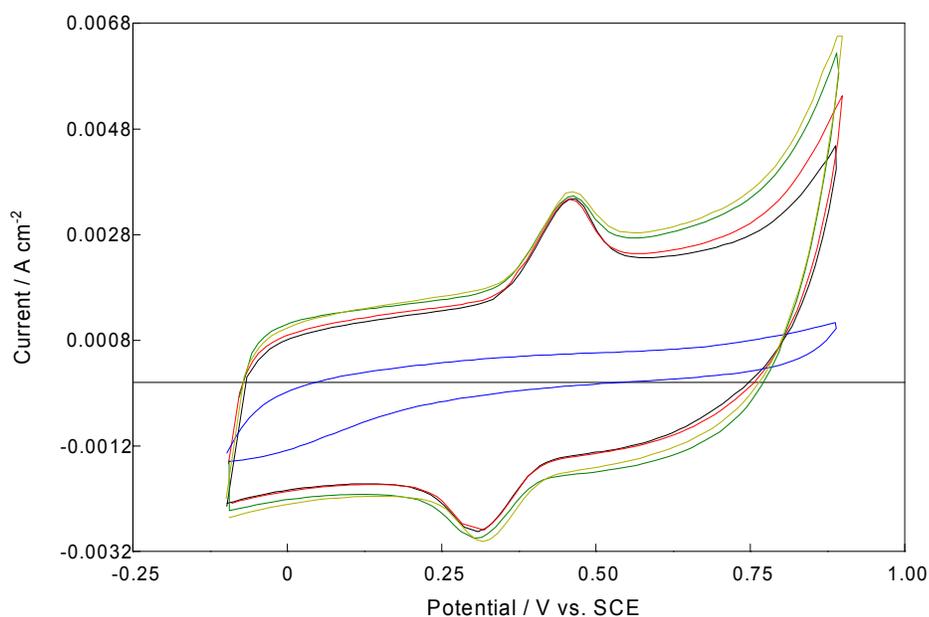
Figure 3.27: Cyclic voltammograms recorded in a 1.0 x 10^{-3} mol dm^{-3} DA / 0.10 mol dm^{-3} Na$_2$SO$_4$ solution (pH~6.0) at a scan rate of 100 mV s^{-1} for PPy-SCD modified electrodes electrosynthesised on a Pt electrode at 0.800 V vs. SCE from 0.01 mol dm^{-3} sulfonated β-cyclodextrin and ▬ 0.01 mol dm^{-3} pyrrole ▬ 0.05 mol dm^{-3} pyrrole ▬ 0.10 mol dm^{-3} pyrrole ▬ 0.20 mol dm^{-3} pyrrole and ▬ 0.30 mol dm^{-3} pyrrole.

3.3.6.3 The Concentration of Sulfonated β-Cyclodextrin

PPy-SCD films were electrosynthesised on a Pt electrode using an oxidation potential of 0.800 V vs. SCE from monomer solutions where the concentration of pyrrole was kept constant and the concentration of sulfonated β-cyclodextrin was varied. The resultant polymers were cycled in a 1.0 x 10^{-3} mol dm^{-3} DA solution and it can be seen from Figure 3.28 and Table 3.6 that the concentration of sulfonated β-cyclodextrin in the monomer solution has little effect on the DA signal. This suggests that the PPy-SCD film formed at the lower sulfonated β-cyclodextrin concentration of 5.0 x 10^{-4} mol dm^{-3} has similar properties, of porosity and doping levels, as the films generated at the higher concentrations of 5.0 x 10^{-2} mol dm^{-3}.
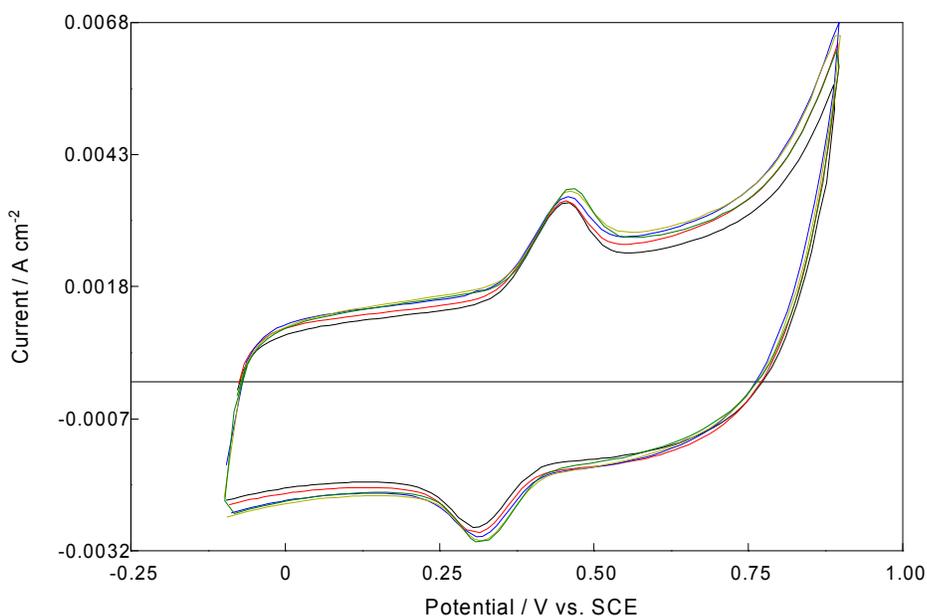
Figure 3.28: Cyclic voltammograms recorded in a 1.0 x 10^{-3} mol dm^{-3} DA / 0.10 mol dm^{-3} Na$_2$SO$_4$ solution (pH~6.0) at a scan rate of 100 mV s^{-1} for PPy-SCD modified electrodes electrosynthesisd on a Pt electrode at 0.800 V vs. SCE from 0.20 mol dm^{-3} pyrrole and ▬ 5.0 x 10^{-4} mol dm^{-3} sulfonated β-cyclodextrin ▬ 1.0 x 10^{-3} mol dm^{-3} sulfonated β-cyclodextrin, ▬ 5.0 x 10^{-3} mol dm^{-3} sulfonated β-cyclodextrin, ▬ 1.0 x 10^{-2} mol dm^{-3} sulfonated β-cyclodextrin and ▬ 5.0 x 10^{-2} mol dm^{-3} sulfonated β-cyclodextrin.

Table 3.6: Oxidation peak currents and potentials obtained at each PPy-SCD modified electrode cycled, at 100 mV s^{-1} in a 1.0 x 10^{-3} mol dm^{-3} DA / 0.10 mol dm^{-3} Na$_2$SO$_4$ solution, pH ~ 6.0. The PPy-SCD films were electrosynthesised at 0.800 V vs. SCE from 0.20 mol dm^{-3} pyrrole with sulfonated β-cyclodextrin as the supporting electrolyte to a constant charge of 0.24 C cm^{-2}.

Concentration of Sulfonated β-Cyclodextrin / mol dm^{-3}	I_p^A / A cm^{-2}	E_p^A / V vs. SCE
5.0 x 10^{-4}	0.001746	0.4604
1.0 x 10^{-3}	0.001732	0.4550
5.0 x 10^{-3}	0.001735	0.4582
1.0 x 10^{-2}	0.001742	0.4599
5.0 x 10^{-2}	0.001745	0.4610

3.3.6.4 The Applied Potential

To investigate the effect of potential, polymer films were electrosynthesised using various oxidation potentials ranging from 0.400 V vs. SCE to 1.000 V vs. SCE. In all cases, the electropolymerisation charge was maintained constant at 0.24 C cm^{-2}, to maintain a near constant film thickness. Then, these polymer films were cycled in a 5.0 x 10^{-3} mol dm^{-3} DA solution and the peak oxidation current of DA was monitored as a function of the potential used in forming the polymer films. These peak oxidation currents are presented in Table 3.7, and plotted as a function of the formation potential in Figure 3.29. It can be seen that the DA oxidation currents increase until a potential greater than or equal to 0.800 V vs. SCE is applied, at which point the oxidation currents decrease significantly. As the potential is increased more PPy will be oxidised and therefore more sulfonated β-cyclodextrin can dope the polymer. Consequently, more DA will be oxidised and this accounts for the increase in the DA peak oxidation currents as the potential is increased. The fact that the currents decrease rapidly after a growth potential greater than 0.800 V vs. SCE has been applied indicates that the polymer films are now over-oxidised. This in turn reduces the ability of the PPy-SCD film to detect DA. It is well known that PPy films can

be over-oxidised at high positive potentials resulting in the loss of conductivity[65]. This fact is investigated further in Section 3.3.6.10.

It can also be seen from Table 3.7 that the DA peak oxidation currents shift to more positive potentials as the potential applied is increased. This shift in the peak potential becomes more significant when a potential greater than or equal to 0.800 V vs. SCE is applied. The shift in peak potential from growing the polymer films at 0.400 V vs. SCE to 0.800 V vs. SCE can be attributed to the fact that more DA will be oxidised at the PPy-SCD film as the applied potential is increased. As a result, a larger and broader peak will be produced by the polymer films grown at the higher potentials. The reason why the peak potentials increase dramatically at applied potentials greater than or equal to 0.800 V vs. SCE is almost certainly because the PPy-SCD film is over-oxidised and as a result the detection of DA is hindered.
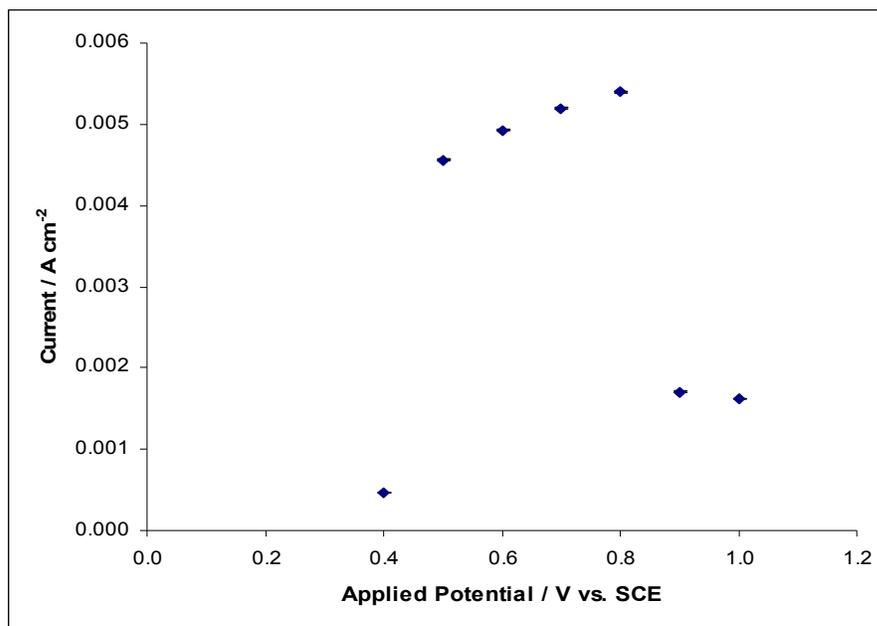
Figure 3.29: Peak oxidation current from the oxidation of 5.0 x 10^{-3} mol dm^{-3} DA at the PPy-SCD film plotted as a function of the potential applied during the growth of the PPy-SCD film (*n*=2). The PPy-SCD films were grown from a monomer solution containing 0.20 mol dm^{-3} pyrrole / 0.01 mol dm^{-3} sulfonated β-cyclodextrin at various potentials until a charge of 0.24 C cm^{-2} was reached.

Table 3.7: Peak oxidation currents and potentials obtained at each PPy-SCD modified electrode, for the oxidation of DA in a 5.0 x 10^{-3} mol dm^{-3} DA / 0.10 mol dm^{-3} Na_2SO_4 solution, cycled at 100 mV s^{-1}. The PPy-SCD films were electrosynthesised from 0.20 mol dm^{-3} pyrrole and 0.01 mol dm^{-3} sulfonated β-cyclodextrin to a constant charge of 0.24 C cm^{-2}.

Applied Potential / V vs. SCE	I_p^A / A cm^{-2}	E_p^A / V vs. SCE
0.4	0.000466 ± 0.000006	0.4447 ± 0.0007
0.5	0.004562 ± 0.000006	0.4874 ± 0.0008
0.6	0.004922 ± 0.000008	0.4886 ± 0.0008
0.7	0.005198 ± 0.000008	0.4911 ± 0.0009
0.8	0.005393 ± 0.000006	0.4923 ± 0.0008
0.9	0.001702 ± 0.000085	0.6327 ± 0.0112
1.0	0.001620 ± 0.000081	0.6410 ± 0.0253

As clearly indicated from these data, the optimum DA signal is obtained when potentials between 0.500 V vs. SCE and 0.800 V vs. SCE are used in the formation of the PPy-SCD film. Therefore, an applied potential of 0.800 V vs. SCE was used to electrodeposit the PPy-SCD films.

3.3.6.5 The Presence of a Supporting Electrolyte in the Monomer Solution

The results from Sections 3.3.4 and 3.3.5.1 confirm that a polymer film grown from a monomer solution containing pyrrole, sulfonated β-cyclodextrin and NaCl is doped with both sulfonated β-cyclodextrin and chloride anions. To examine what effect this has on the DA signal, PPy-SCD films grown in the presence and absence of 0.10 mol dm^{-3} NaCl were cycled in a 1.0 x 10^{-3} mol dm^{-3} DA solution, Figure 3.30. The resulting oxidation peak currents and potentials are shown in Table 3.8. From this table it can be seen that the DA signal produced by the polymer film grown from the monomer solution containing NaCl is

lower than the signal generated by the polymer film grown in the absence of NaCl. In addition, the DA peak potential occurs at a lower potential. This would not be expected, if according to Temsamani *et al.*[38], the anion from the supporting electrolyte is selectively excluded as a dopant anion. Seeing that the oxidation peak currents and potentials detected at a PPy-SCD film grown from a monomer solution containing NaCl are lower than those generated at the PPy-SCD film grown from a solution without NaCl, proves that a certain amount of the chloride anions from the supporting electrolyte are incorporated into the polymer in conjunction with the sulfonated β-cyclodextrin.
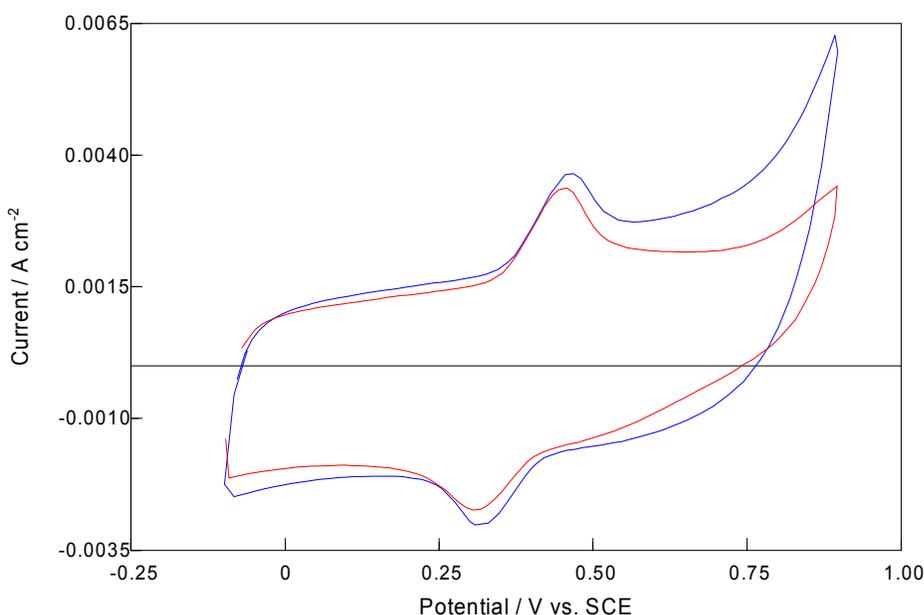
Figure 3.30: Cyclic voltammograms of a PPy-SCD modified electrode electrosynthesisd on a Pt electrode at 0.800 V vs. SCE from a monomer solution containing — 0.20 mol dm^{-3} pyrrole / 0.01 mol dm^{-3} sulfonated β-cyclodextrin and — 0.20 mol dm^{-3} pyrrole / 0.01 mol dm^{-3} sulfonated β-cyclodextrin / 0.10 mol dm^{-3} NaCl, cycled in a 1.0 x 10^{-3} mol dm^{-3} DA / 0.10 mol dm^{-3} Na$_2$SO$_4$ solution (pH~6.0). Scan rate = 100 mV s^{-1}.

Table 3.8: Oxidation peak currents and potentials obtained at each PPy-SCD modified electrode for the oxidation of DA in a 1.0 x 10^{-3} mol dm^{-3} DA / 0.10 mol dm^{-3} Na$_2$SO$_4$ solution.

	I_p^A / A cm^{-2}	E_p^A / V vs. SCE
No Supporting Electrolyte	0.001742 ± 0.000015	0.4599 ± 0.0006
0.10 mol dm^{-3} NaCl Supporting Electrolyte	0.001648 ± 0.000021	0.4540 ± 0.0008

3.3.6.6 The Electrochemical Window

The upper and lower potential limits were varied in order to investigate the effect of the electrochemical window on the DA signal. From Figure 3.31 it can be seen that the DA signal increases as the upper potential limit is increased. There is a three-fold increase in the peak oxidation current on increasing the upper potential from 0.600 to 0.900 V vs. SCE. Once the polymer is synthesised it is likely that the cyclodextrin cavities contain monomer or oligomers and when the upper potential limit is low, these remain within the cavity blocking access to the DA. On the other hand, they are likely to be oxidised and released from the cavity with the application of the higher potentials. This is consistent with the higher rates of DA oxidation, as the cavities are now free to bind with the DA.

A similar trend holds true as the lower potential limit is decreased, as evidenced from Figure 3.32. Again, there is an increase in the peak current on cycling the polymer to lower applied potentials. However, in this case the increase in the oxidation current is less significant. Based on these findings, an electrochemical window of -0.100 V vs. SCE to 0.900 V vs. SCE was selected. These upper and lower limits were chosen based on the fact that cycling the PPy-SCD modified electrodes past an upper potential of 0.900 V vs. SCE would cause the polymer films to over-oxidise, while using potentials lower than -0.100 V vs. SCE would introduce sodium cations into the polymer as it is reduced. As shown in Section 3.5.5.5, the PPy-SCD film facilitates cation exchange, with the ingress of Na$^+$ observed from about -0.200 V vs SCE to -0.800 V vs SCE, Figure 3.23. Indeed, as shown in Figure 3.33, a clear decline in the DA signal is observed when the PPy-SCD film is

cycled down to -0.800 V vs. SCE at which point a high influx of Na^+ is observed, Figure 3.23, Section 3.5.5.5.
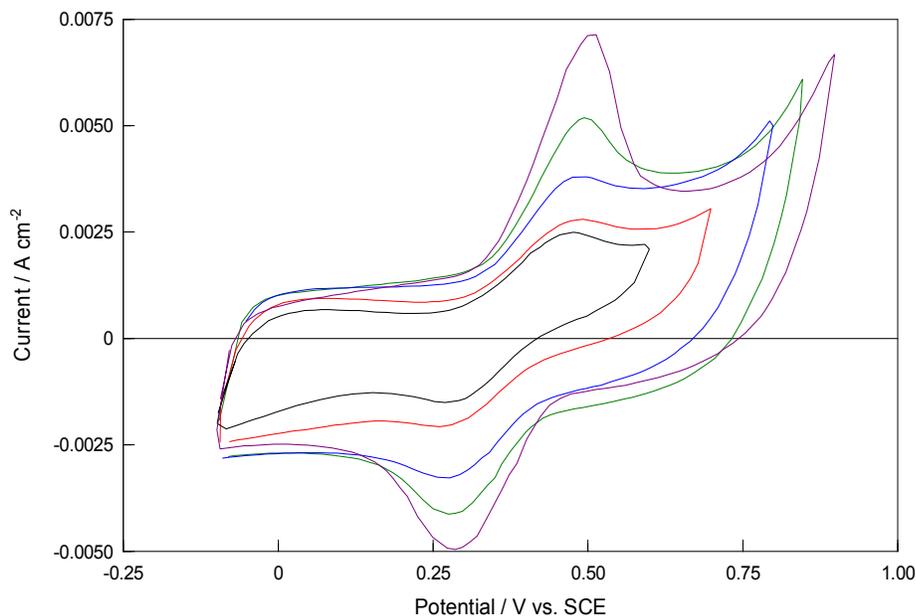

Figure 3.31: Cyclic voltammograms of a PPy-SCD modified electrode electrosynthesisd on a Pt electrode at 0.800 V vs. SCE from 0.20 mol dm^{-3} pyrrole / 0.01 mol dm^{-3} sulfonated β-cyclodextrin in a 5.0 x 10^{-3} mol dm^{-3} DA / 0.10 mol dm^{-3} Na$_2$SO$_4$ solution (pH~6.0) from ▬ -0.100 V vs. SCE to 0.600 V vs. SCE, ▬ -0.100 V vs. SCE to 0.700 V vs. SCE, ▬ -0.100 V vs. SCE to 0.800 V vs. SCE, ▬ -0.100 V vs. SCE to 0.850 V vs. SCE and ▬ -0.100 V vs. SCE to 0.900 V vs. SCE. Scan rate = 100 mV s^{-1}.

It is clearly evident from Figure 3.33 that cycling the PPy-SCD film to potentials where the film is reduced gives rise to a poor DA signal with a reduction in the peak oxidation current and an anodic shift in the peak oxidation potential. In addition to the influx of Na^+ this observation is also consistent with the ladder-doped model proposed by Ingram *et al.*[56] for PPy doped with sulfonated naphthalene. In this study, the authors argued that the rungs of the ladder are held in place by the positively charged PPy backbone. On reduction of the polymer, the structure collapses and the anions are free to bind with the incoming cations. If the PPy-SCD film has a similar structure, then a more open porous structure would be held in place when the polymer is maintained in the oxidised state, enabling the DA molecules to gain easy access to the cyclodextrins. On the other hand, when the polymer is

reduced and the open porous structure collapses, access to the cyclodextrins is now hindered. Even though the polymer is re-oxidised on the forward cycle, the open-porous structure facilitating efficient ion migration within the polymer cannot be regenerated fully. Indeed, Ingram *et al.*[56] suggest that the structural collapse of their polymer is best averted if the polymer is never fully reduced.
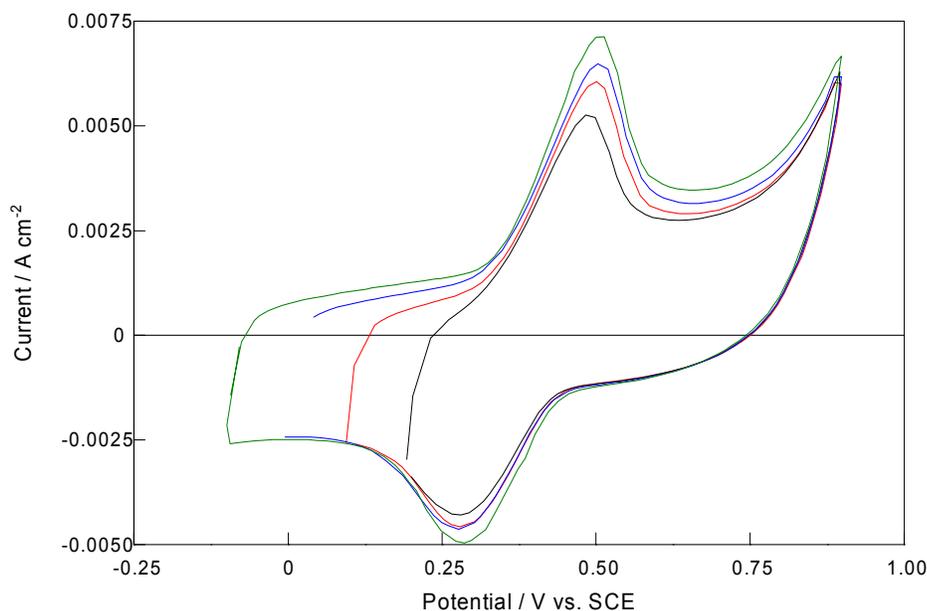
Figure 3.32: Cyclic voltammograms of a PPy-SCD modified electrode electrosynthesisd on a Pt electrode at 0.800 V vs. SCE from 0.20 mol dm^{-3} pyrrole / 0.01 mol dm^{-3} sulfonated β-cyclodextrin in a 5.0 x 10^{-3} mol dm^{-3} DA / 0.10 mol dm^{-3} Na$_2$SO$_4$ solution (pH~6.0) from ▬ 0.200 V vs. SCE to 0.900 V vs. SCE, ▬ 0.100 V vs. SCE to 0.900 V vs. SCE, ▬ 0.000 V vs. SCE to 0.900 V vs. SCE and ▬ -0.100 V vs. SCE to 0.900 V vs. SCE. Scan rate = 100 mV s^{-1}.
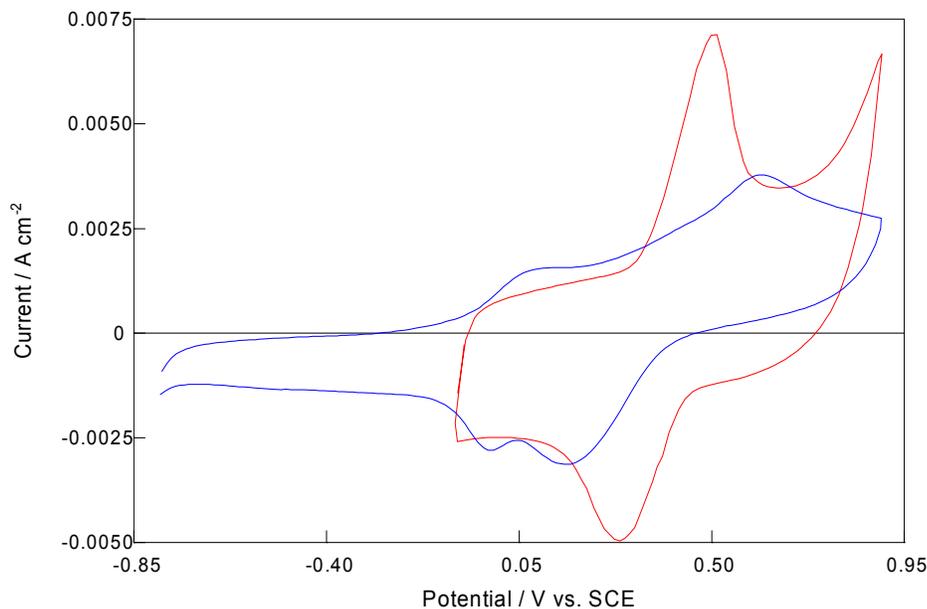
Figure 3.33: Cyclic voltammograms of a PPy-SCD modified electrode electrosynthesisd on a Pt electrode at 0.800 V vs. SCE from 0.20 mol dm^{-3} pyrrole / 0.01 mol dm^{-3} sulfonated β-cyclodextrin in a 5.0 x 10^{-3} mol dm^{-3} DA / 0.10 mol dm^{-3} Na$_2$SO$_4$ solution (pH~6.0) from ▬ -0.100 V vs. SCE to 0.900 V vs. SCE and ▬ -0.800 V vs. SCE to 0.90 V vs. SCE. Scan rate = 100 mV s^{-1}.

3.3.6.7 The Effect of Scan Rate on the Dopamine Signal

The effect of scan rate on the DA signal was investigated using cyclic voltammetry. The PPy-SCD films were grown at 0.800 V vs SCE and then cycled in a 5.0 x 10^{-3} mol dm^{-3} DA solution at different scan rates, in the range of 25 mV s^{-1} to 200 mV s^{-1}. Typical data are shown in Figure 3.34, where it is clear that the scan rate has a prominent influence on both the anodic and cathodic peak currents of DA with the peak currents increasing as the scan rate is increased.

These data were first analysed using the power law relationships in Equations 3.20 and 3.21,

$$I_{p,a} = kv^x \qquad\qquad 3.20$$

$$\log (I_{p,a}) = \log (k) + x\log(v) \qquad\qquad 3.21$$

where, $I_{p,a}$ is the oxidation peak current (A cm^{-2}), k is the proportional constant, v is the scan rate (mV s^{-1}) and x is the exponent of the scan rate. If the charge transport is diffusion controlled then a plot of the logarithm of the current as a function of the logarithm of the scan rate will be linear with a slope of ~0.5. Conversely, if the charge transport is electron transfer controlled then a plot of the logarithm of the current as a function of the logarithm of the scan rate will be linear with a slope of ~1.0[66]. These diagnostic features were applied to the oxidation of DA at the PPy-SCD film using the data presented in Figure 3.34.

The logarithm of the peak oxidation current was computed and plotted as shown in Figure 3.35. Figure 3.35 shows that such a plot is linear with a slope of 0.45. This value is close to the theoretical value of 0.5 indicating that the oxidation of DA is a diffusion-controlled process.
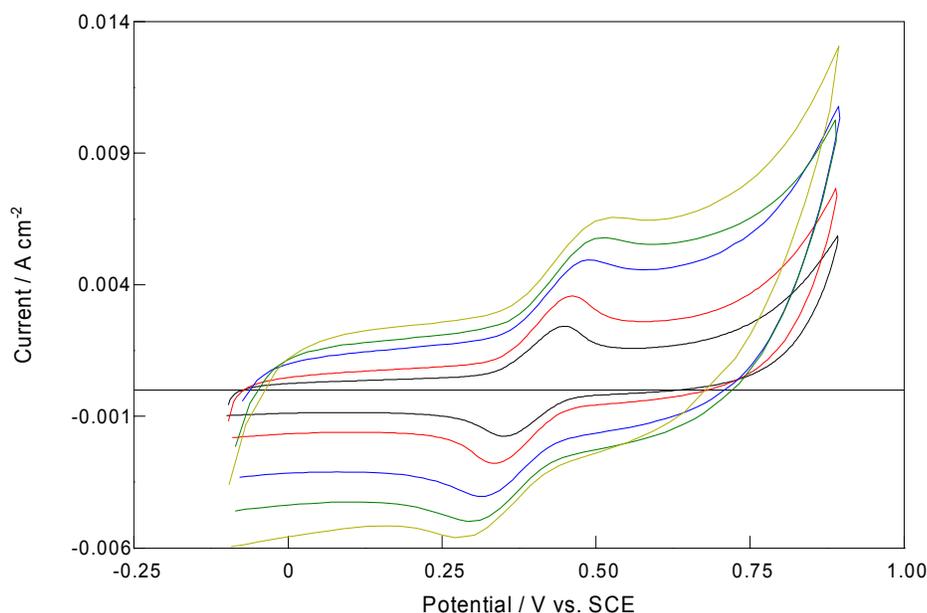
Figure 3.34: Cyclic voltammograms of the PPy-SCD modified electrodes in 5.0 x 10^{-3} mol dm^{-3} DA / 0.10 mol dm^{-3} Na$_2$SO$_4$ at a scan rate of ▬ 200 mV s^{-1}, ▬ 150 mV s^{-1}, ▬ 100 mV s^{-1}, ▬ 50 mV s^{-1} and ▬ 25 mV s^{-1}. Electrochemical Window: –0.100 V vs. SCE to 0.900 V vs. SCE. The PPy-SCD films were grown at 0.800 V vs. SCE from 0.20 mol dm^{-3} pyrrole and 0.01 mol dm^{-3} sulfonated β-cyclodextrin until a charge of 0.24 C cm^{-2} was consumed.
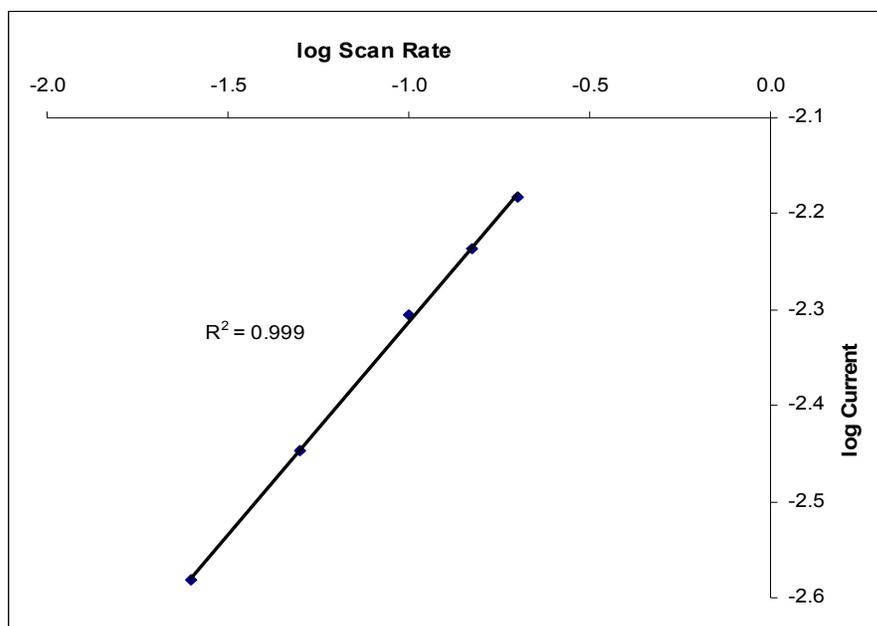
Figure 3.35: Plot of the logarithm of the anodic peak current as a function of the logarithm of the scan rate for the oxidation of 5.0 x 10^{-3} mol dm^{-3} DA in 0.10 mol dm^{-3} sodium sulfate (pH~6.0) at a PPy-SCD film. The PPy-SCD film was grown at 0.800 V vs. SCE from 0.20 mol dm^{-3} pyrrole and 0.01 mol dm^{-3} sulfonated β-cyclodextrin until a charge of 0.24 C cm^{-2} was reached.

The analysis presented in Figure 3.35 is consistent with the diffusion of DA being the rate-determining step in the oxidation of DA. In order to evaluate the diffusion coefficient the anodic peaks currents were plotted as a function of the square root of the scan rate, as shown in Figure 3.36. Two plots are shown in this figure; one gives the peak currents with the background subtracted, while the other gives the total current at the peak potential. A linear relationship between the current and the square root of the scan rate is observed in both cases and this indicates that the oxidation of DA conforms to the Randles-Sevcik equation, Equation 3.22.

$$I_p = (2.69 \text{ x } 10^5)n^{3/2}D^{1/2}v^{1/2}c_o \qquad\qquad 3.22$$

where, I_p is the peak current (A cm^{-2}), n is the electron stoichiometry, D is the diffusion coefficient (cm^2 s^{-1}), v is the scan rate (V s^{-1}) and c_o is the concentration (mol cm^{-3})[60].
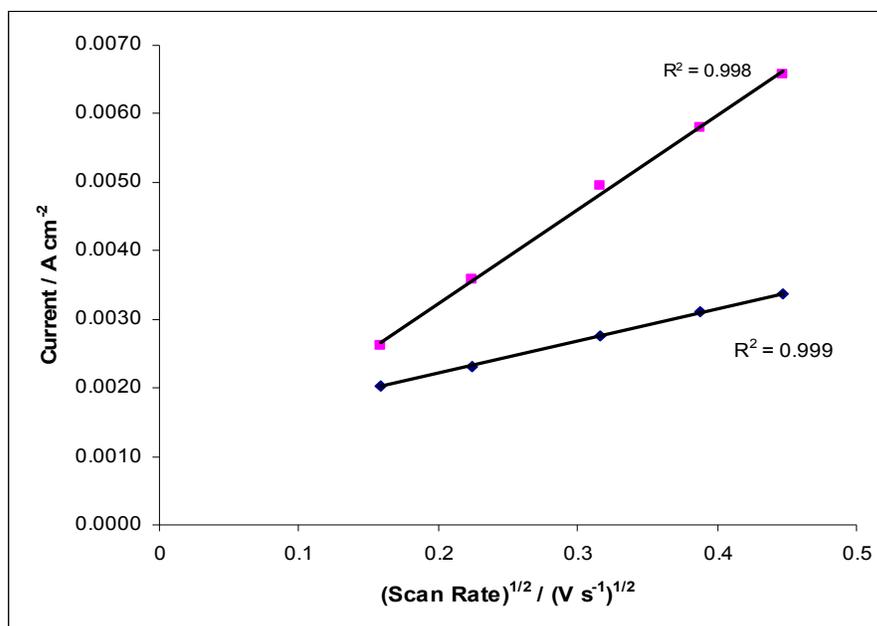
Figure 3.36: The forward peak current as a function of the square root of the scan rate where the currents in ■ have had the background subtracted and the currents in ■ have not had the background subtracted.

Consequently, the diffusion coefficient can be obtained from the slope of the plot. A diffusion coefficient value of 1.52×10^{-6} cm^2 s^{-1} was obtained from the slope of the plot where the background current was subtracted, while a much higher value of 1.29×10^{-5} cm^2 s^{-1} was obtained from the slope of the plot where the total current was plotted. Clearly there is a large variation in the slopes of the plots and the corresponding diffusion coefficients. As shown earlier in Section 3.3.5.4, the PPy-SCD polymer has a very high capacitance and the background current increases considerably at higher scan rates, as clearly evident in Figure 3.24, making the detection of DA more difficult. Based on this fact, the diffusion coefficient of DA can only be estimated as a value which lies in the region of 1.52×10^{-6} cm^2 s^{-1} to 1.29×10^{-5} cm^2 s^{-1}. These values signify that the diffusion of DA is solution based and they compare well to other diffusion coefficient values reported in the literature for DA[67-70], which all range from 10^{-6} to 10^{-5} cm^2 s^{-1}.

3.3.6.8 Reversibility and Kinetics

The reversibility of the system was characterised by comparing the voltammograms to a simple reversible reaction. The peak separation, ΔE_p, for a reversible couple is given by:

$$\Delta E_p = E_p^A - E_p^C = \frac{59}{n} \, \text{mV}$$

$\qquad\qquad\qquad\qquad$ 3.23

where, E_p^A is the peak potential of the oxidation peak, E_p^C is the peak potential of the reduction peak and n is the number of electrons transferred[71]. The ratio of the peak currents for a reversible reaction should be equal to one and the peak potentials should be independent of the scan rate.

The calculated peak separations and the ratio of the peak currents for DA at each of the scan rates are shown in Table 3.9. It can be seen from this table that the peak separations at each of the scan rates are higher than the expected theoretical value of 29.5 mV. Furthermore, the ratio of the peak currents at each scan rate, do not equal one. Moreover, the peak potentials are not independent of scan rate as they increase with increasing scan rate, Table 3.9. This indicates some kinetic limitation in the reaction between the redox sites of the PPy-SCD film and the DA. This kinetic limitation might be associated with the charge propagation within the film, or the chemical interaction between the protonated DA species and the cyclodextrins. However, as shown in Figure 3.36, the oxidation current for DA increases linearly with the square root of the scan rate, suggesting that the reaction is under mass-transfer control. It can be concluded that the electrochemistry of DA at the PPy-SCD modified electrode does not follow ideal reversible behaviour and so is a quasi-reversible process, in agreement with literature reports on the oxidation of DA at other modified electrodes[72, 73].

Table 3.9: Peak oxidation, peak reduction, peak separation and ratio of oxidation and reduction peak currents calculated at various scan rates for the oxidation of DA in a 5.0 x 10^{-3} mol dm^{-3} DA / 0.10 mol dm^{-3} Na$_2$SO$_4$ at a PPy-SCD modified electrode solution. The PPy-SCD films were grown at 0.800 V vs. SCE from 0.20 mol dm^{-3} pyrrole and 0.01 mol dm^{-3} sulfonated β-cyclodextrin until a charge of 0.24 C cm^{-2} was consumed.

Scan Rate / mV s^{-1}	E_p^A / V vs. SCE	E_p^C / V vs. SCE	ΔE_p / mV	I_p^A / I_p^C
25	0.4479	0.3511	97	1.37
50	0.4617	0.3381	124	1.28
100	0.4857	0.3080	178	1.23
150	0.5151	0.2922	223	1.20
200	0.5253	0.2713	254	1.17

In order to obtain some insight into the observed kinetic limitations, further analysis on the oxidation of DA at the PPy-SCD films was performed and the apparent rate constant, k_{DA}, for the oxidation of DA at the film was estimated. This was achieved using rotation disc voltammetry and the Koutecky-Levich equation, Equation 3.24. Here, i_L is the measured limiting current, n is the number of electrons transferred, F is the Faraday constant, A is the electrode area, C_o is the DA concentration, k is the rate constant, Γ is the surface coverage, D is the diffusion coefficient, v is the kinematic viscosity and ω is the rotation speed. According to Equation 3.24 the plot of $1/i_L$ as a function of $1/\omega^{1/2}$ is linear and the rate constant for the oxidation of DA at the PPy-SCD film, k_{DA}, can be obtained from the intercept of this line.

$$\frac{1}{i_L} = \frac{1}{nFAC_ok\Gamma} + \frac{1}{0.62nFAD^{2/3}v^{-1/6}C_o\omega^{1/2}}$$
3.24

The PPy-SCD film was electrodeposited on a Pt rotating disc electrode at 0.800 V vs. SCE until a charge of 0.24 C cm^{-2} had been reached. The electrode was then rotated in a 5.0 x

10^{-3} mol dm^{-3} DA solution at various rotation rates from 200 to 2000 rpm. The limiting current was recorded at 0.700 V vs. SCE for each rotation speed and a Koutecky-Levich plot was generated, Figure 3.37. From this figure it can be seen that a linear Koutecky-Levich relationship exists and consequently the rate constant of the reaction can be determined from the intercept of this line. A value of 1.7 x 10^{-2} cm s^{-1} was obtained for $k\Gamma$ and using the estimated surface coverage from Section 3.3.5.3, 4.3 x 10^{-8} mol cm^{-2}, k was found to be 3.9 x 10^2 mol^{-1} dm^3 s^{-1}. This value for k is reasonably high, indicating a fairly fast electrocatalytic process which is ideal behaviour for any sensor. It also is comparable to the typical rate constants reported in the literature for the oxidation of DA[74-77], which can range from 10^2 to 10^5 M^{-1} s^{-1}. However, the vast majority of the rate constants lie in the 10^2 mol^{-1} dm^3 s^{-1} region[74, 75, 78].
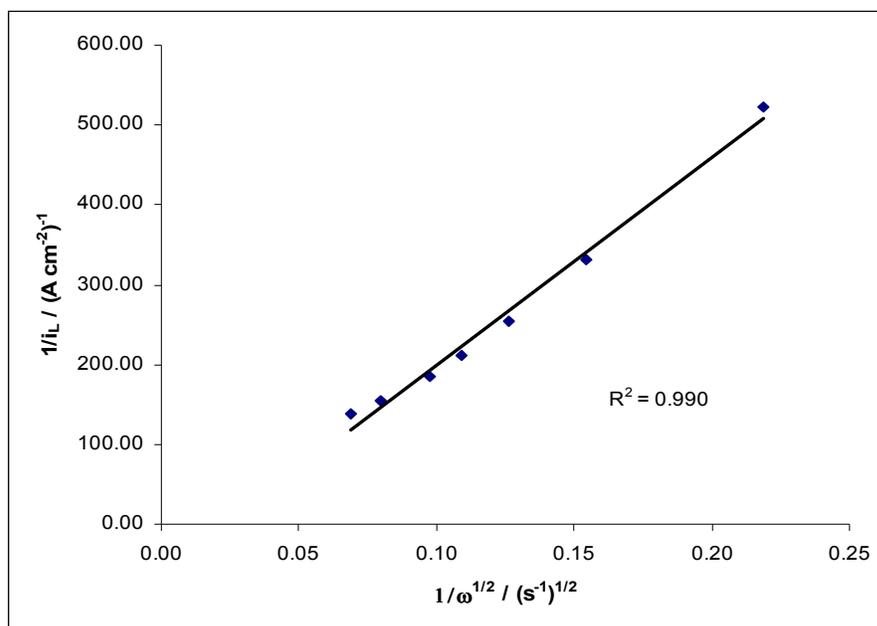
Figure 3.37: Koutecky-Levich plot for 5.0 x 10^{-3} mol dm^{-3} DA / 0.10 mol dm^{-3} Na$_2$SO$_4$ (pH~6.0) at a PPy-SCD modified electrode.

3.3.6.9 The Effect of pH

The effect of the solution pH on the electrochemical signal of DA was examined in the pH range of 3.0 – 6.0. From Table 3.10 it can be seen that there is no real difference in the oxidation peak currents. The oxidation peak potentials do shift slightly to lower values as the pH is increased, Table 3.10. However, this shift is not overly significant given that the shift in the oxidation peak potential per pH unit is only 4.6 mV.

Applying the Nernst equation to the oxidation of DA, gives Equation 3.25. According to Equation 3.25, the peak potential due to the $2e^-/2H^+$ oxidation of DA should vary with pH to give a slope value of 59.1 mV. Obviously, under these experimental conditions, the proton participation in the DA oxidation reaction does not follow normal Nernstian behaviour.

$$E = E° + \frac{0.0591}{2} log \frac{[DA - o - quinone][H^+]^2}{[DA]}$$

3.25

Differential pulse voltammetry was subsequently employed to see if a similar result would be obtained using this more sensitive technique. The parameters used for the differential pulse voltammetry were; pulse amplitude, 50 mV, pulse width 0.07 s, sampling width, 0.03 s, pulse period, 0.30 s and scan rate 5 mV s^{-1}. The ensuing peak potentials are shown in Table 3.11. Again, it can be seen from this table that the peak potentials do not shift as the pH is altered. It is obvious from these results that the DA response at the PPy-SCD modified electrode does not depend on the pH of the solution when the pH is varied from 3.0 to 6.0. However, the DA oxidation peak potentials do shift considerably when the pH of the DA / Na$_2$SO$_4$ solution is lowered further. For example, an oxidation peak potential of 0.5660 V vs. SCE was recorded for a 5.0 x 10^{-3} mol dm^{-3} DA / Na$_2$SO$_4$ solution (pH~1.9) using cyclic voltammetry. This corresponds to a potential difference of 60.5 mV when the pH is lowered from 3.0 to 2.0, which is very close to the theoretical value of 59.1 mV at 25 °C.

The lack of a pH dependence between pH values of 3.0 and 6.0 for the oxidation of DA is unusual. One factor that can be ruled out in this analysis is the level of protonated DA in

solution as the pH is varied from 2.0 to 6.0. This is because the DA will be more or less 100% protonated in this pH region, Figure 3.38. Accordingly, a protonation effect should not be a concern in the analysis. The effect of the pH on the dissociation of DA was calculated using Equation 3.26, a derivation of Equation 5.13 in Chapter 5, Section 5.3.1.

$$[DA^+] = \frac{100}{1+10^{pH-pKa}}$$
3.26
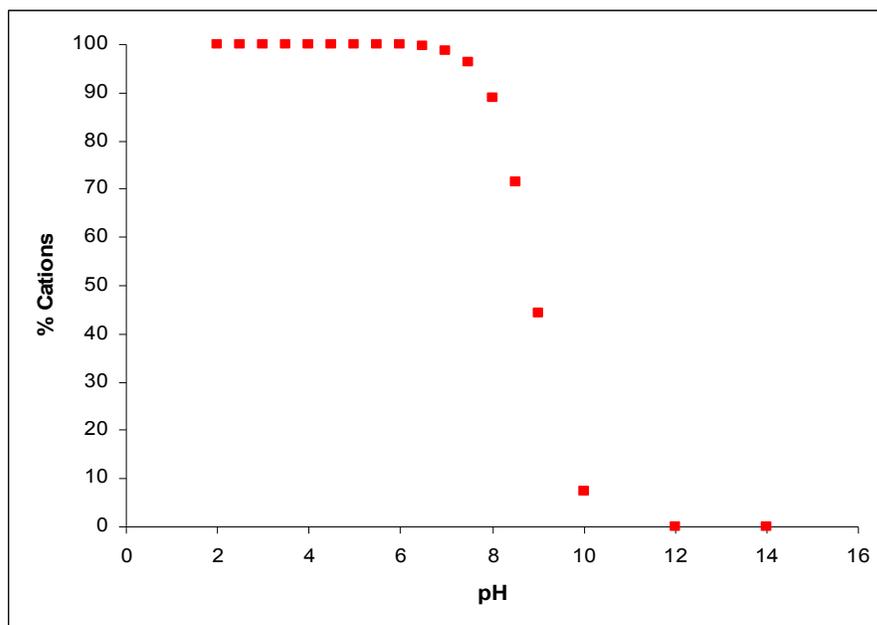
Figure 3.38: The percentage of cations as a function of pH for DA. The percentage of cations for a given pH value was calculated by substituting various pH values into Equation 3.26.

A possible explanation for the lack of a pH dependence between pH 3.0 and 6.0 can be made by considering both the kinetics and the Nernst equation. The Nernst equation, Equation 3.25 (where the concentrations represent the electrode surface concentrations), will be obeyed provided the electron transfer kinetics is sufficiently fast so that equilibrium is attained at each potential applied. It appears at pH 6.0 and using a scan rate of 100 mV s^{-1} that the oxidation of DA is not sufficiently facile on the time scale of the experiment. To test this hypothesis, the effect of decreasing the pH of the DA solution to 2.0 on the rate constant, *k*, was evaluated using the same procedure as outlined in Section 3.3.6.8. Under

these conditions, a value of 2.5×10^3 M^{-1} s^{-1} was determined, which is approximately 4 times higher than the k value obtained when the pH of the DA / Na_2SO_4 solution was 6.0. With this higher rate of electron transfer, equilibrium is achieved on the time scale of the experiment and the Nernst equation is obeyed. This is one possible explanation for the difference observed at pH 2.0 and from pH 3.0 to 6.0. However, this is a complex process which requires further kinetic analysis.

Table 3.10: Oxidation currents and potentials obtained at each PPy-SCD modified electrode for a 5.0×10^{-3} mol dm^{-3} DA / 0.10 mol dm^{-3} Na_2SO_4 solution using cyclic voltammetry at 100 mV s^{-1}. The PPy-SCD films were grown at 0.800 V vs. SCE from 0.20 mol dm^{-3} pyrrole and 0.01 mol dm^{-3} sulfonated β-cyclodextrin until a charge of 0.24 C cm^{-2} was consumed.

pH	I_p^A / A cm^{-2}	E_p^A / V vs. SCE
3.0	0.005385	0.5055
4.0	0.005369	0.5009
5.0	0.005300	0.4967
6.0	0.005393	0.4923

Table 3.11: Oxidation potentials obtained at each PPy-SCD modified electrode for a 5.0×10^{-3} mol dm^{-3} DA / 0.10 mol dm^{-3} Na_2SO_4 solution using differential pulse voltammetry; pulse amplitude, 50 mV, pulse width 0.07 s, sampling width, 0.03 s, pulse period, 0.30 s and scan rate 5 mV s^{-1}. The PPy-SCD films were grown at 0.800 V vs. SCE from 0.20 mol dm^{-3} pyrrole and 0.01 mol dm^{-3} sulfonated β-cyclodextrin until a charge of 0.24 C cm^{-2} was consumed.

pH	E_p^A / V vs. SCE
3.0	0.4100
4.0	0.4100
5.0	0.4100
6.0	0.4100

3.3.6.10 Over-Oxidation and Reduction of the PPy-SCD Film

Cyclic voltammetry was used to investigate whether or not the PPy-SCD film was capable of detecting DA when it was over-oxidised or reduced and if so was the sensing better than at the standard oxidised film. From Figure 3.39 it can be seen that when the polymer film is held at an oxidation potential of 1.00 V vs. SCE for 10 min it loses its ability to detect DA with the DA response at the over-oxidised PPy-SCD film comparable to the response at a bare Pt electrode, Figure 3.1, Section 3.3.1. This is not surprising as the overoxidised PPy film is highly porous.

The DA signal from PPy-SCD films that were held for 10 min at a reduction potential of -0.250 V vs. SCE, -0.500 V vs. SCE and -1.000 V vs. SCE are illustrated in Figure 3.40. From this figure it can be seen that holding the polymer film at a reduction potential of -1.000 V vs. SCE for 10 min results in a very poor DA signal. Under these conditions, the PPy-SCD is reduced prior to cycling in the DA-containing solution. This is in agreement with the results obtained in Section 3.3.6.6, which show that reduction of the polymer gives rise to poor DA oxidation currents. As the holding potential is increased to -0.500 V vs. SCE and then further to -0.250 V vs. SCE, this leads to partially oxidised PPy-SCD films and the DA oxidation current is now higher and the oxidation peak potential is lower.

Nevertheless, it is clear that the DA signal recorded at each of these PPy-SCD films is not as good as the response at the standard PPy-SCD film. Therefore, it can be concluded that the PPy-SCD film detects DA best when it is in the oxidised state.
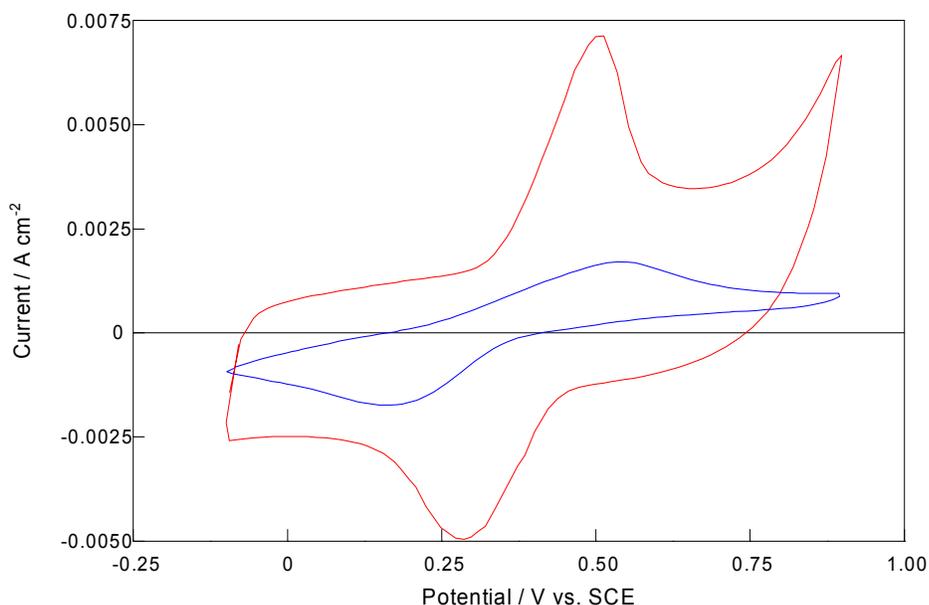
Figure 3.39: Cyclic voltammograms of a — PPy-SCD modified electrode in a 5.0 x 10^{-3} mol dm^{-3} DA / 0.10 mol dm^{-3} Na$_2$SO$_4$ solution (pH~6.0) and a — PPy-SCD modified electrode electrosynthesisd where the film was subsequently held at 1.000 V vs. SCE for 10 min before cycling in a 5.0 x 10^{-3} mol dm^{-3} DA / 0.10 mol dm^{-3} Na$_2$SO$_4$ solution (pH~6.0). Scan rate = 100 mV s^{-1}. Both films were grown from a monomer solution containing 0.20 mol dm^{-3} pyrrole / 0.01 mol dm^{-3} sulfonated β-cyclodextrin at 0.800 V vs. SCE.
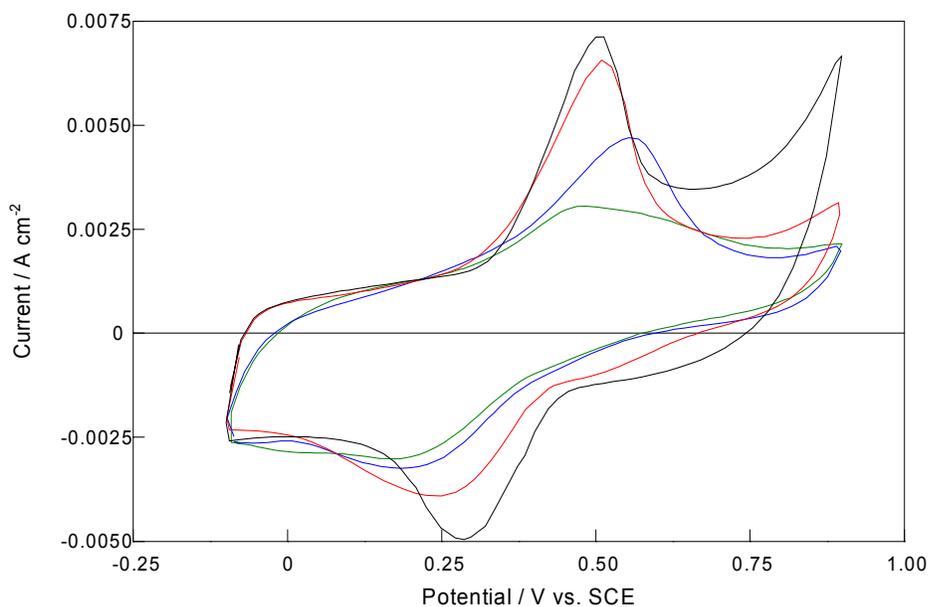
Figure 3.40: Cyclic voltammograms of PPy-SCD films in a 5.0 x 10^{-3} mol dm^{-3} DA / 0.10 mol dm^{-3} Na$_2$SO$_4$ solution (pH~6.0), Scan rate = 100 mV s^{-1}. Films were electrosynthesisd at 0.800 V vs. SCE from a monomer solution containing 0.20 mol dm^{-3} pyrrole / 0.01 mol dm^{-3} sulfonated β-cyclodextrin. Films were reduced at a potential of — -0.250 V vs. SCE, — -0.500 V vs. SCE and — -1.000 V vs. SCE for 10 min prior to analysis, and — no prior reduction.

3.3.6.11 The Electropolymerisation Charge

To inspect the effect of polymer thickness, PPy-SCD films were electrosynthesised on a Pt electrode at 0.800 V vs. SCE until various charges, ranging from 0.24 C cm^{-2} to 1.19 C cm^{-2} were reached. Then, the polymers were cycled in the DA solution and the peak current and potentials were recorded. The peak current is plotted as a function of the electropolymerisation charge in Figure 3.41, while the peak currents and corresponding peak potentials are given in Table 3.12. From Figure 3.41 it can be seen that the optimum DA signal is acquired when a charge of 0.32 C cm^{-2} is used. The peak oxidation current initially increases with charge, reaching a maximum value at 0.32 C cm^{-2}, at which point there is a dramatic fall in the peak currents. This result is unusual in view of the fact that the porosity of a polymer film generally increases as the thickness of the film is increased[79]. Consequently, the surface area that DA can react at will also increase which should result in higher DA currents however this was not the case. The reason why the currents decrease at the higher charges may be connected with the longer polymerisation times need to generate the higher charges. For example, a 160 s polymerisation period is required to generate a charge of 1.20 C cm^{-2}, compared to 43 s to give a charge of 0.32 C cm^{-2}. The results presented in Section 3.3.6.10 show clearly that the DA response at a PPy-SCD film is very weak when the polymer is held at a high oxidation potential for a given length of time. Therefore, the polymer films that are grown at 0.800 V vs. SCE for longer periods of time will have more over-oxidised polymer and accordingly will have an inferior DA signal.

In addition, the potential at which the oxidation of DA takes place is shifted to higher values with increasing charge, as highlighted in Table 3.12. These results clearly show that the polymers grown to higher charges are less efficient in oxidising DA.

Table 3.12: Oxidation currents and potentials obtained at each PPy-SCD modified electrode for a 1.0 x 10^{-3} mol dm^{-3} DA / 0.10 mol dm^{-3} Na$_2$SO$_4$ solution, pH = 6.0, using cyclic voltammetry at 100 mV s^{-1}. The PPy-SCD films were grown at 0.800 V vs. SCE from 0.20 mol dm^{-3} pyrrole and 0.01 mol dm^{-3} sulfonated β-cyclodextrin.

| Charge / C cm^{-2}	I_p^A / A cm^{-2}	E_p^A / V vs. SCE
0.24	0.001742	0.4599
0.28	0.001870	0.4635
0.32	0.001976	0.4679
0.40	0.001739	0.4792
0.56	0.001738	0.4845
0.72	0.001701	0.4895
1.19	0.001632	0.4824
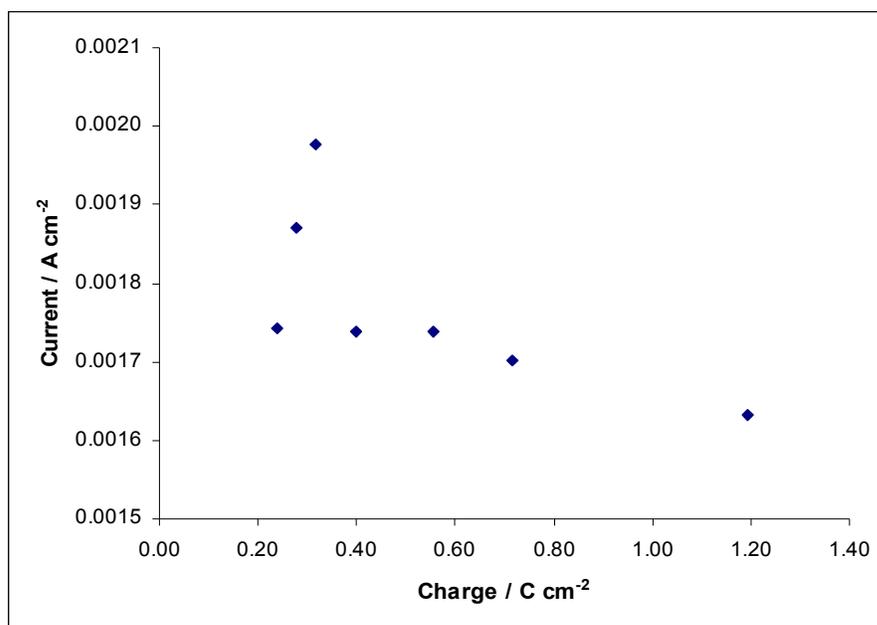
Figure 3.41: The forward peak current plotted as a function of the electropolymerisation charge. Peak currents were measured by cycling the PPy-SCD films in 1.0 x 10^{-3} mol dm^{-3} DA / 0.10 mol dm^{-3} Na$_2$SO$_4$, pH ~ 6.0, at 100 mV s^{-1}. The PPy-SCD films were grown at 0.800 V vs. SCE from 0.20 mol dm^{-3} pyrrole and 0.01 mol dm^{-3} sulfonated β-cyclodextrin.

3.3.6.12 Influence of Oxygen Levels

From searching the literature it can be seen that removal of dissolved oxygen from the solutions is standard practice in the characterisation of most sensors[80-82]. Therefore to inspect if dissolved oxygen had any effect on the DA signal the monomer solutions, the background solutions and the DA solutions were deoxygenating with nitrogen for 15 min and the sensing performance was compared with data recorded without any deoxygenation. From Figure 3.42 it can be seen that purging the solutions with nitrogen does not increase the magnitude or the reversibility of the DA signal and thus dissolved oxygen has no influence.
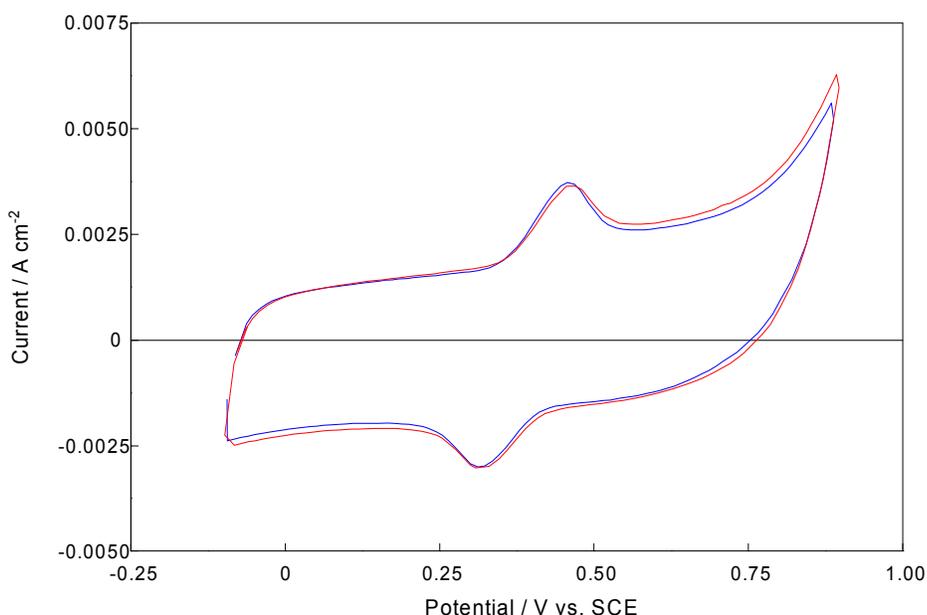
Figure 3.42: Cyclic voltammograms of a ▬ PPy-SCD film electrosynthesisd on a Pt electrode at 0.800 V vs. SCE in a 1.0 x 10^{-3} mol dm^{-3} DA / 0.10 mol dm^{-3} Na$_2$SO$_4$ solution (pH~6.0) where the monomer solution, background solution and DA solution were not deoxygenated with N$_2$ and of a ▬ PPy-SCD film electrosynthesisd on a Pt electrode at 0.800 V vs. SCE in a 1.0 x 10^{-3} mol dm^{-3} DA / 0.10 mol dm^{-3} Na$_2$SO$_4$ solution (pH~6.0) where the monomer solution, background solution and DA solution were deoxygenated with N$_2$. Scan rate = 100 mV s^{-1}. All films were grown from a monomer solution containing 0.20 mol dm^{-3} pyrrole / 0.01 mol dm^{-3} sulfonated β-cyclodextrin.

3.3.6.13 Optimum Conditions

As detailed in the previous sections, various parameters were varied in order to maximise the DA response, using cyclic voltammetry, at the PPy-SCD modified electrode. These parameters and the optimum conditions are summarised in Table 3.13.

Table 3.13: Summary of the parameters varied and the optimum conditions.

Parameter	Optimum Result
Working Electrode	The substrate that the PPy-SCD film is electrosythesised on is not important. Pt electrode chosen.
Concentration of Pyrrole	Concentration of pyrrole only relevant when a very low concentration is used. A concentration of 0.2 mol dm^{-3} was selected.
Concentration of Sulfonated β-Cyclodextrin	Concentration of sulfonated β-cyclodextrin not significant. A concentration of 0.01 mol dm^{-3} was used.
Applied Potential	0.800 V vs. SCE
Presence of a Supporting Electrolyte in the Monomer Solution	Lower DA signal obtained therefore opted for no supporting electrolyte.
Electrochemical Window	-0.100 V vs. SCE to 0.900 V vs. SCE
Scan Rate and Reversibility	Quasi-reversible process 100 mV s^{-1}
Effect of pH	No significant effect on the DA signal. A pH of 6.0 was selected to satisfy physiological conditions.
Over-oxidation and Reduction of the PPy-SCD Film	Both processes resulted in a lower DA signal.
Electropolymerisation Charge	Optimum charge was 0.32 C cm^{-2}
Presence of Oxygen	No effect, therefore the solutions were not deoxygenated.

3.3.7 Dopamine Calibration Curves

In order to obtain detailed information on the sensitivity of the sensor, cyclic voltammetry and constant potential amperometry data were measured using the optimum parameters outlined above.

3.3.7.1 Cyclic Voltammetry

The sensitivity of the PPy-SCD modified electrode was firstly investigated using cyclic voltammetry. The observed peak currents and potentials at each DA concentration are shown in Table 3.14. From this table it can be seen that the oxidation peak currents increase with increasing concentrations of DA and that the oxidation peak potentials shift to more positive potentials. The lowest concentration of DA that could be detected at the PPy-SCD modified electrode using this technique was 4.0×10^{-5} mol dm^{-3}. A curve is obtained over the entire concentration range, Figure 3.43, with a linear region attained at the lower concentrations of DA, Figure 3.44. The linear regression equation was $I_{pa} = 4.00c_{DA}$, with a correlation coefficient of 0.999. The linear response is very important as this is the simplest way to analyse the amount of DA in solution. However, a detection limit of 4.0×10^{-5} mol dm^{-3} DA is very high given that the typical concentrations of DA range from 10^{-8} to 10^{-6} mol dm^{-3} in most biological samples[22]. In a bid to increase the sensitivity of the PPy-SCD modified electrode another technique called constant potential amperometry was employed because amperometry measurements performed under stirred conditions have a much higher current sensitivity than cyclic voltammetry[83].

Table 3.14: Anodic peak currents and potentials (averaged over 5 experiments, error bars provided in Figure 3.43) observed by various DA concentrations in a 0.10 mol dm^{-3} Na$_2$SO$_4$, pH~6.0, supporting electrolyte. The PPy-SCD films were grown with the optimum conditions outlined in Table 3.13.

Conc. of DA / mol dm^{-3}	I_p^A / A cm^{-2}	E_p^A / V vs. SCE
4.0 x 10^{-5}	0.000194	0.4361
5.0 x 10^{-5}	0.000240	0.4390
6.0 x 10^{-5}	0.000283	0.4410
8.0 x 10^{-5}	0.000355	0.4449
1.0 x 10^{-4}	0.000438	0.4469
2.0 x 10^{-4}	0.000600	0.4502
5.0 x 10^{-4}	0.001135	0.4573
7.0 x 10^{-4}	0.001525	0.4621
1.0 x 10^{-3}	0.001976	0.4679
3.0 x 10^{-3}	0.003908	0.4946
5.0 x 10^{-3}	0.005507	0.5060
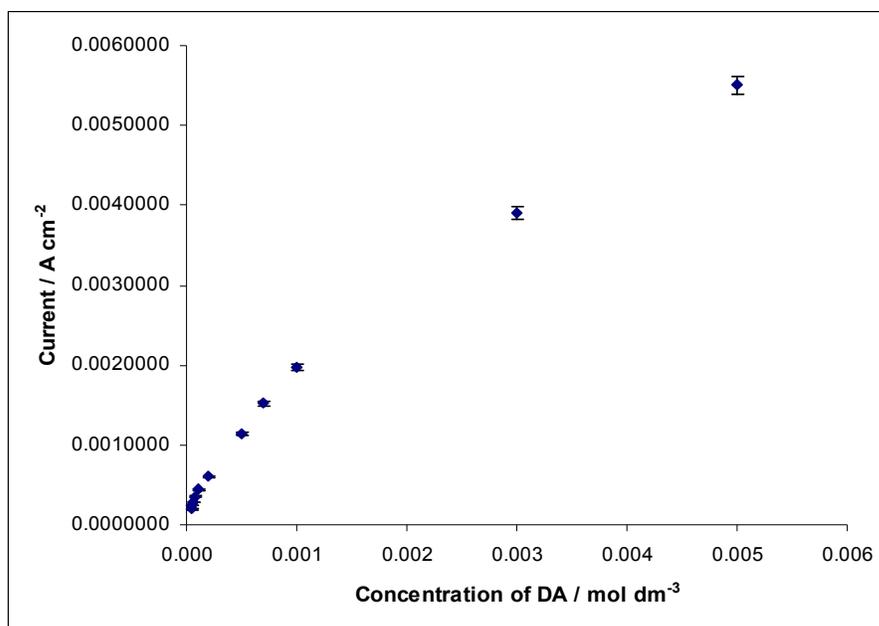
Figure 3.43: The forward peak currents obtained from cyclic voltammetry as a function of the DA concentration (*n*=5). The PPy-SCD films were grown with the optimum conditions outlined in Table 3.13.
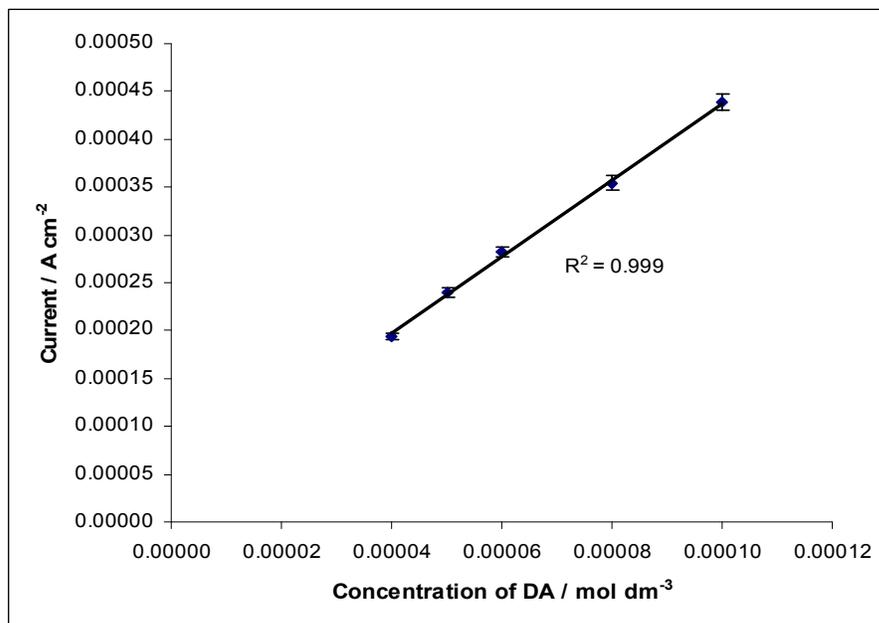
Figure 3.44: The forward peak currents obtained from cyclic voltammetry plotted as a function of the concentration of DA at low concentrations (*n*=5). The PPy-SCD films were grown with the optimum conditions outlined in Table 3.13.

3.3.7.2 Constant Potential Amperometry

A typical plot is presented in Figure 3.45, showing the amperometric response of the PPy-SCD film to successive additions of DA. The response time (time for the signal to increase from 10% to 80%) was less than 3.3 s, which indicates a reasonably quick response of the modified electrode to DA.

The relationship between the measured current and the concentration of DA is shown in Figures 3.46 and 3.47. A curve is obtained over a wide concentration range, Figure 3.46, while a clear linear region is observed at lower concentrations, Figure 3.47. The data in both plots are averaged over four separate determinations. The regression equation was I_{pa} = 0.847c_{DA}, with a correlation coefficient of 0.999. This gives a current to concentration ratio of 0.847 μA μM^{-1}. Using the linear calibration curve, the limit of detection was found to be 3.36 x 10^{-6} mol dm^{-3} DA. This was obtained using the expression,

$$C_m = \frac{3S_b}{m}$$
                                                                                3.27

where C_m is the detection limit, S_b is the standard deviation of the blank response and m is the slope of the linear calibration curve[84].
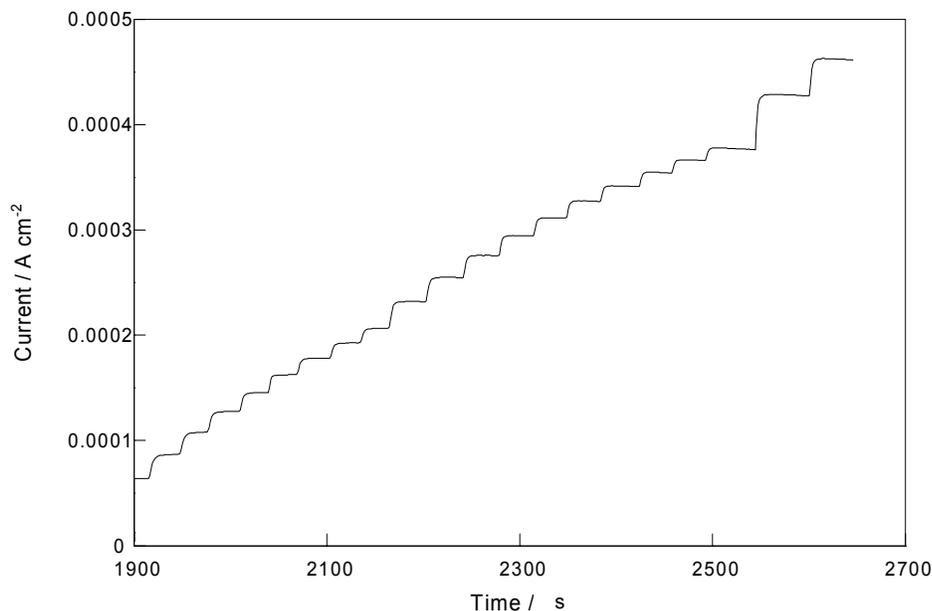
Figure 3.45: Constant potential amperometry, recorded at 0.650 V vs. SCE, for the PPy-SCD films with current plotted as a function of time and as a function of successive additions of DA aliquots ranging from 50 µL to 5 mL. The PPy-SCD films were grown with the optimum conditions outlined in Table 3.12.

Clearly, constant potential amperometry has increased the sensitivity of the sensor dramatically. Although this concentration, 3.36×10^{-6} mol dm^{-3} DA, is not sufficiently low for a viable DA sensor, it may be possible to reach lower detection limits by using pulsed techniques, such as differential pulse voltammetry, or by miniaturising the electrode. The limit of detection of various other electroanalytic methods for DA is shown in Table 3.15. Interestingly, a limit of detection of 4.0×10^{-5} mol dm^{-3} DA, obtained by Ferrreira *et al.*[10], was sufficient enough to detect DA in a pharmaceutical product. Therefore, the PPy-SCD modified electrode may have potential in this area. A means of increasing the sensitivity of the sensor is explored in Chapter 4.
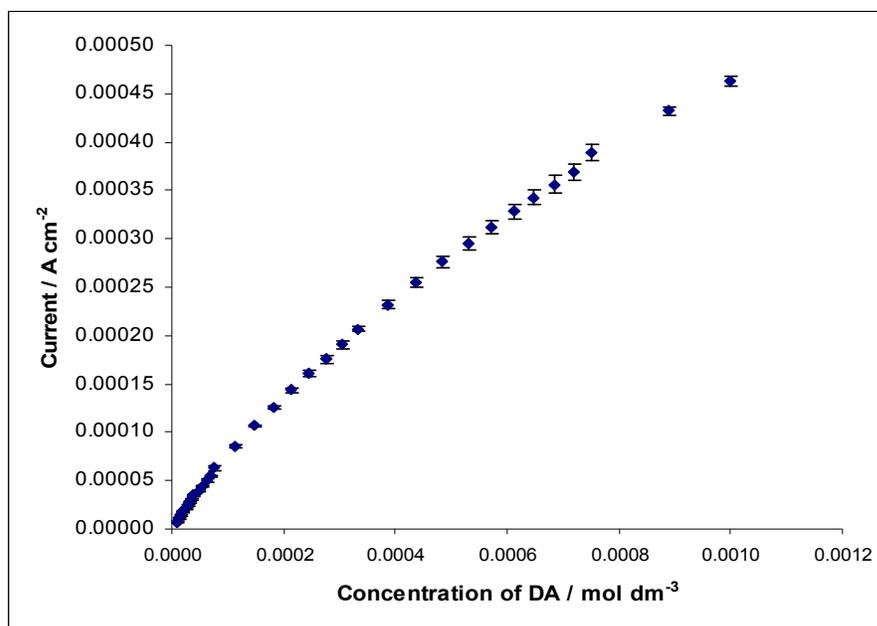
Figure 3.46: Steady-state currents from constant potential amperometry plotted as a function of the DA concentrations (*n*=4). The PPy-SCD films were grown with the optimum conditions outlined in Table 3.13.
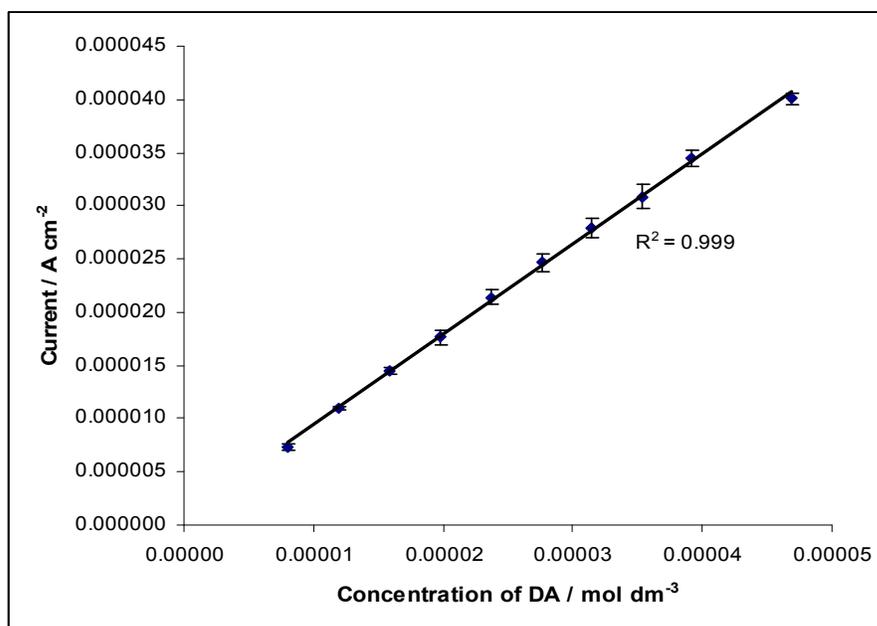
Figure 3.47: Steady-state currents from constant potential amperometry plotted as a function of the linear response of DA at low concentrations (*n*=4). The PPy-SCD films were grown with the optimum conditions outlined in Table 3.13.

Table 3.15: Limit of detection of various other electroanalytic methods for DA.

Reference	Modified Electrode	Limit of Detection / mol dm^{-3}	Method
This Work	Polypyrrole-sulfonated-β-cyclodextrin modified Pt electrode	3.4×10^{-6}	Amperometry
42	Polypyrrole-β-cyclodextrin modified GC electrode	6.0×10^{-6}	Cyclic Voltammetry
85	Multi-wall carbon nanotubes/β-cyclodextrin modified GC electrode	6.7×10^{-6}	Amperometry
86	Bean sprout peroxidase immobilised on a Au electrode modified with self-assembled monolayers of $_L$-cysteine	4.8×10^{-7}	Square Wave Voltammetry
87	β-cyclodextrin-Sonogel-carbon electrode	1.6×10^{-7}	Adsorptive Differential Pulse Voltammetry
88	Self-assembled Au nanoparticles/cysteamine modified GC electrode	4.0×10^{-9}	Differential Pulse Voltammetry
89	β-cyclodextrin/Multi-wall carbon nanotubes/chitosan modified GC electrode	6.0×10^{-8}	Square Wave Voltammetry
90	Screen printed electrode modified with carbon paste (graphite powder dispersed in ionic liquids)	1.2×10^{-6}	Cyclic Voltammetry
91	Zinc oxide/redox mediators modified GC electrode	5.0×10^{-7}	Amperometry
10	Langmuir-Blodgett films from polyaniline/ruthenium complexes on indium-tin-oxide coated glass	5.0×10^{-5}	Cyclic Voltammetry
68	Penicillamine self-assembled monolayer modified Au electrode	4.0×10^{-6}	Cyclic Voltammetry

3.4 Summary of Results

At the beginning of this chapter several PPy films were electrosynthesised at a Pt electrode from monomer solutions containing pyrrole and various dopants and the DA response at each of the PPy films was subsequently examined. PPy films doped with chloride, sulfate, dodecyl sulfate and neutral β cyclodextrin gave very poor responses in comparison to the DA signal at the PPy-SCD film. The fact that the DA response at the PPy-SCD modified electrode is far superior confirms that the sulfonated β-cyclodextrin plays a significant role in the sensing of DA. Furthermore, the peak current measured with pure Pt is considerably smaller confirming that the signal is from the polymer and not the substrate material.

No supporting electrolyte was necessary for the formation of the PPy-SCD film. This ensured that the polymer was only doped by the sulfonated β-cyclodextrin. It was found that both the sulfonated β-cyclodextrin and the anion from the supporting electrolyte doped the polymer when a monomer solution containing both was used. However, the resulting polymer film exhibited a weaker DA oxidation signal. The nucleation of the PPy-SCD film on the Pt was found to be an instantaneous process and the order of the reactions relating to the monomer concentration, α, and to the dopant concentration, β, were found to be 0.7 and 0.4, respectively.

SEM analysis showed an ordered 'cauliflower' structure for the morphology of a PPy-SCD film, while EDX proved that the anionic β-cyclodextrin was indeed incorporated into the polymer film. EDX analysis also verified that both the sulfonated β-cyclodextrin and the anions from a supporting electrolyte were doped into the polymer matrix if a supporting electrolyte was used in the electropolymerisation process. The thickness of a typical PPy-SCD film used in this study was also investigated using a Tencor profilometer. Two identical samples were examined and thicknesses of 510 nm ± 50 nm and 500 nm ± 10 nm were obtained.

The surface coverage of electroactive species at the PPy-SCD film was approximated as 4.3 x 10^{-8} mol cm^{-2} and the capacitance of the PPy-SCD film was found to be 1.2 x 10^{-3} F cm^{-2}. It was also found that the large sulfonated β-cyclodextrin dopant was permanently anchored

within the polymer matrix, giving the system cation exchange properties. In addition, it was established that the doping level in the film was not a simple 1:3 relationship. A much lower doping level close to 1:8 was estimated. Furthermore, the rate constant, k, for the oxidation of DA at the PPy-SCD modified electrode was found the be 3.7 x 10^2 mol^{-1} dm^3 s^{-1} at a pH of 6.0 and 1.2 x 10^3 mol^{-1} dm^3 s^{-1} at a pH of 2.0. These k values are quite high which indicate a reasonably fast electrocatalytic process.

The optimum DA signal was obtained by electrosynthesising the PPy-SCD films at a Pt electrode using an oxidation potential of 0.800 V vs. SCE from an aqueous solution of 0.20 mol dm^{-3} pyrrole and 0.01 mol dm^{-3} sulfonated β-cyclodextrin in H_2O until a charge of 0.32 C cm^{-2} was reached. The resulting polymer films were then cycled in the background electrolyte, Na_2SO_4, between -0.100 V vs. SCE and 0.900 V vs. SCE for 10 cycles at 100 mV s^{-1} and subsequently were transferred to the DA solutions and cycled between the same electrochemical window for the equivalent number of cycles at the same scan rate.

The sensitivity of the sensor was evaluated using both cyclic voltammetry measurements and constant potential amperometry. The lowest concentration of DA that could be detected at the PPy-SCD modified electrode using cyclic voltammetry was 4.0 x 10^{-5} mol dm^{-3} whereas a limit of detection of 3.36 x 10^{-6} mol dm^{-3} DA was found using constant potential amperometry. Although the sensitivity of the PPy-SCD modified electrode is not sufficiently low for a viable *in-vivo* DA sensor, it has excellent selectivity, Chapters 5 and 6, and is particularly easy and cheap to prepare, with an electrosynthesis period of 40 s.

3.5 References

1. M. R. Gluck, L. A. Santana, H. Granson and M. D. Yahr, *Journal of Neural Transmission*, **111**, 713, (2004).
2. J. Lyne, B. D. Kelly and W. T. O'Connor, *Ir. J. Med. Sci.*, **173**, 155, (2004).
3. P. E. M. Phillips, G. D. Stuber, M. Heien, R. M. Wightman and R. M. Carelli, *Nature*, **422**, 614, (2003).
4. R. D. O'Neill, *Sensors*, **5**, 317, (2005).
5. G. S. Wilson and M. A. Johnson, *Chemical Reviews*, **108**, 2462, (2008).
6. E. Koutsilieri, V. ter Meulen and P. Riederer, *Journal of Neural Transmission*, **108**, 767, (2001).
7. Y. Li and X. Lin, *Sens. Actuator B-Chem.*, **115**, 134, (2006).
8. X. Lin, Y. Zhang, W. Chen and P. Wu, *Sens. Actuator B-Chem.*, **122**, 309, (2007).
9. L. Lin, J. Chen, H. Yao, Y. Chen, Y. Zheng and X. Lin, *Bioelectrochemistry*, **73**, 11, (2008).
10. M. Ferreira, L. R. Dinelli, K. Wohnrath, A. A. Batista and O. N. Oliveira, *Thin Solid Films*, **446**, 301, (2004).
11. G. Hu, Y. Liu, J. Zhao, S. Cui, Z. Yang and Y. Zhang, *Bioelectrochemistry*, **69**, 254, (2006).
12. S. M. Chen and W. Y. Chzo, *J. Electroanal. Chem*, **587**, 226, (2006).
13. G. F. Kang and X. Q. Lin, *Electroanalysis*, **18**, 2458, (2006).
14. S. Thiagarajan and S.-M. Chen, *Talanta*, **74**, 212, (2007).
15. P. Shakkthivel and S.-M. Chen, *Biosens. Bioelectron.*, **22**, 1680, (2007).
16. U. E. Majewska, K. Chmurski, K. Biesiada, A. R. Olszyna and R. Bilewicz, *Electroanalysis*, **18**, 1463, (2006).
17. Y. Zhao, Y. Gao, D. Zhan, H. Liu, Q. Zhao, Y. Kou, Y. Shao, M. Li, Q. Zhuang and Z. Zhu, *Talanta*, **66**, 51, (2005).
18. N. J. Ke, S.-S. Lu and S.-H. Cheng, *Electrochemistry Communications*, **8**, 1514, (2006).
19. J. Wang, Y. Wang, H. Lv, F. Hui, Y. Ma, S. Lu, Q. Sha and E. Wang, *J. Electroanal. Chem*, **594**, 59, (2006).
20. J.-B. Raoof, R. Ojani and S. Rashid-Nadimi, *Electrochim. Acta*, **50**, 4694, (2005).
21. R. Hosseinzadeh, R. E. Sabzi and K. Ghasemlu, *Colloids and Surfaces B: Biointerfaces*, **68**, 213, (2009).
22. J. Zheng and X. Zhou, *Bioelectrochemistry*, **70**, 408, (2007).
23. S. Jo, H. Jeong, S. R. Bae and S. Jeon, *Microchem J.*, **88**, 1, (2008).
24. Y. Zhang, G. Jin, Y. Wang and Z. Yang, *Sensors*, **3**, 443, (2003).
25. T. Liu, M. Li and Q. Li, *Talanta*, **63**, 1053, (2004).
26. G. Erdogdu, H. B. Mark and A. E. Karagozler, *Analytical Letters*, **29**, 221, (1996).
27. S. Hou, N. Zheng, H. Feng, X. Li and Z. Yuan, *Anal. Biochem.*, **381**, 179, (2008).
28. R. Zhang, G.-D. Jin, D. Chen and X.-Y. Hu, *Sens. Actuator B-Chem.*, **In Press, Accepted Manuscript**.
29. H. Zhao, Y. Zhang and Z. Yuan, *Anal. Chim. Acta*, **441**, 117, (2001).
30. A. Ramanavicius, A. Ramanaviciene and A. Malinauskas, *Electrochim. Acta*, **51**, 6025, (2006).
31. M. Nishizawa, H. Nozaki, H. Kaji, T. Kitazume, N. Kobayashi, T. Ishibashi and T. Abe, *Biomaterials*, **28**, 1480, (2007).

32.   Y. Z. Zhou, L. J. Zhang, S. L. Chen, S. Y. Dong and X. H. Zheng, *Chinese Chemical Letters*, **20**, 217, (2009).
33.   A. R. Zanganeh and M. K. Amini, *Sens. Actuator B-Chem.*, **135**, 358, (2008).
34.   R. C. Dorf, *CRC Handbook of Engineering Tables*, CRC Press 656, (2004).
35.   C. E. Housecroft and E. C. Constable, *Chemistry: an introduction to organic, inorganic, and physical chemistry*, Pearson Education, 1285, (2006).
36.   R. Chang, *Physical Chemistry for the Biosciences*, University Science Books, 677, (2005).
37.   Y. Li and J. Ouyang, *Synthetic Metals*, **113**, 23, (2000).
38.   K. R. Temsamani, H. B. Mark Jr, W. Kutner and A. M. Stalcup, *J. Solid State Electrochem.*, **6**, 391, (2002).
39.   G. Bidan, C. Lopez, F. Mendes-Viegas and E. Vieil, *Biosens. Bioelectron.*, **9**, 219, (1994).
40.   D. A. Reece, S. F. Ralph and G. G. Wallace, *Journal of Membrane Science*, **249**, 9, (2005).
41.   K. R. Temsamani, O. Ceylan, B. J. Yates, S. Oztemiz, T. P. Gbatu, A. M. Stalcup, H. B. Mark Jr and W. Kutner, *J. Solid State Electrochem.*, **6**, 494, (2002).
42.   N. Izaoumen, D. Bouchta, H. Zejli, M. E. Kaoutit and K. R. Temsamani, *Analytical Letters*, **38**, 1869, (2005).
43.   N. Izaoumen, D. Bouchta, H. Zejli, M. E. Kaoutit, A. M. Stalcup and K. R. Temsamani, *Talanta*, **66**, 111, (2005).
44.   J. Serra Moreno, S. Panero and B. Scrosati, *Electrochim. Acta*, **53**, 2154, (2008).
45.   J. O. Iroh and G. A. Wood, *European Polymer Journal*, **33**, 107, (1997).
46.   B. Scharifker and G. Hills, *Electrochim. Acta*, **28**, 879, (1983).
47.   A. N. Correia, S. A. S. Machado and L. A. Avaca, *J. Electroanal. Chem*, **488**, 110, (2000).
48.   D. Simkunaite, E. Ivaskevic, I. Valsiunas, A. Kalinicenko and A. Steponavicius, *J. Solid State Electrochem.*, **12**, 225, (2008).
49.   G. G. Wallace, G. M. Spinks, L. A. P. Kane-Maguire and P. R. Teasdale, *Conductive Electroactive Polymers: Intelligent Materials Systems*, CRC Press, 237, (2003).
50.   A. F. Diaz, J. I. Castillo, J. A. Logan and W. Y. Lee, *J. Electroanal. Chem*, **129**, 115, (1981).
51.   J. M. Fonner, L. Forciniti, H. Nguyen, J. D. Byrne, Y. F. Kou, J. Syeda-Nawaz and C. E. Schmidt, *Biomedical Materials*, **3**, (2008).
52.   J. Tietje-Girault, C. Ponce de León and F. C. Walsh, *Surface and Coatings Technology*, **201**, 6025, (2007).
53.   A. J. Bard and L. R. Faulkner, *Electrochemical Methods: Fundamentals and Applications*, John Wiley & Sons, Inc, 833, (2001).
54.   V. D. Patake, S. S. Joshi, C. D. Lokhande and O.-S. Joo, *Materials Chemistry and Physics*, **114**, 6, (2009).
55.   S. Suematsu, Y. Oura, H. Tsujimoto, H. Kanno and K. Naoi, *Electrochim. Acta*, **45**, 3813, (2000).
56.   M. D. Ingram, H. Staesche and K. S. Ryder, *Journal of Power Sources*, **129**, 107, (2004).
57.   M. Hepel, *Electrochim. Acta*, **41**, 63, (1996).

58.   G. Bidan, B. Ehui and M. Lapkowski, *Journal of Physics D-Applied Physics*, **21**, 1043, (1988).
59.   R. Ansari Khalkhali, W. E. Price and G. G. Wallace, *Reactive and Functional Polymers*, **56**, 141, (2003).
60.   J. Wang, *Analytical Electrochemistry*, Wiley-Interscience, 250, (2006).
61.   G. Maia, R. M. Torresi, E. A. Ticianelli and F. C. Nart, *Journal of Physical Chemistry*, **100**, 15910, (1996).
62.   C. Debiemme-Chouvy, H. Cachet and C. Deslouis, *Electrochim. Acta*, **51**, 3622, (2006).
63.   A. L. Briseno, A. Baca, Q. Z. Zhou, R. Lai and F. M. Zhou, *Anal. Chim. Acta*, **441**, 123, (2001).
64.   C. K. Baker, Y. J. Qiu and J. R. Reynolds, *Journal of Physical Chemistry*, **95**, 4446, (1991).
65.   L. Özcan, Y. Sahin and H. Türk, *Biosens. Bioelectron.*, **24**, 512, (2008).
66.   Y.-S. Gal, W.-C. Lee, W. S. Lyoo, S.-H. Jin, K. T. Lim, Y.-I. Park and J.-W. Park, *International Journal of Photoenergy* **2008**, 1, (2008).
67.   H.-M. Zhang, N.-Q. Li and Z. Zhu, *Microchem J.*, **64**, 277, (2000).
68.   Q. Wang, D. Dong and N. Li, *Bioelectrochemistry*, **54**, 169, (2001).
69.   K. Farhadi, F. Kheiri and M. Golzan, *Journal of the Brazilian Chemical Society*, **19**, 1405, (2008).
70.   G.-S. Lai, H.-L. Zhang and D.-Y. Han, *Microchim. Acta*, **160**, 233, (2008).
71.   R. Greef, R. Peat, L. M. Peter, D. Pletcher and J. Robinson, *Instrumental Methods in Electrochemistry*, T. J. Kemp, Ellis Horwood Limited, 443, (1985).
72.   P. R. Roy, T. Okajima and T. Ohsaka, *Bioelectrochemistry*, **59**, 11, (2003).
73.   Q. Wang, N. Q. Li and W. Q. Wang, *Analytical Sciences*, **18**, 635, (2002).
74.   H. Razmi, M. Agazadeh and B. Habibi-A, *J. Electroanal. Chem*, **547**, 25, (2003).
75.   D.-M. Zhou, H.-X. Ju and H.-Y. Chen, *J. Electroanal. Chem*, **408**, 219, (1996).
76.   H. X. Ju, J. G. Ni, Y. Gong, H. Y. Chen and D. Leech, *Analytical Letters*, **32**, 2951, (1999).
77.   S. M. Chen, J. Y. Chen and R. Thangamuthu, *Electroanalysis*, **19**, 1531, (2007).
78.   H. Razmi and A. Azadbakht, *Electrochim. Acta*, **50**, 2193, (2005).
79.   S. Carquigny, O. Segut, B. Lakard, F. Lallemand and P. Fievet, *Synthetic Metals*, **158**, 453, (2008).
80.   P. Kannan and S. A. John, *Anal. Biochem.*, **386**, 65, (2009).
81.   D. Zheng, J. Ye, L. Zhou, Y. Zhang and C. Yu, *J. Electroanal. Chem*, **625**, 82, (2009).
82.   S. A. Kumar, C.-F. Tang and S.-M. Chen, *Talanta*, **76**, 997, (2008).
83.   A. Salimi, K. Abdi and G. R. Khayatian, *Microchim. Acta*, **144**, 161, (2004).
84.   D. A. Skoog, F. J. Holler and S. R. Crouch, *Principles of Instrumental Analysis*, Thomson, 1039, (2007).
85.   G. Alarcon-Angeles, B. Perez-Lopez, M. Palomar-Pardave, M. T. Ramirez-Silva, S. Alegret and A. Merkoci, *Carbon*, **46**, 898, (2008).
86.   S. K. Moccelini, S. C. Fernandes and I. C. Vieira, *Sens. Actuator B-Chem.*, **133**, 364, (2008).
87.   N. Izaoumen, L. M. Cubillana-Aguilera, I. Naranjo-Rodríguez, J. L. H.-H. de Cisneros, D. Bouchta, K. R. Temsamani and J. M. Palacios-Santander, *Talanta*, **In Press, Corrected Proof**.

88.   G.-Z. Hu, D.-P. Zhang, W.-L. Wu and Z.-S. Yang, *Colloids and Surfaces B: Biointerfaces*, **62**, 199, (2008).
89.   B. Kong, J. Zeng, G. Luo, S. Luo, W. Wei and J. Li, *Bioelectrochemistry*, **In Press, Corrected Proof**.
90.   D. V. Chernyshov, N. V. Shvedene, E. R. Antipova and I. V. Pletnev, *Anal. Chim. Acta*, **621**, 178, (2008).
91.   C.-F. Tang, S. A. Kumar and S.-M. Chen, *Anal. Biochem.*, **380**, 174, (2008).

Chapter 4

Optimising the Sensitivity and Biocompatibility of the Polypyrrole Sulfonated β-Cyclodextrin Modified Electrode

4.1 Introduction

The ultimate goal of this study is to develop a simple, biocompatible, highly sensitive and selective dopamine (DA) sensor. The results from the previous chapter showed that while the polypyrrole-sulfonated β-cyclodextrin (PPy-SCD) modified electrode was very easy and quick to fabricate, it suffered slightly in sensitivity. The lowest concentration of DA that could be sensed was 3.36×10^{-6} mol dm^{-3}, yet the typical concentrations of DA that exist in most biological samples range from 1.0×10^{-7} mol dm^{-3} to 1.0×10^{-5} mol dm^{-3} DA[1]. In addition to this the characterisation of the PPy-SCD modified electrode was carried out in a sodium sulfate (Na_2SO_4) solution. This is not the most biocompatible electrolyte, especially in terms of an implantable DA sensor.

At the beginning of this chapter a novel approach for increasing the sensitivity of the PPy-SCD film is explored. This involves incorporating nanostructures, in the form of ultrathin fibers generated via electrospinning, into the polymer matrix. The latter stage of the chapter focuses on increasing the biocompatibility of the sensor by applying the PPy-SCD modified electrode to the detection of DA in a phosphate buffered solution. It was found that the electrolyte used for sensing DA at the PPy-SCD modified electrode plays a central role and has a major influence on the peak currents and peak potentials recorded. Accordingly, the effect of the supporting electrolyte on the DA signal is also investigated in this chapter.

4.2 Experimental

The instrumentation and software employed are described in Sections 2.3 and 2.12.1. All the experiments are described in detail in Chapter 2. The electrospinning and electrochemical characterisation of the fibers and the subsequent electropolymerisation of PPy-SCD was carried out in the Intelligent Polymer Research Institute (IPRI) at the University of Wollongong, Australia. In general, the same sample was used in the electrochemical characterisation of the fibers. However, to examine the influence of scan rate a new sample was used for each scan rate inspected.

The PPy-SCD films used to investigate the detection of DA in the phosphate buffer solution and in the other supporting electrolytes were grown at a potential of 0.500 V vs. SCE until a charge of 0.24 C cm^{-2} was consumed from a 0.20 mol dm^{-3} pyrrole / 0.01 mol dm^{-3} sulfonated β-cyclodextrin solution. The background current was subtracted from all the DA currents reported throughout this chapter, unless otherwise stated. In all cases, the modified electrodes were first cycled in the background electrolyte to ensure the release of any pyrrole or oligomers at the surface, then the electrodes were transferred to the DA solutions.

4.3 Results and Discussion

4.3.1 Electrospinning

The ultimate goal of the research visit to the University of Wollongong, Australia was to improve the sensitivity of the DA sensor. In an attempt to achieve this, nanostructures were incorporated into the polymer matrix with the hope of increasing the surface area allowing lower concentrations of DA to be detected. This was investigated by generating ultrathin fibers using an electrospinning approach. Layers of PPy-SCD were electropolymerised onto the fibers and these new materials were then compared with the polymer films described in Chapter 3 for the electrochemical sensing of DA.

4.3.1.1 Electrospinning Process

Electrospinning is a straightforward and inexpensive method of producing nanofibers from polymer solutions with diameters ranging from nanometers to micrometers[2]. The nanofibers have several useful characteristics, such as a large surface area to volume ratio and high porosity and thus have been applied to many areas, such as tissue engineering scaffolds[3], wound dressing materials[4], drug delivery systems[5] and sensors[6]. The principle of electrospinning is based on applying a high electric field to a droplet of polymer solution which causes the formation of an electrified jet that continuously elongates into long thin

fibers due to the electrostatic repulsions between the surface charges and the evaporation of the solvent[7]. The electrospinning set-up is described in detail in Section 2.12.2. A wide variety of polymers have been successfully electrospun into super fine fibers. These include polyvinyl alcohol (PVA)[8-10], polylactic acid (PLA)[11-13], polyethylene oxide (PEO)[14-16] and polystyrene (PS)[17-19] to name a few. In addition, a number of polymer composites and blends, such as, PLA/polyglycolide[20], carboxymethyl chitin/PVA[21] and polyaniline/PEO[22] have also been electrospun. The diameter and morphology of the electrospun fibers are chiefly influenced by the properties of the solution and the experimental conditions. For example, the type of polymer and solvent used together with the overall viscosity, elasticity, conductivity, polarity and surface tension of the solution will play a major role. In terms of the operational conditions, the size and the shape of the fibers will be dependent on the applied electric field, the flow rate and the distance between the collector and the needle tip. Moreover, ambient parameters such as the humidity and temperature of the chamber may also be influential[23].

PLA, Figure 4.1, was chosen as the polymer to be studied, as it possesses a slow biodegradation rate and it is biocompatible[24]. This is necessary, as the biodegradation process may interfere with the sensing ability of the material. PLA is currently used in various biomedical applications such as stents, tissue scaffolds and FDA approved sutures[25].
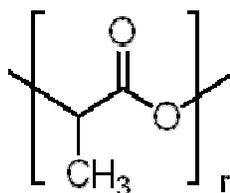
Figure 4.1. Structure of PLA.

In order to achieve an adherent layer of PLA fibers that had smooth surfaces with no bead defects, various experimental parameters were varied and investigated. These included the solvent that the PLA was dissolved in, the concentration of the polymer solution, the

applied voltage and the flow rate for the PLA solution. To examine these variables and their effect on the morphology and diameter of the electrospun fibers, a syringe with a diameter of 4.9 mm and a needle with a diameter of 1.0 mm were used. Furthermore, the collector plate was approximately 10 cm away from the needle tip and a constant supply of air flowed through the chamber during the electrospinning process.

It is well known that the nature of the solvent is important in electrospinning[26]. Typical solvents previously used to electrospin PLA fibers include 1,1,1,3,3,3-hexafluoro-2-propanol (HFIP)[27] and dichloromethane (DCM)[12]. Various solvent systems were firstly examined. 5 w/v% PLA solutions were prepared by mixing PLA in chloroform (CH_3Cl), HFIP or a solvent mixture of CH_3Cl and dimethylformamide (DMF) (70:30). The PLA would not dissolve in the solvent mixture of CH_3Cl:DMF and an attempt to electrospin the PLA from a CH_3Cl solution was unsuccessful because the solution was too viscous for the needle tip. In contrast, the PLA dissolved into the HFIP and the resulting solution was not too viscous. The electrospun material was collected on a glass slide and analysed using an optical microscope.

An optical micrograph of the electrospun material formed with the 5 w/v% PLA and HFIP solution at a flow rate of 0.4 ml h^{-1} and at 15 kV is shown in Figure 4.2. From Figure 4.2 it can be seen that nanoparticles are generated instead of nanofibers. Particles have previously been observed when the polymer concentration is too low[28].

Based on this result the PLA concentration was varied and its effect on the electrospun material was explored. A 20 w/v% PLA solution in HFIP and a 15 w/v% PLA solution in HFIP were prepared. The 20 w/v% PLA solution in HFIP proved to be too viscous for the needle tip, however nanofibers were successfully collected on a glass slide from the 15 w/v% PLA solution in HFIP. This is clearly shown in Figure 4.3(a). However, the presence of beads in the electrospun fibers is obvious. Beading is a common and undesirable problem in electrospinning[29], as the formation of beads reduces the otherwise large surface area.

In a bid to try and reduce or eliminate these beads the same solution was electrospun using similar parameters with the exception of the flow rate which was reduced to 0.2 ml h^{-1}. The resulting optical image is shown in Figure 4.3(b). From this figure it can be seen that the nanofibers produced are free from beads.
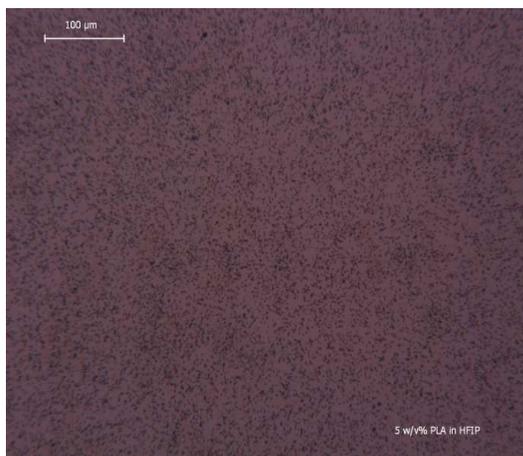
Figure 4.2: Optical microscope image of 5 w/v% PLA in HFIP using a voltage of 15 kV and a flow rate of 0.4 ml h^{-1}.
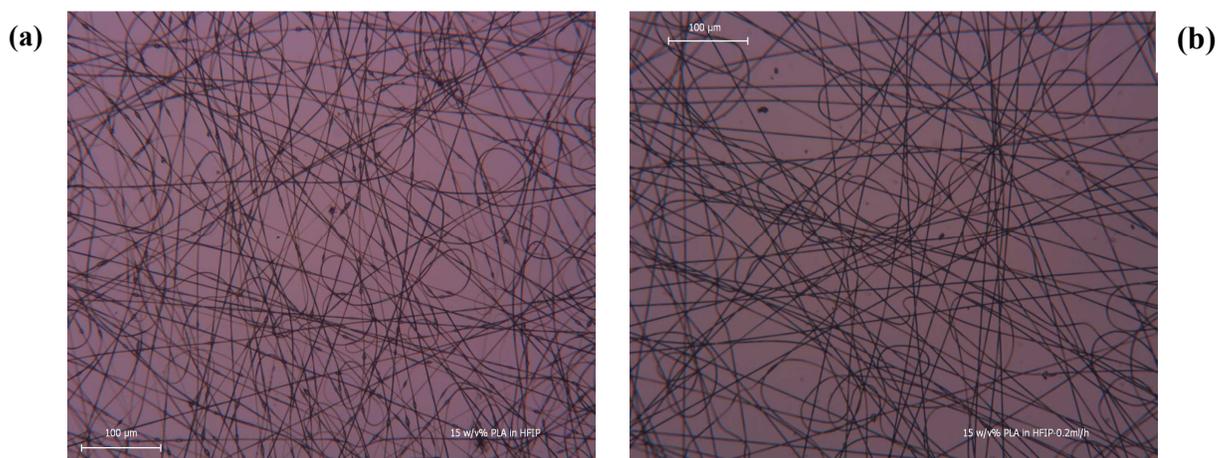
Figure 4.3: (a) Optical microscope image of 15 w/v% PLA in HFIP using a voltage of 15 kV and a flow rate of 0.4 ml h^{-1}. (b) Optical microscope image of 15 w/v% PLA in HFIP using a voltage of 15 kV and a flow rate of 0.2 ml h^{-1}.

Based on the positive results obtained in Figure 4.3(b), several samples were collected from the 15 w/v% PLA solution in HFIP on Au mylar using different voltages and flow rates. The significance of the applied voltage on the diameter of the nanofibers is highlighted in Figures 4.4(a) to (d) and Table 4.1. For these samples the electrospinning process was carried out using applied voltages of 5 kV, 10 kV, 15 kV and 20 kV at a steady flow rate of 0.2 ml h^{-1}. From the SEM images it can be seen that nanofibers were successfully generated at each voltage, however it is clear from Table 4.1 that an applied voltage of 15 kV and 20 kV produced the thinnest fibers. These results correspond well to other literature reports where increasing the applied voltage in the electrospinning process decreased the diameter of the fibers[30-32]. In general, increasing the applied voltage will increase the electrostatic repulsion force on the fluid jet, which favours thinner fiber formation.

To investigate the effect of the flow rate on the diameter of the nanofibers, samples were electrospun at a voltage of 5 kV using various flow rates ranging from 0.2 ml h^{-1} to 1.0 ml h^{-1}. SEM images of the resulting nanofibers are highlighted in Figures 4.5(a) to (d) and the calculated diameters from each of the samples are shown in Table 4.2. It is clear that thinner fibers are produced at a flow rate of 0.2 ml h^{-1}. In addition, beading, although not noticeable from the SEM images shown, was evident at the higher flow rates of 0.6 ml h^{-1} and 1.0 ml h^{-1}.

Table 4.1: Diameters of PLA nanofibers generated at a flow rate of 0.2 ml h^{-1} using various voltages.

Voltage / kV	Diameter / nm
5	693 $\pm$ 35
10	533 $\pm$ 26
15	338 $\pm$ 24
20	391 $\pm$ 47
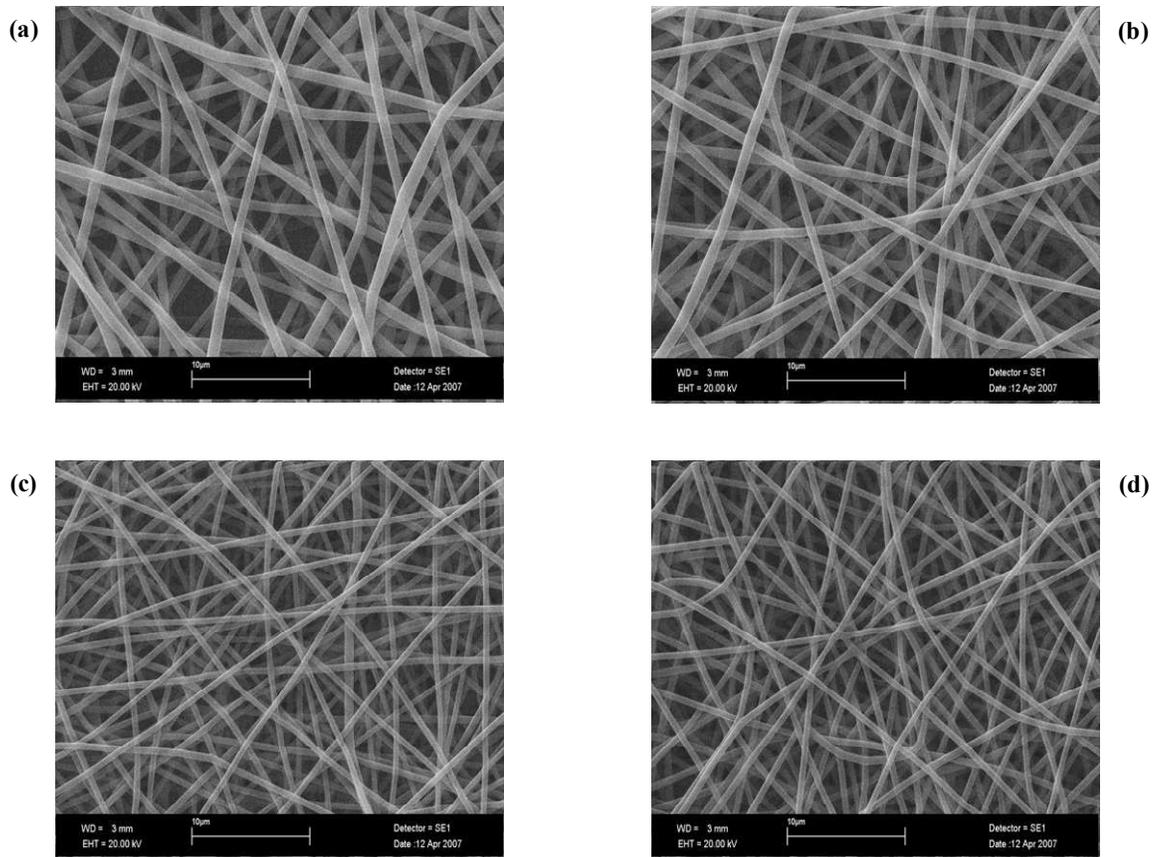
Figure 4.4: (a) SEM micrograph of 15 w/v% PLA in HFIP at a flow rate of 0.2 ml h^{-1} and a voltage of 5 kV. (b) SEM micrograph of 15 w/v% PLA in HFIP at a flow rate of 0.2 ml h^{-1} and a voltage of 10 kV. (c) SEM micrograph of 15 w/v% PLA in HFIP at a flow rate of 0.2 ml h^{-1} and a voltage of 15 kV. (d) SEM micrographs of 15 w/v% PLA in HFIP at a flow rate of 0.2 ml h^{-1} and a voltage of 20 kV.

Table 4.2: Diameters of PLA nanofibers generated at 5 kV at various flow rates.

Flow rate / ml h^{-1}	Diameter / nm
0.2	693 ± 35
0.4	791 ± 18
0.6	866 ± 34
1.0	942 ± 43
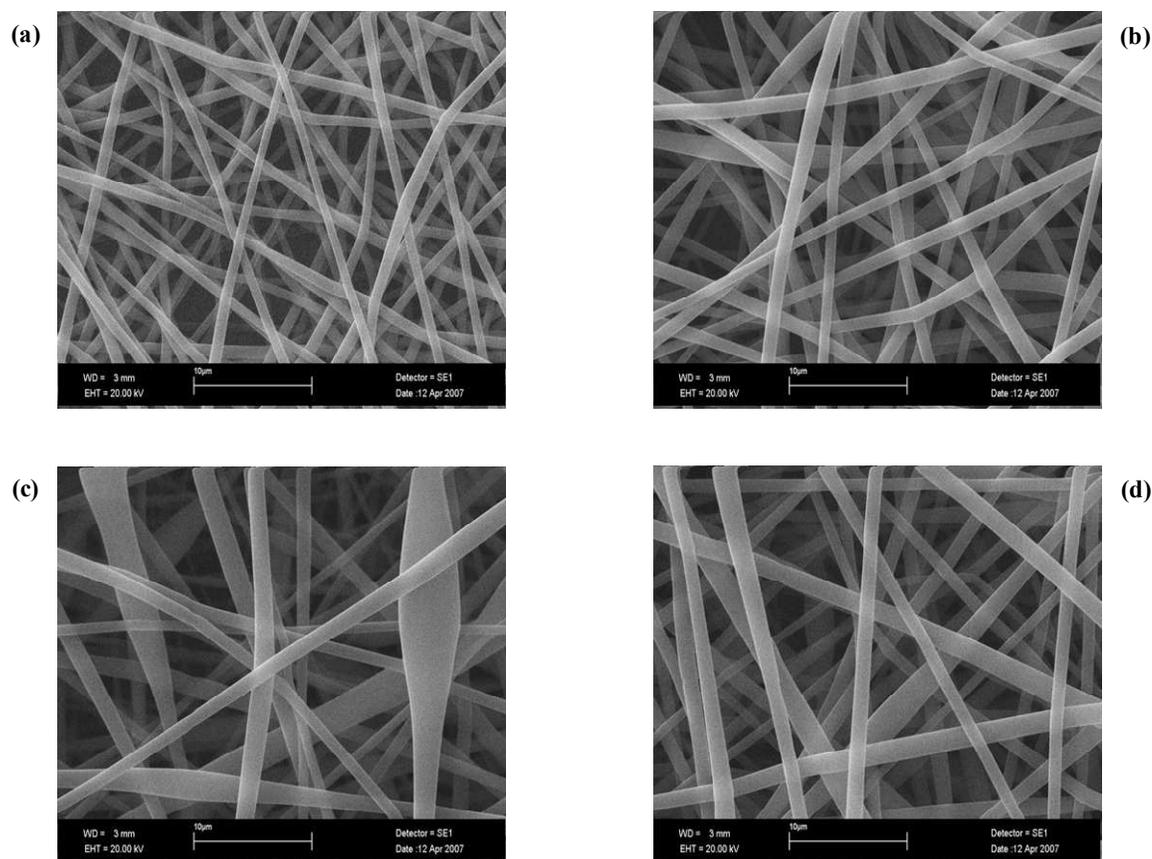
Figure 4.5: (a) SEM micrograph of 15 w/v% PLA in HFIP at a flow rate of 0.2 ml h^{-1} and a voltage of 5 kV. (b) SEM micrograph of 15 w/v% PLA in HFIP at a flow rate of 0.4 ml h^{-1} and a voltage of 5 kV. (c) SEM micrograph of 15 w/v% PLA in HFIP at a flow rate of 0.6 ml h^{-1} and a voltage of 5 kV. (d) SEM micrograph of 15 w/v% PLA in HFIP at a flow rate of 1.0 ml h^{-1} and a voltage of 5 kV.

It is well documented in the literature that the flow rate has an influence on the diameter of the fibers produced. Generally, the diameter of the fibers will increase as the flow rate is increased[33]. For example, Wang and Kumar[34] studied the influence of flow rate on the electrospinning of polyacrylonitrile and found that the fiber diameter increased with increasing flow rate. Also, Park *et al.*[35] observed higher fiber diameters with increasing feed rate. The results obtained with PLA in this study are in good agreement with these previous studies.

The optimum conditions for electrospinning a uniform film of PLA nanofibers are highlighted in Table 4.3. These conditions are based on using a syringe with a diameter of 4.9 mm and a needle with a diameter of 1.0 mm. In addition, the collector plate was

approximately 10 cm away from the syringe tip with a constant supply of air flowing through the chamber during the electrospinning process. The diameter of the nanofibers produced, using these parameters, is roughly 338 ± 24 nm.

Table 4.3: Summary of the optimum conditions for electrospinning PLA nanofibers.

Solvent	HFIP
Polymer concentration	15 w/v%
Flow rate	0.2 ml h^{-1}
Voltage	15 kV

4.3.1.2 Electrochemical Characterisation

The electrochemical characterisation of the PLA nanofibers was achieved in a 0.01 mol dm^{-3} K$_3$FeCN$_6$ / 0.10 mol dm^{-3} KCl solution using cyclic voltammetry. The fibers were electrospun under the optimum conditions given in Table 4.3, where the electrospinning period was varied from 1 to 10 min. The background currents have not been subtracted from any of the currents reported in this section. Typical voltammograms are presented in Figure 4.6, and show a well-defined pair of redox peaks, with an oxidation wave centred at 0.264 V vs. Ag/AgCl, corresponding to the oxidation of ferrocyanide to ferricyanide, and a reduction peak at 0.124 V vs. Ag/AgCl, representing the reduction of ferricyanide to ferrocyanide. From Figure 4.6(a) it can be seen that the PLA nanofibers on the Au mylar give rise to a significant decrease in the measured currents compared to the bare Au mylar electrode. The results obtained from cycling the PLA nanofibers on the gold mylar in the 0.01 mol dm^{-3} K$_3$FeCN$_6$ / KCl solution are amplified in Figure 4.6(b). The currents vary in the order of bare Au mylar > 1 min PLA nanofibers > 3 min PLA nanofibers >10 min PLA nanofibers. This is due to the fact that PLA is an insulating material and therefore as more is generated on the surface of the gold mylar the more insulating the surface will become, blocking access to the gold interface where the FeCN$_6^{3-}$/FeCN$_6^{4-}$ redox reaction takes place.

The effect of scan rate on the cyclic voltammograms was investigated using 1 min electrospun PLA nanofibers, Figure 4.7. From this figure it is clear that the scan rate has a prominent influence on the anodic and cathodic peak currents of the ferricyanide/ferrocyanide couple with the peak currents increasing as the scan rate is increased. The diffusion coefficients corresponding to the oxidation of ferrocyanide to ferricyanide and the ensuing reduction of ferricyanide to ferrocyanide were subsequently evaluated by plotting the anodic peaks currents and cathodic peak currents as a function of the square root of the scan rate, as shown in Figure 4.8. Using the slope from each plot and Equation 3.21, a diffusion coefficient value of 4.35×10^{-8} cm^2 s^{-1} was obtained for the oxidised species while a diffusion coefficient value of 4.12×10^{-8} cm^2 s^{-1} was obtained for the reduced species. These values are significantly lower than the values reported in the literature at a bare Au electrode[36-38], where the diffusion coefficients for $FeCN_6^{3-}$ and $FeCN_6^{4-}$ are in the 10^{-6} cm^2 s^{-1} region. These clear decreases in the diffusion coefficients indicate that the diffusion of the ferricyanide/ferrocyanide to and from the Au surface is hindered by the presence of the nanofibers.

(a)

(b)
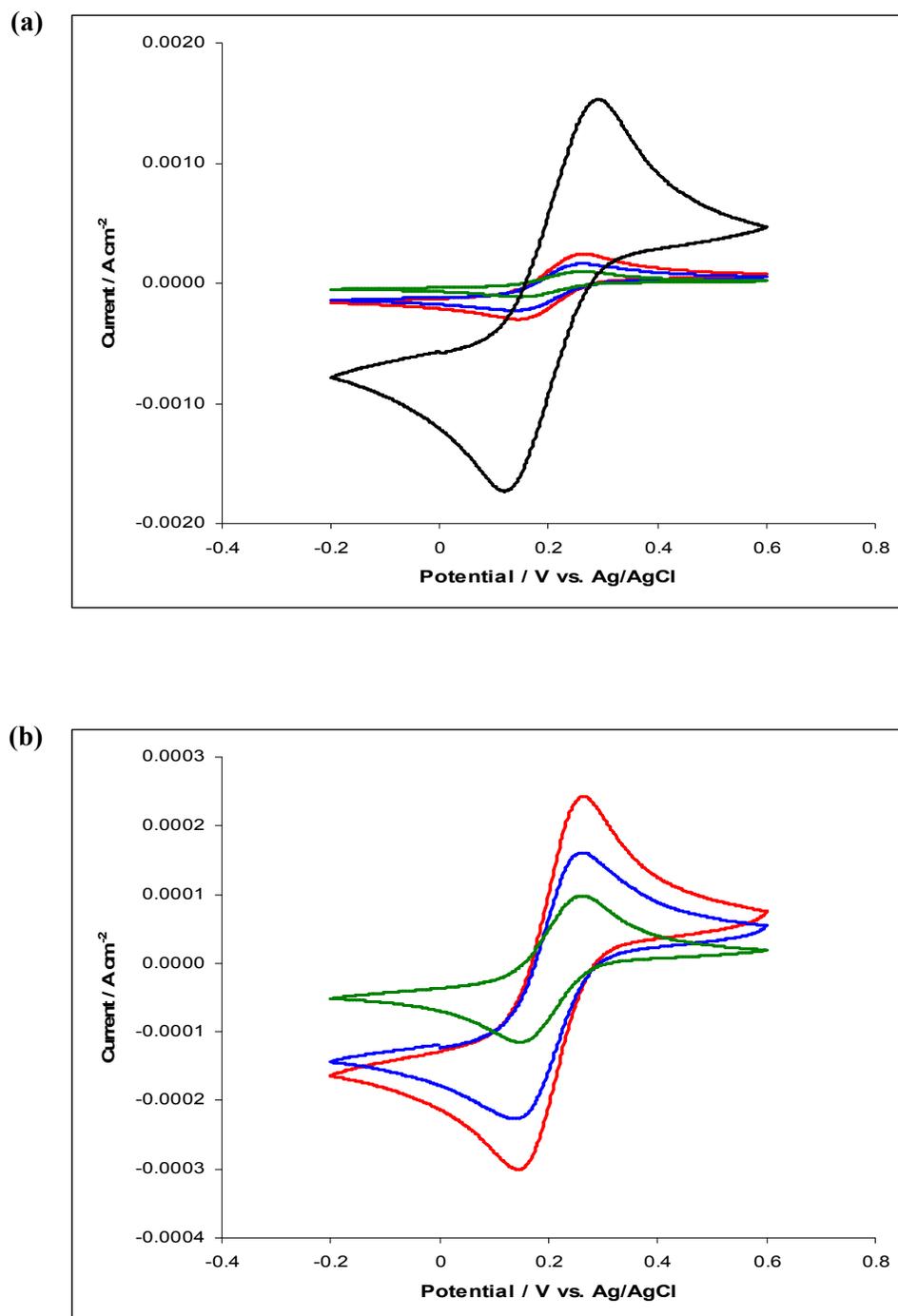
Figure 4.6: (a) Cyclic voltammograms recorded in a 0.01 mol dm^{-3} K$_3$FeCN$_6$ / KCl solution at 100 mV s^{-1} for — bare Au mylar and PLA nanofibers generated on Au mylar for — 1 min, — 3 min and — 10 min electrospinning periods. (b) Cyclic voltammograms recorded in a 0.01 mol dm^{-3} K$_3$FeCN$_6$ / KCl solution at 100 mV s^{-1} for the PLA nanofibers generated on Au mylar for — 1 min, — 3 min and — 10 min electrospinning periods.
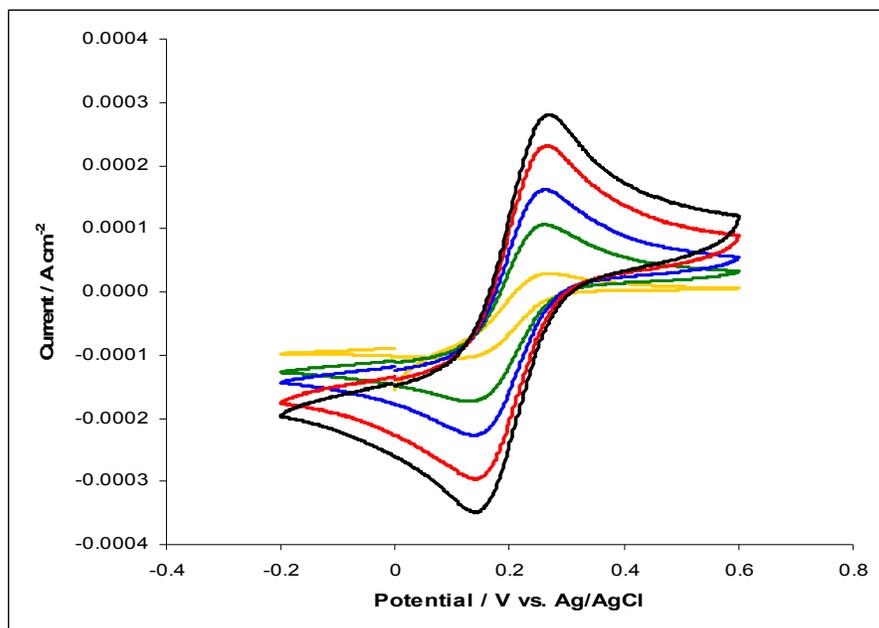
**Figure 4.7: Cyclic voltammograms of the 1 min electrospun PLA nanofibers on Au mylar in 0.01 mol dm^{-3} K$_3$FeCN$_6$/ KCl solution at a scan rate of — 300 mV s^{-1}, — 200 mV s^{-1}, — 100 mV s^{-1}, — 50 mV s^{-1} and — 10 mV s^{-1}.**
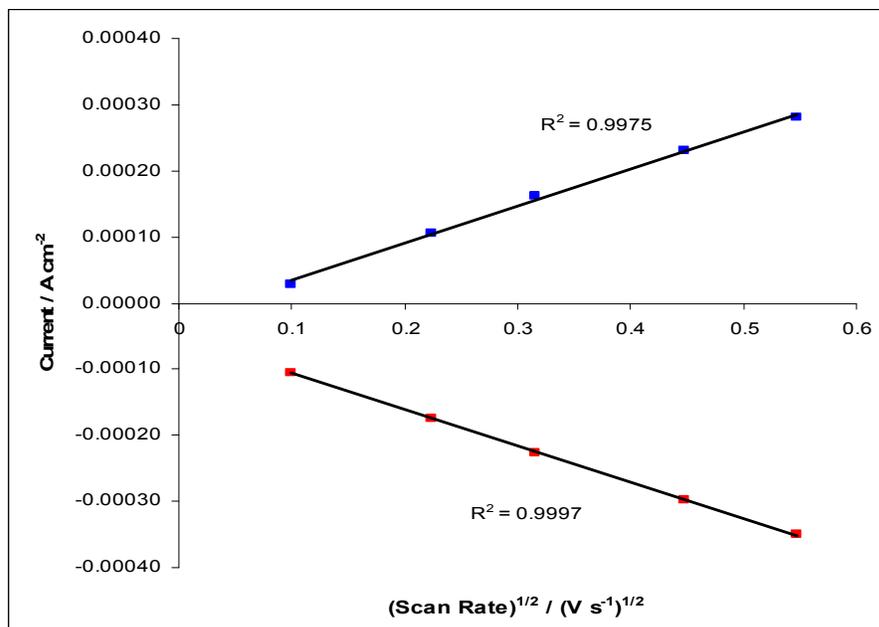
Figure 4.8: The ■ forward peak current and the ■ reverse peak current as a function of the square root of the scan rate.

Next, the stability of the electrospun nanofibers was studied. The upper and lower potential limits used in the cyclic voltammetry were varied to determine their influence, if any, on the stability of the PLA nanofibers. The forward peak current was measured as a function of the upper and lower potential limits, Figures 4.9 (a) and (b), respectively. It can be seen that the peak currents increase as the upper potential limit is increased and as the lower potential limit is decreased. The increase in the peak currents can be attributed to the stability of the PLA nanofibers rather than a genuine increase in the ferricyanide signal as the electrochemical window is increased. With increasing potential limits the adherence of the nanofibers to the surface of the Au mylar is lost exposing a higher surface area of gold.

To confirm this, 1 min PLA electrospun nanofibers were cycled in the K_3FeCN_6 / KCl solution for 100 cycles and cycles 1, 10, 50 and 100 are shown in Figure 4.10. It is obvious from this figure that the currents increase with increasing cycle number. The oxidation current obtained at the 100th cycle, 1.41×10^{-3} A cm^{-2}, is similar to the oxidation current obtained using bare Au mylar, 1.53×10^{-3} A cm^{-2}, suggesting that almost the entire Au mylar surface is available for the oxidation of the ferricyanide at this stage.

Based on these observations, the stability of the PLA nanofibers in the ferricyanide solution was further explored. This was done by immersing a sample of the 20 min electrospun PLA nanofibers in a K_3FeCN_6 / KCl solution and taking cyclic voltammetry scans at regular intervals over a 24-h period. These results are shown in Figure 4.11, where it can be seen that the peak currents increase with the immersion period. Again, this shows a decline in the amount of PLA nanofibers at the surface with increasing immersion period. The peak current is plotted as a function of the immersion period in Figure 4.12, where the rate of exposure of the Au substrate can be seen. From this figure it is evident that the peak currents increase as the immersion period of the PLA nanofibers in the K_3FeCN_6 / KCl solution increases. This is due to the fact that PLA nanofibers are progressively being displaced from the surface of the Au mylar as the experiment advances. Nevertheless, on comparing the data presented in Figures 4.9, 4.10 and 4.11, it can be concluded that cycling the fibers through a potential window gives rise to a higher rate of exposure of the Au substrate, particularly when a lower density of fibers (1 min electrospun fibers) are used.

(a)

(b)
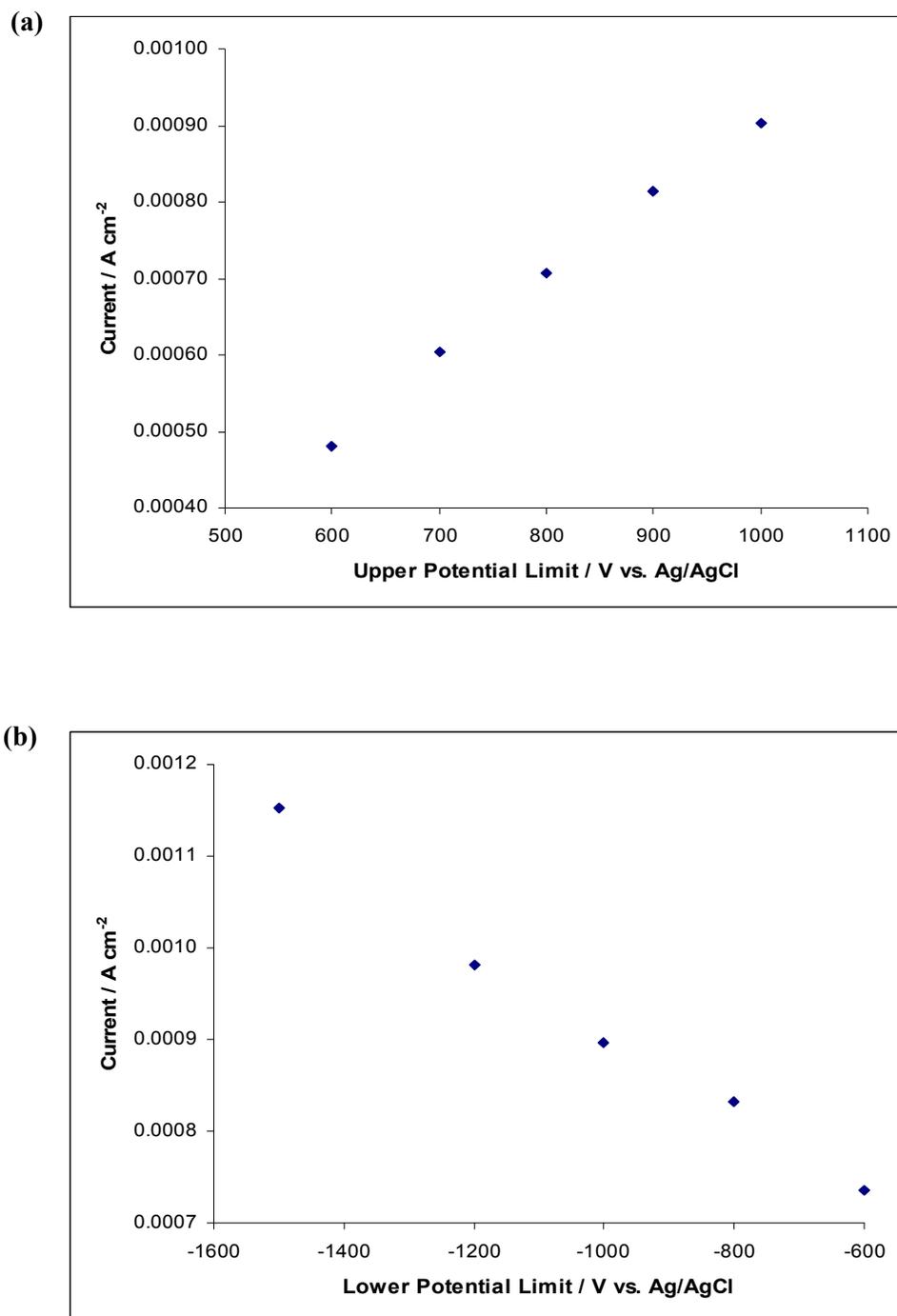
Figure 4.9: (a) The forward peak current for 1 min electrospun PLA nanofibers obtained from cyclic voltammograms in a 0.01 mol dm^{-3} K$_3$FeCN$_6$ / KCl solution at 100 mV s^{-1} as a function of the upper potential limit. Lower potential limit was kept constant at -0.300 V vs. SCE. (b) The forward peak current as a function of the lower potential limit. Upper potential limit was kept constant at 0.600 V vs. SCE.
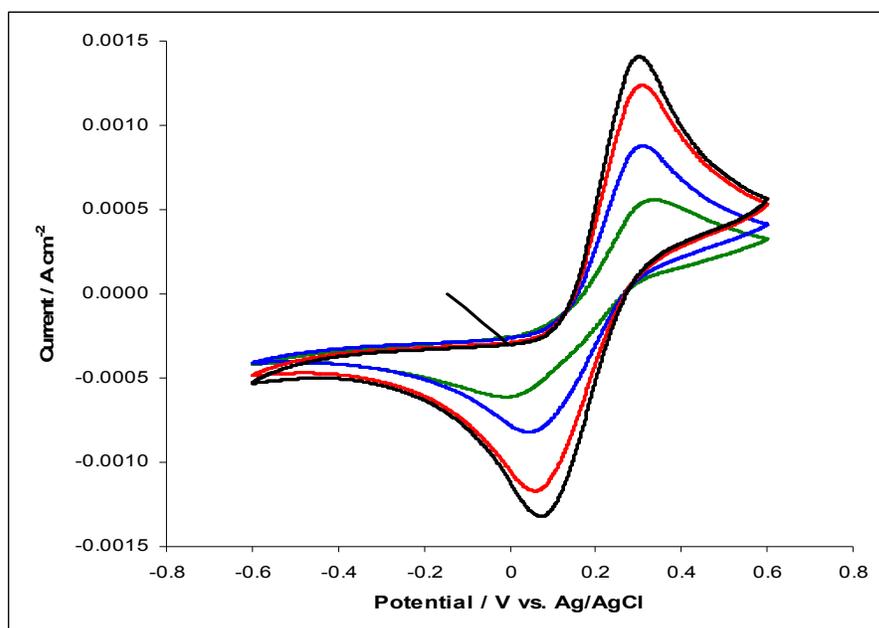
Figure 4.10: Cyclic voltammograms of the 1 min electrospun PLA nanofibers in a 0.01 mol dm^{-3} K$_3$FeCN$_6$ / KCl solution where ▬ is the 1st cycle, ▬ is the 10th cycle, ▬ is the 50th cycle and ▬ is the 100th cycle. Scan rate = 100 mV s^{-1}.
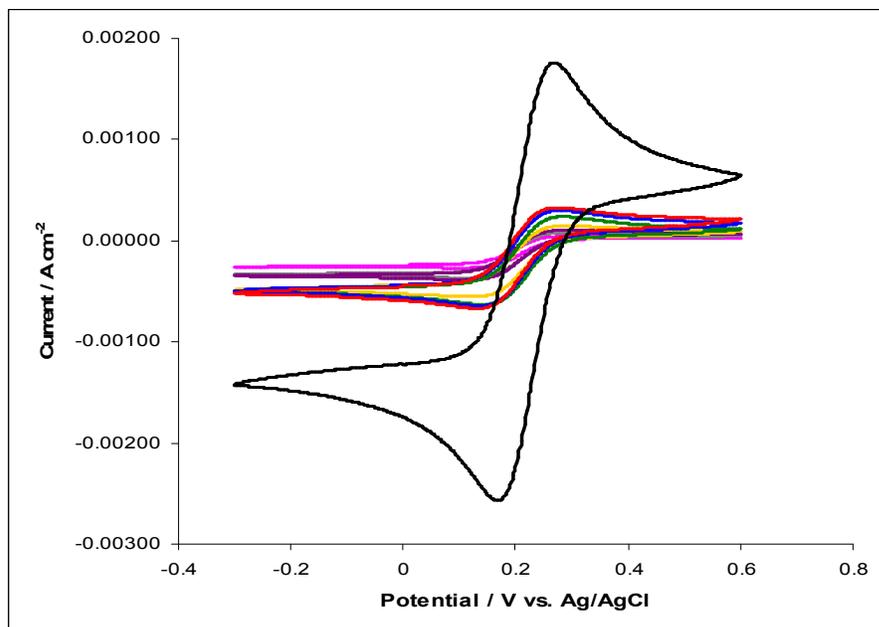
Figure 4.11: Cyclic voltammograms of the 20 min electrospun PLA nanofibers on Au mylar in 0.01 mol dm^{-3} K$_3$FeCN$_6$ / KCl solution after immersion in the solution for ▬ 24 h, ▬ 16 h , ▬ 14 h, ▬ 12 h, ▬ 7 h, ▬ 2 h, ▬ 1 h and ▬ 0 h. Scan Rate = 100 mV s^{-1}.
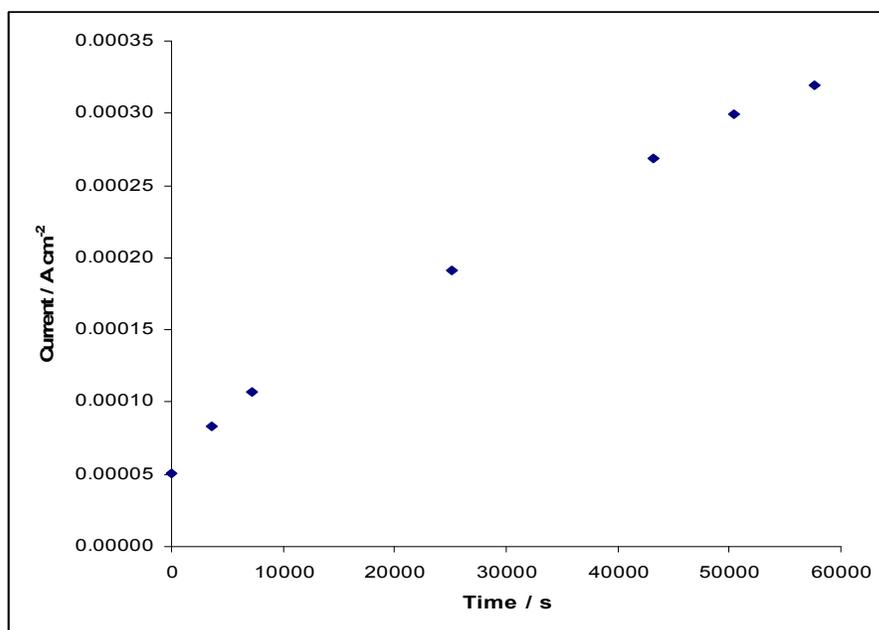
Figure 4.12: The peak currents recorded at 20 min electrospun PLA fibers in a 0.01 mol dm^{-3} K$_3$FeCN$_6$ / KCl solution as a function of the immersion period in the solution. The background current has not been subtracted from these peak currents. Peak currents were measured using cyclic voltammetry with the potential cycled between -0.600 and 0.600 V vs. Ag/AgCl at 100 mV s^{-1}.

4.3.1.3 Polymerisation / Sensing Studies

Constant potential, constant current and cyclic voltammetry were all used in an attempt to electropolymerise a layer of PPy-SCD on the 1 min PLA nanofibers. It was found that the polymer film did not completely coat the surface of the fibers when constant potential or constant current methods were employed. In addition, the polymeric material did not retain the nanostructure properties of the fibers in the regions where the polymer did coat the fibers. Cyclic voltammetry, as a means of growing the PPy-SCD film on the 1 min PLA nanofibers, was more successful. When a large number of cycles were used, typically 100 cycles, complete and uniform coverage of the fibers was observed. Representative cyclic voltammograms are presented in Figure 4.13, where the 10th, 30th, 50th and 100th cycles are shown. Oxidation of the pyrrole can be seen at roughly 0.640 V vs. Ag/AgCl, while the oxidation wave for the PPy-SCD deposited film is clearly visible at approximately -0.200 V vs. Ag/AgCl. It is also interesting to note the increase in the current with increasing cycle number which is consistent with the growth of a highly conducting polymer. Furthermore,

the nanostructured properties of the fibers were maintained, as evident in Figure 4.14. On comparing Figure 4.14 with Figure 4.5, which shows the fibers prior to electropolymerisation, it is obvious that PPy nucleates from the Au substrate and grows around the fibers filling the open spaces. This creates a three dimensional mesh of PPy, and PPy coated nanoscale fibers. The difficulty in forming PPy at these fibers can be explained in terms of the limited access to the gold substrate. Indeed, this is highlighted in Figure 4.6(a) which shows a significant reduction in the oxidation of $FeCN_6^{4-}$ at the fiber coated Au substrates. It is noteworthy to mention that while the electrodeposition of poly(3,4-ethylenedioxythiphene) (PEDOT) onto electrospun nanofibers has been previously reported[39], the electrodeposition of polypyrrole (PPy) or indeed a PPy-SCD film onto nanofibers is a novel concept.
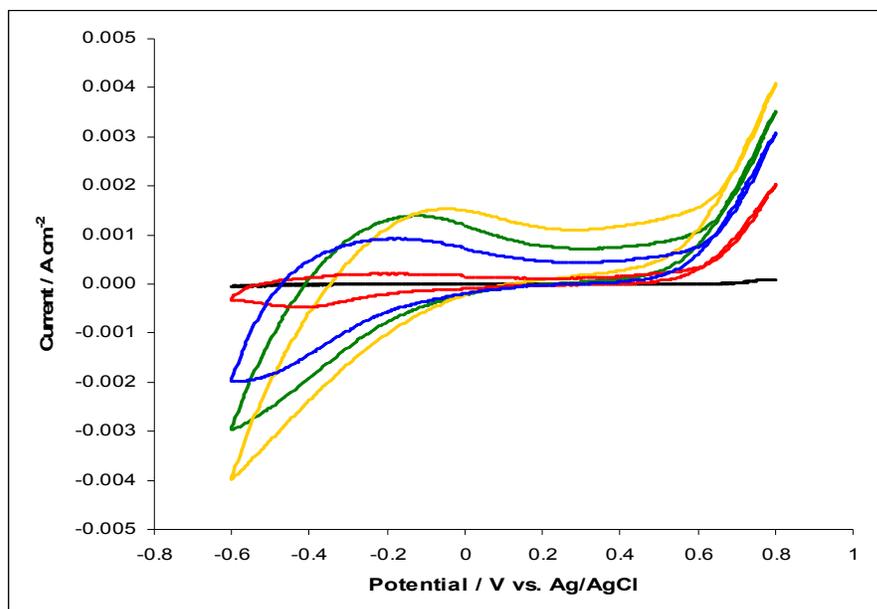
Figure 4.13: Cyclic voltammograms recorded for the electrochemical deposition of PPy-SCD on 1 min PLA where —— is the 1st cycle, —— is the 10th cycle, —— is the 30th cycle, —— is the 50th cycle and —— is the 100th cycle. Scan Rate = 100 mV s^{-1}. Electrochemical window: -0.600 V vs. Ag/AgCl to 0.800 V vs. Ag/AgCl and the electropolymerisation solution was 0.20 mol dm^{-3} pyrrole and 0.01 mol dm^{-3} β-cyclodextrin.
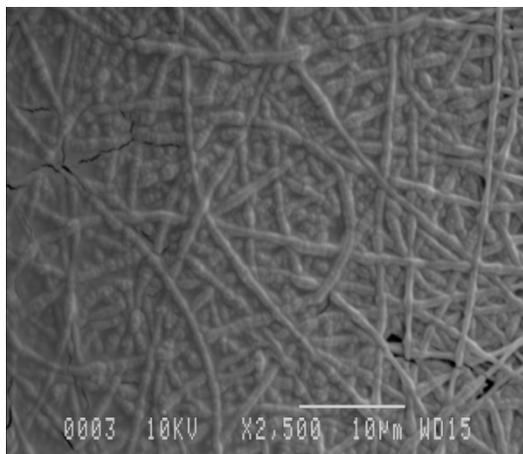
Figure 4.14: SEM micrograph of PPy-SCD film grown on 1 min PLA for 100 cycles using cyclic voltammetry. The PPy-SCD was formed in 0.20 mol dm^{-3} pyrrole and 0.01 mol dm^{-3} sulfonated β-cyclodextrin by cycling from -0.600 to 0.800 V vs. Ag/AgCl at 100 mV s^{-1}.

Once the PPy-SCD films were deposited on the nanofiber substrates they were tested in the electrochemical sensing of DA. The anodic peak currents and potentials obtained for the oxidation of 1.0 x 10^{-4} mol dm^{-3} DA at a PPy-SCD film grown on the 1 min PLA nanofibers and a PPy-SCD film grown on the bare Au substrate, under similar conditions, are compared in Table 4.4. Clearly, there is very little difference in either the DA peak current or peak potential and there is no evidence whatsoever to indicate that the nanofibers are beneficial in the sensing of DA. Furthermore, these currents are significantly lower than those obtained in Chapter 3 using a PPy-SCD modified platinum electrode. This can be attributed to the fact that a high number of cycles are required to electropolymerise the PPy-SCD film on the 1 min PLA nanofibers. The higher the number of cycles used the higher the background current, as evident from Figure 4.13. This in turn will mask the detection of DA.

To try and alleviate this problem, 15 s electrospun fibers were used as only 15 cycles of polymer growth were required to obtain a satisfactory polymer film. A DA oxidation peak current of 2.0 x 10^{-4} A cm^{-2} was recorded at the PPy-SCD film generated on the 15 s electrospun PLA nanofibers while an oxidation peak current of 2.2 x 10^{-4} A cm^{-2} was obtained from a polymer film generated on the bare Au mylar for 15 cycles of polymer growth. In both cases, the same concentration of DA, 1.0 x 10^{-4} mol dm^{-3}, was investigated.

Again, there is little difference between the rate of oxidation of DA at the PPy-SCD film deposited on the fiber coated Au mylar and the bare Au mylar electrodes. Although the peak currents generated by 15 cycles of polymer growth are higher than those generated by 100 cycles of polymer growth, they are still considerably lower than those generated at the PPy-SCD modified platinum electrode.

Table 4.4: Oxidation peak currents and potentials observed at a PPy-SCD film grown on bare Au mylar and a PPy-SCD film grown on 1 min electrospun PLA nanofibers on Au mylar in a 1.0 x 10^{-4} mol dm^{-3} DA / 0.10 mol dm^{-3} Na$_2$SO$_4$ solution.

Material	I_p^A / A cm^{-2}	E_p^A / V vs. Ag/AgCl
PPy-SCD film generated for 100 cycles on bare Au mylar	9.6 x 10^{-5}	0.4460
PPy-SCD film generated for 100 cycles on 1 min electrospun PLA nanofibers	9.8 x 10^{-5}	0.4440

Another approach used to deposit a layer of PPy-SCD on the nanofibers was vapour phase polymerisation. This is a chemical approach that involves coating the surface with a thin layer of oxidant which is subsequently treated with the vapour of the monomer, initialising polymerisation. A detailed account of the vapour phase polymerisation approach is given in Chapter 2, Section 2.12.4. SEM images taken at the interface between polymer growth and no polymer growth prove that not only was polymerisation successful but that the polymer retained the nanostructured properties of the fibers as well. This is clear from the micrograph shown in Figure 4.15. Furthermore, it was possible to coat the entire surface of the fibers. The presence of the oxidation and reduction peaks of PPy, Figure 4.16, at approximately -0.200 V vs. Ag/AgCl and -0.500 V vs. Ag/AgCl, respectively, further confirms that polymerisation was successful using the vapour phase approach.

The PPy-SCD films that were generated using this vapour phase polymerisation process were placed in a 1.0 x 10^{-3} mol dm^{-3} DA solution and cyclic voltammetry was used to

detect the DA. This was then compared to the results obtained from a polymer grown on bare Au mylar under the same conditions. The peak currents densities and peak potentials for the oxidation of DA are compared in Table 4.5 for both polymer systems. It can be seen that the PLA nanofibers are not having any significant effect on the sensitivity of the system.
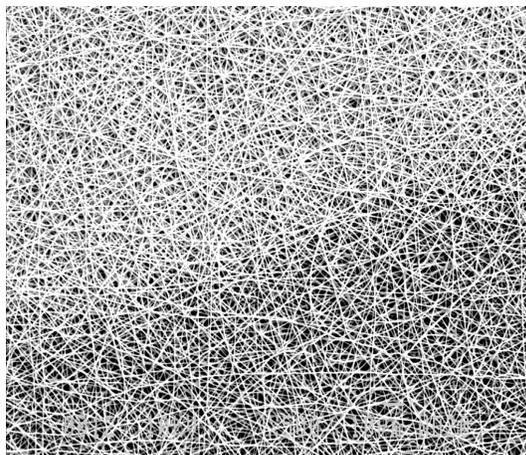
Figure 4.15: SEM image taken at the interface between polymer growth and no polymer growth of PPy-SCD on 1 min PLA nanofibers via vapour phase polymerisation (x500).
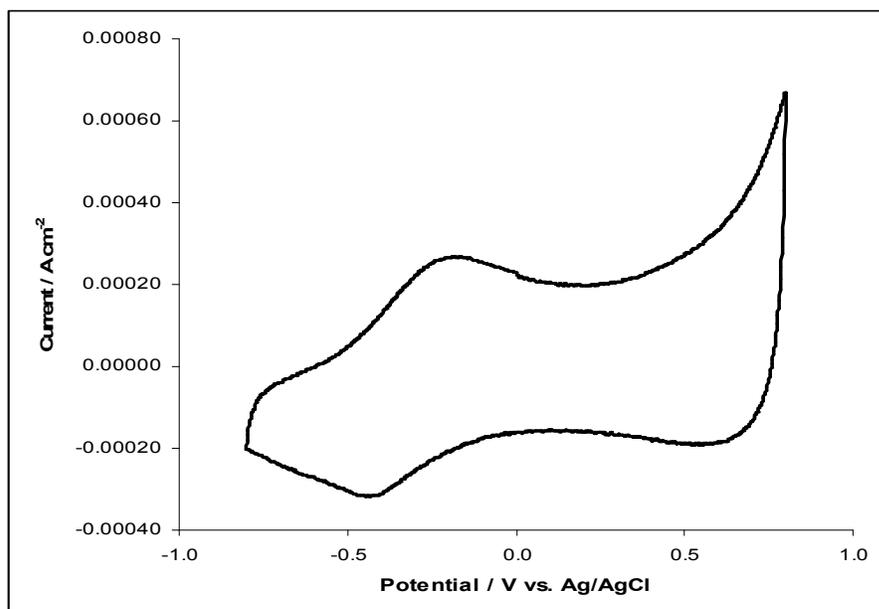
Figure 4.16: Cyclic voltammogram in a 0.10 mol dm^{-3} Na$_2$SO$_4$ solution of the PPy-SCD film deposited on the 1 min PLA nanofibers formed by vapour phase polymerisation.

Table 4.5: Oxidation peak currents and potentials observed at a PPy-SCD film grown on bare Au mylar and a PPy-SCD film grown on 1 min electrospun PLA nanofibers on Au mylar via vapour phase polymerisation in a 1.0 x 10^{-3} mol dm^{-3} DA / 0.10 mol dm^{-3} Na$_2$SO$_4$ solution.

Material	I_p^A / A cm^{-2}	E_p^A / V vs. Ag/AgCl
PPy-SCD film on bare Au mylar	4.8 x 10^{-4}	0.4220
PPy-SCD film on 1 min PLA nanofibers	4.7 x 10^{-4}	0.4220

4.3.2 The Detection of Dopamine in a Phosphate Buffer Solution

A buffer solution is an aqueous solution consisting of a mixture of a weak acid and its conjugate base or a weak base and its conjugate acid. Such solutions are able to maintain a constant pH even after the addition of reasonable amounts of acid and base[40, 41]. The buffering action of a weak acid (HA) and its conjugate base (A$^-$) can be explained by Equations 4.1 and 4.2. The acid is able to neutralise the addition of any OH$^-$ ions by forming undissociated water, Equation 4.1, while the base combines with the added H$^+$ ions removing them from the solution as an undissociated weak acid, Equation 4.2.

$$HA + OH^- \rightleftharpoons H_2O + A^- \qquad\qquad 4.1$$

$$A^- + H_3O^+ \rightleftharpoons H_2O + HA \qquad\qquad 4.2$$
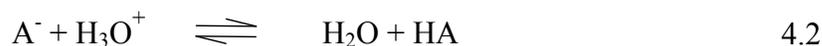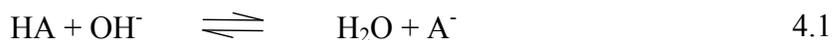
Among the wide variety of buffer solutions available, perhaps one of the most popular and commonly used to characterise biological sensors is the phosphate buffer (PB)[42-45]. The PB is traditionally used because not only is it quick and easy to prepare but it also has a pH range of 5.9 to 8.0[46]. Accordingly, a solution representing the pH of a biological system can be prepared and the pH of the solution can be kept at a constant value.

The effect of using a PB solution and a saline PB solution as possible supporting electrolytes for the detection of DA at the PPy-SCD modified electrode was investigated. The resulting voltammograms recorded using the buffer and saline buffer as the supporting electrolytes are shown in Figure 4.17. In this section the PPy-SCD films were all formed as detailed in the experimental section of this chapter, Section 4.3, at a platinum electrode. The cyclic voltammogram recorded for DA in Na_2SO_4 as the supporting electrolyte is also included in this figure for comparison purposes. From Figure 4.17 it is obvious that lower oxidation currents are generated from the PB solutions in comparison to the Na_2SO_4 solution. In addition, the oxidation of DA in the PB and saline PB solutions occurs at slightly lower potentials. This decrease in the oxidation potential is especially dramatic in the PB solution. This is highlighted further in Table 4.6 where the oxidation currents and corresponding oxidation potentials of DA are tabulated for each of the supporting electrolytes. The peak potential separation, ΔE_p, is also shown.

It can be seen that the DA signal produced by the DA / PB solution is less reversible than that generated by the DA / saline PB solution and DA / Na_2SO_4 solution. The fact that the reversibility of the saline PB solution is different to the PB solution can be attributed to the fact that a considerable amount of NaCl is used to prepare the saline PB solution, Section 2.4. As shown in Figure 4.18, where the cyclic voltammograms of 5.0×10^{-3} mol dm^{-3} DA recorded in a 0.10 mol dm^{-3} NaCl and in a 0.10 mol dm^{-3} saline PB electrolyte are compared, the detection of DA in the saline PB solution is very similar to the DA signal in the pure NaCl electrolyte. Clearly, the presence of the chloride anion has a significant effect on the voltammetry of DA in the PB supporting electrolyte and accounts for the variation in the oxidation currents and the significant difference in the oxidation peak potentials observed between the PB and the saline PB electrolyte.

This phenomenon along with the influence of these and other supporting electrolytes on the oxidation peak currents and potentials of DA is further explored in Section 4.3.3.
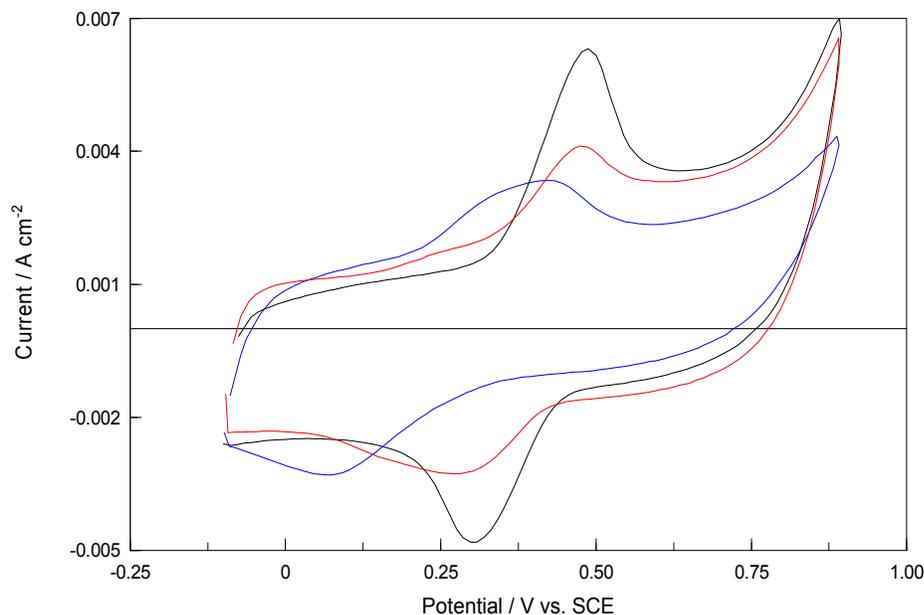
Figure 4.17: Cyclic voltammograms of a PPy-SCD modified electrode in a ▬ 5.0 x 10⁻³ mol dm⁻³ DA / 0.10 mol dm⁻³ Na₂SO₄ solution (pH~6.0), ▬ 5.0 x 10⁻³ mol dm⁻³ DA / 0.10 mol dm⁻³ PB solution (pH~6.0), and a ▬ 5.0 x 10⁻³ mol dm⁻³ DA / 0.10 mol dm⁻³ saline PB solution (pH~6.0). Scan rate = 100 mV s⁻¹.

Table 4.6: The oxidation peak currents and potentials and peak separations calculated for a 5.0 x 10⁻³ mol dm⁻³ DA / 0.10 mol dm⁻³ Na₂SO₄ solution, a 5.0 x 10⁻³ mol dm⁻³ DA / 0.10 mol dm⁻³ PB solution, a 5.0 x 10⁻³ mol dm⁻³ DA / 0.17 mol dm⁻³ saline PB solution and a 5.0 x 10⁻³ mol dm⁻³ DA / 0.10 mol dm⁻³ NaCl solution at the PPy-SCD modified electrode.

Background Solution	I_p^A / A cm⁻²	E_p^A / V vs. SCE	ΔE / V
0.10 mol dm⁻³ Na₂SO₄	0.004562	0.4874	0.1896
0.10 mol dm⁻³ PB	0.001320	0.4111	0.3421
0.17 mol dm⁻³ Saline-PB	0.001557	0.4737	0.2243
0.10 mol dm⁻³ NaCl	0.003825	0.5126	0.2371
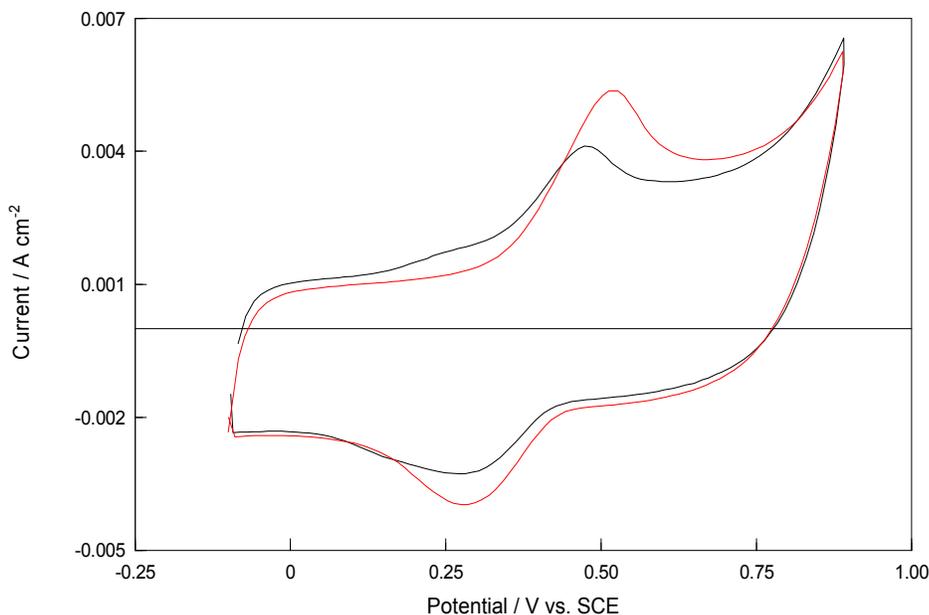
Figure 4.18: Cyclic voltammograms of a PPy-SCD modified electrode in a — 5.0 x 10^{-3} mol dm^{-3} DA / 0.10 mol dm^{-3} NaCl solution (pH~6.0) and a — 5.0 x 10^{-3} mol dm^{-3} DA / 0.10 mol dm^{-3} saline PB solution (pH~6.0). Scan rate = 100 mV s^{-1}.

As shown in Figure 4.17 and Table 4.6, the oxidation of DA in the Na$_2$SO$_4$ supporting electrolyte generates the highest currents and is also more reversible than in any other electrolyte. In a bid to amplify the DA signal in the PB solution and to try and also increase its reversibility, various concentrations of Na$_2$SO$_4$ were added to the 0.10 mol dm^{-3} PB buffer. The results obtained are summarised in Table 4.7, where the peak oxidation current and peak potential for the oxidation of 5.0 x 10^{-3} mol dm^{-3} DA are provided as a function of the concentration of Na$_2$SO$_4$ added to the buffer. The ionic strength of the solution is also provided in the final column of the table.

It can be seen from Table 4.7 that the peak currents increase in the presence of Na$_2$SO$_4$ varying from 1.32 x 10^{-3} A cm^{-2} in the absence of sulfate to 2.00 x 10^{-3} A cm^{-2} in the presence of 0.30 mol dm^{-3} Na$_2$SO$_4$. Also, the oxidation peak potentials decrease by approximately 65 mV on adding 0.30 mol dm^{-3} Na$_2$SO$_4$ to the PB solution. This is somewhat unexpected seeing as the oxidation potential of 5.0 x 10^{-3} mol dm^{-3} DA in pure 0.10 mol dm^{-3} Na$_2$SO$_4$ solution is 0.487 V vs. SCE. However, these variations can be

explained in terms of the ionic strength of the solutions. There is a significant difference in the ionic strength on comparing the PB and the PB sulfate mixtures, Table 4.7.

As shown in Table 4.8, as the molarity of the PB electrolyte is increased there is a corresponding increase in the peak oxidation currents and a decrease in the peak oxidation potential. This result indicates that the decrease in the oxidation potential is due to an increase in the ionic strength of the solutions and that the higher ionic strength solutions improve the charge transfer film kinetics and thus higher oxidation currents are observed. Although increasing the ionic strength of the PB solution results in higher oxidation currents and lower oxidation potentials, the currents are still not as high as those recorded in Na_2SO_4. Therefore, a means of increasing the oxidation currents in the PB solution would be advantageous. The results from Section 3.3.6 showed that the scan rate and the electrochemical window had a significant effect on the DA signal in Na_2SO_4 thus altering these parameters may also have a beneficial influence on the oxidation of DA in the PB solution. Accordingly, a series of experiments was carried out to probe the influence of scan rate and variations in the electrochemical window on the detection of DA in the PB buffer.

Table 4.7: The oxidation peak currents and potentials recorded at the PPy-SCD modified electrode for a 5.0 x 10^{-3} mol dm^{-3} DA / 0.10 mol dm^{-3} PB solution in the absence and presence of Na_2SO_4.

Background Solution / mol dm^{-3}	I_p^A / A cm^{-2}	E_p^A / V vs. SCE	Ionic Strength / mol dm^{-3}
0.10 PB + 0.00 Na_2SO_4	0.001320	0.4111	0.14
0.10 PB + 0.10 Na_2SO_4	0.001862	0.3812	0.44
0.10 PB + 0.20 Na_2SO_4	0.001912	0.3668	0.74
0.10 PB + 0.30 Na_2SO_4	0.002005	0.3469	1.04

Table 4.8: The oxidation peak currents and potentials recorded at the PPy-SCD modified electrode for a 5.0 x 10⁻³ mol dm⁻³ DA / 0.10 mol dm⁻³ PB solution, a 5.0 x 10⁻³ mol dm⁻³ DA / 0.20 mol dm⁻³ PB solution and a 5.0 x 10⁻³ mol dm⁻³ DA / 0.30 mol dm⁻³ PB solution.

Molarity of PBS Solution / mol dm⁻³	I_p^A / A cm⁻²	E_p^A / V vs. SCE	Ionic Strength / mol dm⁻³
0.10 PB	0.001320	0.4111	0.14
0.20 PB	0.001659	0.3994	0.28
0.30 PB	0.001898	0.3876	0.42

Results on the influence of scan rate are summarised in Table 4.9 and representative cyclic voltammograms are depicted in Figure 4.19. As expected, the oxidation peak currents and potentials increase with increasing scan rate. However, the currents recorded at a relatively high scan rate of 300 mV s⁻¹ are still not on a par with those recorded in Na_2SO_4 at 100 mV s⁻¹.

The effects of varying the upper and lower potential limits are shown in Figures 4.20 and 4.21. The data overlaid in Figure 4.20 show the influence of variations in the upper potential limit. There is a general increase in the peak current with increasing potential up to a limit of 0.900 V vs. SCE. However, on polarising the electrode to 1.000 V vs. SCE, the DA signal is lost. This is probably connected to the overoxidation of the polymer film at this higher oxidation potential[47]. For the voltammograms shown in Figure 4.21, the upper potential limit was fixed at 0.900 V vs. SCE and the lower potential limit was varied from -0.100 to -0.800 V vs. SCE. Increasing the lower potential limit to -0.300 and -0.800 V vs. SCE leads to a considerable change in the DA oxidation wave, with a significant increase in the peak oxidation potential, while the reduction peak potential of the dopamine-o-quinone (DOQ) is shifted to lower potentials, leading to considerably less reversible behaviour. From these figures it is clear that an electrochemical window of -0.100 V vs. SCE to 0.900 V vs. SCE provides the best possible DA signal in the PB electrolyte. Therefore, no additional increase in the magnitude of the currents could be obtained by altering the electrochemical window.
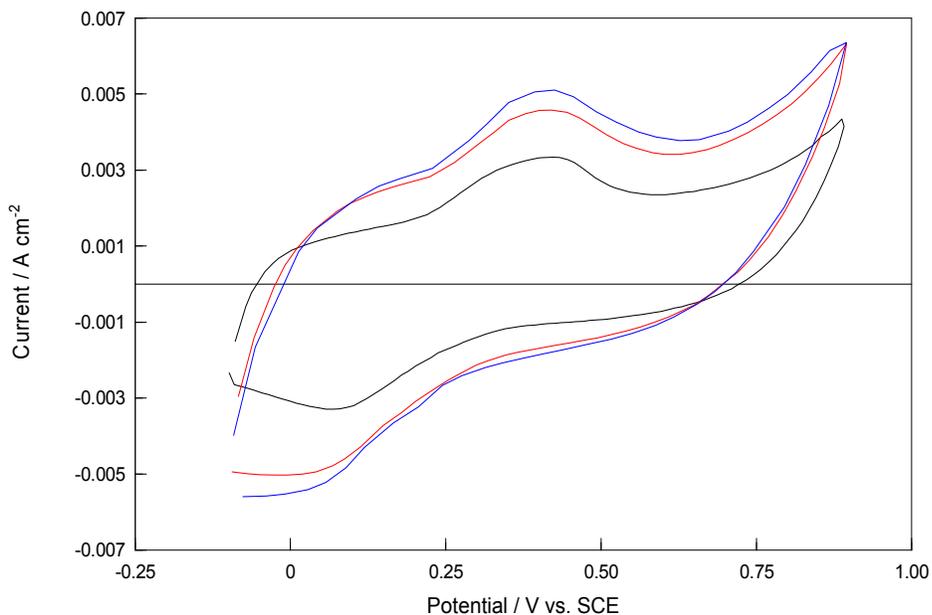
Figure 4.19: Cyclic voltammograms of the PPy-SCD modified electrode in 5.0 x 10^{-3} mol dm^{-3} DA / 0.10 mol dm^{-3} PB solution at a scan rate of ▬ 300 mV s^{-1}, ▬ 200 mV s^{-1} and ▬ 100 mV s^{-1}. Electrochemical Window: −0.100 V vs. SCE to +0.900 V vs. SCE.

Table 4.9: The oxidation peak currents and potentials recorded at the PPy-SCD modified electrode for a 5.0 x 10^{-3} mol dm^{-3} DA / 0.10 mol dm^{-3} PB solution at various scan rates.

Scan Rate / mV s^{-1}	I_p^A / A cm^{-2}	E_p^A / V vs. SCE
100	0.001320	0.4111
200	0.001489	0.4201
300	0.001656	0.4321
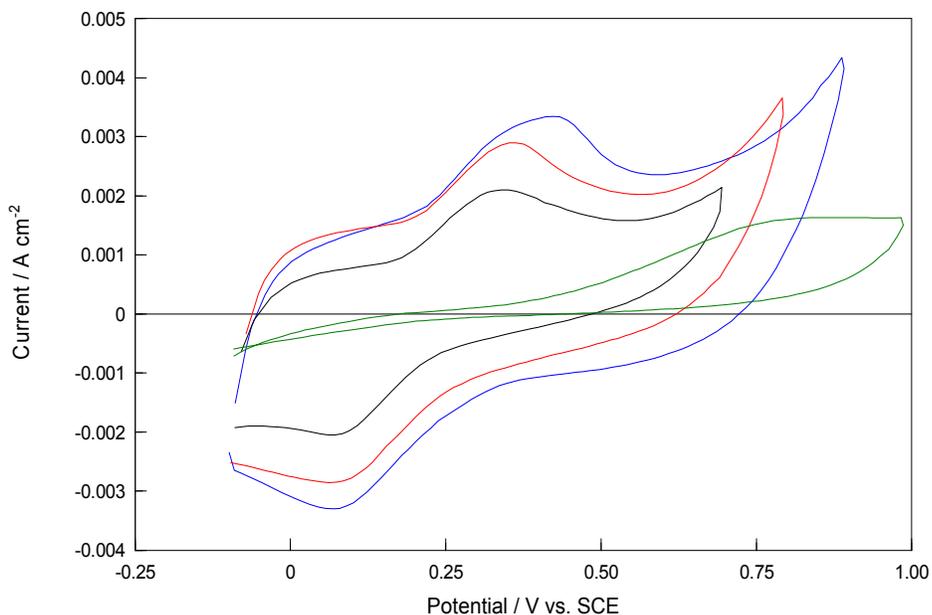
Figure 4.20: Cyclic voltammograms of a PPy-SCD modified electrode in a 5.0 x 10^{-3} mol dm^{-3} DA / 0.10 mol dm^{-3} PB solution (pH~6.0) from ▬ -0.100 V vs. SCE to 0.700 V vs. SCE, ▬ -0.100 V vs. SCE to 0.800 V vs. SCE, ▬ -0.100 V vs. SCE to 0.900 V vs. SCE and ▬ -0.100 V vs. SCE to 1.00 V vs. SCE. Scan rate = 100 mV s^{-1}.
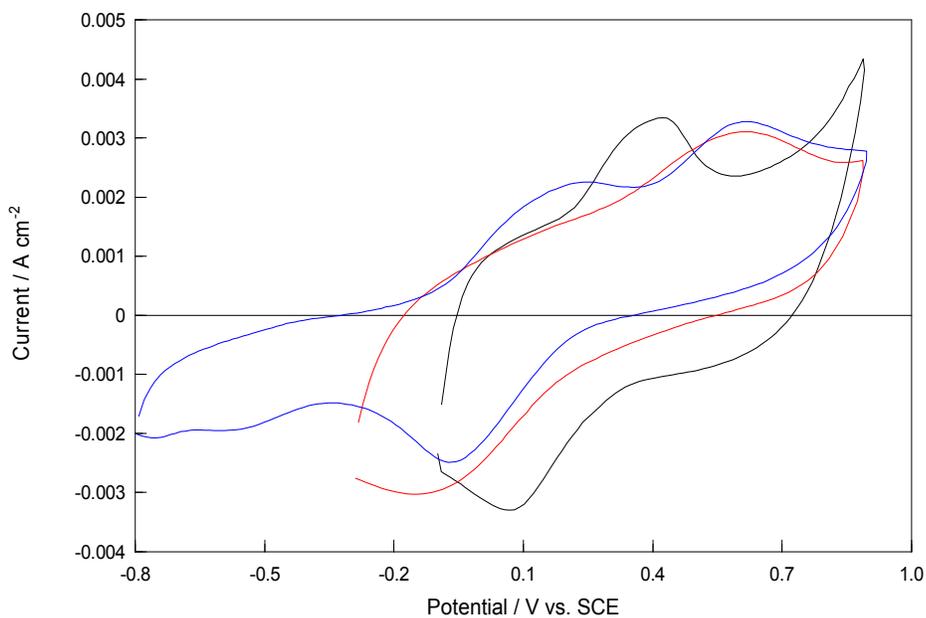
Figure 4.21: Cyclic voltammograms of a PPy-SCD modified electrode in a 5.0 x 10^{-3} mol dm^{-3} DA / 0.10 mol dm^{-3} PB solution (pH~6.0) from ▬ -0.100 V vs. SCE to 0.900 V vs. SCE, ▬ -0.300 V vs. SCE to 0.900 V vs. SCE and ▬ -0.800 V vs. SCE to 0.900 V vs. SCE. Scan rate = 100 mV s^{-1}.

4.3.3 The Role of the Anion in the Supporting Electrolyte on the Dopamine Signal

The results from Section 4.3.2 demonstrated that the supporting electrolyte has a major influence on the DA signal. To investigate this phenomenon further, the oxidation peak currents and potentials of DA in a wide variety of electrolytes were recorded. The effect of using different buffer solutions is highlighted in Table 4.10. From this table it can be seen that lower DA oxidation currents and lower oxidation potentials are obtained with each of the buffer solutions in comparison to the Na_2SO_4 solution, as a supporting electrolyte. Although the ionic strength of the solutions is not constant, Table 4.10, and the ionic strength has a considerable influence on the peak potentials of DA in the phosphate buffer solution, Tables 4.7 and 4.8, Section 4.3.2, these results cannot be explained in terms of ionic strength alone. As evident in Table 4.8 there is a significant reduction in the peak oxidation potential of DA as the ionic strength of the PB solution is increased from 0.14 to 0.42 mol dm^{-3}. However, the same trend is not evident in Table 4.10.

More direct information on the role of ionic strength on the peak oxidation potential of DA can be obtained by plotting the peak oxidation potential as a function of the ionic strength. Typical plots are presented in Figures 4.22 and 4.23 using the data presented in Tables 4.8 and 4.10. There is a clear linear relationship between the peak oxidation potential and the ionic strength for the PB system. Again, this linear relationship, but with a different slope, is observed with the organic buffers and the 0.10 mol dm^{-3} PB solution, highlighted in Table 4.10. Clearly the points corresponding to the higher ionic strengths, i.e., the sulfate and saline PB buffered solutions, are governed by a different relationship.
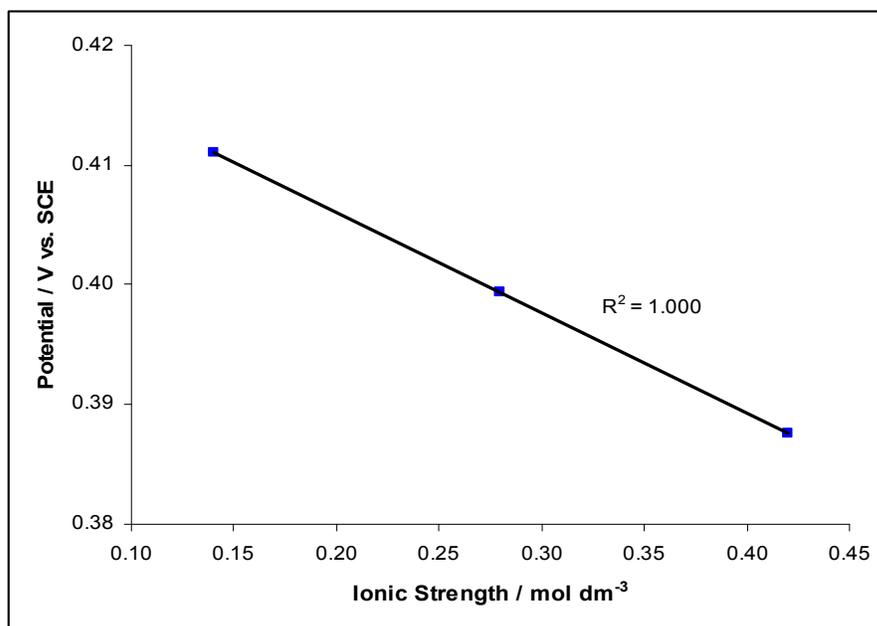
Figure 4.22: The oxidation peak potential as a function of the ionic strength for the PB solutions described in Table 4.8.
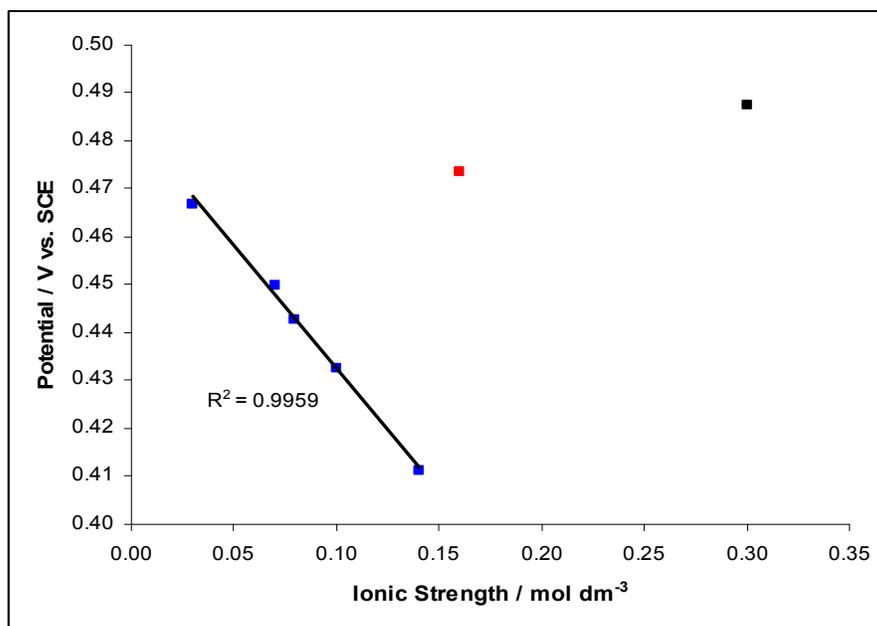

Figure 4.23: The oxidation peak potential as a function of the ionic strength for the ■ organic buffer solutions and the PB solution, the ■ saline PB solution and the ■ Na$_2$SO$_4$ solution described in Table 4.10.

It can be seen from this analysis that the ionic strength is not the only influence on the oxidation of DA. As shown in Figure 4.23, there is a clear reduction in the oxidation peak potential with increasing ionic strength, yet the Na_2SO_4 solution, which gives the highest DA oxidation peak potential, has a higher ionic strength than any of the buffer solutions. Furthermore, in terms of the phosphate buffer solutions it can be seen that the oxidation of DA in the saline phosphate buffer solution occurs at a higher potential than the oxidation of DA in the phosphate buffer solution. This has already been attributed to the fact that an excess amount of NaCl is present in the saline phosphate buffer solution and so it mimics the pure NaCl solution, Table 4.6, rather than the phosphate buffer solution. Confirmation of this comes from the fact that the ionic strength of the saline phosphate buffer solution is higher than the phosphate buffer solution.

Table 4.10: The oxidation peak currents and potentials recorded at the PPy-SCD modified electrode for 5.0 x 10^{-3} mol dm^{-3} DA in various buffer solutions and in a Na_2SO_4 solution and the corresponding ionic strengths of the supporting electrolyte solutions.

Background Solution (pH=6.0)	I_p^A / A cm^{-2}	E_p^A / V vs. SCE	Ionic Strength / mol dm^{-3}
Na_2SO_4	0.004562	0.4874	0.30
Phosphate Buffer	0.001320	0.4111	0.14
Saline-Phosphate Buffer	0.001557	0.4737	0.16
Acetate Buffer	0.002581	0.4326	0.10
Succinate Buffer	0.002017	0.4499	0.07
Maleate Buffer	0.001346	0.4428	0.08
MES Buffer	0.000937	0.4669	0.03

Although ohmic drops, or IR drops, become more significant at low concentrations of electrolyte solutions[48], again this cannot be used to explain the data presented in Figure 4.23, where the peak oxidation potential of DA recorded in the sulfate and the saline phosphate buffer electrolytes is higher than the other buffer systems. However, the IR drop will be more significant in these organic buffers where the ionic strength varies from 0.03 to 0.14 mol dm^{-3}. Indeed, the peak oxidation potentials observed for DA in these organic buffering systems do seem to be governed by the ionic strength of the solution, with the peak potentials recorded decreasing with increasing ionic strength. This suggests that the ionic strength does influence the peak potential of the DA signal, but only when the ionic strength of the solution is low as these organic based buffer solutions have an ionic strength less than or equal to 0.10 mol dm^{-3}. Additional proof of this is again presented in Table 4.11 and Figure 4.24 where it can be seen that the shift in the peak potential is more prominent when the ionic strength of the Na$_2$SO$_4$ solution is lowered.
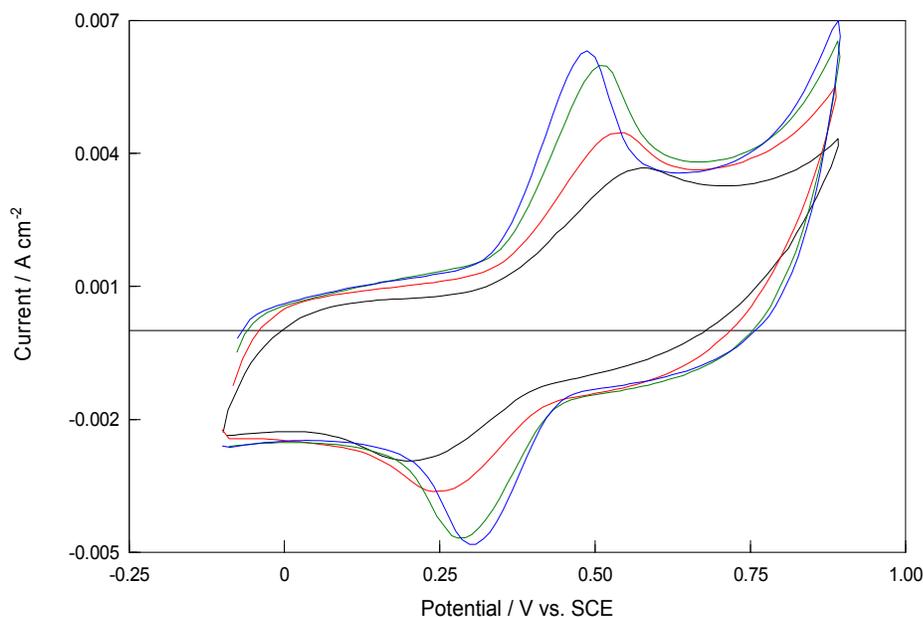
Figure 4.24: Cyclic voltammograms of a PPy-SCD modified electrode in a — 5.0 x 10^{-3} mol dm^{-3} DA / 0.100 mol dm^{-3} Na$_2$SO$_4$ solution (pH~6.0), — 5.0 x 10^{-3} mol dm^{-3} Na$_2$SO$_4$ solution (pH~6.0), — 5.0 x 10^{-3} mol dm^{-3} DA / 0.033 mol dm^{-3} Na$_2$SO$_4$ solution (pH~6.0), — 5.0 x 10^{-3} mol dm^{-3} DA / 0.017 mol dm^{-3} Na$_2$SO$_4$ solution (pH~6.0). Scan rate = 100 mV s^{-1}.

Table 4.11: The oxidation peak currents and potentials recorded at the PPy-SCD modified electrode for 5.0×10^{-3} mol dm^{-3} DA in various Na$_2$SO$_4$ solutions and the corresponding ionic strengths.

Concentration of Na$_2$SO$_4$ / mol dm^{-3} (pH=6.0)	I_p^A / A cm^{-2}	E_p^A / V vs. SCE	Ionic Strength / mol dm^{-3}
0.017	0.002544	0.5744	0.05
0.033	0.002907	0.5469	0.10
0.067	0.004145	0.5063	0.20
0.100	0.004562	0.4874	0.30

Table 4.12: The oxidation peak currents and potentials recorded at the PPy-SCD modified electrode for 5.0×10^{-3} mol dm^{-3} DA in a 0.10 mol dm^{-3} phosphate buffer solution, a 0.10 mol dm^{-3} acetate buffer solution, a 0.10 mol dm^{-3} sodium phosphate solution and a 0.10 mol dm^{-3} sodium acetate solution and their corresponding ionic strengths.

Background Solution / 0.1 mol dm^{-3} (pH=6.0)	I_p^A / A cm^{-2}	E_p^A / V vs. SCE	Ionic Strength / mol dm^{-3}
Phosphate Buffer	0.001320	0.4111	0.14
Acetate Buffer	0.002581	0.4326	0.10
NaH$_2$PO$_4$	0.001381	0.4150	0.10
CH$_3$COONa	0.002434	0.4301	0.10

One factor that can be ruled out is the buffer capacity effect of the buffer solutions. The oxidation peak currents and potentials obtained by the phosphate buffer solution and the acetate buffer solution and related salts are given in Table 4.12. It can be seen that similar currents and potentials are recorded from the buffer solutions and the corresponding salt solutions.

Although some of the findings reported here can be related to the ionic strength of the solution, particularly at low ionic strength, it is also clear that the nature of the anion is important. To probe this further, the DA oxidation peak currents and potentials were recorded in the presence of a number of sodium salts. These results are summarised in Table 4.13. In this set of experiments, the ionic strength was maintained constant and at a sufficiently high value to avoid IR drop contributions, Table 4.13.

It is clear from this table that the optimum DA oxidation signal is obtained using the simple chloride and sulfate systems. The peak currents observed with the sodium acetate solution (CH_3COONa) are higher than those recorded in the sodium oxalate solution ($Na_2C_2O_4$). The fact that the smaller of the two organic based supporting electrolytes produced a higher DA oxidation signal along with the fact that the simple chloride and sulfate solutions generate the best DA signal suggests that perhaps the size of the anion also plays a significant role. However, this does not account for the fact that the oxidation current produced in the disodium phosphate solution (Na_2HPO_4) is lower than the oxidation current produced in the sodium sulfate solution (Na_2SO_4) given that the sulfate and phosphate anions are very similar in size.

Table 4.13: The oxidation peak currents and potentials recorded at the PPy-SCD modified electrode for 5.0 x 10^{-3} mol dm^{-3} DA in various sodium salt solutions and their corresponding ionic strengths.

Background Solution (pH=6.0)	I_p^A / A cm^{-2}	E_p^A / V vs. SCE	Ionic Strength / mol dm^{-3}
0.10 mol dm^{-3} Na_2HPO_4	0.001804	0.4007	0.30
0.30 mol dm^{-3} CH_3COONa	0.002995	0.4130	0.30
0.10 mol dm^{-3} $Na_2C_2O_4$	0.002689	0.4607	0.30
0.30 mol dm^{-3} NaCl	0.004118	0.4787	0.30
0.10 mol dm^{-3} Na_2SO_4	0.004562	0.4874	0.30

Interestingly, there is some evidence in the literature to suggest that the electrochemical behaviour of DA and other catecholamines is affected by the presence of anions with carboxylate groups[49]. The interactions between the carboxylate anions and the DA are poorly understood, however, they have been associated with the oxidation products of DA. For example, Winter *et al.*[50] suggest that the citrate anion stabilises the oxidation products of DA, while other reports[51] show that the addition of EDTA to the supporting electrolyte inhibits the formation of polymeric species from the DA oxidation reaction. In addition, large shifts in the DA oxidation peak potential and current have been observed in the presence of sodium dodecyl sulfate, which exerts a micellar effect[52]. These observations have been explained in terms of the adsorption of the surfactant at the electrode surface to form a negatively charged surface which attracts the protonated DA and stabilises the quinone cation. These studies highlight the role of electrostatic interactions and their influence on the peak oxidation potentials and currents recorded for the oxidation of DA.

The succinate, maleate, oxalate and acetate buffers/salts have anions with one or two carboxylate groups and the solutions prepared with these salts may have some stabilisation effects on the oxidation products of DA, as suggested by Winter and co-workers[49]. The reduction peak potential of the DA-o-quinone in the acetate, succinate and maleate buffer solutions occurs at 0.025 V vs. SCE, 0.016 V vs. SCE and 0.017 V vs. SCE, respectively. In contrast, the reduction peak potential of the DA-o-quinone in the sulfate solution occurs at approximately 0.298 V vs. SCE. The lower reduction potentials of the DA-o-quinone in the organic buffer solutions implies that it may indeed be stabilised by the carboxylic groups that each of these solutions contain. The fact that the reduction of the DA-o-quinone in the succinate and maleate buffer solutions, which both contain two carboxylate groups, is lower than in the acetate buffer solution, which contains only one carboxylate group, highlights this. It is clear from Table 4.10 that the DA oxidation peak potentials recorded in these organic buffer solutions are lower than those recorded in the simple sulfate solution. Therefore, the lower reduction peak potentials observed in the organic buffer solutions may be attributable to this. However, the separation in the reduction peak potentials between these buffer solutions and the Na_2SO_4 solution is significantly higher than the separation in the oxidation peak potentials, Table 4.14. This further suggests that the carboxylate groups are perhaps stabilising the oxidation product of the DA.

On the other hand, the sulfate and chloride anions may have a stabilisation effect on the protonated DA, through electrostatic interactions with the protonated amine. This is consistent with the higher oxidation potentials recorded for DA in the presence of chloride and sulfate anions, which is very obvious in Figure 4.23, and cannot be explained in terms of ionic strength and conductivity of the solution.

Table 4.14: The potential difference between the oxidation and reduction of DA in a Na_2SO_4 solution and an acetate, succinate and maleate buffer solution.

Buffer Solution	$E_p{}^A{}_{\text{DA/sodium sulfate solution}} - E_p{}^A{}_{\text{DA/buffer solution}} /$ V	$E_p{}^C{}_{\text{DA/sodium sulfate solution}} - E_p{}^C{}_{\text{DA/buffer solution}} /$ V
Acetate	0.055	0.273
Succinate	0.038	0.282
Maleate	0.045	0.280

The results in this section show clearly that the supporting electrolyte has a major influence on the DA signal. The magnitude of the DA oxidation peak and the location of the peak potential vary as the supporting electrolyte is changed. This phenomenon is very difficult to explain with various factors, including electrostatic interactions, the size, nature and ionic strengths of the solutions all having an influence on the recorded DA signal. One thing that is clear is that the oxidation of DA is far superior in the Na_2SO_4 solution followed closely by the NaCl solution. The fact that the chloride solution generates similar DA currents and potentials to the Na_2SO_4 solution means that a saline based electrolyte can be used to detect DA at the PPy-SCD modified electrode, thus increasing the biological applications of the sensor. However, as most of the characterisation studies were carried out in the Na_2SO_4 solution it was decided to continue using this solution, although several studies were carried out with the chloride and buffered electrolytes for comparison purposes (these data are not shown).

4.4 Summary of Results

The main aims of this chapter were to try and improve the sensitivity of the PPy-SCD material and to also increase its biocompatibility.

The results presented show clearly that incorporating nanostructures into the polymer matrix in an attempt to improve the sensitivity of the sensor is not a viable approach. Electrochemical techniques, such as constant current and constant potential were unable to be used to grow the PPy-SCD films onto the fibers due to fact that the fibers were too dense and prevented the pyrrole monomer from oxidising at the Au interface. In some experiments the polymer was deposited onto small areas, but a uniform polymer coating could not be achieved.

This was also evident with cyclic voltammetry when a low number of cycles were employed to grow the PPy-SCD films onto the fibers. Again, this was explained in terms of the nucleation of the polymer at the Au mylar surface and as a result the sections of the surface where the fibers are dense are very difficult to coat. However, using a high number of cycles a continuous coating of the polymer was obtained, while maintaining the structure of the underlying fibers.

However, the oxidation of DA was similar in the presence and absence of the nanofibers. Moreover, the detection signal of DA became compromised on increasing the number of polymer growth cycles. This gave rise to an increase in the background current, masking the detection of DA. In an attempt to reduce the background current fewer nanofibers were electrospun onto the Au mylar and less polymer was deposited at the electrospun surface. Also, vapour phase polymerisation was used to deposit small amounts of the PPy-SCD film onto the fibers. However, in both cases, there was no evidence to suggest that the fibers were beneficial in the electrochemical sensing of DA.

In relation to the supporting electrolyte, it was found that a NaCl solution could be used as a supporting electrolyte. This solution practically matched the performance of the Na_2SO_4 solution. Consequently, the PPy-SCD modified electrode should thrive in most biological samples where the content of saline in these samples is very high. In addition to NaCl,

various other supporting electrolytes, including the phosphate buffer solution, were also investigated. The DA peak currents and potentials obtained from these electrolytes were noticeably lower. It was difficult to explain these observations, with contributions from the ionic strength, size and nature of the anions in the solutions.

4.5 References

1. J. Zheng and X. Zhou, *Bioelectrochemistry*, **70**, 408, (2007).
2. J. Xu, J. Zhang, W. Gao, H. Liang, H. Wang and J. Li, *Materials Letters*, **63**, 658, (2009).
3. H.-J. Jin, J. Chen, V. Karageorgiou, G. H. Altman and D. L. Kaplan, *Biomaterials*, **25**, 1039, (2004).
4. A. Schneider, X. Y. Wang, D. L. Kaplan, J. A. Garlick and C. Egles, *Acta Biomaterialia*, **In Press, Corrected Proof**.
5. E.-R. Kenawy, F. I. Abdel-Hay, M. H. El-Newehy and G. E. Wnek, *Materials Chemistry and Physics*, **113**, 296, (2009).
6. W. Zheng, Z. Li, H. Zhang, W. Wang, Y. Wang and C. Wang, *Materials Research Bulletin*, **In Press, Corrected Proof**.
7. D. Li and Y. N. Xia, *Advanced Materials*, **16**, 1151, (2004).
8. Y. Hong, T. Shang, Y. Li, L. Wang, C. Wang, X. Chen and X. Jing, *Journal of Membrane Science*, **276**, 1, (2006).
9. K. K. H. Wong, J. L. Hutter, M. Zinke-Allmang and W. Wan, *European Polymer Journal*, **In Press, Corrected Proof**.
10. B. Ding, H. Y. Kim, S. C. Lee, D. R. Lee and K. J. Choi, *Fibers and Polymers*, **3**, 73, (2002).
11. X. Zong, K. Kim, D. Fang, S. Ran, B. S. Hsiao and B. Chu, *Polymer*, **43**, 4403, (2002).
12. M. Bognitzki, W. Czado, T. Frese, A. Schaper, M. Hellwig, M. Steinhart, A. Greiner and J. H. Wendorff, *Advanced Materials*, **13**, 70, (2001).
13. F. Yang, R. Murugan, S. Wang and S. Ramakrishna, *Biomaterials*, **26**, 2603, (2005).
14. J. M. Deitzel, J. D. Kleinmeyer, J. K. Hirvonen and N. C. Beck Tan, *Polymer*, **42**, 8163, (2001).
15. S. Tripatanasuwan, Z. Zhong and D. H. Reneker, *Polymer*, **48**, 5742, (2007).
16. S. A. Theron, A. L. Yarin, E. Zussman and E. Kroll, *Polymer*, **46**, 2889, (2005).
17. T. Uyar and F. Besenbacher, *Polymer*, **49**, 5336, (2008).
18. C. L. Casper, J. S. Stephens, N. G. Tassi, D. B. Chase and J. F. Rabolt, *Macromolecules*, **37**, 573, (2004).
19. G. Eda and S. Shivkumar, *Journal of Materials Science*, **41**, 5704, (2006).
20. S. G. Kumbar, S. P. Nukavarapu, R. James, L. S. Nair and C. T. Laurencin, *Biomaterials*, **29**, 4100, (2008).
21. K. T. Shalumon, N. S. Binulal, N. Selvamurugan, S. V. Nair, D. Menon, T. Furuike, H. Tamura and R. Jayakumar, *Carbohydrate Polymers*, **In Press, Accepted Manuscript**.
22. I. D. Norris, M. M. Shaker, F. K. Ko and A. G. MacDiarmid, *Synthetic Metals*, **114**, 109, (2000).
23. Z.-M. Huang, Y. Z. Zhang, M. Kotaki and S. Ramakrishna, *Composites Science and Technology*, **63**, 2223, (2003).
24. Y. Gong, Q. Zhou, C. Gao and J. Shen, *Acta Biomaterialia*, **3**, 531, (2007).
25. B. Gupta, N. Revagade and J. Hilborn, *Progress in Polymer Science*, **32**, 455, (2007).

26. S. Ramakrishna, T.-C. Lim, W.-E. Teo, K. Fujihara and Z. Ma*, An Introduction to Electrospinning and Nanofibers*, World Scientific, 382, (2005).
27. Y. You, S. Won Lee, S. Jin Lee and W. H. Park, *Materials Letters*, **60**, 1331, (2006).
28. J. Liu and S. Kumar, *Polymer*, **46**, 3211, (2005).
29. H. Fong, I. Chun and D. H. Reneker, *Polymer*, **40**, 4585, (1999).
30. V. Beachley and X. Wen, *Materials Science and Engineering: C*, **In Press, Corrected Proof**.
31. C. J. Buchko, L. C. Chen, Y. Shen and D. C. Martin, *Polymer*, **40**, 7397, (1999).
32. Y. Liu, J. Chen, V. Misoska and G. G. Wallace, *Reactive and Functional Polymers*, **67**, 461, (2007).
33. U. S. Sajeev, K. A. Anand, D. Menon and S. Nair, *Bulletin of Materials Science*, **31**, 343, (2008).
34. T. Wang and S. Kumar, *Journal of Applied Polymer Science*, **102**, 1023, (2006).
35. J. Y. Park, I. H. Lee and G. N. Bea, *Journal of Industrial and Engineering Chemistry*, **14**, 707, (2008).
36. M. E. G. Lyons and G. P. Keeley, *Sensors*, **6**, 1791, (2006).
37. C. Ribaut, K. Reybier, B. Torbiero, J. Launay, A. Valentin, O. Reynes, P. L. Fabre and F. Nepveu, *IRBM*, **29**, 141, (2008).
38. E. Sabatani, J. Cohenboulakia, M. Bruening and I. Rubinstein, *Langmuir*, **9**, 2974, (1993).
39. M. R. Abidian, D. H. Kim and D. C. Martin, *Advanced Materials*, **18**, 405, (2006).
40. R. Chang*, Physical Chemistry for the Chemical and Biological Sciences*, University Science Books, 1018, (2000).
41. A. T. Florence and D. Attwood*, Physicochemical Principles of Pharmacy*, Pharmaceutical Press, 492, (2006).
42. R. N. Goyal and S. P. Singh, *Carbon*, **46**, 1556, (2008).
43. Y. Chen, L.-R. Guo, W. Chen, X.-J. Yang, B. Jin, L.-M. Zheng and X.-H. Xia, *Bioelectrochemistry*, **In Press, Corrected Proof**.
44. W. J. Kang, L. M. Niu and L. Ma, *Chin. Chem. Lett.*, (2008).
45. I. R. W. Z. de Oliveira, A. Neves and I. C. Vieira, *Sens. Actuator B-Chem.*, **129**, 424, (2008).
46. H. J. Arnikar, S. S. Kadam and K. N. Gujar*, Essentials of Physical Chemistry and Pharmacy*, Orient Blackswan, 384, (1992).
47. L. Özcan, Y. Sahin and H. Türk, *Biosens. Bioelectron.*, **24**, 512, (2008).
48. R. Woods, P. E. Richardson, F. M. Doyle and E. S. I. E. a. E. E. Division*, Proceedings of the Fourth International Symposium on Electrochemistry in Mineral and Metal Processing: 4th International Symposium*, The Electrochemical Society, 460, (1996).
49. E. Winter, R. M. de Carvalho, L. T. Kubota and S. Rath, *Journal of the Brazilian Chemical Society*, **14**, 564, (2003).
50. E. Winter, L. Codognoto and S. Rath, *Electrochim. Acta*, **51**, 1282, (2006).
51. R. M. de Carvalho, L. T. Kubota and S. Rath, *J. Electroanal. Chem*, **548**, 19, (2003).
52. X.-L. Wen, Y.-H. Jia and Z.-L. Liu, *Talanta*, **50**, 1027, (1999).

Chapter 5

Interference from Ascorbic Acid and

Epinephrine and Mechanism of Sensing

5.1 Introduction

The ability to determine dopamine (DA) in the presence of other species found in the living organism has been a major goal of electroanalytical research. The majority of these compounds are electroactive and possess the ability to oxidise in the same, or similar, potential region as DA, masking the detection of DA using electrochemical approaches. Furthermore, these compounds are normally present in concentrations that are higher than DA in the living organism. Some electroactive compounds that commonly cause problems include ascorbic acid (AA), epinephrine (EP), 3,4-dihydroxyphenylacetic acid (DOPAC), 5-hydroxytryptamine (serotonin, 5-HT) and uric acid (UA). Electroinactive, or poor electroactive species, such as glutamic acid (Glu) and aspartic acid (Asp) are also problematic as it is the predominant opinion that these can foul the sensor by adhering to the outer surface[1, 2].

In order to accurately determine DA, a sensor must be exclusive to DA detection in the presence of other species, especially AA and catechol metabolites. The effect of such species on the determination of DA was first observed by Kissinge and co-workers[3]. They noted that the recorded voltammetric peaks were due to a number of different compounds oxidising at similar potentials, and that AA, not DA, was the principal contributor. Since then, various approaches have been used in an attempt to resolve this problem, as discussed in Chapter 1 and further in this chapter. In the first part of this chapter, AA and EP have been investigated to examine their effect, if any, on the determination of DA at the polypyrrole-sulfonated β-cyclodextrin (PPy-SCD) modified electrode.

In the latter sections of this chapter, the mechanism of how the PPy-SCD modified electrode is sensing the DA is explored. This could be due to the formation of an inclusion complex between the DA and the sulfonated β-cyclodextrin or to the oxidation of DA at the polypyrrole (PPy) film, or alternatively to a combination of both. It is well known from the literature that cyclodextrins form inclusion complexes with a wide variety of guest molecules[4]. The formation of an inclusion complex will depend primarily on the size of the guest and the size of the cavity of the cyclodextrin and on the polarity of the guest molecule[5, 6]. The polarity of the guest molecule is a critical parameter due to the

hydrophobic nature of the internal cavity of the cyclodextrin[7]. Various other factors such as hydrogen bonding, electrostatic interactions, van der Waals forces and the displacement of the polar water molecules from the cyclodextrin cavity will also influence the formation of an inclusion complex[8, 9]. The internal cavity of the β-cyclodextrin is approximately 7.8 Å[10], but an inclusion complex can still form if only the hydrophobic part of the molecule enters the cavity[11]. Therefore, hydrophobic moieties of the DA may include in the cavity of the sulfonated β-cyclodextrin. The significance of the electrostatic interactions between the cationic DA and the anionic sulfonated groups on the β-cyclodextrin has also been investigated. Prior to this, Michaelis-Menten analysis and Lineweaver-Burk analysis were used to establish if there was any interaction, either due to complexation or electrostatic interactions, between the DA and the sulfonated β-cyclodextrin. Finally, an explanation for the interference or lack thereof due to AA or EP in the determination of DA at the PPy-SCD modified electrode is provided.

5.2 Experimental

The instrumentation and software employed are described in Section 2.3. All chemicals, electrochemical experiments and solutions are described in detail in Chapter 2. The PPy films used in this chapter were electrosynthesised at a platinum (Pt) electrode using a potential of 0.800 V vs. SCE from a monomer solution containing 0.20 mol dm^{-3} pyrrole and 0.01 mol dm^{-3} dopant electrolyte until a charge of 0.24 C cm^{-2} had been reached, unless otherwise stated. The errors in the interference section are reported as a percentage of the mean values and are given from lowest percentage error to highest percentage error with *n* representing the number of experiments carried out. The errors in the current measurements were calculated using Equation 5.1. Also, in some of the comparisons in this section, the pH of the pure DA solutions is slightly higher than the pH of the combined solutions, but it has been shown in Section 3.3.6.9 that the DA signal (oxidation current and potential) does not change in the pH range of 4 to 6 for the PPy-SCD-modified electrode when cyclic voltammetry is used at a scan rate of 100 mV s^{-1} in a Na$_2$SO$_4$ supporting electrolyte. The average peak currents and potentials of each concentration of DA are given in Tables 5.1

and 5.2, respectively, and are the values used in the comparisons throughout Sections 5.3.1 and 5.3.2. It is important to stress that the background currents have not been subtracted in this chapter unless otherwise stated. The errors in the complex formation constants were calculated using the LINEST function in Microsoft Excel$^{®}$, while Sigmaplot software was used to determine accurate values for K_m and I_{max}.

$$Standard\ Error = \frac{Standard\ Deviation \div \sqrt{n}}{Mean\ Current\ of\ n} \times \frac{100}{1} \qquad 5.1$$

Table 5.1: Peak oxidation currents observed for various DA concentrations in a 0.10 mol dm^{-3} Na$_2$SO$_4$, pH~6.0, supporting electrolyte.

Conc. of DA / mol dm^{-3}	I_p^A 1 / A cm^{-2}	I_p^A 2 / A cm^{-2}	I_p^A 3 / A cm^{-2}	I_p^A 4 / A cm^{-2}	Mean I_p^A / A cm^{-2}
6.0 x 10^{-5}	0.001836	0.001856	0.001820	0.001847	**0.001840**
7.0 x 10^{-5}	0.001894	0.001871	0.001906	0.001855	**0.001881**
8.0 x 10^{-5}	0.001921	0.001913	0.001920	0.001916	**0.001918**
9.0 x 10^{-5}	0.001969	0.001943	0.001946	0.001979	**0.001959**
1.0 x 10^{-4}	0.002041	0.002000	0.002001	0.002046	**0.002014**
2.0 x 10^{-4}	0.002190	0.002209	0.002270	0.002193	**0.002216**
3.0 x 10^{-4}	0.002529	0.002499	0.002446	0.002378	**0.002463**
5.0 x 10^{-4}	0.002902	0.002894	0.002875	0.002882	**0.002888**
1.0 x 10^{-3}	0.003648	0.003668	0.003651	0.003645	**0.003653**

Table 5.2: Peak oxidation potentials of various DA concentrations (6.0 x 10^{-5} to 1.0 x 10^{-3} mol dm^{-3}) in a 0.10 mol dm^{-3} Na$_2$SO$_4$, pH~6.0, supporting electrolyte.

Conc. of DA / mol dm^{-3}	E_p^A 1 / V vs. SCE	E_p^A 2 / V vs. SCE	E_p^A 3 / V vs. SCE	E_p^A 4 / V vs. SCE	Mean E_p^A / V vs. SCE
6.0 x 10^{-5}	0.4229	0.4230	0.4235	0.4325	**0.4255**
7.0 x 10^{-5}	0.4281	0.4302	0.4255	0.4311	**0.4287**
8.0 x 10^{-5}	0.4256	0.4357	0.4344	0.4334	**0.4323**
9.0 x 10^{-5}	0.4354	0.4361	0.4357	0.4345	**0.4354**
1.0 x 10^{-4}	0.4353	0.4348	0.4319	0.4437	**0.4364**
2.0 x 10^{-4}	0.4369	0.4405	0.4383	0.4369	**0.4381**
3.0 x 10^{-4}	0.4385	0.4467	0.4425	0.4364	**0.4410**
5.0 x 10^{-4}	0.4475	0.4483	0.4428	0.4444	**0.4458**
1.0 x 10^{-3}	0.4588	0.4606	0.4583	0.4594	**0.4593**

5.3 Results and Discussion

5.3.1 Interference of Ascorbic Acid (AA)

AA, Figure 5.1, is a sugar acid with antioxidant properties and it is the most problematic interfering compound in electrochemical DA detection. It coexists with DA in most biological systems at concentrations that are several hundred times higher than DA. The typical concentration of DA is 10^{-8} to 10^{-6} mol dm^{-3} while AA concentrations as high as 10^{-4} mol dm^{-3} have been reported[12]. It is also electroactive and can be easily oxidised having a range of $E_{1/2}$ values between -100 to 400 mV vs. SCE[13] on most solid electrodes. This lies in the same potential region as DA, which has a range of $E_{1/2}$ values between 100

to 250 mV vs. SCE for various electrode substrates[13], and accordingly AA dominates the signal observed. In addition, the products of AA oxidation foul the electrode surface causing a decrease in the peak currents at most solid electrodes[14]. Furthermore, AA reacts with the oxidised DA product (dopamine-o-quinone, DOQ) which is generated through the electrochemical oxidation of DA. This reaction leads to the oxidation of AA and the regeneration of DA. The catalytic regeneration of DA makes it available for further electrochemical oxidation, and thus complicates the analyses. The mechanism of this reaction has been explained by Bilewicz *et al.*[14] and by Zhang and Jiang[15]. It involves a redox reaction between the oxidised DA product (DOQ) and AA which results in the oxidation of AA and the regeneration of initial DA. This DA can then be re-oxidised at the electrode surface generating a greater signal than expected for a given concentration of DA. This mechanism is outlined in Scheme 5.1.
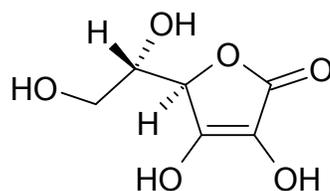
Figure 5.1: Structure of AA
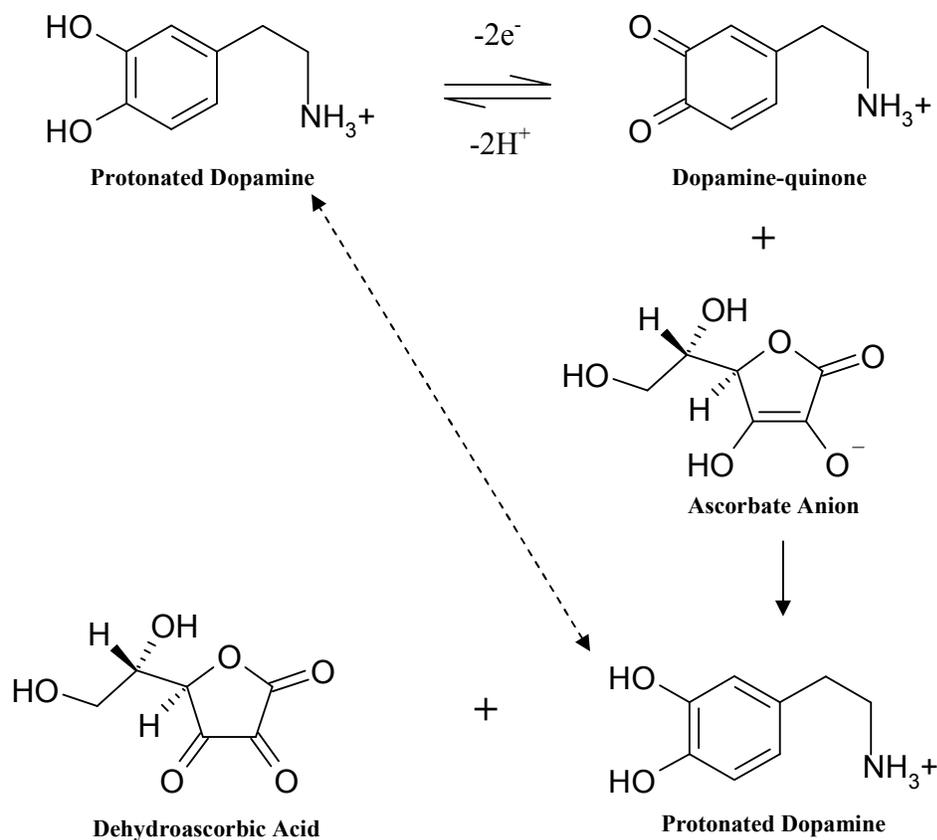
Scheme 5.1: Mechanism of the electrocatalytic oxidation of AA by DA[14, 15].

In Figure 5.2(a), the cyclic voltammograms of a bare Pt electrode and a PPy-SCD film cycled in 1.0×10^{-3} mol dm^{-3} AA are compared. In both cases, the potential is cycled in the potential range where AA is known to oxidise. It can be seen that AA is oxidised at a bare Pt electrode as the oxidation current of the AA solution is higher than that of the solution containing no AA at potentials higher than 0.160 V vs. SCE. No oxidation is observed for AA at the PPy-SCD modified electrode. When AA and DA are simultaneously mixed in the same solution, only the DA peak is detected at the PPy-SCD electrode, giving very good selectivity. Figure 5.2(b) highlights this, where the voltammogram recorded for DA in the presence of AA is identical to that obtained in DA alone. This can be attributed to the negative charges of the sulfonated groups on the β-cyclodextrin. Although the charge on the sulfonated groups may be balanced by an equal and opposite charge from the oxidised polypyrrole backbone (PPy$^+$), the –SO$_3^-$ pendants will provide a highly negative local

charge. Furthermore, as discussed in Section 3.3.5.5, free $-SO_3^-$ groups are likely to exist at the PPy-SCD surface. AA will exist to some extent as an anion ($pK_a = 4.10$)[16] at the pH of the experiment (pH = 4.3) and so will be repelled from the surface by the negatively charged sulfonated groups on the β-cyclodextrin. The dissociation of AA is shown in Scheme 5.2. The percentage of AA that is negatively charged at the pH of the experiment can be calculated using Equation 5.13. From this equation it was found that approximately 62% of the AA is negatively charged at a pH of 4.3. As the percentage of anions is relatively high we would not expect an inclusion complex to be formed due to the repulsion between the anionic AA and the anionic sulfonated β-cyclodextrin. In addition, the neutral AA should not be attracted to the negatively charged interface. Therefore, the formation of a host-guest complex between AA and the sulfonated β-cyclodextrin is very unlikely. This phenomenon is further investigated in Section 5.3.7.
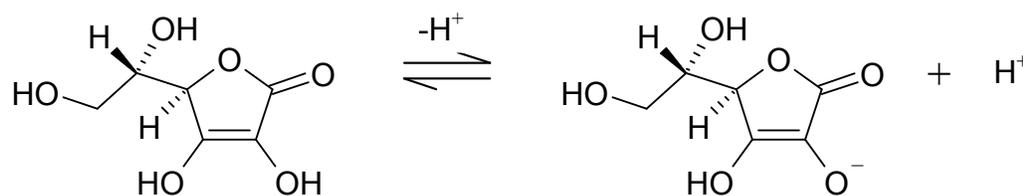
Scheme 5.2: Dissociation of AA.

Equation 5.13 was also used to investigate the effect of pH on the dissociation of AA. This equation was obtained by describing the dissociation of AA in terms of the degree of dissociation, α, and then using the well known Henderson Hasselbalch equation, as detailed in Equations 5.2 to 5.13. The influence of pH on the % of anions in solution is highlighted in Figure 5.3, where various pH values were substituted into Equation 5.13 and the percentage of anions was plotted as a function of the pH. From Figure 5.3 it can be seen that AA will be predominately neutral at low pH values, but becomes more anionic in nature as the pH of the solution is increased. At pH values in the vicinity of 6.0, close to 100% of the AA molecules exist in the anionic form.

Dissociation of AA	$AA \; \rightleftharpoons \; AA^- + H^+$ $(1\text{-}\alpha) \qquad \alpha \qquad \alpha$	5.2
Equilibrium Constant	$K = \dfrac{[AA^-][H^+]}{[AA]}$	5.3
Taking log of both sides	$\log K = \log[H^+] + \log \dfrac{[AA^-]}{[AA]}$	5.4
Henderson Hasselbalch Equation	$pH = pK_a + \log \dfrac{[AA^-]}{[AA]}$	5.5
Rearranging Equation 5.5	$pH - pK_a = \log \dfrac{[AA^-]}{[AA]}$	5.6
Taking antilog of both sides	$10^{pH-pK_a} = \dfrac{[AA^-]}{[AA]}$	5.7
Substituting α for AA⁻ and 1-α for AA	$10^{pH-pK_a} = \dfrac{\alpha}{1-\alpha}$	5.8
Taking the reciprocal of Equation 5.8	$10^{pK_a-pH} = \dfrac{1-\alpha}{\alpha}$	5.9
Rearranging Equation 5.9	$10^{pK_a-pH} = \dfrac{1}{\alpha} - \dfrac{\alpha}{\alpha}$	5.10
Rearranging Equation 5.10	$\dfrac{1}{\alpha} = 10^{pK_a-pH} + 1$	5.11
Therefore	$\alpha = \dfrac{1}{1 + 10^{pK_a-pH}}$	5.12
% Anions	$[AA^-] = \dfrac{100}{1 + 10^{pK_a-pH}}$	5.13

(a)

(b)
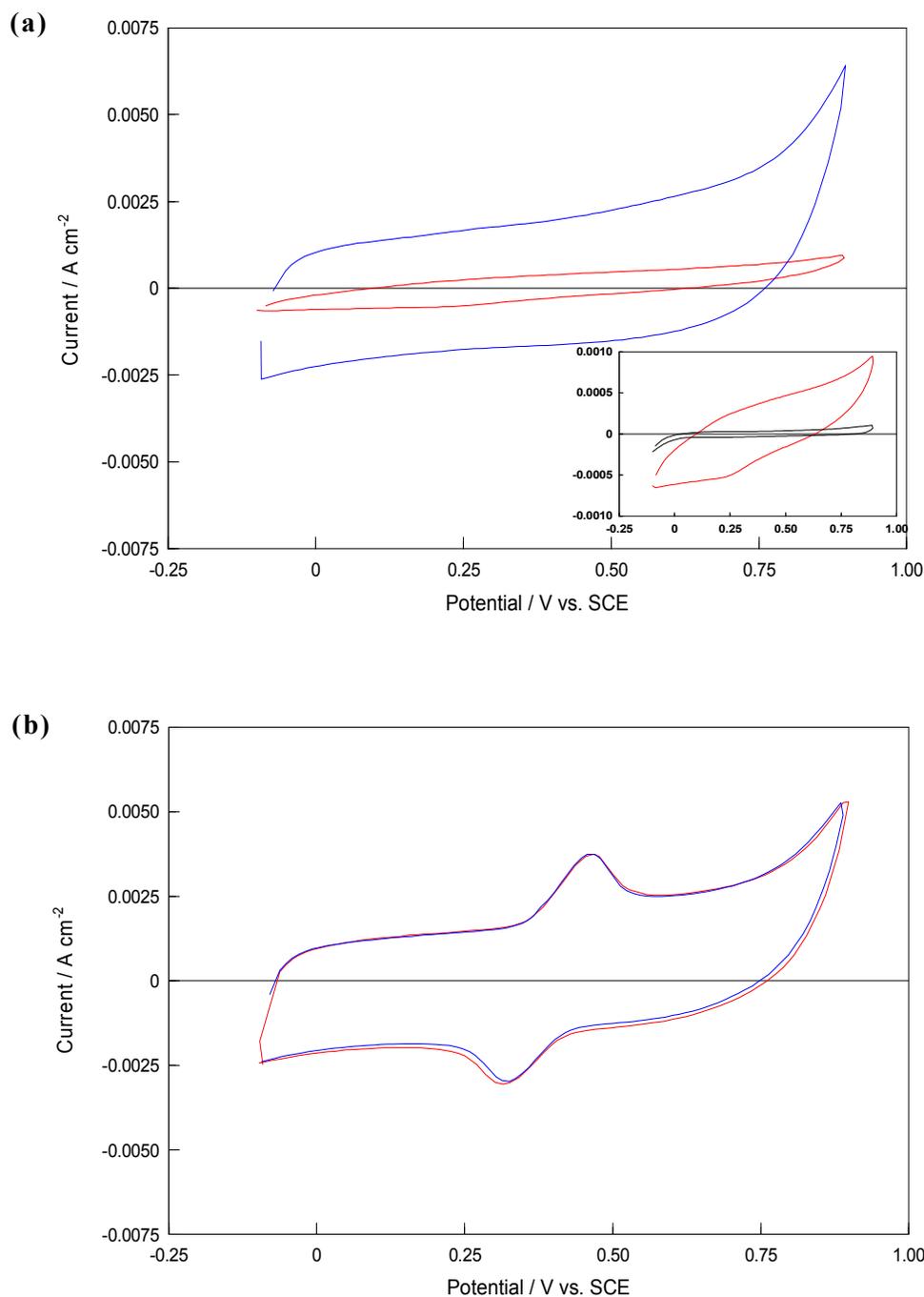
Figure 5.2: (a) Cyclic voltammograms of a ▬ bare Pt electrode and a ▬ PPy-SCD modified electrode in a 1.0×10^{-3} mol dm^{-3} AA / 0.10 mol dm^{-3} Na$_2$SO$_4$ solution (pH~4.3). Scan rate = 100 mV s^{-1}. Inset: Cyclic voltammograms of the bare Pt electrode in a ▬ 0.10 mol dm^{-3} Na$_2$SO$_4$ solution and in a ▬ 1.0×10^{-3} mol dm^{-3} AA / 0.10 mol dm^{-3} Na$_2$SO$_4$ solution; scan rate = 100 mV s^{-1}. Axes are identical to Figure 5.2(a). (b) Cyclic voltammograms of the PPy-SCD modified electrode in a ▬ 1.0×10^{-3} mol dm^{-3} DA / 0.10 mol dm^{-3} Na$_2$SO$_4$ solution (pH~6.0) and in a ▬ 1.0×10^{-3} mol dm^{-3} DA / 1.0×10^{-3} mol dm^{-3} AA / 0.10 mol dm^{-3} Na$_2$SO$_4$ solution (pH~4.3). Scan rate = 100 mV s^{-1}.
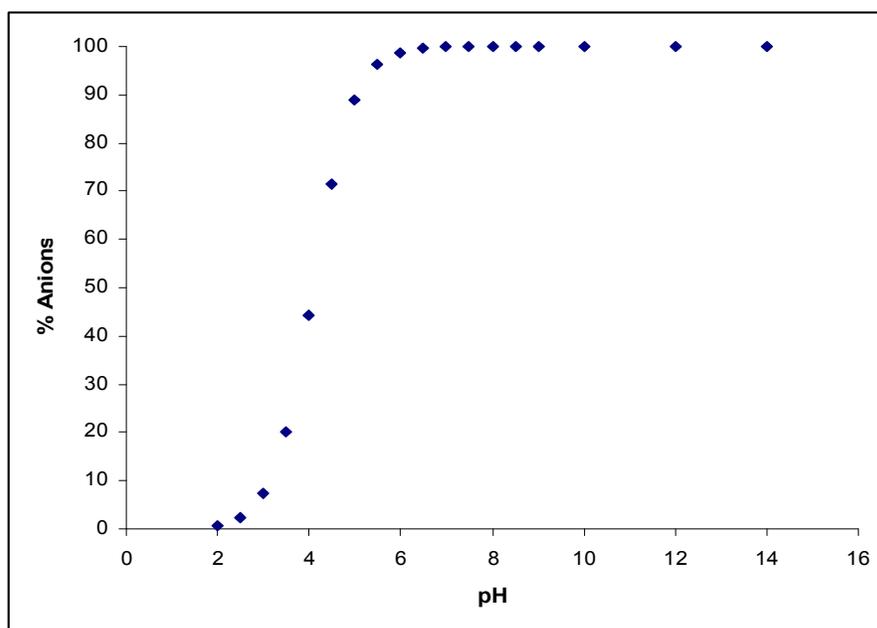
Figure 5.3: The percentage of anions as a function of pH for AA. The percentage of anions for a given pH was calculated by substituting various pH values into Equation 5.13.

The influence of AA on the DA oxidation peak currents is summarised in Table 5.3 and the current data are also plotted with error bars in Figure 5.4. In both cases, the peak currents obtained for the oxidation of DA in the presence of 1.0×10^{-3} mol dm^{-3} AA solution, at a pH of 4.3, are presented. On comparing these data to the mean currents provided in Table 5.1, it can be seen that the DA current signal is not affected by the presence of AA. Also, irrespective of the concentration of DA, there is no evidence of any increase in the DA oxidation current as a result of the solution reaction between DOQ and AA, Scheme 5.1. A more direct comparison of the DA oxidation currents in the absence and presence of AA is provided in Figure 5.5, where the peak oxidation currents of DA are shown as a function of the DA concentration with and without the presence of AA. Again, it is clear that there is no interference from the AA. As already mentioned, this is probably due to the anionic AA, which is kept at a sufficient distance from the interface by the local negative charges of the PPy-SCD film. This enables the reduction of the DOQ back to DA during the reduction cycle of the voltammogram and thus avoids any, or little, regeneration of the DA through the AA catalysed reaction.

Table 5.3: Peak currents observed when a fixed concentration of 1.0 x 10^{-3} mol dm^{-3} AA was added to various DA concentrations in a 0.10 mol dm^{-3} Na$_2$SO$_4$, pH~4.3, supporting electrolyte.

Conc. of DA / mol dm^{-3}	I_p^A 1 / A cm^{-2}	I_p^A 2 / A cm^{-2}	I_p^A 3 / A cm^{-2}	Mean I_p^A / A cm^{-2}
6.0 x 10^{-5}	0.001843	0.001823	0.001839	**0.001835**
8.0 x 10^{-5}	0.001917	0.001924	0.001920	**0.001920**
1.0 x 10^{-4}	0.002026	0.002018	0.002016	**0.002020**
3.0 x 10^{-4}	0.002483	0.002410	0.002508	**0.002467**
5.0 x 10^{-4}	0.002884	0.002906	0.002866	**0.002885**
1.0 x 10^{-3}	0.003641	0.003664	0.003663	**0.003656**
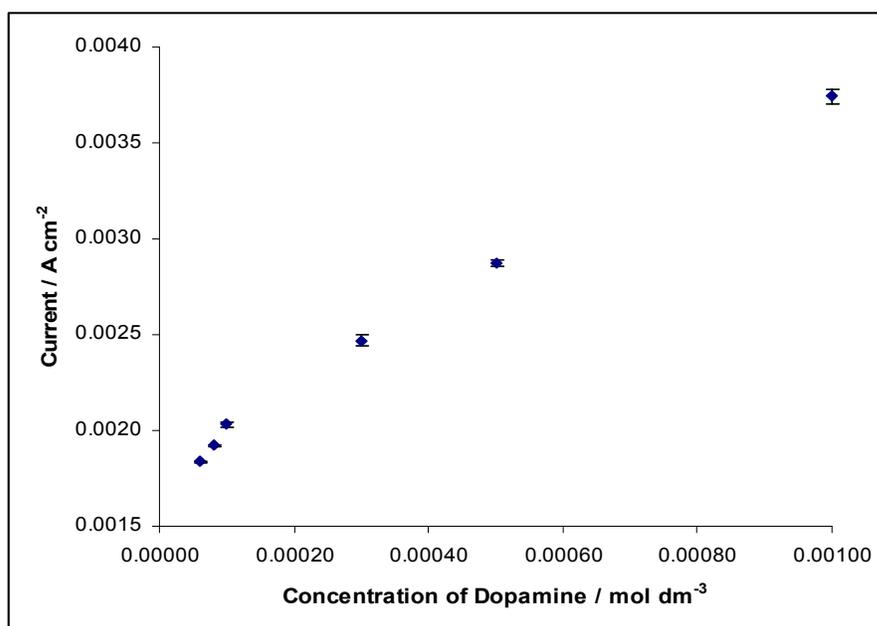
Figure 5.4: Calibration plot of the mean peak current of DA as a function of the concentration of DA where 1.0 x 10^{-3} mol dm^{-3} AA was added to each DA solution in a 0.10 mol dm^{-3} Na$_2$SO$_4$, pH~4.3, supporting electrolyte (*n*=3).
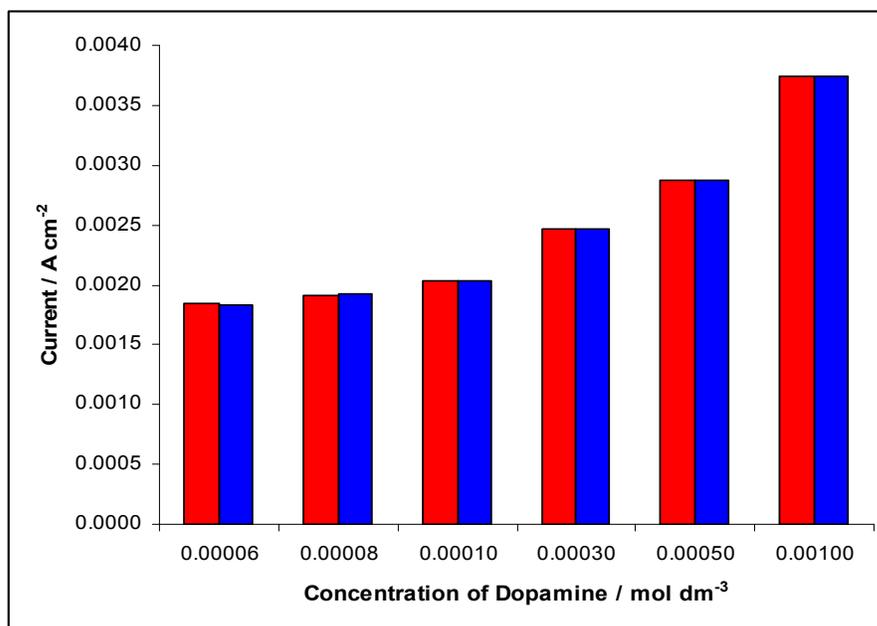
Figure 5.5: Peak current, from the cyclic voltammograms, of DA as a function of the concentration of DA in the ■ presence (*n*=3) and ■ absence (*n*=4) of 1.0×10^{-3} mol dm^{-3} AA in a 0.10 mol dm^{-3} Na$_2$SO$_4$, pH~4.3, supporting electrolyte.

Table 5.4 summarises the DA peak potentials obtained by detecting a range of DA concentrations (6.0×10^{-5} to 1.0×10^{-3} mol dm^{-3}) in a fixed concentration of AA (1.0×10^{-3} mol dm^{-3}). The mean potentials were then compared to the potentials observed for pure DA oxidation and this is illustrated in Figure 5.6. It can be seen that the presence of AA does not interfere with the potential of the DA oxidation signal.

Table 5.4: Peak oxidation potentials of various DA concentrations (6.0 x 10⁻⁵ to 1.0 x 10⁻³ mol dm⁻³) in a fixed concentration of 1.0 x 10⁻³ mol dm⁻³ AA in a 0.10 mol dm⁻³ Na₂SO₄, pH~4.3, supporting electrolyte.

Conc. of DA / mol dm⁻³	E_p^A 1 / V vs. SCE	E_p^A 2 / V vs. SCE	E_p^A 3 / V vs. SCE	Mean E_p^A / V vs. SCE
6.0×10^{-5}	0.4224	0.4249	0.4279	**0.4251**
8.0×10^{-5}	0.4326	0.4322	0.4320	**0.4323**
1.0×10^{-4}	0.4359	0.4383	0.4338	**0.4360**
3.0×10^{-4}	0.4388	0.4387	0.4429	**0.4401**
5.0×10^{-4}	0.4437	0.4433	0.4469	**0.4446**
1.0×10^{-3}	0.4650	0.4575	0.4549	**0.4591**
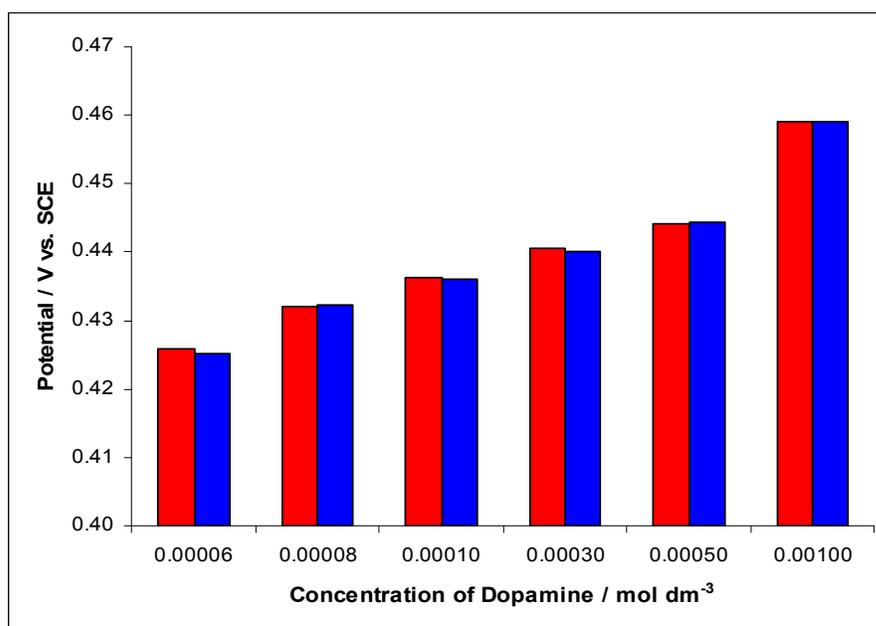
Figure 5.6: Peak potentials of DA oxidation for a range of DA concentrations (6.0 x 10⁻⁵ to 1.0 x 10⁻³ mol dm⁻³) obtained using cyclic voltammetry at a scan rate of 100 mV s⁻¹, of DA in the ■ presence (*n*=3) and ■ absence (*n*=4) of 1.0 x 10⁻³ mol dm⁻³ AA in a 0.10 mol dm⁻³ Na₂SO₄, pH~4.3, supporting electrolyte.

A higher concentration of AA was also investigated. In this case, a 1.0 x 10^{-2} mol dm^{-3} AA solution with a pH of 3.4 was used. The cyclic voltammograms of a bare Pt electrode and a PPy-SCD film cycled in 1.0 x 10^{-2} mol dm^{-3} AA are compared in Figure 5.7. This concentration of AA is significantly higher than the typical concentrations of AA found in most biological samples and is also higher than most concentrations studied in the literature. It can be seen that this concentration of AA is easily oxidised at the bare Pt electrode giving an oxidation wave at 0.580 V vs. SCE. However, no oxidation peak was observed at the PPy-SCD modified electrode on increasing the AA concentration to 1.0 x 10^{-2} mol dm^{-3}. The presence of the polymer has resulted in the oxidation of AA being eliminated.
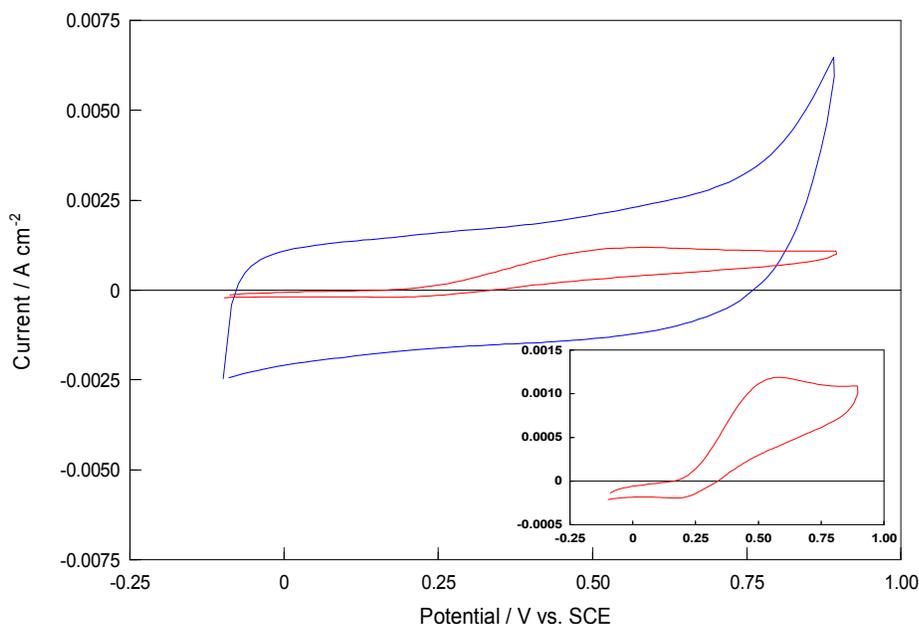
Figure 5.7: Cyclic voltammograms of a ━ bare Pt electrode and a ━ PPy-SCD modified electrode in a 0.01 mol dm^{-3} AA / 0.10 mol dm^{-3} Na$_2$SO$_4$ solution (pH~3.4). Scan rate = 100 mV s^{-1}. Inset: Amplification of the cyclic voltammogram at the bare Pt electrode. Axes are identical to Figure 5.7.

The influence of 1.0 x 10^{-2} mol dm^{-3} AA on the DA oxidation peak currents and peak potentials is summarised in Table 5.5, where the peak currents and peak potentials obtained with pure 1.0 x 10^{-3} mol dm^{-3} DA are compared to the values measured when 1.0 x 10^{-2} mol

dm^{-3} AA solution is present. It can be seen that the presence of 1.0 x 10^{-2} mol dm^{-3} AA has no affect on the DA peak currents or potentials, which is surprising given the high concentration of AA.

Table 5.5: A comparison of the mean peak oxidation currents and potentials of a 1.0 x 10^{-3} mol dm^{-3} DA / 0.10 mol dm^{-3} Na$_2$SO$_4$ solution, pH~6.0 and a 1.0 x 10^{-3} mol dm^{-3} DA / 0.01 mol dm^{-3} AA / 0.10 mol dm^{-3} Na$_2$SO$_4$ solution, pH~3.4.

	Mean I_p^A / A cm^{-2}	Mean E_p^A / V vs. SCE
1.0 x 10^{-3} mol dm^{-3} DA	0.003653	0.4593
1.0 x 10^{-3} mol dm^{-3} DA and 1.0 x 10^{-2} mol dm^{-3} AA	0.003647	0.4597

These results show clearly that both 1.0 x 10^{-3} mol dm^{-3} AA and 1.0 x 10^{-2} mol dm^{-3} AA do not interfere with the detection of DA, with the PPy-SCD films developed in this work eliminating the signal from AA. The good performance of the sensor at both concentrations of AA can be attributed to the anionic nature of AA, as previously outlined in this section.

AA exists as a negatively charged species at pH 7.4[13], Figure 5.3, and therefore materials that repel anions can separate or eliminate the interference of AA and have been used to modify electrodes in the design of various sensors. The most common approach is the use of Nafion®, a permselective membrane, which repels the negatively charged AA anion from the electrode surface, thus enabling the discrimination of the AA and DA oxidation waves[17, 18].

Other examples of modified electrodes that separate the oxidation waves of AA and DA are carbon nanotubes[19], poly(sulfosalicyclic acid) and poly(vinyl alcohol) modified glassy carbon electrodes[16, 20], gels containing an ionic liquid and multiwalled carbon nanotubes[21], polymer/metal nanoparticles[22, 23], self-assembled monolayers[24, 25] and overoxidised polymers[26]. Table 5.6 summarises the obtained findings of the said literature.

As shown in Table 5.6 the PPy-SCD modified electrode compares very well with the literature, eliminating interference at high AA:DA ratios. Other materials, especially those reported by Zheng and Zhou[12] and Won *et al.*[27] come close to the performance of the PPy-SCD sensor. For example, Zheng and Zhou[12] have shown that a 4.0 x 10^{-3} mol dm^{-3} AA solution has no electrochemical response at a carbon paste electrode modified by a sodium dodecyl sulfate monolayer. Furthermore, when this concentration of AA is present in a 4.0 x 10^{-5} mol dm^{-3} DA solution, there is no obvious change in the oxidation current of DA due to the electrocatalytic oxidation effect of AA.

Won *et al.*[27] claim that there is virtually no change in the oxidation current of DA in the presence of 3.0 x 10^{-3} mol dm^{-3} AA. The modified electrode used in this case was an electrochemically activated GC electrode modified with a Cu-(3-mercaptopropyl) trimethoxy silane-complex, further coated by a thin layer of Nafion[®]. However, no experimental evidence was given in this paper to back up these claims.

In recent years there has been much interest in the design of selective DA sensors based on cyclodextrins. For example, Alarcon-Angeles *et al.*[28] have modified a GC electrode with a multi-walled carbon nanotubes / neutral β-cyclodextrin film. This electrode was capable of separating the anodic peaks of a mixed solution of DA (0 - 5.0 x 10^{-4} mol dm^{-3}) and AA (8.0 x 10^{-4} mol dm^{-3}) with the presence of AA having no effect on the response to DA. In comparison to these materials, the PPy-SCD modified electrode can eliminate the interference of AA and this is likely to be connected with the anionic character of the sulfonated cyclodextrin.

Thiolated cyclodextrins have also been employed to try and alleviate the selectivity concern of AA and DA. For example, Majewska *et al.*[14] used self-assembled monolayers of a thiolated-α-cyclodextrin with a positively charged cysteamine, while Fragoso *et al.*[29] used self-assembled monolayers of a thiolated-β-cyclodextrin. Majewska *et al.*[14] used a preelectrolysis step that resulted in the resolution of the DA and AA oxidation peaks, while Fragoso *et al.*[29] found that a 10-fold excess of AA did not interfere in the detection of DA.

Table 5.6: Quoted literature results that investigate the effect of AA in the determination of DA.

Reference	Ratio of [AA]:[DA]	Result
PPy-SCD film	1–17:1	No interference
10	1:1	AA and DA oxidation peaks resolved
11	3–50:1	AA and DA oxidation peaks resolved
12	20:1	AA and DA oxidation peaks resolved
13	5:1	AA and DA oxidation peaks resolved
14	8:1	AA and DA oxidation peaks resolved
15	25000–250000:1	AA and DA oxidation peaks resolved
16	1.5:1	AA and DA oxidation peaks resolved
17	1:1	AA and DA oxidation peaks resolved
18	1.04:1	AA and DA oxidation peaks resolved
20	600:1	AA and DA oxidation peaks resolved

There are several other methods of detecting DA selectively in the presence of AA without the use of modified electrodes. One successful approach is to use electrochemistry at the interface between two immiscible electrolyte solutions[30, 31]. Berduque *et al.*[30] found that a large excess of AA did not affect the electrochemical response of DA and Beni *et al.*[31] concluded that AA had no influence on the determination of DA. However, this approach can never be used as an in-vivo sensing method.

In summary, the PPy-SCD modified electrode, which gives highly reproducible results and eliminates the interference from AA, has potential in the design of an *in-vivo* DA sensor.

This new sensor compares very favourably with the best performing sensors currently available and, as shown in Table 5.6, has the added advantage of eliminating the signal from AA at relatively high ratios of AA to DA.

5.3.2 Interference of Epinephrine (EP, Adrenaline)

EP, Figure 5.8, is one of the most important neurotransmitters in the mammalian central nervous system[32]. It is also known to be an important hormone[33] and abnormalities in the concentration levels of EP are symptoms of several diseases[34]. It is a key interfering compound in the selective detection of DA. EP and DA are structurally similar and frequently exist together in natural samples[35]. Their oxidation potentials are very close to each other on most solid electrodes[36]. This results in an overlapping voltammetric response making it difficult to differentiate between them electrochemically. Furthermore, the final product of EP oxidation can be easily transformed into a polymer[37]. This reaction leads to the electrode surface being blocked making the determination of DA in the presence of EP very complicated.
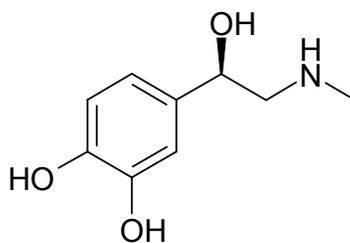
Figure 5.8: Structure of EP

The results obtained from cycling a bare Pt electrode and a PPy-SCD electrode in a 1.0×10^{-3} mol dm^{-3} EP solution in a supporting Na$_2$SO$_4$ electrolyte, are compared in Figure 5.9(a). It can be seen that EP is easily oxidised at the bare Pt electrode giving an oxidation wave at 0.460 V vs. SCE. An oxidation and reduction peak was observed at 0.470 V vs. SCE and 0.350 V vs. SCE, respectively, at the PPy-SCD modified electrode. This is in the

same potential region where DA oxidises. The reason why EP is oxidised at the PPy-SCD modified electrode can be attributed to the fact that EP will exist as a positively charged species at the pH of the experiment (pH = 5.7) as the pKa of EP[38] is approximately 9.8. Scheme 5.3 illustrates the protonation of EP. Therefore, the cation will be attracted to the negatively charged sulfonated groups on the β-cyclodextrin. EP can then in turn form a supramolecular inclusion complex with the sulfonated β-cyclodextrin. This is further investigated in Section 5.3.8.

In Figure 5.9(b), the cyclic voltammograms of a PPy-SCD modifed electrode cycled in a pure DA solution and a mixed solution of EP and DA are compared. It can be seen that only one oxidation and reduction peak is observed and that the currents recorded from the mixed solution of EP and DA are higher than that of DA alone. This suggests that both DA and EP are detected concurrently resulting in an overlapping voltammetric response. This is because EP and DA are oxidised at similar potentials at the PPy-SCD modified electrode.
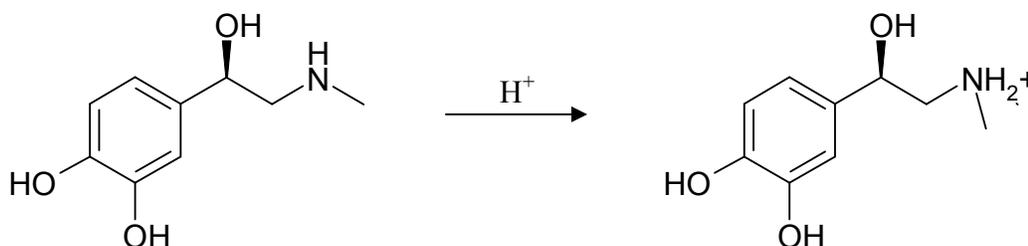
Scheme 5.3: The protonation of EP.

(a)

(b)
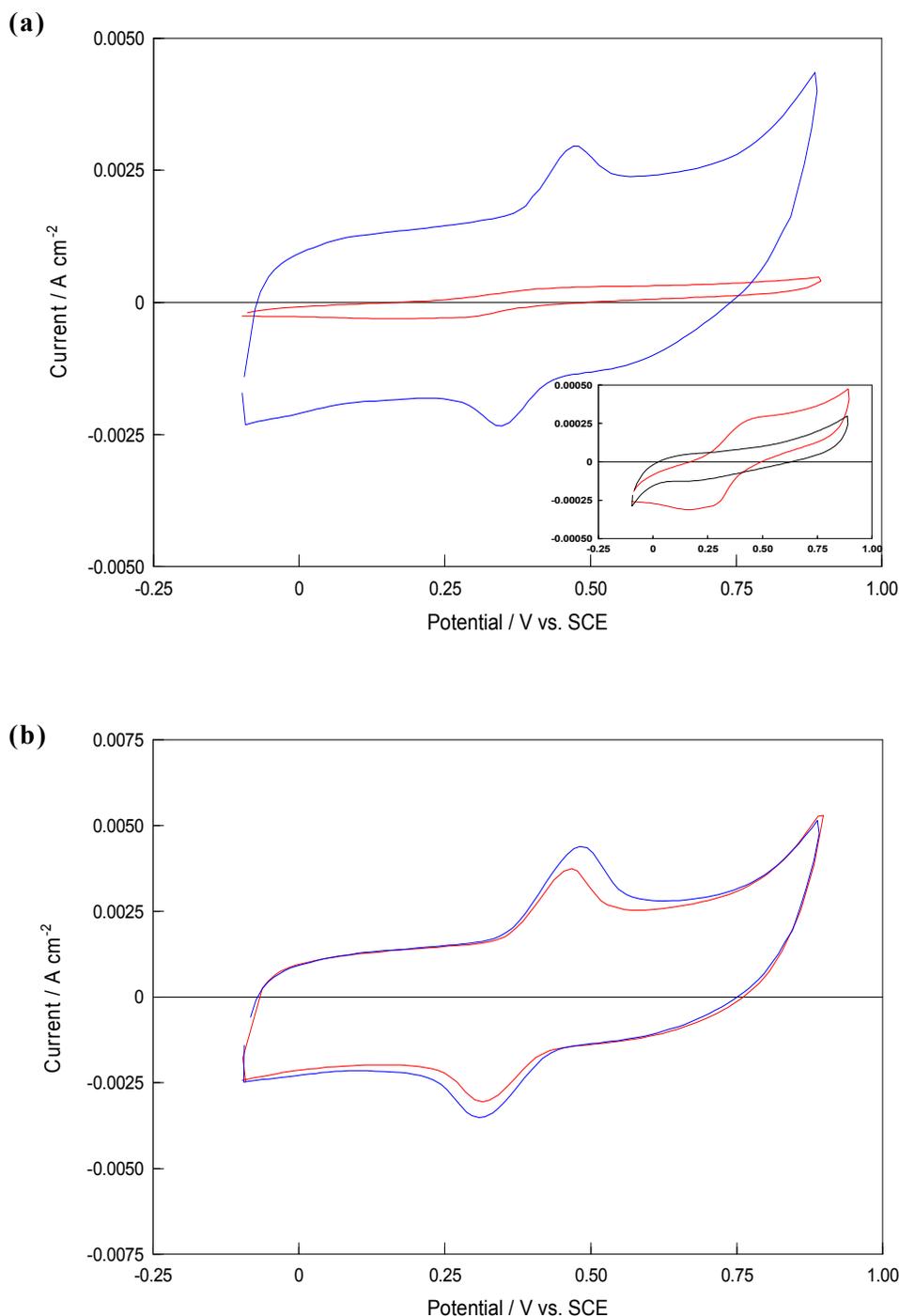
Figure 5.9: (a) Cyclic voltammograms of a ▬ bare Pt electrode and a ▬ PPy-SCD modified electrode in a 1.0 x 10^{-3} mol dm^{-3} EP / 0.10 mol dm^{-3} Na$_2$SO$_4$ solution (pH~5.7). Scan rate = 100 mV s^{-1}. Inset: Cyclic voltammograms of the bare Pt electrode in a ▬ 0.10 mol dm^{-3} Na$_2$SO$_4$ solution and in a ▬ 1.0 x 10^{-3} mol dm^{-3} EP / 0.10 mol dm^{-3} Na$_2$SO$_4$ solution; scan rate = 100 mV s^{-1}. Axes are identical to Figure 5.9(a). (b) Cyclic voltammograms of the PPy-SCD modified electrode in a ▬ 1.0 x 10^{-3} mol dm^{-3} DA / 0.10 mol dm^{-3} Na$_2$SO$_4$ solution (pH~6.0) and in a ▬ 1.0 x 10^{-3} mol dm^{-3} DA / 1.0 x 10^{-3} mol dm^{-3} EP / 0.10 mol dm^{-3} Na$_2$SO$_4$ solution (pH~5.7). Scan rate = 100 mV s^{-1}.

The DA peak oxidation currents observed when a fixed concentration of EP (1.0 x 10^{-3} mol dm^{-3}) was mixed with varying concentrations of DA (7.0 x 10^{-5} to 1.0 x 10^{-3} mol dm^{-3}) are shown in Table 5.7. The mean peak current, the standard deviation and the standard error were calculated from these data. The calculated errors range from 0.68 to 2.34% of the mean value with $n = 3$. These low errors show good agreement over the three replicate EP experiments. In Figure 5.10 the mean peak current is plotted as a function of the DA concentration with a constant amount of added EP (1.0 x 10^{-3} mol dm^{-3}). The current increases with increasing concentration of DA, in a manner similar to that observed in Figure 5.4, however, the currents are higher, indicating interference from the EP.

Table 5.7: Peak currents observed when a fixed concentration of 1.0 x 10^{-3} mol dm^{-3} EP was added to various DA concentrations in a 0.10 mol dm^{-3} Na$_2$SO$_4$, pH~5.7, supporting electrolyte.

Conc. of DA / mol dm^{-3}	I_p^A 1 / A cm^{-2}	I_p^A 2 / A cm^{-2}	I_p^A 3 / A cm^{-2}	Mean I_p^A / A cm^{-2}
7.0 x 10^{-5}	0.002689	0.002664	0.002800	**0.002717**
9.0 x 10^{-5}	0.002953	0.002752	0.002956	**0.002887**
2.0 x 10^{-4}	0.003157	0.003106	0.003178	**0.003147**
5.0 x 10^{-4}	0.003599	0.003496	0.003636	**0.003577**
1.0 x 10^{-3}	0.004169	0.004102	0.004395	**0.004222**

The influence of 1.0 x 10^{-3} mol dm^{-3} EP on the DA oxidation peak currents is summarised in Figure 5.11, where the magnitude of the peak currents obtained with pure DA are compared to the values measured when 1.0 x 10^{-3} mol dm^{-3} EP solution is present. Again, it can be seen that in the presence of 1.0 x 10^{-3} mol dm^{-3} EP, the DA peak currents have increased in intensity. The reason for this is that both DA and EP are detected simultaneously, resulting in an overlapping voltammetric response.
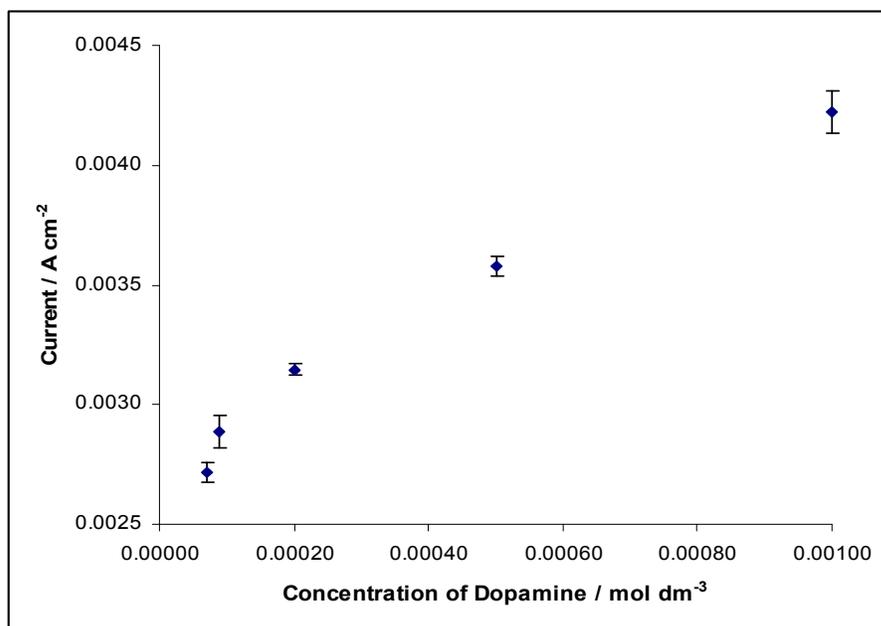
Figure 5.10: Calibration plot of the mean peak current of DA as a function of the concentration of DA where 1.0 x 10^{-3} mol dm^{-3} EP was added to each DA solution in a 0.10 mol dm^{-3} Na$_2$SO$_4$, pH~5.7, supporting electrolyte (*n*=3).
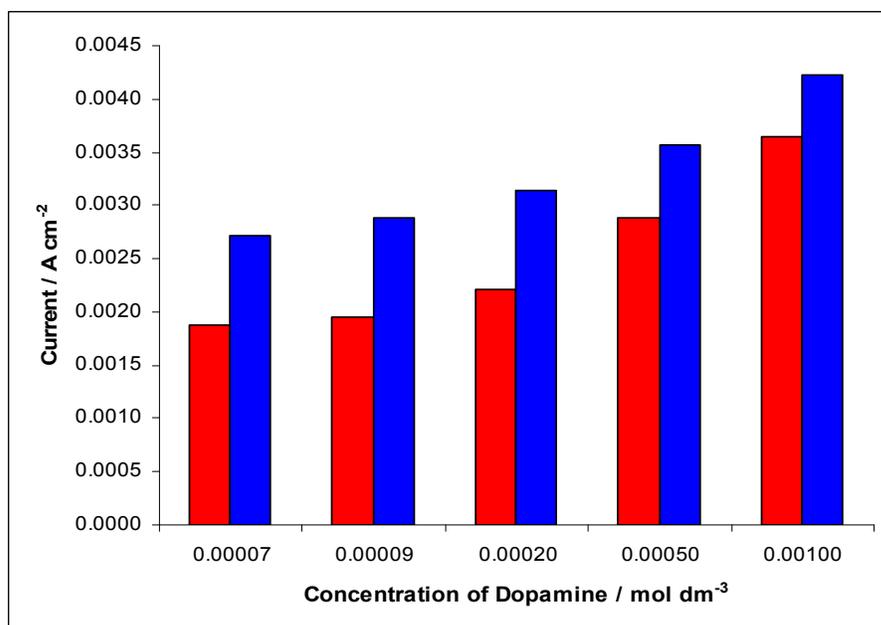
Figure 5.11: Peak current, from the cyclic voltammograms, of DA as a function of the concentration of DA in the ■ presence (*n*=3) and ■ absence (*n*=4) of 1.0 x 10^{-3} mol dm^{-3} EP in a 0.10 mol dm^{-3} Na$_2$SO$_4$, pH~5.7, supporting electrolyte.

The DA oxidation peak potentials for the same experiment were also recorded and are shown in Table 5.8. The mean potentials were then compared to the potentials observed for pure DA and this is illustrated in Figure 5.12. It can be seen that the presence of 1.0×10^{-3} mol dm^{-3} EP with DA has shifted the peak currents to more positive potentials. Again, this shift is due to DA and EP being detected concurrently resulting in an overlapping voltammetric response.

These results show clearly that 1.0×10^{-3} mol dm^{-3} EP does interfere in the electrochemical detection of DA. This can be attributed to the cationic nature of EP, as previously outlined in this section.

Table 5.8: Peak oxidation potentials of various DA concentrations (7.0×10^{-5} to 1.0×10^{-3} mol dm^{-3}) in a fixed concentration of 1.0×10^{-3} mol dm^{-3} EP in a 0.10 mol dm^{-3} Na$_2$SO$_4$, pH~5.7, supporting electrolyte.

Conc. of DA / mol dm^{-3}	E_p^A 1 / V vs. SCE	E_p^A 2 / V vs. SCE	E_p^A 3 / V vs. SCE	Mean E_p^A / V vs. SCE
7.0×10^{-5}	0.4729	0.4734	0.4745	**0.4736**
9.0×10^{-5}	0.4741	0.4758	0.4764	**0.4754**
2.0×10^{-4}	0.4762	0.4811	0.4723	**0.4765**
5.0×10^{-4}	0.4711	0.4833	0.4782	**0.4775**
1.0×10^{-3}	0.4791	0.4811	0.4765	**0.4789**
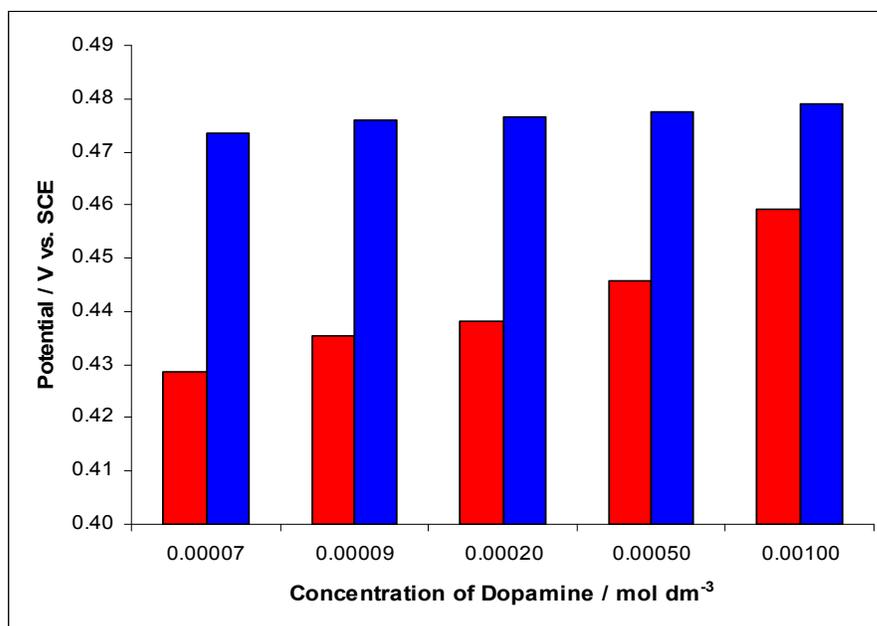
Figure 5.12: Peak potentials of DA oxidation for a range of DA concentrations (7.0 x 10^{-5} to 1.0 x 10^{-3} mol dm^{-3}) obtained using cyclic voltammetry at a scan rate of 100 mV s^{-1} in the ■ presence (*n*=3) and ■ absence (*n*=4) of 1.0 x 10^{-3} mol dm^{-3} EP in a 0.10 mol dm^{-3} Na$_2$SO$_4$, pH~5.7, supporting electrolyte.

There are no reports, to the best of our knowledge, on the manufacture of a modified electrode that can selectively detect DA in the presence of EP. However, various modified electrodes have been developed in an attempt to simultaneously determine EP and DA. These materials generally work by analysing the cathodic peak currents of DA and EP. This approach cannot be used with the PPy-SCD modified electrode as only one reduction peak is observed in the voltammogram in Figure 5.9(b). Table 5.9 summarises the different materials found in the literature that are somewhat successful in the simultaneous detection of DA and EP. In most cases the analysis is focussed on the reduction, or cathodic, peak currents.

Various other materials and techniques have been employed for the determination of DA and EP in samples. These methods usually work by simultaneously detecting DA and EP rather than eliminating EP. Examples of such techniques include capillary electrophoresis using carbon nanotube paste electrodes[39], flow injection analysis and high-performance liquid chromatography with chemiluminescence detection[40], post-column terbium

complexation and sensitised fluorescence detection using high-performance liquid chromatography[41] and peroxidase-based spectrophotometric methods[42]. However, these techniques can never be used for real-time, *in-vivo* sensing. In summary, the PPy-SCD modified electrode cannot eliminate the interference from EP.

Table 5.9: Various materials in the literature that are capable of simultaneously detecting DA and EP.

Reference	Electrode	Result
35	Carbon paste electrode modified with poly($_L$-arginine)	Anodic peaks overlapped. Determination using cathodic peak currents.
43	Glassy carbon electrode modified with poly(caffeic acid)	Anodic peaks overlapped. Determination using anodic and cathodic peak currents.
44	Poly(neutral red) film modified electrodes	Anodic peaks overlapped. Determination using cathodic peak currents.
45	Glassy carbon electrode modified with poly(2,6-pyridine dicarboxylic acid)	Anodic peaks overlapped. Determination using cathodic peak currents.
46	Graphite electrode modified with multi-wall carbon nanotube	Anodic peaks overlapped. Determination using cathodic peak currents.
47	Nickelous macrocyclic complex film modified electrode	Anodic peaks separated. Determination using anodic peak currents.
48	α-cylcodextrin incorporated carbon nanotube-coated pyrolytic graphite electrode	Anodic peaks overlapped. Determination using cathodic peak currents.

5.3.3 Michaelis-Menten Kinetics and Lineweaver-Burk Analysis

Michaelis-Menten kinetics describes the kinetic properties of many enzymes[49]. It involves the enzyme (E) binding to a substrate (S) to form an enzyme-substrate complex (E-S). The enzyme and substrate are in fast equilibrium with the enzyme-substrate complex, which then dissociates to generate free enzyme and the substrate is converted to a product (P). This may be described by Equation 5.14,

$$[E] + [S] \quad \underset{k_{-1}}{\overset{k_1}{\rightleftharpoons}} \quad [E\text{-}S] \quad \xrightarrow{k_2} \quad [E] + [P] \qquad \qquad 5.14$$
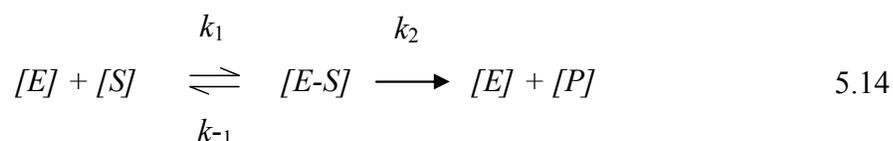
where k_1, k_{-1} are rate constants for the association of substrate and enzyme and the dissociation of substrate from the enzyme, respectively. k_2 is the rate constant for the dissociation of converted substrate (product). Two major assumptions are made in this analysis. The first is that there must be a vast excess of substrate so that *[S] >> [E]* and the second is that the *[E-S]* complex is formed and broken down at the same rate, *i.e.*, the system is at steady-state conditions[50].

The Michaelis-Menten equation describes the relationship between the rate of substrate conversion by an enzyme and the concentration of the substrate and is given by Equation 5.15. In this equation, V is the rate of substrate conversion, V_{max} is the maximum rate of substrate conversion, [S] is the substrate concentration and K_m is the Michaelis constant[51].

$$V = \frac{V_{max}[S]}{K_m + [S]} \qquad \qquad 5.15$$

where
$$K_m = \frac{k_{-1} + k_2}{k_1} \qquad \qquad 5.16$$

and
$$V_{max} = k_2([E] + [E - S]) \qquad \qquad 5.17$$

In order to determine the rate of substrate conversion (V), experiments must be carried out where the substrate concentration, ([S]), is increased until the maximum rate of substrate conversion, (V_{max}), is reached. At this point, the enzyme active sites are saturated with substrate. V will increase with increasing [S], asymptotically approaching $V_{max,}$ as shown in Figure 5.13. This is known as a Michaelis plot. The V_{max} asymptote is never reached therefore an accurate determination of V_{max} is not possible. Instead, the Michaelis constant (K_m) can be used to describe the kinetics of the reaction, if the data fit the hyperbolic curve. K_m is equivalent to the substrate concentration, [S], at which the V reaches half of the V_{max} value. Since V_{max} cannot be accurately determined, an estimate of V_{max} is used to determine K_m. K_m approximates how tightly the substrate is bound to the enzyme. A low K_m value indicates tight binding, whereas a high K_m value suggests weak binding. Typical K_m values for enzyme systems range from micromolar to millimolar[52].
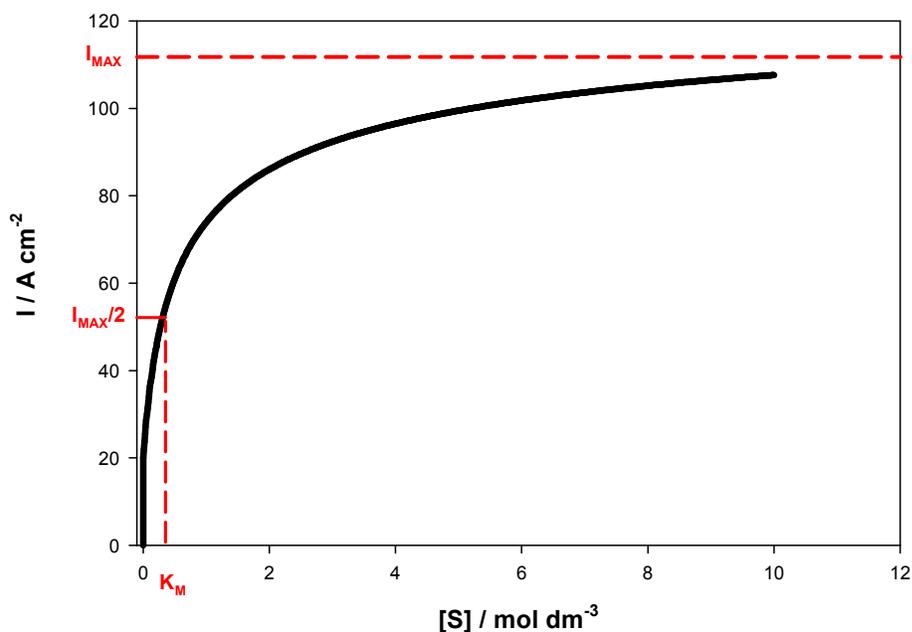
**Figure 5.13: Typical Michaelis plot for an enzyme showing the relationship between the concentration of substrate, ([S]), and the rate of the conversion, (V). I_{max} and K_m are highlighted in red on the graph.**

In order to see if there was any binding interaction between the DA and the PPy-SCD film the Michaelis-Menten equation was applied to the constant potential amperometry data for DA from Chapter 3, Section 3.3.7.2. In this case V is equal to the current, I, and subsequently V_{max} is equal to I_{max}. It can be seen from Figure 5.14 that the curve obeys the Michaelis-Menten equation with a correlation coefficient of 0.9992. The Michaelis constant, K_m, and the maximum current, I_{max}, were determined from this curve with values of 1.53 x 10^{-3} mol dm^{-3} and 1.17 x 10^{-3} A cm^{-2}, respectively. As this value of K_m is relatively high this would suggest that the DA interacts weakly with the PPy-SCD film.

It can be seen from Figure 5.14 that the curve does not approach a true I_{max}. Therefore, the K_m value determined can only be taken as an estimate of the binding between DA and the PPy-SCD electrode. Theoretically, higher concentrations of DA should have been investigated. However, 1.0 x 10^{-3} mol dm^{-3} DA is significantly higher than typical concentrations of DA found in biological samples. In this respect, the data obtained from the curve are acceptable as it is the lower concentrations of DA that are of interest.
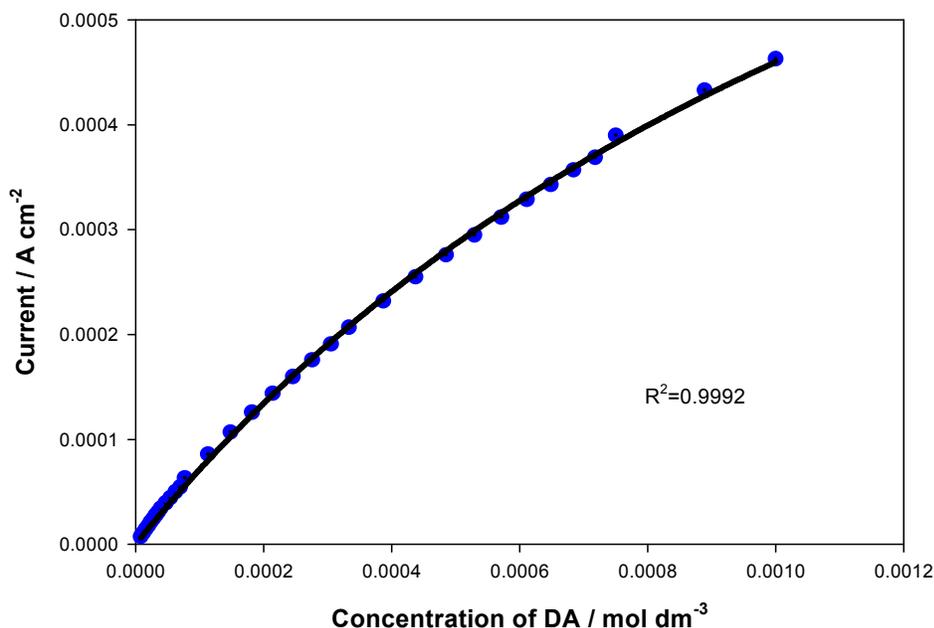
Figure 5.14: Michaelis plot of the currents recorded from the constant potential amperometry data, presented in Chapter 3, versus the concentration of DA, (n = 4), at the PPy-SCD modified electrode at a rotation speed of 2000 rpm and a constant holding potential of +0.650 V vs. SCE.

As already mentioned, there are limitations in the quantitative analysis of the Michaelis-Menten equation. This is due to the fact that V_{max} is never really reached therefore V_{max} and hence K_m values calculated from this curve are approximate. A more practical way to determine V_{max} and K_m, although still not ideal, is to convert the data into a linear Lineweaver-Burk plot[53]. The Lineweaver-Burk equation, shown in Equation 5.18, is a linear transformation of the Michaelis-Menten equation generated by taking the reciprocal of both sides.

$$\frac{1}{V} = \frac{1}{V_{max}} + \frac{K_m}{V_{max}[S]}$$

5.18

A plot of $1/V$ versus $1/[S]$ yields a straight line, as shown in Figure 5.15. The y-intercept of this graph is equivalent to the inverse of V_{max} and the x-intercept of this graph represents $-1/K_m$. In terms of the DA-PPy-SCD system, V will be equal to the current, I, and V_{max} is equivalent to I_{max}. A plot $1/I$ versus $1/[DA]$ is illustrated in Figure 5.16. It can be seen that the data fit the Lineweaver-Burk equation with a correlation coefficient of 0.9997. Values of K_m and I_{max} were estimated as 6.34 x 10^{-4} mol dm^{-3} and 5.89 x 10^{-4} A cm^{-2}, respectively, from this analysis. These values are somewhat lower than the values evaluated using the Michaelis-Menten equation. Even though the K_m value estimated from the Lineweaver-Burk equation is lower than the K_m value obtained using the Michaelis-Menten equation, it is still quite a high K_m value. This indicates that the binding interaction between the DA and the PPy-SCD film is relatively weak, confirming the outcome from the Michaelis-Menten analysis.
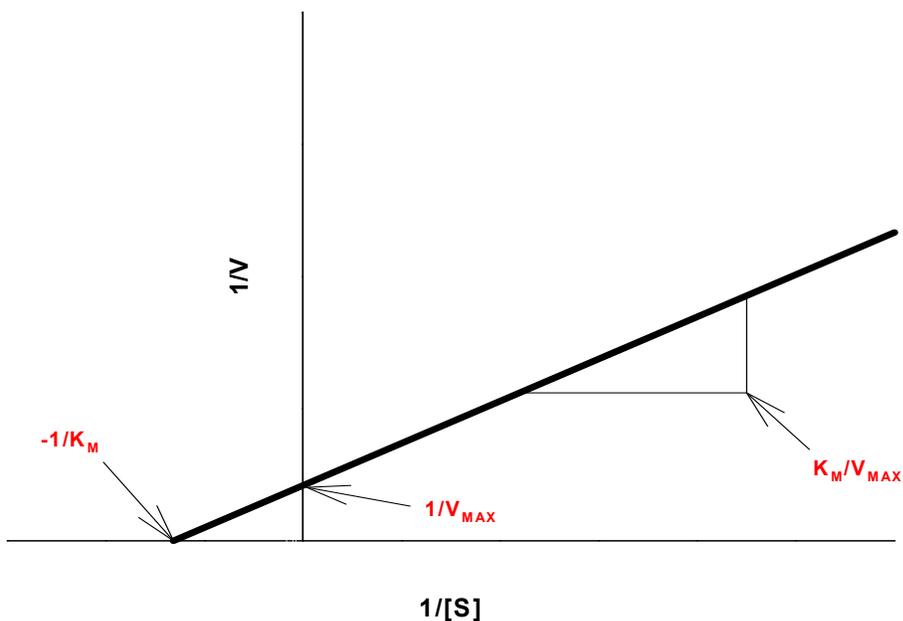
Figure 5.15: Typical Lineweaver-Burk plot for an enzyme showing the relationship between the concentration of substrate ([S]) and the rate of the conversion (V). V_{max} **and** K_m **are highlighted in red on the graph.**
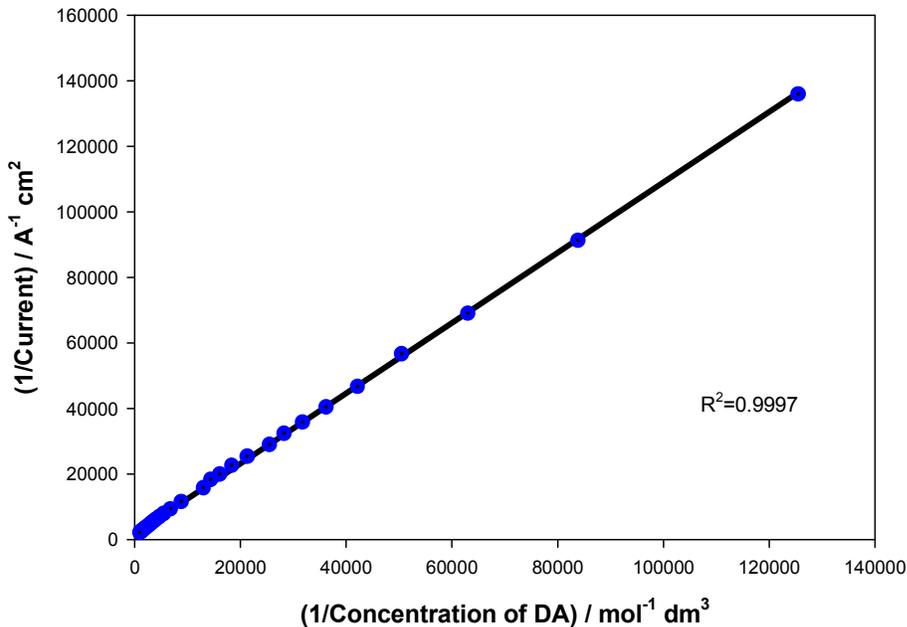
Figure 5.16: Lineweaver-Burk plot of the currents recorded from the constant potential amperometry data, presented in Chapter 3, versus the concentration of DA, (n = 4), at the PPy-SCD modified electrode at a rotation speed of 2000 rpm and a constant holding potential of +0.650 V vs. SCE.

Even though the PPy-SCD film is not an enzyme, the Michaelis-Menten equation and the Lineweaver-Burk equation can be applied to this system to gauge if there is any binding interaction between it and the DA. This is because cyclodextrins can mimic enzyme-catalysed reactions and this has been well documented in the literature[54]. The PPy-SCD and DA binding can be summarised in Equation 5.19, where the PPy-SCD is equivalent to the enzyme, (E), DA is equivalent to the substrate, (S), and the binding of the PPy-SCD with DA, ([PPy-SCD-DA]), can be correlated with the enzyme substrate complex, [E-S], Equation 5.14.

$$[PPy\text{-}SCD] + [DA] \underset{k_{-1}}{\overset{k_1}{\rightleftharpoons}} [PPy\text{-}SCD\text{-}DA] \xrightarrow{k_2} [PPy\text{-}SCD] + [Ox\text{-}DA] \quad 5.19$$
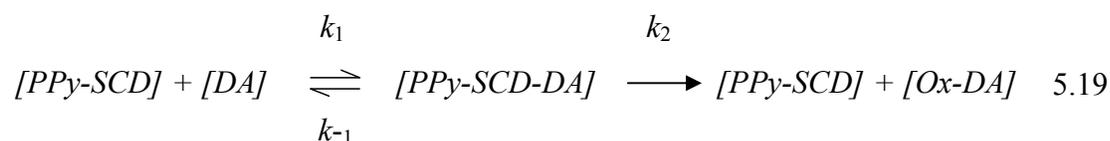
As the K_m values calculated from the Michaelis-Menten equation and the Lineweaver-Burk equation are relatively high this suggests that there is a weak interaction between the DA and the sulfonated β-cyclodextrin. This means that the complex can then easily dissociate into free polymer and the oxidised DA product, DOQ, as described in Equation 5.19.

The Michaelis-Menten equation has been used to characterise the kinetics between many enzymes and substrates. Wang *et al.*[55] used the Michaelis-Menten equation to evaluate the affinity of sertraline, desmethylsertraline, bupropion and its three major metabolites and verapamil for P-glycoprotein. The authors found that sertraline, desmethylsertraline and verapamil had a high affinity for P-glycoprotein with K_m values of 4.70×10^{-6} mol dm^{-3}, 6.50×10^{-6} mol dm^{-3} and 8.70×10^{-6} mol dm^{-3} determined for each, respectively. Bupropion and its three major metabolites had a weak affinity for P-glycoprotein with K_m values of 2.70×10^{-3} mol dm^{-3}, 3.20×10^{-4} mol dm^{-3}, 2.10×10^{-3} mol dm^{-3} and 1.10×10^{-4} mol dm^{-3}. The higher K_m values described by Wang *et al.*[55] are very comparable to the K_m value obtained between the DA and the PPy-SCD film. This supports the earlier statement that the complex formed between the DA and the polymer is relatively weak.

The Lineweaver-Burk equation has also been used to analyse the kinetics between enzymes and substrates. Tu and Chen[56] and Wititsuwannakul *et al.*[57] determined the K_m value

between DA and polyphenol oxidase (PPO) using the Lineweaver-Burk equation. Wititsuwannakul *et al.*[57] determined this value in solution using two PPOs, PPO-I and PPO-II, reporting K_m values of 2.08 x 10^{-3} mol dm^{-3} for PPO-I and DA, and 2.12 x 10^{-3} mol dm^{-3} for PPO-II and DA. Tu and Chen[56] used immobilised PPO to determine the K_m value. The PPO was immobilised in a β-cyclodextrin polymer that had tetramethylbenzidine and ferrocene included in its cavity. A K_m value of 6.90 x 10^{-6} mol dm^{-3} was found between the DA and the immobilised PPO. The K_m value reported by Wititsuwannakul *et al.*[57] is in good agreement with the K_m value calculated for DA and the PPy-SCD film, while the K_m value evaluated by Tu and Chen[56] is much lower.

Another factor that needs to be considered is that the PPy-SCD film is immobilised onto an electrode surface whereas the enzymes investigated by Wang *et al.*[55] and Wititsuwannakul *et al.*[57] are in solution. The kinetics of immobilised enzymes may be different from those measured for the same enzyme in free solution. Therefore, the K_m value obtained between the DA and the PPy-SCD film and the K_m values evaluated by Wang *et al.*[55] and Wititsuwannakul *et al.*[57] cannot be directly compared, as they are two different systems. In general the K_m value will increase if the enzyme is immobilised. However, it has been shown that the K_m value of an immobilised enzyme can equal the K_m value of the free enzyme[58] or even be lower[59], depending on the type of enzyme, support and substrate. Wang *et al.*[60], Bhatia *et al.*[61] and Duggal and Buchholz[62] all observed the phenomena of the K_m value increasing. The change in the affinity of the enzyme to the substrate can result from a number of factors, including structural changes which can lower the accessibility of the substrate to the active site[63], diffusion limitations, or interactions with the support[64].

To the best of our knowledge, there are no reports on the evaluation of a K_m value between DA and a PPy film doped with sulfonated β-cyclodextrin. This analysis clearly shows that there is some binding interaction between the DA and the PPy-CD film.

5.3.4 Complexation between Dopamine and the Sulfonated β-Cyclodextrin and an Investigation into the Mechanism of Sensing at the PPy-SCD Modified Electrode

The results acquired from the Michaelis-Menten kinetics and the Lineweaver-Burk analyses indicate that there is some kind of interaction between the DA and the PPy-SCD film. This interaction could arise solely from DA forming an inclusion complex with the sulfonated β-cyclodextrin. On the other hand, the interaction could be purely electrostatic, with the negatively charged sulfonated groups on the cyclodextrin attracting the cationic DA. Alternatively, it could be a combination of both these effects.

Cyclodextrins are well-known for their ability to include a variety of guest molecules into their cavities[65]. Inclusion usually occurs without the formation of any covalent bonds[66]. The type of compounds that can be included into the cavity and the stability of the inclusion complex depends on a number of factors, such as the size of the cavity, the shape of the guest molecules, electrostatic interactions and hydrophobic forces[8]. In particular, compounds usually need to be hydrophobic in nature to be included. This is because cyclodextrins have a hydrophobic internal cavity which will allow the hydrophobic guest molecule, or hydrophobic moieties in the guest molecule, to incorporate[67]. In general, the apolar part of the molecule will bind with the internal surface of the cyclodextrin, while the hydrophilic part of the molecule remains as far as possible on the outer face of the complex[11]. Therefore, the hydrophobic component of DA may form an inclusion complex with the hydrophobic internal cavity of the sulfonated β-cyclodextrin.

In terms of the interaction being a mixture of complexation and electrostatic contributions, it has already been shown in the literature that electrostatic interactions will affect the stability of an inclusion complex. Hbaieb *et al.*[68] obtained enhanced complexation for anions when the β-cyclodextrin was functionalised with cationic amino groups. Therefore, the stability of the inclusion complex, if one is formed, between DA and the β-cyclodextrin, will possibly be increased by the presence of the sulfonated groups. Alternatively, purely electrostatic interactions might only occur because the cationic DA is attracted to the

anionic sulfonated groups. In either situation both electrostatic interactions and complexation will be important in the sensing of DA.

Cyclic voltammetry was firstly used to investigate if an inclusion complex was formed between the DA and the sulfonated β-cyclodextrin in solution. These data were recorded with a fixed concentration of DA, 5.0×10^{-4} mol dm^{-3}, at a glassy carbon (GC) electrode in a buffered citrate-phosphate, pH 6.0, solution. The concentration of the sulfonated cyclodextrin was varied from 2.0×10^{-2} mol dm^{-3} to 2.5×10^{-3} mol dm^{-3} to give DA-containing solutions with an excess of the anionic sulfonated β-cyclodextrin. The voltammograms recorded for the pure DA solution were then compared with the data recorded in the presence of the sufonated β-cyclodextrin. Figure 5.17 shows the effect of the sulfonated β-cyclodextrin on the cyclic voltammetry of DA. The solutions of DA in the presence of varying concentrations of sulfonated β-cyclodextrin produce similar electrochemical characteristics as the free DA, but the anodic peak potentials are shifted to more positive potentials. The peak currents, also, decrease with increasing concentrations of sulfonated β-cyclodextrin. This reduction in the peak current and the anodic shift of the peak potentials for the oxidation of the analyte are indicative of the formation of inclusion complexes[5, 69]. The shift in the peak potentials reveals that the DA is more difficult to oxidise in the presence of the sulfonated β-cyclodextrin because it is included in the hydrophobic cavity. The decrease in the peak currents is consistent with a lower diffusion coefficient of the included DA compared to that of free DA. The sulfonated β-cyclodextrin is large and bulky and this will give rise to a measurable decrease in the diffusion coefficient of the encapsulated DA.

Interestingly, there is no change in the potential at which the DOQ is reduced and converted back to DA with increasing concentrations of the sulfonated β-cyclodextrin. This can be seen from the position of the peak reduction potentials in Figure 5.17. For example, the peak potential is 0.064 V vs. SCE in the absence of the sulfonated β-cyclodextrin and 0.060 V vs. SCE in the presence of the 0.02 mol dm^3 sulfonated β-cyclodextrin. These observations illustrate that once the included DA is converted to DOQ, it is expelled from the cavity. The polymer and sulfonated β-cyclodextrin sites are then regenerated leaving them available for more reactions.

The complex formation constant, K, between the DA and the sulfonated β-cyclodextrin was evaluated using Equation 5.20. In this analysis, C_p represents the concentration of sulfonated β-cyclodextrin, A is the proportional constant, i_o and i are the peak currents without and with sulfonated β-cyclodextrin, respectively, and K is the complex formation constant[70]. A plot of $1/C_p$ versus $1/(1-i/i_o)$ yields a straight line, as shown in Figure 5.18, with a correlation coefficient of 0.9997. The intercept of the graph is equivalent to the complex formation constant, K. A complex formation constant, K, of 199.54 ± 4.88 mol^{-1} dm^3 was retrieved from this analysis.
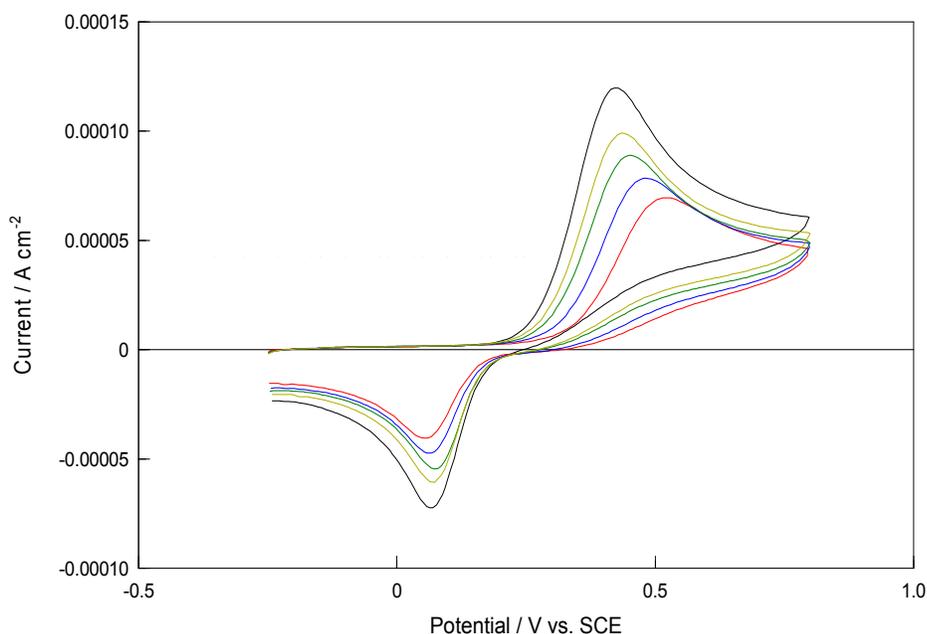
Figure 5.17: Cyclic voltammograms of a bare GC electrode in a ▬ 5.0 x 10^{-4} mol dm^{-3} DA / 0.30 mol dm^{-3} citrate phosphate buffer solution and in a ▬ 5.0 x 10^{-4} mol dm^{-3} DA / 0.02 mol dm^{-3} sulfonated β-cyclodextrin / 0.30 mol dm^{-3} citrate phosphate buffer solution, ▬ 5.0 x 10^{-4} mol dm^{-3} DA / 0.010 mol dm^{-3} sulfonated β-cyclodextrin / 0.30 mol dm^{-3} citrate phosphate buffer solution, ▬ 5.0 x 10^{-4} mol dm^{-3} DA / 5.0 x 10^{-3} mol dm^{-3} sulfonated β-cyclodextrin / 0.30 mol dm^{-3} citrate phosphate buffer solution and in a ▬ 5.0 x 10^{-4} mol dm^{-3} DA / 2.5 x 10^{-3} mol dm^{-3} sulfonated β-cyclodextrin / 0.30 mol dm^{-3} citrate phosphate buffer solution (pH of all solutions ~ 6.0). Scan rate = 50 mV s^{-1}. Electrochemical Window: -0.250 V vs. SCE to 0.800 V vs. SCE.

$$\frac{1}{C_p} = K \frac{(1\text{-}A)}{1-i/i_o} \text{-}K \qquad\qquad 5.20$$
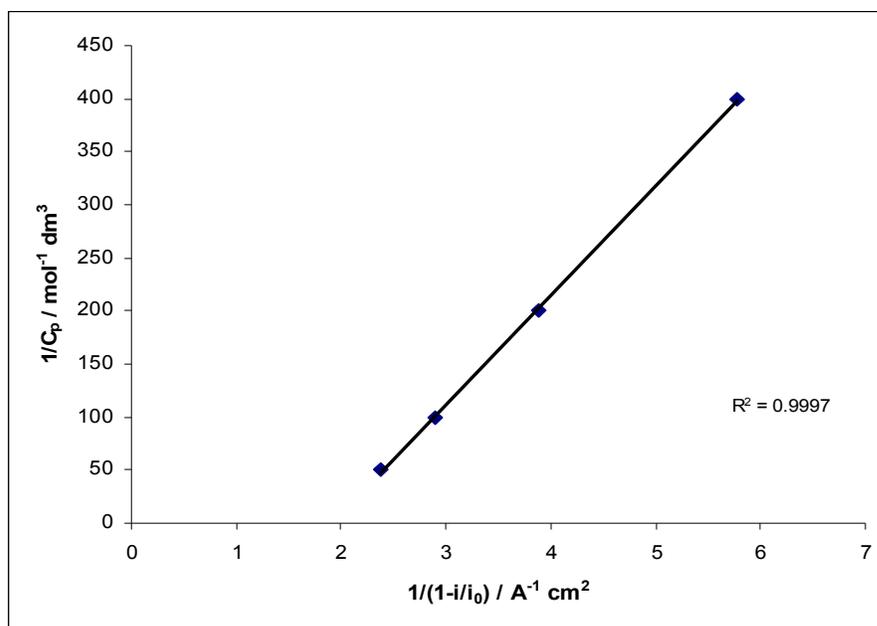
Figure 5.18: Plot of 1/C versus 1/(1-i/i₀). Data taken from the voltammetry plots presented in Figure 5.17.

Equation 5.20 is subject to some stipulations. The concentration of cyclodextrin, C_p, must be larger than the total concentration (C_t) of DA in solution and a 1:1 association complex must be formed. In this analysis, the cyclodextrin concentration was maintained in large excess, satisfying the first condition. Consequently, as the experimental data correspond well to Equation 5.20, this may suggest that a 1:1 association complex is formed between the DA and the sulfonated β-cyclodextrin. This will be further investigated in Section 5.3.5.

To further prove complexation rotation disc voltammetry was carried out on the DA and sulfonated β-cyclodextrin in solution. Again, these data were recorded with a GC electrode in a citrate-phosphate buffer (pH 6.0). The DA concentration was maintained at a constant value of 5.0×10^{-4} mol dm⁻³, while the sulfonated β-cyclodextrin concentration was kept in excess, ranging from 2.5×10^{-3} mol dm⁻³ to 2.0×10^{-2} mol dm⁻³. Rotation rates were varied from 50 to 2000 rpm. Figure 5.19 shows the effect of the sulfonated β-cyclodextrin on the rotation disc voltammetry of DA, with a rotation speed of 500 rpm. It can be seen that the half-wave potentials continue to shift to more positive potentials and that the limiting currents decrease as the sulfonated β-cyclodextrin concentration is increased. Similar data

were recorded at higher rotation rates. This confirms the results obtained from cyclic voltammetry.
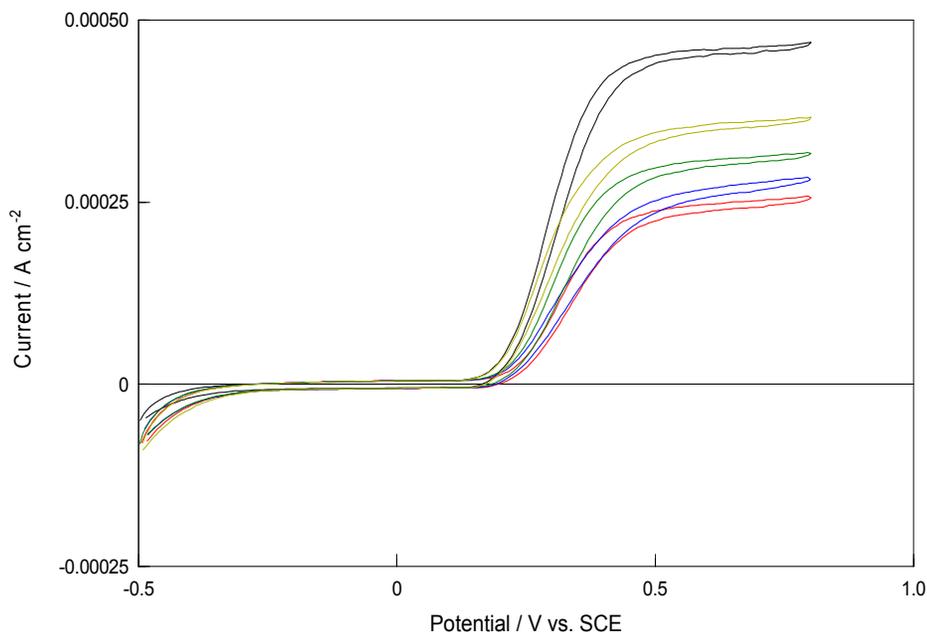
Figure 5.19: Rotation disc voltammograms of a bare GC electrode in a ▬ 5.0 x 10^{-4} mol dm^{-3} DA / 0.30 mol dm^{-3} citrate phosphate buffer solution and in a ▬ 5.0 x 10^{-4} mol dm^{-3} DA / 0.02 mol dm^{-3} sulfonated β-cyclodextrin / 0.30 mol dm^{-3} citrate phosphate buffer solution, ▬ 5.0 x 10^{-4} mol dm^{-3} DA / 0.01 mol dm^{-3} sulfonated β-cyclodextrin / 0.30 mol dm^{-3} citrate phosphate buffer solution, ▬ 5.0 x 10^{-4} mol dm^{-3} DA / 5.0 x 10^{-3} mol dm^{-3} sulfonated β-cyclodextrin / 0.30 mol dm^{-3} citrate phosphate buffer solution and in a ▬ 5.0 x 10^{-4} mol dm^{-3} DA / 2.5 x 10^{-3} mol dm^{-3} sulfonated β-cyclodextrin / 0.30 mol dm^{-3} citrate phosphate buffer solution (pH of all solutions~6.0). Rotation Speed = 500 rpm. Scan Rate = 50 mV s^{-1}. Electrochemical Window: -0.500 V vs. SCE to 0.800 V vs. SCE.

The complex formation constant, *K*, between the DA and the sulfonated β-cyclodextrin was determined using Equation 5.21, which was originally proposed by Galus[69]. Here, *F* is the Faraday constant, *R* is the gas constant, *T* is the temperature, $(E_{1/2})_{app}$ and $(E_{1/2})_f$ are the half-wave potentials in the presence and absence of the sulfonated β-cyclodextrin, respectively. *K* is the complex formation constant and D_c and D_f are the diffusion coefficients in the presence and absence of the sulfonated β-cyclodextrin, respectively.

$$\frac{F}{RT}\left\{\left(E_{\frac{1}{2}}\right)_{app} - \left(E_{\frac{1}{2}}\right)_{f}\right\} = ln\,(1 + K[SCD]) + ln\,(\frac{D_c}{D_f})^{1/2} \qquad 5.21$$

The diffusion coefficients were evaluated using Equation 5.22, also known as the Levich equation. The Levich equation describes the current at a rotating disc electrode, where i_L is the limiting current, n is the number of electrons transferred, F is the Faraday constant, A is the electrode area, D is the diffusion coefficient, ω is the rotation speed, v is the kinematic viscosity and C is the concentration of reactant in solution.

$$i_L = (0.62)nFAD^{2/3}\omega^{1/2}v^{-1/6}C_0 \qquad 5.22$$

The limiting currents for DA and for DA in the presence of the various concentrations of sulfonated β-cyclodextrin were measured and plotted against the square root of the rotation speed. DA, with and without the sulfonated β-cyclodextrin, resulted in good linear Levich plots with zero intercepts, as illustrated in Figure 5.20. The diffusion coefficients were calculated using Equation 5.22 and the slopes from each of the linear plots in Figure 5.20. The kinematic viscosity of the system was taken to be 0.01 cm^2 s^{-1}. Table 5.10 shows the calculated diffusion coefficient values and the half-wave potentials for DA and DA in the presence of various concentrations of sulfonated β-cyclodextrin. A clear decrease in the diffusion coefficient is observed with increasing concentration of the sulfonated β-cyclodextrin. The value of the ratio, D_c/D_f is 0.42, where D_c corresponds to the diffusion coefficient with a large excess of sulfonated β-cyclodextrin. This is in very good agreement with ratios found in the literature for the complexation of ferrocenes with neutral cyclodextrins[69]. A complex formation constant of 240.18 ± 5.87 mol^{-1} dm^3 was determined using Equation 5.21 and the data presented in Table 5.10. This is in good agreement with the value obtained from the cyclic voltammetry data, Figure 5.17.
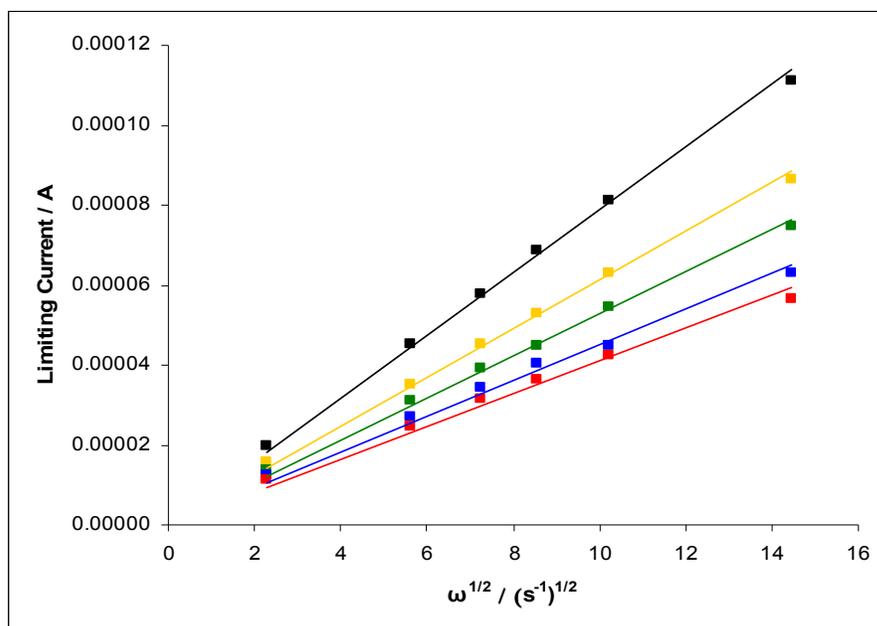
Figure 5.20: Levich plots of the recorded limiting currents from a ▬ 5.0 x 10⁻⁴ mol dm⁻³ DA / 0.30 mol dm⁻³ citrate phosphate buffer solution, a ▬ 5.0 x 10⁻⁴ mol dm⁻³ DA / 0.02 mol dm⁻³ sulfonated β-cyclodextrin / 0.30 mol dm⁻³ citrate phosphate buffer solution, a ▬ 5.0 x 10⁻⁴ mol dm⁻³ DA / 0.01 mol dm⁻³ sulfonated β-cyclodextrin / 0.30 mol dm⁻³ citrate phosphate buffer solution, a ▬ 5.0 x 10⁻⁴ mol dm⁻³ DA / 5.0 x 10⁻³ mol dm⁻³ sulfonated β-cyclodextrin / 0.30 mol dm⁻³ citrate phosphate buffer solution from a ▬ 5.0 x 10⁻⁴ mol dm⁻³ DA / 2.5 x 10³ mol dm⁻³ sulfonated β-cyclodextrin / 0.30 mol dm⁻³ citrate phosphate buffer solution as a function of the square root of the rotation speed; pH of all solutions ~6.0. The limiting currents were recorded at 0.65 V vs. SCE. Rotation Speeds = 50, 300, 500, 700, 1000 and 2000 rpm.

Table 5.10: Diffusion coefficient values and the half-wave potentials for DA and DA in the presence of various concentrations of sulfonated β-cyclodextrin in a citrate-phosphate buffer, pH 6.0.

Concentration of Sulfonated β-Cyclodextrin / mol dm⁻³	Diffusion Coefficient / cm² s⁻¹	Half Wave Potentials / V vs. SCE
0	1.07×10^{-5}	0.2953
2.5×10^{-3}	7.31×10^{-6}	0.2838
5.0×10^{-3}	5.87×10^{-6}	0.3018
1.0×10^{-2}	4.64×10^{-6}	0.3151
2.0×10^{-2}	4.03×10^{-6}	0.3231

The results presented in this section so far confirm that an inclusion complex is formed between DA and the sulfonated β-cyclodextrin. Therefore, the interaction between the DA and the sulfonated β-cyclodextrin cannot be purely electrostatic. However, as already mentioned, electrostatic interactions may play an important role in the stability of the inclusion complex.

In an attempt to determine the role, if any, that electrostatic interactions play rotation disc voltammetry was used to see if an inclusion complex was formed between DA and the neutral β-cyclodextrin in solution. Figure 5.21 shows the effect of the neutral β-cyclodextrin on the rotation disc voltammetry of DA. These data were recorded at 50 rpm and therefore, the distinct limiting currents observed in Figure 5.19 are not seen. A large excess of the neutral cyclodextrin was used. As evident from Figure 5.21, there is little evidence of complexation between the DA and the neutral β-cyclodextrin. The half-wave potentials do not shift to more positive potentials and the currents do not decrease in the presence of a high concentration of the neutral β-cyclodextrin. This is very different to that observed in Figures 5.17 or 5.19 with the sulfonated β-cyclodextrin. This indicates that electrostatic interactions between the anionic sulfonated groups on the cyclodextrin and the cationic DA are crucial in the formation of a complex between the sulfonated β-cyclodextrin and the DA. Further evidence to support the role of electrostatic interactions comes from the fact that a polymer doped with the neutral β-cyclodextrin cannot detect DA as efficiently as the PPy-SCD modified electrode, as shown in Section 3.3.2.
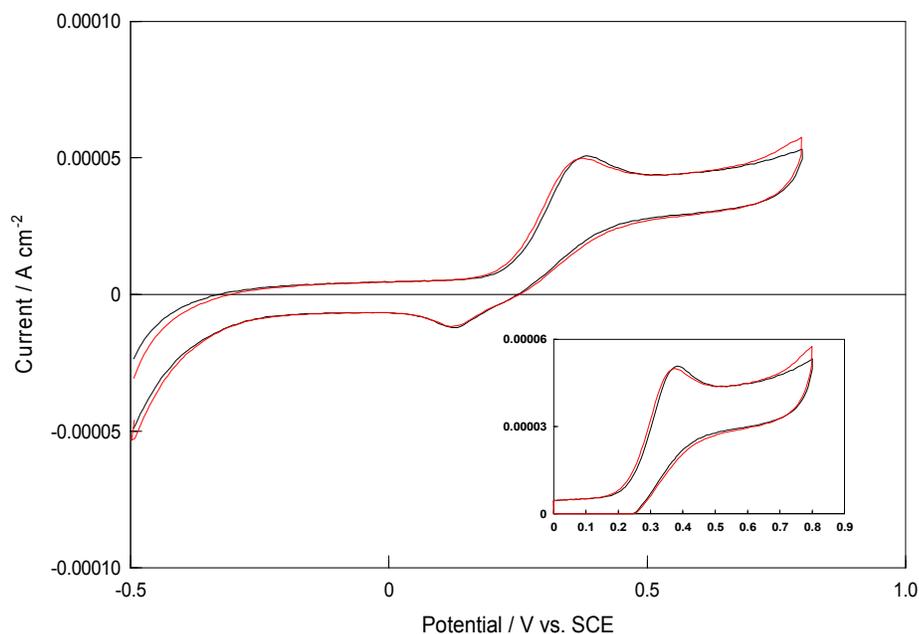
Figure 5.21: Rotation disk voltammograms of a bare GC electrode in a ▬ 1.0 x 10^{-4} mol dm^{-3} DA / 0.30 mol dm^{-3} citrate phosphate buffer solution and in a ▬ 1.0 x 10^{-4} mol dm^{-3} DA / 2.0 x 10^{-3} mol dm^{-3} neutral β-cyclodextrin / 0.30 mol dm^{-3} citrate phosphate buffer solution. (pH of all solutions ~6.0). Rotation Speed = 50 rpm. Inset: Magnification of the oxidation region. Axes are identical to Figure 5.21. Electrochemical Window: -0.500 V vs. SCE to 0.800 V vs. SCE.

According to the above results, the oxidation of DA can be attributed to the formation of an inclusion complex with the sulfonated β-cyclodextrin incorporated as a dopant within the PPy matrix. However, there will be regions of the polymer matrix, that are free from the large sulfonated β-cyclodextrin dopant and accordingly, the oxidation of DA may also occur at these regions, *i.e.*, at the PPy film. To investigate if the oxidation of DA was due solely to the formation of an inclusion complex, or if it was a combination of both oxidation at the polymer film and complexation with the sulfonated β-cyclodextrins, the polymer film was altered so that there were no inclusion sites within the polymer matrix. Sodium dodecyl sulfate (SDS) was chosen as a dopant for the PPy film instead of the sulfonated β-cyclodextrin. This polymer film (PPy-SDS) was then used to investigate if DA could be sensed. As shown in Figure 5.22, SDS contains sulfated groups. However, unlike the sulfonated β-cyclodextrin, it has no cavity for complexation of the DA. The resultant voltammogram recorded on cycling a PPy-SDS modified electrode in a DA solution is illustrated in Figure 5.23. It can be seen from this figure that the DA is oxidised at the SDS

doped polymer film. However, when the cyclic voltammogram recorded at the PPy-SDS modified electrode is compared to the cyclic voltammogram obtained for the same concentration of DA at the PPy-SCD modified electrode, it is obvious that the oxidation of DA is vastly improved by the presence of the sulfonated β-cyclodextrin. This is depicted in Figure 5.24. Indeed, similar results were obtained with PPy films doped with chloride or sulfate; in all cases the oxidation of DA was poor at these films. Therefore, even though the oxidation of DA occurs at the PPy-SCD modified electrode via the formation of an inclusion complex and to some extent at the PPy film, as evidenced from the data presented in Figure 5.24, it appears that complexation plays a more dominant role in the shape of the well-defined DA signal.
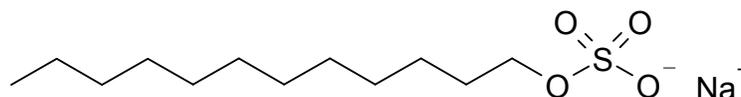
Figure 5.22: Structure of SDS
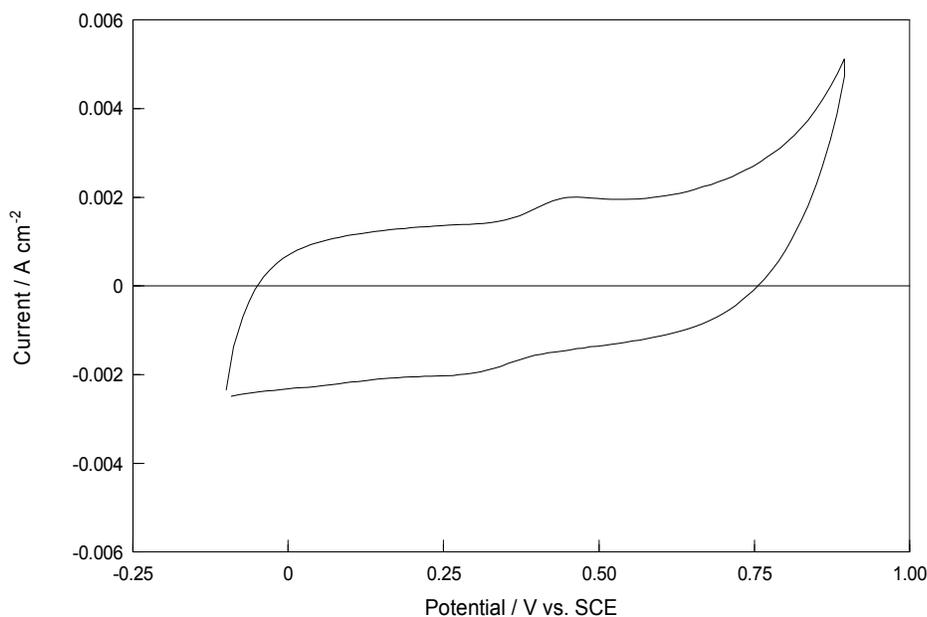
Figure 5.23: Cyclic voltammogram of a PPy-SDS modified electrode in a 1.0 x 10^{-3} mol dm^{-3} DA / 0.10 mol dm^{-3} Na$_2$SO$_4$ solution (pH~6.0). Scan rate = 100 mV s^{-1}.
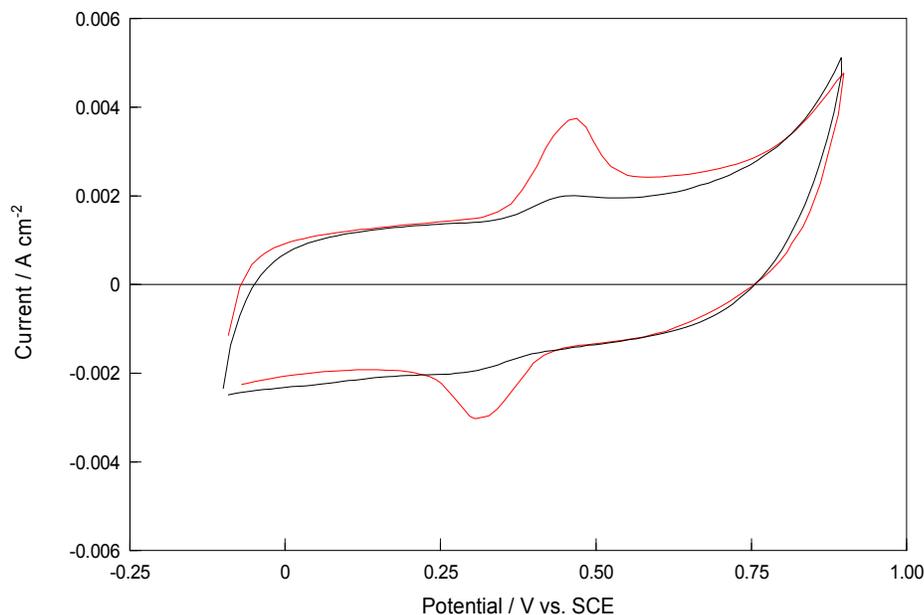
Figure 5.24: Cyclic voltammograms of a ▬ PPy-SDS modifed electrode and a ▬ PPy-SCD modified electrode in a 1.0 x 10^{-3} mol dm^{-3} DA / 0.10 mol dm^{-3} Na$_2$SO$_4$ solution (pH~6.0). Scan rate = 100 mV s^{-1}.

Another feature of the representative cyclic voltammograms of DA at the PPy-SCD and PPy-SDS modified electrodes is that the oxidation and reduction peak currents of DA at the PPy-SDS modified electrode are very similar in magnitude, to give a quasi-reversible system with $I_p^A / I_p^C = 1.0$. However, the oxidation and reduction peak currents of DA at the PPy-SCD modified electrode are somewhat different. This is highlighted in Table 5.11, where the ratios of the oxidation and reduction peak currents of DA at the PPy-SCD and PPy-SDS modified electrodes are compared, together with the peak separation, $\Delta E = (E_{pa} - E_{pc})$. The peak separation values are similar, deviating to a similar degree from the ideal reversible behaviour, where $\Delta E = 0.0592/n$.   The ratio, I_p^A / I_p^C, at the PPy-SCD modified electrode is considerably higher than 1.0, signifying that not all the DOQ, produced during the oxidation of DA, is reduced at the electrode surface. This can be explained in terms of the higher concentration gradient at the PPy-SCD modified electrode compared to that at the PPy-SDS modified electrode. More DA is oxidised at the PPy-SCD modified electrode to give a higher concentration of DOQ and a higher concentration gradient for the diffusion of DOQ from the interface. The effect of the concentration gradient at the PPy-SCD

modified electrode is shown in Table 5.11(a), where the ratio of the oxidation and reduction peak currents of DA approached unity as the concentration of DA decreased. However, the diffusion of the DOQ is more efficient from the PPy-SCD modified electrode than from the PPy-SDS modified electrode. For example, a concentration of 7.0 x 10^{-5} mol dm^{-3} DA at the PPy-SCD modified electrode produced a similar oxidation current to that of a 1.0 x 10^{-3} mol dm^{-3} DA solution at the PPy-SDS modified electrode. However, the I_p^A / I_p^C ratio of the 7.0 x 10^{-5} mol dm^{-3} DA solution at the PPy-SCD modified electrode was 1.14 compared to 0.99 for the 1.0 x 10^{-3} mol dm^{-3} DA solution at the PPy-SDS modified electrode. This indicates that the concentration gradient is not solely responsible for the enhanced diffusion of the DOQ at the PPy-SCD modified electrode. Another factor that could have an influence on the diffusion rate of the DOQ at the PPy-SCD modified electrode might be the arrangement of the sulfonated β-cyclodextrins in the polymer matrix. If some of the sulfonated β-cyclodextrins at the surface of the polymer, point into the double layer, then the oxidised DA, DOQ, would be able to diffuse away from the electrode surface more rapidly and more efficiently, and would account for the observations in Table 5.11(b).

Table 5.11(a): The ratio of the oxidation and reduction peak currents for various concentrations of DA at the PPy-SCD modified electrode.

Conc. of DA / mol dm^{-3}	I_p^A / I_p^C
1.0 x 10^{-3}	1.22
5.0 x 10^{-4}	1.19
2.0 x 10^{-4}	1.17
9.0 x 10^{-5}	1.15
7.0 x 10^{-5}	1.14

Table 5.11(b): Peak separation values and the ratio of the oxidation and reduction peak currents of a 1.0 x 10^{-3} mol dm^{-3} DA solution at the PPy-SCD and PPy-SDS modified electrodes.

	PPy-SCD	PPy-SDS
I_p^A / I_p^C	1.22	1.02
ΔE / V	0.15	0.13

5.3.5 Job's Plot Analysis and Stoichiometry of the Inclusion Complex

The stoichiometry of the DA and sulfonated β-cyclodextrin complex was determined by the Job's method using a spectrophotometric approach. To carry this out, solutions of DA and sulfonated β-cyclodextrin were made up keeping the total molar concentration of the DA and the sulfonated β-cyclodextrin constant, while the mole ratio of DA was varied from 0.0 to 1.0. Further details on these solutions and compositions are presented in Section 2.11.4. The absorbance of each solution was then measured. Typical UV spectral data are presented in Figure 5.25. In a solution containing no sulfonated β-cyclodextrin, the absorbance of the solution is due exclusively to the DA, to give the characteristic λmax of 280 nm. As the concentration of the sulfonated β-cyclodextrin increased, or the mole fraction of DA is decreased, the absorbance at 280 nm decreases. The absorbance from about 240 to 270 nm is due to an impurity in the sulfonated β-cyclodextrin. However, the absorbance of the sulfonated β-cyclodextrin at 280 nm is negligible.

To generate the Job's plot the mole fraction and the change in the absorbance (*ΔA*) were calculated using Equations 5.23 and 5.24. A plot of the mole fraction versus the change in the absorbance times the mole fraction is shown in Figure 5.26. The maximum absorbance occurs at a mole fraction of 0.5 which indicates the formation of a 1:1 host-guest complex between the DA and the sulfonated β-cyclodextrin.

$$Mole\ Fraction = \frac{[DA]}{[DA] + [SCD]}$$
<div align="right">5.23</div>

$$\Delta A = A_{DA} - A_{DA+SCD}$$
<div align="right">5.24</div>
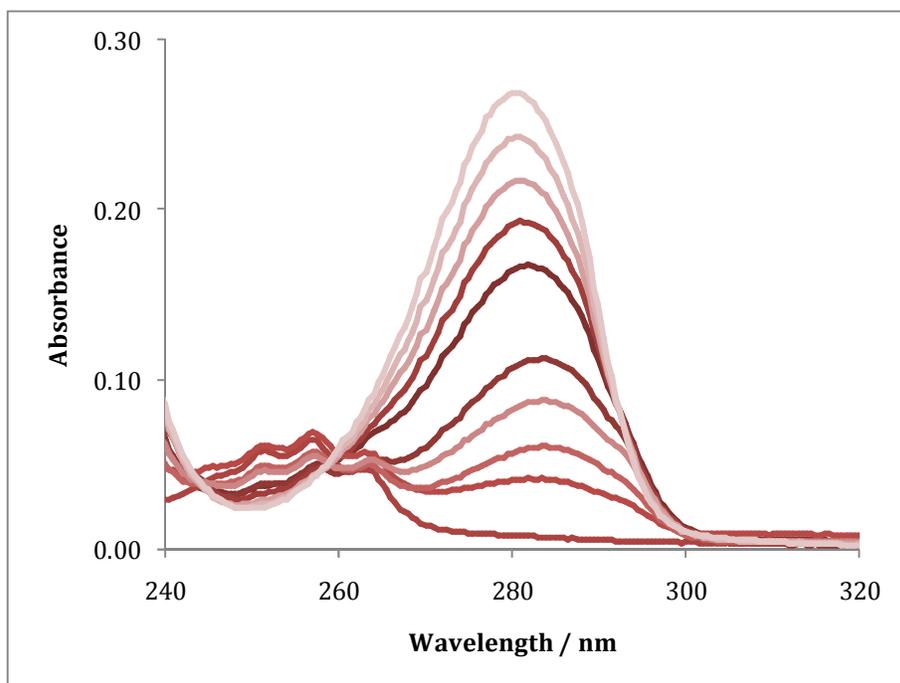
Figure 5.25: UV spectra for the Job's plot titration curve with sulfonated β-cyclodextrin and DA. From low to high absorbance values, the mole fraction of DA increases from 0.0 to 1.0, in increments of 0.1.
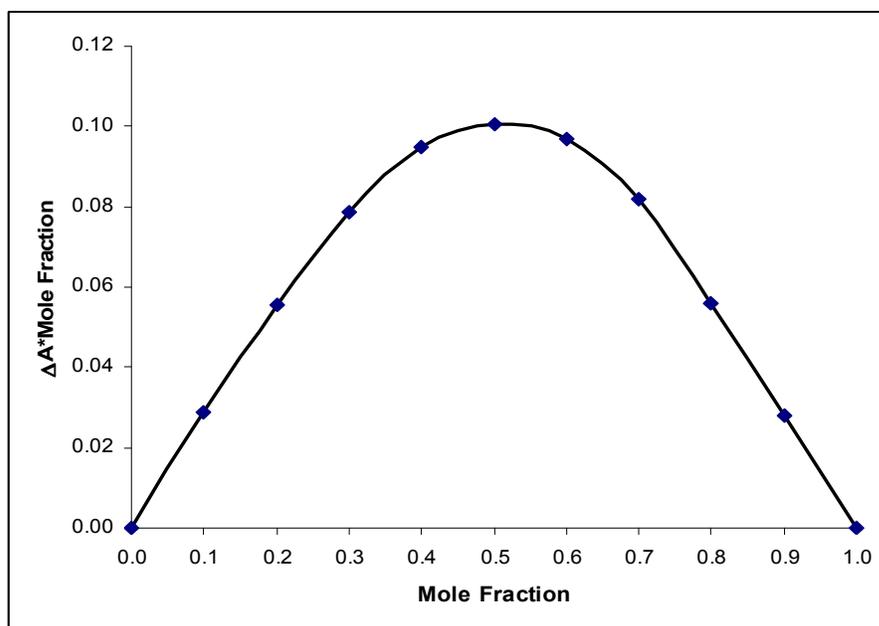
Figure 5.26: Job's plot generated for the DA and the sulfonated β-cyclodextrin system at 298 K, pH~6.0. Absorbance data were taken at 280.5 nm.

It is clear from the results above that a 1:1 inclusion complex is formed between the DA and the sulfonated β-cyclodextrin. The ratio of DA to sulfonated β-cyclodextrin at the maximum absorbance represents the stoichiometry of the complex. As the maximum absorbance occurs at a mole fraction of 0.5, this indicates that a 1:1 complex is formed between the DA and the sulfonated β-cyclodextrin.

There are no reports, to the best of our knowledge, on the stoichiometry of the DA-sulfonated β-cyclodextrin complex. However, Zhou *et al.*[71] determined a 1:1 stoichiometry for the DA and neutral β-cyclodextrin complex, which agrees well with the findings reported here.

5.3.6 NMR Analysis

The manner in which the DA is included, or encapsulated, inside the cavity of the sulfonated β-cyclodextrin was investigated further using nuclear magnetic resonance spectrometry (^{1}H NMR) and the results of this investigation are reported in this section. The environment of individual atoms can be examined and probed using ^{1}H NMR and many researchers have used this method to aid with, or determine, complexation between guest molecules and cyclodextrins[72, 73]. The ^{1}H NMR spectra of the DA, the sulfonated β-cyclodextrin and the mixture of DA and sulfonated β-cyclodextrin are shown in Figure 5.27. As the cyclodextrin is charged, these data were recorded in D_2O and in the presence of 0.1 mol dm^{-3} KCl to buffer the ionic strength. It can be seen that the ^{1}H NMR spectrum of the DA produced clear, well resolved signals, whereas, the ^{1}H NMR spectrum of the sulfonated β-cyclodextrin is very complicated. This is due to the fact that the sulfonated β-cyclodextrin sample is a mixture of substituted cyclodextrins, with the degrees of substitution varying between 7 and 11. This made it very difficult to follow the chemical shifts of the cyclodextrin protons and so the analysis was confined to the guest protons. In particular, the chemical shifts of the protons in the aromatic region can be followed as these are due to the DA molecule and are not complicated from the sulfonated β-cyclodextrin. This is a good region to investigate as the relatively hydrophobic phenol ring of the DA

molecule is more than likely the moiety that includes within the cavity of the sulfonated β-cyclodextrin.
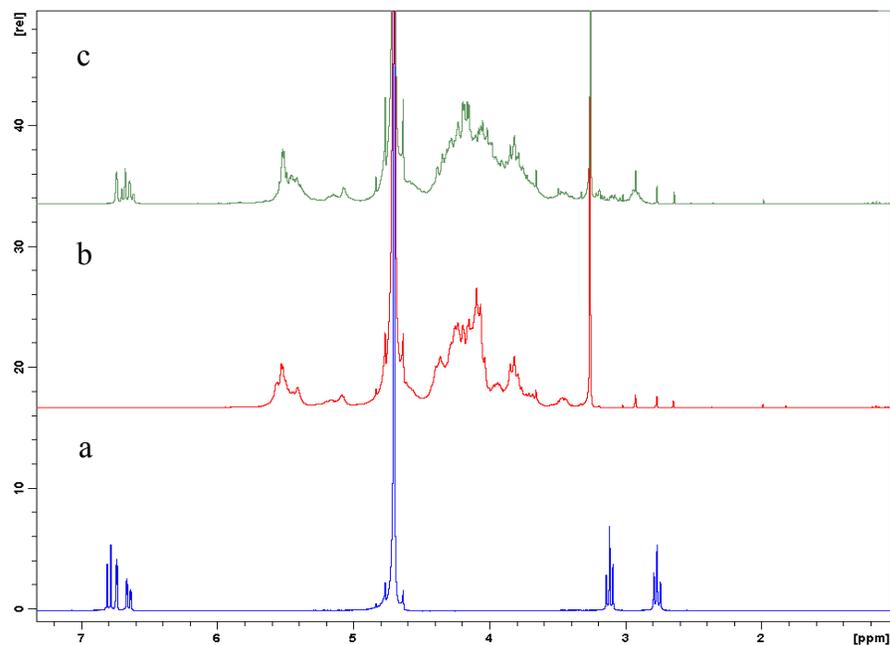
Figure 5.27: ^{1}**H NMR spectra (in D$_2$O and 0.10 mol dm^{-3} KCl) of (a) 5.0 x 10^{-3} mol dm^{-3} DA, (b) 0.02 mol dm^{-3} sulfonated β-cyclodextrin and (c) 5.0 x 10^{-3} mol dm^{-3} DA and 0.02 mol dm^{-3} sulfonated β-cyclodextrin in a solution. NMR experiment was carried out by Gillian Hendy.**

The ^{1}H NMR spectra of the aromatic region of pure DA and the mixture of DA and sulfonated β-cyclodextrin are shown in Figure 5.28. The ^{1}H NMR spectra of the aromatic region of pure DA shows two doublets and a doublet of doublets corresponding to the H_a, H_c and H_b protons, respectively, as indicated in Figure 5.29. It can be seen from Figure 5.28 that the H_a and H_b protons have shifted upfield whereas, the H_c proton remains stationary. This suggests that the H_a and H_b protons are influenced by the sulfonated β-cyclodextrin and are included in the cavity. On the other hand, the H_c proton remains outside the cavity. It was also observed that the H_a proton underwent greater displacement than the H_b proton so it is reasonable to speculate that the H_a proton will be more deeply included within the cavity of the sulfonated β-cyclodextrin. Therefore, the DA will include in the cavity of the sulfonated β-cyclodextrin according to the schematic provided in Figure 5.30. With this

arrangement, the cationic group is maintained outside the cavity and is likely to be electrostatically attracted to the anionic sulfonated groups on the rim of the cavity. In addition, the hydrophilic OH groups are only slightly included to give a stable inclusion complex between the DA and the sulfonated β-cyclodextrin. These NMR data are in good agreement with the cyclic voltammetry and RDE measurements, Section 5.3.4, Michaelis-Menten analysis, Section 5.3.3, and UV spectroscopy measurements, Section 5.3.5, provided earlier and confirm the formation of an inclusion complex between DA and the sulfonated β-cyclodextrin.
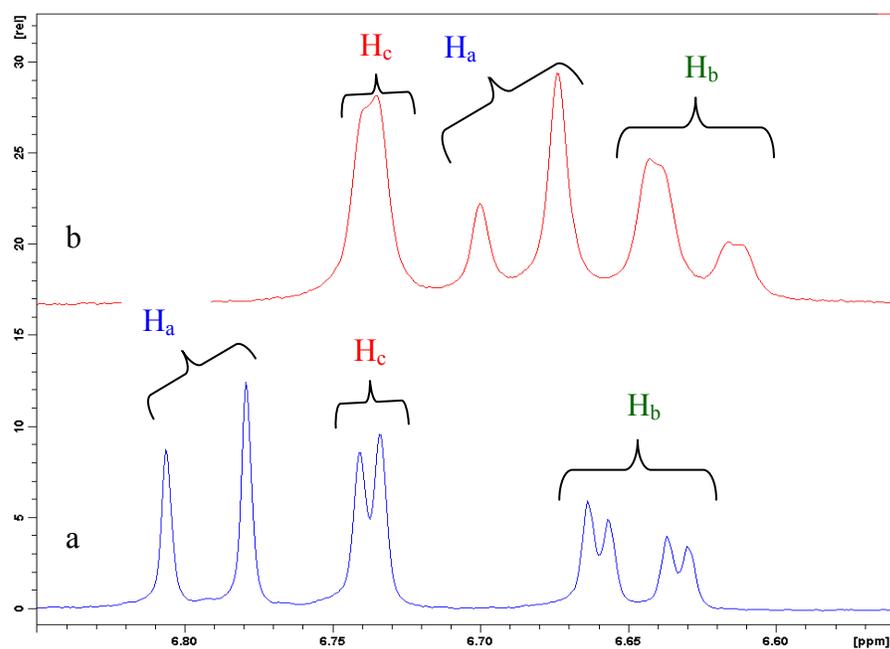
Figure 5.28: Extract of the aromatic part of the ^{1}H NMR spectra of (a) 5.0 x 10^{-3} mol dm^{-3} DA and (b) 5.0 x 10^{-3} mol dm^{-3} DA and 0.02 mol dm^{-3} sulfonated β-cyclodextrin in a 0.10 mol dm^{-3} KCl solution. Analysis carried out by Gillian Hendy.
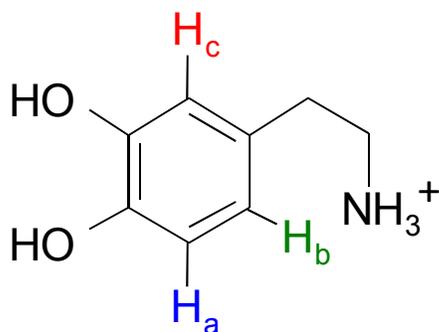
Figure 5.29: Structure of DA and designation of the protons in Figure 5.28.
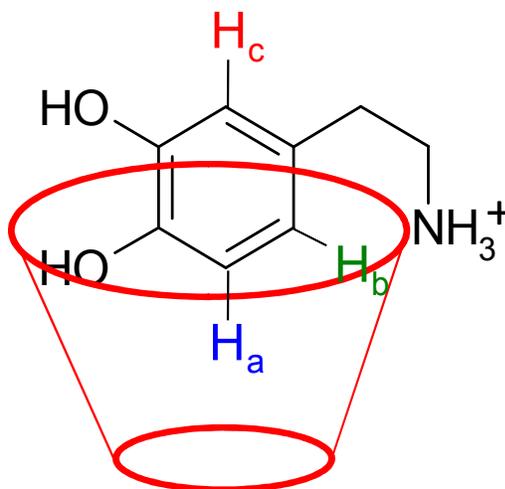
Figure 5.30: A schematic of the inclusion complex formed between the DA and the sulfonated β-cyclodextrin.

5.3.7 Complexation between Ascorbic Acid and the Sulfonated β-Cyclodextrin

The results presented in Section 5.3.1 show clearly that both 1.0×10^{-3} mol dm^{-3} AA and 1.0×10^{-2} mol dm^{-3} AA are not oxidised at the PPy-SCD modified electrode. This result was not surprising as the formation of a host-guest complex between AA and the sulfonated β-cyclodextrin is very unlikely. Based on electrostatic interactions, the anionic AA should be repelled from the anionic sulfonated β-cyclodextrin and the neutral AA should not be attracted to the negatively charged sulfonated β-cyclodextrin. In addition, AA is not

especially hydrophobic and so should not be attracted to the hydrophobic cavity of the sulfonated β-cyclodextrin. To confirm these claims, cyclic voltammetry was used to investigate if an inclusion complex was formed between the AA and the sulfonated β-cyclodextrin at a pH of 4.3 and 3.4, mimicking the pH of the 1.0×10^{-3} mol dm^{-3} AA and 1.0×10^{-2} mol dm^{-3} AA solutions, respectively. Representative data are shown in Figures 5.31 and 5.32 for solution pH values of 4.3 and 3.4, respectively. These data were recorded at a bare GC electrode. A citrate-phosphate buffer solution, (pH values of 3.4 and 4.3) was used as the supporting electrolyte and the concentration of AA was 5.0×10^{-4} mol dm^{-3}, while the concentration of the sulfonated β-cyclodextrin was maintained in excess, at 0.01 mol dm^{-3}. It is obvious from these plots, that no inclusion complex is formed between the AA and the sulfonated β-cyclodextrin at either pH value. At a pH of 3.4, Figure 5.32, there is a slight decrease in the current. However, there is no shift in the potential. As complexation can only be established if there is a shift in the oxidation potential, it is clear that AA does not form an inclusion complex with the sulfonated β-cyclodextrin.

A PPy-SDS modified electrode was also used to examine if the PPy film doped with a simple dopant could oxidise AA. Cyclic voltammograms showing the electrochemical behaviour of the PPy-SDS film in a 0.01 mol dm^{-3} AA and in a 1.0×10^{-3} mol dm^{-3} AA sulfate containing solution are shown in Figure 5.33. There is no evidence for the oxidation of AA, even at the higher concentration. Indeed, similar data were recorded for PPy films doped with chloride and sulfate anions.
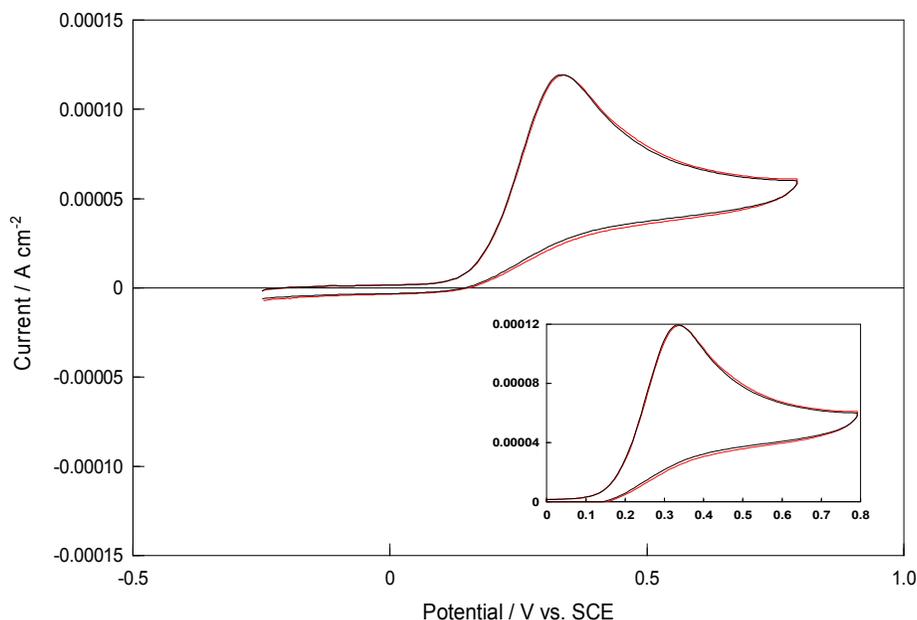
Figure 5.31: Cyclic voltammograms of a bare GC electrode in a — 5.0 x 10⁻⁴ mol dm⁻³ AA / 0.30 mol dm⁻³ citrate phosphate buffer solution and in a — 5.0 x 10⁻⁴ mol dm⁻³ AA / 0.010 mol dm⁻³ sulfonated β-cyclodextrin / 0.30 mol dm⁻³ citrate phosphate buffer solution (pH of all solutions ~4.3). Scan rate = 50 mV s⁻¹. Inset: Magnification of the oxidation region. Axes are identical to Figure 5.31. Electrochemical Window: -0.250 V vs. SCE to 0.800 V vs. SCE.
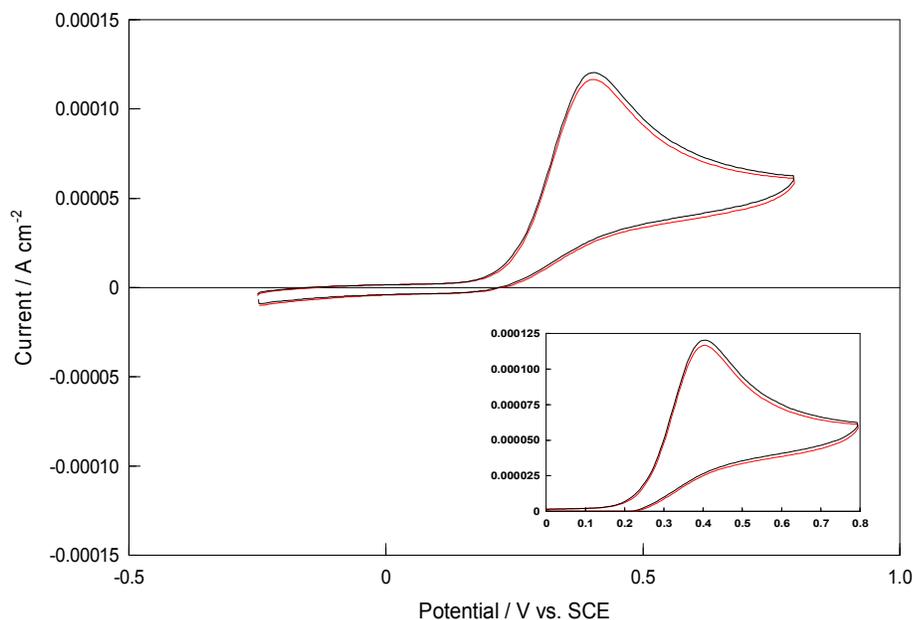
Figure 5.32: Cyclic voltammograms of a bare GC electrode in a — 5.0 x 10⁻⁴ mol dm⁻³ AA / 0.30 mol dm⁻³ citrate phosphate buffer solution and in a — 5.0 x 10⁻⁴ mol dm⁻³ AA / 0.01 mol dm⁻³ sulfonated β-cyclodextrin / 0.30 mol dm⁻³ citrate phosphate buffer solution (pH of all solutions ~3.4). Scan rate = 50 mV s⁻¹. Inset: Magnification of the oxidation region. Axes are identical to Figure 5.32. Electrochemical Window: -0.250 V vs. SCE to 0.800 V vs. SCE.
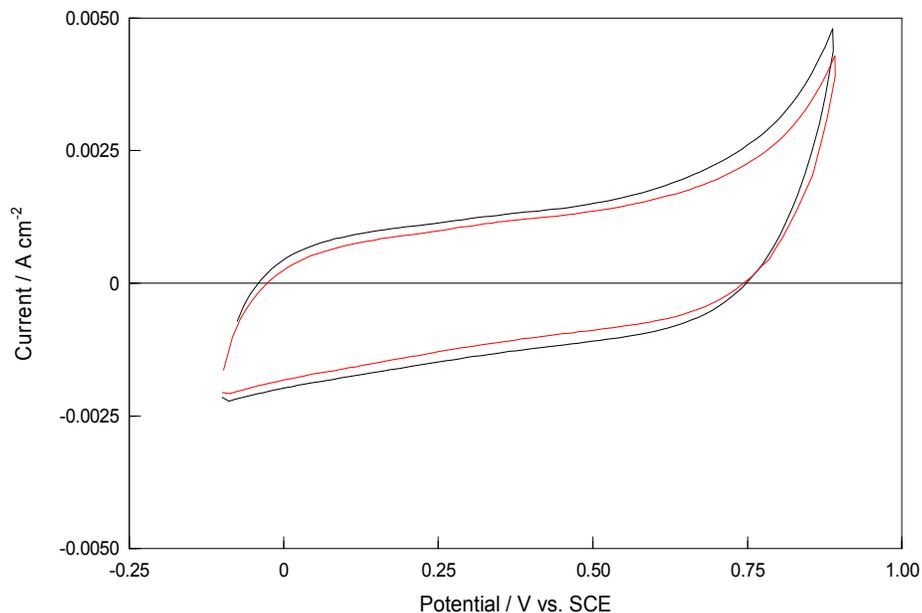
Figure 5.33: Cyclic voltammograms of a PPy-SDS modified electrode in a ▬ 0.010 mol dm^{-3} AA / 0.10 mol dm^{-3} Na$_2$SO$_4$ solution (pH of solution ~3.4) and in a ▬ 1.0 x 10^{-3} mol dm^{-3} AA / 0.10 mol dm^{-3} Na$_2$SO$_4$ solution (pH of solution ~4.3). Scan rate = 100 mV s^{-1}.

The results presented in this section confirm that no inclusion complex is formed between the AA and the sulfonated β-cyclodextrin. In addition, neither concentration of AA (1.0 x 10^{-3} mol dm^{-3} AA or 1.0 x 10^{-2} mol dm^{-3} AA) was detected at the PPy-SDS modified electrode. This explains why both 1.0 x 10^{-3} mol dm^{-3} AA and 1.0 x 10^{-2} mol dm^{-3} AA are not oxidised at the PPy-SCD modified electrode.

To the best of our knowledge, there are no reports in the literature that have examined the complexation between AA and a sulfonated β-cyclodextrin. There have been reports on the formation of an inclusion complex between AA and a neutral-β-cyclodextrin by Manzanares and co-workers[74]. This is in contrast to the findings of Terekhova *et al.*[75] who observed no complexation between AA and neutral-β-cyclodextrin. Manzanares *et al.*[74] showed that the neutral-β-cyclodextrin formed an inclusion complex with the neutral AA and with the negatively charged AA, however the anionic AA had less affinity for the neutral-β-cyclodextrin. The affinity of the AA for the sulfonated β-cyclodextrin will be even less than that of the neutral-β-cyclodextrin due to the presence of the negatively charged sulfonated groups on the β-cyclodextrin.

5.3.8 Complexation between Epinephrine and the Sulfonated β-Cyclodextrin

As already discussed in Section 5.3.2, EP is easily oxidised at the PPy-SCD modified electrode giving an oxidation and reduction peak at approximately 0.470 V vs. SCE and 0.350 V vs. SCE, respectively. One reason why EP is detected at the PPy-SCD modified electrode could be that the negatively charged sulfonated β-cyclodextrin is attracting the cationic EP and consequently a complex is formed between the two.

Cyclic voltammetry was used to investigate if this was the case and the results are shown in Figure 5.34. These data were recorded with a 5.0 x 10^{-4} mol dm^{-3} solution of EP in a supporting citrate-phosphate electrolyte solution at a GC electrode, in the absence and presence of a large excess, 0.01 mol dm^{-3}, of sulfonated β-cyclodextrin. From Figure 5.34 it can be seen that an excess of the sulfonated β-cyclodextrin gives rise to a reduction in the EP peak oxidation current and also to a shift of the oxidation peak potential to more positive values. This is indicative of complexation and has already been explained in detail in Section 5.3.4. The degree to which the EP peak current decreases and the extent of the potential shift, in the presence of the sulfonated β-cyclodextrin, are similar to that observed with the cationic DA and this is highlighted in Table 5.12.

This is not surprising as the structures of EP and DA are similar in that both compounds contain a relatively hydrophobic phenol ring that can complex with the hydrophobic internal cavity of the sulfonated β-cyclodextrin. In addition, both compounds are predominantly cationic. Therefore, the oxidation of EP at the PPy-SCD modified electrode can be attributed to the formation of an inclusion complex between EP and the sulfonated β-cyclodextrin. As previously shown with DA, the PPy film is also able to oxidise the EP, and EP is oxidised at the film to the same extent as DA. This is highlighted in Figure 5.35 where it can be seen that EP is oxidised at the PPy-SDS modified electrode. A comparison of this result to the oxidation of EP at the PPy-SCD modified electrode is illustrated in the inset of Figure 5.35. It is clear from this comparison that both the anodic and cathodic peaks of the EP redox reaction are enhanced by the presence of the sulfonated β-cyclodextrin. Therefore, the detection of EP at the PPy-SCD modified electrode can be

attributed to both complexation with the cyclodextrin cavity and oxidation at the polymer film.
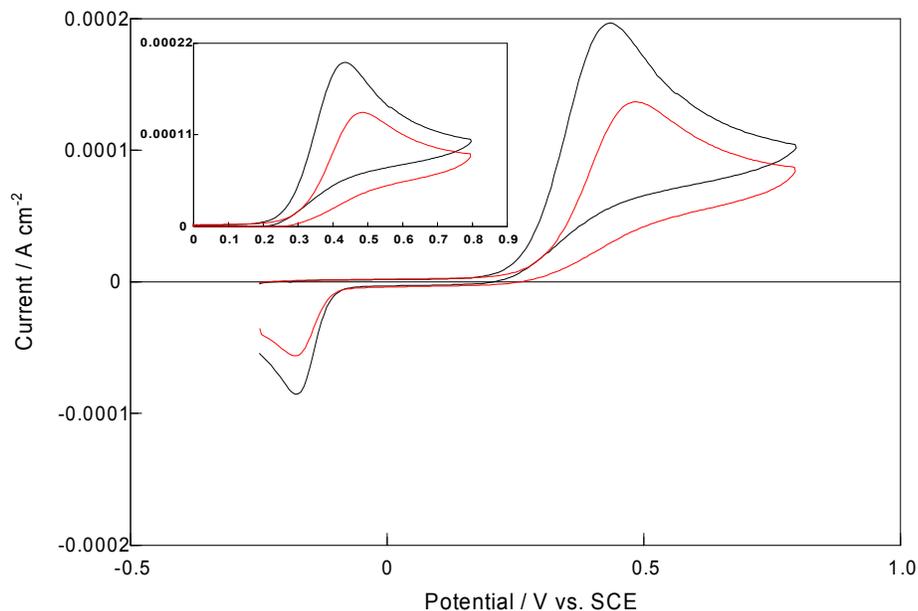
Figure 5.34: Cyclic voltammograms of a bare GC electrode in a ━ 5.0 x 10⁻⁴ mol dm⁻³ EP / 0.30 mol dm⁻³ citrate phosphate buffer solution and in a ━ 5.0 x 10⁻⁴ mol dm⁻³ EP / 0.01 mol dm⁻³ sulfonated β-cyclodextrin / 0.30 mol dm⁻³ citrate phosphate buffer solution (pH of all solutions ~6.0). Scan rate = 50 mV s⁻¹. Inset: Magnification of the oxidation region. Axes are identical to Figure 5.34. Electrochemical Window: -0.250 V vs. SCE to 0.800 V vs. SCE.

Table 5.12: Peak potential shifts and ratio of peak currents for the oxidation of the DA and EP systems in the presence of 0.01 mol dm⁻³ sulfonated β-cyclodextrin in a 0.30 mol dm⁻³ citrate phosphate, pH~4.5, buffer. Concentrations of DA and EP were 5.0 x 10⁻⁴ mol dm⁻³.

$E_p^A{}_{DA+CD} - E_p^A{}_{DA}$ / V vs.SCE	$E_p^A{}_{EP+CD} - E_p^A{}_{EP}$ / V vs.SCE	$I_p^A{}_{DA} : I_p^A{}_{DA+CD}$	$I_p^A{}_{EP} : I_p^A{}_{EP+CD}$
0.059	0.051	1.52 : 1	1.44 : 1
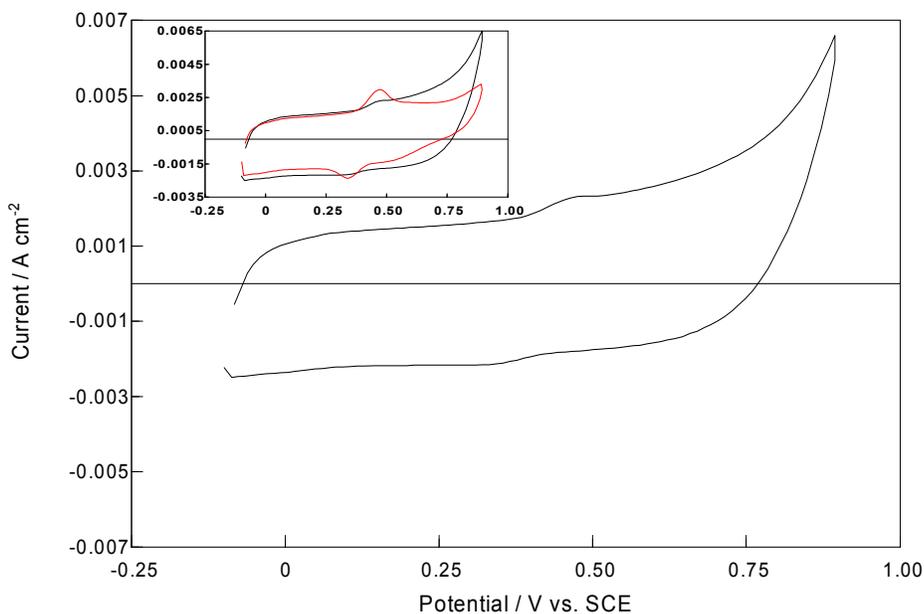
Figure 5.35: Cyclic voltammogram of a PPy-SDS modified electrode in a 1.0×10^{-3} mol dm^{-3} EP / 0.10 mol dm^{-3} Na$_2$SO$_4$ solution (pH~6.0). Scan rate = 100 mV s^{-1}. Inset: Cyclic voltammograms of a — PPy-SDS modifed electrode and a — PPy-SCD modified electrode in a 1.0×10^{-3} mol dm^{-3} EP / 0.10 mol dm^{-3} Na$_2$SO$_4$ solution (pH~6.0). Scan rate = 100 mV s^{-1}. Axes are identical to those in Figure 5.35.

Although the structures of EP and DA are similar, the oxidation signal of EP at the PPy-SCD modified electrode is slightly lower than that of DA. The oxidation current observed for 1.0×10^{-3} mol dm^{-3} DA at the PPy-SCD modified electrode is approximately 0.0037 A cm^{-2}, whereas the oxidation current observed for the same concentration of EP is roughly 0.0029 A cm^{-2}. The oxidation of DA and EP are similar at a bare Pt electrode and at a PPy film and thus the slightly lower oxidation signal of the EP at the PPy-SCD film must be connected with the extent of complexation. In particular, the manner in which EP includes within the cavity of the sulfonated β-cyclodextrin may explain the slightly lower oxidation currents. As already discussed in Section 5.3.6, for the inclusion complex formed between DA and the sulfonated β-cyclodextrin, one hydroxy group will be included within the cavity, Figure 5.30. On the other hand, the inclusion complex formed between the EP and the sulfonated β-cyclodextrin may have two hydrophilic hydroxy groups included within the cavity, as shown in the schematic in Figure 5.36. This would reduce the hydrophobicity of the guest and as a result the EP would be attracted to a lesser degree than the DA to the hydrophobic cavity of the sulfonated β-cyclodextrin. Consequently, less EP will be

oxidised at the PPy-SCD modified electrode. The formation of an inclusion complex between the EP and the sulfonated β-cyclodextrin, where only one hydrophilic hydroxy group is included, is possible. However, the fact that EP is oxidised to a lesser extent at the PPy-SCD modified electrode and forms a slightly weaker inclusion complex with the sulfonated β-cyclodextrin may suggest that two hydrophilic hydroxy groups are included in the cavity of the sulfonated β-cyclodextrin.
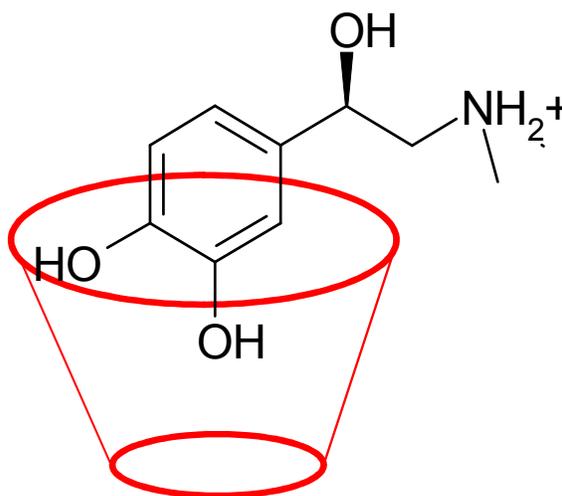
Figure 5.36: One possible inclusion complex formed between the DA and the sulfonated β-cyclodextrin.

The results presented in this section show that an inclusion complex is indeed formed between EP and the sulfonated β-cyclodextrin. However, the manner in which the EP is included within the cavity is likely to be different to that of the DA system. There are no reports, to the best of our knowledge, which have examined the complexation between EP and the sulfonated β-cyclodextrin. There have been reports on the formation of an inclusion complex between EP and a PPy/neutral-β-cyclodextrin film by Izaoumen and co-workers[8]. However, the authors provided no direct evidence to support the formation of an inclusion complex.

5.4 Summary of Results

A summary of the key results obtained in this chapter is given in this section. The main objectives of this chapter were to investigate the effect, if any, that AA and EP have on the determination of DA at the PPy-SCD modified electrode and to investigate the mechanism of how the PPy-SCD modified electrode is sensing DA; either via the formation of an inclusion complex with the sulfonated β-cyclodextrin, electrostatic interactions with the anionic sulfonated groups on the sulfonated β-cyclodextrin, or the oxidation of DA at the PPy film or alternatively a combination of these parameters.

Michaelis-Menten kinetics and Lineweaver-Burk analysis confirmed that there was some kind of interaction between the DA and the PPy-SCD film. Based on the magnitude of the Km values obtained, this was described as a relatively weak binding interaction. Furthermore, the good agreement between the Michaelis-Menten theory and the data recorded for the oxidation of DA at the PPy-SCD modified electrode suggests that the DA-sulfonated β-cyclodextrin complex is converted into the product, DOQ, and free sulfonated β-cyclodextrin. The regenerated sulfonated β-cyclodextrin is then available for further binding with the DA.

The cyclic voltammetry and rotation disc voltammetry results, from Section 5.3.4, verified that this binding interaction was due to the formation of a host-guest complex between the DA and the sulfonated β-cyclodextrin in solution, with complex formation constants of 199.54 ± 4.88 mol^{-1} dm^3 and 240.18 ± 5.87 mol^{-1} dm^3 obtained, respectively, from cyclic voltammetry and rotation disc voltammetry. The two different techniques produced very comparable complex formation constants, confirming the validity of the electrochemical approaches. The calculated complex formation constants are small in comparison to other substances that are well known to form strong inclusion complexes with cyclodextrins. For example, a complex formation constant of approximately 3530 ± 350 mol^{-1} dm^3 has been evaluated for the inclusion complex between ferrocene and the neutral β-cyclodextrin[76]. Therefore, a complex formation constant in the region of 200 mol^{-1} dm^3 suggests weak complexation, which is consistent with the weak binding interactions deduced from the Michaelis-Menten and Lineweaver-Burk analysis. Interestingly, the reduction potential of

the DOQ was not influenced by the presence of a large excess of sulfonated β-cyclodextrin. Again, this is in good agreement with the Michaelis-Menten theory, where the analysis is based on the regeneration of the enzyme (sulfonated β-cyclodextrin). Accordingly, once the DA is oxidised, to the DOQ, it is expelled from the cavity.

Using UV spectroscopy, in conjunction with the Job's method, it was found that a 1:1 association complex was formed between the DA and the sulfonated β-cyclodextrin. Further studies using ^{1}H NMR confirmed that the DA was included within the cavity of the sulfonated β-cyclodextrin through the reasonably hydrophobic phenol ring. It is well known that cyclodextrins will only tend to form inclusion complexes with guest molecules that are hydrophobic, or guest molecules that have hydrophobic groups/regions. This is because cyclodextrins have a hydrophobic internal cavity that will attract hydrophobic compounds. DA is not a highly hydrophobic molecule. However, the phenol ring, in its structure, will have some degree of hydrophobicity. The rather weak nature of the complexation can be attributed to the fact that the phenol ring contains hydrophilic OH groups; one of which is included in the cavity.

The role that electrostatic interactions play was also investigated. It was determined that electrostatic interactions increase the stability of the inclusion complex formed between the DA and the sulfonated β-cyclodextrin. No apparent inclusion complex was formed between the neutral β-cyclodextrin and the DA, and even using fluorescence spectrometry, a significantly more sensitive technique than cyclic voltammetry, Zhou *et al.*[71] only calculated a binding constant of 95.06 mol^{-1} dm^3 for the inclusion complex formed between the neutral β-cyclodextrin and the DA. This value is lower than the values calculated in this study for the inclusion complex formed between the DA and the sulfonated β-cyclodextrin. It appears that the electrostatic interactions between the anionic sulfonated groups on the rim of the cyclodextrin and the cationic group of the DA molecule enhance the complexation between the cyclodextrin and the DA. Indeed, the NMR studies support the idea that the protonated amine group on the DA molecule remains outside the cavity and is bound through electrostatic interactions with the anionic sulfonated groups on the rim. Further evidence to support the importance of the electrostatic interactions comes from the fact that a polymer doped with the neutral β-cyclodextrin cannot detect DA as efficiently as

the PPy-SCD modified electrode, as shown in Section 3.3.2. These findings are in agreement with the work reported by Okimoto *et al.*[77] who showed that the anionic sulfobutylether β-cyclodextrin forms more stable inclusion complexes with cationic drugs than with the neutral 2-hydroxypropyl-β-cyclodextrin.

Using a PPy-SDS modified electrode it was found that the PPy film, regions of the film that are free from the sulfonated β-cyclodextrin dopant, was also capable of oxidising the DA. Consequently, the mode of sensing is a combination of both complexation, enhanced through electrostatic interactions, and oxidation at the polymer film. However, the oxidation currents obtained for a given concentration of DA at the PPy-SDS modified electrode were considerably lower than the signal obtained for the same concentration of DA at the PPy-SCD modified electrode. This was attributed to the formation of an inclusion complex between the DA molecule and the sulfonated β-cyclodextrin dopant, enabling more efficient oxidation of DA at the modified electrode. It was also found that the DOQ was diffusing from the surface of the PPy-SCD modified electrode more efficiently than from the surface of the PPy-SDS modified electrode. This was attributed to the higher rate of oxidation of DA at the PPy-SCD electrode and consequently, the higher concentration gradients of the DOQ.

The results presented in Sections 5.3.1 show clearly that AA, even at a considerable high concentration of 0.01 mol dm^{-3}, does not interfere in the electrochemical detection of DA at the PPy-SCD modified electrode. AA is not oxidised at the PPy film nor does it form an inclusion complex with the sulfonated β-cyclodextrin. This was confirmed in Section 5.3.7 using rotating disc voltammetry. Based on the polarity of the AA molecule it would seem an unlikely candidate to include within the cavity of a cyclodextrin, however there are some reports in the literature that provide evidence for the formation of an inclusion complex between cyclodextrins and AA[74, 78]. In most of these cases, the unionised form of AA interacts more strongly with the cavity than the ionised form of AA. Nevertheless, AA is less likely to include within the cavity of the sulfonated β-cyclodextrin due to the presence of the negatively charged sulfonated groups on the β-cyclodextrin and this was confirmed in Section 5.3.7.

On the other hand, EP is oxidised at the PPy film and does form an inclusion complex with the sulfonated β-cyclodextrin. Consequently, it is oxidised at the PPy-SCD modified electrode. It is oxidised in the same potential region as DA and a mixed solution of EP and DA results in an overlapping voltammetric response. This result is not surprising, as EP is similar in chemical structure and polarity to DA.

EP was oxidised at the PPy-SDS modified electrode to the same degree as DA and formed an inclusion complex with the sulfonated β-cyclodextrin. A slightly weaker inclusion complex is formed between EP and the sulfonated β-cyclodextrin in comparison to the one formed between the sulfonated β-cyclodextrin and the DA, resulting in a lower oxidation signal for EP than DA at the PPy-SCD modified electrode. This was explained in terms of the moiety of EP that includes within the cavity of the sulfonated β-cyclodextrin; it is likely to be less hydrophobic than the moiety of DA that includes within the cavity.

In summary, the electrochemical sensing of DA is a combination of both oxidation at the PPy film and complexation with the sulfonated β-cyclodextrin, incorporated within the PPy matrix as a dopant. The stability of the inclusion complex formed is enhanced by the presence of the anionic sulfonated groups on the β-cyclodextrin, which give rise to electrostatic interactions with the protonated group on DA. The PPy-SCD modified electrode can eliminate the interference of AA, even at a concentration of 1.0×10^{-2} mol dm^{-3}, giving very good selectivity for the detection of DA in the presence of AA. However, the PPy-SCD film cannot eliminate the interference from EP, as EP forms an inclusion complex with the sulfonated β-cyclodextrin and it is oxidised in the same potential region as DA. Therefore, the sensor cannot be used to discriminate between the presence of DA and EP.

5.5 References

1.   R. Gifford, J. J. Kehoe, S. L. Barnes, B. A. Kornilayev, M. A. Alterman and G. S. Wilson, Biomaterials, **27**, 2587, (2006).
2.   N. Wisniewski, F. Moussy and W. M. Reichert, Fresenius J. Anal. Chem., **366**, 611, (2000).
3.   P. T. Kissinge, J. B. Hart and R. N. Adams, Brain Research, **55**, 209, (1973).
4.   B. Kong, J. Zeng, G. Luo, S. Luo, W. Wei and J. Li, Bioelectrochemistry, **In Press, Corrected Proof**.
5.   X.-J. Dang, M.-Y. Nie, T. Jian and H.-L. Li, J. Electroanal. Chem, **448**, 61, (1998).
6.   C. Danel, N. Azaroual, A. Brunel, D. Lannoy, G. Vermeersch, P. Odou and C. Vaccher, J. Chromatogr. A, **1215**, 185, (2008).
7.   J. Mrozek, B. Banecki, E. Sikorska, A. Skwierawska, J. Karolczak and W. Wiczk, Chemical Physics, **354**, 58, (2008).
8.   N. Izaoumen, D. Bouchta, H. Zejli, M. E. Kaoutit, A. M. Stalcup and K. R. Temsamani, Talanta, **66**, 111, (2005).
9.   A. Afkhami and L. Khalafi, Anal. Chim. Acta, **599**, 241, (2007).
10.   C. Retna Raj and R. Ramaraj, Electrochim. Acta, **44**, 2685, (1999).
11.   E. Alvira, J. A. Mayoral and J. I. García, Chem. Phys. Lett., **245**, 335, (1995).
12.   J. Zheng and X. Zhou, Bioelectrochemistry, **70**, 408, (2007).
13.   J. P. Lowry and R. D. O'Neill, Encyclopedia of Sensors, Neuroanalytical Chemistry In Vivo Using Electrochemical Sensors, C. A. Grimes, E. C. Dicky, and M. V. Pishko, American Scientific Publishers, **10**, 1, (2006).
14.   U. E. Majewska, K. Chmurski, K. Biesiada, A. R. Olszyna and R. Bilewicz, Electroanalysis, **18**, 1463, (2006).
15.   L. Zhang and X. Jiang, J. Electroanal. Chem., **583**, 292, (2005).
16.   H. Zhao, Y. Zhang and Z. Yuan, Anal. Chim. Acta, **441**, 117, (2001).
17.   D. Zheng, J. Ye, L. Zhou, Y. Zhang and C. Yu, J. Electroanal. Chem, **625**, 82, (2009).
18.   S. Yuan, W. Chen and S. Hu, Materials Science and Engineering: C, **25**, 479, (2005).
19.   M. Zhang, K. Gong, H. Zhang and L. Mao, Biosens. Bioelectron., **20**, 1270, (2005).
20.   Y. Li and X. Lin, Sens. Actuator B-Chem., **115**, 134, (2006).
21.   Q. Zhuang, Z. Zhu, Y. Zhao, Y. Gao, D. Zhan, H. Liu, Q. Zhao, Y. Kou, Y. Shao and M. Li, Talanta, **66**, 51, (2005).
22.   J. Mathiyarasu, S. Senthilkumar, K. L. N. Phani and V. Yegnaraman, Materials Letters, **62**, 571, (2008).
23.   A. I. Gopalan, K.-P. Lee, K. M. Manesh, P. Santhosh, J. H. Kim and J. S. Kang, Talanta, **71**, 1774, (2007).
24.   R. K. Shervedani, M. Bagherzadeh and S. A. Mozaffari, Sens. Actuator B-Chem., **115**, 614, (2006).
25.   L. Zhang, J. Jia, X. Zou and S. Dong, Electroanalysis, **16**, 1413, (2004).
26.   Y. Li, P. Wang, L. Wang and X. Lin, Biosens. Bioelectron., **22**, 3120, (2007).
27.   M.-S. Won, M. A. Rahman, N.-H. Kwon, D. R. Shankaran and Y.-B. Shim, Electroanalysis, **17**, 2231, (2005).
28.   G. Alarcon-Angeles, B. Perez-Lopez, M. Palomar-Pardave, M. T. Ramirez-Silva, S. Alegret and A. Merkoci, Carbon, **46**, 898, (2008).

29.   A. Fragoso, E. Almirall, R. Cao, L. Echegoyen and R. G. Jonte, Chem. Commun., **19**, 2230, (2004).
30.   A. Berduque, R. Zazpe and D. W. M. Arrigan, Anal. Chim. Acta, **611**, 156, (2008).
31.   V. Beni, M. Ghita and D. W. M. Arrigan, Biosens. Bioelectron., **20**, 2097, (2005).
32.   Y. Zeng, J. Yang and K. Wu, Electrochim. Acta, **53**, 4615, (2008).
33.   S. H. Kim, J. W. Lee and I.-H. Yeo, Electrochim. Acta, **45**, 2889, (2000).
34.   W. Cheng, G. Jin and Y. Zhang, Russian Journal of Electrochemistry, **41**, 940, (2005).
35.   M. Wei and S. Deng-Ming, Chinese Journal of Analytical Chemistry, **35**, 66, (2007).
36.   X. H. Liu, Y. Zhang, G. F. Zuo and X. Q. Lu, Chinese Chemical Letters, **17**, 657, (2006).
37.   T. Luczak, Electroanalysis, **20**, 1317, (2008).
38.   E. Dempsey, A. Kennedy, N. Fay and T. McCormac, Electroanalysis, **15**, 1835, (2003).
39.   M. Chicharro, A. Sánchez, E. Bermejo, A. Zapardiel, M. D. Rubianes and G. A. Rivas, Anal. Chim. Acta, **543**, 84, (2005).
40.   E. Nalewajko, A. Wiszowata and A. Kojlo, J. Pharm. Biomed. Anal., **43**, 1673, (2007).
41.   M. A. Fotopoulou and P. C. Ioannou, Anal. Chim. Acta, **462**, 179, (2002).
42.   M. Zhu, X. Huang, J. Li and H. Shen, Anal. Chim. Acta, **357**, 261, (1997).
43.   N. B. Li, W. Ren and H. Q. Luo, Electroanalysis, **19**, 1496, (2007).
44.   Y. Sun, B. Ye and X. Zhou, Chin. J. Anal. Chem., **26**, 506, (1998).
45.   X.-C. He, P. Li and J.-Y. Mo, J. Instrum. Anal., **19**, 19, (2000).
46.   G. Wang, Z. Wang, S. Xiao, Y. Wang and G. Luo, Chin. J. Anal. Chem., **31**, 1281, (2003).
47.   R. Liang, J. Qiu, T. Huang, J. Mo and P. Cai, J. Instrum. Anal., **21**, 31, (2002).
48.   G.-Y. Wang, X.-J. Liu, G.-A. Luo and Z.-H. Wang, Chinese Journal of Chemistry, **23**, 297, (2005).
49.   S. W. Runge, B. J. F. Hill and W. M. Moran, Life Sciences Education, **5**, 348, (2006).
50.   L. Buckberry and P. Teesdale, Essentials of Biological Chemistry, John Wiley & Sons, Ltd, **1**, 145, (2001).
51.   Michaelis-Menten Kinetics, Department of Chemistry, Davidson College NC, http://www.chm.davidson.edu/erstevens/Michaelis/Michaelis.html.
52.   Introduction to Enzymes and Catalysis, Biochemistry 3521, Fordham University, http://dwb4.unl.edu/Chem/CHEM869P/CHEM869PLinks/www.fordham.edu/Biochem_3521/lect10/lect10.html.
53.   Enzyme kinetics and the Michaelis-Menten equation, Biochemistry Department, University   of   Leicester, http://www.le.ac.uk/by/teach/biochemweb/tutorials/michment2print.html.
54.   R. Kataky and E. Morgan, *Biosens. Bioelectron.*, **18**, 1407, (2003).
55.   J. S. Wang, H. J. Zhu, B. B. Gibson, J. S. Markowitz, J. L. Donovan and C. L. DeVane, *Biological & Pharmaceutical Bulletin*, **31**, 231, (2008).
56.   Y. F. Tu and H. Y. Chen, *Anal. Biochem.*, **299**, 71, (2001).
57.   D. Wititsuwannakul, N. Chareonthiphakorn, M. Pace and R. Wititsuwannakul, *Phytochemistry*, **61**, 115, (2002).

58. C. M. Hooijmans, M. L. Stoop, M. Boon and K. C. A. M. Luyben, *Biotechnol. Bioeng.*, **40**, 16, (1992).
59. Z.-X. Tang, J.-Q. Qian and L.-E. Shi, *Materials Letters*, **61**, 37, (2007).
60. W. Wang, L. Deng, Z. H. Peng and X. Xiao, *Enzyme and Microbial Technology*, **40**, 255, (2007).
61. R. B. Bhatia, C. J. Brinker, A. K. Gupta and A. K. Singh, *Chem. Mater.*, **12**, 2434, (2000).
62. S. K. Duggal and K. Buchholz, *Eur J Appl Microbiol Biotechnol*, **16**, 81, (1982).
63. S. A. Çetinus, H. N. Öztop and D. Saraydın, *Enzyme and Microbial Technology*, **41**, 447, (2007).
64. P. He, G. Greenway and S. J. Haswell, *Nanotechnology*, **19**, (2008).
65. P. Fini, R. Loseto, L. Catucci, P. Cosma and A. Agostiano, *Bioelectrochemistry*, **70**, 44, (2007).
66. C. Retna Raj and R. Ramaraj, *Electrochim. Acta*, **44**, 279, (1998).
67. C. Yáñez, R. Salazar, L. J. Núñez-Vergara and J. A. Squella, *Journal of Pharmaceutical and Biomedical Analysis*, **35**, 51, (2004).
68. S. Hbaieb, R. Kalfat, Y. Chevalier, N. Amdouni and H. Parrot-Lopez, *Mater. Sci. Eng. C-Biomimetic Supramol. Syst.*, **28**, 697, (2008).
69. E. Coutouli-Argyropoulou, A. Kelaidopoulou, C. Sideris and G. Kokkinidis, *J. Electroanal. Chem*, **477**, 130, (1999).
70. G.-C. Zhao, J.-J. Zhu, J.-J. Zhang and H.-Y. Chen, *Anal. Chim. Acta*, **394**, 337, (1999).
71. Y. Y. Zhou, C. Liu, H. P. Yu, H. W. Xu, Q. Lu and L. Wang, *Spectroscopy Letters*, **39**, 409, (2006).
72. G. Uccello-Barretta, F. Balzano, D. Paolino, R. Ciaccio and S. Guccione, *Bioorganic & Medicinal Chemistry*, **13**, 6502, (2005).
73. M. Zhang, J. Li, L. Zhang and J. Chao, *Spectroc. Acta Pt. A-Molec. Biomolec. Spectr.*, **71**, 1891, (2009).
74. M. I. Manzanares, V. Solís and R. H. de Rossi, *J. Electroanal. Chem*, **407**, 141, (1996).
75. I. V. Terekhova, O. V. Kulikov, R. S. Kumeev, M. Y. Nikiforov and G. A. Al'per, *Russian Journal of Coordination Chemistry*, **31**, 218, (2005).
76. D. Osella, A. Carretta, C. Nervi, M. Ravera and R. Gobetto, *Organometallics*, **19**, 2791, (2000).
77. K. Okimoto, R. A. Rajewski, K. Uekama, J. A. Jona and V. J. Stella, *Pharmaceutical Research*, **13**, 256, (1996).
78. C. Garnero and M. Longhi, *Journal of Pharmaceutical and Biomedical Analysis*, **45**, 536, (2007).

Chapter 6

Interfering Compounds

6.1 Introduction

One of the major difficulties in the electrochemical detection of dopamine (DA) is the presence of a wide array of interfering compounds. This has already been discussed to some extent in Chapter 5, where the influence of ascorbic acid (AA) and epinephrine (EP) on the determination of DA at the polypyrrole sulfonated β-cyclodextrin (PPy-SCD) modified electrode was examined.

In this chapter a wide variety of other interfering compounds have been investigated. These include the purine metabolite uric acid (UA), the 5-hydroxytryptamine (serotonin, 5-HT) neurotransmitter and its metabolite, 5-hydroxyindole acetic acid (5HIAA) and the key metabolites of DA, 3,4-dihydroxyphenylacetic acid (DOPAC) and homovanillic acid (HVA). In addition, several amino acids, including glutamic acid (Glu) and aspartic acid (Asp), have been examined to establish their effect, if any, on the determination of DA at the PPy-SCD modified electrode.

6.2 Experimental

The instrumentation and software employed are described in Section 2.3. In these experiments the PPy-SCD film was electro-synthesised as outlined in Section 2.7 using a potential of 0.800 V vs. SCE until a charge of 0.24 C cm^{-2} was reached. In each experiment a fresh PPy-SCD film was used. The response of every interfering compound was firstly investigated at a Pt substrate and then at the PPy-SCD modified Pt electrode. The peak currents and peak potentials for the oxidation of DA in the presence of each interfering compound were recorded where the concentration ratio of interfering compound to DA varied from 1.0:1.0 to 14.3:1.0. This ratio was used for all the interfering compounds apart from UA. The concentration of UA was reduced ten-fold because UA has a lower solubility in water. For this reason, the concentration ratio of UA to DA also decreased by a factor of ten. The errors are reported as a percentage of the mean values and are given from lowest percentage error to highest percentage error with *n* representing the number of experiments

carried out. The errors in the peak currents were calculated using Equation 6.1. The pH of the combined solution of DA and interfering compound was not altered unless otherwise specified. A comparison is then made between the mean oxidation currents and mean oxidation potentials of DA with and without the possible interferent. In some of the comparisons, the pH of the pure DA solution is slightly higher than the pH of the combined solutions, but it has been shown in Sections 3.3.6.9 that the DA signal at the PPy-SCD modified electrode does not change with small changes in pH when cyclic voltammetry is used at a scan rate of 100 mV s^{-1}. The average peak currents and average peak potentials obtained with pure DA at the PPy-SCD modified electrode are shown in Chapter 5 in Tables 5.1 and 5.2, respectively, and these are the values used in the comparisons throughout this chapter. The background currents have not been subtracted in this chapter unless otherwise stated.

$$Standard\ Error = \frac{Standard\ Deviation \div \sqrt{n}}{Mean\ Current\ of\ n} \times \frac{100}{1} \qquad 6.1$$

6.3 Results and Discussion

The potential interfering compounds in this chapter were selected based on their electroactivity and their projected structure in solution. Using a range of electroactive/electroinactive interfering compounds that will either be neutral, cationic, zwitterionic or anionic at the pH of the experiment should provide more information on the role that complexation and electrostatic interactions play at the PPy-SCD modified electrode. The majority of the compounds chosen are well-known interferents in DA detection, however, a large number, including HVA and 5-HIAA, have not been explored before using modified electrodes.

UA, Asp, Glu, 5-HIAA, DOPAC and HVA are all electroactive and will be negatively charged (or exist as zwitterions in the case of the amino acids) at the pH of the experiment.

Histamine (HA), 5-HT and acetaminophen (ACOP) are also electroactive, but HA and 5-HT will be positively charged while ACOP will be neutral. Electroinactive compounds investigated include aminobutyric acid (GABA), acetylcholine (Ach) and glycine (Gly). Both GABA and Gly will be in their zwitterionic forms at the pH of the experiment, while Ach will be a cationic species.

6.3.1 Uric Acid (UA)

UA, Figure 6.1, is the primary end product of purine metabolism in the human body. Abnormalities in the concentration levels of UA have been linked to several diseases such as gout, hyperuricemia and Lesch-Nyan syndrome[1]. Enhanced urate levels have also been associated with diseases such as leukaemia and pneumonia[2]. UA and DA exist together in most natural samples, however the concentration of UA is generally 100-1000 times higher than that of DA[3]. Furthermore, UA is electroactive having a range of $E_{1/2}$ values between 300 to 400 mV vs. SCE on most solid electrodes[4]. Therefore, UA has an overlapping oxidation potential with DA at most conventional electrodes. These problems make UA a very challenging interfering compound in the selective detection of DA.

The dissociation of UA involves keto-enol tautomerism and Jimenez and Alderete[5] have shown that the deprotonation of UA, in an aqueous medium, occurs through the proton loss at one of the monohydroxy tautomers, as shown in Scheme 6.1.
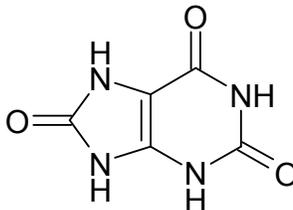
Figure 6.1: Structure of UA.
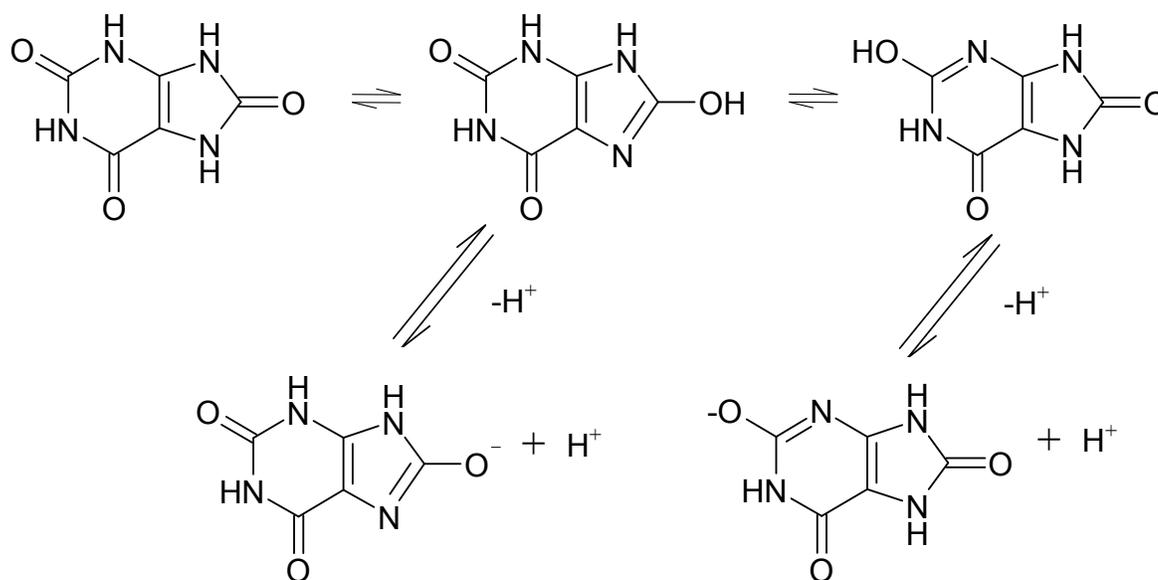
Scheme 6.1: Dissociation of UA[5].

In Figure 6.2(a), the cyclic voltammograms of a bare Pt electrode and a PPy-SCD film cycled in 1.0×10^{-4} mol dm^{-3} UA are compared. It can be seen that UA is slightly oxidised at the bare Pt electrode, as the oxidation current of the UA solution is higher than that of the solution containing no UA at potentials higher than 0.16 V vs. SCE. No oxidation is observed for UA at the PPy-SCD modified electrode.

When UA and DA are simultaneously mixed in the same solution, only DA is detected at the PPy-SCD electrode, giving very good selectivity. Figure 6.2(b) highlights this and the voltammogram recorded is identical to that obtained with DA alone. One possible reason for this is that UA will exist, to some extent, as a mixture of a neutral and an anionic species ($pK_a = 5.4$)[6] at the pH of the experiment (pH = 5.2), Scheme 6.1. The anion will be repelled from the surface, while, conversely, DA which exists as a cation ($pK_b = 8.87$) will be attracted to the interface. In addition, the sulfonated β-cyclodextrin is unlikely to form a supramolecular inclusion complex with UA, as approximately 40% of the UA is negatively charged. This percentage was calculated using Equation 5.13 from Chapter 5.

(a)

(b)
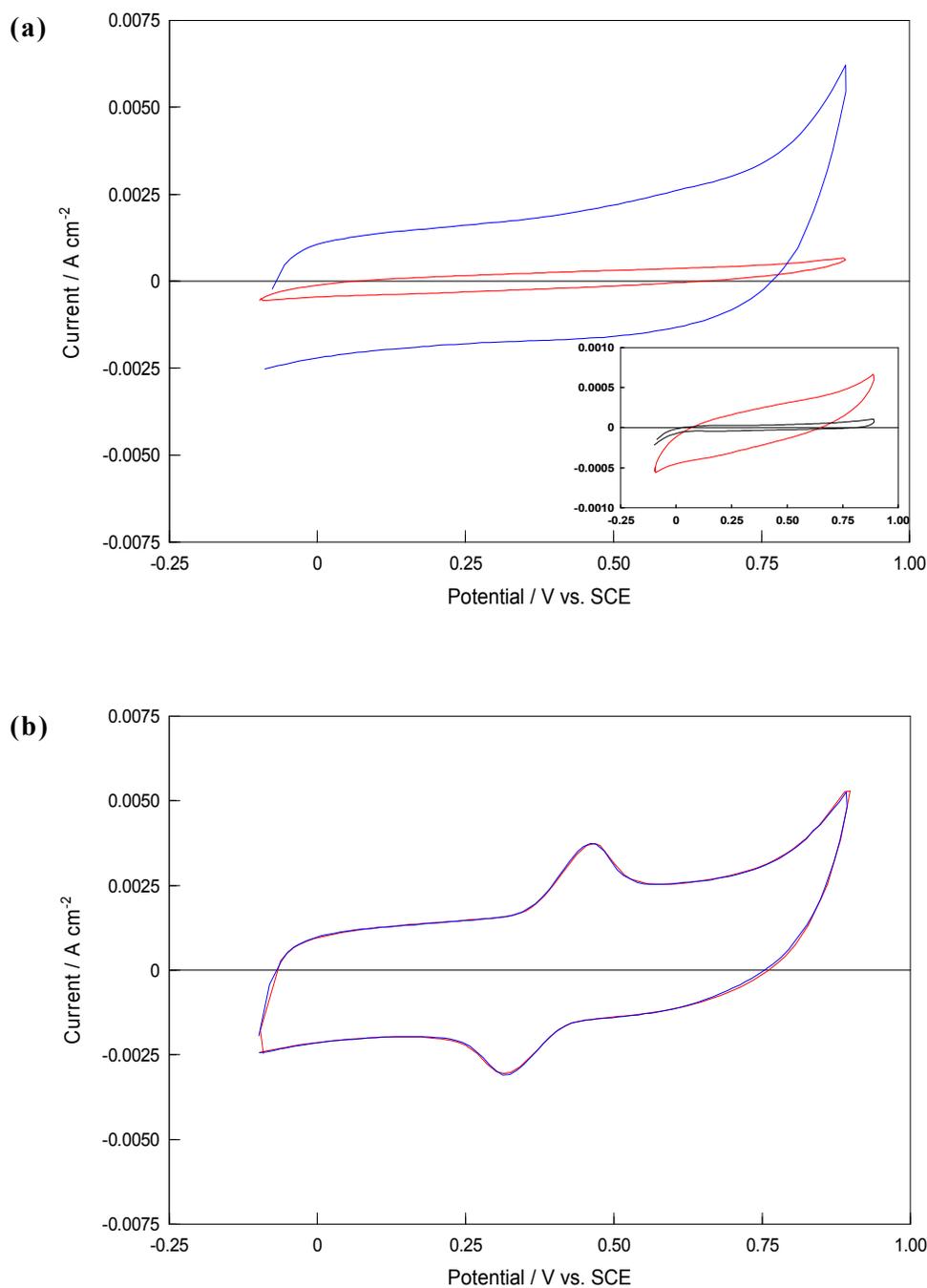
Figure 6.2: (a) Cyclic voltammograms of a ▬ bare Pt electrode and a ▬ PPy-SCD modified electrode in a 1.0 x 10^{-4} mol dm^{-3} UA / 0.10 mol dm^{-3} Na$_2$SO$_4$ solution (pH~5.2). Scan rate = 100 mV s^{-1}. Inset: Cyclic voltammograms of the bare Pt electrode in a ▬ 0.10 mol dm^{-3} Na$_2$SO$_4$ solution and in a ▬ 1.0 x 10^{-4} mol dm^{-3} UA / 0.10 mol dm^{-3} Na$_2$SO$_4$ solution. Scan rate = 100 mV s^{-1}. Axes are identical to Figure 6.2(a). (b) Cyclic voltammograms of the PPy-SCD modified electrode in a ▬ 1.0 x 10^{-3} mol dm^{-3} DA / 0.10 mol dm^{-3} Na$_2$SO$_4$ solution (pH~6.0) and in a ▬ 1.0 x 10^{-4} mol dm^{-3} DA / 1.0 x 10^{-4} mol dm^{-3} UA / 0.10 mol dm^{-3} Na$_2$SO$_4$ solution (pH~5.2). Scan rate = 100 mV s^{-1}.

In order to clearly establish the degree of complexation, if any, between UA and the sulfonated β-cyclodextrin, a series of cyclic voltammetry experiments was performed at a bare glassy carbon (GC) electrode in a citrate phosphate buffer with a 5.0 x 10^{-4} mol dm^{-3} UA solution in the absence and presence of an excess of the sulfonated β-cyclodextrin. These data were recorded at pH values of 5.2 and 3.3, to alter the extent of dissociation of the UA molecule.

Figure 6.3 highlights the fact that no inclusion complex is formed between UA and the sulfonated β-cyclodextrin at a pH of 5.2. An excess of the sulfonated β-cyclodextrin has not caused the peak currents to decrease or to shift to higher potentials, as expected for the formation of an inclusion complex, as discussed in Chapter 5.

In order to see what role electrostatic interactions play between the UA and the sulfonated β-cyclodextrin in terms of a host-guest complex, the pH was reduced to 3.3. This meant that less than 1% of the UA was negatively charged and so complexation between UA and the sulfonated β-cyclodextrin would not be restricted electrostatically. Figure 6.4 shows that at this pH no complexation occurs. This indicates that electrostatic interactions alone do not influence the formation of a host-guest complex between UA and the sulfonated β-cyclodextrin. An alternative explanation is connected to the hydrophobic character of UA. As discussed in Chapter 5, the phenol rings of DA and EP are non polar and hydrophobic, while the presence of the heteroatoms within the UA ring and the hydroxyl groups, Scheme 6.1, reduce the hydrophobicity to give a more polar UA molecule. This, in turn, will reduce the driving force for complexation in the hydrophobic cavity of the cyclodextrin.

On searching the literature three papers were found that mention the formation of an inclusion complex between UA and a β-cyclodextrin[7-9]. However, in all three cases, no direct evidence to support the formation of an inclusion complex was provided.
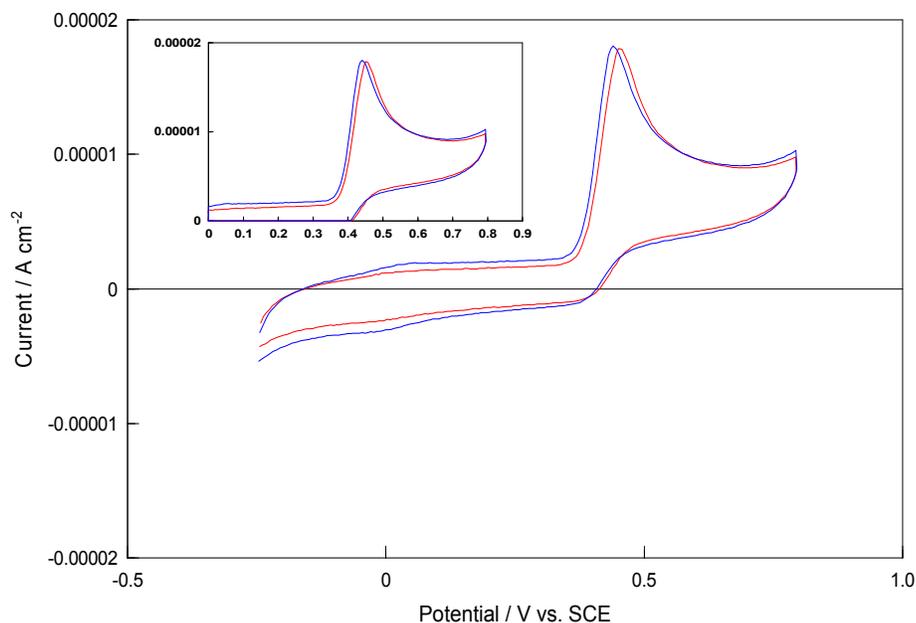
Figure 6.3: Cyclic voltammograms of a bare GC electrode in a ▬ 5.0 x 10^{-4} mol dm^{-3} UA / 0.30 mol dm^{-3} citrate phosphate buffer solution (pH~5.2) and in a ▬ 5.0 x 10^{-4} mol dm^{-3} UA / 0.01 mol dm^{-3} sulfonated β-cyclodextrin / 0.30 mol dm^{-3} citrate phosphate buffer solution (pH~5.2). Scan rate = 50 mV s^{-1}. Inset: Magnification of the oxidation region. Axes are identical to Figure 6.3. Electrochemical Window: -0.250 V vs. SCE to 0.800 V vs. SCE.
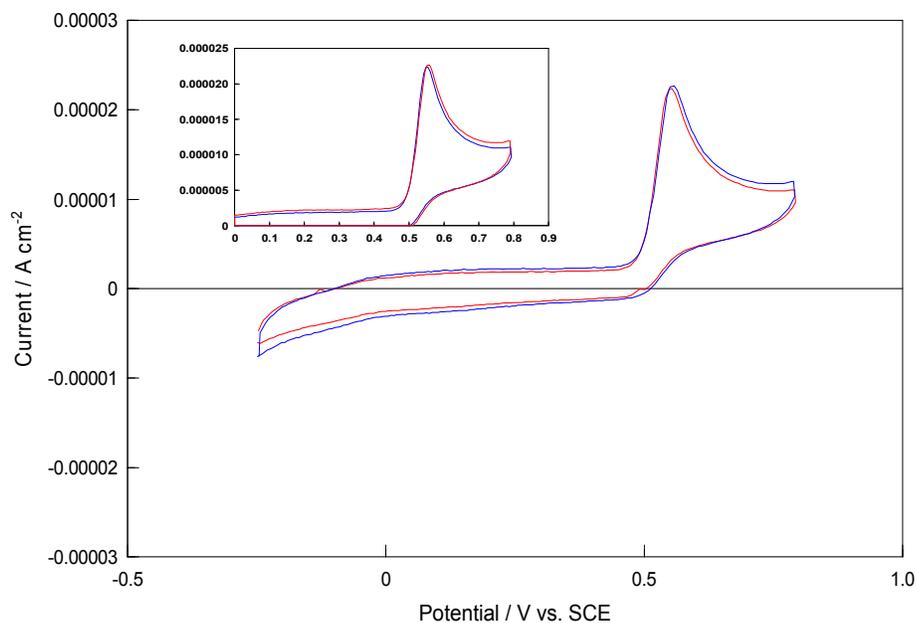
Figure 6.4: Cyclic voltammograms of a bare GC electrode in a ▬ 5.0 x 10^{-4} mol dm^{-3} UA / 0.30 mol dm^{-3} citrate phosphate buffer solution (pH~3.3) and in a ▬ 5.0 x 10^{-4} mol dm^{-3} UA / 0.01 mol dm^{-3} sulfonated β-cyclodextrin / 0.30 mol dm^{-3} citrate phosphate buffer solution (pH~3.3). Scan rate = 50 mV s^{-1}. Inset: Magnification of the oxidation region. Axes are identical to Figure 6.4. Electrochemical Window: -0.250 V vs. SCE to 0.800 V vs. SCE.

The DA peak currents and peak potentials observed when a fixed concentration of UA (1.0 x 10^{-4} mol dm^{-3}) was mixed with varying concentrations of DA (7.0 x 10^{-5} - 1.0 x 10^{-3} mol dm^{-3}) are shown in Table 6.1. In this table the mean values are presented. The errors range from 0.32 to 1.82% of the mean value, with $n = 3$, indicating very good reproducibility from experiment to experiment. In Figure 6.5, the mean peak current is plotted as a function of the DA concentration to give the characteristic calibration curve observed for DA, Section 3.3.7.

Table 6.1: Peak currents and peak oxidation potentials observed when a fixed concentration of 1.0 x 10^{-4} mol dm^{-3} UA was added to various DA concentrations in a 0.10 mol dm^{-3} Na_2SO_4, pH~5.2, supporting electrolyte ($n=3$).

Conc. of DA / mol dm^{-3}	Mean I_p^A/ mA cm^{-2}	Mean E_p^A / mV vs. SCE
7.0 x 10^{-5}	1.888 ± 0.003	429.2 ± 0.8
9.0 x 10^{-5}	1.955 ± 0.001	435.3 ± 0.5
2.0 x 10^{-4}	2.211 ± 0.006	438.7 ± 0.2
5.0 x 10^{-4}	2.886 ± 0.008	445.3 ± 0.4
1.0 x 10^{-3}	3.653 ± 0.009	459.2 ± 0.3

The influence of UA on the DA oxidation peak currents is summarised in Figure 6.6, where the magnitude of the peak currents obtained with pure DA is compared to the values measured when 1.0 x 10^{-4} mol dm^{-3} UA solution is present. It can be seen that the DA signal is not affected by the presence of UA. Identical peak currents for the oxidation of DA are obtained regardless of the excess amount of UA added to the DA solution.

The mean potentials, given in Table 6.1, were then compared to the potentials observed for pure DA oxidation and this is illustrated in Figure 6.7. It can be seen that the presence of UA does not interfere with the potential of the DA oxidation signal.
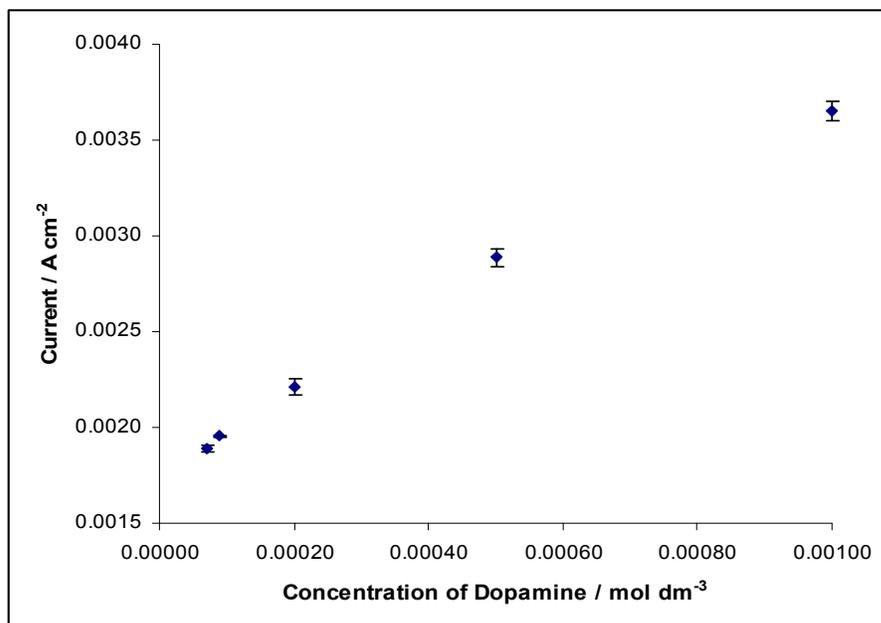
Figure 6.5: Calibration plot of the mean peak current of DA as a function of the concentration of DA where 1.0 x 10^{-4} mol dm^{-3} UA was added to each DA solution in a 0.10 mol dm^{-3} Na$_2$SO$_4$, pH~5.2, supporting electrolyte (n=3).
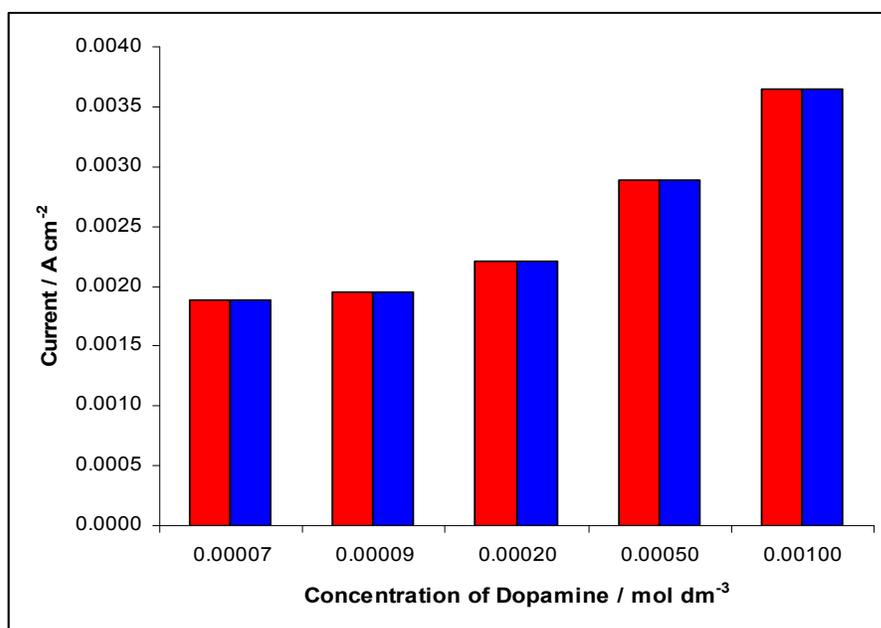
Figure 6.6: Peak currents, from the cyclic voltammograms, of DA as a function of the concentration of DA in the ■ presence (n=3) and ■ absence (n=4) of 1.0 x 10^{-4} mol dm^{-3} UA in a 0.10 mol dm^{-3} Na$_2$SO$_4$, pH~5.2, supporting electrolyte.
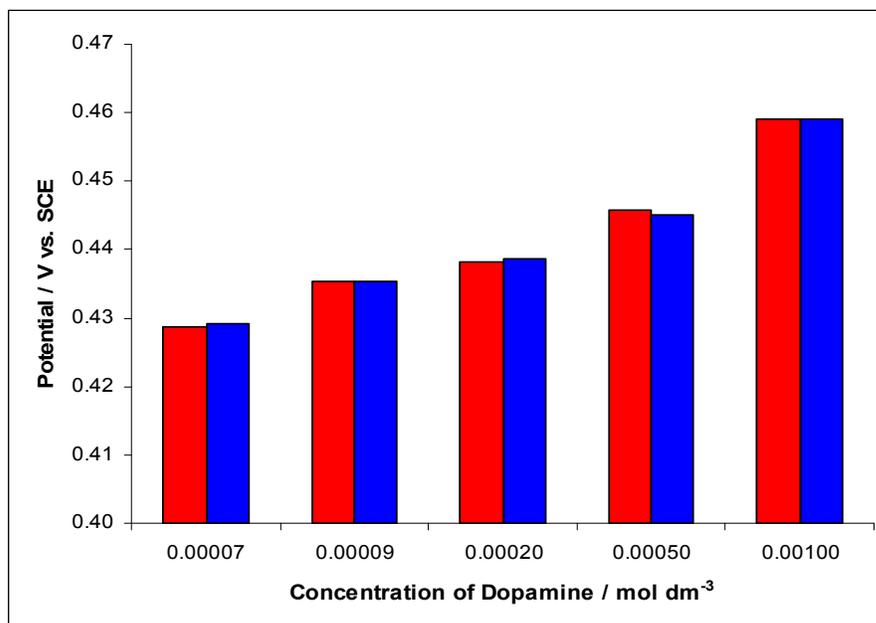
Figure 6.7: Peak potentials of DA oxidation for a range of DA concentrations (7.0 x 10^{-5} - 1.0 x 10^{-3} mol dm^{-3}) obtained using cyclic voltammetry, in the ■ presence (*n*=3) and ■ absence (*n*=4) of 1.0 x 10^{-4} mol dm^{-3} UA in a 0.10 mol dm^{-3} Na$_2$SO$_4$, pH~5.2, supporting electrolyte.

The results in this section show clearly that 1.0 x 10^{-4} mol dm^{-3} UA is not an interferent, eliminating the signal of UA. This can be attributed to the non hydrophobic character of UA and also to the anionic nature of the molecule. At physiological pH 7.4, UA exists as an anion[4], and therefore materials that repel anions can separate or eliminate the interference of UA. One common strategy is to modify the electrode surface with a permselective polymer film. Nafion®[10, 11] and melanin-type[12] polymer films have previously been used to reject the negatively charged UA.

On the whole, the modified electrodes described in the literature usually function by separating the oxidation waves of UA and DA. Table 6.2 summarises the various materials found in the literature that are capable of doing this. In contrast to these materials, the PPy-SCD film can eliminate the interference of UA at ratios of UA:DA ranging from 0.1-1.4:1.

Table 6.2: Materials, reported in the literature, which are capable of resolving the oxidation peaks of UA and DA.

Reference	Ratio of [UA]:[DA]	Material
13	1:0.33	Evans blue modified glassy carbon electrode
14	1:1	Poly-chromotrope 2B modified glassy carbon electrode
15	1:0.5	Melanin modified pyrolytic graphite electrode
16	100-5000:1	Platinum electrode modified with single-walled carbon nanotubes and phytic acid
17	1:1	Carbon nanofiber modified carbon paste electrode
18	5:1	DNA immobilised in an overoxidised polypyrrole film on a carbon fiber electrode
19	1:1	Overoxidised polypyrrole with incorporated single-walled carbon nanotubes on a glassy carbon electrode
20	1:1	Glassy carbon electrode coated with choline and gold nanoparticles
21	0.13-2.33:1	Carbon ionic liquid electrode
3	2:1	Carbon paste electrode modified with palladium nanoparticle-loaded carbon nanofibers
1	5.7:1	Platinum and gold nanoparticles with L-cysteine on a glassy carbon electrode
22	1:1	Poly(3-methylthiophene) modified glassy carbon electrode coated with nafion/single-walled carbon nanotubes
23	1:0.4	Glassy carbon electrode modified with ferrocene single-walled carbon nanotubes
24	2.5:1	Glassy carbon electrode modified with p-nitobenzenazo resorcinol

Other materials that come close to the performance of the PPy-SCD sensor are those developed by Rocha and Carapuca[10] and Luczak[25]. Rocha and Carapuca[10] have shown that a 1.05 x 10^{-3} mol dm^{-3} UA solution has no electrochemical response at a Nafion$^®$-coated GC electrode. Furthermore, when 1.0 x 10^{-3} mol dm^{-3} of UA is present in a 4.9 x 10^{-4} mol dm^{-3} DA solution, there is no noticeable difference in the oxidation peak current of DA. Luczak[25] used an overoxidised DA polymer film to show that the DA oxidation peak current remained unaltered in the presence of 1.0 x 10^{-3} mol dm^{-3} UA.

There are several other methods of detecting DA selectively in the presence of UA without the use of modified electrodes. One approach is to use flow injection analysis. Leu and Lin[26] used flow injection analysis with $LiMn_2O_4$ for the determination of DA but found negligible interference, 2%, from UA. Nevertheless, this approach cannot be used as an *in-vivo* sensor for real-time analysis.

There are no reports, to the best of our knowledge, on the use of cyclodextrins for the selective detection of DA in the presence of UA, or for the simultaneous detection of DA and UA. In summary, the PPy-SCD modified electrode eliminates the interference from UA and has potential in the design of an *in-vivo* DA sensor.

6.3.2 Aspartic Acid (Asp) and Glutamic Acid (Glu)

Asp and Glu, Figures 6.8 and 6.9, are non-essential amino acids that serve as major excitatory neurotransmitters in the brain and both exhibit relatively poor electroactivity[4,27]. Therefore, they will coexist with DA in most biological samples. In addition to this, amino acids are well known to foul electrodes by adhering to the surface, causing a decline in the sensor signal[28]. For these reasons, Asp and Glu were investigated as interferents to see if they had any effect on the performance of the PPy-SCD modified electrode.
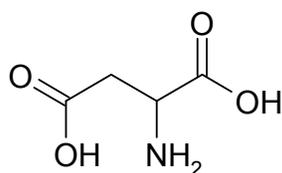
Figure 6.8: Structure of Asp   **Figure 6.9: Structure of Glu**
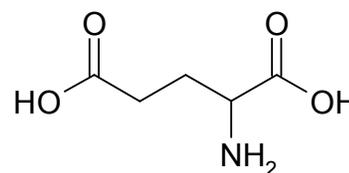
The electroactivity of Asp and Glu at a bare Pt electrode was first investigated in the sulfate supporting electrolyte by cycling the Pt electrode in a 1.0×10^{-3} mol dm^{-3} solution of Asp and in a 1.0×10^{-3} mol dm^{-3} solution of Glu. Representative cyclic voltammograms are shown in the inset in Figure 6.10 for the Asp. Nearly identical voltammograms (not shown here) were recorded for the Glu, as both amino acids have similar and related chemical structures, Figures 6.8 and 6.9. The oxidation of the amino acid occurs from approximately 0.400 V vs. SCE to 0.800 V vs. SCE. In addition, a reduction wave, centred at 0.230 V vs. SCE, is clearly visible.
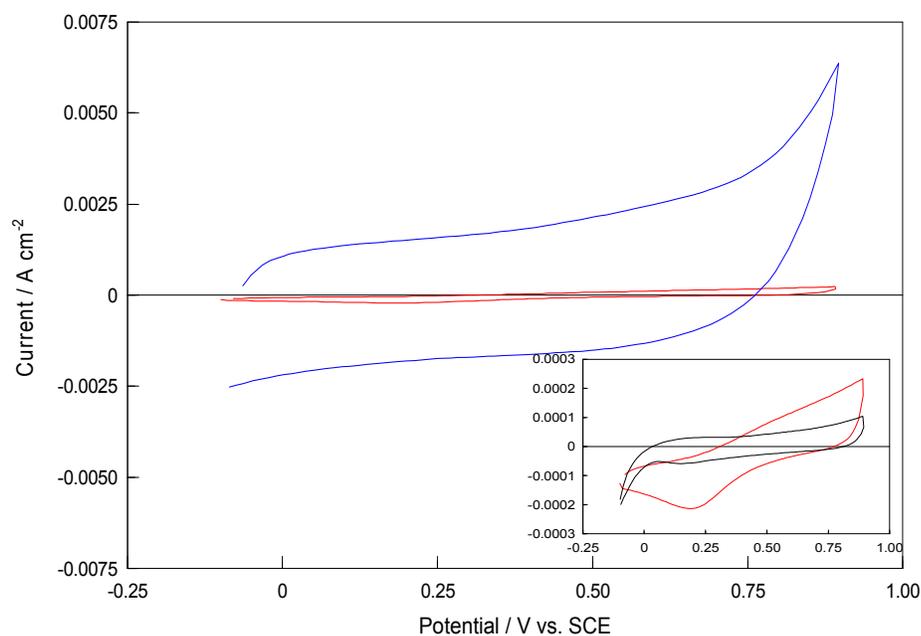
Figure 6.10: Cyclic voltammograms of a — bare Pt electrode and a — PPy-SCD modified electrode in a 1.0×10^{-3} mol dm^{-3} Asp / 0.10 mol dm^{-3} Na$_2$SO$_4$ solution (pH~4.0). Scan rate = 100 mV s^{-1}. Inset: Cyclic voltammograms of the bare Pt electrode in a — 0.10 mol dm^{-3} Na$_2$SO$_4$ solution and in a — 1.0×10^{-3} mol dm^{-3} Asp / 0.10 mol dm^{-3} Na$_2$SO$_4$ solution. Scan rate = 100 mV s^{-1}. Axes are identical to Figure 6.10.

The electroactivity of Asp or Glu is not observed at the PPy-SCD modified electrode, as shown in Figure 6.10. There is no evidence of either the oxidation or reduction waves, observed at the platinum electrode. However, the background current of the PPy-SCD is significantly higher than the oxidation and reduction currents of Asp and Glu at the Pt substrate, making it difficult to detect Asp and Glu at this PPy-SCD modified Pt electrode. Next, the PPy-SCD modified electrode was cycled in a solution of DA with and without the presence of Asp or Glu. Typical data are presented in Figure 6.11(a) and 6.11(b), where the cyclic voltammogram recorded in a 1.0×10^{-3} mol dm^{-3} DA solution is compared with the corresponding voltammograms recorded in the combined solutions, 1.0×10^{-3} mol dm^3 DA with 1.0×10^{-3} mol dm^{-3} Asp or 1.0×10^{-3} mol dm^3 DA with 1.0×10^{-3} mol dm^{-3} Glu. It is clear from this comparison that the oxidation of DA and the subsequent reduction of the dopamine-o-quinone (DOQ) are not affected by the presence of Asp or Glu.

In order to explore this further, the concentration ratio of Asp/Glu to DA in the combined solution was varied from 1.0 (1.0×10^{-3} mol dm^{-3} DA and 1.0×10^{-3} mol dm^{-3} Asp/Glu) to 14.3 (7.0×10^{-5} mol dm^{-3} DA and 1.0×10^{-3} mol dm^{-3} Asp/Glu) and the peak currents and peak potentials for the oxidation of DA were measured as a function of the concentration of DA. A total of five separate measurements were carried out for each Asp/DA mixture, while three separate measurements were carried out for each Glu/DA mixture. In Figures 6.12(a) and (b), the peak oxidation currents of DA are plotted as a function of the DA concentration with a fixed 1.0×10^{-3} mol dm^{-3} solution of Asp or with a fixed 1.0×10^{-3} mol dm^{-3} solution of Glu. The error bars for the DA oxidation currents in the presence of Asp range between 0.92 to 1.48%, while the error bars in the presence of Glu range between 0.58 to 2.90%. These low errors show good agreement over the five replicate Asp experiments and three replicate Glu experiments. The calibration plots are very similar to that presented in Figure 6.5, showing that the Asp and Glu have very little effect on the oxidation of DA, regardless of the concentration of DA. A more direct comparison between the oxidation currents and potentials of DA with and without Asp is provided in Figures 6.13(a) and 6.14(a). The same comparison with and without Glu is shown in Figures 6.13(b) and 6.14(b). These data clearly show that both Asp and Glu exert no influence on

the signal of DA. Identical currents to pure DA are measured, regardless of the excess amount of Asp or Glu present in the solution, at each concentration of DA.
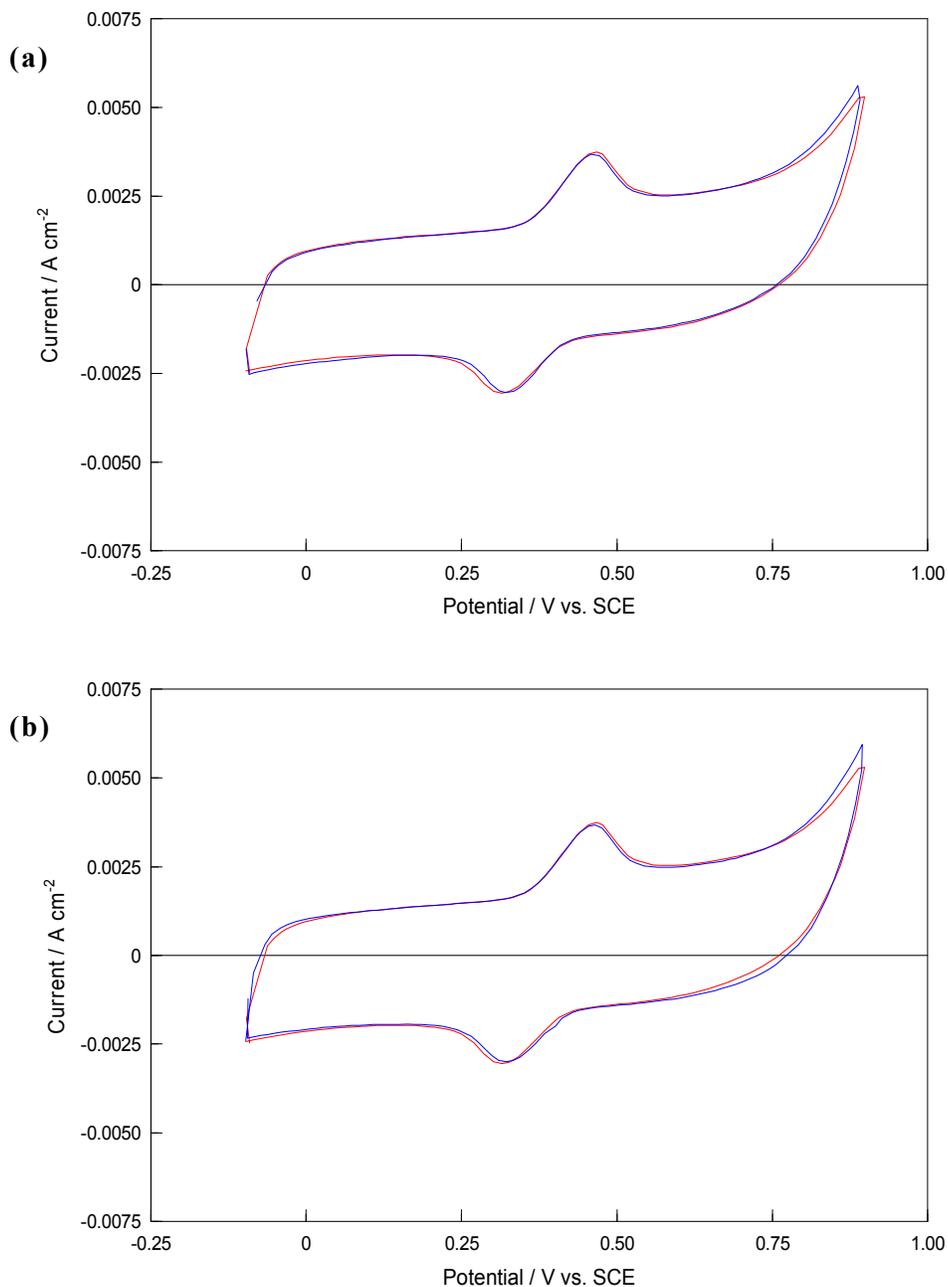
Figure 6.11: (a) Cyclic voltammograms of the PPy-SCD modified electrode in a — 1.0 x 10^{-3} mol dm^{-3} DA / 0.10 mol dm^{-3} Na$_2$SO$_4$ solution (pH~6.0) and in a — 1.0 x 10^{-3} mol dm^{-3} DA / 1.0 x 10^{-3} mol dm^{-3} Asp / 0.10 mol dm^{-3} Na$_2$SO$_4$ solution (pH~4.0). Scan rate = 100 mV s^{-1}. (b) Cyclic voltammograms of the PPy-SCD modified electrode in a — 1.0 x 10^{-3} mol dm^{-3} DA / 0.10 mol dm^{-3} Na$_2$SO$_4$ solution (pH~6.0) and in a — 1.0 x 10^{-3} mol dm^{-3} DA / 1.0 x 10^{-3} mol dm^{-3} Glu / 0.10 mol dm^{-3} Na$_2$SO$_4$ solution (pH~4.1). Scan rate = 100 mV s^{-1}.

(a)

(b)
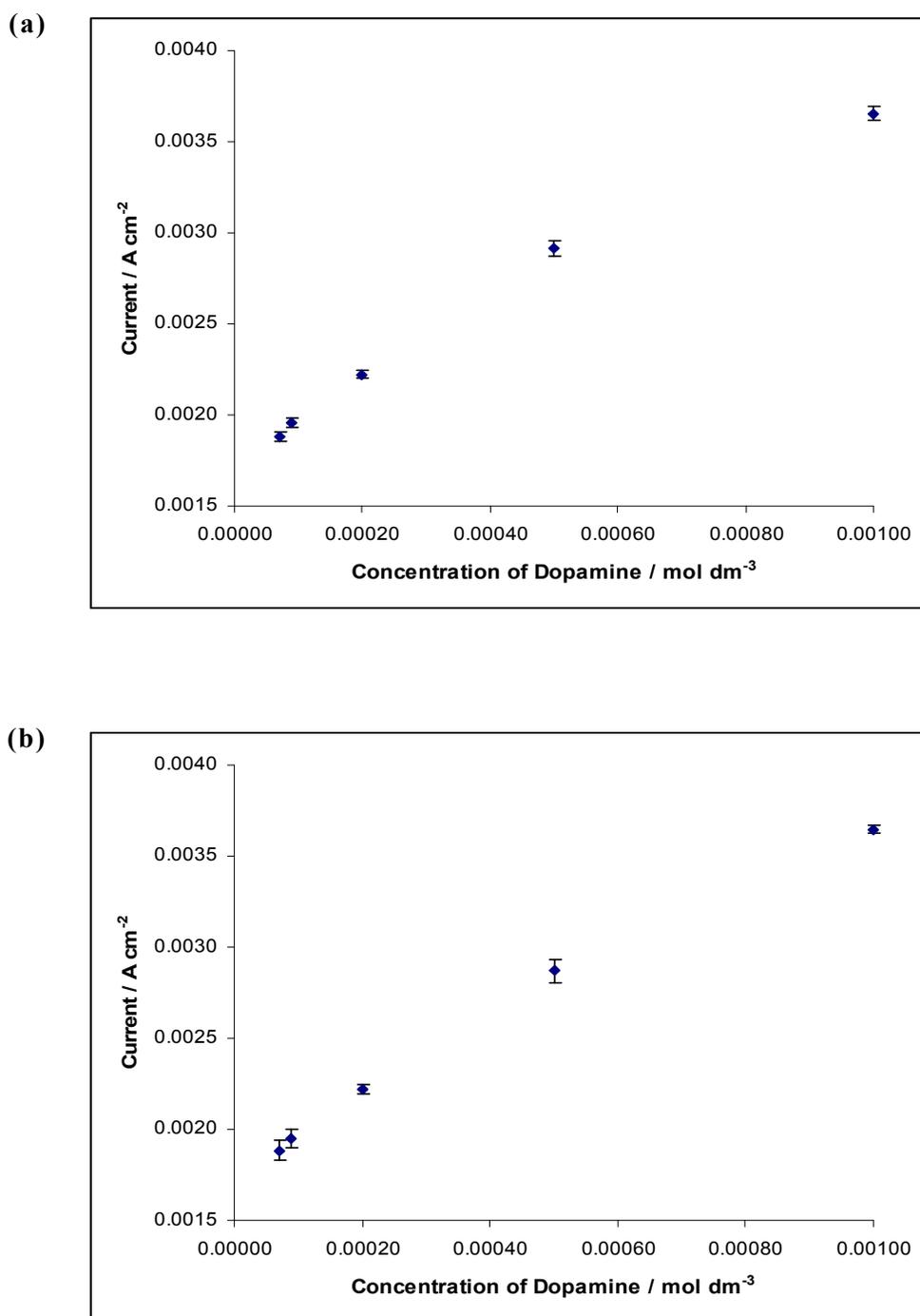
Figure 6.12: (a) Calibration plot of the mean peak oxidation current of DA as a function of the concentration of DA where 1.0 x 10^{-3} mol dm^{-3} Asp was added to each DA solution in a 0.10 mol dm^{-3} Na$_2$SO$_4$, pH~4.0, supporting electrolyte (*n*=5). (b) Calibration plot of the mean peak oxidation current of DA as a function of the concentration of DA where 1.0 x 10^{-3} mol dm^{-3} Glu was added to each DA solution in a 0.10 mol dm^{-3} Na$_2$SO$_4$, pH~4.1, supporting electrolyte (*n*=3).

(a)

(b)
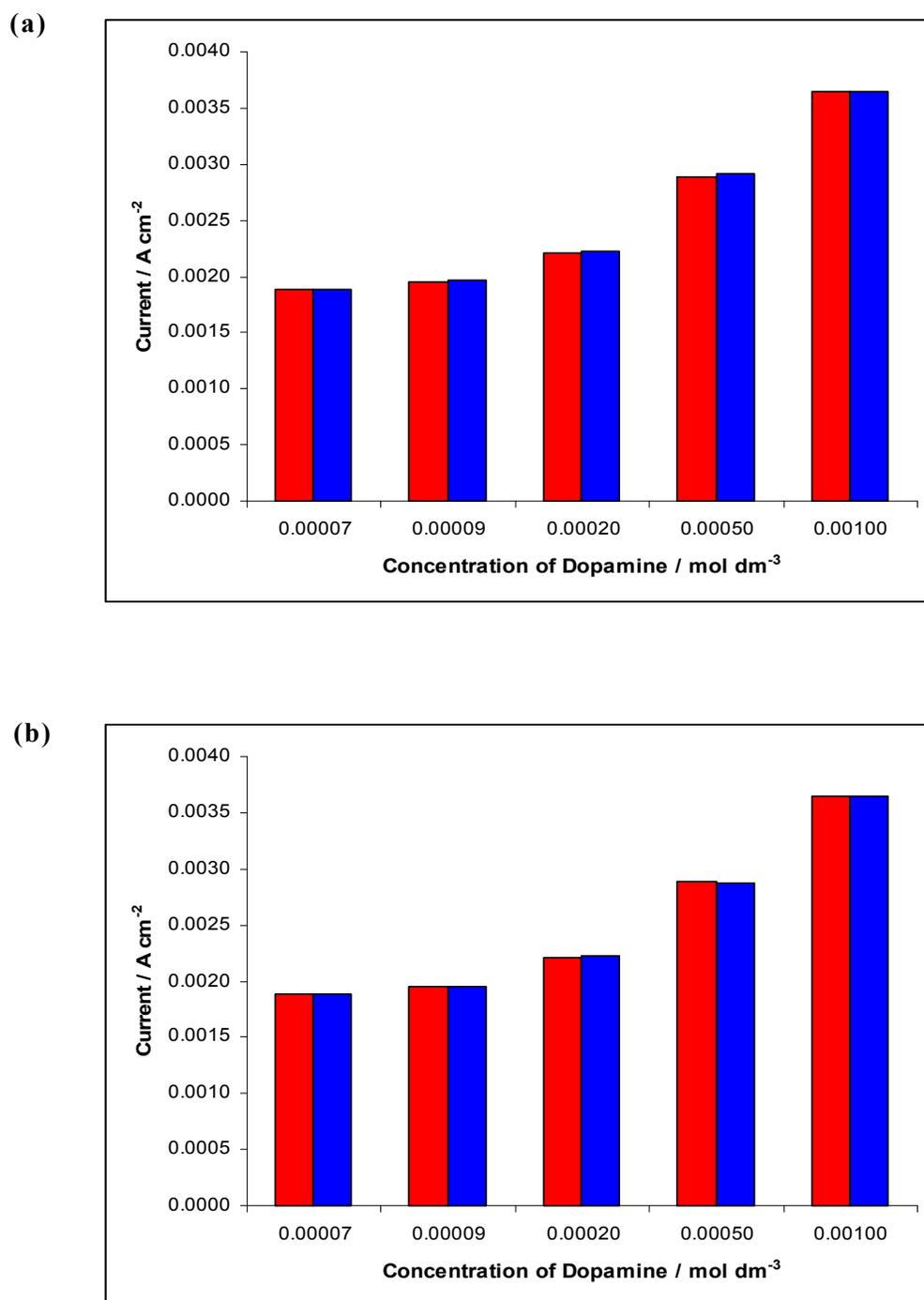
Figure 6.13: (a) Peak oxidation currents, from the cyclic voltammograms, of DA as a function of the concentration of DA in the ■ presence (*n*=5) and ■ absence (*n*=4) of 1.0 x 10^{-3} mol dm^{-3} Asp in a 0.10 mol dm^{-3} Na$_2$SO$_4$, pH~4.0, supporting electrolyte. (b) Peak currents, from the cyclic voltammograms, of DA as a function of the concentration of DA in the ■ presence (*n*=3) and ■ absence (*n*=4) of 1.0 x 10^{-3} mol dm^{-3} Glu in a 0.10 mol dm^{-3} Na$_2$SO$_4$, pH~4.1, supporting electrolyte.

(a)

(b)
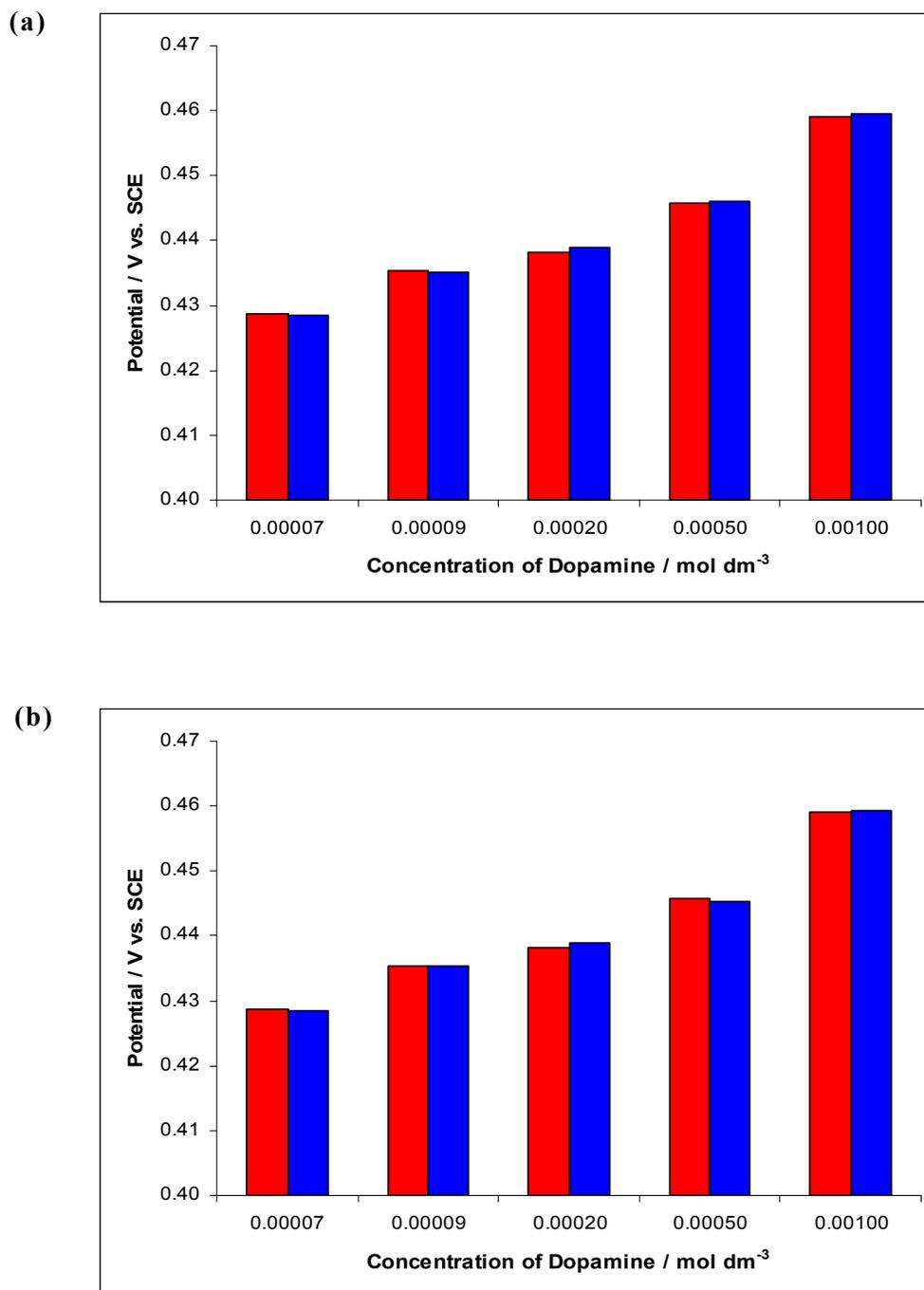
Figure 6.14: (a) Peak potentials of DA oxidation for a range of DA concentrations (7.0×10^{-5} - 1.0×10^{-3} mol dm^{-3}) obtained using cyclic voltammetry, in the ■ presence (*n*=5) and ■ absence (*n*=4) of 1.0×10^{-3} mol dm^{-3} Asp in a 0.10 mol dm^{-3} Na$_2$SO$_4$, pH~4.0, supporting electrolyte. (b) Peak potentials of DA oxidation for a range of DA concentrations (7.0×10^{-5} - 1.0×10^{-3} mol dm^{-3}) obtained using cyclic voltammetry, in the ■ presence (*n*=3) and ■ absence (*n*=4) of 1.0×10^{-3} mol dm^{-3} Glu in a 0.10 mol dm^{-3} Na$_2$SO$_4$, pH~4.1, supporting electrolyte.

Although the oxidation currents observed with Asp and Glu at the Pt electrode (inset in Figure 6.10 are low, approximately 0.0001 A cm^{-2} at 0.500 V vs. SCE, this current value is significantly higher than the standard errors in the DA oxidation currents measured for the 7.0 x 10^{-5} mol dm^{-3} DA solution. Accordingly, if the Asp or Glu was oxidised at the PPy-SCD, higher peak currents for the DA oxidation wave, particularly at the lower DA concentration, would be expected. Clearly this is not the case, lending support to the fact that Asp and Glu are not detected at the PPy-SCD modified electrode. Indeed, there was no evidence of a reduction wave from the oxidised Asp or Glu, which has a higher peak current at the pure Pt surface (Figure 6.10), in any of the voltammograms recorded for the PPy-SCD in the DA-containing solutions.

As discussed earlier with UA, electrostatic interactions are important in the electrochemical sensing as the PPy-SCD modified electrode is highly charged with ionised sulfonated groups. Asp and Glu are amino acids and depending on the pH of the solution, they can exist in one of three forms to give a cationic, a zwitterionic or an anionic species, as detailed in Schemes 6.2 and 6.3, respectively. At the pH of the experiment (pH = 4.0) Asp will exist mainly in the zwitterionic form (pK_a of α-COOH is 2.1). In addition, the carboxylic group on the side chain (pKa of the ionisable side chain is 3.9) is ionised to give a polar structure which will be predominantly anionic. Glu will be in the exact same form as Asp. Accordingly, Asp and Glu should be repelled by the anionic sulfonated groups on the cyclodextrin.
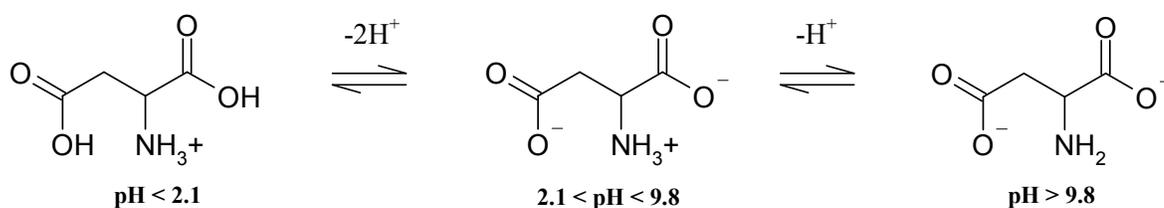
Scheme 6.2: The cationic, zwitterionic and anionic forms of Asp[29].
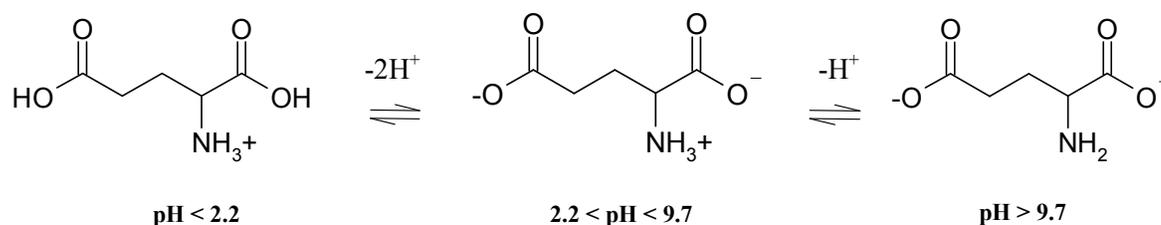
Scheme 6.3: The cationic, zwitterionic and anionic forms of Glu[29].

In relation to inclusion complexation, it is well known in the literature that inclusion complexes are only formed between aromatic amino acids, for example tyrosine and cyclodextrins[30]. In addition, the anionic character of the Asp and Glu would inhibit the formation of an inclusion complex with the anionic sulfonated cyclodextrin. It has already been shown in the literature that electrostatic interactions affect the stability of an inclusion complex[31] and these electrostatic interactions would be highly unfavourable in the case of the polar Asp system at a pH of 4.0 and the polar Glu system at a pH of 4.1.

As already noted in this section, both Asp and Glu are amino acids and therefore are capable of fouling the electrode surface. This may cause the DA signal to diminish rapidly and eventually disappear. In order to determine if Asp or Glu were poisoning the electrode surface the DA peak currents obtained in the presence of 1.0×10^{-3} mol dm^{-3} Asp or Glu over ten cycles were compared to the currents obtained by pure DA. Figure 6.15 shows the results obtained in the presence of Glu. From Figure 6.15 it can be seen that Glu is not fouling the electrode surface as the DA peak currents in the presence of Glu mimic that of pure DA. The same result was also found for Asp.

In summary, the PPy-SCD electrode eliminates the interference of Asp and Glu in the electrochemical detection of DA and offers advantages over the existing methodologies. Some of the existing materials and techniques employed for the analysis of DA in the presence of Asp and Glu are summarised in Table 6.3. These approaches are largely based on chromatography measurements and while they are successful in detecting DA, these approaches can never be used for real-time in-vivo sensing.
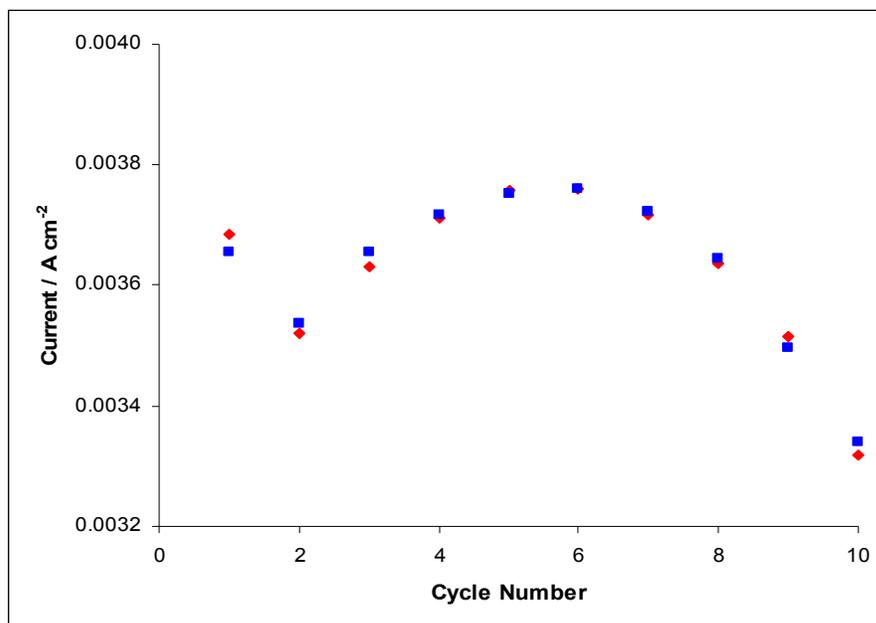
Figure 6.15: Peak oxidation currents of DA, from the cyclic voltammograms, of 1.0×10^{-3} mol dm^{-3} DA as a function of the cycle number in the ■ presence (*n=3*) and ■ absence (*n=3*) of 1.0×10^{-3} mol dm^{-3} Glu in a 0.10 mol dm^{-3} Na_2SO_4, pH~4.1, supporting electrolyte.

Table 6.3: Materials in the literature that are capable of simultaneously detecting DA and Asp or DA and Glu or that can selectively detect DA in the presence of Asp or Glu.

Reference	Technique	Result
26	Flow injection analysis with $LiMn_2O_4$	Selective
32	Hydrophilic interaction chromatography coupled to tandem-mass spectrometry	Simultaneous
33	Capillary electrophoresis with laser-induced fluorescence	Simultaneous
34	Microdialysis together with high performance liquid chromatography	Simultaneous
35	Microdialysis and capillary electrophoresis with laser-induced fluorescence	Simultaneous
36	GC tandem-mass spectrometry with electron capture	Simultaneous
37	Capillary electrophoresis with laser-induced fluorescence	Simultaneous

To the best of our knowledge, there are no reports on the selective detection of DA in the presence of Asp or indeed on the simultaneous detection of DA and Asp using modified electrodes. However, the interference of Glu has been investigated by Kooshki and Shams[38] and Lin and Gong[39]. Kooshki and Shams[38] found that a 25-fold excess of Glu did not interfere in the signal of 4.0 x 10^{-7} mol dm^{-3} DA using a carbon paste electrode modified with titanium phosphated silica gel. However, no experimental evidence was provided in the paper to verify this result. In contrast, Lin and Gong[39] have shown that a 150-fold excess of Glu does interfere with the peak current of 1.0 x 10^{-5} mol dm^{-3} DA at a glassy carbon electrode modified with a 5,5-ditetradecyl-2-(2-trimethyl-ammonioethyl)-1,3-dioxane bromide self-assembled bilayer membrane. Clearly, the PPy-SCD has potential for the electrochemical sensing of DA, eliminating any interference from Asp and Glu. Furthermore, these amino acids do not appear to foul the electrode.

6.3.3 Aminobutyric Acid (GABA)

GABA, Figure 6.16, is an electroinactive, non-protein amino acid and is the chief inhibitory neurotransmitter in the central nervous system[40]. The concentration of GABA in the brain is greater than most other neurotransmitters, including DA. Therefore, GABA was investigated in order to determine its effect, if any, on the function of the PPy-SCD modified electrode.
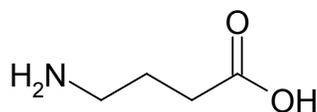
Figure 6.16: Structure of GABA

As expected, no electrochemical redox activity for GABA was observed at the bare platinum electrode. The cyclic voltammogram of a 1.0 x 10^{-3} mol dm^{-3} solution of GABA,

in 0.10 mol dm^{-3} Na$_2$SO$_4$, was also recorded at a PPy-SCD modified electrode. Again there was no evidence of any electrochemical activity of GABA at the PPy-SCD modified electrode.

GABA is a zwitterion at the pH of the experiment and so carries a positive charge on the amine group and a negative charge on the terminal oxygen. The cationic, zwitterionic and anionic forms of GABA are shown in Scheme 6.4. Although GABA is not electroactive, the possible interaction of the amine group on GABA with the negatively charged sulfonated groups on the β-cyclodextrin could foul the electrode surface, or block access to the cyclodextrin cavities, causing the DA signal to diminish.

Scheme 6.4: The cationic, zwitterionic and anionic forms of GABA[29].

The performance of the PPy-SCD sensor to the detection of DA was examined in the presence of GABA. Equivalent voltammograms for the redox behaviour of DA, in the absence and presence of GABA, at the PPy-SCD modified electrode, were observed and are shown in Figure 6.17. GABA does not interfere with the DA signal and the familiar, well defined, anodic and cathodic peaks of DA are retained. This would suggest that no lasting interaction between GABA and the sulfonated β-cyclodextrin exists, and that the sulfonated β-cyclodextrin sites in the film are free to bind to DA.

As with Asp and Glu, the formation of an inclusion complex between GABA and the sulfonated β-cyclodextrin is also very unlikely due to the non hydrophobic nature of the GABA. Also, on repetitive cycling, the polarisation curves for a given concentration of DA mixed with GABA corresponded to the polarisation curves for a given concentration of

pure DA. As discussed earlier with Glu, this indicates that electrode fouling by GABA does not occur.

The cyclic voltammetric oxidation current outputs were recorded for five concentrations of DA in the presence of GABA. From these data, the mean peak current, the standard deviation and the standard errors were calculated. The standard errors, which ranged from 0.38 to 2.98%, reflect the excellent reproducibility of the PPy-SCD films. These mean peak currents for DA oxidation in the presence of 1.0×10^{-3} mol dm^{-3} GABA, are plotted as a function of the concentration of DA, and are shown in Figure 6.18.

The curve presented in Figure 6.18 is very similar to the calibration curves presented in Figures 6.5 and 6.12, indicating little effect from GABA. The influence of GABA on the DA oxidation peak currents is further highlighted in the histogram in Figure 6.19. In this figure, it is clear that a 1.0×10^{-3} mol dm^{-3} concentration of GABA has no effect on the DA oxidation currents at the PPy-SCD modified electrode, even at low DA concentrations.

A visual comparison between the peak oxidation potentials of DA, recorded in the absence and presence of GABA, is made in the form of a histogram, in Figure 6.20. Again, it is clear from this figure that GABA does not alter the peak oxidation potentials of DA.
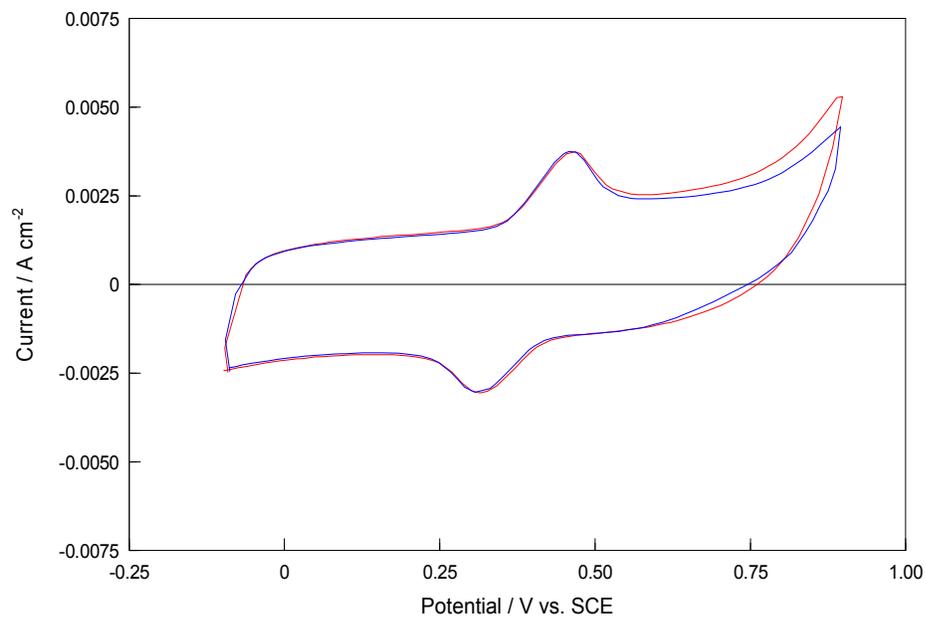
Figure 6.17: Cyclic voltammograms of the PPy-SCD modified electrode in a — 1.0 x 10^{-3} mol dm^{-3} DA / 0.10 mol dm^{-3} Na$_2$SO$_4$ solution (pH~6.0) and in a — 1.0 x 10^{-3} mol dm^{-3} DA / 1.0 x 10^{-3} mol dm^{-3} GABA / 0.10 mol dm^{-3} Na$_2$SO$_4$ solution (pH~6.0). Scan rate = 100 mV s^{-1}.
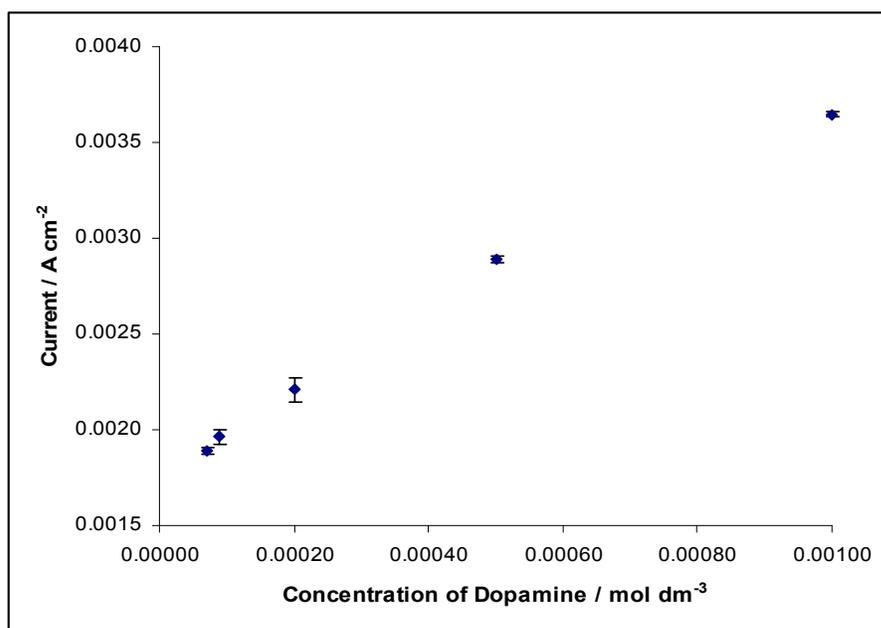
Figure 6.18: Calibration plot of the mean oxidation peak current of DA as a function of the concentration of DA where 1.0 x 10^{-3} mol dm^{-3} GABA was added to each DA solution in a 0.10 mol dm^{-3} Na$_2$SO$_4$, pH~6.0, supporting electrolyte (*n*=4).
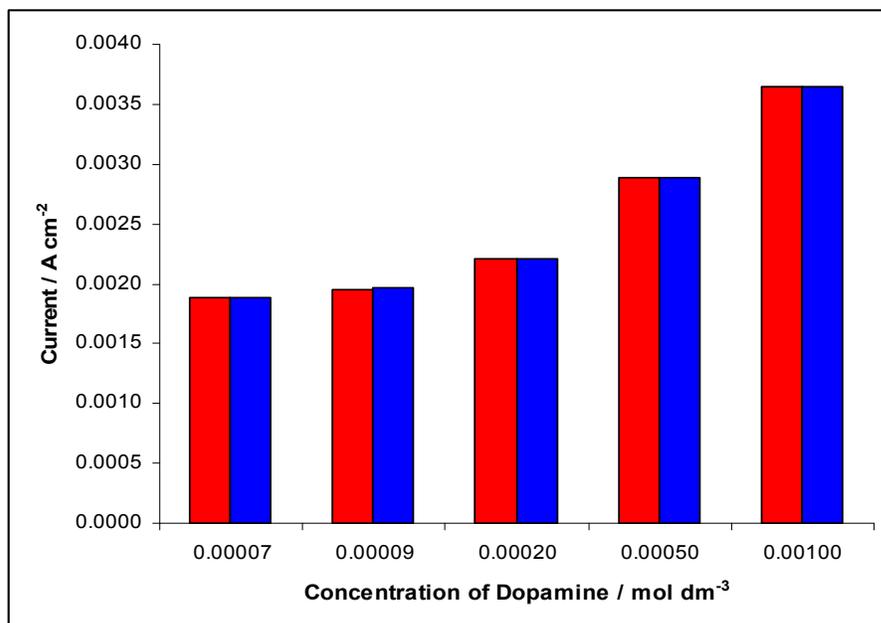
Figure 6.19: Peak oxidation currents of DA, from the cyclic voltammograms, of DA as a function of the concentration of DA in the ■ presence (*n*=4) and ■ absence (*n*=4) of 1.0 x 10^{-3} mol dm^{-3} GABA in a 0.10 mol dm^{-3} Na$_2$SO$_4$, pH~6.0, supporting electrolyte.
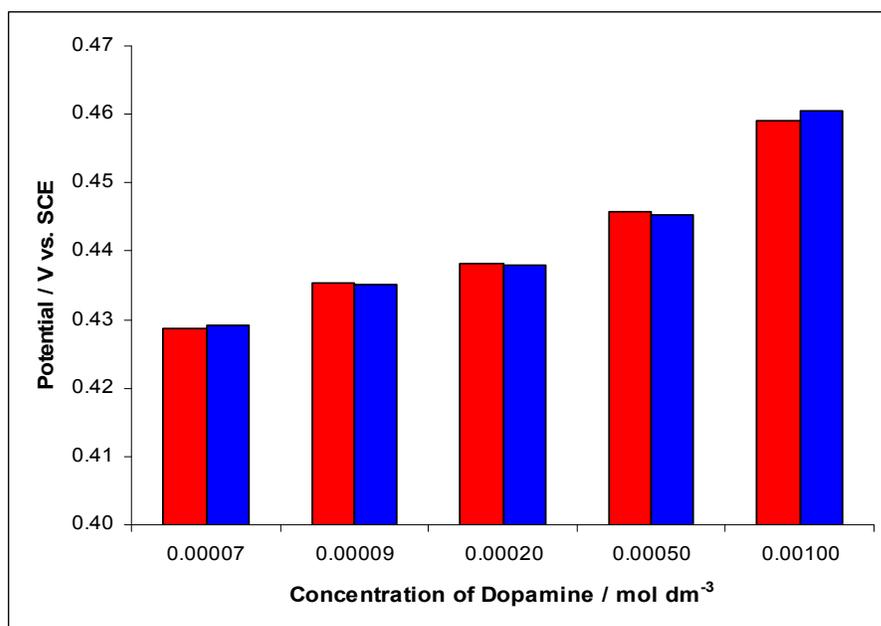
Figure 6.20: Peak potentials of DA oxidation for a range of DA concentrations (7.0 x 10^{-5} - 1.0 x 10^{-3} mol dm^{-3}) obtained using cyclic voltammetry, in the ■ presence (*n*=4) and ■ absence (*n*=4) of 1.0 x 10^{-3} mol dm^{-3} GABA in a 0.10 mol dm^{-3} Na$_2$SO$_4$, pH~6.0, supporting electrolyte.

The data outlined for DA oxidation peak currents and potentials in the presence of GABA suggest that no other solution phenomena are occurring, for example DA-GABA ion-pairing, and thus it can be concluded that GABA exhibits no interference on the oxidation of DA at the PPy-SCD electrode.

The approaches taken in the literature to date for the detection of GABA and DA in samples have been non-electrochemical due to the electroinactivity of GABA. Consequently, these methods are not suitable for real-time in-vivo detection, but nevertheless deserve to be mentioned. The authors Leu and Lin[26] eliminated the interference of GABA in the detection of DA using flow injection analysis with $LiMn_2O_4$. Simultaneous detection of DA and GABA was achieved by Zhao and Suo[41]. These authors used high-performance liquid chromatography with fluorescence detection and on-line mass spectrometric identification following derivatisation with 1,2-benzo-3,4-dihydrocarbazole-9-ethyl chloroformate. In conclusion, the PPy-SCD can detect DA in the presence of GABA, thus improving its worth as a possible real-time *in-vivo* sensor.

6.3.4 Acetylcholine (Ach)

Ach, Figure 6.21, is a key neurotransmitter in both the peripheral nervous system and the central nervous system[42]. It plays an important role in various functions, such as learning and memory formation and development and maintenance of addiction[43]. As Ach coexists with DA, it may interfere with the detection of DA at the PPy-modified electrode if the sensor were to be applied to an in-vivo environment. Furthermore, Ach will remain a positively charged compound in solution and so there may be competition between the cationic DA and cationic Ach at the PPy-SCD modified electrode.
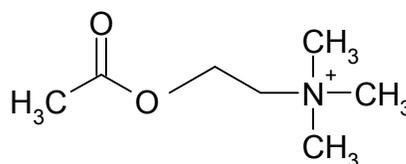
Figure 6.21: Structure of Ach

Using cyclic voltammetry it was found that Ach is not oxidised at a bare Pt electrode or at the PPy-SCD modified electrode. This is not surprising as Ach is not an electroactive species. When the PPy-SCD modified electrode is cycled in a solution containing 1.0×10^{-3} mol dm^{-3} Ach and 1.0×10^{-3} mol dm^{-3} DA, only the oxidation and reduction peaks of DA are detected. The voltammogram recorded in the mixed Ach and DA solution is identical to that recorded in DA alone, as illustrated in Figure 6.22, and as a result it can be concluded that Ach is not an interferent in the detection of DA. On the basis of electrostatic interactions, some interference would be expected from Ach, however this is not the case. Many electroinactive interferents can adhere to bare/modified electrode surfaces causing a decrease in background current and, ultimately, the cessation of analyte detection signals. The risk of this happening is increased with Ach, as it is positively charged and consequently will be attracted to the negatively charged interface. However, our data indicate that electrode fouling due to Ach is not prominent, with the currents, in the presence and absence of Ach, following the same trend.
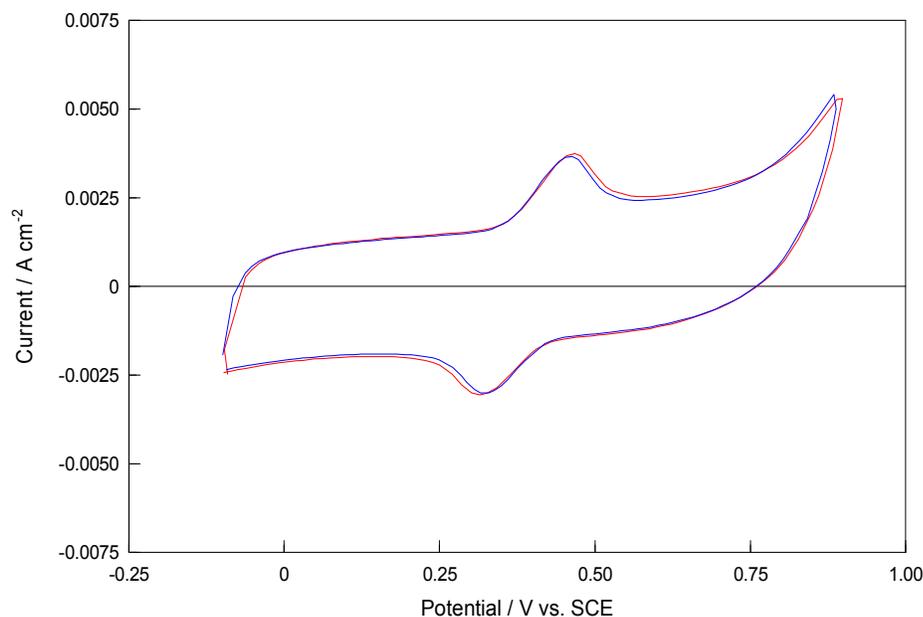
Figure 6.22: Cyclic voltammograms of the PPy-SCD modified electrode in a — 1.0×10^{-3} mol dm^{-3} DA / 0.10 mol dm^{-3} Na$_2$SO$_4$ solution (pH~6.0) and in a — 1.0×10^{-3} mol dm^{-3} DA / 1.0×10^{-3} mol dm^{-3} Ach / 0.10 mol dm^{-3} Na$_2$SO$_4$ solution (pH~5.4). Scan rate = 100 mV s^{-1}.

The peak oxidation currents and peak oxidation potentials obtained when a fixed concentration of Ach was mixed with varying concentrations of DA were measured. Two separate measurements were carried out and errors ranging from 0.66 to 2.42% were found demonstrating good agreement between the experiments. The mean peak current was plotted as a function of the DA concentration and the resulting trace is shown in Figure 6.23. These mean values were then compared, in the form of histograms in Figures 6.24 and 6.25, to the mean values obtained with pure DA oxidation. It can be seen from these figures that a 1.0×10^{-3} mol dm^{-3} Ach has no influence on the DA peak currents or peak potentials, regardless of the concentration of DA.

To review, the results in this section show clearly that 1.0×10^{-3} mol dm^{-3} Ach does not interfere with the determination of DA at the PPy-SCD modified electrode and therefore, the modified electrode has potential in the design of an *in-vivo* DA sensor.
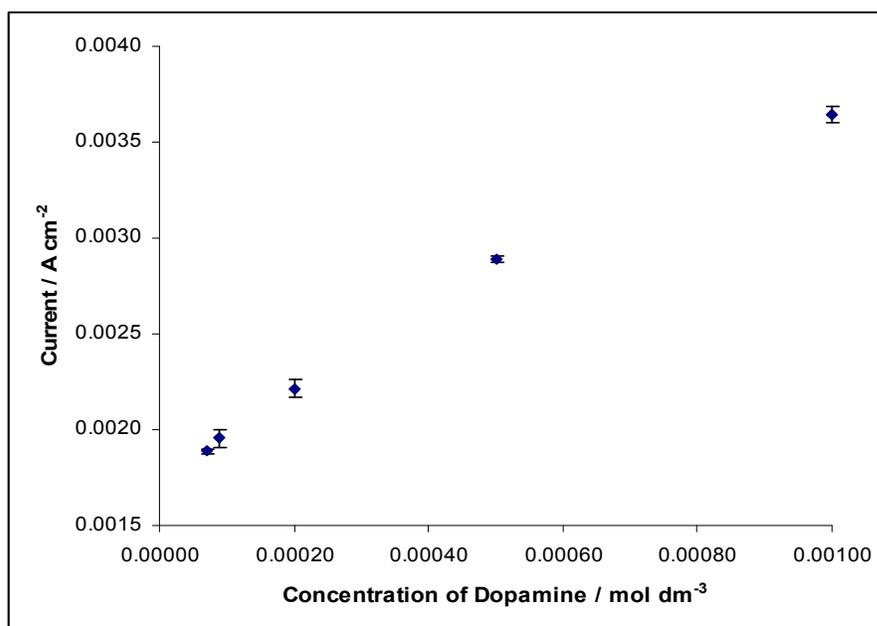
Figure 6.23: Calibration plot of the mean peak oxidation current of DA as a function of the concentration of DA where 1.0×10^{-3} mol dm^{-3} Ach was added to each DA solution in a 0.10 mol dm^{-3} Na$_2$SO$_4$, pH~5.4, supporting electrolyte (n=2).
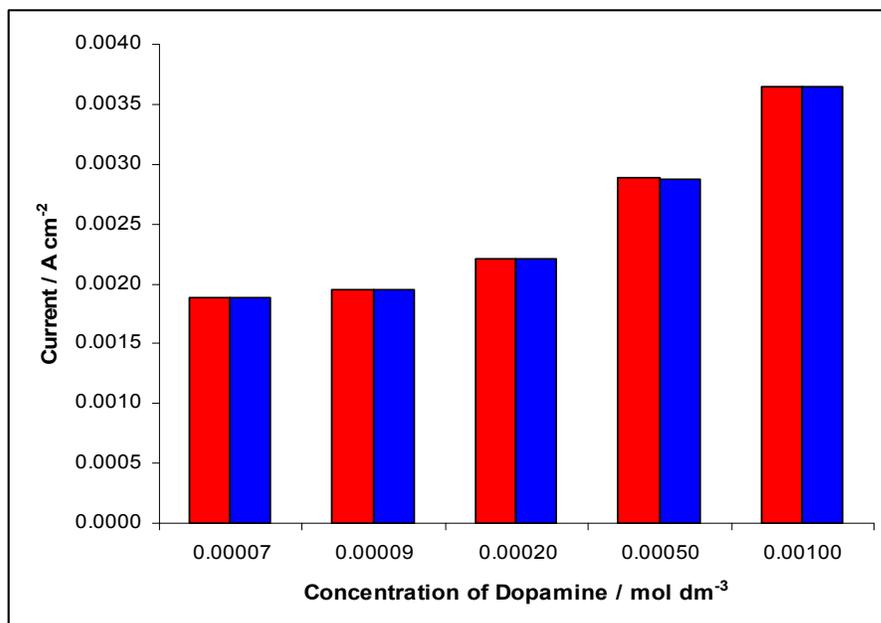
Figure 6.24: Peak oxidation currents, from the cyclic voltammograms, of DA as a function of the concentration of DA in the ■ presence (*n*=2) and ■ absence (*n*=4) of 1.0 x 10^{-3} mol dm^{-3} Ach in a 0.10 mol dm^{-3} Na$_2$SO$_4$, pH~5.4, supporting electrolyte.
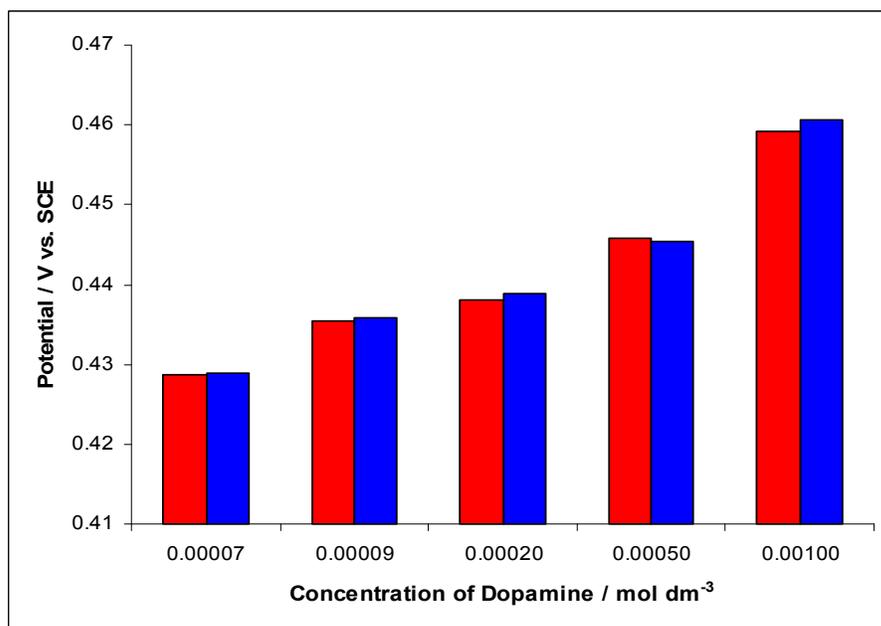
Figure 6.25: Peak potentials of DA oxidation for a range of DA concentrations (7.0 x 10^{-5} - 1.0 x 10^{-3} mol dm^{-3}) obtained using cyclic voltammetry, in the ■ presence (*n*=2) and ■ absence (*n*=4) of 1.0 x 10^{-3} mol dm^{-3} Ach in a 0.10 mol dm^{-3} Na$_2$SO$_4$, pH~5.4, supporting electrolyte.

To the best of our knowledge, there are no reports on the selective electrochemical detection of DA in the presence of Ach, or for the simultaneous detection of DA and Ach at a modified electrode. Several non-electrochemical techniques have been reported in the literature, but it is noteworthy to mention that these methods cannot be used for real-time, in-vivo measurements. Examples of such techniques include flow injection analysis[26], capillary electrophoresis combined with microelectrospray-tandem mass spectrometry[44] and hydrophilic interaction chromatography coupled with tandem-mass spectrometry[32]. Another approach is to use electrochemistry at the interface between two immiscible electrolyte solutions[45]. Using this approach, Beni *et al.*[45] showed that the determination of DA could not be evaluated in the presence of Ach as the transfer peaks occurred at the same potential and as a consequence the signals overlapped.

6.3.5 Glycine (Gly)

Gly, Figure 6.26, is a non-essential amino acid that serves as an inhibitory neurotransmitter in the central nervous system[46]. It is an essential intermediate in the metabolism of purines and porphyrins[47]. Structurally, Gly is the smallest of the amino acids, but like all other amino acids, it is capable of fouling the electrode surface[28]. It is also less polar than Asp and Glu. Furthermore, Gly will coexist with DA within the central nervous system. For these reasons, Gly may interfere with the detection of DA at the PPy-modified electrode if the sensor were to be applied to an in-vivo environment.
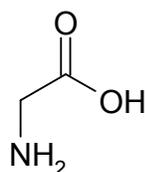
Figure 6.26: Structure of Gly

It was observed using cyclic voltammetry that Gly was not oxidised at a bare Pt electrode and no oxidation was observed for Gly at the PPy-SCD modified electrode. Figure 6.27 shows that when Gly and DA are simultaneously mixed in the same solution, only the DA peak is detected at the PPy-SCD electrode. The cyclic voltammogram recorded is identical to that of DA alone, indicating that the performance of the sensor is not affected by the presence of Gly.

Depending on the pH of the experiment Gly will either be cationic, zwitterionic or anionic. The three forms are shown in Scheme 6.5 and it can be seen that Gly will exist in the zwitterionic form at the pH of the experiment (pH = 5.8). As discussed earlier with UA, Gly is not detected because the negatively charged groups on Gly probably maintain it at a sufficient distance from the interface. This will prevent the possible interaction of the amine group on Gly with the negatively charged sulfonated groups. Although Gly is less polar than Glu and Asp, it is still not sufficiently hydrophobic and so the formation of an inclusion complex between Gly and the sulfonated β-cyclodextrin is very unlikely. In addition, no electrode fouling from Gly was evident, with the DA peak currents in the presence of Gly following the same trend as the currents of pure DA, as a function of cycle number.
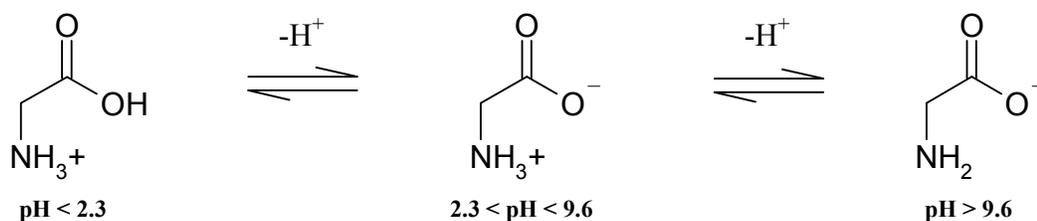
Scheme 6.5: The cationic, zwitterionic and anionic forms of Gly[29].
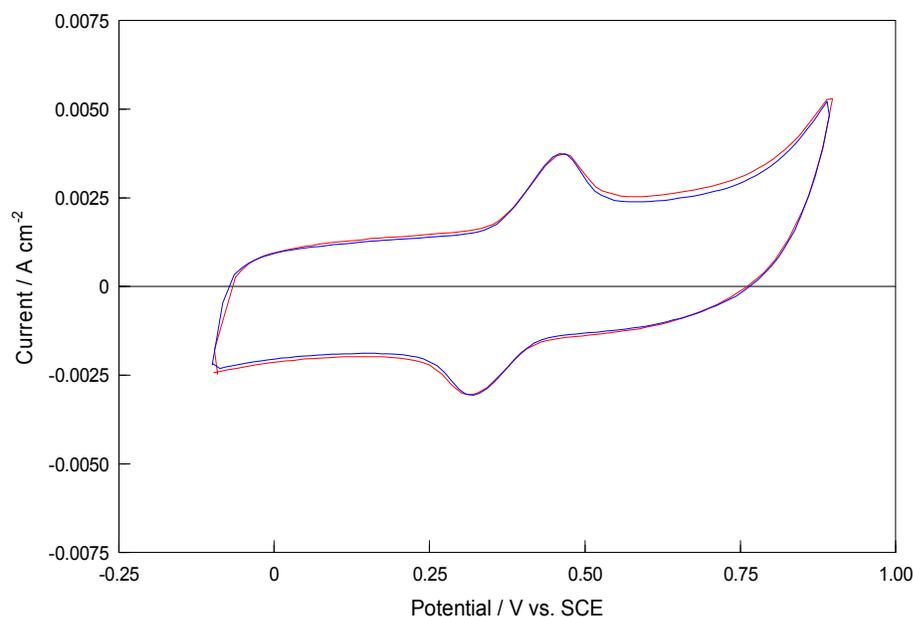
Figure 6.27: Cyclic voltammograms of the PPy-SCD modified electrode in a ▬ 1.0×10^{-3} mol dm^{-3} DA / 0.10 mol dm^{-3} Na$_2$SO$_4$ solution (pH~6.0) and in a ▬ 1.0×10^{-3} mol dm^{-3} DA / 1.0×10^{-3} mol dm^{-3} Gly / 0.10 mol dm^{-3} Na$_2$SO$_4$ solution (pH~5.8). Scan rate = 100 mV s^{-1}.

The DA peak currents observed when a fixed concentration of Gly (1.0×10^{-3} mol dm^{-3}) was mixed with varying concentrations of DA (7.0×10^{-5} - 1.0×10^{-3} mol dm^{-3}) were measured and are plotted as a function of the DA concentration in Figure 6.28. Good reproducibility between the experiments was obtained, as highlighted by the height of the error bars, which range from 0.03 to 1.45% of the mean value with *n* = 2. The low errors clearly show that nearly identical PPy-SCD films can be synthesised in each experiment. As evident from the plot, a calibration curve, which is very similar to those presented earlier in Figures 6.5, 6.12 and 6.18 is obtained.

The influence of Gly on the DA oxidation peak currents is summarised in Figure 6.29, where the magnitude of the peak currents obtained with pure DA are compared to the values measured when 1.0×10^{-3} mol dm^{-3} Gly solution is present. It can be seen that the DA signal is not affected by the presence of Gly.
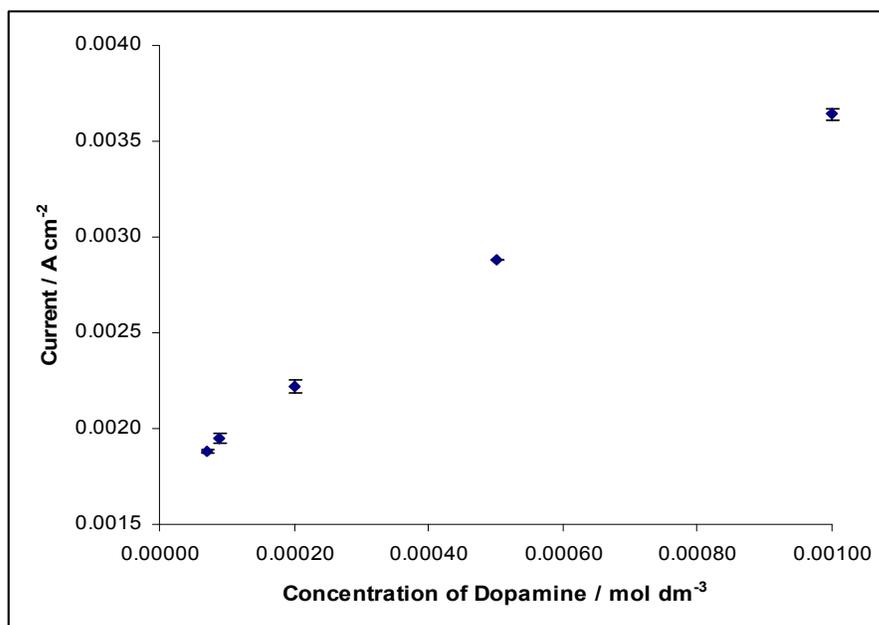
Figure 6.28: Calibration plot of the mean peak oxidation current of DA as a function of the concentration of DA where 1.0 x 10^{-3} mol dm^{-3} Gly was added to each DA solution in a 0.10 mol dm^{-3} Na$_2$SO$_4$, pH~5.8, supporting electrolyte (*n*=2).
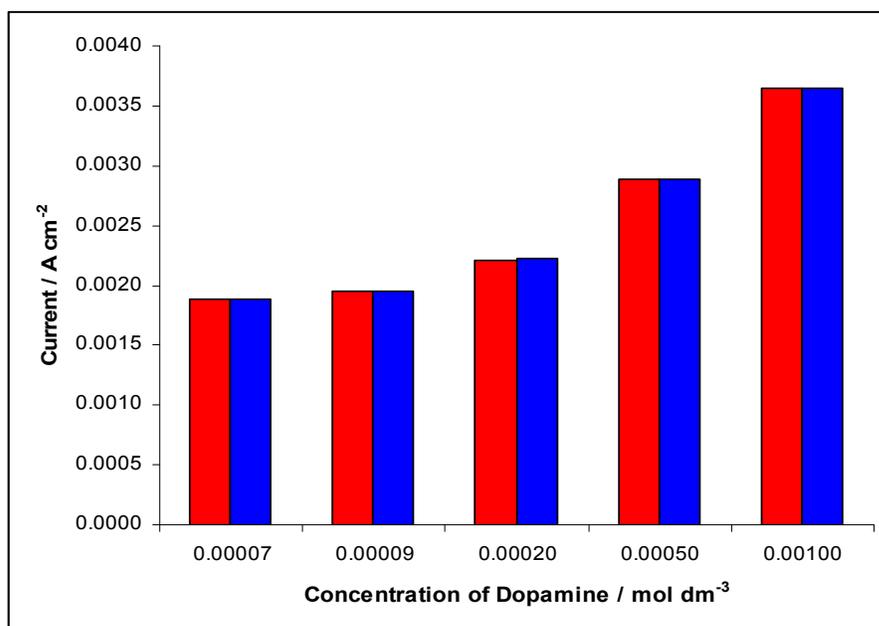

Figure 6.29: Peak oxidation currents, from the cyclic voltammograms, of DA as a function of the concentration of DA in the ■ presence (*n*=2) and ■ absence (*n*=4) of 1.0 x 10^{-3} mol dm^{-3} Gly in a 0.10 mol dm^{-3} Na$_2$SO$_4$, pH~5.8, supporting electrolyte.

The mean potentials were then compared to the potentials observed for pure DA oxidation and this is illustrated in Figure 6.30. It can be seen that the presence of Gly does not interfere with the potential of the DA oxidation signal.

The effect of lowering the pH of the Gly solution was also investigated. A 1.0×10^{-3} mol dm^{-3} Gly solution was lowered to a pH of 1.9. At this pH, Gly will exist predominately as a cation, as evident from Scheme 6.5. Consequently, there may be increased competition between the cationic DA and the predominately cationic Gly at the PPy-SCD modified electrode. Therefore, at a pH of 1.9, Gly may pose as a larger interferent threat than at a pH of 5.8. The electroactivity of Gly (pH~1.9) at a bare Pt electrode and a PPy-SCD modified electrode was investigated by cycling both electrodes in a 1.0×10^{-3} mol dm^{-3} solution of Gly, in an acidified sulfate supporting electrolyte. The voltammograms recorded are shown in Figure 6.31. It can be seen that while Gly is oxidised at a bare Pt electrode, giving a low oxidation currents at potentials higher than 0.550 V vs. SCE, under these acidic conditions, no oxidation is observed for Gly at the PPy-SCD modified electrode.
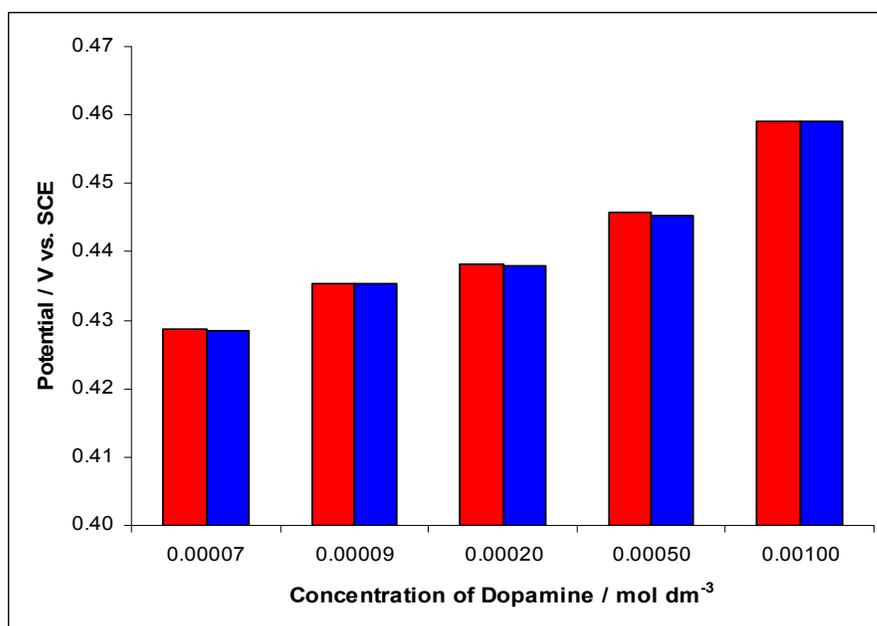

Figure 6.30: Peak potentials of DA oxidation for a range of DA concentrations (7.0×10^{-5} - 1.0×10^{-3} mol dm^{-3}) obtained using cyclic voltammetry, in the ■ presence (*n*=2) and ■ absence (*n*=4) of 1.0×10^{-3} mol dm^{-3} Gly in a 0.10 mol dm^{-3} Na$_2$SO$_4$, pH~5.8, supporting electrolyte.
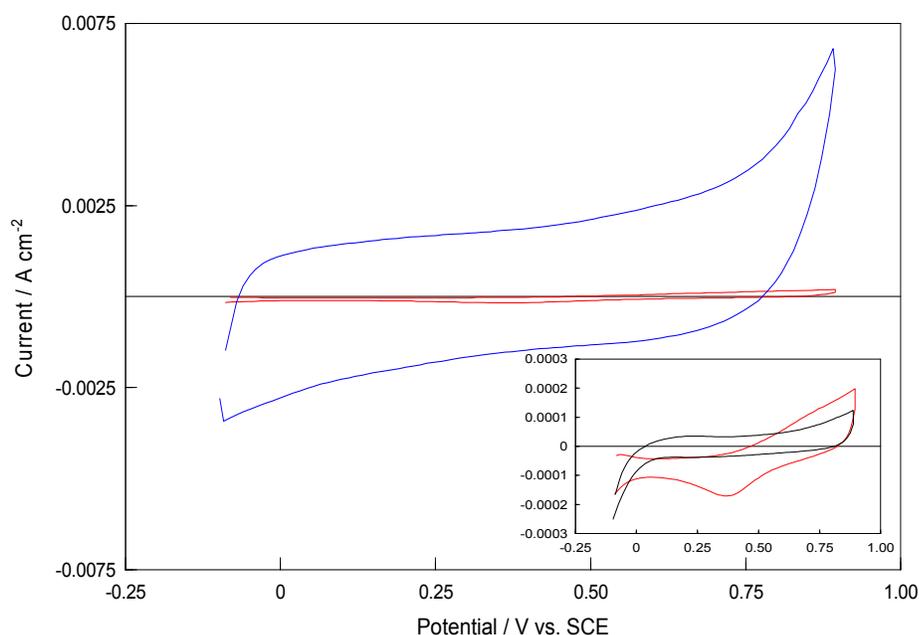
Figure 6.31: Cyclic voltammograms of a ▬ **bare Pt electrode and a** ▬ **PPy-SCD modified electrode in a 1.0 x 10^{-3} mol dm^{-3} Gly / 0.10 mol dm^{-3} Na$_2$SO$_4$ solution (pH~1.9). Scan rate = 100 mV s^{-1}. Inset: Cyclic voltammograms of the bare Pt electrode in a** ▬ **0.10 mol dm^{-3} Na$_2$SO$_4$ solution and in a** ▬ **1.0 x 10^{-3} mol dm^{-3} Gly / 0.10 mol dm^{-3} Na$_2$SO$_4$ solution. Scan rate = 100 mV s^{-1}. Axes are identical to Figure 6.31.**

When Gly and DA were simultaneously mixed in the same solution and the pH of the solution was adjusted to 1.9, only the DA peak was detected at the PPy-SCD electrode. Cyclic voltammograms similar to those shown in Figure 6.27 were obtained, except for the fact that the DA redox reaction was more reversible, under the acidic conditions. The peak currents and peak potentials for the oxidation of DA from mixed acidic solutions of Gly and DA, where the concentration ratios of Gly to DA varied from 1.0 (1.0 x 10^{-3} mol dm^{-3} DA and 1.0 x 10^{-3} mol dm^{-3} Gly) to 14.3 (7.0 x 10^{-5} mol dm^{-3} DA and 1.0 x 10^{-3} mol dm^{-3} Gly), were measured as a function of the concentration of DA. The influence of Gly on the DA oxidation peak currents and peak potentials is highlighted in Figures 6.32 and 6.33, respectively. The magnitude of the peak oxidation currents and the corresponding peak potentials obtained with pure DA (pH~1.9) are identical to the values measured when 1.0 x 10^{-3} mol dm^{-3} Gly solution (pH~1.9) is present. This clearly shows that the cationic Gly is not an interferent in the electrochemical sensing of DA. Clearly, the cationic Gly does not compete with the protonated DA during the oxidation of DA at the PPy-SCD electrode.
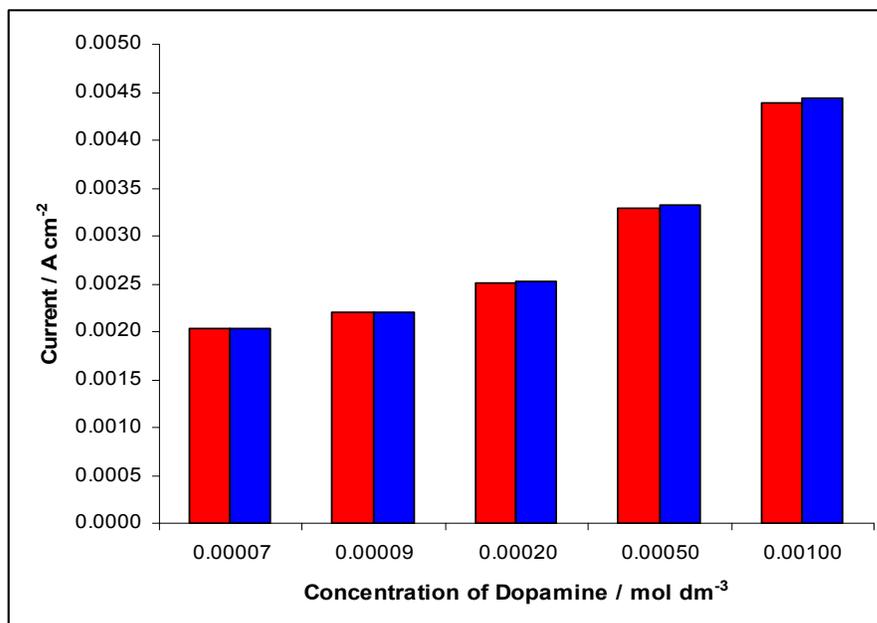
Figure 6.32: Peak oxidation currents, from the cyclic voltammograms, of DA as a function of the concentration of DA in the ■ presence (*n*=2) and ■ absence (*n*=2) of 1.0 x 10^{-3} mol dm^{-3} Gly in a 0.10 mol dm^{-3} Na$_2$SO$_4$, pH~1.9, supporting electrolyte.
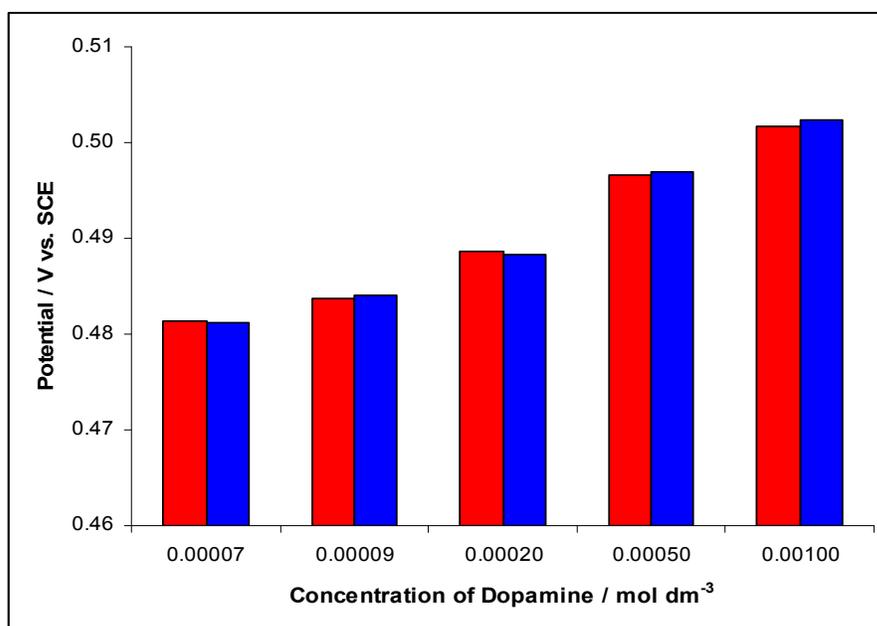
Figure 6.33: Peak potentials of DA oxidation for a range of DA concentrations (7.0 x 10^{-5} - 1.0 x 10^{-3} mol dm^{-3}) obtained using cyclic voltammetry, in the ■ presence (*n*=2) and ■ absence (*n*=2) of 1.0 x 10^{-3} mol dm^{-3} Gly in a 0.10 mol dm^{-3} Na$_2$SO$_4$, pH~1.9, supporting electrolyte.

In summary, the PPy-SCD electrode eliminates the interference of Gly, regardless of whether it is cationic or in the zwitterion form, in the electrochemical detection of DA and offers advantages over the existing methodologies. To date, the approaches reported in the literature have all been based on techniques that are not suitable for real-time, in-vivo detection. One such approach reported is that by McKenzie *et al.*[48], where the authors used automated capillary liquid chromatography to simultaneously determine DA and Gly. There appears to be no reports in the literature on the use of modified electrodes for the selective detection of DA in the presence of Gly, or indeed for the simultaneous detection of DA and Gly.

To conclude, the PPy-SCD modified electrode eliminates any interference from Gly and so could be used as a possible in-vivo DA sensor.

6.3.6 Histamine (HA)

HA, Figure 6.34, is an important neurotransmitter in the peripheral tissues and the central nervous system[49]. It is believed to be involved in the regulation of arousal state, locomotor activity, cardiovascular control, water intake, food intake and memory function[50]. Since HA coexists with DA, HA could interfere with the detection of DA at the PPy-modified electrode. Therefore, HA was investigated in order to determine its effect, if any, on the performance of the PPy-SCD modified electrode in the electrochemical sensing of DA.
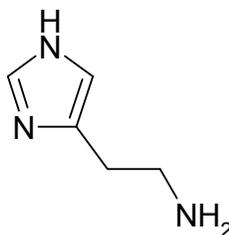
Figure 6.34: Structure of HA

The pH of 1.0×10^{-3} mol dm^{-3} HA is 10.0. This caused the DA to oxidise in solution immediately when the mixed solutions were prepared and as a result lower currents were observed at the PPy-SCD modified electrode in comparison to pure DA. Consequently, the pH of the HA solution was adjusted to 4.5. Typical cyclic voltammograms for a 1.0×10^{-3} mol dm^{-3} solution of HA (pH~4.5), in 0.10 mol dm^{-3} Na$_2$SO$_4$, at a bare Pt electrode and a PPy-SCD modified electrode are shown in Figure 6.35(a). The HA is oxidised at a bare Pt electrode but no electrochemical redox activity was observed for HA at the PPy-SCD modified electrode. According to Scheme 6.6, HA exists as a positively charged species at a pH of 4.5. Therefore, some interference might be expected from the HA. In Figure 6.35(b) it can be seen that the cyclic voltammogram of a mixed solution of HA and DA (pH~4.5) is the same as the cyclic voltammogram of pure DA (pH~6.0). This suggests that HA does not interfere with the DA signal. As no interference is exhibited from HA, this implies that no host guest complex forms between HA and the sulfonated β-cyclodextrin
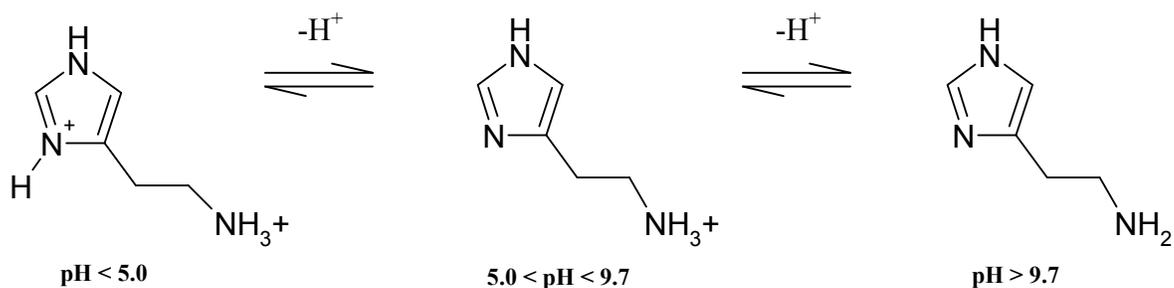
Scheme 6.6: The equilibrium of HA[29].
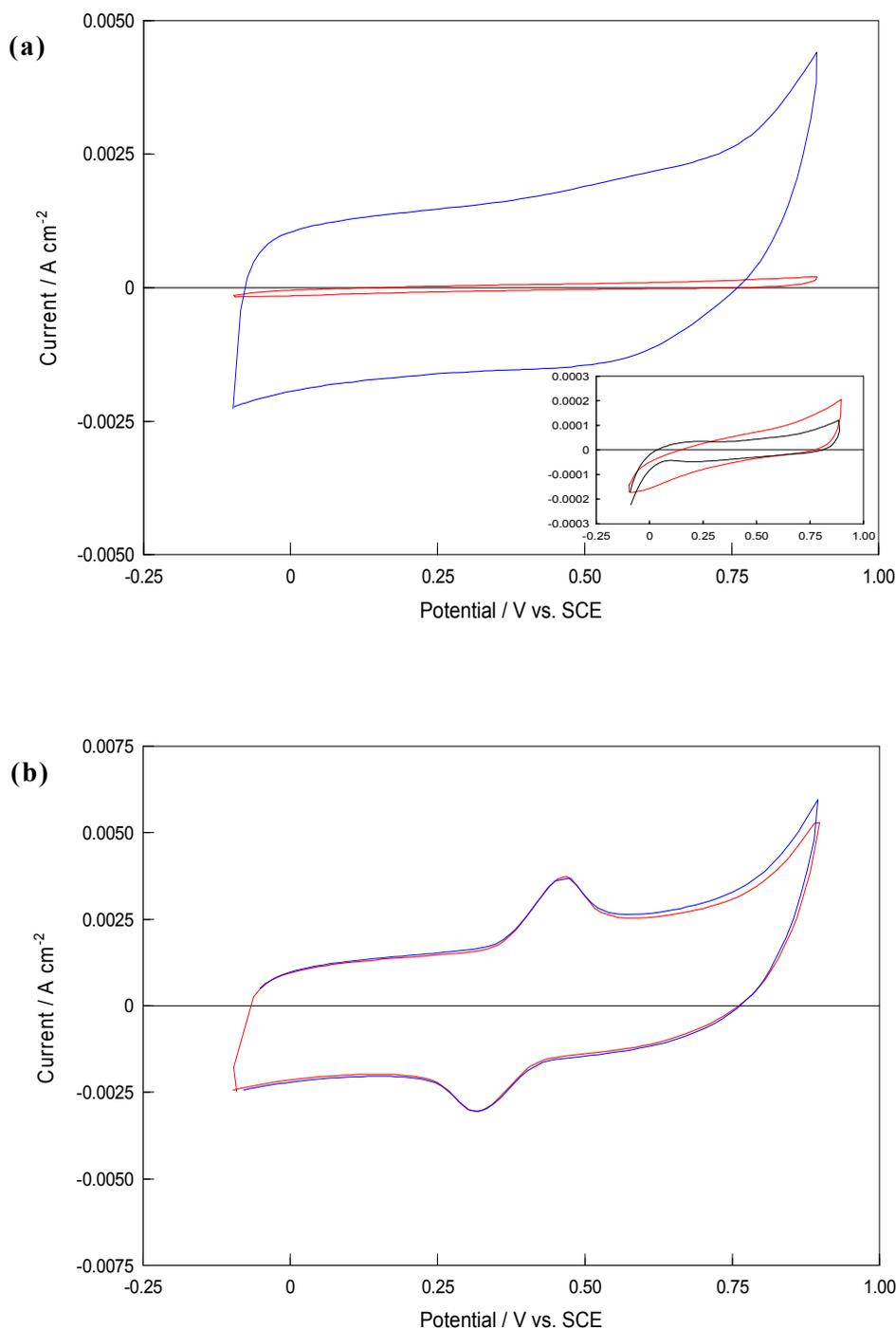
Figure 6.35: (a) Cyclic voltammograms of a ▬ **bare Pt electrode and a** ▬ **PPy-SCD modified electrode in a 1.0 x 10⁻³ mol dm⁻³ HA / 0.10 mol dm⁻³ Na₂SO₄ solution (pH~4.5). Scan rate = 100 mV s⁻¹. Inset: Cyclic voltammograms of the bare Pt electrode in a** ▬ **0.10 mol dm⁻³ Na₂SO₄ solution and in a** ▬ **1.0 x 10⁻³ mol dm⁻³ HA / 0.10 mol dm⁻³ Na₂SO₄ solution. Scan rate = 100 mV s⁻¹. Axes are identical to Figure 6.35(a). (b) Cyclic voltammograms of the PPy-SCD modified electrode in a** ▬ **1.0 x 10⁻³ mol dm⁻³ DA / 0.10 mol dm⁻³ Na₂SO₄ solution (pH~6.0) and in a** ▬ **1.0 x 10⁻³ mol dm⁻³ DA / 1.0 x 10⁻³ mol dm⁻³ HA / 0.10 mol dm⁻³ Na₂SO₄ solution (pH~4.5). Scan rate = 100 mV s⁻¹.**

The cyclic voltammetric oxidation current outputs, recorded for various concentrations of DA in the presence of HA, were recorded. In these experiments the pH of the solution was adjusted to 4.5. From these data, the mean peak current, the standard deviation and the standard errors were calculated. These mean peak currents for DA oxidation in the presence of 1.0×10^{-3} mol dm^{-3} HA, were plotted as a function of the concentration of DA and this plot is shown in Figure 6.36. The standard errors calculated, ranging from 0.03 to 0.33%, reflect the excellent reproducibility of the PPy-SCD films. The influence of HA on the DA oxidation peak currents is further highlighted in the histogram in Figure 6.37. As shown, a 1.0×10^{-3} mol dm^{-3} concentration of HA has no effect on the DA oxidation currents at the PPy-SCD modified electrode, even at low DA concentrations.

The peak oxidation potentials, obtained from the aforementioned solution mixture were compared with the peak potentials of DA without HA, and are plotted in Figure 6.38, which clearly shows that HA does not interfere with the potential of the DA oxidation signal.
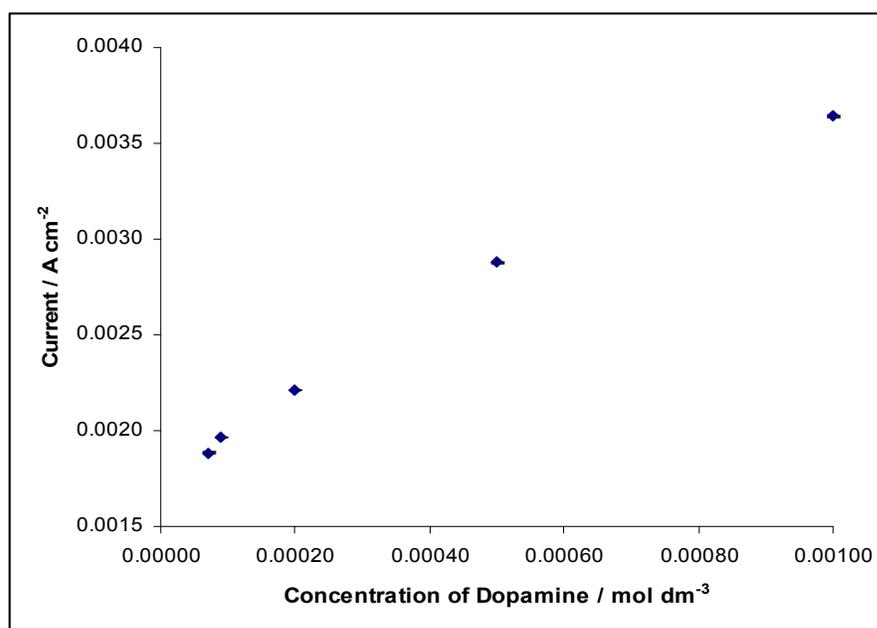
Figure 6.36: Calibration plot of the mean peak current of DA as a function of the concentration of DA where 1.0×10^{-3} mol dm^{-3} HA was added to each DA solution in a 0.10 mol dm^{-3} Na$_2$SO$_4$, pH~4.5, supporting electrolyte (n=3).
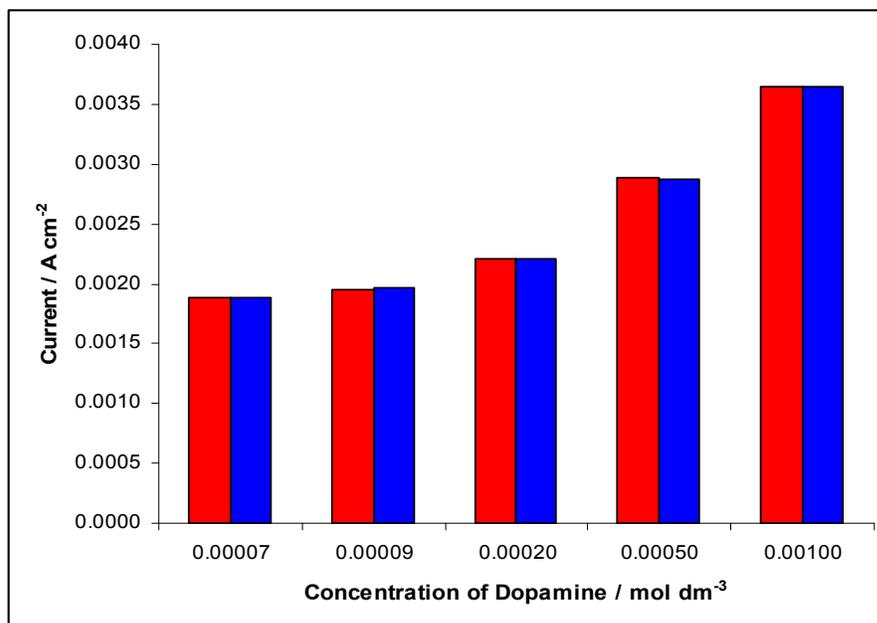
Figure 6.37: Peak oxidation currents, from the cyclic voltammograms, of DA as a function of the concentration of DA in the ■ presence (*n*=3) and ■ absence (*n*=4) of 1.0 x 10^{-3} mol dm^{-3} HA in a 0.10 mol dm^{-3} Na$_2$SO$_4$, pH~4.5, supporting electrolyte.
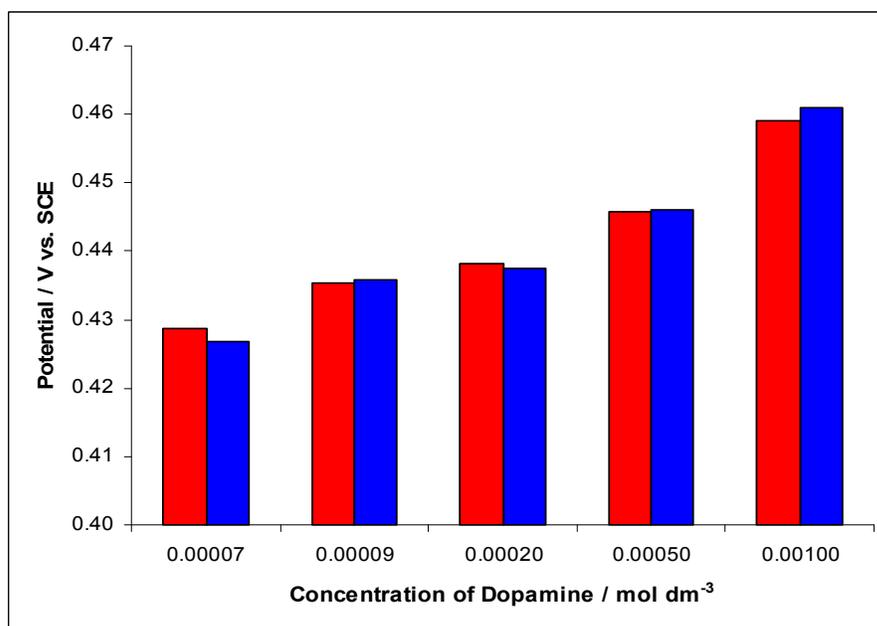
Figure 6.38: Peak potentials of DA oxidation for a range of DA concentrations (7.0 x 10^{-5} - 1.0 x 10^{-3} mol dm^{-3}) obtained using cyclic voltammetry, in the ■ presence (*n*=3) and ■ absence (*n*=4) of 1.0 x 10^{-3} mol dm^{-3} HA in a 0.10 mol dm^{-3} Na$_2$SO$_4$, pH~4.5, supporting electrolyte.

The results presented and discussed in this section show that the PPy-SCD modified electrode eliminates the interference of 1.0×10^{-3} mol dm^{-3} HA.

Most of the existing materials and techniques employed for the analysis of DA in the presence of HA are largely based on chromatography measurements[51] and while they are successful in detecting DA, these approaches can never be used for real-time in-vivo sensing. There are no reports, to the best of our knowledge, on the selective detection of DA in the presence of HA, or for the simultaneous detection of DA and HA, at a modified electrode that can be used as an in-vivo sensor for real-time analysis.

In summary, the PPy-SCD modified electrode can eliminate the interference of HA in the electrochemical detection of DA.

6.3.7 Acetaminophen (Paracetamol, ACOP)

ACOP, Figure 6.39, is a common analgesic anti-pyretic agent and can be used as an alternative drug for those who are sensitive to aspirin[52]. It is a phenolic compound and it is well known that these compounds can foul solid state electrodes[53]. In addition, ACOP is electrochemically active[54]. These issues make ACOP a possible interferent that could complicate the selective measurement of DA in biological samples.
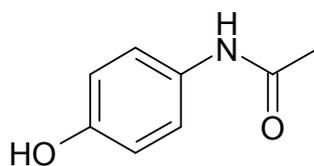
Figure 6.39: Structure of ACOP

The electroactivity of ACOP at a bare Pt electrode was investigated in the sulfate supporting electrolyte by cycling the Pt electrode in a 1.0×10^{-3} mol dm^{-3} solution of

ACOP. Representative cyclic voltammograms are shown in the inset in Figures 6.40(a). It can be seen that ACOP is oxidised at the bare Pt electrode giving an oxidation wave at approximately 0.680 V vs. SCE. The electroactivity of ACOP was also inspected at the PPy-SCD modified electrode, as shown in Figure 6.40(a), where again a small oxidation peak is evident at 0.640 V vs. SCE. Although, the oxidation current of ACOP is relatively low at the Pt electrode, the oxidation of ACOP can be observed clearly at the PPy-SCD electrode.

The PPy-SCD sensor performance to the detection of DA was then examined in the presence of a fixed concentration of ACOP. It can be seen in Figure 6.40(b) that the oxidation of ACOP and the oxidation of DA and the subsequent reduction of the DOQ can all be detected. Nevertheless, the oxidation peaks are well resolved and the oxidation peak of DA is not affected by the presence of ACOP. This means that the simultaneous determination of DA can still be achieved in the presence of 1.0×10^{-3} mol dm^{-3} ACOP.

ACOP will exist predominantly as a neutral species (pKa = 9.56) at the pH of the experiment (pH = 6.0) and for that reason, ACOP should not be attracted by the anionic sulfonated groups on the β-cyclodextrin. As already discussed in Chapter 5, the mechanism of sensing is a mixture of oxidation at the polymer film and complexation with the sulfonated β-cyclodextrin, which is incorporated within the polyprrrole matrix, as a dopant. Therefore, ACOP must be oxidised by one or both of these processes.

In order to explore the possibility that ACOP is independently oxidised by the polypyrrole matrix, the sulfonated β-cyclodextrin dopant was replaced with SDS, as detailed in Section 5.3.4. This SDS-doped polypyrrole film was cycled in a solution of 1.0×10^{-3} mol dm^{-3} ACOP in a supporting Na_2SO_4 electrolyte. The resultant voltammogram is presented in Figure 6.41, while a direct comparison between the electrochemical behaviour and oxidation of ACOP at the PPy-SCD and PPy-SDS electrodes is shown in the inset in Figure 6.41.
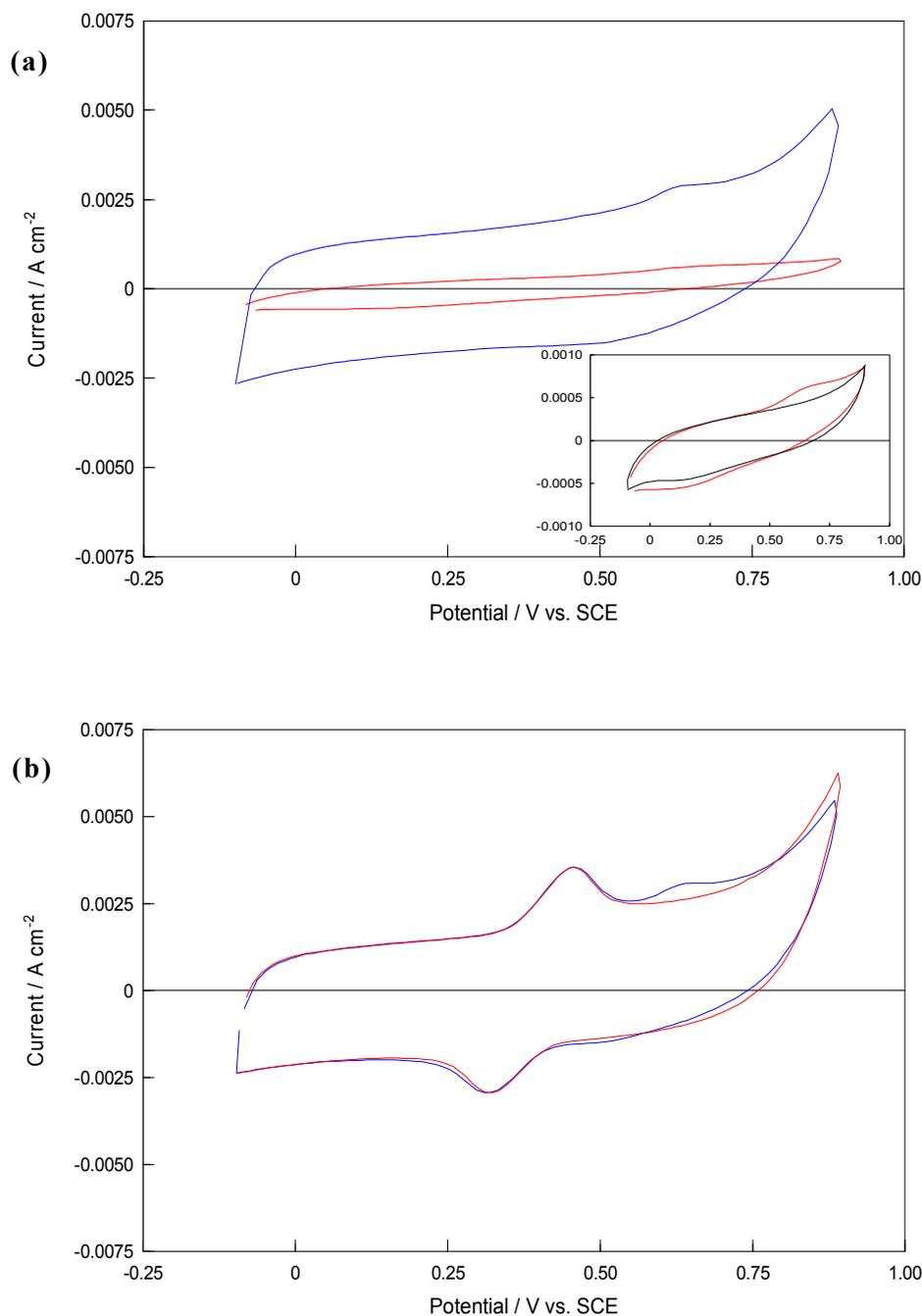
Figure 6.40: **(a) Cyclic voltammograms of a — bare Pt electrode and a — PPy-SCD modified electrode in a 1.0 x 10^{-3} mol dm^{-3} ACOP / 0.10 mol dm^{-3} Na$_2$SO$_4$ solution (pH~6.0). Scan rate = 100 mV s^{-1}. Inset: Cyclic voltammograms of the bare Pt electrode in a — 0.10 mol dm^{-3} Na$_2$SO$_4$ solution and in a — 1.0 x 10^{-3} mol dm^{-3} ACOP / 0.10 mol dm^{-3} Na$_2$SO$_4$ solution. Scan rate = 100 mV s^{-1}. Axes are identical to Figure 6.40(a). (b) Cyclic voltammograms of the PPy-SCD modified electrode in a — 1.0 x 10^{-3} mol dm^{-3} DA / 0.10 mol dm^{-3} Na$_2$SO$_4$ solution (pH~6.0) and in a — 1.0 x 10^{-3} mol dm^{-3} DA / 1.0 x 10^{-3} mol dm^{-3} ACOP / 0.10 mol dm^{-3} Na$_2$SO$_4$ solution (pH~6.0). Scan rate = 100 mV s^{-1}.**
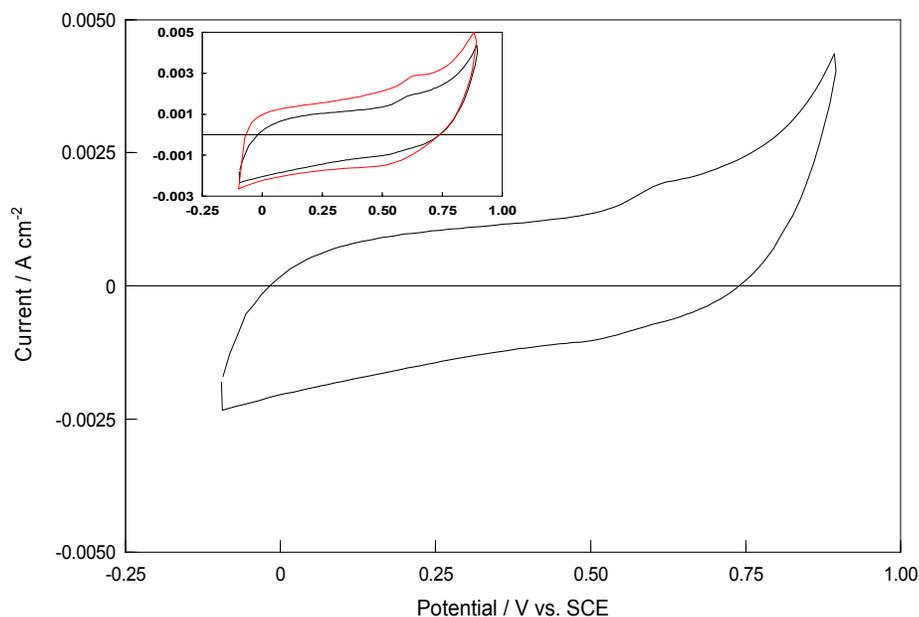
Figure 6.41: Cyclic voltammogram of a PPy-SDS modified electrode in a 1.0 x 10^{-3} mol dm^{-3} ACOP / 0.10 mol dm^{-3} Na$_2$SO$_4$ solution (pH~6.0). Scan rate = 100 mV s^{-1}. Inset: Cyclic voltammograms of a ▬ PPy-SDS modifed electrode and a ▬ PPy-SCD modified electrode in a 1.0 x 10^{-3} mol dm^{-3} ACOP / 0.10 mol dm^{-3} Na$_2$SO$_4$ solution (pH~6.0). Scan rate = 100 mV s^{-1}. Axes are identical to Figure 6.41.

From Figure 6.41 it can be seen that the polypyrrole film (PPy-SDS) can oxidise the ACOP, giving an oxidation wave at around 0.61 V(SCE). This occurs at a slighter lower potential than the oxidation of ACOP at the PPy-SCD modified electrode. In addition, ACOP is oxidised at the PPy-SDS polymer film to the lesser degree than at the PPy-SCD modified electrode. The oxidation current observed for 1.0 x 10^{-3} mol dm^{-3} ACOP at the PPy-SCD modified electrode is approximately 0.0029 A cm^{-2}, whereas the oxidation current observed for the same concentration of ACOP at the PPy-SDS modified electrode is roughly 0.0019 A cm^{-2}. Consequently, the ACOP oxidation signal is enhanced at the PPy-SCD modified electrode and this must be connected to the presence of the cyclodextrin.

Next, a set of experiments was performed in an attempt to establish whether or not the ACOP forms an inclusion complex with the sulfonated β-cyclodextrin. This involved a study on the cyclic voltammetry of ACOP at a bare GC electrode in the presence and absence of a large excess of the sulfonated β-cyclodextrin. A citrate phosphate buffer, pH

6.0, was used as the supporting electrolyte. At this pH, the ACOP will exist as a neutral species in solution. Typical voltammograms are presented in Figure 6.42. A clear oxidation wave for the ACOP can be seen, with a peak potential at approximately 0.520 V vs. SCE. On addition of a large excess of the sulfonated β-cyclodextrin to the electrolyte solution, it is seen that there is a small decrease in the peak oxidation current and a small shift in the peak current to more positive potentials. This indicates weak complexation between the ACOP and the sulfonated β-cyclodextrin.

In particular, the extent of complexation between ACOP and the sulfonated β-cyclodextrin is considerably weaker than that observed in Chapter 5 between the DA and the sulfonated β-cyclodextrin. This is probably due to the fact that ACOP is neutral and so will not be electrostatically attracted to the anionic sulfonated β-cyclodextrin. This will result in the formation of a weaker inclusion complex than the one formed between the protonated DA and the anionic sulfonated β-cyclodextrin.
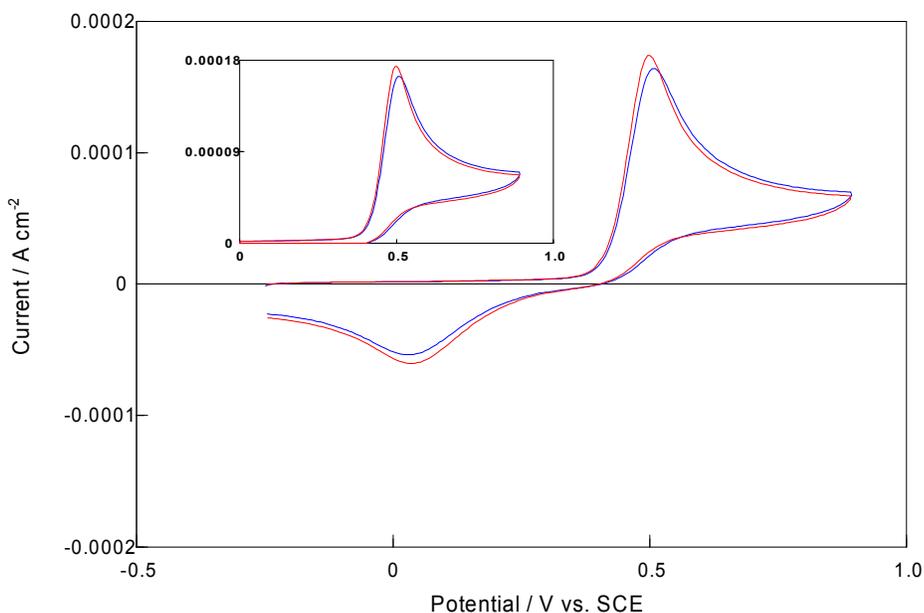
Figure 6.42: Cyclic voltammograms of a bare GC electrode in a ▬ 5.0 x 10^{-4} mol dm^{-3} ACOP / 0.30 mol dm^{-3} citrate phosphate buffer solution (pH~6.0) and in a ▬ 5.0 x 10^{-4} mol dm^{-3} ACOP / 0.01 mol dm^{-3} sulfonated β-cyclodextrin / 0.30 mol dm^{-3} citrate phosphate buffer solution (pH~6.0). Scan rate = 50 mV s^{-1}. Electrochemical window: -0.250 to 0.900 V vs. SCE. Inset: Magnification of the oxidation region. Axes are identical to Figure 6.42.

The DA peak currents observed when a fixed concentration of ACOP (1.0×10^{-3} mol dm^{-3}) was added to varying concentrations of DA were evaluated. A total of three separate measurements were carried out for each mixture and the average values were computed. Good agreement between the three replicate experiments was obtained. This can be seen clearly from the data plotted in Figure 6.43, where the peak oxidation currents of DA, with error bars which range between 0.25 to 2.98%, are plotted as a function of the DA concentration with a fixed 1.0×10^{-3} mol dm^{-3} solution of ACOP, to give the characteristic calibration curve.

A more direct comparison between the oxidation peak currents and peak potentials of DA, with and without ACOP, is provided in Figures 6.44 and 6.45. These plots clearly show that ACOP is exerting no influence on the oxidation signal of DA.
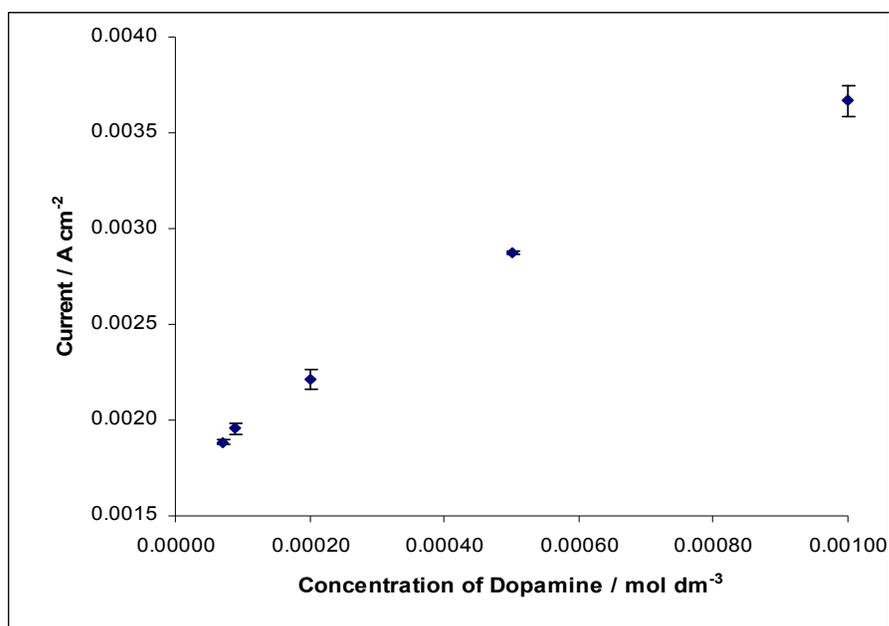
Figure 6.43: Calibration plot of the mean peak oxidation currents of DA as a function of the concentration of DA where 1.0×10^{-3} mol dm^{-3} ACOP was added to each DA solution in a 0.10 mol dm^{-3} Na$_2$SO$_4$, pH~6.0, supporting electrolyte ($n=3$).
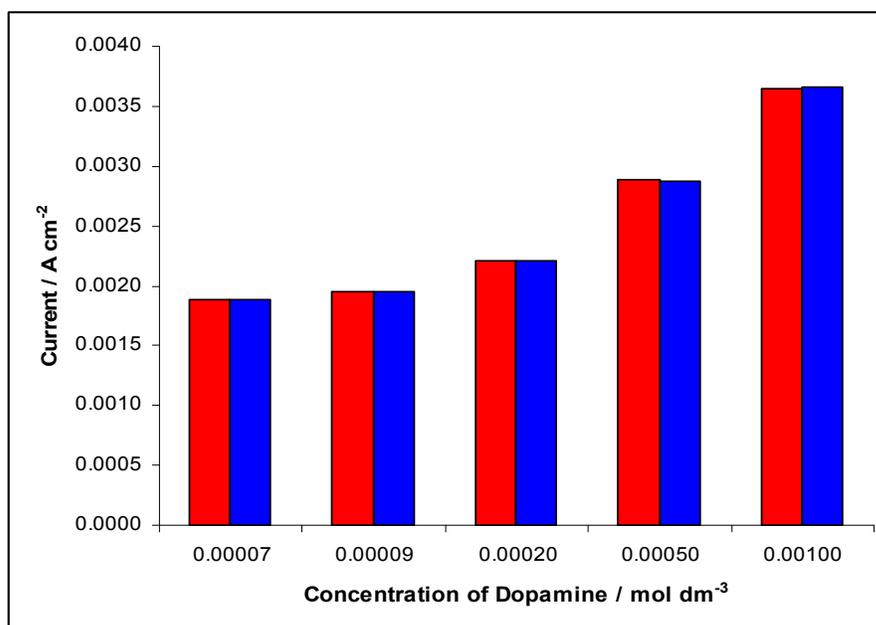
Figure 6.44: Peak currents, from the cyclic voltammograms, of DA as a function of the concentration of DA in the ■ presence (*n*=3) and ■ absence (*n*=4) of 1.0 x 10^{-3} mol dm^{-3} ACOP in a 0.10 mol dm^{-3} Na$_2$SO$_4$, pH~6.0, supporting electrolyte.
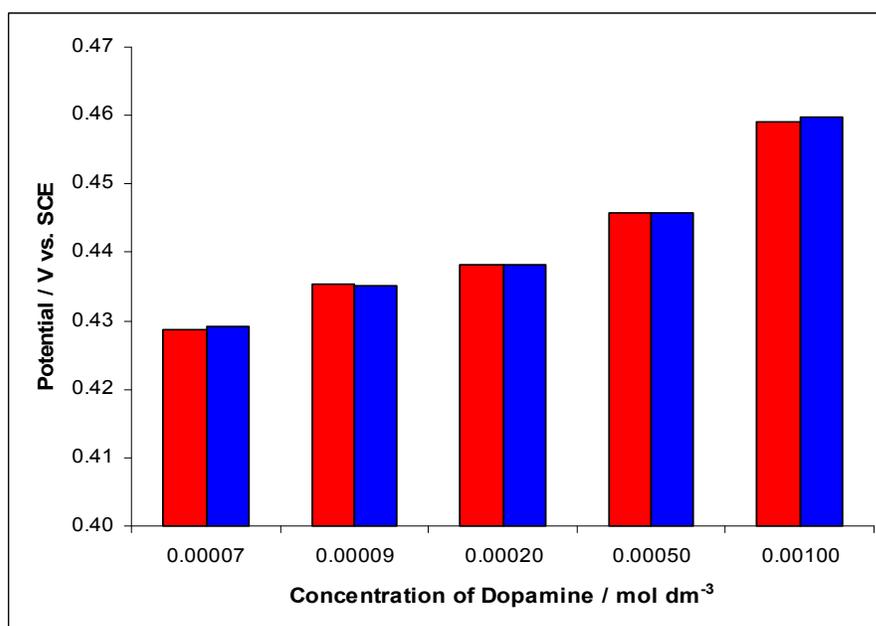

Figure 6.45: Peak oxidation potentials of DA oxidation for a range of DA concentrations (7.0 x 10^{-5} - 1.0 x 10^{-3} mol dm^{-3}) obtained using cyclic voltammetry, in the ■ presence (*n*=3) and ■ absence (*n*=4) of 1.0 x 10^{-3} mol dm^{-3} ACOP in a 0.10 mol dm^{-3} Na$_2$SO$_4$, pH~6.0, supporting electrolyte.

The results presented in this section show that while 1.0×10^{-3} mol dm^{-3} ACOP is detected at the PPy-SCD modified electrode, it does not interfere with the electrochemical determination of DA. The oxidation peaks of DA and ACOP are well resolved with ACOP having no effect on the DA signal.

Other modified electrodes capable of separating the anodic peaks of ACOP and DA are those developed by Wang et al.[55] and Kumar et al.[56]. Wang et al.[55] used a GC electrode modified with carbon-coated nickel magnetic nanoparticles to separate the anodic peaks of a mixed solution of DA (1.0×10^{-4} mol dm^{-3}) and ACOP (1.0×10^{-3} mol dm^{-3}). Kumar et al.[56] were also able to resolve the oxidation waves of ACOP (2.0×10^{-5} mol dm^{-3}) and DA ($0 - 2.0 \times 10^{-5}$ mol dm^{-3}) using a GC electrode modified with nano-TiO$_2$ particles and poly(acid yellow 9). Modified electrodes have also been developed by Li and Jing[57] and Jia et al.[58] for the selective detection of ACOP, where DA has been investigated as a possible interferent. The electrodes developed were able to eliminate the interference of DA up to a 10-fold and 50-fold excess over the concentration of ACOP.

Other materials and techniques have been employed for the determination of DA and ACOP in samples. However, these can not be used for real-time, in-vivo sensing. One technique reported in the literature that attempts to eliminate the interference of ACOP in the determination of DA is that reported by Milczarek and Ciszewski[59]. The authors used electropolymerised films derived from guaiacol and its derivatives in conjunction with flow-injection analysis to try and eliminate the interference of ACOP.

In summary, ACOP does not interfere in the electrochemical detection of DA at the PPy-SCD modified electrode and therefore, the modified electrode has potential in the design of an *in-vivo* DA sensor.

6.3.8 5-Hydroxytryptamine (Serotonin, 5-HT) and 5-Hydroxyindole Acetic Acid (5HIAA)

5-HT, Figure 6.46, is a monoamine neurotransmitter in the central nervous system and plays a significant role in various pharmacological, physical and biological processes[60]. It can be protonated in aqueous solution, as illustrated in Scheme 6.7. It is a major interfering compound in the selective detection of DA. This is because 5-HT and DA coexist in biological systems and it has been shown that they influence each other in their respective activities[61]. In addition, 5-HT is electroactive and the voltammetric responses of DA and 5-HT at bare electrodes overlap[62]. 5-HIAA, Figure 6.47, is an important product of 5-HT breakdown[63]. Likewise, 5-HIAA is electroactive, oxidising in the same potential region as DA[4]. For these reasons, 5-HT and 5-HIAA were investigated to see if they had any effect on the performance of the PPy-SCD modified electrode in the electrochemical sensing of DA.
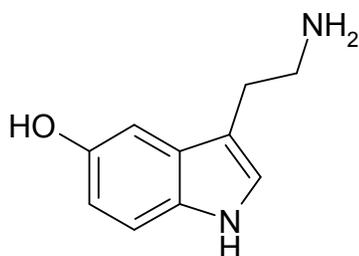

**Figure 6.46: Structure of 5-HT**   **Figure 6.47: Structure of 5HIAA**
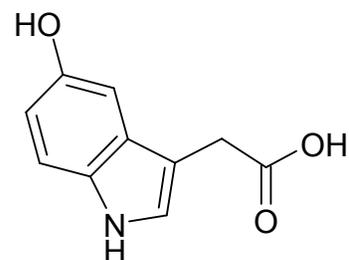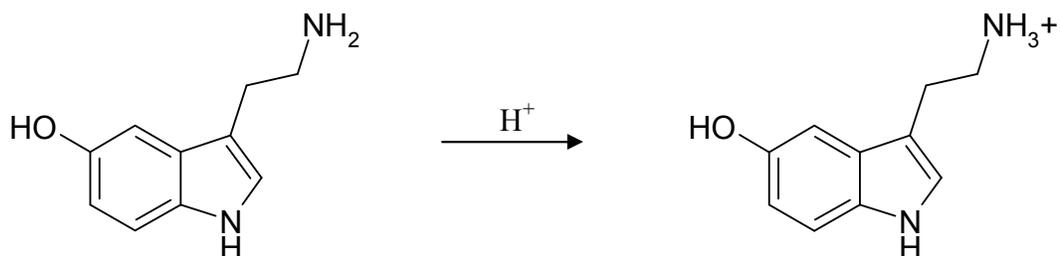

Scheme 6.7: Protonation of 5-HT.

The cyclic voltammograms of a bare Pt electrode and a PPy-SCD modified electrode cycled in a 1.0 x 10^{-3} mol dm^{-3} 5-HT solution are shown in Figure 6.48(a), while the corresponding data recorded in a 1.0 x 10^{-3} mol dm^{-3} 5-HIAA solution are compared in Figures 6.48(b). It can be seen that 5-HT is oxidised at the bare Pt electrode giving a broad oxidation wave centred at 0.600 V vs. SCE. Three oxidation peaks are observed for 5-HT at the PPy-SCD modified electrode, at approximately 0.100 V vs. SCE, 0.330 V vs. SCE and 0.590 V vs. SCE. However, these oxidation signals are weak.

As shown in Figure 6.48(b), 5-HIAA is also easily oxidised at the bare Pt electrode showing a broad oxidation wave and a corresponding reduction wave at lower potentials. No obvious oxidation seems to be observed for 5-HIAA at the PPy-SCD modified electrode. However, if the oxidation region of 5-HIAA at the PPy-SCD modified electrode is magnified, three broad peaks can be distinguished at around 0.110 V vs. SCE, 0.340 V vs. SCE and 0.540 V vs. SCE, which are quite similar to that observed with 5-HT.
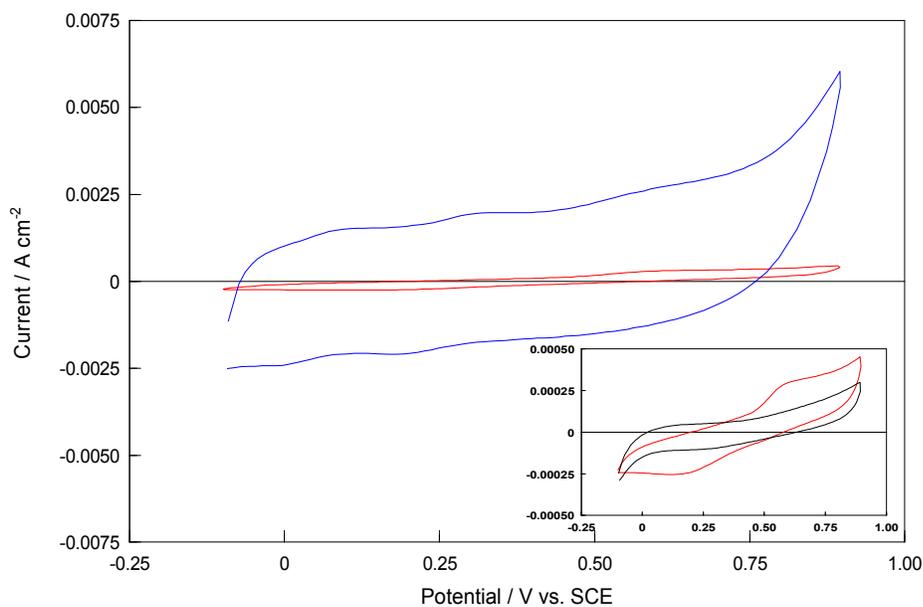

Figure 6.48(a): Cyclic voltammograms of a — bare Pt electrode and a — PPy-SCD modified electrode in a 1.0 x 10^{-3} mol dm^{-3} 5-HT / 0.10 mol dm^{-3} Na$_2$SO$_4$ solution (pH~4.5). Scan rate = 100 mV s^{-1}. Inset: Cyclic voltammograms of the bare Pt electrode in a — 0.10 mol dm^{-3} Na$_2$SO$_4$ solution and in a — 1.0 x 10^{-3} mol dm^{-3} 5-HT / 0.10 mol dm^{-3} Na$_2$SO$_4$ solution. Scan rate = 100 mV s^{-1}. Axes are identical to Figure 6.48(a).
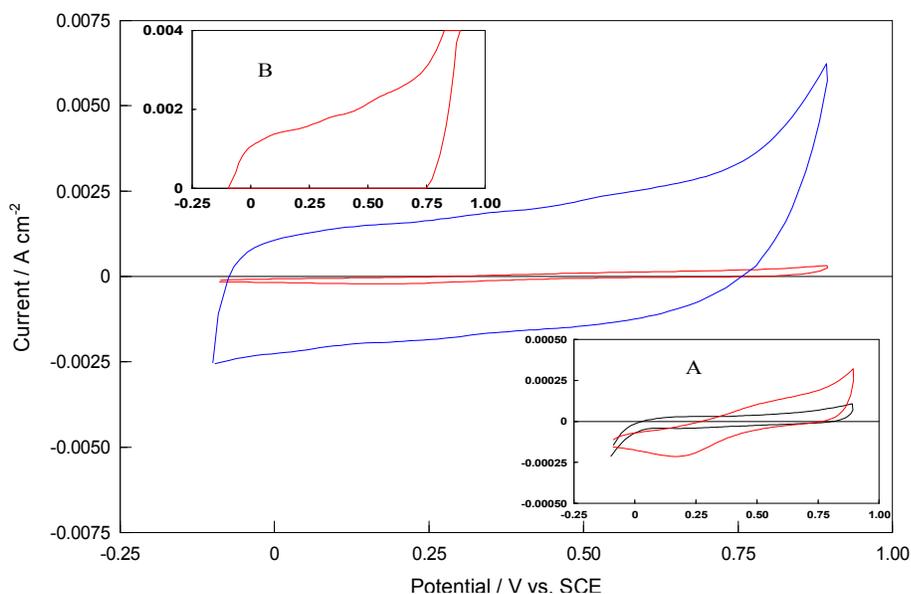
Figure 6.48(b): Cyclic voltammograms of a — bare Pt electrode and a — PPy-SCD modified electrode in a 1.0 x 10^{-3} mol dm^{-3} 5-HIAA / 0.10 mol dm^{-3} Na$_2$SO$_4$ solution (pH~4.1). Scan rate = 100 mV s^{-1}. Inset(A): Cyclic voltammograms of the bare Pt electrode in a — 0.10 mol dm^{-3} Na$_2$SO$_4$ solution and in a — 1.0 x 10^{-3} mol dm^{-3} 5-HIAA / 0.10 mol dm^{-3} Na$_2$SO$_4$ solution. Scan rate = 100 mV s^{-1}. Axes are identical to Figure 6.48(b). Inset(B): Magnification of the oxidation region of the cyclic voltammogram of a — PPy-SCD modified electrode in a 1.0 x 10^{-3} mol dm^{-3} 5-HIAA / 0.10 mol dm^{-3} Na$_2$SO$_4$ solution (pH~4.1). Axes are identical to Figure 6.48(b).

In order to explore the origin of this detection for both the 5-HT and the 5-HIAA, the electrochemical behaviour of the two compounds at the SDS-doped polypyrrole film was firstly investigated. In Figure 6.49(a), the electrochemical behaviour of 5-HT and 5-HIAA are compared at the PPy-SDS film, where cyclic voltammograms recorded in a 1.0 x 10^{-3} mol dm^{-3} 5-HT solution, or in a 1.0 x 10^{-3} mol dm^{-3} 5-HIAA solution, are shown. Similar data are presented, for comparative purposes, at the PPy-SCD polymer film in Figure 6.49(b).

For, the PPy-SDS system, the pH was maintained in the vicinity of 4.1 to 4.5 and a 0.10 mol dm^{-3} Na$_2$SO$_4$ supporting electrolyte was used. Although it is somewhat difficult to conclude from Figure 6.49(a) and (b), due to the magnitude of the oxidation peaks, the 5-HT is oxidised at the PPy-SDS modified electrode at approximately 0.340 V vs. SCE and 0.540 V vs. SCE, giving two oxidation waves. The oxidation currents at the PPy-SDS modified electrode are somewhat lower that the oxidation currents measured at the PPy-

SCD modified electrode, Figure 6.49(b). Furthermore, the electrochemistry of 5-HT at the PPy-SCD film resulted in three oxidation peaks. This indicates that the sulfonated β cyclodextrin plays some role in the electrochemical behaviour of 5-HT.

5-HT will exist predominantly as a cation (pK_b = 9.97)[64] at the pH of the experiment (pH = 4.50), therefore, the cation may be attracted to the electrode surface, particularly when the anionic sulfonated β cyclodextrin is used as a dopant. The electrochemical behaviour of 5-HT at a GC electrode was studied in the absence and presence of an excess of sulfonated β cyclodextrin in an attempt to establish if the cationic 5-HT molecule has the ability to form an inclusion complex with the anionic sulfonated β cyclodextrin. As evident from Figure 6.50, it is clear that 5-HT can indeed form a host-guest complex with the sulfonated-β-cyclodextrin. An excess of the sulfonated-β-cyclodextrin gives rise to a decrease in the peak oxidation currents and, more importantly, to an anodic shift of the peak oxidation potential. This is indicative of complexation and has previously been explained in detail in Chapter 5.
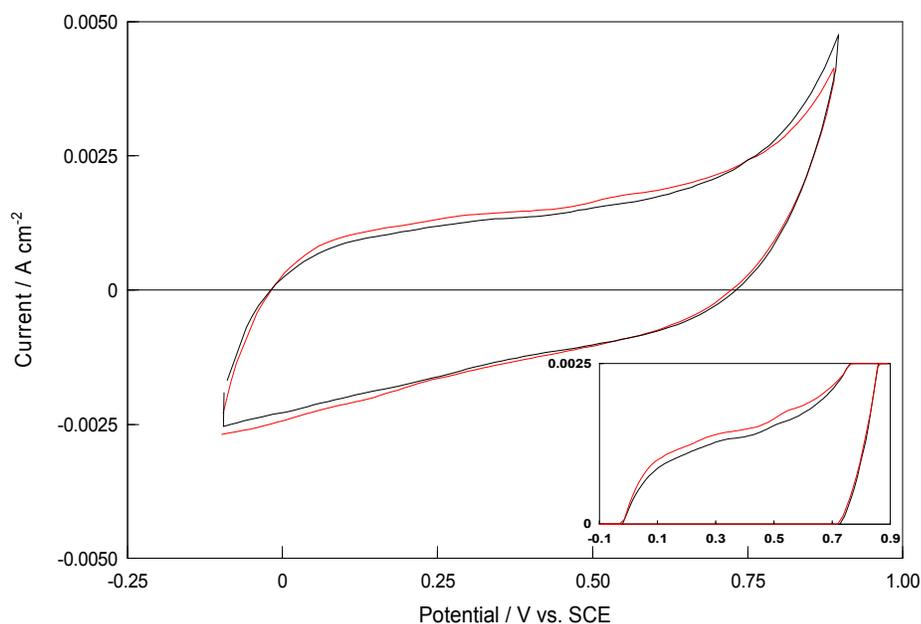
Figure 6.49(a): Cyclic voltammogram of a PPy-SDS modified electrode in a ▬ 1.0 x 10^{-3} mol dm^{-3} 5-HIAA / 0.10 mol dm^{-3} Na$_2$SO$_4$ solution (pH~4.1) and in a ▬ 1.0 x 10^{-3} mol dm^{-3} 5-HT / 0.10 mol dm^{-3} Na$_2$SO$_4$ solution (pH~4.5). Scan rate = 100 mV s^{-1}. Inset: Magnification of the oxidation regions. Axes are identical to Figure 6.49.
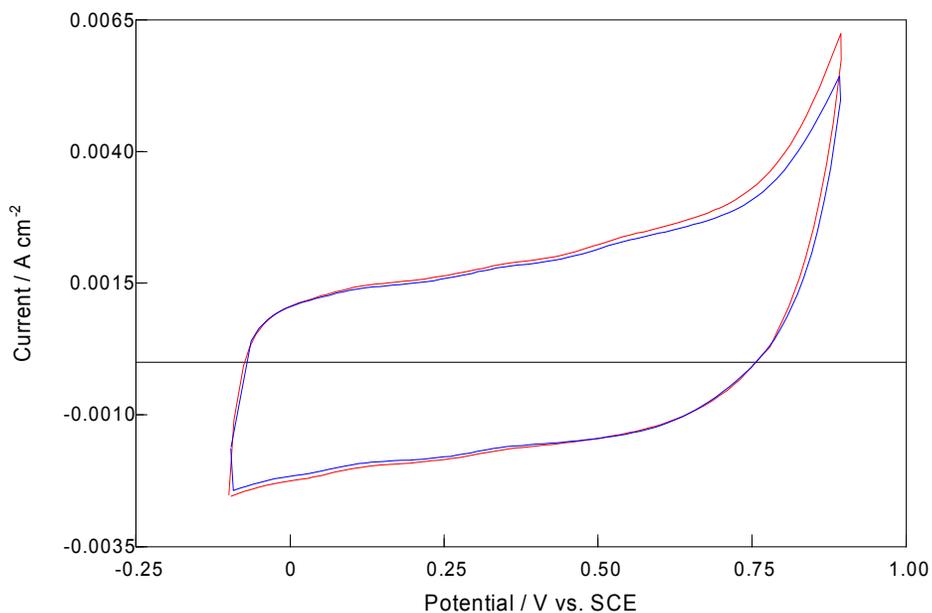
Figure 6.49(b): Cyclic voltammogram of a PPy-SCD modified electrode in a ▬ 1.0 x 10^{-3} mol dm^{-3} 5-HIAA / 0.10 mol dm^{-3} Na$_2$SO$_4$ solution (pH~4.1) and in a ▬ 1.0 x 10^{-3} mol dm^{-3} 5-HT / 0.10 mol dm^{-3} Na$_2$SO$_4$ solution (pH~6.1). Scan rate = 100 mV s^{-1}.
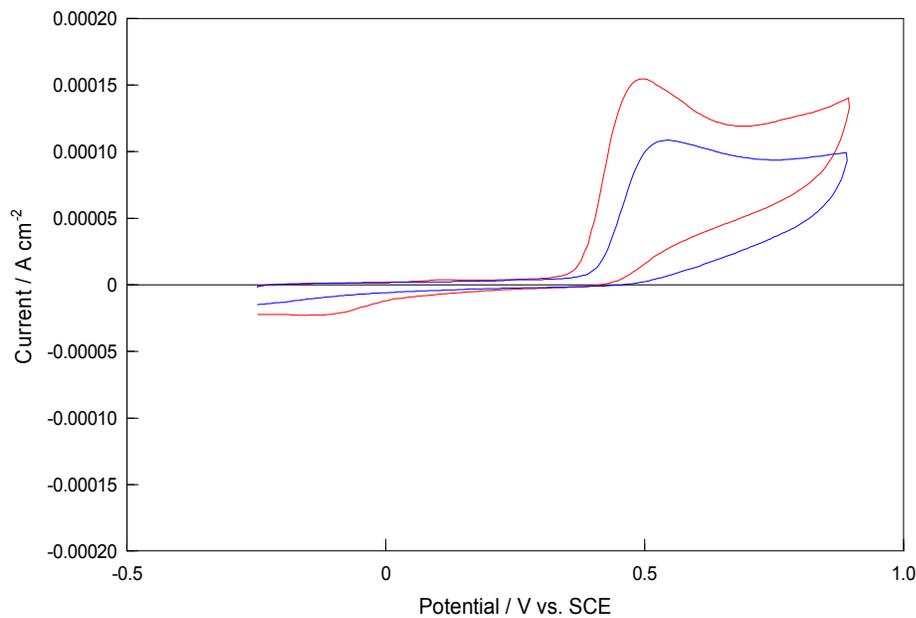

Figure 6.50: Cyclic voltammograms of a bare GC electrode in a ▬ 5.0 x 10^{-4} mol dm^{-3} 5-HT / 0.30 mol dm^{-3} citrate phosphate buffer solution (pH~4.5) and in a ▬ 5.0 x 10^{-4} mol dm^{-3} 5-HT / 0.01 mol dm^{-3} sulfonated β-cyclodextrin / 0.30 mol dm^{-3} citrate phosphate buffer solution (pH~4.5). Scan rate = 50 mV s^{-1}. Electrochemical window: -0.250 to 0.900 V vs. SCE.

It is also worth mentioning that the degree to which the 5-HT peak current decreases and the peak is shifted to more noble potentials is comparable to that of the cationic DA. This is highlighted in Table 6.4 and shows that a relatively strong inclusion complex is formed between 5-HT and the sulfonated β cyclodextrin. Based on the extent of the potential shift, it can be concluded that the DA forms a slightly stronger host-guest inclusion complex with the sulfonated β-cyclodextrin. Nevertheless, the relatively strong inclusion complex formed between 5-HT and the sulfonated β-cyclodextrin accounts for the detection of 5-HT at the PPy-SCD film.

Table 6.4: A comparison of the decrease and shift in the peak oxidation currents of 5.0 x 10^{-4} mol dm^{-3} DA and 5.0 x 10^{-4} 5-HT in the presence of 0.01 mol dm^{-3} sulfonated β-cyclodextrin in a 0.30 mol dm^{-3} citrate phosphate, pH~4.5 buffer solution.

$E_p^A{}_{DA+CD} - E_p^A{}_{DA}$ / V vs.SCE	$E_p^A{}_{5-HT+CD} - E_p^A{}_{5-HT}$ / V vs.SCE	$I_p^A{}_{DA} : I_p^A{}_{DA+CD}$	$I_p^A{}_{5-HT} : I_p^A{}_{5-HT+CD}$
0.059	0.055	1.52 : 1	1.45 : 1

The detection of 5-HIAA at the PPy-SCD modified electrode is slightly harder to explain. The pKa of 5-HIAA[65] is approximately 4.5, therefore it will exist as a mixture of negatively charged species and a neutral entity at the pH of the experiment (pH = 4.1). The dissociation of 5-HIAA is shown in Scheme 6.8. Approximately 30% of the 5-HIAA is negatively charged, at pH = 4.1 giving electrostatic repulsion between the anionic 5-HIAA and the anionic sulfonated β-cyclodextrin. In addition, the neutral 5-HIAA should not be attracted to the negatively charged macrocycle interface, and thus the formation of a host-guest complex between 5-HIAA and the sulfonated β-cyclodextrin is unlikely.
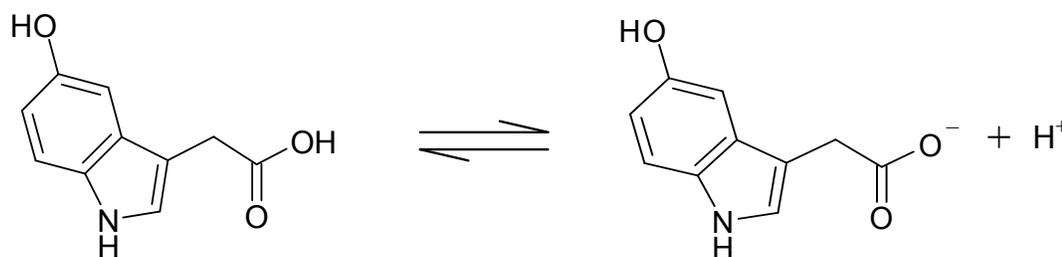
Scheme 6.8: Dissociation of 5-HIAA.

Similarly to 5-HT, 5-HIAA is oxidised at the SDS-doped polypyrrole film, as illustrated in Figure 6.49(a). Again, it is oxidised at this SDS-doped polypyrrole film to a lesser extent than at the PPy-SCD modified electrode. This shows that while the 5-HIAA is oxidised at the polypyrrole film, the rate of oxidation is enhanced when the polymer is doped with the anionic sulfonated β cyclodextrins.

On studying the complexation properties of 5-HIAA with the sulfonated β cyclodextrin, it was found, as shown in Figure 6.51(a), that a very weak inclusion complex is formed between the 5-HIAA and the sulfonated β-cyclodextrin. Although, there is a reasonable decrease in the oxidation current, there is only a small ennoblement of the peak oxidation potential. As with ACOP, it is noticeable that the complexation between 5-HIAA and the sulfonated β-cyclodextrin is considerably weaker than that observed with DA or 5-HT. In order to further investigate the extent of complexation between the anionic/neutral 5-HIAA and the anionic sulfonated β-cyclodextrin, the pH of the 5-HIAA solution was increased to 6.1. At this pH, about 98% of the 5-HIAA is negatively charged. Figure 6.51(b) shows that at this pH weak complexation still occurs. A comparison of the complexation between 5-HIAA and the sulfonated β-cyclodextrin at pH 4.1 and 6.1 is made in Table 6.5, where it can be seen that the strength of the inclusion complex formed at both pH values is similar. This indicates that the carboxylate anion on the 5-HIAA is maintained at a sufficient distance from the negatively charged sulfonated groups, preventing electrostatic repulsion.

The formation of a weak inclusion complex between the sulfonated β cyclodextrin and 5-HIAA can be attributed to the fact that 5-HIAA is not electrostatically attracted to the

negatively charged sulfonated groups on the β-cyclodextrin. However, there may be a kinetic component to the complexation and in order to investigate this phenomenon, the cyclic voltammetry data were recorded as a function of time. Cyclic voltammograms of the 5.0×10^{-4} mol dm^{-3} 5-HIAA, with excess sulfonated β-cyclodextrin, were recorded at various time intervals. Representative data are provided in Figure 6.52. Nearly identical voltammograms are recorded following 10, 60 and 100 min immersion time. This clearly shows that the host-guest complex is formed within the first 10 min and that there is a limited kinetic effect to the formation of the weak inclusion complex between 5-HIAA and the sulfonated β cyclodextrin.

When 5-HT and DA are simultaneously mixed in the same solution, three oxidation peaks are detected at the PPy-SCD electrode, as highlighted in Figure 6.53(a). The oxidation peaks observed for pure 5-HT at the PPy-SCD modified electrode at 0.100 V vs. SCE and 0.340 V vs. SCE are still visible, while the oxidation peak at 0.610 V vs. SCE is now suppressed. The oxidation peak at approximately 0.460 V vs. SCE corresponds to the oxidation of DA and it can be seen that the currents recorded for mixed solutions of 1.0×10^{-3} mol dm^{-3} DA and 1.0×10^{-3} mol dm^{-3} 5-HT are lower than that of 1.0×10^{-3} mol dm^{-3} DA alone. Figure 6.53(b) shows that when 5-HIAA and DA are simultaneously mixed in the same solution, only the DA peak is detected at the PPy-SCD electrode. Similarly to 5-HT, it can be seen that the currents recorded for mixed solutions of 1.0×10^{-3} mol dm^{-3} DA and 1.0×10^{-3} mol dm^{-3} 5-HIAA are lower than that of pure 1.0×10^{-3} mol dm^{-3} DA.

(a)

(b)
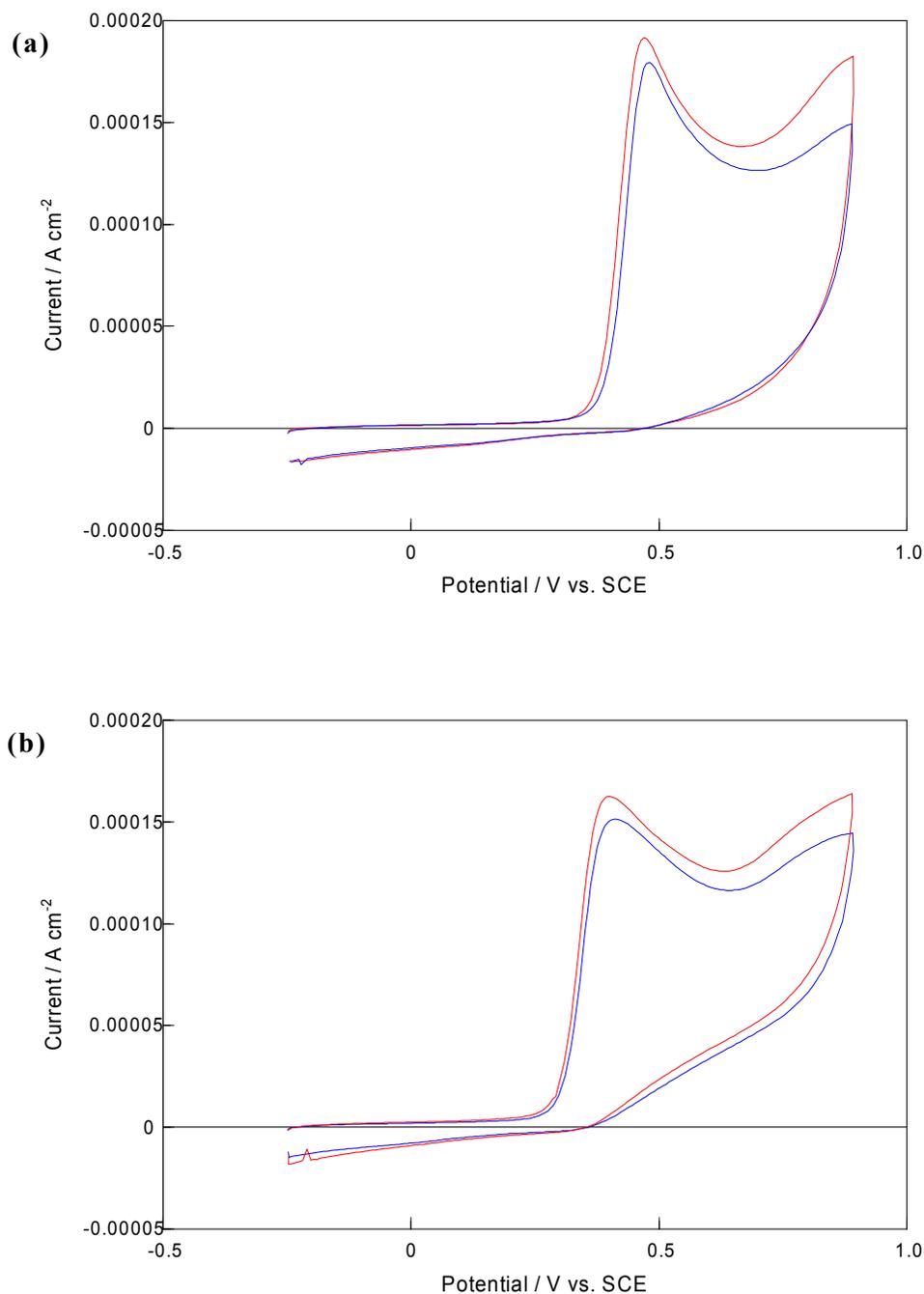
Figure 6.51: (a) Cyclic voltammograms of a bare GC electrode in a ▬ **5.0 x 10^{-4} mol dm^{-3} 5-HIAA / 0.30 mol dm^{-3} citrate phosphate buffer solution (pH ~4.1) and in a** ▬ **5.0 x 10^{-4} mol dm^{-3} 5-HIAA / 0.010 mol dm^{-3} sulfonated β-cyclodextrin / 0.30 mol dm^{-3} citrate phosphate buffer solution (pH ~4.1). Scan rate = 50 mV s^{-1}. Electrochemical window: -0.250 to 0.900 V vs. SCE. (b) Cyclic voltammograms of a bare GC electrode in a** ▬ **5.0 x 10^{-4} mol dm^{-3} 5-HIAA / 0.30 mol dm^{-3} citrate phosphate buffer solution (pH ~6.1) and in a** ▬ **5.0 x 10^{-4} mol dm^{-3} 5-HIAA / 0.010 mol dm^{-3} sulfonated β-cyclodextrin / 0.30 mol dm^{-3} citrate phosphate buffer solution (pH ~6.1). Electrochemical window: -0.250 to 0.900 V vs. SCE.**

Table 6.5: A Comparison of the decrease and shift in the peak currents of 5.0 x 10^{-4} mol dm^{-3} 5-HIAA in the presence of 0.01 mol dm^{-3} sulfonated β-cyclodextrin in a 0.30 mol dm^{-3} citrate phosphate solution at pH values of 4.1 and 6.1.

E_p^{A} 5-HIAA+CD (pH 4.1) $-$ E_p^{A} 5-HIAA (pH 4.1) / V vs.SCE	E_p^{A} 5-HIAA+CD (pH 6.1) $-$ E_p^{A} 5-HIAA (pH 6.1) / V vs.SCE	I_p^{A} 5-HIAA (pH 4.1) : I_p^{A} 5-HIAA+CD (pH 4.1)	I_p^{A} 5-HIAA (pH 6.1) : I_p^{A} 5-HIAA+CD (pH 6.1)
0.011	0.013	1.07 : 1	1.07 : 1
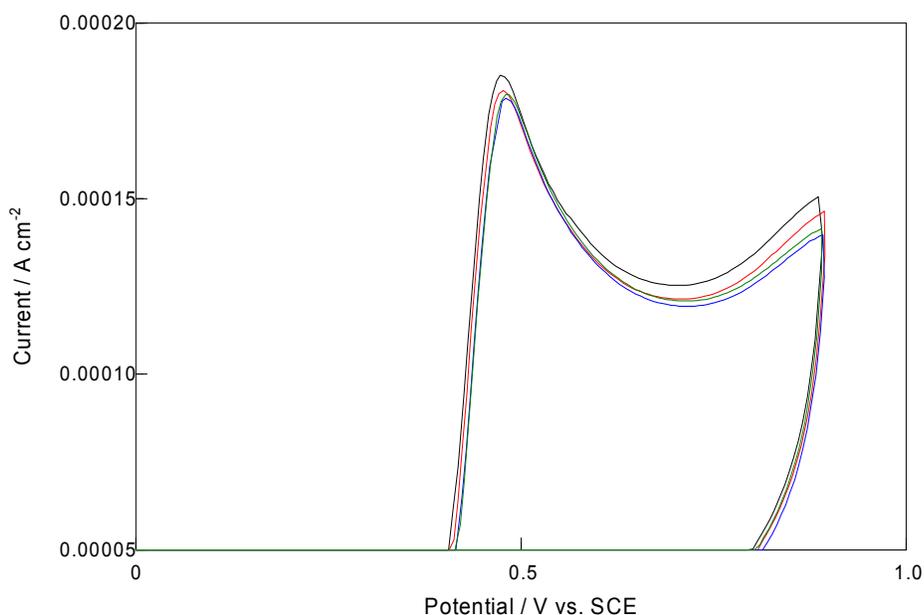
Figure 6.52: Cyclic voltammograms of a bare GC electrode in a 5.0 x 10^{-4} mol dm^{-3} 5-HIAA / 0.01 mol dm^{-3} sulfonated β-cyclodextrin / 0.30 mol dm^{-3} citrate phosphate buffer solution (pH~4.1) at — 0, — 10, — 60 and — 120 mins. Scan rate = 50 mV s^{-1}. Electrochemical window: -0.250 to 0.900 V vs. SCE.

The DA peak currents observed when a fixed concentration of 5-HT or 5-HIAA (1.0 x 10^{-3} mol dm^{-3}) was mixed with varying concentrations of DA (7.0 x 10^{-5} - 1.0 x 10^{-3} mol dm^{-3}) were measured and the mean peak currents and the standard errors, ranging from 0.19 to 2.77% of the mean value; n = 3 were computed. The mean peak current is plotted as a function of the DA concentration in the presence of either 5-HT or 5-HIAA in Figures 6.54(a) and (b), respectively.
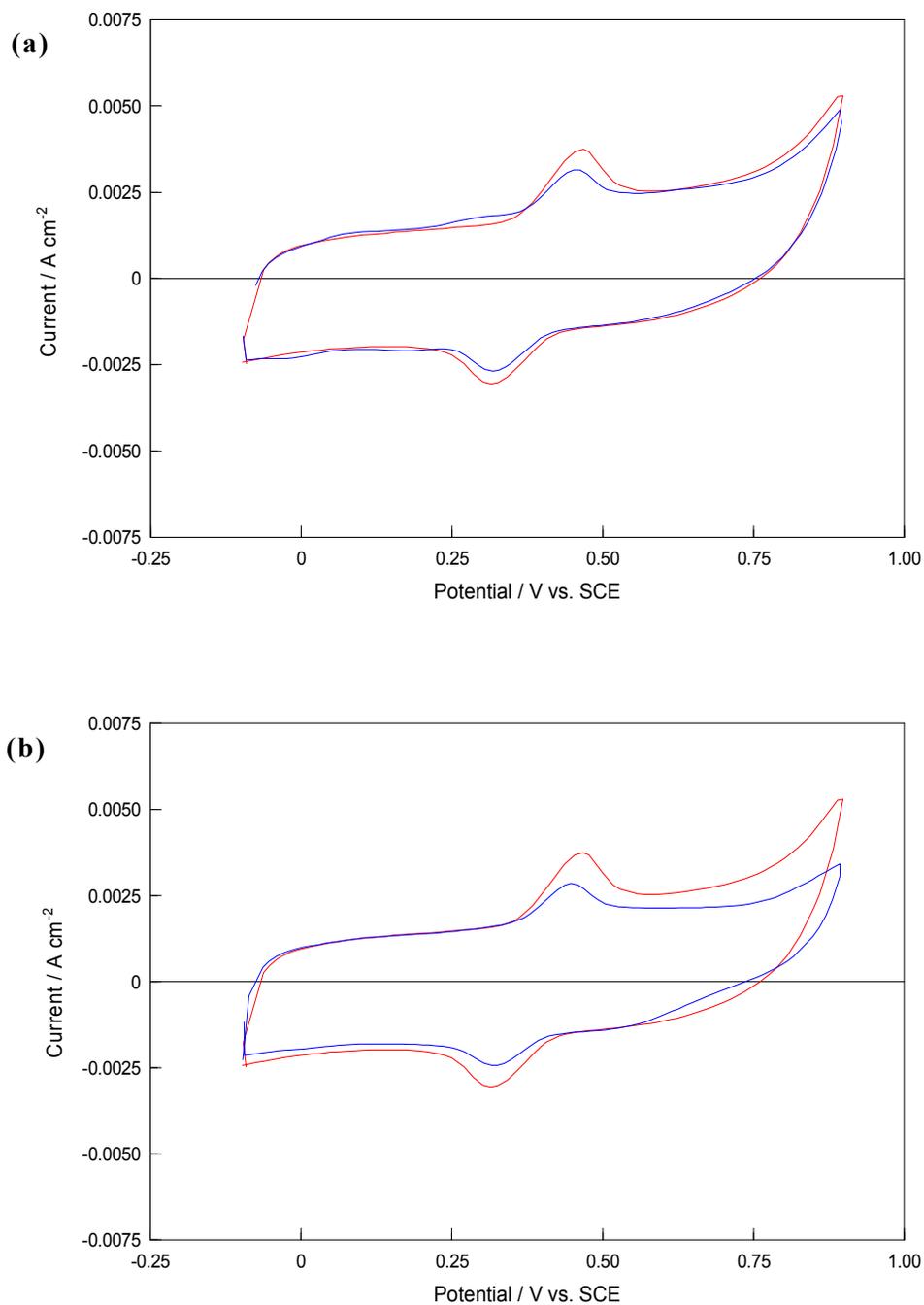
Figure 6.53: (a) Cyclic voltammograms of the PPy-SCD modified electrode in a ━ **1.0 x 10⁻³ mol dm⁻³ DA / 0.10 mol dm⁻³ Na₂SO₄ solution (pH~6.0) and in a** ━ **1.0 x 10⁻³ mol dm⁻³ DA / 1.0 x 10⁻³ mol dm⁻³ 5-HT / 0.10 mol dm⁻³ Na₂SO₄ solution (pH~4.5). Scan rate = 100 mV s⁻¹. (b) Cyclic voltammograms of the PPy-SCD modified electrode in a** ━ **1.0 x 10⁻³ mol dm⁻³ DA / 0.10 mol dm⁻³ Na₂SO₄ solution (pH~6.0) and in a** ━ **1.0 x 10⁻³ mol dm⁻³ DA / 1.0 x 10⁻³ mol dm⁻³ 5-HIAA / 0.10 mol dm⁻³ Na₂SO₄ solution (pH~4.1). Scan rate = 100 mV s⁻¹.**

(a)

(b)

**Figure 6.54: (a) Calibration plot of the mean peak current of DA as a function of the concentration of DA where 1.0 x 10^{-3} mol dm^{-3} 5-HT was added to each DA solution in a 0.10 mol dm^{-3} Na$_2$SO$_4$, pH~4.5, supporting electrolyte (*n*=3). (b) Calibration plot of the mean peak current of DA as a function of the concentration of DA where 1.0 x 10^{-3} mol dm^{-3} 5-HIAA was added to each DA solution in a 0.10 mol dm^{-3} Na$_2$SO$_4$, pH~4.1, supporting electrolyte (*n*=3).**

The influence of 5-HT and 5-HIAA on the DA oxidation peak currents is summarised in Figures 6.55(a) and (b), respectively, where the magnitude of the peak oxidation currents obtained with pure DA are compared to the values measured when 1.0×10^{-3} mol dm^{-3} 5-HT solution, or 1.0×10^{-3} mol dm^{-3} 5-HIAA solution, is present. It can be seen that for the lower concentrations of DA, the DA currents are not affected by the presence of 5-HT or 5-HIAA. However, in the presence of 1.0×10^{-3} mol dm^{-3} 5-HT or 1.0×10^{-3} mol dm^{-3} 5-HIAA, the DA peak currents for the higher concentrations of DA decrease in intensity, giving interference at the higher DA concentrations, but not with the lower concentrations.

This unusual behaviour may be connected to the rather complex oxidation of 5-HT, which results in the formation of several products. These products have the potential to foul the electrode surface. To investigate if this was the case, the oxidation peak currents obtained from a pure 1.0×10^{-3} mol dm^{-3} DA solution and a 1.0×10^{-3} mol dm^{-3} DA solution mixed with 1.0×10^{-3} mol dm^{-3} 5-HT were plotted as a function of cycle number. A similar analysis was carried out for pure 7.0×10^{-5} mol dm^{-3} DA and 7.0×10^{-5} mol dm^{-3} DA mixed with 1.0×10^{-3} mol dm^{-3} 5-HT. The results are shown in Figures 6.56(a) and (b), respectively. In Figure 6.56(a) it can be seen that the DA peak currents obtained in the presence of 1.0×10^{-3} mol dm^{-3} 5-HT do not follow the same pattern as those measured for pure DA. The currents continuously decrease with cycle number rather than reaching a maximum and then decreasing, as observed in the pure DA solution. In contrast, the DA peak currents obtained for a 7.0×10^{-5} mol dm^{-3} DA and 1.0×10^{-3} mol dm^{-3} 5-HT solution do follow the same trend as that observed with pure 7.0×10^{-5} mol dm^{-3} DA. This suggests that the electrode is indeed poisoned by the by-products of 5-HT oxidation, but only in the presence of relatively high concentrations of DA. A similar effect was observed with 5-HIAA. This is not surprising as 5-HIAA is a metabolite of 5-HT.

(a)

(b)
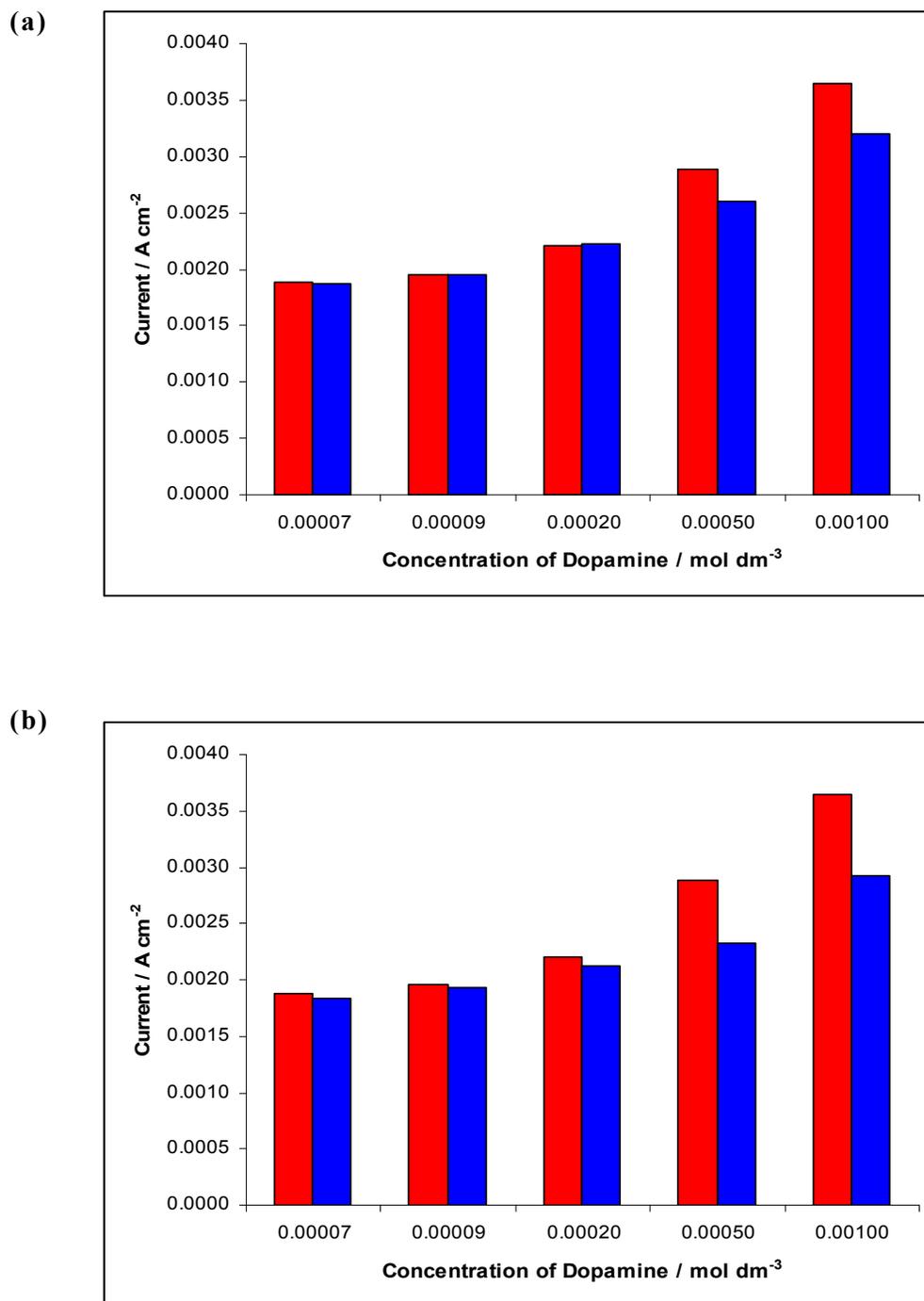
Figure 6.55: (a) Peak currents, from the cyclic voltammograms, of DA as a function of the concentration of DA in the ■ presence (*n*=3) and ■ absence (*n*=4) of 1.0 x 10^{-3} mol dm^{-3} 5-HT in a 0.10 mol dm^{-3} Na_2SO_4, pH~4.5, supporting electrolyte. (b) Peak currents, from the cyclic voltammograms, of DA as a function of the concentration of DA in the ■ presence (*n*=3) and ■ absence (*n*=4) of 1.0 x 10^{-3} mol dm^{-3} 5-HIAA in a 0.10 mol dm^{-3} Na_2SO_4, pH~4.1, supporting electrolyte.

(a)

(b)

**Figure 6.56: (a) Peak currents, from the cyclic voltammograms, of 1.0 x 10^{-3} mol dm^{-3} DA as a function of the cycle number in the ■ presence (*n*=3) and ■ absence (*n*=3) of 1.0 x 10^{-3} mol dm^{-3} 5-HT in a 0.10 mol dm^{-3} Na$_2$SO$_4$, pH~4.5, supporting electrolyte. (b) Peak currents, from the cyclic voltammograms, of 7.0 x 10^{-5} mol dm^{-3} DA as a function of the cycle number in the ■ presence (*n*=3) and ■ absence (*n*=3) of 1.0 x 10^{-3} mol dm^{-3} 5-HT in a 0.10 mol dm^{-3} Na$_2$SO$_4$, pH~4.1, supporting electrolyte.**

The DA oxidation peak potentials in the presence of 1.0×10^{-3} mol dm^{-3} 5-HT solution or 1.0×10^{-3} mol dm^{-3} 5-HIAA solution were also recorded and the mean potentials were then compared to the potentials observed for pure DA and this is illustrated in Figures 6.57(a) and (b) for the 5-HT and 5-HIAA systems, respectively. It can be seen that the presence of 5-HT does not interfere with the potential of the DA oxidation signal. The presence of 5-HIAA has a slightly different result than 5-HT on the potential of DA oxidation. It does not interfere with the potentials of the DA oxidation signals for the lower concentrations of DA but it has shifted the peak potentials of the higher concentrations of DA to more negative values.

These results show clearly that while 1.0×10^{-3} mol dm^{-3} 5-HT and 1.0×10^{-3} mol dm^{-3} 5-HIAA are not interferents at concentrations of 2.0×10^{-4} mol dm^{-3} DA or lower, they do interfere in the electrochemical detection of DA at higher concentrations of DA. It is noteworthy to mention that the concentrations of 5-HT and 5-HIAA (1.0×10^{-3} mol dm^{-3}) investigated in this interference study are considerably higher than the typical concentrations of 5-HT and 5-HIAA found in most biological systems. In terms of an implantable, *in-vivo* sensor, the typical concentrations of 5-HT and 5-HIAA in the brain extracellular fluid are up to 5 times lower than that of DA[4]. More importantly, the concentrations of DA that exist in this environment are significantly lower than the concentrations of DA affected by the presence of 5-HT and 5-HIAA in this section. Therefore, the PPy-SCD modified electrode can eliminate the interference of 5-HT and 5-HIAA for analyte compositions similar to biological samples. This is because 5-HT and 5-HIAA do not influence the peak current signals or potentials of the lower concentrations of DA and these are the essential concentrations of DA that will be monitored in any biological system.

(a)

(b)
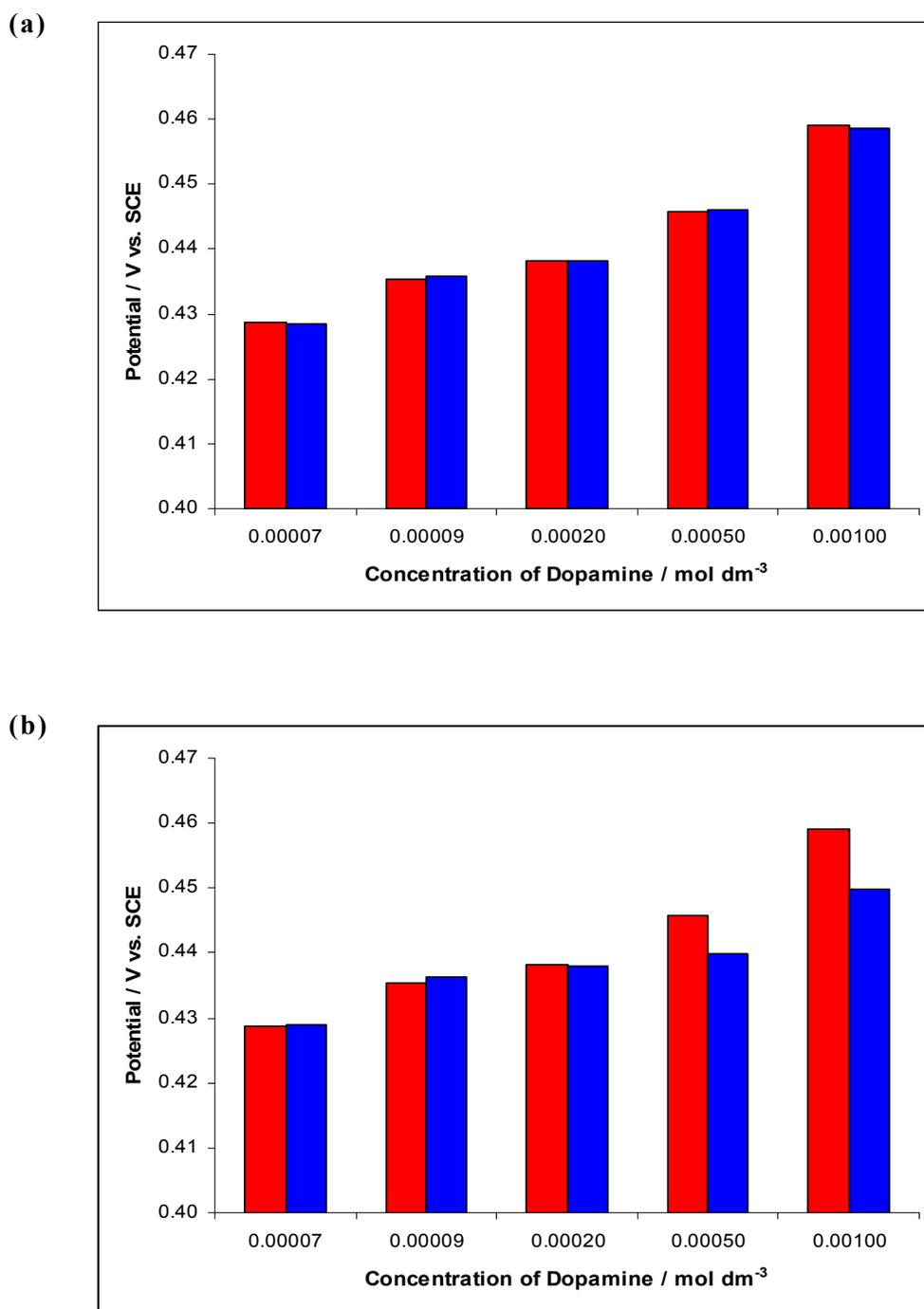
Figure 6.57: (a) Peak potentials of DA oxidation for a range of DA concentrations (7.0 x 10^{-5} - 1.0 x 10^{-3} mol dm^{-3}) obtained using cyclic voltammetry, in the ■ presence (*n*=3) and ■ absence (*n*=4) of 1.0 x 10^{-3} mol dm^{-3} 5-HT in a 0.10 mol dm^{-3} Na$_2$SO$_4$, pH~4.5, supporting electrolyte. (b) Peak potentials of DA oxidation for a range of DA concentrations (7.0 x 10^{-5} - 1.0 x 10^{-3} mol dm^{-3}) obtained using cyclic voltammetry, in the ■ presence (*n*=3) and ■ absence (*n*=4) of 1.0 x 10^{-3} mol dm^{-3} 5-HIAA in a 0.10 mol dm^{-3} Na$_2$SO$_4$, pH~4.1, supporting electrolyte.

There are no reports, to the best of our knowledge, on the manufacture of a modified electrode that can selectively detect DA in the presence of 5-HT or 5-HIAA. However, modified electrodes have been developed to simultaneously detect 5-HT and DA. Table 6.6 summarises the various electrode materials found in the literature that are capable of the simultaneous detection of 5-HT and DA. There appears to be no reports in the literature on the use of modified electrodes for the simultaneous detection of DA and 5-HIAA. Various other techniques have been used to detect DA and 5-HIAA together in samples. These methods are usually based around chromatography[66, 67] and so can not be used for real-time, *in-vivo* sensing.

Table 6.6: Materials in the literature that are capable of simultaneously detecting 5-HT and DA.

Reference	Material
60	Indium tin oxide electrode modified with gold nanoparticles
61	Gold nanoclusters on a insulating overoxidised-polypyrrole film on a glassy carbon electrode
62	Glassy carbon electrode modified with a carbon nanotube film
68	Poly(phenosafranine) modified glassy carbon electrode
69	Poly(o-phenylenediamine) modified glassy carbon electrode
70	Carbon fiber microelectrode modified with an inner layer of gold nanoparticles and an outer layer of calf thymus ds-DNA
71	Graphite electrode modified with intercalating carbon nanotubes
72	Acetylcholine modified glassy carbon electrode
73	5,5-ditetradecyl-2-(2-trimethylammonioethyl)-1,3-dioxane bromide self assembled lipid bilayer membrane modified glassy carbon electrode
74	Unmodified edge plane pyrolytic graphite electrode
75	Carbon fiber electrode modified with overoxidised polypyrrole and calf-thymus DNA

There are several other methods of simultaneously detecting DA and 5-HT without the use of modified electrodes. One approach is to use capillary electrophoresis. Maruszak _et al._[76] used capillary electrophoresis with a carboxymethyl-β-cyclodextrin chiral selector to separate DA and 5-HT. Nevertheless, this approach can not be used as an _in-vivo_ sensor for real-time analysis.

In summary, the PPy-SCD modified electrode eliminates the interference from 1.0×10^{-3} mol dm^{-3} 5-HT and 1.0×10^{-3} mol dm^{-3} 5-HIAA at concentrations of DA that would be investigated in real samples. Therefore, the PPy-SCD modified electrode may well have potential in the design of a DA sensor that could be used in real biological samples.

6.3.9 3,4-Dihydroxyphenylacetic Acid (DOPAC) and Homovanillic Acid (HVA)

DOPAC, Figure 6.58, is an important metabolite of DA[77]. It is a key interfering compound in the selective detection of DA. DOPAC and DA are structurally and chemically similar and frequently exist together in biological fluids[78]. Furthermore DOPAC is electroactive having a range of $E_{1/2}$ values between 100 to 250 mV vs. SCE[4] on most solid electrodes and this lies in the same potential region as DA is oxidised. HVA, Figure 6.59, is an electroactive[4], metabolite of DA[79]. Similarly to DOPAC, HVA and DA exist together in most natural samples. These problems make HVA and DOPAC very challenging interfering compounds in the selective detection of DA.
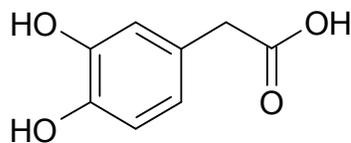

Figure 6.58: Structure of DOPAC   Figure 6.59: Structure of HVA
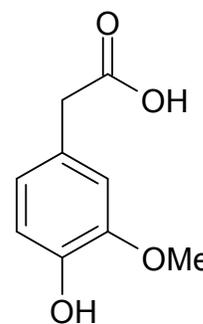
The electroactivity of DOPAC and HVA at a bare Pt electrode was firstly investigated in the sulfate supporting electrolyte by cycling the Pt electrode in a 1.0×10^{-3} mol dm^{-3} solution of DOPAC and in a 1.0×10^{-3} mol dm^{-3} solution of HVA. Representative cyclic voltammograms are shown in the inset in Figures 6.60(a) and 6.60(b) for the DOPAC and HVA systems, respectively. The oxidation of DOPAC occurs at approximately 0.520 V vs. SCE, while the oxidation of HVA occurs at 0.790 V vs. SCE. In addition, a reduction wave, centred at 0.170 V vs. SCE, is clearly visible for both compounds. In terms of the electroactivity of DOPAC and HVA at the PPy-SCD modified electrode, one oxidation peak was observed at 0.450 V vs. SCE for DOPAC, whereas two oxidation peaks are observed for HVA at approximately 0.440 V vs. SCE and 0.660 V vs. SCE.

Next, the PPy-SCD modified electrode was cycled in a solution of DA with and without the presence of DOPAC or HVA. Typical data are presented in Figures 6.61(a) and 6.61(b), where the cyclic voltammogram recorded in a 1.0×10^{-3} mol dm^{-3} DA solution is compared with the corresponding voltammograms recorded in the combined solutions, 1.0×10^{-3} mol dm^{3} DA with 1.0×10^{-3} mol dm^{-3} DOPAC or 1.0×10^{-3} mol dm^{3} DA with 1.0×10^{-3} mol dm^{-3} HVA. It can be seen that the currents recorded from the mixed solutions of DA with DOPAC, and DA with HVA are higher than that of DA alone. This shows that both DA and the DOPAC and HVA interferents are detected concurrently, resulting in an overlapping voltammetric responses.

In order to explore this further, the concentration ratios of DOPAC/HVA to DA in the combined solutions were varied from 1.0 (1.0×10^{-3} mol dm^{-3} DA and 1.0×10^{-3} mol dm^{-3} DOPAC/HVA) to 14.3 (7.0×10^{-5} mol dm^{-3} DA and 1.0×10^{-3} mol dm^{-3} DOPAC/HVA) and the peak currents and peak potentials for the oxidation of DA were measured. A total of three separate measurements were carried out for each DOPAC/DA mixture and HVA/DA mixture and the average values were computed. These data are plotted in Figures 6.62(a) and (b) and show good agreement between the replicate experiments. The error bars in the presence of DOPAC range between 0.96 to 2.82%, while the error bars in the presence of HVA range between 0.68 to 1.64%.
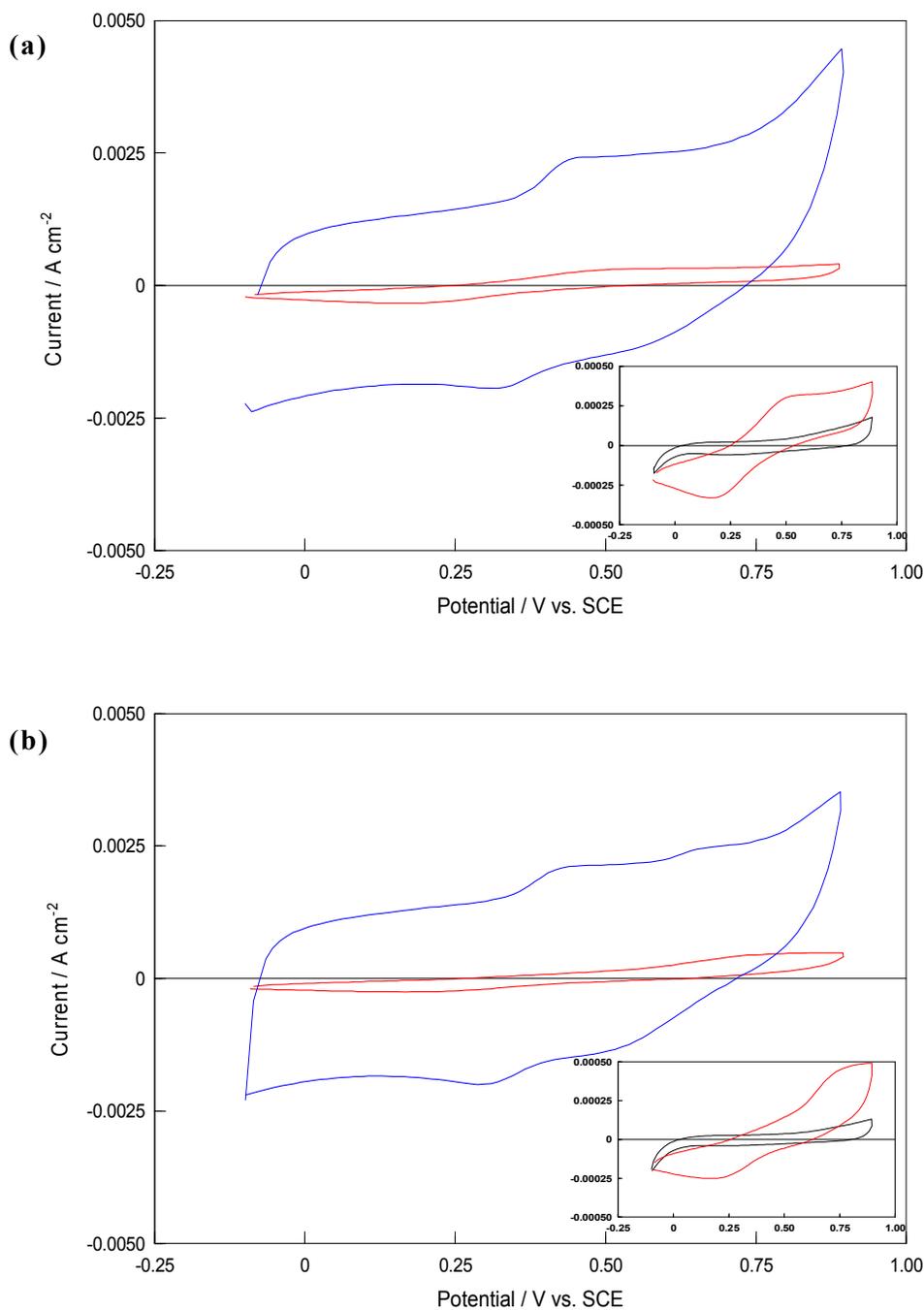
Figure 6.60: (a) Cyclic voltammograms of a — bare Pt electrode and a — PPy-SCD modified electrode in a 1.0 x 10^{-3} mol dm^{-3} DOPAC / 0.10 mol dm^{-3} Na$_2$SO$_4$ solution (pH~4.1). Scan rate = 100 mV s^{-1}. Inset: Cyclic voltammograms of the bare Pt electrode in a — 0.10 mol dm^{-3} Na$_2$SO$_4$ solution and in a — 1.0 x 10^{-3} mol dm^{-3} DOPAC / 0.10 mol dm^{-3} Na$_2$SO$_4$ solution. Scan rate = 100 mV s^{-1}. Axes are identical to Figure 6.60(a). (b) Cyclic voltammograms of a — bare Pt electrode and a — PPy-SCD modified electrode in a 1.0 x 10^{-3} mol dm^{-3} HVA / 0.10 mol dm^{-3} Na$_2$SO$_4$ solution (pH~4.0). Scan rate = 100 mV s^{-1}. Inset: Cyclic voltammograms of the bare Pt electrode in a — 0.10 mol dm^{-3} Na$_2$SO$_4$ solution and in a — 1.0 x 10^{-3} mol dm^{-3} HVA / 0.10 mol dm^{-3} Na$_2$SO$_4$ solution. Scan rate = 100 mV s^{-1}. Axes are identical to Figure 6.60(b).
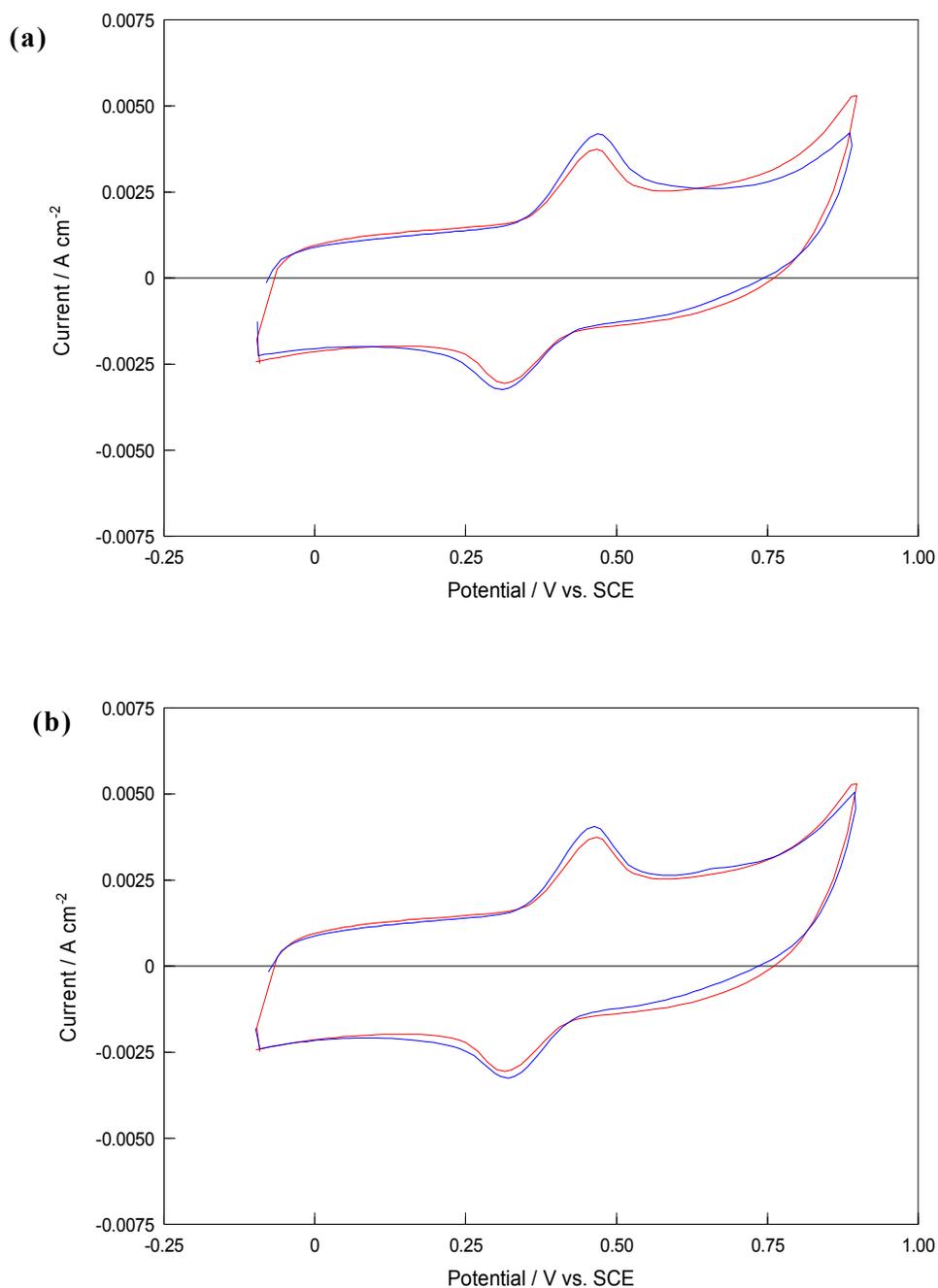
Figure 6.61: (a) Cyclic voltammograms of the PPy-SCD modified electrode in a — 1.0 x 10^{-3} mol dm^{-3} DA / 0.10 mol dm^{-3} Na$_2$SO$_4$ solution (pH~6.0) and in a — 1.0 x 10^{-3} mol dm^{-3} DA / 1.0 x 10^{-3} mol dm^{-3} DOPAC / 0.10 mol dm^{-3} Na$_2$SO$_4$ solution (pH~4.1). Scan rate = 100 mV s^{-1}. (b) Cyclic voltammograms of the PPy-SCD modified electrode in a — 1.0 x 10^{-3} mol dm^{-3} DA / 0.10 mol dm^{-3} Na$_2$SO$_4$ solution (pH~6.0) and in a — 1.0 x 10^{-3} mol dm^{-3} DA / 1.0 x 10^{-3} mol dm^{-3} HVA / 0.10 mol dm^{-3} Na$_2$SO$_4$ solution (pH~4.0). Scan rate = 100 mV s^{-1}.

(a)

(b)

Figure 6.62: (a) Calibration plot of the mean peak oxidation current of DA as a function of the concentration of DA where 1.0 x 10^{-3} mol dm^{-3} DOPAC was added to each DA solution in a 0.10 mol dm^{-3} Na$_2$SO$_4$, pH~4.1, supporting electrolyte (*n*=3). (b) Calibration plot of the mean peak current of DA as a function of the concentration of DA where 1.0 x 10^{-3} mol dm^{-3} HVA was added to each DA solution in a 0.10 mol dm^{-3} Na$_2$SO$_4$, pH~4.0, supporting electrolyte (*n*=3).

A more direct comparison between the oxidation currents and potentials of DA with and without DOPAC is provided in Figures 6.63(a) and 6.64(a), respectively. The same comparison with and without HVA is shown in Figures 6.63(b) and 6.64(b), respectively. These data clearly show that both DOPAC and HVA have an influence on the signal of DA. The DA peak currents increase in intensity and the peak potentials shift to more positive potentials. This is consistent with the oxidation of both HVA and DA and also DOPAC and DA at similar potentials, to give one combined signal.

As discussed throughout this chapter, electrostatic interactions are important in the electrochemical sensing, as the PPy-SCD modified electrode is highly charged with ionised sulfonated groups. DOPAC and HVA are phenolic compounds and depending on the pH of the solution, can dissociate into their anions, as detailed in Scheme 6.9 and Scheme 6.10. At the pH that the DOPAC experiments are carried out (pH = 4.1), approximately 35% of the DOPAC ($pK_a = 4.4$)[65] is negatively charged. Roughly 30% of the HVA ($pK_a = 4.4$)[65] is negatively charged at the pH of the HVA experiments, which was set at 4.0. As discussed with the 5-HIAA system, the DOPAC and HVA should be repelled by the anionic sulfonated groups on the cyclodextrin. However, Figures 6.65(a) and 6.65(b) show that DOPAC and HVA form a weak inclusion complex with the sulfonated β-cyclodextrin, as evidenced from the small shift in peak potential and small reduction in the peak oxidation current. In addition, both DOPAC and HVA are oxidised at the polypyrrole film in the absence of the sulfonated β cyclodextrin as a dopant (PPy-SDS) and this coupled with the complexation may explain why DOPAC and HVA are oxidised at the PPy-SCD modified electrode.

(a)

(b)
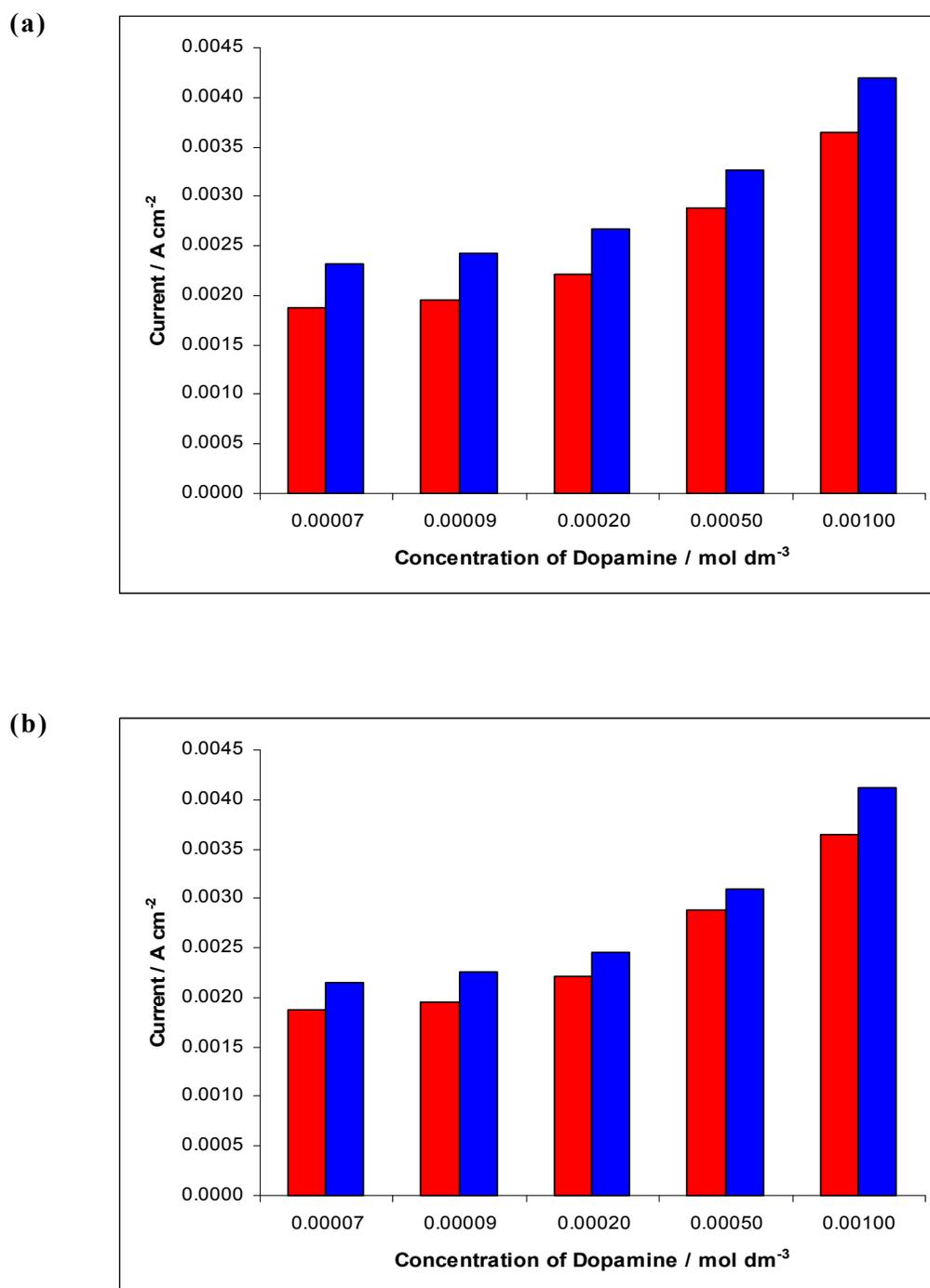
Figure 6.63: (a) Peak currents, from the cyclic voltammograms, of DA as a function of the concentration of DA in the ■ presence ($n=3$) and ■ absence ($n=4$) of 1.0×10^{-3} mol dm^{-3} DOPAC in a 0.10 mol dm^{-3} Na$_2$SO$_4$, pH~4.1, supporting electrolyte. (b) Peak currents, from the cyclic voltammograms, of DA as a function of the concentration of DA in the ■ presence ($n=3$) and ■ absence ($n=4$) of 1.0×10^{-3} mol dm^{-3} HVA in a 0.10 mol dm^{-3} Na$_2$SO$_4$, pH~4.0, supporting electrolyte.

(a)

(b)
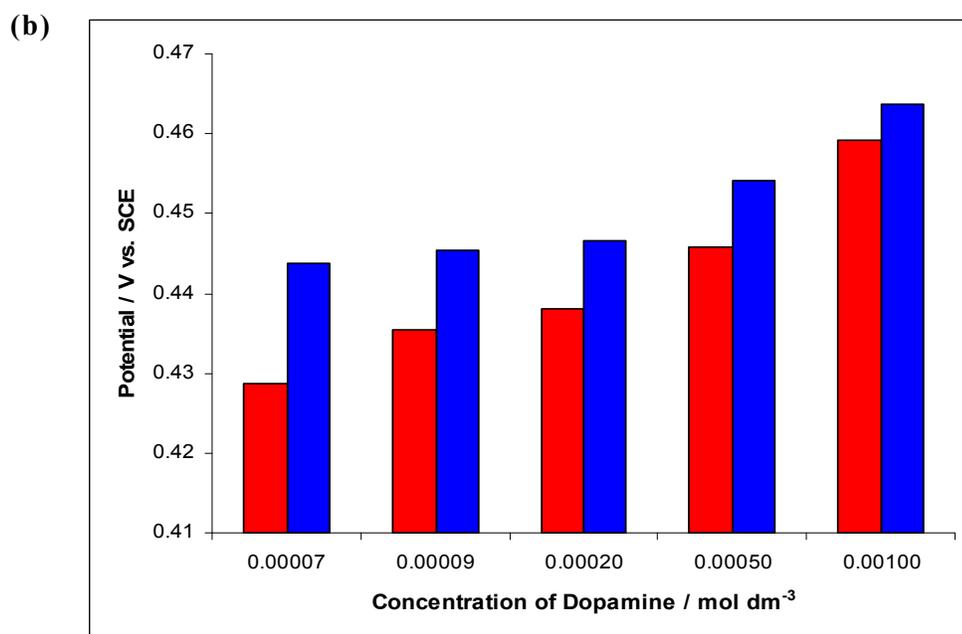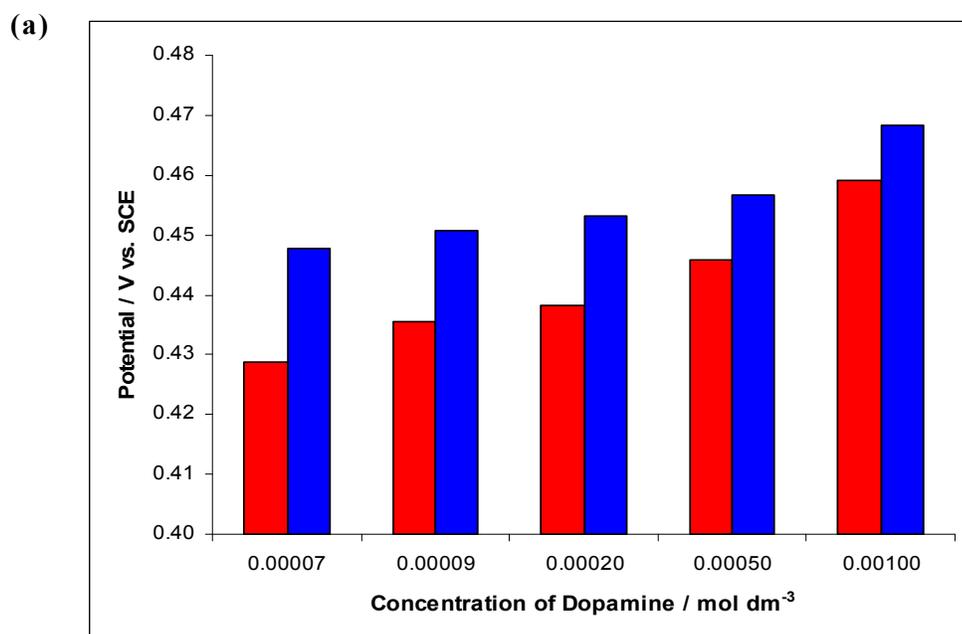
Figure 6.64: (a) Peak potentials of DA oxidation for a range of DA concentrations (7.0 x 10^{-5} -1.0 x 10^{-3} mol dm^{-3}) obtained using cyclic voltammetry, in the ■ presence (*n*=3) and ■ absence (*n*=4) of 1.0 x 10^{-3} mol dm^{-3} DOPAC in a 0.10 mol dm^{-3} Na$_2$SO$_4$, pH~4.1, supporting electrolyte. (b) Peak potentials of DA oxidation for a range of DA concentrations (7.0 x 10^{-5} – 1.0 x 10^{-3} mol dm^{-3}) obtained using cyclic voltammetry, in the ■ presence (*n*=3) and ■ absence (*n*=4) of 1.0 x 10^{-3} mol dm^{-3} HVA in a 0.10 mol dm^{-3} Na$_2$SO$_4$, pH~4.0, supporting electrolyte.

Similarly to 5-HIAA, a weak host-guest complex was formed when the pH of the DOPAC and HVA solutions was increased to 6.7. At this pH over 99% of the DOPAC and HVA molecules are negatively charged. This suggests that the anionic carboxylate groups on DOPAC and HVA are maintained at a sufficient distance from the negatively charged interface, avoiding the strong electrostatic repulsion between the ionised carboxylate groups and the sulfonated groups on the cyclodextrin. Therefore, DOPAC and HVA are not sufficiently repelled from the surface, allowing moieties in the molecules to include within the cavity of the sulfonated β-cyclodextrin.
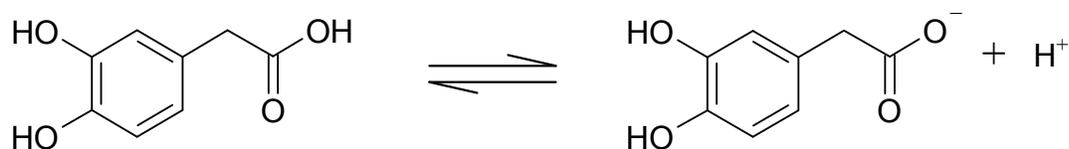
Scheme 6.9: Dissociation of DOPAC.
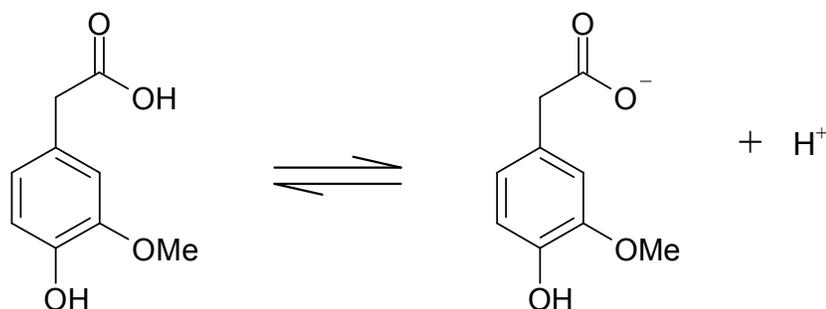
Scheme 6.10: Dissociation of HVA.

These results show clearly that 1.0×10^{-3} mol dm^{-3} DOPAC and 1.0×10^{-3} mol dm^{-3} HVA do interfere in the electrochemical detection of DA. This can be attributed to the ability of the sulfonated β-cyclodextrin to form a weak host-guest complex with DOPAC and HVA.
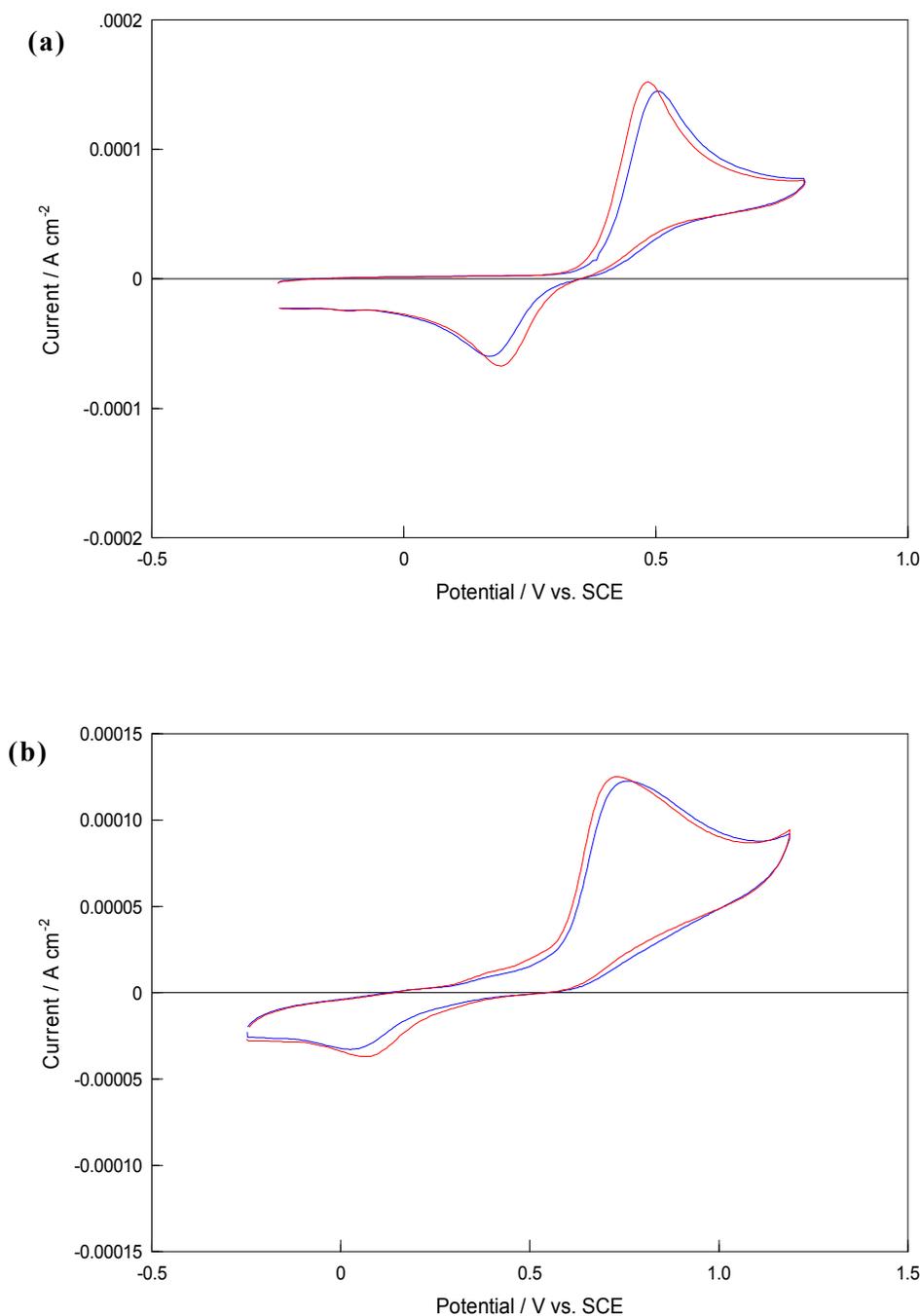
Figure 6.65: (a) Cyclic voltammograms of a bare GC electrode in a ▬ 5.0 x 10⁻⁴ mol dm⁻³ DOPAC / 0.30 mol dm⁻³ citrate phosphate buffer solution (pH~4.1) and in a ▬ 5.0 x 10⁻⁴ mol dm⁻³ DOPAC / 0.01 mol dm⁻³ sulfonated β-cyclodextrin / 0.30 mol dm⁻³ citrate phosphate buffer solution (pH~4.1). Scan rate = 50 mV s⁻¹. Electrochemical window: -0.250 to 0.800 V vs. SCE. (b) Cyclic voltammograms of a bare GC electrode in a ▬ 5.0 x 10⁻⁴ mol dm⁻³ HVA / 0.30 mol dm⁻³ citrate phosphate buffer solution (pH~4.0) and in a ▬ 5.0 x 10⁻⁴ mol dm⁻³ HVA / 0.01 mol dm⁻³ sulfonated β-cyclodextrin / 0.30 mol dm⁻³ citrate phosphate buffer solution (pH~4.0). Scan rate = 50 mV s⁻¹. Electrochemical window: -0.250 to +1.200 V vs. SCE.

There have been a number of modified electrodes developed for the determination of DA, where DOPAC has been investigated as a possible interferent. Examples include electrodes developed by Lin and Gong[39] and Mo and Ogorevc[80]. Lin and Gong[39] have shown that a 200-fold excess of DOPAC had no effect on the peak current of 1.0×10^{-6} mol dm^{-3} DA at a GC electrode modified with a 5,5-ditetradecyl-2-(2-trimethyl-ammonioethyl)-1,3-dioxane bromide self-assembled bilayer membrane. Mo and Ogorevc[80] achieved a similar result using an overoxidised poly(1,2-phenylenediamine) coated carbon fiber microelectrode. A 100-fold excess of DOPAC did not interfere with the measurement of 1.0×10^{-7} mol dm^{-3} DA. However, no experimental evidence was given in either paper to back up these claims. There are no reports, to the best of our knowledge, on the manufacture of a modified electrode that can selectively detect DA in the presence of HVA, or that can simultaneously detect DA and HVA. The approaches taken in the literature to date, for the detection of HVA and DA in samples, are largely based on high performance liquid chromatography with electrochemical detection[81-83]. While they are successful in detecting DA, these approaches can never be used for real-time *in-vivo* sensing. Methods that are not suitable for real-time, *in-vivo* detection have also been employed to analyse DA and DOPAC mutually. Microchip capillary electrophoresis with cellulose-DNA-modified screen-printed electrodes[84] is one such method that has been used.

6.4 Comparisons

A summary of the results obtained is provided in Table 6.7, while the chemical structures of the compounds are provided in Table 6.8. These compounds were selected because they are all potential interferents in the sensing of DA and they have different sizes and in some cases they have chemical structures that are very different to DA, while in other cases they have structures that are similar to that of DA. These compounds differ in polarity and hydrophobicity, and exist in solution in various forms, cationic, anionic to zwitterionic. Consequently, by comparing the results a greater insight into the role that complexation and electrostatic interactions play in the sensing of compounds at the PPy-SCD modified electrode may be obtained.

Table 6.7: Summary of the results obtained from the interferents investigated in this Chapter.

Interferent	Result
Uric Acid (UA)	Interference Eliminated
Aspartic Acid (Asp)	Interference Eliminated
Aminobutyric Acid (GABA)	Interference Eliminated
Acetylcholine (Ach)	Interference Eliminated
Glutamic Acid (Glu)	Interference Eliminated
Glycine (Gly)	Interference Eliminated
Histamine (HA)	Interference Eliminated
Acetaminophenol (ACOP)	DA and ACOP detected simultaneously with ACOP having no effect on DA signal
5-Hydroxyindole Acetic Acid (5-HIAA)	No interference on DA signal at lower concentrations of DA. Interference at higher concentrations.
5-Hydroxytryptamine (5-HT)	No interference on DA signal at lower concentrations of DA. Interference at high concentrations.
3,4-Dihydroxyphenylacetic Acid (DOPAC)	Interference Not Eliminated
Homovanillic Acid (HVA)	Interference Not Eliminated

Table 6.8: Summary of the chemical structure of the interfering compounds. The compounds highlighted in red are electroinactive while the rest are all electroactive.

Uric Acid (UA) Anionic	Aspartic Acid (Asp) Predominately Negative	Glutamic Acid (Glu) Predominately Negative
Aminobutyric Acid (GABA) **Zwitterionic**	**Acetylcholine (Ach)** **Cationic**	**Glycine (Gly)** **Zwitterionic**
Histamine (HA) Cationic	Acetaminophenol (ACOP) Neutral	5-Hydroxytryptamine (5-HT) Cationic
5-Hydroxyindole Acetic Acid **(5-HIAA)** **Anionic/Neutral**	**3,4-Dihydroxyphenylacetic Acid** **(DOPAC)** **Anionic/Neutral**	**Homovanillic Acid (HVA)** **Anionic/Neutral**
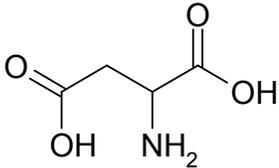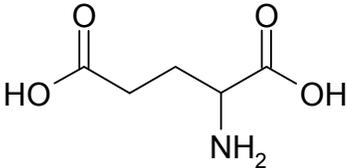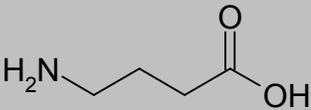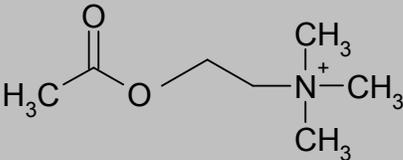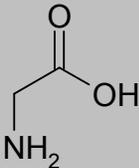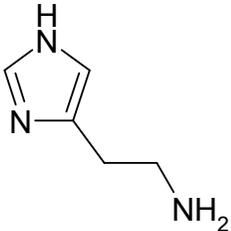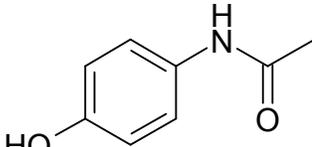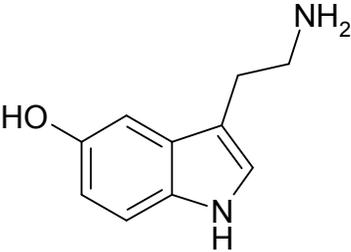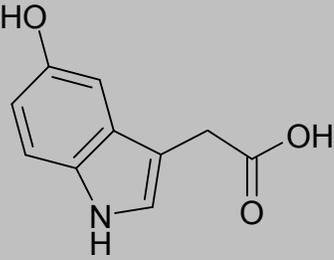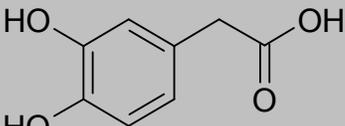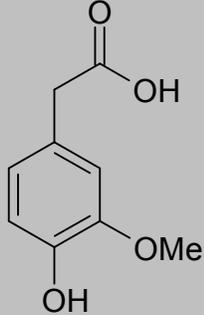
It is well known from the literature that the main driving force for complex formation is the displacement of water molecules from the cavity by more hydrophobic guest molecules, assuming that there is a fit between the size of the guest and the cavity of the cyclodextrin[85]. For β-cyclodextrins, this cavity is typically between 6.0 and 6.5 Å, but an inclusion complex can still form if only part of the molecule enters the cavity. Once inside the cavity, the conformation of the guest molecule may alter under the weak van der Waals forces that exist. However, the energetically favourable interactions are the displacement of the polar water molecules from the hydrophobic (apolar) cavity. Once outside the cavity, the displaced water forms hydrogen bonds with the neighbouring water molecules. On the other hand, the repulsive interactions between the guest and the aqueous environment are reduced as the guest enters the cavity.

Based on these hydrophobic interactions, it is not surprising that UA and the polar amino acids, Asp and Glu do not form inclusion complexes. Although Gly is commonly described as a non-polar amino acid, it has polar amino and carboxylic groups making it too polar for the hydrophobic cavity of the cyclodextrin. GABA is also polar, and the inclusion complex is unlikely to be favoured energetically. Interestingly, in a recent study using hydrophilic interaction chromatography, Zhang *et al.*[32], found that Ach, 5-HT, DA, GABA, Glu and Asp eluted out in turn from the hydrophilic column, indicating that the amino acids are of higher polarity, whereas Ach and 5-HT are comparable to DA. This is in good agreement with the results obtained with 5-HT. As shown in Figure 6.49(a), 5-HT forms an inclusion complex with the sulfonated β-cyclodextrin. Indeed, the degree of complexation is similar to that observed with DA. However, Ach, which has similar polarity, does not appear to interfere in the detection of DA. This suggests that while hydrophobicity is important, other interactions are also contributing to the formation, or non-formation, of an inclusion complex with the anionic sulfonated β-cyclodextrin.

Direct evidence to support the role of electrostatic interactions in promoting an inclusion complex comes from the 5-HT, ACOP, DOPAC, HVA and 5-HIAA experiments. 5-HT is cationic and although the molecule is larger than DA, it forms an inclusion complex with the sulfonated β-cyclodextrin. As discussed in Chapter 5, the amine group on the DA

remains outside the cavity and the electrostatic interactions between the protonated amine group and the sulfonated groups on the β-cyclodextrin increase the stability of the inclusion complex. It is interesting to compare the extent of the complexation of the anionic sulfonated β-cyclodextrin with the cationic DA and cationic 5-HT with that observed with the anionic sulfonated β-cyclodextrin and the neutral ACOP, neutral or anionic 5-HIAA, DOPAC and HVA molecules. All four (ACOP, 5-HIAA, DOPAC and HVA) have a 6-membered aromatic ring, similar to 5-HT and DA. When the pH is adjusted so that the neutral or un-dissociated species predominate, then a weak inclusion complex is observed. This suggests that the aromatic ring enters the cavity, but the lack of a cationic group to attract the sulfonated groups on the ring of the β-cyclodextrin leads to a very weak inclusion complex. It is also noteworthy to mention that the peaks observed for the oxidation of 1.0×10^{-3} mol dm^{-3} 5-HIAA, DOPAC and HVA at the PPy-SCD modified electrode are noticeably less than the oxidation peaks observed for an equivalent concentration of DA. This is also seen with ACOP, which oxidises at potentials that are higher than DA, Figure 6.40(a). The oxidation signal of 5-HT at the PPy-SCD modified electrode is also lower than that of DA but this is probably due to the fact that a stronger inclusion complex is formed between the DA and the sulfonated β-cyclodextrin than between the 5-HT and sulfonated β-cyclodextrin. However, the oxidation of these compounds at a bare Pt electrode yields similar, if not higher peak currents. This indicates a clear relationship between the electrochemical sensing event and the degree of complexation.

The results obtained with the cationic HA and Ach are more difficult to rationalise, as these are cationic species. The Ach should have sufficient hydrophobicity to include within the sulfonated β-cyclodextrin cavity, through the ester group. However, the positively charged nitrogen, surrounded by three methyl groups may be too large to sit outside the cavity and bind electrostatically with the sulfonated groups. It is unlikely that this end of the molecule would enter the cavity. Although Ach is not electroactive, it could nevertheless block the cavity of the sulfonated β-cyclodextrin and limit the detection of DA. This was not observed in any experiments suggesting that an inclusion complex is not formed, most likely due to steric effects at the charged nitrogen. HA is electroactive, but is only oxidised

at relatively high potentials, Figure 6.35. In this case, the positively charged nitrogen on the amine group is not sterically hindered, however, the protonated nitrogen on the ring will not favour complexation and at the pH of the experiment (pH = 4.5) this form will predominate, while the concentration of the non-protonated ring structure, Scheme 6.6, will be lower.

It is clearly evident from the experiments carried out with the PPy-SDS electrode, that ACOP, 5-HT and 5-HIAA are oxidised, although only to a small extent, when the polymer is doped with a simple dopant, which is unable to act as a host system. In all cases, higher oxidation currents were observed when the polypyrrole film was doped with the sulfonated β-cyclodextrin. Again, this confirms the role of the sulfonated β-cyclodextrin in the electrochemical detection of these analytes.

It is also significant to mention that none of the amino acids poisoned the electrode surface. Amino acids are well known to foul electrodes by adhering to the surface, causing a decline in the sensor signal[28]. This was not observed with Asp, Glu, GABA or Gly.

In summary, UA, Asp, Glu, GABA, Ach, Glu, Gly, and HA are not oxidised at the PPy-SCD modified electrode, attributable to the fact that no complexation occurs between these compounds and the sulfonated β-cyclodextrin. As a result, they do not interfere in the electrochemical detection of DA at the PPy-SCD modified electrode. This is due to the nature of each compound in solution and their hydrophobic character or in the case of Ach, steric hindrance. ACOP, 5-HT, 5-HIAA, DOPAC and HVA do form an inclusion complex with the sulfonated β-cyclodextrin. This is because they all contain a relatively hydrophobic phenol ring that will be attracted to the hydrophobic internal cavity of the cyclodextrin. The degree to which these compounds include in the cavity depends on their form in solution with species that are predominately cationic forming the more stable inclusion complexes. Although, ACOP, 5-HT and 5-HIAA are oxidised at the PPy-SCD modified electrode, they do not interfere in the electrochemical detection of DA. This is because they are not oxidised in the same potential region as DA. The higher concentrations of DA are affected by 5-HT and 5-HIAA, due to the electrode poisoning, however for concentrations similar to biological samples they do not interfere. In contrast,

DOPAC and HVA are oxidised in the same potential region and as a result interfere in the determination of DA at the PPy-SCD modified electrode.

6.5 Summary of Results

It has been demonstrated in this chapter that the PPy-SCD modified electrode can effectively block the interference of a wide range of interferents including UA, Asp, GABA, Ach, Glu, Gly, HA and ACOP. The interference of 5-HIAA and 5-HT depends on the concentration of DA, and is not an issue at low DA concentrations. However, the interference of DOPAC and HVA could not be eliminated. The mechanism of sensing has been determined to be a combination of complexation, electrostatic interactions and oxidation at the polymer film, with cationic compounds that are hydrophobic, producing the strongest inclusion complexes and highest oxidation signals.

6.6 References

1.   S. Thiagarajan and S.-M. Chen, *Talanta*, **74**, 212, (2007).
2.   E. Miland, A. J. M. Ordieres, P. T. Blanco, M. R. Smyth and C. O. Fagain, *Talanta*, **43**, 785, (1996).
3.   J. Huang, Y. Liu, H. Hou and T. You, *Biosens. Bioelectron.*, **xxx**, xxx, (2008).
4.   J. P. Lowry and R. D. O'Neill, *Encyclopedia of Sensors, Neuroanalytical Chemistry In Vivo Using Electrochemical Sensors*, C. A. Grimes, E. C. Dicky, and M. V. Pishko, American Scientific Publishers, **10**, 1, (2006).
5.   V. Jiménez and J. B. Alderete, *Journal of Molecular Structure-THEOCHEM*, **755**, 209, (2005).
6.   J.-M. Zen, J.-J. Jou and G. Ilangovan, *Analyst*, **123**, 1345, (1998).
7.   S. G. Wu, T. L. Wang, Z. Y. Gao, H. H. Xu, B. N. Zhou and C. Q. Wang, *Biosens. Bioelectron.*, **23**, 1776, (2008).
8.   M. Ramirez-Berriozabal, L. Galicia, S. Gutierrez-Granados, J. S. Cortes and P. Herrasti, *Electroanalysis*, **20**, 1678, (2008).
9.   Z. H. Wang, Y. M. Wang and G. Luo, *Analyst*, **127**, 1353, (2002).
10.   L. S. Rocha and H. M. Carapuca, *Bioelectrochemistry*, **69**, 258, (2006).
11.   F. O. Brown and J. P. Lowry, *Analyst*, **128**, 700, (2003).
12.   M. D. Rubianes and G. A. Rivas, *Anal. Chim. Acta*, **440**, 99, (2001).
13.   L. Lin, J. Chen, H. Yao, Y. Chen, Y. Zheng and X. Lin, *Bioelectrochemistry*, **73**, 11, (2008).
14.   X. Lin, Q. Zhuang, J. Chen, S. Zhang and Y. Zheng, *Sens. Actuator B-Chem.*, **125**, 240, (2007).
15.   R. P. d. Silva, A. W. O. Lima and S. H. P. Serrano, *Anal. Chim. Acta*, **612**, 89, (2008).
16.   S. Jo, H. Jeong, S. R. Bae and S. Jeon, *Microchem J.*, **88**, 1, (2008).
17.   Y. Liu, J. Huang, H. Hou and T. You, *Electrochem. Commun.*, **10**, 1431, (2008).
18.   X. Jiang and X. Lin, *Analyst*, **130**, 391, (2005).
19.   Y. Li, P. Wang, L. Wang and X. Lin, *Biosens. Bioelectron.*, **22**, 3120, (2007).
20.   P. Wang, Y. Li, X. Huang and L. Wang, *Talanta*, **73**, 431, (2007).
21.   A. Safavi, N. Maleki, O. Moradlou and F. Tajabadi, *Anal. Biochem.*, **359**, 224, (2006).
22.   H.-S. Wang, T.-H. Li, W.-L. Jia and H.-Y. Xu, *Biosens. Bioelectron.*, **22**, 664, (2006).
23.   S. Jiao, M. Li, C. Wang, D. Chen and B. Fang, *Electrochim. Acta*, **52**, 5939, (2007).
24.   X. Lin, Y. Zhang, W. Chen and P. Wu, *Sens. Actuator B-Chem.*, **122**, 309, (2007).
25.   T. Luczak, *Electrochim. Acta*, **53**, 5725, (2008).
26.   H. J. Leu and M. S. Lin, *Electroanalysis*, **18**, 307, (2006).
27.   Y. Song, Y. Feng, X. Lu, S. Zhao, C.-W. Liu and Y.-M. Liu, *Neurosci. Lett.*, **445**, 53, (2008).
28.   R. Gifford, J. J. Kehoe, S. L. Barnes, B. A. Kornilayev, M. A. Alterman and G. S. Wilson, *Biomaterials*, **27**, 2587, (2006).
29.   pKa Data Compiled by R. Williams, Peterson Laboratory, Penn State Chemistry Department, http://research.chem.psu.edu/brpgroup/pKa_compilation.pdf.

30. M. Shanmugam, D. Ramesh, V. Nagalakshmi, R. Kavitha, R. Rajamohan and T. Stalin, *Spectro. Acta Pt. A-Molec. Biomolec. Spectr.*, **71**, 125, (2008).

31. S. Hbaieb, R. Kalfat, Y. Chevalier, N. Amdouni and H. Parrot-Lopez, *Mater. Sci. Eng. C-Biomimetic Supramol. Syst.*, **28**, 697, (2008).

32. X. Zhang, A. Rauch, H. Lee, H. Xiao, G. Rainer and N. K. Logothetis, *Rapid Commun. Mass Spectrom.*, **21**, 3621, (2007).

33. Z. Chen, J. Wu, G. B. Baker, M. Parent and N. J. Dovichi, *J. Chromatogr. A*, **914**, 293, (2001).

34. M. F. Olive, K. K. Mehmert and C. W. Hodge, *Brain Res. Protoc.*, **5**, 16, (2000).

35. S. Parrot, V. Sauvinet, V. Riban, A. Depaulis, B. Renaud and L. Denoroy, *J. Neurosci. Methods*, **140**, 29, (2004).

36. J. A. Eckstein, G. M. Ammerman, J. M. Reveles and B. L. Ackermann, *J. Mass Spectrom.*, **43**, 782, (2008).

37. L. Bert, F. Robert, L. Denoroy, L. Stoppini and B. Renaud, *J. Chromatogr. A*, **755**, 99, (1996).

38. M. Kooshki and E. Shams, *Anal. Chim. Acta*, **587**, 110, (2007).

39. X. Lin and J. Gong, *Anal. Chim. Acta*, **507**, 255, (2004).

40. M. v. d. Zeyden, W. H. Oldenziel, K. Rea, T. I. Cremers and B. H. Westerink, *Pharmacol. Biochem. Behav.*, **90**, 135, (2008).

41. X.-E. Zhao and Y.-R. Suo, *Talanta*, **76**, 690, (2008).

42. S. Li, C.-C. Liu and T.-C. Chou, *Biosens. Bioelectron.*, **20**, 9, (2004).

43. M. Yang, Y. Yang, Y. Yang, G. Shen and R. Yu, *Anal. Chim. Acta*, **530**, 205, (2005).

44. E. M. Javerfalk-Hoyes, U. Bondesson, D. Westerlund and P. E. Andren, *Electrophoresis*, **20**, 1527, (1999).

45. V. Beni, M. Ghita and D. W. M. Arrigan, *Biosens. Bioelectron.*, **20**, 2097, (2005).

46. J. R. Cooper, F. E. Bloom and R. H. Roth*, The Biochemical Basis of Neuropharmacology*, Oxford University Press **Chapter 6**, 105, (2003).

47. M. Vidotti, S. I. C. d. Torresi and L. T. Kubota, *Sens. Actuator B-Chem.*, **In Press, Corrected Proof**.

48. J. A. M. McKenzie, C. J. Watson, R. D. Rostand, I. German, S. R. Witowski and R. T. Kennedy, *J. Chromatogr. A*, **962**, 105, (2002).

49. S. Oguri and Y. Yoneya, *J. Chromatogr. B*, **781**, 165, (2002).

50. Y. Miyamoto, R. Yoshimoto, M. Yumoto, A. Ishihara, K. Takahashi, H. Kotani, A. Kanatani and S. Tokita, *Anal. Biochem.*, **334**, 89, (2004).

51. B. M. De Borba and J. S. Rohrer, *J. Chromatogr. A*, **1155**, 22, (2007).

52. J.-M. Zen and Y.-S. Ting, *Anal. Chim. Acta*, **342**, 175, (1997).

53. R. M. de Carvalho, R. S. Freire, S. Rath and L. T. Kubota, *J. Pharm. Biomed. Anal.*, **34**, 871, (2004).

54. C. Wang, C. Li, F. Wang and C. Wang, *Microchim. Acta*, **155**, 365, (2006).

55. S.-F. Wang, F. Xie and R.-F. Hu, *Sens. Actuator B-Chem.*, **123**, 495, (2007).

56. S. A. Kumar, C.-F. Tang and S.-M. Chen, *Talanta*, **76**, 997, (2008).

57. M. Li and L. Jing, *Electrochim. Acta*, **52**, 3250, (2007).

58. L. Jia, X.-H. Zhang, Q. Li and S.-F. Wang, *J Anal Chem*, **62**, 266, (2007).

59. G. Milczarek and A. Ciszewski, *Electroanalysis*, **15**, 529, (2003).

60. R. N. Goyal, V. K. Gupta, M. Oyama and N. Bachheti, *Talanta*, **72**, 976, (2007).

61.   J. Li and X. Lin, *Sens. Actuator B-Chem.*, **124**, 486, (2007).
62.   K. Wu, J. Fei and S. Hu, *Anal. Biochem.*, **318**, 100, (2003).
63.   R. N. Goyal, M. Oyama, V. K. Gupta, S. P. Singh and R. A. Sharma, *Sens. Actuator B-Chem.*, **134**, 816, (2008).
64.   J. Pratuangdejkul, W. Nosoongnoen, G.-A. Guérin, S. Loric, M. Conti, J.-M. Launay and P. Manivet, *Chem. Phys. Lett.*, **420**, 538, (2006).
65.   H. Sirén, R. Kuldvee, T. Karla, T. Ekström and M.-L. Riekkola, *J. Chromatogr. A*, **1068**, 89, (2005).
66.   J.-C. Alvarez, D. Bothua, I. Collignon, C. Advenier and O. Spreux-Varoquaux, *Biomed. Chromatogr.*, **13**, 293, (1999).
67.   K. Fujino, T. Yoshitake, J. Kehr, H. Nohta and M. Yamaguchi, *J. Chromatogr. A*, **1012**, 169, (2003).
68.   T. Selvaraju and R. Ramaraj, *Electrochem. Commun.*, **5**, 667, (2003).
69.   T. Selvaraju and R. Ramaraj, *J. Appl. Electrochem.*, **33**, 759, (2003).
70.   L. Lu, S. Wang and X. Lin, *Anal. Sci.*, **20**, 1131, (2004).
71.   Z.-h. Wang, Q.-l. Liang, Y.-m. Wang and G.-a. Luo, *J. Electroanal. Chem.*, **540**, 129, (2003).
72.   G.-P. Jin, X.-Q. Lin and J.-m. Gong, *J. Electroanal. Chem.*, **569**, 135, (2004).
73.   J.-M. Gong and X.-Q. Lin, *Anal. Sci.*, **20**, 905, (2004).
74.   R. T. Kachoosangi and R. G. Compton, *Anal. Bioanal. Chem.*, **387**, 2793, (2007).
75.   X. Jiang and X. Lin, *Anal. Chim. Acta*, **537**, 145, (2005).
76.   W. Maruszak, M. Trojanowicz, M. Margasinska and H. Engelhardt, *J. Chromatogr. A*, **926**, 327, (2001).
77.   C. R. Raj and T. Ohsaka, *Electroanalysis*, **14**, 679, (2002).
78.   P. R. Roy, M. S. Saha, T. Okajima, S.-G. Park, A. Fujishima and T. Ohsaka, *Electroanalysis*, **16**, 1777, (2004).
79.   T. Selvaraju and R. Ramaraj, *Electrochim. Acta*, **52**, 2998, (2007).
80.   J.-W. Mo and B. Ogorevc, *Anal. Chem.*, **73**, 1196, (2001).
81.   M. A. Vicente-Torres, P. Gil-Loyzaga, F. Carricondo and M. V. Bartolomé, *J. Neurosci. Methods*, **119**, 31, (2002).
82.   F. Xu, M. Gao, G. Shi, L. Wang, W. Zhang, J. Xue, L. Jin and J. Jin, *Anal. Chim. Acta*, **439**, 239, (2001).
83.   T. Sasaki, T. Fukushima, M. Ohishi and T. Toyo'oka, *Biomed. Chromatogr.*, **22**, 888, (2008).
84.   M. Johirul, A. Shiddiky, R.-E. Kim and Y.-B. Shim, *Electrophoresis*, **26**, 3043, (2005).
85.   B. Fang, W. Zhang, X. Kan, H. Tao, X. Deng and M. Li, *Sens. Actuator B-Chem.*, **117**, 230, (2006).

Chapter 7

Conclusion

7.1 General Conclusions

The ultimate goal of this Ph.D. research programme was to develop a simple, biocompatible, highly sensitive and selective dopamine (DA) sensor. A polypyrrole-sulfonated β-cyclodextrin (PPy-SCD) modified electrode was employed to try and accomplish this aim.

The PPy-SCD film was fabricated on a platinum (Pt) electrode from a solution of pyrrole and sulfonated β-cyclodextrin using a potentiostatic mode of electropolymerisation. In general, an oxidation potential of 0.800 V vs. SCE was applied to the Pt electrode until a particular charge was consumed. The electrosynthesis period of the polymer film was extremely fast using this oxidation potential with 0.20 mol dm^{-3} pyrrole and 0.01 mol dm^{-3} sulfonated β-cyclodextrin. For example, it took approximately 40 s for the PPy-SCD film to reach the most commonly used charge throughout this study, 0.24 C cm^{-2}. This fast rate of electropolymerisation was explained in terms of the high conductivity of the sulfonated β-cyclodextrin; the conductivity of the sulfonated β-cyclodextrin was four times higher than the conductivity of an equimolar NaCl solution. Consequently, no supporting electrolyte was necessary for the formation of the PPy-SCD film, ensuring that the polymer was only doped by the sulfonated β-cyclodextrin. The fact the anionic sulfonated β-cyclodextrin was doped into the polypyrrole was confirmed by EDX and SEM images showed that the PPy-SCD film had an ordered 'cauliflower' morphology.

The nucleation of the PPy-SCD film on the Pt was found to be an instantaneous process using a series of relationships derived by Scharifker and Hills[1]. Studies on the kinetics of the electropolymerisation reaction showed that the order of the reaction with respect to the pyrrole concentration, *α*, was 0.7, while a lower value of 0.4 was obtained for *β*, the partial order of the reaction for the SCD dopant anion. These fractional values of the partial orders are consistent with a complex electropolymerisation process and are in good agreement with previous literature reports on the electropolymerisation of pyrrole from simple dopant anions[2, 3].

The capacitance of the PPy-SCD film was high and was found to be 1.2 x 10^{-3} F cm^{-2}, compared to the capacitance of 6.1 x 10^{-4} F cm^{-2} for an equivalent PPy-Cl film. This two-

fold increase in the capacitance is consistent with the storage of considerably more negative charge in the PPy-SCD films due to the presence of free sulfonated groups in the films, which in turn enhances the concentration of cations bound within the polymer. Using EQCM measurements, it was shown that a simple 1:3 dopant ratio between the sulfonated β-cyclodextrin and the pyrrole is not possible in these PPy-SCD films. Instead, the doping ratio was estimated to be 1:8 or a 12.5% doping level. Again, it was concluded that some free sulfonated groups without any charge compensation are present within the PPy-SCD films. It was also found that the large sulfonated β-cyclodextrin dopant was permanently anchored within the polymer matrix, giving the system cation exchange properties.

Although pyrrole is a known toxin, its corresponding polymer form, polypyrrole, is highly biocompatible[4, 5]. In addition, toxicity studies have shown that the sulfonated β-cyclodextrin is harmless when it is orally or parenterally administered[6]. Consequently, the PPy-SCD films are likely to exhibit good biocompatibility properties. It is noteworthy to mention that the formation of a PPy-SCD film is not an entirely novel concept, having previously been reported by Temsamani *et al.*[7], Bidan *et al.*[8] and Reece *et al.*[9]. However, in the case of Temsamani *et al.*[7] a supporting electrolyte was used and it is unlikely that the polymer is doped solely by the sulfonated β-cyclodextrin. Moreover, to the best of our knowledge, the application of such a film to sense DA has never been reported.

The PPy-SCD film displayed excellent sensitivity to DA in comparison to the other polypyrrole modified electrodes studied in this research. These included polypyrrole films doped with chloride, sulfate, dodecyl sulfate and neutral β-cyclodextrin which all gave very weak responses. In general, the DA response at the PPy-SCD modified electrode was carried out in a sulfate supporting electrolyte. However, it was found that similar results could be obtained using a saline based electrolyte, thus increasing the biological applications of the sensor. A limit of detection of 3.36×10^{-6} mol dm^{-3} DA was estabilished using constant potential amperometry.

It was also possible to detect DA using cyclic voltammetry. However, in this case, the electrochemical window had a significant effect on the DA oxidation current. There was a three-fold increase in the peak oxidation current on increasing the upper potential limit

from 0.600 to 0.900 V vs. SCE. This was attributed to the oxidation and release of pyrrole oligomers from the CD cavities with the application of the higher potentials. Higher rates of DA oxidation were subsequently observed, as the free cavities were available to bind with the DA.

Using cyclic voltammetry and the Randles-Sevcik equation, it was shown that the diffusion of DA was the rate-determining step in the oxidation of DA. The diffusion coefficient of DA was estimated to lie in the region of 1.52×10^{-6} cm^2 s^{-1} to 1.29×10^{-5} cm^2 s^{-1}. The high capacitance of the PPy-SCD film made it difficult to extract the exact diffusion coefficient. Studies on the kinetics and reversibility of the DA oxidation reaction at the PPy-SCD film showed that the electrochemistry of DA at the PPy-SCD modified electrode did not follow ideal reversible behaviour. Instead, it resembles a quasi-reversible process, in agreement with numerous literature reports on the oxidation of DA at other modified electrodes[10, 11]. Using RDE measurements and the Koutechy-Levich analysis, the rate constant, k_{DA}, for the oxidation of DA at the film was estimated as 3.7×10^2 mol^{-1} dm^3 s^{-1} at a pH value of 6.0.

The usual peak potential-pH shift in the electrochemical detection of DA was not observed using cyclic voltammetry. Applying the Nernst equation to the oxidation of DA, which can be described as a 2e$^-$/2H$^+$ transfer, the slope of the peak potential-pH plot should approach a value of 59.1 mV. However, this was not observed in the pH range from 3.0 to 6.0 suggesting that the proton participation in the DA oxidation reaction does not follow normal Nernstian behaviour. Interestingly, the 59.1 mV per pH unit was observed between pH values of 1.0 and 2.0. It is very difficult to explain this phenomenon, however, a higher rate constant for the oxidation of DA at the PPy-SCD film was calculated at a pH of 2.0 compared with the value observed at a pH of 6.0 which may indicate some kinetic effect.

An attempt to increase the sensitivity further by incorporating nanostructures into the polymer matrix was unsuccessful. Ultrathin PLA (Poly(L-lactide) acid) fibers were successfully generated at a Au substrate using an electrospinning approach. However, it proved difficult to electropolymerise the PPy-SCD films onto the fiber deposit. This was due to the fact that the fibers were dense and prevented the pyrrole monomer from oxidising at the Au interface. Nevertheless, using cyclic voltammetry with a high number

of cycles, a continuous coating of the PPy-SCD film was obtained, while maintaining the structure of the underlying PLA fibers. However, the oxidation of DA was similar in the presence and absence of the nanofibers.

Although the sensitivity obtained using constant potential amperometry is not sufficiently high, given that the concentration of DA ranges from 10^{-8} to 10^{-6} mol dm^{-3} in most biological samples[12], it compares very well to the detection limits reported at several other modified electrodes[13-17].

The superior sensing abilities of the PPy-SCD film compared to other PPy doped films were attributed to the fact that a 1:1 host-guest complex is formed between the DA and the sulfonated β-cyclodextrin. This was confirmed using both cyclic voltammetry and rotating disc voltammetry with complex formation constants of 199.54 ± 4.88 mol^{-1} dm^3 and 240.18 ± 5.87 mol^{-1} dm^3 calculated, respectively. NMR analysis further revealed that the relatively hydrophobic phenol ring present in DA included within the cavity of the sulfonated β-cyclodextrin. In addition, it was found that electrostatic interactions between the anionic sulfonated groups on the β-cyclodextrin and the protonated group on DA enhanced the stability of the inclusion complex formed. Indeed, the NMR studies supported the idea that the protonated amine group on the DA molecule remains outside the cavity and is bound through electrostatic interactions with the anionic sulfonated groups on the rim. Furthermore, no apparent inclusion complex was formed between the neutral β-cyclodextrin and the DA.

Michaelis-Menten kinetics and Lineweaver-Burk analysis also confirmed that there was a clear interaction between the DA and the PPy-SCD film. A K_m value of 1.53 x 10^{-3} mol dm^{-3} and 6.34 x 10^{-4} mol dm^{-3} was obtained using the Michaelis-Menten equation and the Lineweaver-Burk equation. These K_m values indicate a relatively weak binding interaction, consistent with the magnitude of the formation constant. Furthermore, the good agreement between the Michaelis-Menten theory and the data recorded for the oxidation of DA at the PPy-SCD modified electrode suggests that the DA-sulfonated β-cyclodextrin complex is converted into the product, dopamine-o-quinone, and free sulfonated β-cyclodextrin. The

regenerated sulfonated β-cyclodextrin is then available for further binding with other DA molecules.

The effects of the anionic sulfonated groups were particularly apparent with ascorbic acid (AA), the most challenging interfering compound in the determination of DA. It was found that 1.0×10^{-3} mol dm^{-3} AA and 1.0×10^{-2} mol dm^{-3} AA did not interfere with the detection of DA. This was attributed to the fact that the negatively charged sulfonated groups on the β-cyclodextrin repel the negatively charged AA from the surface of the PPy-SCD. In addition, AA is not especially hydrophobic and so is not attracted to the hydrophobic cavity of the sulfonated β-cyclodextrin. These factors in turn prevented the AA from forming an inclusion complex with the sulfonated β-cyclodextrin. This was also the case for other anionic / zwitterionic interfering compounds, including uric acid (UA), aspartic acid (Asp), glutamic acid (Glu), aminobutyric acid (GABA) and glycine (Gly).

Other anionic interfering compounds examined in this study were the key metabolites of DA, 3,4-dihydroxyphenylacetic acid (DOPAC) and homovanillic acid (HVA) and the metabolite of the 5-hydroxytryptamine (serotonin, 5-HT) neurotransmitter, 5-hydroxyindole acetic acid (5HIAA). Based on electrostatic interactions, these compounds should not be attracted to the negatively charged sulfonated β-cyclodextrin and thus should not include within the cavity of the cyclodextrin. However, weak complexation was observed for all three. This is due to the fact that the anionic carboxylate groups on the 5-HIAA, DOPAC and HVA are maintained at a sufficient distance from the negatively charged interface, avoiding the strong electrostatic repulsion between the ionised carboxylate groups and the sulfonated groups on the cyclodextrin. Thus, the phenol ring that each compound possesses can include in the cavity, but the lack of a cationic group to attract the sulfonated groups on the ring of the β-cyclodextrin leads to the formation of a very weak inclusion complex. This was also found to be the case for the neutral acetaminophen (ACOP). In terms of the selective determination of DA, interference was only observed from DOPAC and HVA over the range of DA concentrations investigated (7.0×10^{-5} mol dm^{-3} - 1.0×10^{-3} mol dm^{-3}). 5-HIAA did not interfere in the electrochemical

detection of DA at concentrations of 2.0 x 10^{-4} mol dm^{-3} DA or lower, while ACOP exhibited no interference.

Similarly to 5-HIAA, 5-HT only impeded in the detection of DA at the PPy-SCD modified electrode at concentrations higher than 2.0 x 10^{-4} mol dm^{-3} DA. However, in this case, 5-HT is cationic in nature and a relatively strong inclusion complex was formed between 5-HT and the sulfonated β-cyclodextrin, comparable to that between the DA and the sulfonated β-cyclodextrin. The influence of epinephrine (Ep), histamine (HA) and acetylcholine (Ach), which are positively charged at the pH of their respective experiments, were also investigated. No interference was observed from HA or Ach. This is probably because neither the HA nor the Ach form an inclusion complex with the sulfonated β-cyclodextrin. In contrast, Ep does include in the cavity of the sulfonated β-cyclodextrin and as a result interferes in the electrochemical detection of DA.

In summary, the PPy-SCD has excellent selectivity, effectively blocking the interference of several major interfering compounds. In total, fourteen interfering compounds were investigated and only three of these, DOPAC, HVA and EP, interfered in the detection of DA. The film is fabricated using biocompatible materials and is particularly easy to prepare, with an electrosynthesis period of approximately 40 s. In terms of potential applications for *in-vivo* sensing, the material does suffer slightly in sensitivity. However, a concentration limit of 3.36 x 10^{-6} mol dm^{-3} is sufficiently sensitive to detect DA at concentrations induced in pharmaceutical products.

As mentioned previously in Chapter 3, lower detection limits may be attained by miniaturising the electrode (~0.1 mm). This is because the current passing through the cell using these microelectrodes is very low and hence the problems of *IR* drop are greatly reduced. Also, the capacitance current decreases much more than the faradaic current leading to a significant improvement in the ratio of faradaic / non-faradaic current[18]. Furthermore, it has been well reported in the literature that these microelectrodes can be conveniently placed in the body with little disruption for real time measurements[19]. Therefore, by using microelectrodes instead of large macroelectrodes, the *in-vivo*

application of the PPy-SCD modified electrode for the sensing of DA may be achieved which would be a significant accomplishment in electroanalytical chemistry.

7.2 References

1.   B. Scharifker and G. Hills, *Electrochim. Acta*, **28**, 879, (1983).
2.   J. Serra Moreno, S. Panero and B. Scrosati, *Electrochim. Acta*, **53**, 2154, (2008).
3.   J. O. Iroh and G. A. Wood, *European Polymer Journal*, **33**, 107, (1997).
4.   M. Nishizawa, H. Nozaki, H. Kaji, T. Kitazume, N. Kobayashi, T. Ishibashi and T. Abe, *Biomaterials*, **28**, 1480, (2007).
5.   E. De Giglio, M. R. Guascito, L. Sabbatini and G. Zambonin, *Biomaterials*, **22**, 2609, (2001).
6.   E. M. M. Del Valle, *Process Biochemistry*, **39**, 1033, (2004).
7.   K. R. Temsamani, H. B. Mark Jr, W. Kutner and A. M. Stalcup, *J. Solid State Electrochem.*, **6**, 391, (2002).
8.   G. Bidan, C. Lopez, F. Mendes-Viegas and E. Vieil, *Biosens. Bioelectron.*, **9**, 219, (1994).
9.   D. A. Reece, S. F. Ralph and G. G. Wallace, *Journal of Membrane Science*, **249**, 9, (2005).
10.   P. R. Roy, T. Okajima and T. Ohsaka, *Bioelectrochemistry*, **59**, 11, (2003).
11.   Q. Wang, N. Q. Li and W. Q. Wang, *Analytical Sciences*, **18**, 635, (2002).
12.   J. Zheng and X. Zhou, *Bioelectrochemistry*, **70**, 408, (2007).
13.   N. Izaoumen, D. Bouchta, H. Zejli, M. E. Kaoutit and K. R. Temsamani, *Analytical Letters*, **38**, 1869, (2005).
14.   G. Alarcon-Angeles, B. Perez-Lopez, M. Palomar-Pardave, M. T. Ramirez-Silva, S. Alegret and A. Merkoci, *Carbon*, **46**, 898, (2008).
15.   D. V. Chernyshov, N. V. Shvedene, E. R. Antipova and I. V. Pletnev, *Anal. Chim. Acta*, **621**, 178, (2008).
16.   Q. Wang, D. Dong and N. Li, *Bioelectrochemistry*, **54**, 169, (2001).
17.   M. Ferreira, L. R. Dinelli, K. Wohnrath, A. A. Batista and O. N. Oliveira, *Thin Solid Films*, **446**, 301, (2004).
18.   R. Greef, R. Peat, L. M. Peter, D. Pletcher and J. Robinson*, Instrumental Methods in Electrochemistry*, T. J. Kemp, Ellis Horwood Limited, 443, (1985).
19.   J. P. Lowry and R. D. O'Neill, *Encyclopedia of Sensors, Neuroanalytical Chemistry In Vivo Using Electrochemical Sensors*, C. A. Grimes, E. C. Dicky, and M. V. Pishko, American Scientific Publishers, **10**, 1, (2006).